



HAL
open science

Clinical, preclinical and translational approaches of orodental anomalies associated with rare diseases

Supawich Morkmued

► **To cite this version:**

Supawich Morkmued. Clinical, preclinical and translational approaches of orodental anomalies associated with rare diseases. Development Biology. Université de Strasbourg, 2017. English. NNT : 2017STRAJ040 . tel-02939373

HAL Id: tel-02939373

<https://theses.hal.science/tel-02939373v1>

Submitted on 15 Sep 2020

HAL is a multi-disciplinary open access archive for the deposit and dissemination of scientific research documents, whether they are published or not. The documents may come from teaching and research institutions in France or abroad, or from public or private research centers.

L'archive ouverte pluridisciplinaire **HAL**, est destinée au dépôt et à la diffusion de documents scientifiques de niveau recherche, publiés ou non, émanant des établissements d'enseignement et de recherche français ou étrangers, des laboratoires publics ou privés.



UNIVERSITÉ DE STRASBOURG



ÉCOLE DOCTORALE DES SCIENCES DE LA VIE ET DE LA SANTÉ

Institut de génétique et de biologie moléculaire et cellulaire IGBMC,

CNRS-UdS UMR7104, Inserm U964

THÈSE présentée par :

Supawich MORKMUED

soutenue le : **8 septembre 2017**

pour obtenir le grade de : **Docteur de l'Université de Strasbourg**

Discipline/ Spécialité : **Biologie des organismes : développement et physiologie**

Approches cliniques, précliniques et translationnelles des anomalies bucco-dentaires associées aux maladies rares

THÈSE dirigée par :

[Mme **BLOCH-ZUPAN** Agnès]

Professeur, Université de Strasbourg

RAPPORTEURS :

[M **KLEIN** Ophir]

Professeur, University of California San Francisco, USA

[Mme **BABAJKO** Sylvie]

Docteure, Centre de Recherche des Cordeliers, Paris

AUTRES MEMBRES DU JURY :

[M **MARK** Manuel]

Professeur, IGBMC, Illkirch

[M **PIPPENGER** Benjamin]

Docteur, Institut Straumann AG, SWITZERLAND

[Mme **PITIPHAT** Waranuch]

Professeur, Khon Kaen University, THAILAND

[Mme **NIEDERREITHER** Karen]

Docteur, IGBMC, Illkirch



UNIVERSITY OF STRASBOURG



DOCTORAL SCHOOL OF LIFE AND HEALTH SCIENCES

**The Institute of Genetics and Molecular and Cellular Biology IGBMC,
CNRS-UdS UMR7104, Inserm U964**

THESIS presented by :

Supawich MORKMUED

Defended on : **8 september 2017**

For obtained the grade of: **Doctor of University of Strasbourg**
Discipline/ Specialty: **Biology of organisms: development and physiology**

**Clinical, preclinical and translational
approaches of orodental anomalies
associated with rare diseases**

THESIS directed by:

[Mme **BLOCH-ZUPAN Agnès**] Professor, University of Strasbourg

REPORTERS :

[M **KLEIN Ophir**] Professor, University of California San Francisco, USA
[Mme **BABAJKO Sylvie**] Doctor, the Cordeliers Research Centre (CRC), Paris

OTHER JURY MEMBERS :

[M **MARK Manuel**] Professor, IGBMC, Illkirch
[M **PIPPENGER Benjamin**] Doctor, Institut Straumann AG, SWITZERLAND
[Mme **PITIPHAT Waranuch**] Professor, Khon Kaen University, THAILAND
[Mme **NIEDERREITHER Karen**] Doctor, IGBMC, Illkirch

REMERCIEMENTS

Comme vous le savez, je suis venu en France il y a cinq ans pour obtenir ma thèse. En septembre s'achèvera cette étape qui sera pour moi une expérience inoubliable et j'aimerais remercier toutes les personnes qui ont rendu cela possible.

Tout d'abord, je veux exprimer ma plus profonde gratitude **au Pr Madame Agnès BLOCH-ZUPAN** pour avoir été mon principal superviseur. Elle m'a donné de nombreuses occasions de m'exprimer et de progresser en tant que chercheur, dentiste, conférencier et m'a même accueilli en France au début de mon séjour. Elle m'a fourni des ressources scientifiques exceptionnelles, un soutien continu ainsi qu'un mentorat et un excellent environnement de travail. Son engagement envers la recherche et le traitement des patients atteints de maladies rares est exceptionnel. Le Pr. BLOCH-ZUPAN m'a également donné des conseils personnels et des clés pour comprendre la culture française et le système académique français. Je suis venu vous dire, chère Agnès, que je m'en vais, comme dit la chanson, avec un immense sentiment de reconnaissance pour vous.

Je suis aussi extrêmement reconnaissant envers **la Docteure Karen NIEDERREITHER**, un co-superviseur qui possède une expertise considérable dans la recherche sur les rétinoïdes et la biologie du développement de la souris. Elle a toujours partagé ses expériences et aidé à diriger mon projet pour faire avancer efficacement mes travaux et mon développement intellectuel. Son engagement personnel pour l'excellence dans la science m'a beaucoup inspiré.

Je tiens à exprimer tous mes remerciements aux membres du Comité consultatif de Mi-thèse:

Le Pr. Ekkehart LAUSCH, Université de Fribourg, pour ses contributions en tant que membre externe du comité de thèse. C'est un merveilleux clinicien et chercheur qui m'a fourni des connaissances en biologie du développement et pour le traitement des patients. Sa carrière est très certainement un exemple pour mon avenir professionnel.

Le Dr Stéphane VINCENT, pour avoir éclairé mes recherches de son expertise en biologie et pour être un excellent chercheur.

Le Dr François CLAUSS, pour son soutien dans mes travaux et pour avoir partagé son expertise dans les expériences chirurgicales sur les souris, à la fois l'implant dentaire et la guérison (modèle d'extraction dentaire) à la faculté de médecine. Il m'a énormément aidé techniquement et intellectuellement à faire avancer mes recherches. J'apprécie particulièrement nos expériences conjointes et nos discussions approfondies.

Je tiens à remercier **le Professeur Ophir KLEIN**, de l'Université de Californie à San Francisco, aux États-Unis, et **la Docteure Sylvie BABAJKO**, du Centre de Recherche des Cordeliers de Paris pour avoir fait partie du jury de thèse de doctorat en tant que rapporteurs de ce travail.

Je tiens aussi à exprimer ma gratitude **au Professeur Manuel MARK**, de l'IGBMC, de l'Université de Strasbourg, **au Dr Benjamin PIPPENGER** de l'Institut Straumann AG et **au Dr Waranuch PITIPHAT** de l'Université de Khon Kaen pour avoir accepté d'être membres de ce jury de thèse. Je leur en suis très reconnaissant et suis très honoré de leur participation.

Je tiens également à remercier toutes les personnes qui m'ont encouragé et soutenu tout au long de la formation doctorale. J'ai reçu un soutien et une formation considérables et diversifiés pour des expériences et des discussions scientifiques et je remercie les personnes suivantes pour leur générosité dans le partage des connaissances et du matériel expérimental :

Tout d'abord, j'aimerais remercier deux ingénieurs talentueux : **Brigitte SCHUHBAUR** et **Valérie FRAULOB** qui m'ont aidé avec leur assistance de laboratoire et leurs conseils techniques. J'ai appris beaucoup de leurs expériences scientifiques et générales. Surtout, leur amitié m'a été précieuse tout au long des événements sociaux et de ma vie au laboratoire. Je ne trouve pas de mots suffisants pour les remercier toutes les deux.

Le Pr Dr Pascal DOLLE pour ses conseils, son soutien et son expertise en préparation de manuscrits. Cela a également favorisé mon avancement professionnel.

Je remercie tous les membres de l'équipe DOLLE, les membres actuels et passés du laboratoire :

Le Dr. Virginie LAUGEL-HAUSHALTER, pour m'avoir fait bénéficier de son engagement personnel et de sa technique du profilage biologique ;

Le Dr. Marie PASCHAKI, pour le soutien en biologie moléculaire et en génétique de souris ;

Le Dr. Anna NIEWIADOMSKA-CIMICKA, pour le soutien en biochimie des protéines, l'analyse des protéines, l'analyse des données de séquençage et pour sa gentillesse ;

Le Dr Carole HAUSHALTER, pour son soutien en biologie moléculaire, génétique de souris et pour sa belle amitié ;

Le Dr Muriel RHINN, pour m'avoir fourni un enseignement fondamental dans la manipulation de la souris et la biochimie ;

Le Dr Wojciech KREZEL, Ania PODLESNY, Marion CIACIA, le Dr Samir LAOUINA, Claire HUBER, Thomas HEID, le Dr Elyette BROLY et le Dr. Rose MBEDE NGA MVONDO pour le soutien en sciences de la biologie et avec qui j'ai partagé de beaux moments pendant ma vie de doctorat.

Je remercie les autres membres de l'IGBMC, de l'Institut clinique de la souris ICS, de la plate-forme d'histopathologie, de la plate-forme de microarray et de la génomique, de la phénotypisation et de la plate-forme d'imagerie μ CT. Je tiens à remercier également les membres de la Faculté de médecine et de chirurgie dentaire de l'Université de Strasbourg:

Le Dr. Megana PRASAD, pour son enseignement fondamental dans les analyses de génétique humaine. Son expertise dans la recherche m'inspirera et elle sera un modèle pour moi ;

Le Dr Mathilde HUCKERT, pour le soutien et l'amitié en clinique d'odontologie pédiatrique, de la Faculté de chirurgie dentaire et du Pôle de médecine et chirurgie bucco-dentaire des Hôpitaux Universitaires de Strasbourg.;

Le Mr. Joseph HEMMERLE et le Mr. Eric MATHIEU, pour avoir donné son soutien lors des expériences et des résultats de microscopie électronique ;

Marzena KAWCZYNSKI, pour l'assistance dans la base de données, les échantillons salivaires et pour avoir su créer un environnement de travail joyeux lors de nombreux événements ;

Le Dr. Alexandru PARLOG, pour avoir donné son enseignement fondamental et pour sa contribution utile dans la recherche osseuse ;

Le Dr. Bernard JOST, pour son soutien lors des expériences de séquençage et de l'analyse bioinformatique ;

Le Dr. Olivia WENDLING, pour la formation en histologie, en immunofluorescence et le projet "Phenomin" pour la souris ;

Le Dr. Isabelle GONCALVES DA CRUZ, pour son soutien dans la zone de phénotypage de souris de l'ICS et la formation de micro-CT ;

Le Dr. Johan H van Es et le Dr. Hans Clevers, de Koninklijke Nederlandse Akademie van Wetenschappen, Amsterdam, Pays-Bas pour avoir fourni la souris Smoc2-Cre-GFP.

Je suis très reconnaissant envers le doyen de la Faculté de Chirurgie Dentaire de Strasbourg –**le Pr Madame Corinne TADDEI-GROSS**, et l'ancien doyen de la faculté de médecine dentaire, l'Université de Khon Kaen, en Thaïlande, **le Dr Waranuch PITIPHAT** et **le Dr Nawarat WARA-ASWAPATI CHAROEN**, ainsi que mon ancien chef du département pédiatrique, **le Dr. Patimaporn PUNGCHANCHAIKUL**, pour m'avoir encouragé à m'engager dans l'enseignement supérieur en dentisterie académique, et donc pour soutenir mon parcours dans la formation doctorale.

Concernant le soutien financier, je suis très heureux d'avoir pu bénéficier de la bourse franco-thaïlandaise et de la bourse de l'Université de Khon Kaen afin de faire face à mes dépenses en France tout au long de la durée du doctorat. Je remercie aussi les financements de l'Institut d'Études Avancées de l'Université de Strasbourg

(USIAS), INTERREG IV et INTERREG V (FEDER) RARENET pour leur soutien à la recherche.

Merci à **Alexandre HERNANDEZ** pour son aide dans toutes mes démarches administratives, dans l'apprentissage de la langue française et la découverte de la culture française.

Merci à tous mes amis thaïlandais PJoke, Boat, New, Mod, Chinchar, Wanchun, Eve, Toei, Nhum, Roger, Tum et Ake en Thaïlande et Sae, Fair, NTum, Paew, PPek, PNan, PYim, PPim, San, Et NTaddy en France pour leur soutien continu, avec qui j'ai partagé des moments inoubliables et pour m'avoir encouragé dans mon travail. Je leur souhaite de très belles choses dans leur avenir.

Ces remerciements ne seraient pas complets si je ne parlais pas de ma famille, de son soutien et de son attention constante. Je souhaite exprimer ma plus grande reconnaissance à mes parents, même si je ne formule jamais mes sentiments directement. Bien qu'ils sachent combien j'apprécie leur temps et leurs efforts, il est important que je souligne ce soutien à la fin de ma thèse. Je suis si heureux de grandir dans cette famille et j'ai beaucoup apprécié leur récente visite en Europe.

Enfin, je voudrais évoquer quelqu'un qui a pris une place fondamentale dans ma vie. Grâce à elle, j'ai eu l'énergie de mener mes activités jusqu'à leur terme et la force d'obtenir mon doctorat. Il s'agit de ma future femme, **le Dr Preeyarat PLONGNIRAS**. Elle est ma meilleure amie et partenaire dans la vie. Je sais combien ses encouragements et son soutien sont précieux, et j'espère une vie merveilleuse avec elle. En Thaïlande et à l'étranger, elle m'a enchanté avec son joli sourire, son rire et son amour.

ACKNOWLEDGEMENTS

At the completion of my thesis, I would like to thank all those people who made this possible and an unforgettable experience for me.

First of all, I would like to express my deepest sense of gratitude to my supervisor Pr. Agnès BLOCH-ZUPAN for being my primary supervisor. She has given me many opportunities to develop as a researcher, dentist, lecturer, and even has hosted me in France at the beginning. She has provided me with exceptional scientific resources, continuous support and mentoring, and a great working environment. Her commitment to the research and treatment of rare diseases patients is exceptional. Pr. Agnès also has given me personal guidance and support for life in understanding French culture and the French academic system, which I am deeply grateful for.

I am extremely grateful and thank Dr. Karen NIEDERREITHER, a co-supervisor with considerable expertise in retinoid signaling and mouse developmental biology research. She has always shared her experiences and helped direct my project to efficiently advance my work and intellectual development. Her personal commitment to excellence in science has greatly inspired me and is very much appreciated.

I would like to express my appreciation to all of the members of my Thesis Advisory Committee Meetings:

Pr. Ekkehart LAUSCH, Freiburg University, for his contributions as an external mid-thesis committee member. He is actively a wonderful clinician and a researcher who provided me knowledge in both developmental biology and patient treatment. His professional career inspires me on how to move forward for my future.

Dr. Stéphane VINCENT, for his essential vision on my research from his expertise in biology from his experience as an excellent researcher.

Dr. François CLAUSS, for supporting my research and sharing his expertise in mouse surgical experiments, both dental implant and wound healing (tooth extraction

models). He has helped me technically and intellectually to advance my research tremendously. I especially appreciate our joint experiences and in depth discussions.

I would like to thank Prof. Ophir KLEIN, from University of California, San Francisco, USA and Dr. Sylvie BABAJKO, from the Centre de Recherche des Cordeliers, Paris for being part of the PhD thesis committee, acting as external reviewers of this PhD thesis.

I would like to thank Prof. Manuel MARK, from IGBMC, University of Strasbourg, Dr. Benjamin PIPPENGER from Institut Straumann AG, and Dr. Waranuch PITIPHAT from Khon Kaen University, for accepting to be members of this PhD thesis committee. I am grateful and honored by their participation.

I also would like to thank all individuals who encouraged and supported me throughout the doctoral training. I have received tremendous, diverse support and training and want to thank the following individuals for their generosity of sharing knowledge and experimental materials.

Firstly, I would like to thank 2 talented engineers; Brigitte SCHUHBAUR and Valérie FRAULOB, who have helped offering laboratory assistance and technical advice. I have learned a tremendous amount from your scientific and general experiences. Their friendships are invaluable. I find no words sufficient to thank both of you.

Dr. Pascal DOLLE for his advice, support, and expertise in manuscript preparation, which has been invaluable in my professional advancement.

I am thankful to everyone in DOLLE team, present and past members of laboratory;

Dr. Virginie LAUGEL-HAUSHALTER, for inspiring me with her personal commitment and biological excellence in genetic profiling.

Dr. Marie PASCHAKI, for support in molecular biology and mouse genetics.

Dr. Anna NIEWIADOMSKA-CIMICKA, for support in protein biochemistry, protein analysis, sequencing data analysis, and for her kindly friendship.

Dr. Carole HAUSHALTER, for support in molecular biology, mouse genetics, and for her wonderful friendship.

Dr. Muriel RHINN, for providing fundamental teaching in mouse manipulation and biochemistry.

Dr. Wojciech KREZEL, Ania PODLESNY, Marion CIACIA, Dr. Samir LAQUINA, Claire HUBER, Thomas HEID, Dr. Elyette BROLY, and Dr. Rose MBEDE NGA MVONDO for support in biology science and sharing nice moments during my PhD life.

I thank other members at IGBMC, ICS mouse facility, histopathology platform, microarray and genomics platform, phenotyping and μ CT imaging platform. I would like to thank also the members at medical and dental faculties of the Université de Strasbourg;

Dr. Megana PRASAD, for providing fundamental teaching in human mutational analyses. Her expertise in genetic research inspires me.

Dr. Mathilde HUCKERT, for support and friendship in pediatric clinic at the Strasbourg Faculty of Dentistry and Teaching Hospital.

Mr. Joseph HEMMERLE and Mr. Eric MATHIEU, for providing fundamental discussions and useful scanning electron microscopy results.

Marzena KAWCZYNSKI, for support in database, salivary samples and for creating an amazing work environment during many events.

Dr. Alexandru PARLOG, for providing fundamental teaching and useful discussions in bone research.

Dr. Bernard JOST, for support of sequencing experiments and bioinformatic analysis.

Dr. Olivia WENDLING, for providing the histology, immunofluorescence, and Phenomin mouse database information.

Dr. Isabelle GONCALVES DA CRUZ, for her support in mouse phenotype area and micro-CT training.

Drs. Johan H van Es and Hans Clevers, from Koninklijke Nederlandse Akademie van Wetenschappen, Amsterdam, Netherlands for providing the Smoc2-Cre-GFP mice.

I am very grateful to the current Dean of the Faculté de Chirurgie Dentaire de Strasbourg -Corinne TADDEI-GROSS, the current and former Dean of the faculty of dentistry at Khon Kaen University, Thailand- Dr. Waranuch PITIPHAT and Dr. Nawarat WARA-ASWAPATI CHAROEN. My former head of the pediatric department, Dr. Patimaporn PUNGCHANCHAIKUL. These individuals have inspired me and supported my commitment to higher education in academic dentistry.

For financial support, I am grateful to the Franco-Thai scholarship and Khon Kaen University. These scholarships have supported my living expenses in France. In addition, I am grateful to University of Strasbourg Institute of Advanced Studies (USIAS), INTERREG IV and V (ERDF funding) RARENET funding to support research expenses.

Thanks to Alexandre HERNANDEZ for his help in French language, and French discovery.

Thanks all my Thai friends PJoke, Boat, New, Mod, Chinchar, Wanchun, Eve, Toei, Nhum, Roger, Tum, and Ake in Thailand and Sae, Fair, NTum, Paew, PPek, PNan, PYim, PPim, San, and NTaddy in France for their continuous support, sharing unforgettable moments, and encouragement.

These acknowledgments would not be complete without thanking my family for their constant support. I want to express my deepest appreciation to my parents. They have guided me from the youngest age, and have been my role model. Their constant faith and hard-working ethics has inspired me.

Finally, I would like to mention the most important lady in my life, my future wife, Dr Preeyarat PLONGNIRAS. She is my best friend and partner in life. I appreciate her encouragement and support, and look forward to a wonderful life together. In Thailand and abroad, she has enchanted me with her cute smile, laughter, and love. Personally, I look forward to a bright future with her.

TABLE DES MATIÈRES (CONTENTS)

REMERCIEMENTS.....	3
ACKNOWLEDGEMENTS	8
TABLE DES MATIÈRES (CONTENTS).....	12
Liste des tableaux (List of tables)	14
Liste des figures (List of figures)	15
Liste des Abréviations (List of Abbreviations).....	16
INTRODUCTION	18
CONTEXTE ET COMMENTAIRE (BACKGROUND AND SIGNIFICANCE)	21
Part I Tooth development.....	22
I.1 The mouse dentition	23
I.2 Sequential stages of odontogenesis	25
I.2.1 The origin of ectodermal tissue and appendages	25
I.2.2 Initiation of dental development.....	26
I.2.3 Dental morphogenesis	28
I.2.4 How the tooth begins to differentiate into defined tooth lineages	29
Part II Signaling pathways involved in tooth development.....	34
II.1 Transcription factors critical in tooth patterning	35
II.2 The TGF- β /BMP pathway.....	39
II.3 FGFs	45
II.4 WNTs	47
II.5 NF- κ B/TNF Pathway.....	49
II.6 The Sonic hedgehog pathway	52
II.7 Notch.....	55
Part III Retinoids	56
III.1 The general role of vitamin A	57
III.2 Clinical use of retinoids and the worldwide role in public health	58
III.3 How RA is obtained from dietary sources, stored in liver, and transported to the cell	59
III.4 Target Cell Uptake, Intracellular Metabolism, Cytoplasmic and Nuclear Receptors Mediating Vitamin A Effects.....	62
III.5 The function of retinoic acid as a transcriptional regulator.....	63
III.6 Vitamin A Deficiency and Excess.....	72

III.7 Associations between vitamin A and evident effect on bone mass in humans	73
III.8 Mechanism of RA effects on bone development	74
Part IV Dental anomalies.....	77
IV.1 Definitions.....	78
IV.2 Environmental factors altering tooth development.....	78
IV.3 Dental anomalies in rare genetic diseases	83
IV.3.1 Hypodontia/Oligodontia.....	83
IV.3.2 Supernumerary teeth or hyperdontia	85
IV.3.3 Microdontia.....	85
IV.3.4 Heritable dentin conditions	86
IV.3.5 Dentin Dysplasia	86
IV.3.6 Amelogenesis Imperfecta	87
IV.4 A focus on rare diseases through human genetics and mimicking mouse models.....	89
Résumé de la thèse	95
RÉSULTATS (RESULTS)	101
(i) Environmental factors.....	102
Retinoic Acid Excess Impairs Amelogenesis Inducing Enamel Defects	103
(ii) Genetic factors	129
Enamel and dental anomalies in latent-transforming growth factor beta-binding protein 3 mutant mice	130
Craniofacial and tooth abnormalities in Sparc-related modular calcium-binding protein 2 (<i>Smoc2</i>) mutant mice.....	148
CONCLUSIONS-DISCUSSION-PERSPECTIVES	169
ANNEXES (APPENDIX).....	178
Liste des annexes (List of appendix).....	179
RÉFÉRENCES BIBLIOGRAPHIQUES (REFERENCES).....	285
Résumé.....	310
Résumé en anglais.....	310

Liste des tableaux (List of tables)

Table 1 Summary of phenotypes resulting from targeted inactivation of retinoid signaling pathway components in mice.....	70
Table 2 RA response elements, either activating or repressing retinoid targets, and their respective physiological roles.....	71
Table 3 Environmental factors related to dental hard tissue formation/anomalies; pre-clinical studies.....	80
Table 4 Human rare diseases and their phenotypes.....	90

Liste des figures (List of figures)

Figure 1 The human and mouse dental morphology and a fate of dental development.....	24
Figure 2 Signaling cascades during epithelial-mesenchymal interaction.....	27
Figure 3 Ectodermal appendages development during its initial stages.....	27
Figure 4 Normal enamel prism of lower incisor in mouse.....	31
Figure 5 Pattern of gene expression in the developing tooth.....	35
Figure 6 Schematic representation of the Bmp and Tgf- β signaling pathways.....	40
Figure 7 TGF- β synthesis and activation.....	43
Figure 8 Schematic representation of Fgf signaling pathway.....	45
Figure 9 Schematic representation of Wnt signaling pathway.....	48
Figure 10 Schematic representation of Eda signaling pathway.....	50
Figure 11 Schematic representation of Notch, Wnt, and Shh signaling cascades....	53
Figure 12 The fate of vitamin A transportation.....	60
Figure 13 Intracellular regulation of retinoid signaling.....	64
Figure 14 RA signaling mechanism.....	66
Figure 15 The model of Hypervitaminosis A.....	75

Liste des Abréviations (List of Abbreviations)

A		E	
AD	Autosomal dominant	E	Embryonic stage
ADH	Alcohol dehydrogenase	ED	Ectodermal dysplasia
AI	Amelogenesis Imperfecta	EDA	Ectodysplasin A
AKT	AKT serine/threonine kinase	Edar	Ectodysplasin A receptor
Alk2	(Acvr1) activin A receptor, type 1	Edaradd	EDAR (ectodysplasin-A receptor)-associated death domain
ALP	Alkaline phosphatase	Enam	Enamelin
α SMA	Alpha-smooth actin	ERDF	The EU-funded project
Ambn	Ameloblastin	F	
Amel	Amelogenin	FACS	Fluorescence activated cell sorting
AML	Acute myelogenous leukemia	FDA	Food and Drug Administration
APC/CK1 α	APC, WNT signaling pathway regulator	FGF	Fibroblast growth factor
APL	Acute promyelocytic leukemia	Foxi3	Forkhead box I3
AR	Autosomal recessive	G	
ATRA	All-trans RA	Gli	GLI family zinc finger
B		GPCR	G-protein coupled receptor
Barx	BARX homeobox	Grem	Gremlin
BCO	beta-carotene oxygenase	GSK-3 β	Glycogen synthase kinase 3 beta
BMD	Bone mineral density	H	
BMP	Bone morphogenetic protein	H3K27me3	Histone H3 lysine 27 trimethylation
BMPR	Bone morphogenetic protein receptor	HAT	Histone acetylase
BPA	Bisphenol A	HDAC	Histone deacetylase
BRONJ	Bisphosphonate-induced osteonecrosis of the jaw	HED	Hypohidrotic Ectodermal Dysplasia
C		Hes1	Hes family bHLH transcription factor 1
CCD	Cleidocranial Dysplasia	HOX	Homeobox
ChIP-Seq	Whole-genome chromatin immunoprecipitation-sequencing	Hoxb1	Homeobox B1
COL1A1	Collagen type I alpha 1 chain	HSP	Heat shock promoter
COL1A2	Collagen type I alpha 2 chain	HSPM	Hypomineralized Second Primary Molars
CRBP	Cellular retinol binding protein	I	
CTNNB1	Catenin beta 1	ICS	Mouse Clinical Institute/Institute Clinique De La Souris
CYP26	Cytochrome P450 26	IEE	Inner enamel epithelium
D		IFN	Interferon
DD	Dentin Dysplasia	IKK	Inhibitor of κ B kinase
DI	Dentinogenesis Imperfecta	I κ B	Inhibitors of κ B
DKK	Dickkopf	IL	Interleukin
Dll	Distal-less	ILK	Integrin-linked Kinase
Dlx	Distal-Less/Dlx homeobox gene	IMPC	International Mouse Phenotyping Consortium
DMP1	Dentin matrix protein 1	J	
DRs	Direct repeats	Jag	Jagged
Dspp	Dentin sialophosphoprotein	JNK	(Mapk8) mitogen-activated protein kinase 8

K

K5-Ikk β Overexpressing IKK β under the control of the keratin 5 promoter
 KLK4 Kallikrein-related peptidase 4

L

Lef1 Lymphoid enhancer binding factor 1
 Lhx LIM homeobox
 LRP Low density lipoprotein
 LTBP3 Latent transforming growth factor-beta binding protein 3

M

MAPK/ERK Mitogen-activated protein kinase
 MIH Molar Incisor Hypomineralization
 miRNA MicroRNA
 MMP20 Matrix metalloproteinase 20
 Msx Msh homeobox

N

NCOA Nuclear receptor co-activator
 NCOR Nuclear receptor co-repressor
 NF- κ B Nuclear factor kappa B
 NICD Notch intracellular domain containing portion
 NIK (Map3k14) mitogen-activated protein kinase kinase kinase 14

O

OCN Osteocalcin
 OI Osteogenesis Imperfecta

P

Pax Paired box
 PCNA Mitosis-specific phosphorylated histone immunohistochemistry
 PECAM Platelet endothelial cell adhesion molecule
 Pitx Paired-like homeodomain transcription factor
 PRC2 Polycomb repressive complex 2
 Ptch1 Patch1

R

RA Retinoic acid
 RALDH Retinaldehyde dehydrogenases
 RANKL Receptor activator of nuclear factor kappa-B ligand
 RAR Retinoic acid receptor
 RARE Retinoic acid-response element
 RAR α RA receptor alpha
 RBP Retinol binding protein
 RDH10 Retinol dehydrogenase 10
 RT-PCR Real-time reverse transcription polymerase chain reaction

Runx2 Runt-domain containing transcription factor 2
 RXR Retinoid X receptors

S

SEM Scanning electron microscope
 SFRP4 Secreted frizzled related protein 4
 SHH Sonic hedgehog
 Smad SMAD family member
 smo Smoothened
 Smoc2 Sparc-related modular calcium-binding protein 2
 Sostdc1 Sclerostin domain containing 1
 SOX3 SRY (sex determining region Y)-box 3
 Sp6 Trans-acting transcription factor 6
 Stra6 Stimulating retinoic acid gene 6

T

TCF/LEF Transcription factor/Lymphoid enhancer binding factor
 TDO Tricho-Dento-Osseous
 TGF- β Transforming growth factor beta
 TNF Tumour necrosis factor
 TRAP Tartrate Resistant Acid Phosphatase
 TUNEL Terminal deoxynucleotidyl transferase dUTP nick end labeling

U

USIAS The University of Strasbourg Institute for Advanced Study

V

VAD Vitamin A deficiency
 VEGF Vascular endothelial growth factor

W

Wise (Sostdc1) sclerostin domain containing 1
 WT Wild-type

INTRODUCTION

During mammalian evolution head morphogenesis is both a conserved and complex process. The vertebrate skull is a complexly designed, evolutionarily quite ancient structure. Within mammals, the overall shape of the skull shows important conserved components, species-specific variations, along with hereditarily conserved individual components[1]. Craniofacial and orodental developmental anomalies are often clear aspects of rare diseases or syndromes. These diseases encompass about 7000 different entities, affecting 4 million people in France, and almost 25 million in Europe. By definition, rare diseases affect less than one person in 2000 and for ~80%, are genetically driven. Among the over than 5000 known syndromes, more than 700 have a craniofacial and/or orodental phenotype[2, 3]. About 250 (of the 700) genetic diseases display cleft lip/palate symptoms. Novel rare diseases and corresponding mutated genes will thus be essential to understand genetic signaling pathways regulating craniofacial and dental development, and provide clues to understand organogenesis to develop future clinical approaches.

Tooth development/anomalies is an excellent model organogenesis to understand how a given mutated gene can alter tooth morphogenesis and/or terminal differentiation of post-mitotic cells, events leading to the formation and mineralization of dentin, enamel, cement. It is also a system to decipher/epigenetics, including genetic interactions with environment. The tooth is indeed an excellent marker of environmental assaults, which when taking place during the early mineralization process (prior tooth eruption within the oral cavity) can have permanent effects. A combination of genetic background and susceptibility to environment may modulate any given phenotype.

Mouse models dentition, despite intrinsic differences reproduces dental anomalies encountered in human rare diseases. These models are a powerful approach to increase our understanding of human disease, through advancing our understanding of fundamental biological mechanisms[4].

This PhD thesis will first present as background information dental development and the main pathways involved, with a focus on retinoids. It will then discuss dental anomalies in relationship with environmental assaults and rare diseases.

The experimental work (presented in published papers) begins with investigations on the role of environment, by examining the developmental effects of excess retinoic acid on enamel formation. The next two papers explore the craniofacial and orodental phenotype of 2 rare diseases transgenic animal models. Enamel and dental anomalies in latent transforming growth factor- β binding protein 3 (*Ltbp3*) mutant mice are examined. Lastly, a manuscript in preparation on the craniofacial and tooth abnormalities in Sparc-related modular calcium-binding protein 2 (*Smoc2*) mutant mice is presented.

These rare disease mouse models were selected based on sequencing data from families and patients enrolled in the Strasbourg University and Hospital Reference Center for orodental rare diseases. These investigations have taken place in collaboration with O-Rares, within the ERDF funding framework of the Interreg IV Offensive Sciences and the Interreg V RARENET projects.

**CONTEXTE ET COMMENTAIRE
(BACKGROUND AND SIGNIFICANCE)**

Part I

Tooth development

Teeth are composite organs with both an epithelial (the enamel organ) and a mesenchymal compartment (papilla, pulp). They use epithelio-mesenchymal interactions to drive their development. The same conserved signaling pathways that regulate most aspects of embryonic development are required for tooth development.

Odontogenesis starts as neural crest cells individualize and migrate towards the first branchial arch to interact with the oral ectoderm, and initiate in specific location and timing the beginning stages of tooth development. Tooth development then progresses through different stages from dental lamina to individual placodes, then through bud, cap, bell stages, to set up the crown and direct later root morphogenesis. Timely controlled terminal differentiation of odontoblasts and ameloblasts begins, leading to the patterning of dentin and enamel matrix. This is followed by further maturation in the mineralization processes. The alveolar bone and the periodontium develop concomitantly.

Most of our current knowledge on the molecular and genetic basis of tooth development has come from mouse studies. Extensive investigations into the molecular regulation of tooth formation have been carried out with many genetically engineered mouse models[5, 6].

Developmental anomalies include changes in the number, shape, size, and/or composite tooth structure. These changes may also be visualized through the color or structural integrity of dental hard tissues such as dentin, enamel, cementum, alveolar bone. In addition the eruption and/or resorption of teeth are also linked to stage-specific morphological and molecular events and pathways.

1.1 The mouse dentition

Mouse teeth have a unique, conserved organization. This is shown in Figure 1. In each quadrant, a single incisor is separated from three molars by a gap (or toothless region) called the diastema. Hence rodents such as mice display a reduced number of teeth (compared to humans). Mice also have a single set of teeth. Rodent teeth are considered to be deciduous teeth that do not undergo replacement[7, 8], whereas humans have two sets of teeth[9]. The potential for tooth replacement in mice appears to have been retained[8, 10, 11]. Rodent incisors are different from

humans because they grow continuously throughout the life of the animal, a property assigned to the presence of stem cells populations in their cervical loops. Enamel is present only on the labial side of the incisor, considered as a crown analogue. The lingual side is covered with dentin and represents the root analogue.

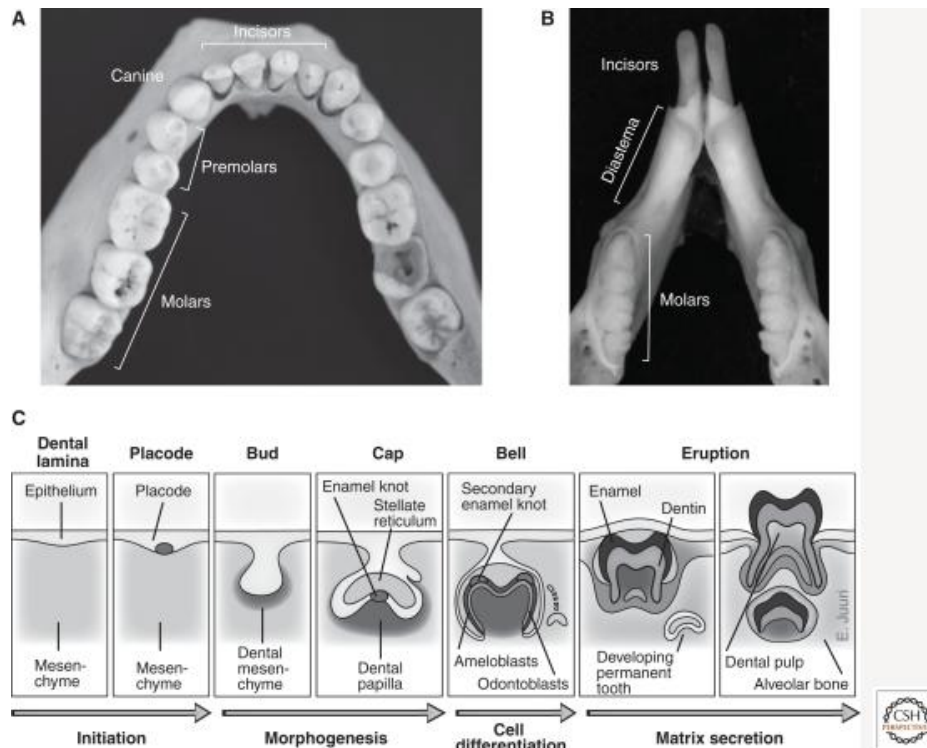


Figure 1 The human and mouse dental morphology and a fate of dental development.

(A) (B) The human permanent dentition, in comparison with the mouse. Mice have a toothless diastema separating incisor and molars in each half of the jaw.

(C) Dental development begins from a thickening of the epithelium, where the growing epithelium then forms bud. Then, the dental mesenchyme condenses underlying the tooth epithelial bud. At the morphogenesis stage, the epithelial tissue transforms to cap and bell shapes. The signaling centers, called primary and secondary enamel knots, in the enamel organ control the growth and the shape of the tooth. At the tooth differentiation stage, enamel-secreting ameloblasts and dentin-secreting odontoblasts mature from epithelial and mesenchymal cells, respectively. (source [12])

I.2 Sequential stages of odontogenesis

Odontogenesis occurs in sequential stages. To recapitulate, this begins with tooth initiation, induction of epithelial placodes (seen as localized thickening of the oral ectoderm), followed by bud, cap, and bell morphogenetic stages. Subsequently, the terminal differentiation of odontoblasts and ameloblasts is observed (Figure 1). Next, root formation and tooth eruption occur. The appearance of sub-regional tooth-types (incisors and molars) can be distinguished by the unique shape of the crown and root, as well as a defined cusp patterns. Studies of developing mouse teeth suggest that cusp initiation and patterning in tooth germs is a process that repeatedly re-utilizes conserved developmental pathways[13-17].

I.2.1 The origin of ectodermal tissue and appendages

During early embryogenesis the ectoderm is the external germ layer. The epidermis develops from the surface ectoderm[18]. Epidermis-derived structures include the skin and other stratified epithelia such as the oral epithelium. Subsequently, these tissues diversify to specialized structures (called ectodermal appendages) that include mammary glands, salivary glands, hair follicles, and teeth. These ectodermal appendages all develop through similar mechanisms, involving precise crosstalk between the epithelium and mesenchyme, and often sharing common morphological features during early organogenesis[19].

The cephalic neural crest

Teeth are ectomesenchymal organs derived from oral ectoderm and neural crest cells ectomesenchyme. The level of origin within the crest for lower incisors and lower and upper molars is identical, namely the caudal part of the midbrain/rostral hindbrain. These cells all migrate toward the first branchial arch. Cells originating from the forebrain and rostral midbrain also migrate towards the frontonasal process and the intermaxillary process to participate to the development of the upper incisors.

1.2.2 Initiation of dental development

Teeth are initiated from the dental lamina, a stripe of stratified epithelium, first visualized at mouse embryonic stage (E) 11. This dental lamina is of epithelial origin (oral ectoderm). Localized epithelial thickenings (placodes) within the dental lamina mark the initiating tooth, which then buds into the underlying mesenchyme.

Dental placode formation can be visualized by *Pitx2* expression. This transcription factor serves as a specific, early marker of dental epithelium, whose expression persists in all epithelial cells of the developing tooth until crown morphogenesis[20]. Reciprocal epithelial–mesenchymal cross-tissue interactions induce and regulate tooth morphogenesis[21]. Tooth-generating oral regions have a so-called odontogenic potential.

Classical tissue recombination experiments have shown that the odontogenic potential first resides in the epithelium at the placode stage[9]. Hence, mouse oral epithelial region (between E9 and E11.5) can induce tooth formation in non-dental mesenchyme[22, 23]. After E11.5 the odontogenic potential shifts to the dental mesenchyme, so this mesenchyme can induce non-dental epithelia to become teeth[24]. In parallel, the ability of the epithelium to induce tooth appears lost at this stage. The shift in odontogenic potential to mesenchyme temporally occurs at the placode stage[24, 25]. The dental lamina expresses many transcription factors and signal molecules such as fibroblast growth factors (FGFs), bone morphogenetic proteins (BMPs), sonic hedgehog (SHH), and WNT signals that regulate dental identity. Gene restricted to the placodes or early signaling centers include *Pitx2* and *Foxi3*, along with many other signaling pathway molecules (including *Shh*, *Wnt*, *Bmp*, *Fgfs*-notably *Fgf20*)[12, 26, 27]. Early combined actions of these factors increase proliferation producing the tooth bud. Some of these factors are involved in mediating the shift of odontogenic potential to the mesenchyme (Figure 2) (reviewed in [21]).

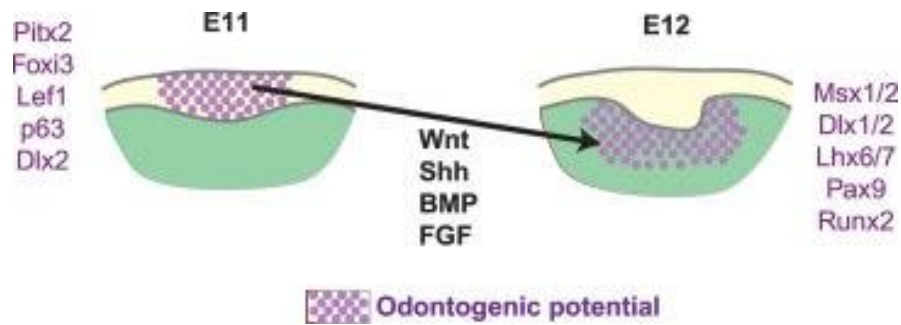


Figure 2 Signaling cascades during epithelial-mesenchymal interaction.

The capacity to initiate teeth first resides in the oral epithelium of E10 and E11 stage mouse embryos (dental lamina stage). This capacity shifts at the placode stage (E12) to the surrounding neural crest-derived mesenchyme. This is simultaneous with dental mesenchyme condensation. The epithelial/mesenchymal odontogenic potential was defined through tissue recombination experiments (source [21])

Teeth develop as epithelial appendages and share many of the same regulatory mechanisms with other ectodermally-derived organs during their initial formation and morphogenesis[12] (Figure 3). During odontogenesis, specific cells secrete signaling molecules at defined sites which often initiate defined transcriptional cascades[28].

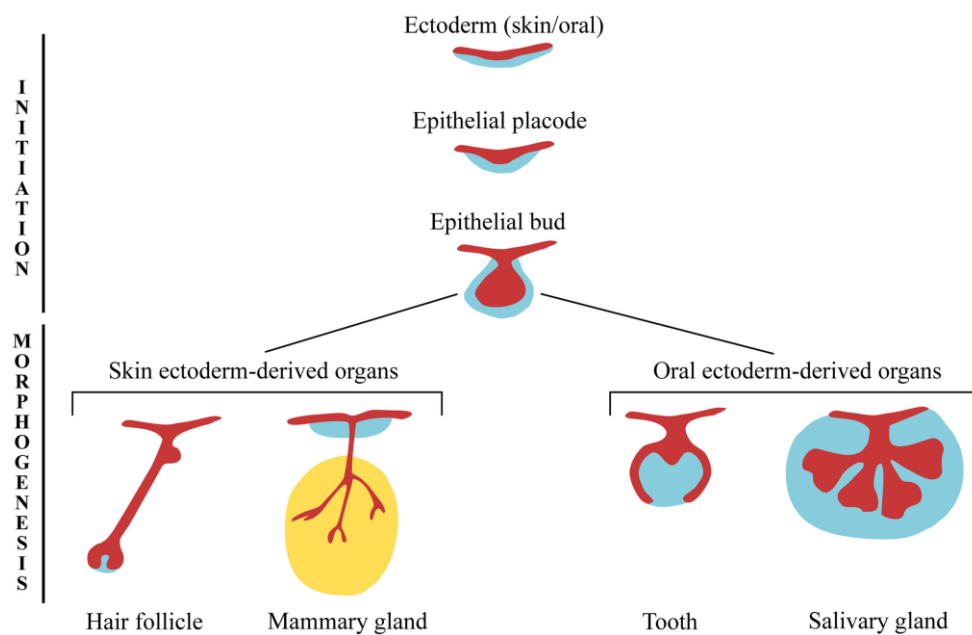


Figure 3 Ectodermal appendages development during its initial stages.

Ectoderm-derived structures initiate from embryonic ectoderm, mainly due to mesenchymal-derived signals. Epithelial placodes appear and subsequently grow into the surrounding mesenchyme. These early developmental events are similar in all ectodermal organs. At later stages, epithelial buds undergo different morphogenetic configurations, resulting in the formation of more specialized structures. (source [29])

1.2.3 Dental morphogenesis

During the transition from the bud to cap stage, a signaling center called the primary enamel knot is formed from a transient cluster of dental epithelial cells[30]. The primary knot establishes the crown base, regulates the pattern of tooth cusps, and directs the projections of enamel and dentin on the occlusal surface. In teeth with multiple cusps (such as the molars) secondary enamel knots appear early at the bell stage, positioned at the tips of future cusps. The secondary knots coordinate cusp patterning by inducing terminal differentiation of the adjacent mesenchymal-derived odontoblasts. Additional enamel knots (which result in additional cusps) can form outside the zones of inhibition of previously formed enamel knots. This process is dynamic. The patterning of cusps is not predetermined, so the size, shape and location of the first-forming cusps regulates the appearance of later-forming cusps[15]. Under this patterning cascade model of cusp development[14], a small change early in tooth germ growth results in large alterations in the fully formed crown, particularly in the total number of cusps.

After performing their function, enamel knots disintegrate through cell apoptosis. Gradients of signaling molecules, including those belonging to the Bmp, Fgf, Wnt, Shh, and NF- κ B signaling pathways[13], originate from and act around the knot, functioning as inducers, mediators, and inhibitors to determine correct formation of tooth shape and crown patterning. These reiterative signaling molecules are indispensable throughout the process of micropatterning (cusp size and cusp number) and macropatterning (tooth size and tooth number). In mice more than 80 genes have been reported to be expressed, in and surrounding the knot (<http://bite-it.helsinki.fi>), suggesting their complex integration and interactions. Alterations of

these fine-tuned interactions lead to alterations of cusp patterning and tooth morphology. These types of dental anomalies are observed in a number of animal models, and are sometimes seen in analogous patient rare disease cases.

I.2.4 How the tooth begins to differentiate into defined tooth lineages

Dentin and enamel are mineralized tissues produced at the late bell stage of tooth development by two different tooth-specific post-mitotic cells: the mesenchyme-derived odontoblasts that produce dentin and the epithelial ameloblasts that produce enamel matrix proteins. Morphological and molecular events occurring during dentinogenesis and amelogenesis will be described.

I.2.4.1 Dentin development (dentinogenesis)

Dentin is the substructure of enamel, and its flexibility reduces tooth damage by absorbing force. Dentin has about 60% mineral content and is a tissue very similar to bone. It has an intricate network of dentinal tubules and is filled with dentinal fluid and odontoblastic processes that are thought to play a role in the neurosensory function of teeth[31]. Dentin acts throughout life as a protective barrier, with reparative responses to environmental assaults. Dentin also can function to secrete sclerotic dentin, which upon attack from dental carries or chewing forces blocks and protects dentinal tubules. Sclerotic dentin appears translucent due to calcification, occurring with aging or injury.

Odontoblasts are specialized ciliated cells [32], who function in the formation of dentin. Odontoblast differentiation follows a defined temporospatial gradient from the cusp tip towards the cervical area of the tooth, an event induced by the inner dental epithelial (IEE) cells. Odontoblasts synthesize dentin matrix proteins [33]. Collagens (I, type I trimer, III, V, VI) are abundant odontoblast components. Non-collagen components of odontoblasts include osteonectin, osteocalcin, and SIBLINGs (Small Integrin-Binding Ligand, N-linked Glycoproteins), osteopontin, bone sialoprotein (BSP), dentin matrix protein 1 (DMP1), and dentin sialophosphoproteins (DSPP or DSP and DPP)[34]. Other molecules which contribute to dentin formation include the proteoglycans, serum proteins such as albumin, enamel proteins such as amelogenins and matrix metalloproteinases (MMPs)[35].

The collagen molecules communicate with a variety of non-collagenous proteins to aid initiate and regulate the mineral deposition in these tissues. DSPP is the most abundant and well-known non-collagenous protein. It is a highly phosphorylated protein, which can attach to the type 1 collagen fibril, regulating collagen deposition at specific sites[31, 33].

Mutations in either type I collagen or linked proteins can cause hereditary dentin defects like *Dentinogenesis Imperfecta* (DI). Many mutations are found in these manners and are often associated with Osteogenesis Imperfecta (OI), a group of hereditary defects associated with bone fragility/anomalies. By the way, only some collagen mutations result in dentin defects[31, 33].

I.2.4.2 Enamel development (amelogenesis)

Dental enamel is the hardest and the most densely mineralised tissue of the body (95% in weight) mainly composed of calcium hydroxyapatite crystallites. Its strength is not only linked to its great mineral content, but also to the sophisticated-arranged organization of enamel crystallites and substructures. Thus, enamel formation necessitates an elaborately regulated orchestration of cellular and chemical events during amelogenesis to properly make enamel with the certain mineral composition and organization[36]. Genetic aberrations or environmental disturbances during this process are able to cause developmental enamel defects[37, 38].

Ameloblasts differentiate, within the enamel organ, at bell stage, from IEE. Their differentiation follows the same temporospatial gradient as odontoblasts, but with a different timeframe. Amelogenesis proceeds in the presence of predentin/dentin and after disappearance of the basement membrane (stages when odontoblasts are functional).

Ameloblast synthesize, participate in mineralization and resorb the enamel matrix proteins during the maturation stage[37]. Amelogenesis can be segmented in five stages, including the initial or pre-secretory stage, secretory stage, transitional stage, maturation stage, and post-maturation stage. First, a layer of IEE adjacent to the underlying ectomesenchyme starts to differentiate into ameloblastic cells, they

withdraw from the cell cycle, elongate, polarize and develop the protein synthesis organites. Pre-secretory ameloblasts differentiate into secretory ameloblasts which deposit a protein matrix. Hence, the enamel matrix acts as a provisional protein scaffold on which enamel crystals are able to form[39]. Differentiating pre-ameloblasts stretch cytoplasmic projections through the basement membrane, which is then gradually degraded. These pre-secretory stage ameloblasts provide an appropriate environment for subsequent matrix and ion deposition. During the secretory stage, the ameloblasts become columnar-shape cells and secrete tremendous amounts of enamel matrix proteins such as Amelogenin (Amel), Ameloblastin (Ambn), and Enamelin (Enam).

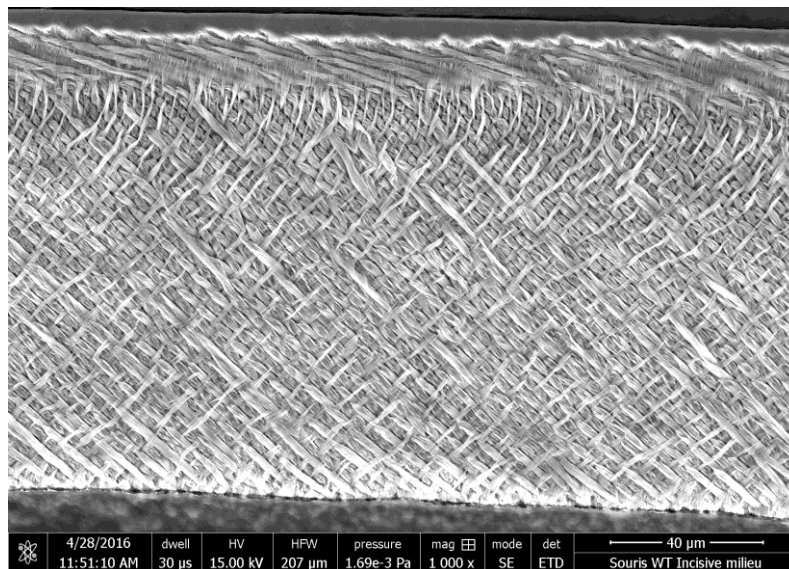


Figure 4 Normal enamel prism of lower incisor in mouse.

Scanning electron microscopic (SEM) analyses of lower incisors from 7 week-old wild-type (WT) mice shown the characteristic enamel rod/interrod structure. More detailed analyses of these enamel microstructure reveals a pattern of interlocking enamel prisms at the erupted portion of the incisor (where enamel is mature). This enamel prism pattern reveals normal thickness of decussations in its criss-crossing pattern. (Images from Supawich Morkmued (2016) collaborated with Pr Joseph Hemmerlé and Dr Eric Mathieu)

During initial enamel secretion, ameloblasts move away from the dentino-enamel junction (DEJ), to permit extension of enamel crystal ribbons and to enable

appositional growth (first as aprismatic enamel, then as prismatic enamel (ameloblasts with Tomes process), and finally as aprismatic surface enamel (stages in human enamel formation))[36]. This progression establishes the thickness of the enamel and serves as a mold for orientating enamel crystals. When the enamel reaches its maximum thickness, then secretory-stage ameloblasts withdraw their cytoplasmic processes and turn into a shorted columnar-shape transition-stage, under which a basement membrane reforms. Subsequently, the transition-stage ameloblasts further shorten into cuboidal maturation-stage ameloblasts, which begin adjusting between ruffle and smooth-ended cells at the surface of enamel. During this maturation stage, the enamel matrix proteins are then degraded by enamel proteases such as kallikrein-related peptidase 4 (KLK4) and matrix metalloproteinase 20 (MMP20). Thus, these proteases permit enamel to degrade matrix and to serve space for additional mineral deposition at the areas of future enamel crystallites, which increases the strength of the enamel[36, 37] (Figure 4). Finally, the enamel is able to exchange mineral ions of the saliva and oral fluid after eruption, which can affect the composition of the external layers of enamel. Hence, the enamel development is elaborately regulated and, still, highly susceptible to either environmental or genetic influences.

1.2.4.3 Dental Pulp

The tooth mesenchyme is subsequently termed dental pulp at the bell stage, as terminal differentiation of odontoblasts proceeds. The dental pulp is mainly a vital tissue comprised of odontoblastic cells, fibroblastic cells, blood vessels, nerves, and a multiplex extracellular matrix. The pulp provides a neurosensory function as well as a reparative potential of dentin[40]. Hence, the dental pulp can increase production of dentin, in a process called reparative or sclerotic dentin production, to protect and isolate essential vital pulp from the injury or noxious stimuli[41]. The pulp is maintained depositing small amounts of new dentin throughout life, as a part of pulp normal physiology[42]. The pulp chamber is gradually reduced with aging. It crucial to keep healthy dental pulp until the termination of root formation and development of the root walls. If the pulp dies in an immature tooth that lacks full root formation, the tooth will likely die. Enamel and dentin are of sufficient thickness to retain the massive forces transmitted from the crown during function.

I.2.4.4 Root formation

Root formation occurs after crown development. Outer dental epithelium of the prospective crown-root boundary, instead of differentiating into ameloblasts become Hertwig's epithelial root sheath (HERS) –a structure that grows and migrates downward guiding the formation of root. This process also induces odontoblasts differentiation, producing root dentin. Essential regulators of bone and dentin differentiation, such as *Osterix*, appear to have roles during root elongation. Hence, dental-specific ablation of *Osterix* produces mice with short tooth roots[43]. *Tgfr2*, *Bmp2*, and *Ptc1* also appear required for root elongation[44-46]. Thus, HERS has a limited growth potential, which defines the length of the root. In addition, the expression of ameloblastin in HERS may trigger normal root differentiation[47]. The disintegration of HERS leads up to the formation of an epithelial mesh called epithelial rests of Malassez. These are odontogenic epithelium within the matrix of the periodontal ligament, supporting tissue-homeostasis or periodontal ligament regeneration potentially acting as a stem-cell like population[48].

Part II

Signaling pathways involved in tooth development

Orchestrated signaling cascades regulate tooth development. Uncovering the molecular details of signaling networks regulating interactions between epithelial and mesenchymal cells within the epithelio-mesenchymal interactions during tooth morphogenesis has been the subject of intensive investigation (reviewed in [9]).

These events include developmentally programmed inter- and extra-cellular growth factor signaling, transcription factor DNA binding, and cell cycle modulation. These signals can be altered in pathological conditions, or by environmental agents - often by events adversely altering tooth patterning and/or differentiation[49].

II.1 Transcription factors critical in tooth patterning

The initial patterning, as well as the coordinated interplay of signals at each step of tooth development is greatly dependent on the actions of numerous transcription factors. For example, during the initiation of tooth development epithelial FGF8 and BMP4 within the oral ectoderm and dental lamina induce the expression of many transcription factors, including *Barx1*, *Dlx1*, *Dlx2*, *Msx1*, *Msx2*, *Pax9*, *Pitx1*, and *Pitx2*[50-52]. The expression in the prospective mesenchyme of many non-classical or divergent homeobox (HOX) -containing genes, such as *Barx1*, *Dlx1*, *Dlx2*, *Dlx3*, *Dlx4*, *Dlx5*, *Dlx6*, *Lhx6*, *Lhx7*, *Msx1*, and *Msx2*[53-55] (Figure 5), led to the proposal of the odontogenic homeobox code model. This model postulates that expression of a specific combinations of homeobox gene directs the formation of specific tooth types[56].

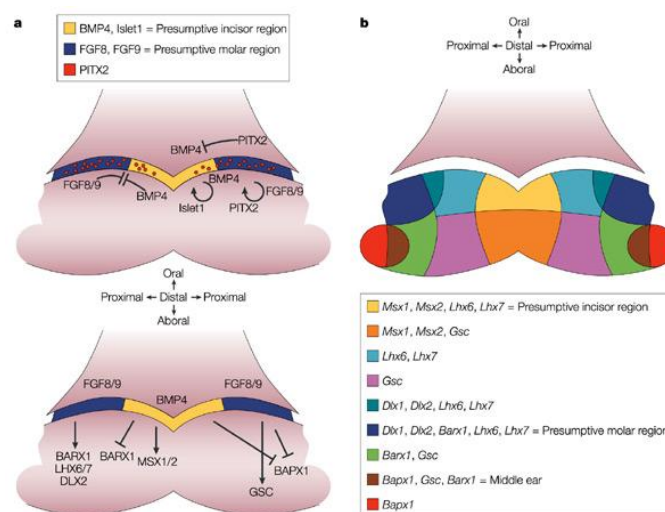


Figure 5 Pattern of gene expression in the developing tooth.

(a) The early dental signaling at the mandibular arch stage. Inductive signaling occurs between the epithelium and the mesenchyme, and within the epithelium at E10.5. Both positive auto-regulatory loops and mutual repression within the epithelium causes the formation of tight boundaries of gene expression, which establish the presumptive incisor and molar tooth fields. Members of different proteins in the epithelium regulate the expression of a variety of divergent homeobox genes. This results in a complicated pattern of gene expression in the mesenchyme in all directions.

(b) The early tooth homeobox model. The expression network of homeobox genes in the jaws produces a homeobox code that may determine tooth type. (source [57])

Pitx2

Paired-like homeodomain transcription factor 2 (*Pitx2*) is a member of the PITX homeobox family encoding a bicoid class of homeodomain proteins. This transcription factor[58] appears an important upstream regulator of the transcriptional hierarchy in early tooth development. At murine E8.5, prior to any morphological signs of tooth development, *Pitx2* is expressed in the stomatodeal epithelium (the precursor to oral and dental epithelium). Accordingly, *Pitx2* is considered to be the earliest transcription factor expressed during tooth development[51, 59]. *Pitx2*^{hd-/-} mandibular teeth arrested as tooth buds, and maxillary teeth arrested at the placode stage[60].

Dlx

Distal-Less/Dlx homeobox (*Dlx*) genes function as homeobox genes with explicit roles in patterning structures such as the developing limb[61]. Several studies have shown that alterations in DLX signaling pathways can cause variations in tooth number. Such studies indicate mechanisms that may have determined tooth number during mammalian evolution. An example of tooth loss in cypriniform fishes (including zebrafish) was correlated with the loss of *dlx2a* and *dlx2b* expression in the oral odontogenic epithelium[62]. Because DLX genes are required for tooth development in mice[63], changes in trans-acting regulators of DLX genes, which might be

downstream of FGF signaling, have been suggested as candidates responsible for the loss of fish pharyngeal oral teeth[62]. Additionally, a region in the upstream regulatory element of *dlx2b* was retained that conducts specific expression in the oral epithelium. The retention of this cis-regulatory element is believed to be due to its requirement in other tissues, being as *Dlx* genes have pleiotropic effects in other organs[64]. These studies suggest that tooth lost from specific regions may be relatively easy to reacquire during evolution[64].

The normal early developmental function of other distal-less genes such as *Dlx3* in odontogenesis remains unclear (potentially owing to functional redundancy between other *Dlx* family members). The loss of *Dlx3* in the neural crest diminishes both odontoblast differentiation and dentin production. *Dlx3* mutant mice have brittle teeth and hypoplastic dentin. *Dspp* is decreased in *Dlx3* mutant odontoblasts[65]. Hence *Dlx3* appears essential in regulating dentin production. It also promotes the gene expression of enamel matrix proteins during amelogenesis[66]. In addition, *DLX3* is mostly involved cases of Tricho-dento-osseous (TDO) syndrome, an autosomal dominant disorder characterized by abnormalities in the thickness and density of bones and teeth[67, 68].

Msx1

Msh homeobox 1 (*Msx1*) is a protein that in humans is encoded by the *MSX1* gene[69]. Homozygous *Msx1*-deficient mice show complete secondary cleft palate, a failure of incisor development, and an arrest in molar development beginning at bud-stage[70].

Pax9

Pax9 is a member of the paired box (PAX) family of transcription factors that encodes for a paired domain-containing transcription factor which plays a major role in the development of mammal dentition. *Pax9* expression has been revealed to specifically mark the mesenchymal regions at prospective sites of tooth formation beginning at E10[50]. In human, it has been associated with selective tooth agenesis, which mainly involves the posterior teeth. In mouse, the lack of *Pax9* causes an arrest in dental development beginning at the bud stage[71]. Molecularly *Pax9* may

act together with *Msx1*, allowing the dental mesenchyme to maintain expression of *Bmp4*, which is crucial for establishing the enamel knot[72, 73]. Recently, it was shown that during early tooth formation, mesenchymal condensation alone could regulate expression of *Msx1* and *Pax9*, as well as that of *Bmp4*[74].

Runx2

RUNX2 encodes a runt-domain containing transcription factor (Runx) that is critical for bone development, hence *Runx2* mutation blocks skeletal ossification, severely disrupting tooth formation[75-77]. *Runx2* is expressed in the dental mesenchyme during the bud and cap stages, and regulates Fgf signaling from the dental epithelium to mesenchyme[75, 78, 79]. *Runx2* mutant mice show tooth developmental arrest at late bud stages[75], accompanied by large reduction or absence of expression of *Fgf3* in the dental mesenchyme, and of *Shh*, *Edar*, and *p21* in the enamel knot[79]. In addition, Runx2 controls continued tooth growth and morphogenesis beyond the cap stage through its activation of *Fgf3* and *Fgf10* expression in the dental papilla[79, 80].

MicroRNAs

MicroRNAs (miRNAs) are 19- to 25-nt noncoding small single-stranded RNAs that negatively regulate gene expression by binding target mRNAs, which is known to be essential for the fine-tuning signaling pathways in development. The involvement of miRNAs in various ectodermal derivatives has been demonstrated in skin[81, 82], hair[83], and teeth[84-87]. The presence of many miRNAs at a single site (potentially acting in a redundant manner) complicate the elucidation of their function. A clear strategy to elucidate miRNA function is the tissue-specific deletion of DICER, which abolishes all miRNAs processing. Functionally the deletion of *dicer* in using *Pitx2-Cre* (the earliest marker of tooth) changed both molar and incisor patterning, disrupted ameloblast development, and expanded the cervical loop[84]. Enamel-specific deletion of DICER revealed somewhat mild changes in tooth shape and enamel differentiation[86]. The expression of miRNAs in distinct regions of the mouse incisor and pulp was profiled using microarray experiments, laying the groundwork for future investigations[86, 87]. miRNA synthesis is tightly controlled, as it guides development

and can be altered in congenital malformations such as DiGeorge syndrome (reviewed in [88]).

II.2 The TGF- β /BMP pathway

BMP

Bone morphogenetic proteins (BMPs) are a family of growth factors functioning to induce the formation of bone and cartilage. Because of the interactions between alveolar bone and tooth, they have obvious roles in tooth development. They also appear to have tooth-specific functions. BMPs play roles at multiple stages during odontogenesis. For example, BMP4, in particular, is an important mediator of signaling between epithelial and mesenchymal tissues[89]. Additionally, in the developing mouse tooth, several *Bmp* genes, including *Bmp-2*, *-3*, *-4*, and *-7*, are expressed in either epithelial or mesenchymal components[90] (Figure 6).

They have important physiological actions as dysregulated BMP signaling can lead to numerous congenital diseases such as Osteogenesis imperfecta, type XIII (OMIM; 614856) or Brachydactyly, type A2 (OMIM; 112600). BMP alterations mark diverse pathological processes including (for example) facial clefting, anophthalmia-microphthalmia, retinal dystrophy, myopia, poly- and/or syndactyly[91, 92].

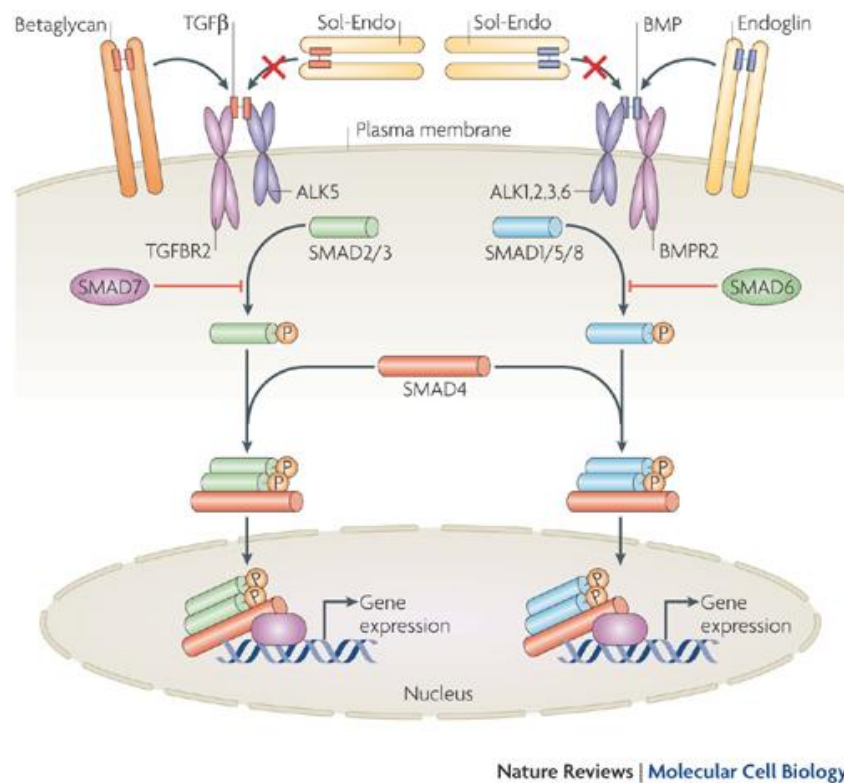


Figure 6 Schematic representation of the Bmp and Tgf- β signaling pathways.

BMP is part of the TGF- β superfamily, its signals transduced into cells by a serine-threonine kinase transmembrane receptor binding with one of the 3 type I receptors (BMPR-IA, BMPR-IB, and Alk2). Its ligand-binding induces receptor in turn phosphorylating target intracellular Smads, mainly Smads-1, -5, and -8, in the cytoplasm. Tgf- β targets mainly Smads-2 and -3 through Tgf- β receptors and Alk5. These phosphorylated Smads (pSmads) then bind to the common Smad4 to control nuclear gene expression (source [93])

BMP roles in tooth initiation

The antagonism between Fgf and Bmp appears to determine the tooth-bud site and tooth type during initiation of the tooth bud. BMP signaling in the oral epithelium antagonizes FGF signaling, the later thought to determine the sites of tooth formation[50-52]. Thus mesenchymal BMP4 regulates *Fgf8* expression[51] and is critical for the establishment of presumptive incisor and molar tooth field, for the

transition from the tooth bud to cap stage, and for induction of the epithelium enamel knot[72, 73]. The inactivation of *activin* or *Bmpr1a* (in either epithelium or mesenchyme) also results in the arrest of tooth development after the bud stage[94-96].

BMP roles in tooth number, tooth morphology, and size

Collectively the BMP signaling pathway regulates tooth formation. Overexpression of the BMP inhibitor Noggin arrests tooth development at the lamina to bud initiation stage of tooth morphogenesis[97]. While relatively little is known regarding the molecular mechanisms in which BMP alterations affect dental morphology, decreasing BMP signaling in the incisor region can lead an incisor to acquire a molar-like phenotype[98]. The relative size of mouse molars can also be influenced by overall BMP levels[99]. Specifically events of BMP activation and inhibition occur successively between developing teeth[100]. Mutation of the BMP inhibitor gremlin (*Grem2*) is associated with human tooth agenesis, microdontia, short tooth roots, taurodontism, sparse, and slow-growing hair[101]. Consistently, *Grem2* mutant mice have small, malformed maxillary and mandibular incisors[102].

BMP roles in tooth differentiation

During odontoblastic differentiation, BMP2 mediates DSPP gene expression and odontoblast differentiation via the heterotrimeric transcription factor Y[103]. In addition, the down-stream effectors of BMP/TGF- β signaling, such as SMAD4 also play a role during tooth differentiation events[104].

Ameloblast differentiation is controlled by antagonistic actions of BMP4 and activin A[94]. The asymmetrically expression of the BMP inhibitor follistatin also regulates the labial-lingual patterning of enamel formation[105]. The continuous growth and enamel deposition in mouse incisors can be modulated by the net levels of Fgf, Activin, and Bmp signaling in the epithelial stem cell niche[106].

TGF- β

Transforming growth factors beta (TGF- β) is part of a super-family of growth factors that regulates a broad range of cell growth, differentiation, and extracellular morphogenetic events[107]. The essential functions of the TGF- β superfamily involve

actions during tooth crown patterning and tooth root development (Figure 6). Their importance is further highlighted in studies investigating Smad-dependent and Smad-independent pathways regulating tissue-tissue interactions during patterning of tooth crown and root (reviewed in [108]).

TGF- β roles in tooth differentiation

TGF- β proteins are thought to play an important role in the morphogenesis of developing teeth[109]. Both TGF- β 1 and TGF- β 3 are produced by the enamel organ and activated by components of the basement membrane[110]. Inhibiting TGF- β signaling stops ameloblast enamel secretion[111, 112] and inactivation of the *Tgfb2* gene increases odontogenic epithelial cell proliferation[113]. *TGF- β -RII cKO* and *TGF- β 1* over-expression exhibits a tooth phenotype at the early stage of enamel formation[112, 114]. *Tgf- β receptor II* conditional knockout mice also show enamel attrition with thinner crystals[114]. In addition, TGF- β -activating SMAD2, 3 and TGF- β -inhibiting SMAD7 are found both in the enamel epithelium and dental mesenchyme. Their mutations produce a variety of tooth phenotypes, such as a reduction of enamel related to their roles in ameloblastic function and tooth morphogenesis[109, 115].

In addition, dosage-dependent effects of TGF- β expression are observed. Transgenic overexpression of TGF- β 1 in early secretory stage ameloblasts (via *dentin TGF- β 1* transgene overexpression) triggers dentin adhesion process detachment, ossification of dentin, and the formation of cyst-like structures formed from enamel matrix-like proteins[112]. An independent strategy of dental-targeted overexpression of TGF- β 1 using a *Dspp-Tgf- β 1* transgene produced a dentin dysplasia-like phenotype[116]. TGF- β 2 overexpression driven by an osteocalcin promoter (expressing in the dental mesenchyme) alters the dentin matrix, reducing dentin hardness and elasticity[117].

Modulation/activation of TGF- β via LTBP

In addition, TGF- β family interacting proteins play roles in the production and degradation of the extracellular matrix. TGF- β s are secreted in the form of latent high molecular mass complexes that contain other proteins [118]. Among their associated

factors are latent TGF-beta binding proteins (LTBPs) (Figure 7). To date, 4 members of the LTBP family (LTBP1, 2, 3, 4) are known. LTBPs are important regulators of TGF- β bioavailability and action. They also interact with other extracellular proteins, including microfibrils and elastic fibers [119]. The mouse LTBP polypeptide forms a complex with the TGF- β 1 precursor [119]. LTBP3 allows latent TGF- β complexes to be targeted to connective tissue matrices and cells [120, 121]. The observation of bone abnormalities in *Ltbp-3*-null mice supports the role of LTBP3 in modulating TGF- β bioavailability [122]. *Ltbp3* mutants, much like *Ltbp1* null mice, develop discernible craniofacial abnormalities [123]. Human *LTBP2* polymorphisms may underlie bone mineral density defects and fracture risk [124]. A recessive mutation in human *LTBP4* causes multi-organ defects that include craniofacial malformations[125].

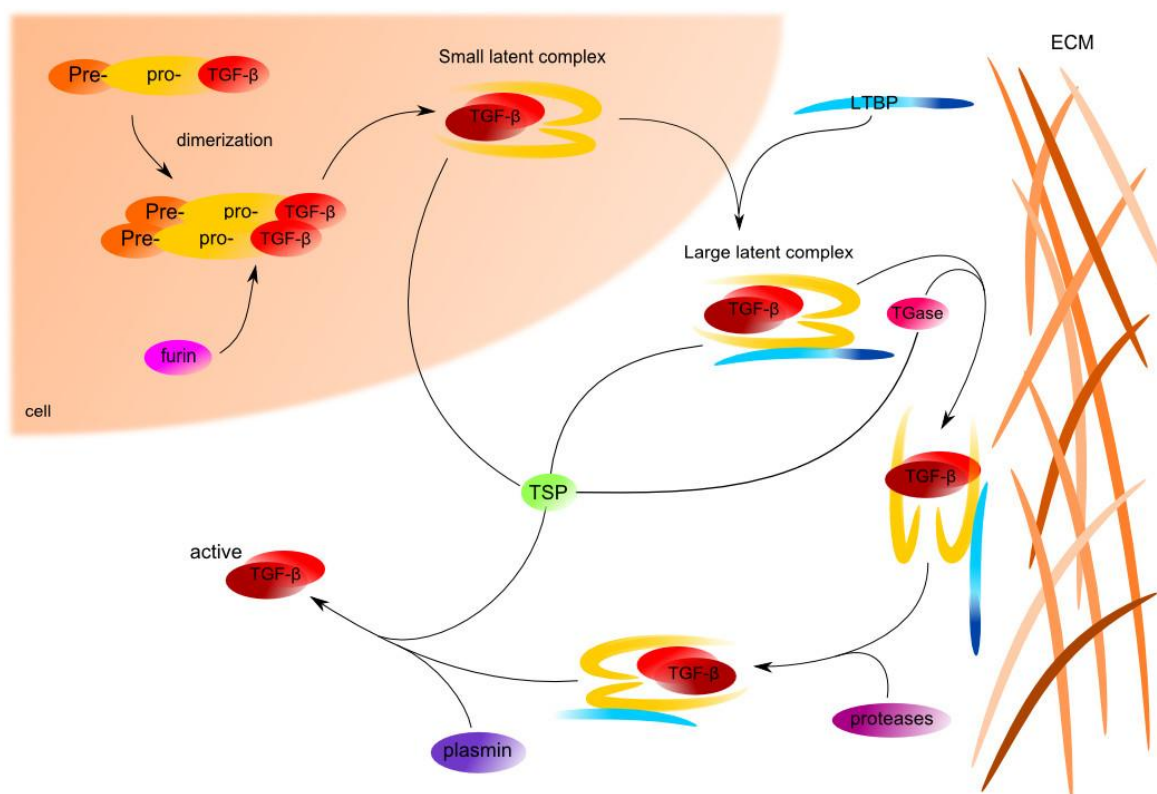


Figure 7 TGF- β synthesis and activation.

TGF- β s are synthesized as inactive precursors that contain unprocessed regions. Processing of inactive forms starts with a proteolytic cleavage that removes signal peptide from pre-pro-TGF- β s forms. After dimerization, TGF- β s are cleaved by proteases into terminal mature peptides and N-terminal Latency Associated Peptides. TGF- β s with Latency Associated Peptides form small latent complexes that are transported to extracellular matrix where they can further covalently bind to latent TGF- β binding protein (LTBP) to form a large latent complexes. LTBP is able to connect inactive TGF- β forms to extracellular matrix (ECM) proteins. This interaction is further supported by covalent transglutaminase-induced crosslinks. Activation of TGF- β starts with release of large latent complexes from ECM by proteases. Then, the mature protein is cleaved from LTBP, which is provided *in vitro* by acidic condition, pH or plasmin, or *in vivo* by thrombospondin. Once the active TGF- β family member is released from the ECM, it is capable of signaling. (Source [126])

LTBP3, has been defined as a member of the LTBP family, which serve to regulate TGF- β bioavailability and signaling by interacting with other extracellular proteins[119] (Figure 7). These proteins function to allow latent TGF- β protein complexes to have an altered conformation, and thus be targeted to connective tissue matrices and cells[121]. Mutations in human *LTBP3* result in patients with short stature, vertebral and skull bone alterations, oligodontia[127], and mitral valve prolapse[128]. In a collaborative report examining patients with *LTBP3* mutations, we observed a range of recessive hypomorphic mutations (producing alterations including gene deletion, nonsense, and aberrant splice mutations) causing developmental abnormalities such as short stature, brachyolmia, and hypoplastic Amelogenesis Imperfecta (AI) (OMIM; 601216)[129]. Investigating the dental phenotype of the *Ltbp3*^{-/-} mouse model demonstrated very thin or absent enamel in both incisors and molars[129] and confirmed this animal model to be reliable to study the pathophysiology of Verloes Bourguignon syndrome. The full description of the tooth-specific morphological alterations in the *Ltbp3*^{-/-} mutant mouse[130] is reported in this thesis in results section page 130.

II.3 FGFs

Fibroblast growth factors, or FGFs, are a vital family of numerous growth factors, with members involved in angiogenesis, wound healing, embryonic development, and various endocrine signaling pathways. FGFs are major actors in the processes of proliferation and differentiation of diverse cells and tissues (Figure 8) (for a general review see [131]; for skeletal-specific functions see [132]).

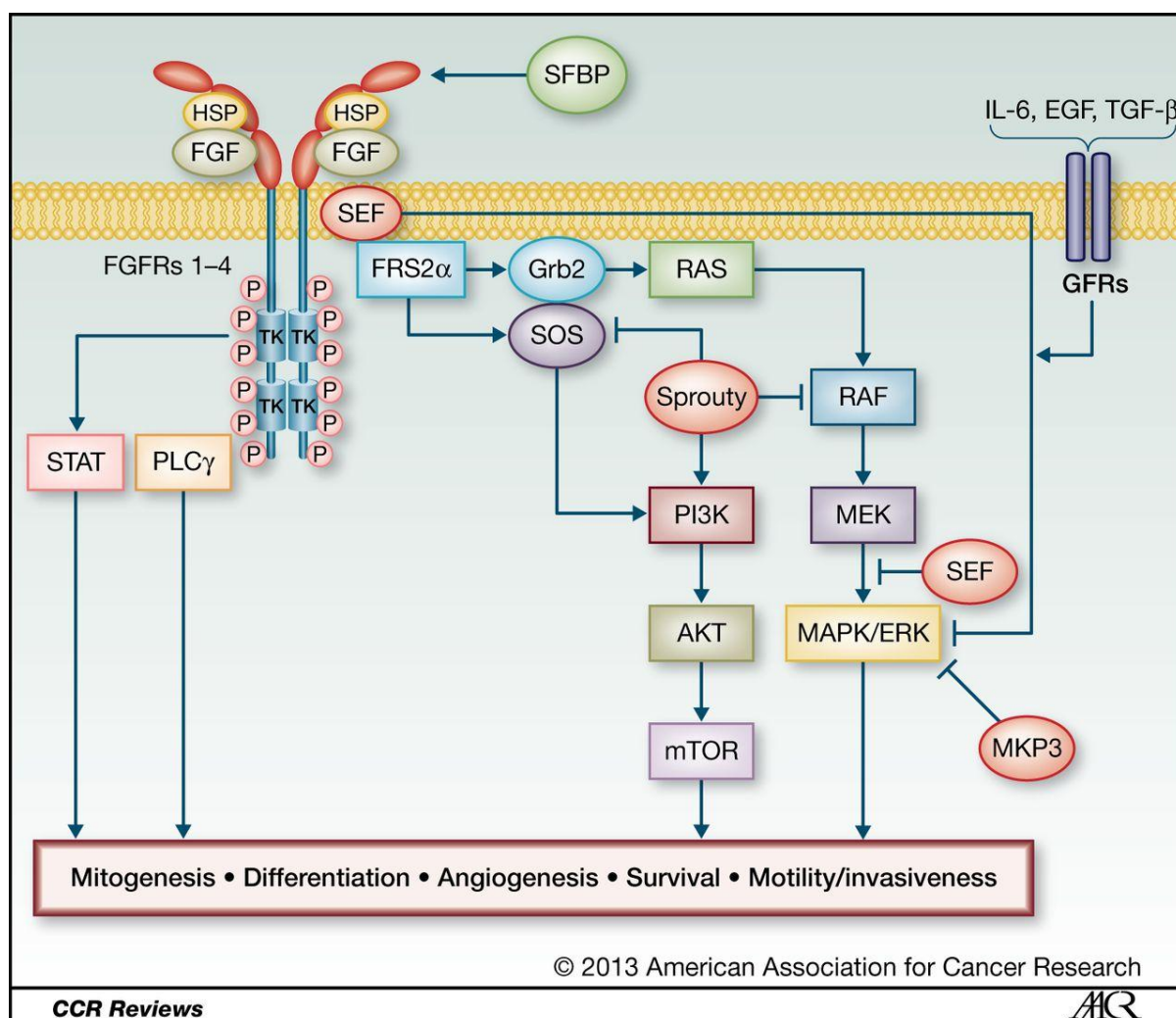


Figure 8 Schematic representation of Fgf signaling pathway.

FGF signaling pathway is regulated at numerous levels. Heparan sulfate proteoglycans play both as co-receptors and modulators of ligand bioavailability. The main signaling pathways downstream of its receptor activation are the Janus kinase/signal transducer and activator of transcription, phosphoinositide phospholipase C, phosphatidylinositol 3-kinase and mitogen-activated protein kinase/extracellular signal-regulated kinase (MAPK/ERK). In addition, Sprouty proteins provide a negative-feedback mechanism to decrease or terminate FGF signaling (source [133]).

FGF roles in tooth number, size and morphology

Fgf8 and *Fgf9* are among the earliest genes to be expressed in the oral epithelium. The conditional inactivation of *Fgf8* in ectoderm caused defects in structures derived from the first pharyngeal arch, including teeth, jaws, lateral skull wall, and middle ear, as well as part of the tongue and other soft tissues[134].

The mice with an inactivation of *Fgf8* specific to the rostral branchial arch showed hypoplastic 1st branchial arch development along with an absence of molars (proximal structures), but in which the distal-most structures (such as lower incisors) were present. These results suggested a model in which the proximal derivatives of the first pharyngeal arch primordium are specified by FGF8, but the distal-most region depends on other signaling molecules for its outgrowth and patterning[134].

In mice over-expressing a dominant negative form of *Fgfr2b*, tooth development did not progress beyond the bud stage[135]. *Fgf4* and *Fgf9*, which are expressed in the enamel knot, are thought to stimulate proliferation in adjacent epithelial and mesenchymal tissues[136, 137]. Deletion of *Fgf3* and *Fgf10* in mice results in smaller teeth with aberrant cusp morphology[106], but individually these genes appear redundant, and did not appear to be individually required for ameloblast differentiation[106, 138]. FGF3 deletion in human has craniofacial defects with microdontia (OMIM; 610706). The role of FGF signaling is evolutionarily conserved and is involved in zebrafish tooth morphogenesis. Decreases in FGF signaling have been proposed to lead to the loss of oral teeth[62, 139].

The sprouty family of genes/proteins is inhibitors of FGF signaling. Members include Sprouty 1, 2, and 4, which are expressed on the labial regions of the tooth during development and in the adult cervical loop. The inactivation of the FGF–inhibitors Sprouty 2 and 4 produces a net increase in FGF signaling, in turn altering the stem cell cervical loop producing the generation of ectopic lingual surface incisor enamel[140]. In addition, alterations in MAPK/ERK cascade can reflect additional roles of the FGF pathway in evolutionarily controlling the number of teeth, which results in the formation of supernumerary teeth in front of the first molar[141]. Indeed, an evolutionary reduction in proliferation in the toothless diastema (potentially due to reductions in net levels of FGF), may account for evolutionary reductions in tooth number[142]. Additional examples of decreases in Sprouty gene dosage leading to increasing numbers of incisors have been reported[143].

II.4 WNTs

The Wnt signaling pathway comprises several signal transduction pathways made up of proteins that signal through cell surface receptors. The main three Wnt signaling pathways have been characterized: the canonical Wnt pathway, the noncanonical planar cell polarity pathway, and the noncanonical Wnt/calcium pathway. All pathways are activated by Wnt-protein ligands binding to Frizzled family receptors. Receptor binding triggers recruitment of the downstream intracellular target Dishevelled[144]. The canonical Wnt pathway leads to regulation of gene transcription via stabilized β -catenin interacting and inducing TCF/LEF activation in the promoter of Wnt-responsive target genes. The non-canonical Wnt planar cell polarity pathway regulates the cytoskeleton that is required for the shape of the cell. Another component of non-canonical Wnt can be via the regulation of calcium concentrations, through calcium release within the cell. The actions of the Wnt signaling pathways specific to the bone formation and/or resorption are summarized in Figure 9.

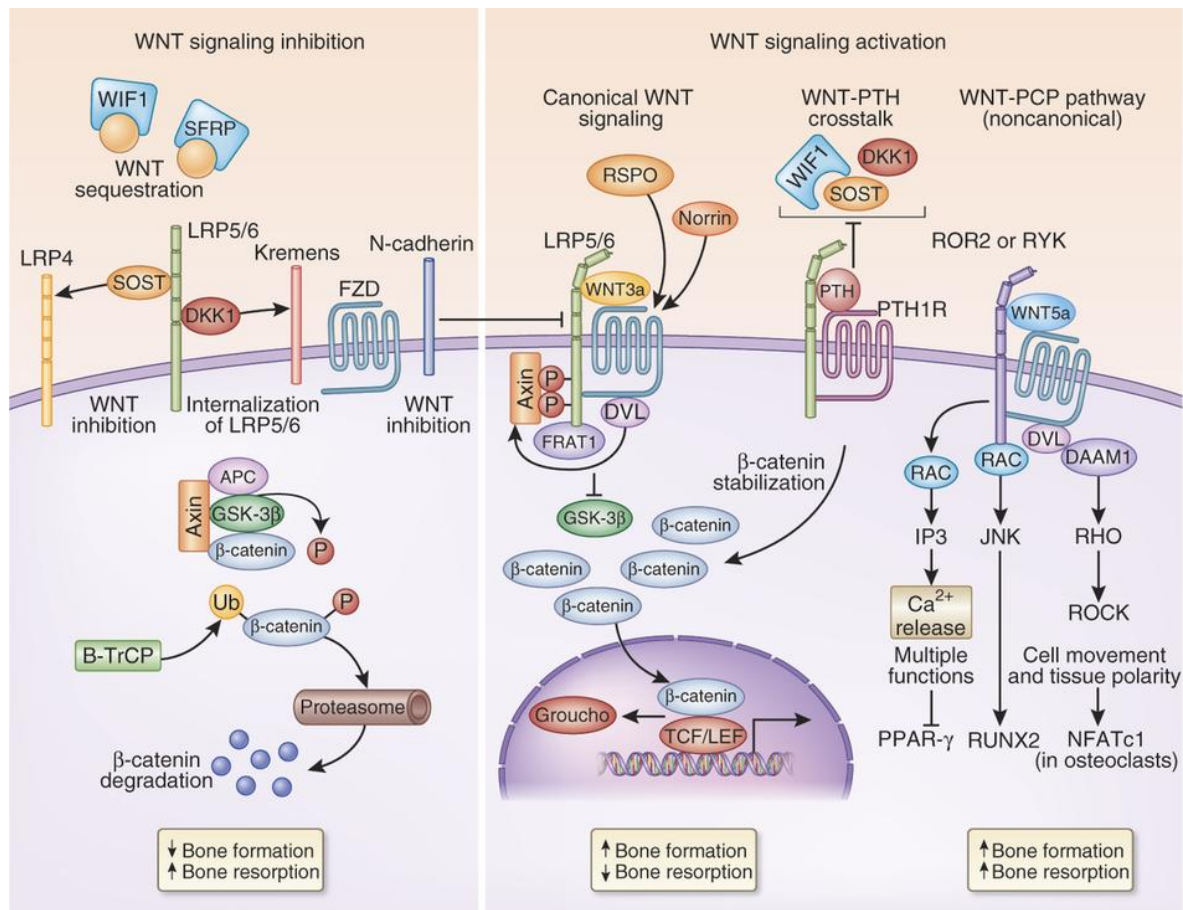


Figure 9 Schematic representation of Wnt signaling pathway.

Wnt proteins are secreted glycoproteins or ligands that transduce extracellular message to intracellular signaling cascade by binding through frizzled receptors. In the absence of this ligand (off state), β -catenin is sequestered by a complex of molecules such as Axin1, 2/APC/CK1 α and GSK-3 β , which is commonly known as destruction complex. Phosphorylation of β -catenin within this complex leads to ubiquitin and proteasomal mediated degradation process. In the presence of WNT ligand (on state), WNT protein binds to frizzled receptors along with its LRP5/6 co-receptor complex resulting in interruption of the destruction complex. This will inhibit GSK-3 β activity which in turn causes cytosolic accumulation of β -catenin, subsequently causing nuclear translocation resulting in target genes activation. In addition, Wnt pathway is inhibited by Dickkopf 1(DKK1), a soluble Wnt inhibitor, activated by NF- κ B (source [145]).

WNT roles in tooth number

The alteration and modulation of WNT signaling leads to variations in tooth number, either increases or decreases in the overall number of teeth. Several of these studies demonstrated that dental epithelium-overexpression of Wnt produces multiple tooth invaginations by augmenting β -catenin, hence causing the formation of extra enamel knots and ultimately, supernumerary teeth[146-149]. Multiple ectopic teeth in the molar region were observed after constitutive activation of the transcriptional effector CTNNB1 (catenin β 1)[146, 150]. Epithelial mis-expression of *Lef1*, the binding partner of CTNNB1, led to multiple tooth-like structures in the murine incisor region[151].

Inactivation of WNT antagonists such as *Apc*[148, 152] and *Sostdc1*[17, 153, 154] led to increases in the number of teeth. Overexpression of the WNT agonist *Sp6* also caused an augmentation in WNT signaling and mice with over 50 teeth[147]. Inversely, there is evidence in humans that decreases in WNT signaling lead to tooth loss[155-157]. Collectively the mechanism by which WNT signaling regulates tooth number appears quite complex because of the large number of Wnt targets and regulators. Further studies appear required for further clarification of this signaling pathway.

WNT roles in tooth morphology

Molar shape can also be regulated by WNT modulation. For example *Lrp4*, encodes a protein which may be a regulator of Wnt signaling. *Lrp4*-null mice exhibited enamel grooves on the labial surface of incisors with similar molecular characteristics as molar cusps, suggesting that WNT signaling may be involved in cusp formation[49].

II.5 NF- κ B/TNF Pathway

Ectodysplasin A (EDA), a transmembrane protein, is a tumor necrosis factor (TNF) superfamily member, whose downstream signaling is transduced by the inhibitor of κ B kinase (IKK) complex and inhibitors of κ B (I κ B) to activate the transcription factor NF- κ B (Figure 10). NF- κ B signaling is involved in a wide range of

cellular processes and at each stage the different family members must be tightly regulated for each function[158, 159].

It is evident that Ectodysplasin/ NF- κ B signaling is involved in the shaping of teeth on a number of different levels. This signaling pathway is quite important during odontogenesis, particularly in the number of teeth as well as the formation of cusps[158].

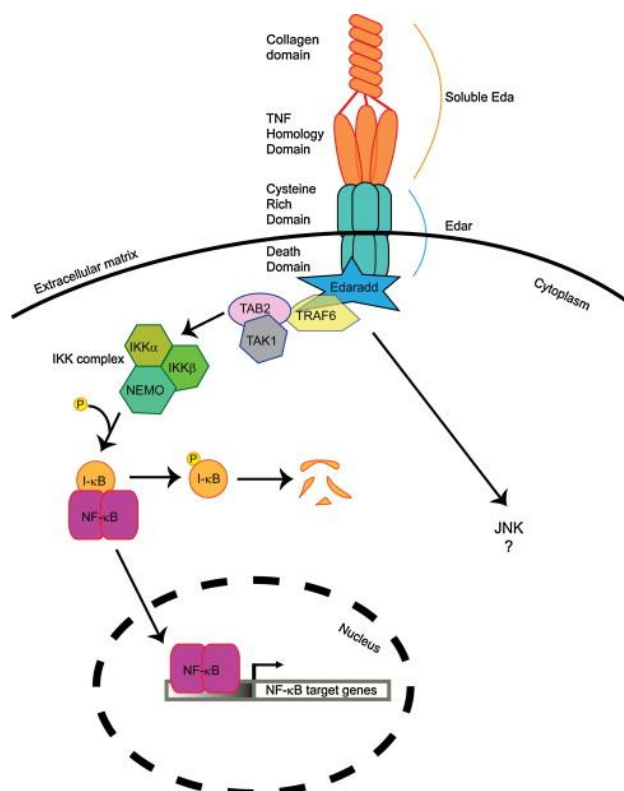


Figure 10 Schematic representation of Eda signaling pathway.

The binding of the ligand Ectodysplasin (EDA-A1) to the TNF-receptor Edar leads to the formation of a complex containing Edaradd, complex. This activates the IKK complex either directly or via activation of NIK (JNK), which in turn phosphorylates IKK. Activation of the IKK complex regulates ubiquitination and proteasomal degradation of the inhibitory proteins I κ B and to the launching of the NF- κ B transcription factor. NF- κ B translocates into the nucleus, where it switches on the transcription of target genes. (source [160])

EDA plays an essential role in the development of ectodermal tissue such as skin[161]. During early odontogenesis, EDA signaling is crucial for determining the size of the tooth field and the number of teeth generated. *Eda* is expressed in oral and dental epithelium throughout tooth formation, whereas *Edar* (*ectodysplasin A receptor*) and *Edaradd* (EDAR Associated Death Domain) are expressed in the enamel knot. Mice with mutations in *Eda*, *Edar* or *Edaradd* (initially found as the spontaneous mutants *tabby*, *downless*, and *crinkled*, respectively) all have a decrease in tooth number and abnormal cusp morphology[158]. The enamel knots in *tabby* or *crinkled* mutants are smaller[162, 163], whereas loss of *Edar* in *downless* mice led to the formation of an elongated-rope like enamel knot[164]. EDA signaling also affects tooth shape[165].

Hypohidrotic Ectodermal Dysplasia (HED) is a rare congenital disorder, affecting organs of ectodermal origin, including teeth, hair and sweat glands. Defects in *EDA*, *EDAR*, and *EDARADD* cause HED in both humans and mice. These 3 genes are involved in NF- κ B activation[166].

EDA roles in tooth number, size and morphology

Mutations in *Eda* or *Edar* resulted in formation of smaller teeth and frequently the absence of third molars[167]. In contrast, increased levels of *Eda* expression or expression of a constitutively active form of *Edar*, led to the formation of a supernumerary tooth in the diastema region[168, 169]. The overexpression of *Edar*, but not of *Eda* resulted in formation of extra cusps[168, 169]. The loss of function of *Eda* has distinct effects on tooth size and morphology, compared to the *Edar* mutation. This may be due to activation of the EDA2R pathway which is specific to *Eda*, whereas *Edar* receptor appears to interact with a yet unidentified protein, and/or to a ligand-independent activity for EDAR[170]. In zebrafish, mutations in *eda* and *edar* led to defects in other ectodermal structures, such as scales and glands, and partial or complete loss of pharyngeal teeth[171].

Mice overexpressing IKK β , an essential component of the NF- κ B pathway, under the control of the keratin 5 promoter (K5-Ikk β) produces supernumerary incisors, whose formation was accompanied by up-regulation of canonical Wnt signaling. Apoptosis that is normally observed in wild-type incisor epithelium was reduced in K5-Ikk β mice. The supernumerary incisors in K5-Ikk β mice were found to

phenocopy extra incisors in mice with mutations of Wnt inhibitor, *Wise*. Excess NF- κ B activity thus induces an ectopic odontogenesis program that is usually suppressed under physiological conditions[172].

The NF- κ B pathway may activate the odonto/osteogenic differentiation of stem cells from apical papilla and regulate some markers such as ALP, RUNX2, Osterix, OCN, DSPP, and DMP1[173]. The receptor activator of NF- κ B ligand, RANKL, is one of the key regulatory molecules in osteoclast formation. Characterization of RANKL expression in rat molars indicates a potential function during tooth movement[174]. Transactivation of NF- κ B by phosphorylation of the p65 component of NF- κ B at amino acid 536 plays a role in osteoclast differentiation stimulated by RANKL. This transactivation pathway is produced rapidly in response to orthodontic stimuli and mechanical insults, and may be important in bone remodeling associated with orthodontic tooth movement. This may involve a cross-regulation of osteoblasts or the periodontal stromal cells via osteoclasts[175].

II.6 The Sonic hedgehog pathway

Sonic hedgehog (SHH) is one of three protein effectors of the mammalian signaling pathway family called hedgehog, with important developmental actions in the regulation of limb morphogenesis and the patterning/organization of the forming brain. Shh is indeed the best established example of a classical developmental morphogen, a molecule that can signal in a concentration-dependent manner[176] (Figure 11). During initiation of tooth formation, *Shh* is expressed in specific regions of the epithelium of the molar and incisal placodes[177]. Analysis of expression of the receptor *Ptch1* and the transcription factor *Gli1*, which are both downstream targets of SHH signaling, show that SHH signals to the mesenchyme as well as the epithelium[178, 179].

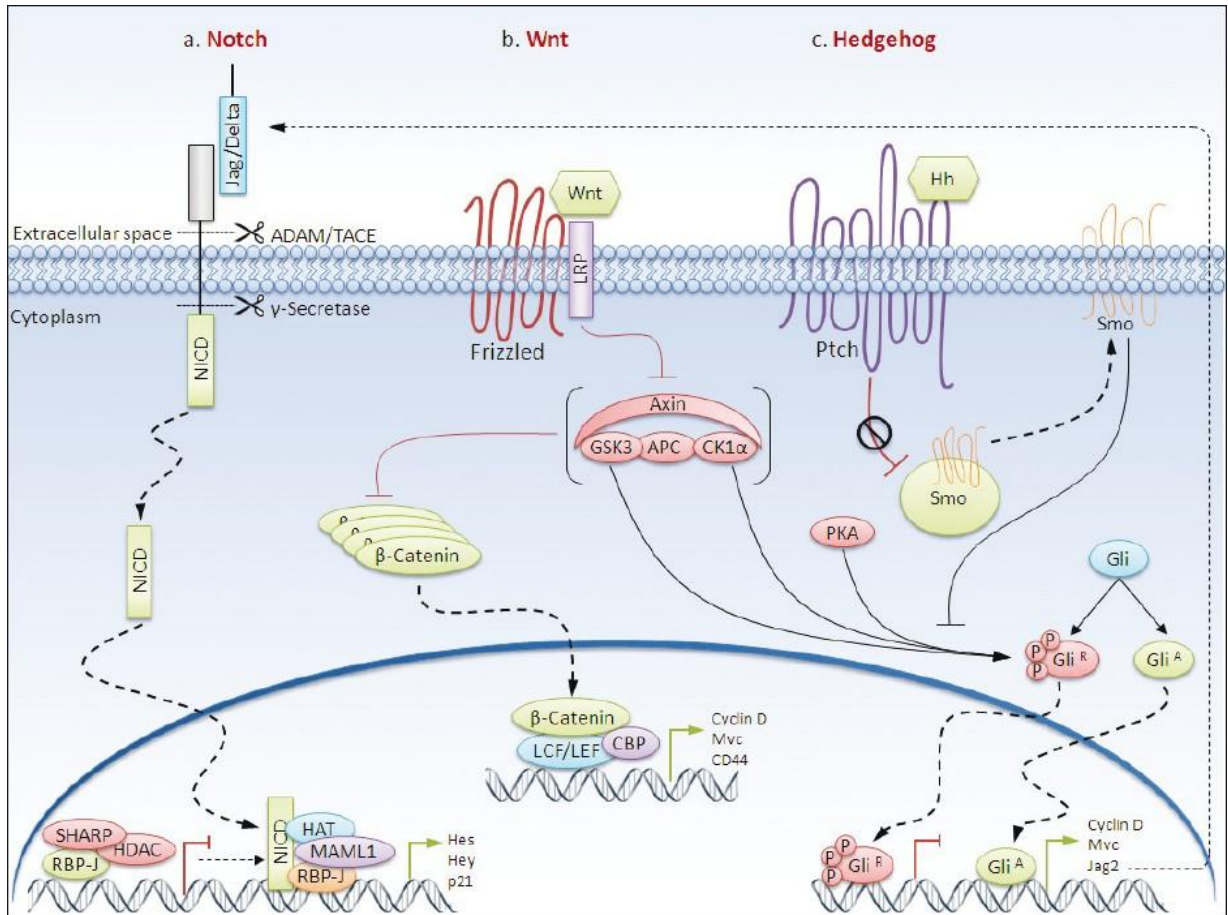


Figure 11 Schematic representation of Notch, Wnt, and Shh signaling cascades.

(a) Notch signaling pathway: Notch receptor is composed of an extracellular ligand binding domain, a single transmembrane spanning region, and intracellular domain. Activation of notch signaling takes place through binding of delta ligand with notch receptor between neighboring cells. Upon ligand binding to notch receptor, it will undergo a conformational change that allows cleavage at extracellular portion. Subsequently, the intracellular portion of notch will be cleaved by gamma-secretase, an intramembrane protease thereby releasing notch intracellular domain containing portion (NICD).

(b) Wnt signaling pathway: Wnt proteins ligands transduces extracellular message to intracellular signaling cascade through the binding of frizzled receptors. In the absence of this ligand, β -catenin is sequestered. Phosphorylation of β -catenin within this complex leads to ubiquitin and proteosomal mediated degradation process. See Figure 9 for a more detailed description.

(c) Shh signaling pathway: Sonic hedgehog (Shh) is a secreted and lipid modified ligand that binds to a transmembrane spanning receptor known as Patched (Ptch) leading to subsequent signal transduction events. In the absence of Shh ligand, Ptch will constitutively repress Smoothed (Smo), another transmembrane spanning protein, having homology similar to G-protein coupled receptor (GPCR). Upon Shh ligand binding to Ptch, Smo inhibition by Ptch will be released, which subsequently leads to activation of downstream GLI (Gli1, 2, 3) family of transcription factors. (source [180])

SHH roles in tooth initiation

At the early stage of tooth development, the mitogenic activity of Shh is thought to stimulate proliferation in the placode epithelium, which enables invagination into the underlying mesenchyme and initiation of the epithelial bud[178, 181]. In the diastema region, it was previously observed that the tooth primordium

was present, but failed to further develop because of a lack of maintained *Shh* expression[182-185].

In zebrafish, *Shh* signaling is necessary continuously throughout tooth development from initiation to mineralization stages[186]. Despite gene duplications and differences in tooth location comparing the mice and zebrafish models, the role of *Shh* signaling in tooth development seems to be conserved between these two species[186].

SHH roles in tooth size, morphology, differentiation

Shh expression is maintained at the tip of the epithelial bud and becomes down-regulated towards the end of the bud stage. It is also re-induced in the enamel knot and continues to be expressed in the epithelium throughout ameloblast differentiation. *Shh* from the enamel knot controls crown formation, by increasing tissue proliferation in both epithelial and adjacent mesenchymal sites[187]. Conditional inactivation of *Shh* or inhibition of signaling using an antibody against *Shh* revealed that *Shh* signaling regulates tooth separation, size, and morphology, as well as cytological organization of matrix secreting cells[188-190].

II.7 Notch

Components of the Notch signaling pathway include four transmembrane Notch receptors (*Notch1-4*) and 5 transmembrane ligands (*Jag1*, *Jag2*, *Dll1*, *Dll3*, and *Dll4*), that are expressed during tooth development and affect several aspects of tooth formation (Figure 11). Notch signaling was demonstrated to regulate tooth morphogenesis and ameloblast differentiation[191]. *Jag1* and the downstream target of Notch signaling, *Hes1* are expressed at the epithelium and ameloblasts, with signaling roles link to enamel differentiation[192]. Inactivation of the Notch-interacting domain of *JAG2* in mice caused abnormal molar shapes, additional cusps, and inhibition of ameloblast differentiation due to alterations in the enamel knot[191].

Part III

Retinoids

III.1 The general role of vitamin A

Vitamin A was known to be the first fat soluble vitamin. More than a century after discovery of vitamin A and β -carotene, these compounds have been investigated to understand the molecular basis of their profound effects and broad roles in human health. Retinoic acid (RA) is recognized as the active component of vitamin A. It carries out many of its diverse actions, in part by playing as the ligand for RA receptor mediated signaling. Thus, RA-induces the expression of a large number of either direct or indirect target genes[193], partially explaining diverse retinoid actions. In addition, nutritionally there are numerous different forms of natural vitamin A (collectively known as retinoids) including β -caretinoid, along with a variety of metabolic intermediates, including retinaldehyde, and the transcriptional activator of retinoic acid receptors –the ligand all- trans-retinoic acid. There are a variety of physiological roles of retinoids, including promoting vision, inducing cell differentiation, supporting reproduction, and maintaining overall cell growth. RA also has important effects on stem cell differentiation, notably in neuroepithelial progenitors (reviewed in [194]). Hence, retinoids are vital micronutrients that have to be taken from the diet as either preformed vitamin A or as the pro-vitamin A caretinoid.

Vitamin A plays important roles during development or homeostasis of different events system or organs such as, eye, skin, growth, reproduction, brain, vascularization, bone. Interestingly, developmental defects occur not only under conditions of deficiency but exposure to excess vitamin A or its active form, RA, is equally deleterious for embryonic development[195]. Thus, too little or too much vitamin A disrupts embryonic development[195]. While vitamin A is generally found in multi-vitamins formula, the premise that increased admission of vitamin A is a primary causative factor in osteoporosis and fracture in developed/industrialized countries such as the United States, and in Scandinavia, is still under debate. The highly intake of vitamin A in diets such as animal liver may be potentially harmful but population-based evidence for effects of vitamin A deficiency also exists. The utility of experimental models to understand broad human epidemiological data is in order. Hence, excessive, as well as insufficient, levels of retinol intake may be associated with compromised bone health.

III.2 Clinical use of retinoids and the worldwide role in public health

During last decade, retinoids have been used widely for the treatment of acne. Tretinoin (all-*trans* RA), isotretinoin (13-*cis* RA), and tazarotene are FDA approved retinoids for the treatment of acne, which have been shown anti-bacterial effect against the *P. acnes* organism[196, 197]. Retinoids have actions inducing cell differentiation, hence are powerful agents to induce neoplastic differentiation. For example, acute promyelocytic leukemia (APL) is a subtype of acute myelogenous leukemia (AML). In APL white blood cells are transformed as cancer cells, with an abnormal accumulation of immature granulocytes called promyelocytes[198]. This disease is produced by RA receptor alpha (RAR α) gene fusion with the promyelocytic oncogene (PML) and is distinguished from other forms of AML by its responsiveness to all-*trans* RA (ATRA; also known as tretinoin) therapy. This is thus a highly curable disease, currently treatment with both ATRA and arsenic resulted in complete remission of all 77 patients investigated[199].

Regarding other types of cancer, both natural and synthetic retinoids have been investigated at the pre-clinical research for anti-cancer activities[200]. The strategy to develop specific synthetic retinoid derivatives, with the potential to target different biological activities-such as anti-proliferative activity[201, 202], inducing apoptosis[203], inhibiting activity of human breast cancer[204], and cytotoxicity or growth inhibitory shown in a variety human cancer cell lines[205-210], has been achieved by modifying the hydrophobic, linker, or hydrophilic moieties of RA. In addition, the development of imaging agents for hybrid compounds containing retinoids to detect multiple human cancer xenografts, would open a new avenue to study the epigenetic biology in cancer (reviewed in [211]). These compounds could have additional applications in neuronal diseases[212]. In addition, the retinoid AM80 has an anti-diabetic activity[213] and seems useful for treatment of Alzheimer's disease[214], where it significantly reduced brain glial activation and neuronal loss, improving spatial learning and memory[215]. Since retinoids have potent actions regulating the stem cell differentiation, they may have clear applications in stem-cell based regenerative technologies[216]. Retinoids may thus have major applications in

the field of biomedicine and including for the repair, replacement or regeneration of cells, tissues, and/or organs.

The importance of retinoid regenerative therapy has been studied in a wide range of diseases including the induction of pro-nephric tubule-like structures from animal caps by combination of activin and RA in kidney diseases[217]. RA also regulates differentiation of the secondary heart field[218, 219], induces dermal proliferation reduces skin wrinkling[220], and normalizes retinal astrocytes in retinal disorders[221, 222]. In neurodegenerative diseases, retinoid use is largely at the experimental stage. Notably, in postpartum Alzheimer's disease patients Raldh2 levels were reduced, stating a potential role of dysregulated RA signaling in the etiology of neurodegenerative diseases[223].

Because of the essential role of this nutrient, extensive investigations on how vitamin A is absorbed and handled by the body, specifically regarding skeletal biology[224] or in the entire body[225] have been reviewed. Vitamin A deficiency (VAD), effects of hypervitaminosis A, general actions of vitamin A, and mechanisms are described in the next sections.

III.3 How RA is obtained from dietary sources, stored in liver, and transported to the cell

Vitamin A is acquired from the diet either as preformed vitamin A or as provitamin A carotenoids[226, 227]. Preformed vitamin A is ingested as long-chained fatty acids of retinol or retinyl esters in foods such as liver, eggs, milk, butter, and fortified cereals. Provitamin A carotenoids (eg, β -carotene, α -carotene, and β -cryptoxanthin) are found in vegetables such as carrots, spinach, and pumpkins. Ingestion of β -carotene is thought to consider for over 75% of the provitamin A carotenoid intake in the United States. A retinol activity equivalent is equal to 1 μ g retinol or 12 μ g β -carotene. Approximate total vitamin A intake in the United States averages 600 μ g retinol activity equivalents per day. Hence, about 70–75% is thought to be due to the consumption of preformed vitamin A.

Dietary retinyl esters are hydrolyzed by pancreatic and intestinal enzymes. Then, free retinol is absorbed by intestinal mucosal cells (i.e. enterocytes)[228, 229]

(Figure 12). Retinol is insoluble in water. However, in the enterocyte, retinol is bound by cellular retinol binding protein (CRBP) II, which is thought to bind most retinol in intestinal cells; it is 1 of 6 known retinoid binding proteins[227]. About 50% of provitamin A carotenoid is taken up in mucosa cells, and about 50% is oxidized to retinal and then reduced to retinol[230]. Retinol derived from both retinyl esters and provitamin A carotenoids is esterified with long-chain fatty acids. The retinyl esters and intact carotenoids are incorporated with other lipids (eg, cholesterol, cholesterol esters, and triglycerides) into chylomicrons which are carried by lymphatic system[231]. Some unesterified retinol is thought to be absorbed directly by the portal system. The presence of fat in the diet helps vitamin A absorption. Fat activates enzymes responsible for hydrolyzing dietary retinyl esters to increase micelle formation for solubilization of retinol and carotenoids in the intestinal lumen, which thus increases chylomicron formation[226].

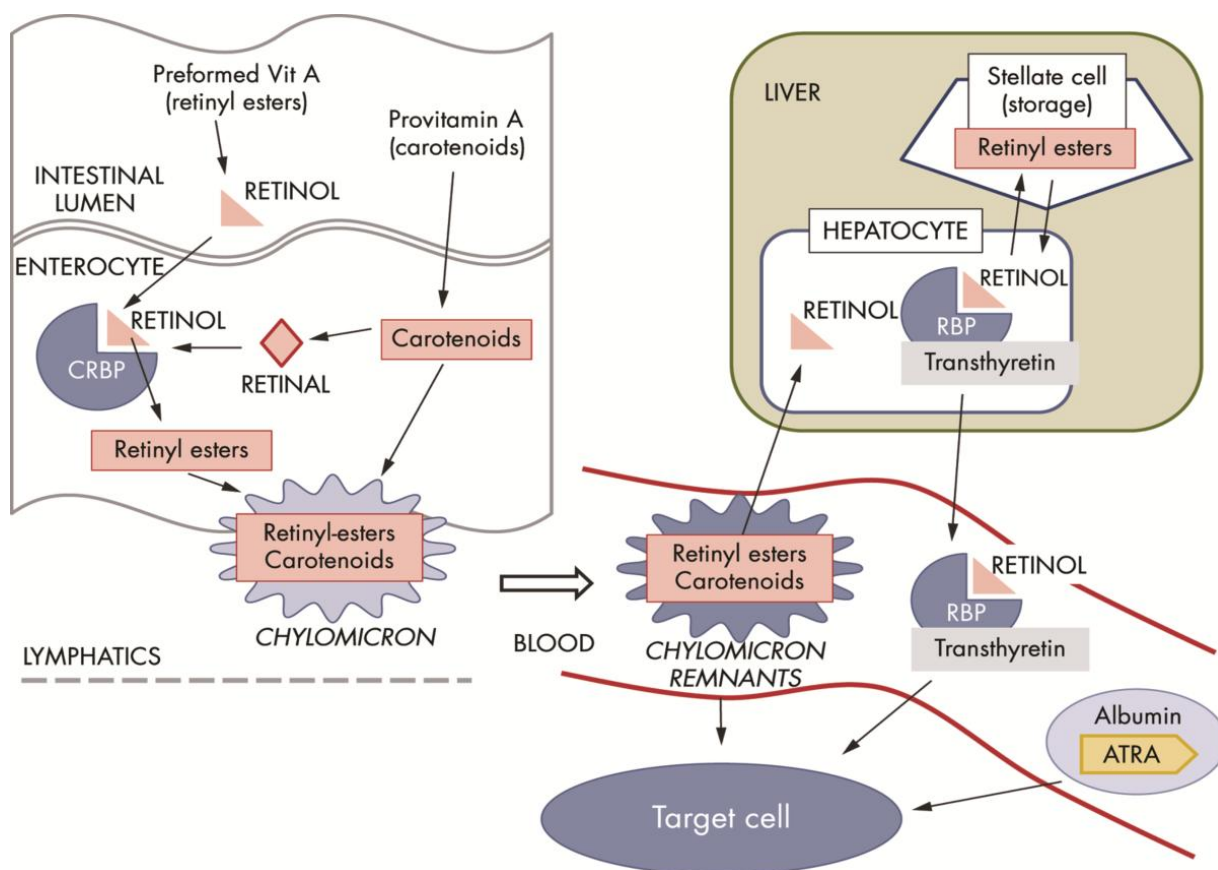


Figure 12 The fate of vitamin A transportation.

Vitamin A is obtained from the diet as retinyl esters or carotenoids. Retinyl esters and carotenoids are incorporated into chylomicrons, which can deliver retinoids directly to target cells. The liver acts as the major organ for clearance of chylomicron remnants. Within the hepatocytes, retinyl esters are hydrolyzed to retinol and bound to RBP. Retinol-RBP is transported via the blood to target cells. If retinol is not used, it can be stored in liver stellate cells in the form of retinyl esters. Retinoids reach target cells principally as retinol-RBP, but retinyl esters and carotenoids can be transported by chylomicrons and ATRA can be bound to albumin (source [224]).

In the bloodstream, chylomicron remnants containing retinyl esters are formed after hydrolysis of chylomicron triglyceride by lipoprotein lipase and addition of apolipoprotein E[227]. Hepatocytes get the retinoid remnants by receptor-mediated endocytosis and retinyl esters are thereby hydrolyzed[232]. If retinol is not needed, it is re-esterified and retained in liver stellate cells. The liver serves as the main storage depot of vitamin A, stocking approximately 70% of total body stores. Smaller amounts of retinyl esters, as well as carotenoids, are also carried by chylomicrons and remnants to extra-hepatic tissues for use and storage[227].

After hydrolysis of retinyl esters in liver stellate cells, it is supposed that retinol is transported back to hepatocytes and bound by retinol binding protein (RBP)[233]. After binding with RBP, the retinol-RBP complex is able to enter the circulation, where it binds with transthyretin, a larger protein that is also synthesized in the liver[234]. Binding of retinol-RBP to transthyretin is important to prevent the clearance by kidney[235]. In the fasting state, most retinoids in the circulation (>95%) are thought to exist as retinol-RBP. However, in the postprandial state, chylomicron retinyl esters is a significant proportion of total circulating retinoid[236].

III.4 Target Cell Uptake, Intracellular Metabolism, Cytoplasmic and Nuclear Receptors Mediating Vitamin A Effects

Pioneering studies of rodents that were nourished with a vitamin A deficient diet first described the VAD syndrome affecting many organ systems as a complex neonatal syndrome[237]. During the next decades, RA was shown to be a ligand for several nuclear receptors, by this way directly controlling the transcriptional activity of target genes. Targeted disruption of the murine RA receptor (RAR) genes revealed principally redundant roles; homozygous disruption of two RARs was necessary to induce abnormalities that add to those of VAD syndrome (reviewed in [238]). Gene-disruption studies confirmed that RARs play roles *in vivo* as heterodimers with retinoid X receptors (RXRs), nuclear receptors that bind the 9-*cis*-RA stereoisomer[239]. Several experimental approaches have been used to investigate functions of retinoid signaling during early embryogenesis. These were carried out in various species, using both gain-of-function strategies (to study stage-specific or region-specific effects of excess RA signaling) and approaches to reduce retinoid signaling for example; through dietary VAD, through loss of function or pharmacological inhibition of synthesizing enzymes or RARs, and through dominant-negative RARs. RA was shown to control embryonic anterior–posterior patterning, in particular by regulating the expression of specific homeobox genes (Hox genes)[240, 241]. These have sequential functions in, for example, neural tube patterning. Here active RA (synthesized predominantly by the enzyme Raldh2), diffuses from predominantly the mesoderm to regulate embryonic-stage growth and patterning of neuronal, notably the posterior hindbrain and embryonic spinal cord[194, 242]. At later stages (E11.5-14.5) RA generated by specific brachial and lumbar spinal cord motor-neuron progenitors regulates the initiation of limb-innervating motor neurons[194, 243]. RA has also been considered as a putative morphogen regulating antero-posterior patterning and digit specification in tetrapod limbs[244] and in regeneration of amphibian limbs[245]. Additionally, functions of RA have been shown for many developing tissues or organ systems including the facial region and forebrain[246-248], the eye[249, 250], and the inner ear[251]. Hence, RA also regulates cardiac morphogenesis and differentiation[252] and is associated in the

development of several organs undergoing budding morphogenesis, especially the lung[233], kidney[253], and pancreas[254].

III.5 The function of retinoic acid as a transcriptional regulator

RA metabolic pathways

The canonical synthesis pathway

The canonical pathway for embryonic RA synthesis has been investigated for well over a decade, largely through gene-targeting studies of several critical murine retinaldehyde or RA synthesizing enzymes. This pathway is conserved in placental embryos, for which plasma-circulating retinol is the main source of retinoids. It is also conserved in oviparous species that store retinol in the egg yolk. Through either yolk sac or placental transfer, retinol is taken up by RBP[239], which is expressed in the embryonic visceral endoderm from pre-gastrulation stages (Figure 13). Although the existence of a cell-surface RBP receptor (which mediates absorption of retinol) has been known for decades, only recently has RBP been identified as the ligand capable of binding to and stimulating retinoic acid gene 6 (*Stra6*) cell membrane signaling (Figure 13). A gene initially cloned in a screen for RA-inducible genes[236]. This gene displays intricate expression patterns during development, presumably indicating tissues to that retinol is preferentially communicated[255]. In human, homozygous mutations of *STRA6* have been found to cause a syndrome combining anophthalmia, heart defects, lung hypoplasia and mental retardation[256]. This indeed is the first model of a retinoid signaling pathway mutation causing developmental abnormalities in humans.

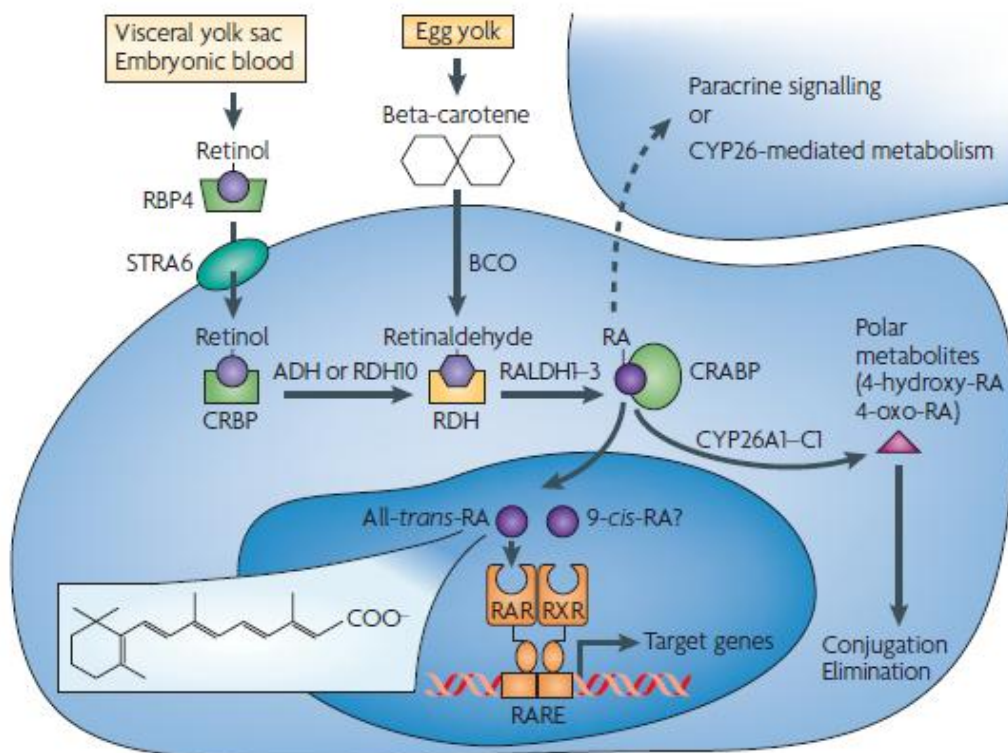


Figure 13 Intracellular regulation of retinoid signaling.

Retinoid sources comprise circulating retinol and carotenoid. Retinol is obtained by embryonic retinol binding protein 4 (RBP4), imported intracellularly by the receptor protein stimulated by retinoic acid 6 (STRA6), and modified into retinaldehyde, principally by retinol dehydrogenase 10 (RDH10). Cleavage of β -carotene by β -carotene oxygenase (BCO) enzyme(s) directly produces retinaldehyde. Retinaldehyde dehydrogenases (RALDH1 to RALDH3) then produce retinoic acid (RA), which plays as a nuclear ligand for nuclear receptors (heterodimers of RA receptors (RARs) and retinoid X receptors (RXRs) to control transcriptional activity of target genes. ATRA is the main *in vivo* RAR ligand. In cells expressing cytochrome P450 26 (CYP26) enzymes, RA is changed into more polar compounds, which are subject to extra metabolism and elimination. However, RA can act in an intracrine manner in cells and also has evidence for non-cell-autonomous actions such as paracrine effects on neighboring cells. (source [257])

Two sequential reactions are necessary to first convert retinol to retinaldehyde, then finally RA. Retinol to retinaldehyde conversion is catalyzed by two

enzyme families, the cytosolic alcohol dehydrogenases (ADHs) and microsomal retinol dehydrogenases (RDHs) (Figure 13). Gene-knockout studies originally implied that this reaction takes place ubiquitously in the embryo, and is mainly due to ADH7 (ADH3)[258]. However, mutation of RDH10 in mice has been shown to result in lethal developmental abnormalities which are characteristic of a RA-deficiency phenotype[259]. This finding has changed our view of the regulation of embryonic RA synthesis, showing a first level of control due to the presence of RDH10 in specific tissues, which prepares the retinoid precursor for tissue-enriched synthesis by retinaldehydes[259, 260]. Some RA synthesis persists in *Rdh10* mutants, indicating other enzymes such as ADH7 can give rise to retinaldehyde (although at quite low levels[259]).

The last step in this pathway is the oxidation of retinaldehyde into RA, and it is well founded that this step gives rise to tissue-specific patterns of RA synthesis (Figure 13). It is performed by three retinaldehyde dehydrogenases (RALDH1, RALDH2, and RALDH3; the corresponding genes are named *Aldh1a1–3*). The murine mutations of *Raldh2* lead to embryonic lethal phenotypes[261, 262], whereas RALDH3 acts at a later fetal stage producing neonatal lethality[261]. RALDHs exhibit distinct expression patterns that attentively correlate with the dynamics of RA signaling, as assayed by the action of murine RA-responsive reporter transgenes[263, 264]. RALDH2, is firstly expressed and induced in the primitive streak and mesodermal cells during gastrulation, is restricted to the posterior embryonic region[265]. Later mesodermal differentiation, RALDH2 remains tight to prospective cervical and trunk levels. *Raldh2* knockout mice indicated this enzyme is responsible for all RA production during early embryogenesis, until E9.0 when RALDH3 begins its expression in the forebrain[248]. Its absence affects many developing systems such as forebrain, hindbrain, heart, forelimbs and somites[248, 252, 266-271], sites also affected by dietary VAD[272], or aldehyde dehydrogenase inhibitors in rodent and other species[246, 273]. RALDH3 has different functions at later stages of eye and nasal development[261]. *Raldh1* mouse mutants are viable, and this enzyme has been shown to play a redundant role with RALDH3, especially during eye development[249, 250].

Tissue-specific RA metabolism

The region-specific and complex effects of excess RA in diverse species emphasize the significance of strictly controlling its distribution. Although the regulation of its synthesis is patently crucial, a supplementary level of control exists in the form of specific RA-metabolizing enzymes. Cytochrome P450 26 (CYP26) A1 was firstly recognized as a RA-inducible gene output, the prototypic member of a cytochrome P450 subfamily is able to transform RA into more polar derivatives[274]. Inconsequentially, additional enzymes with similar activity were cloned, namely CYP26B1 and CYP26C1[275, 276]. While it has been debated whether CYP26 products are active retinoids, *in vivo* data indicate the role of Cyp26a1 is to eliminate bioactive RA from specific tissues[277]. All three CYP26 genes have precise expression domains during embryogenesis. Targeted mutation of *Cyp26a1* and *Cyp26b1* causes developmental abnormalities similar to effects of teratogenic RA excesses[278-280]. Thus, a major function of CYP26 enzymes may be to guard proliferative progenitors, or stem cells from the differentiating effects of RA.

Transcriptional regulation of RA receptor signaling

RA-generating cells release RA, which is absorbed by neighboring cells. Hence, while RA signaling is predominantly paracrine[281], RA may function in an autocrine mode during spermatogenesis[282]. Signal transduction requires binding of RA to a nuclear RAR, which forms a heterodimer complex with RXR. RAR–RXR regulates transcription by binding to DNA at RA–response elements (RAREs) located in enhancer regions of RA target genes[257, 281] (Figure 14).

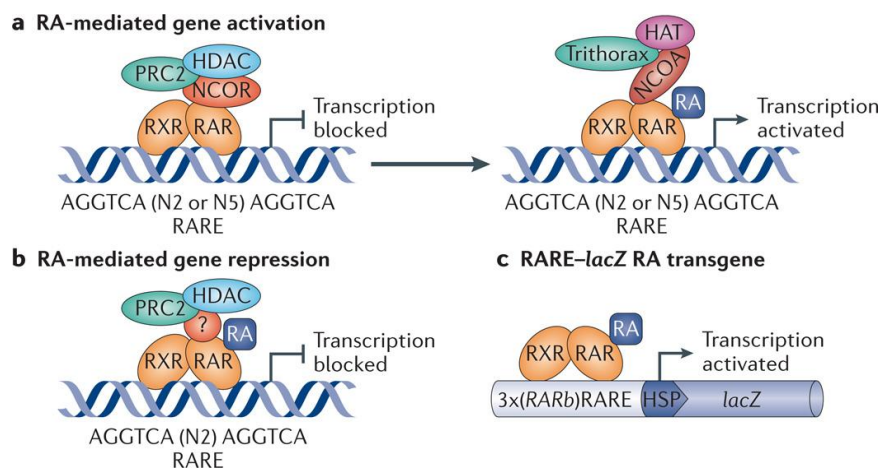


Figure 14 RA signaling mechanism.

RA binds to RAR in an RXR heterodimer complex bound to RAREs near target genes, effecting in regulation of transcription.

(a) For genes activated by RA, the absence of RA allows co-repressors of the nuclear receptor co-repressor (NCOR) family to bind to RAR and recruit repressive factors such as Polycomb repressive complex 2 (PRC2) and histone deacetylase (HDAC), whereas the presence of RA releases co-repressors and allows co-activators of the nuclear receptor co-activator (NCOA) family to bind to RAR and recruit activating factors such as Trithorax and histone acetylase (HAT).

(b) For genes repressed by RA, for example *Fgf8*, the presence of RA allows RAR to recruit PRC2 and HDAC. Nevertheless, in this case, its co-regulators are unknown.

(c) The RARE-*lacZ* RA-reporter transgene, which is usually used to detect RA activity *in vivo*, consists of three tandem RAREs situated upstream of a basal heat shock promoter (HSP) directing *lacZ* gene cassette expression, expressing the β -galactosidase reporter. (source [281])

During classical RA-dependent gene activation, unliganded RAR–RXR heterodimers bind to RARE sequences and suppress transcription of their associated genes. Hence these targets are silenced, except during activation by RA ligand binding[283-286]. Nevertheless, additional co-regulators and epigenetic changes take part during retinoid transcriptional regulation. In the repressive unliganded state, the RAR–RXR heterodimer recruits co-repressors such as nuclear receptor co-repressor 1 (NCOR1) and NCOR2, which successively recruit histone deacetylase (HDAC) protein complexes and Polycomb repressive complex 2 (PRC2). This results in histone H3 lysine 27 trimethylation (H3K27me3), chromatin condensation, and gene silencing[287-289] (Figure 14). RA binding to RAR–RXR induces a conformational change in the heterodimer, which initiates the substitution of repressive factors by co-activators such as nuclear receptor co-activator 1 (NCOA1), NCOA2, or NCOA3. These co-activators recruit histone acetylase (HAT) complexes and Trithorax proteins, which mediate H3K4me3, chromatin relaxation and gene activation[290, 291] (Figure 14). During activation, co-activators bind to RAR, not RXR, which is consistent with RA-liganded RAR being the main regulatory component of RAR–RXR heterodimers[292]. Although there are exceptions to the

classical model, for example RARE sequences upstream of *Fgf8* and homeobox B1 (*Hoxb1*) mediate gene repression[293, 294] (Figure 14).

Functional RAREs normally are present near the proximal 3' regions of genes which need RA for normal expression during development. The characteristic consensus RA response element consist of hexameric direct repeats (DRs) with interspacing of 2 bp (DR2 elements) or 5 bp (DR5 elements) (Table 1), contrary to vitamin D and thyroid hormone response elements, which respectively characteristically display DR3 and DR4 configurations[295, 296]. Other hexameric repeat configurations have been also found to bind to RARs in cell line studies[297], but still their *in vivo* significance is unclear. The DR1 element has been proposed to act as a RARE on the basis of *in vitro* studies in which RA function was induced by high levels of exogenous RA and overexpression of RAR[298], but there is absence of evidence for DR1 elements regulating RA signaling *in vivo* (Table 1).

For both the DR5 and DR2 elements the optimal consensus is a 5'-(A/G)G(G/T)TCA-3' sequence arranged as a palindrome, allowing the most efficient RAR binding[299] (Figure 14). In some cases it is unclear what defines whether a RARE has a repressing or an activating function. The repressive RAREs upstream of *Hoxb1* and *Fgf8* and also in the mouse *Wnt8a*, are DR2 elements, but many activating RAREs also have DR2 spacing, whereas others have DR5 spacing. Hence, even if DR2 spacing is required for repressive RAREs, RARE modality appears to necessitate other factors such as related partner enhancer elements or specific co-regulators[300].

Gene regulation by RA

RA performs by binding to RARs, which are members of the nuclear receptor superfamily[301]. There are RAR α , RAR β , and RAR γ that are conserved throughout vertebrates and that mainly bind all-trans-RA. RARs play in heterodimeric combinations with retinoid X receptors (RXR α , RXR β and RXR γ). RXRs bind 9-cis-RA, a ligand which is not essential for developmental, hence cannot rescue RA deficient *Raldh2* phenotypes[302]. RXRs appear to play roles as scaffolding proteins to aid DNA binding of the RAR-RXR complex[303]. RAR α , RXR α and RXR β receptors have rather ubiquitous expression patterns, whereas RAR β , RAR γ and RXR γ exhibit more complex and tissue-specific expression domains (reviewed in

[304]). Therefore, most tissues are potential targets of retinoid activities, while different heterodimeric complexes are able to transduce the RA signal. Murine gene knockout studies showed a large degree of functional redundancy between RAR/RXR heterodimers, with developmental abnormalities generally occurring when two receptors are inactivated in combination, except in the occurrence of RXR α mutants that die in utero owing to heart defects[305] (Table 2).

In the nucleus, RAR/RXR dimers bind to DNA motifs known as RAREs as described[193]. RAR/RXRs are able to bind RAREs, yet in the absence of ligand they recruit co-repressor complexes and produce target gene repression. Conversely, RA ligand binding induces a conformational change that causes the recruitment of co-activator complexes and the release of co-repressors. These events initiate chromatin remodeling that de-compacts the chromatin and assists the assembly of the transcription pre-initiation complex. Thus, whole-genome chromatin immunoprecipitation-sequencing (ChIP-Seq) study carried out in ES cells proposed that the presence of RA may induce de novo RAR/RXR binding to large RAREs, which are not bound by unliganded receptors[306].

Many RAR target genes have been identified[193], including genes from within the retinoid pathway, such as *Rarb*, *Crbp1/2* (*Rbp1/2*), *Crabp1/2*, and *Cyp26a1*. Included in this list are several members of the Hox gene family, including *Hoxa1*, *Hoxb1*, *Hoxb4* and *Hoxd4*, harboring RAREs, the function of which has been shown *in vivo*[307]. There are numerous novel putative target genes rising through genetic and genomic profiling of novel genes binding RARs and/or with evolutionarily conserved RAREs[308, 309].

Gene(s)*	Stage of lethality	Loss-of-function phenotype	Main references
<i>Adh1</i>	Viable	Postnatal increase in vitamin A toxicity	Deltour et al., 1999b; Molotkov et al., 2002b
<i>Adh5</i>	Postnatal	Growth deficiency, vitamin A toxicity	Deltour et al., 1999b; Molotkov et al., 2002a; Molotkov et al., 2002b
<i>Adh7</i>	Viable	Sensitivity to vitamin A deficiency	Deltour et al., 1999a; Deltour et al., 1999b
<i>Rdh5</i>	Viable	Vision: delay in dark adaptation	Driessen et al., 2000
<i>Rdh10</i>	E10.5-14.5	Small optic vesicles/eyes; abnormal hindbrain and posterior branchial arches; abnormal heart tube; small forelimb buds; defects in organogenesis (lung, gut, pancreas, kidney)	Cunningham et al., 2011; Sandell et al., 2007; Rhinn et al., 2011
<i>Raldh1</i>	Viable	No abnormality reported	Fan et al., 2003; Matt et al., 2005
<i>Raldh2</i>	E9.5-10.5	Hypoplastic optic vesicles; abnormal hindbrain ('anteriorisation'), lack of posterior branchial arches; impaired heart looping and chamber differentiation; truncation of body axis, asymmetry in somite formation; absence of limb buds; defects in organogenesis (lung, gut, pancreas, kidney)	Mic et al., 2002; Niederreither et al., 1999; Niederreither et al., 2001; Niederreither et al., 2000; Ribes et al., 2009; Ribes et al., 2006; Sirbu and Duester, 2006; Vermot et al., 2005
<i>Raldh3</i>	Neonatal	Shortening of ventral retina; nasal abnormality (choanal atresia); altered GABAergic neuronal differentiation in forebrain basal ganglia	Chatzi et al., 2011; Dupé et al., 2003; Matt et al., 2005; Molotkov et al., 2006
<i>Cyp26a1</i>	Neonatal	Abnormal hindbrain ('posteriorisation'); truncation of posterior body, sometimes with sirenomelia ('mermaid-like tail'); vertebral transformations	Abu-Abed et al., 2001; Sakai et al., 2001
<i>Cyp26b1</i>	Neonatal	Limb defects (abnormal distal skeleton and cartilage maturation); craniofacial abnormalities (reduced maxilla and mandible, cleft palate); gonadal abnormalities (premature meiosis, apoptosis of male germ cells)	Bowles et al., 2006; MacLean et al., 2009; MacLean et al., 2007; Yashiro et al., 2004
<i>Cyp26c1</i>	Viable	No abnormality reported	Uehara et al., 2007
<i>Cyp26a1;Cyp26c1</i>	E9.5-10.5	Reduced forebrain and midbrain, hindbrain expansion; deficiency in cranial neural crest	Uehara et al., 2007
<i>Rara</i>	Postnatal (variable)	Growth deficiency; vertebral transformations/abnormalities; malformed laryngeal cartilages; webbed digits (variable); male sterility (degeneration of testis germinal epithelium)	Ghyselinck et al., 1997; Lufkin et al., 1993
<i>Rarb</i>	Viable	Growth deficiency; vertebral transformations/abnormalities; ocular abnormality (retrolenticular membrane); locomotor behavioural defects	Ghyselinck et al., 1997; Krezel et al., 1998
<i>Rarg</i>	Postnatal (variable)	Growth deficiency; vertebral transformations/abnormalities; malformed laryngeal and tracheal cartilages	Chapellier et al., 2002; Ghyselinck et al., 1997; Lohnes et al., 1993
		Webbed digits (variable); abnormal differentiation of keratinocytes; male sterility (abnormal seminal vesicle and prostate epithelia)	
<i>Rara;Rarb</i>	Neonatal	Abnormal hindbrain patterning (abnormal r5-r7); absence/abnormality of posterior branchial arch derivatives (thymus, parathyroids) and salivary glands; heart outflow tract and large vessel abnormalities; severe laryngeal/tracheal abnormalities; lung hypoplasia, lack of oesophagotracheal separation; kidney and female genital tract abnormalities	Batourina et al., 2001; Dupé et al., 1999; Ghyselinck et al., 1997; Lohnes et al., 1994; Mendelsohn et al., 1994
<i>Rara;Rarg</i>	E12.5 to neonatal	Abnormal hindbrain patterning ('anteriorisation'); absence/abnormality of posterior branchial arch derivatives (thymus, parathyroids) and salivary glands; eye defects (retinal coloboma, absence of lens); heart outflow tract and large vessel abnormalities, myocardial hypoplasia; severe laryngeal/tracheal abnormalities; craniofacial and limb skeletal defects; kidney, male and female genital tract abnormalities	Ghyselinck et al., 1997; Lohnes et al., 1994; Mendelsohn et al., 1994; Wendling et al., 2001
<i>Rxra</i>	E13.5-16.5	Heart outflow tract and large vessel abnormalities, myocardial hypoplasia; eye defects (shortening of ventral retinal abnormal cornea); placental defect (disorganisation of labyrinthine zone)	Gruber et al., 1996; Kastner et al., 1994; Merki et al., 2005; Sapin et al., 1997; Sucov et al., 1994
<i>Rxrb</i>	Partial perinatal lethality	Male sterility (abnormal Sertoli cells, impaired spermatozoid production)	Kastner et al., 1996
<i>Rxrg</i>	Viable	Behavioural and depression-like defects	Krezel et al., 1998; Krzyzosiak et al., 2010
<i>Rxra;Rxrb</i>	E9.5-10.5	Truncation of posterior body; abnormal nasal region and posterior branchial arches; abnormal heart tube; placental defect (absence of labyrinthine zone)	Wendling et al., 1999

*All phenotypes refer to homozygous germline mutants with gene disruptions generated in embryonic stem (ES) cells. Some examples of compound (double homozygous null) mutations leading to severe embryonic abnormalities are also given. The double mutations were generated through mouse intercrosses, except for *Cyp26a1;Cyp26c1*, for which the two neighbouring genes were deleted in ES cells.

Table 1 Summary of phenotypes resulting from targeted inactivation of retinoid signaling pathway components in mice. (source [308])

Gene	Function during development	Modality	Type	RARE sequence 5'–3' consensus ³⁵ :			Refs
				AGGTCA G T	N?	AGGTCA G T	
<i>Cdx1-5'</i>	Somitogenesis and neurogenesis	Activating	DR2*	GGGTCG	TG	ACCCCT [‡]	110
		Activating	IR0*	GGGTCG		TGACCC	–
<i>Cdx1-3'</i>	Somitogenesis and neurogenesis	Activating	DR2	GGGTCA	AG	AGTTCA	111
<i>Cyp26a1</i>	Degradation of excess RA	Activating	DR5	AGTTCA	CCCAA	AGTTCA	97
<i>Dbx1</i>	Spinal cord interneuron development	Activating	DR2	TGTTCA	GC	TATTCA [‡]	123,162
<i>Drd2</i>	Forebrain striatum development	Activating	DR3	GGGTCA	CCC	TGGCCA	131,132
<i>Epo</i>	Liver erythropoiesis and cardiac growth	Activating	DR2	GGGTCA	AG	AGGTCA	138
<i>Fgf8</i>	Body axis extension, somitogenesis and forelimb initiation	Repressive	DR2	GGGTCA	GC	AGTTCA [‡]	30
<i>Hnf1b</i>	Hindbrain development	Activating	DR5	GGGTCA	CATTG	TGGTCA [‡]	163
<i>Hoxa1</i>	Hindbrain development	Activating	DR5	GGTTCA	CCGAA	AGTTCA [‡]	164,165
<i>Hoxb1-5'</i>	Hindbrain development	Repressive	DR2	AGGGCA	AG	AGTTCA [‡]	31
<i>Hoxb1-3'</i>	Hindbrain development	Activating	DR2	AGGTAA	AA	AGGTCA [‡]	166
<i>Hoxb1-3'</i>	Foregut and hindbrain development	Activating	DR5	GGTTCA	TAGAG	AGTTCA [‡]	167
<i>Hoxa3</i>	Hindbrain development	Activating	DR5	GGTTCA	AGAAG	AGTTCA	115,168
<i>Hoxb3</i>	Hindbrain development	Activating	DR5	GGTTCA	AGAAG	AGTTCA	115,168
<i>Hoxd3</i>	Hindbrain development	Activating	DR5	GGTTCA	AGCAG	AGTTCA	168
<i>Hoxa4-5'</i>	Hindbrain, spinal cord, gut, lung and kidney development	Activating	DR5	AGGTGA	ACTTC	AGGTCA [‡]	115,169
<i>Hoxa4-3'</i>	Hindbrain and spinal cord development	Activating	DR5	AGTTCA	CCGAG	AGGACA	115,168
<i>Hoxb4-5'</i>	Hindbrain and spinal cord development	Activating	DR5	GGGTGA	ACCGC	AGGTCA	170
<i>Hoxb4-3'</i>	Hindbrain and spinal cord development	Activating	DR5	AGTTCA	TGGAG	AGGCCA [‡]	115,170,171
<i>Hoxc4-5'</i>	Hindbrain and spinal cord development	Activating	DR5	AGGTGA	AATGC	AGGTCA	168
<i>Hoxc4-3'</i>	Hindbrain and spinal cord development	Activating	DR5	GGTTCA	CGGGA	AGGACA	168
<i>Hoxd4-5'</i>	Anterior somite development	Activating	DR5	AGGTGA	AATGC	AGGTCA [‡]	172
<i>Hoxd4-3'</i>	Hindbrain and spinal cord development	Activating	DR5	GGTTCA	CCCAG	AGGACA [‡]	115,173
<i>Hoxb5</i>	Hindbrain and spinal cord development	Activating	DR5	GGATCA	CGCAG	AGGTCA [‡]	170,174
<i>Mmp11</i>	Limb interdigital development (two RAREs 200 bp apart)	Activating	DR2	AGGTCC	TG	AGTTCA	88,89,175
		Activating	DR2	AGGTCC	CG	AGTTCA	88,89,175
<i>Ngn2</i>	Spinal cord development (two RAREs 52 bp apart)	Activating	DR5	AGTTCA	CGCTA	TGGACA [‡]	122
		Activating	DR2	AGAACA	AA	AGCTCA [‡]	122
<i>pou5f3</i>	Maintainence of pluripotency	Repressive	DR2	CATTCA	CA	AATTCA [‡]	100
<i>Pax6</i>	Spinal cord and motor neuron development	Activating	DR2	AGTTCA	GT	TAGTCA	44,98,123
<i>Pitx2</i>	Perioptic mesenchyme growth in the eye	Activating	DR5	AATTCA	TTAGA	AAGTCA	129
<i>Rarb</i>	RA signalling	Activating	DR5	GGTTCA	CCGAA	AGTTCA [‡]	176
<i>Stra8</i>	Male meiosis	Activating	DR2	GGGTGA	AA	AGGTCA	16,144
<i>Tgm2</i>	Limb interdigital development	Activating	DR5	AGGTCC	CAGTG	GGGTCA	88,177
<i>Wnt8a</i>	Body axis extension and somitogenesis	Repressive	DR2	AGATCA	GA	AGTTCA	119

Table 2 RA response elements, either activating or repressing retinoid targets, and their respective physiological roles. RAREs frequently occur near the 5' proximal region of genes which require RA for their normal expression in embryo or adult. (source [300])

III.6 Vitamin A Deficiency and Excess

At present, vitamin A deficiency (VAD) is still an issue in developing countries, and its supplementation has had a huge impact worldwide, enhancing vision and immune functions, and also rescuing innumerable lives at a minimal price per patient[310]. As described, there has been prevalent use of retinoids for treatment of several skin conditions such as acne[311] and for different cancers, including APL, head and neck squamous cell carcinoma, Kaposi's sarcoma, ovarian carcinoma, and neuroblastoma[312].

Assessing vitamin A status in individuals is yet rather difficult. The regular methods utilize measuring serum retinol and retinyl ester concentrations. Vitamin A is generally stored in the liver and released as needed bound to RBP, so determining of the serum retinol level is quite an insensitive method for defining vitamin A status, except when levels are exceedingly low or high[313]. Serum levels of retinol usually increase with age, so normal conditions in adults are approximately 1–3 $\mu\text{mol/L}$. Serum concentrations of retinol $<1.05 \mu\text{mol/L}$ point out potentially inadequate vitamin A status, and concentrations $<0.70 \mu\text{mol/L}$ point out deficiency[314, 315]. However, the level of serum retinol is not linked with hepatic vitamin A storage, and additional methods, including dose-response tests and isotope dilution assays, have been advanced which are better indicators of vitamin A reserves in liver[313, 316]. Hence, measurement of serum retinol levels is inadequate for determining vitamin A status with clinical or subclinical toxicity[317]. Serum retinyl esters have been proposed as an alternative marker for chronic hypervitaminosis A[318, 319]. Serum retinyl ester levels of exceeding 10% of total serum vitamin A (retinol plus retinyl esters) or 0.2 $\mu\text{mol/L}$ have been proposed to give thought to excess retinol stores and potential toxicity[320]. Serum retinyl esters increases with age, an effect probably due to increased intestinal uptake and reduced clearance of chylomicron remnants[319-321].

Excessive consummation of preformed vitamin A or retinoid derivatives can lead to hypervitaminosis A. Hypervitaminosis A is not generally a result of increased intake of provitamin A carotenoids such as β -carotene, because β -carotene to retinol conversion is under negative feedback[322]. Thus, carotenemia and yellowing of the

skin are present with elevated intake of carotenes, but these alterations are easily reversible[323].

III.7 Associations between vitamin A and evident effect on bone mass in humans

An important finding in this current thesis and work on the adverse effects of RA excess on enamel formation[324], was the capacity of fetal RA to rapidly reduce skeletal bone ossification. Clinically the consumption of excess, notably from dietary supplementation with multivitamins may contribute to skeletal fragility or osteoporosis. This is a heated debate. The actually recommended daily allowance (RDA) of vitamin A is 900 µg/day in adult males and 700 µg/day in adult, non-pregnant or non-lactating females, likely producing no ill effects. But it is not clear if these subtle increases in vitamin A levels have a physiological role. In animal models, though, in which the RA synthesizing enzyme *Raldh1* is absent (slightly reducing RA endogenous RA levels) mice clearly show higher trabecular and cortical bone mass, correlating with increased BMP2, RUNX2 and alkaline phosphatase, demonstrating clear targets whereby RA excess perturb bone formation[325].

Acute illness due to hypervitaminosis A characterized by peeling of the skin, vomiting, convulsions, headache, and diarrhea is rarely seen[225]. Clinical studies investigating the association between vitamin A and fracture risk of bone or osteoporosis have provided conflicting evidence, showing that vitamin A is both beneficial and harmful to bone health (see [224] for an extensive review). The osteoporosis/bone health effects of increased consumption of vitamin A in human populations is rather unclear, with increased[326-334], decreased[335-338], and/or no associations[339-345] to fracture risk and bone mineral density (BMD) all reported[346, 347]. Conversely to the individual observations, a meta-analysis of prospective studies has proposed that elevated retinol intake and high blood retinol levels have no effect on total fractures, but remarkably enhance the risk of hip fracture[348].

Specific skeletal effects reported in human case studies indicate retinoids increase cortical bone resorption, augment skeletal and joint pain, and cause premature epiphyseal closure[349].

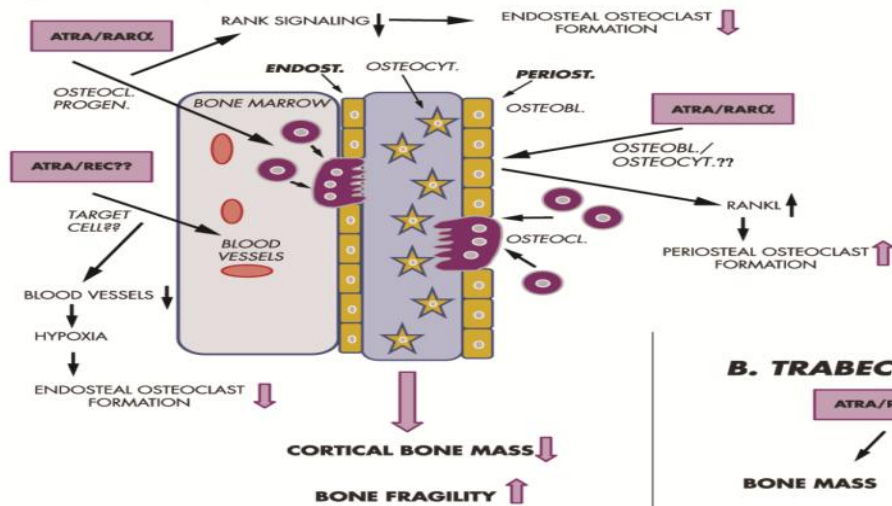
Typical skeletal alterations due to hypervitaminosis A found in animal investigations are thinning of the cortex of long bones and elevated frequency of fracture. For example, short-term studies in rodents treated with high concentrations of retinoids suggest that cortical bone thinning owes mainly to activation of subperiosteal resorption[350]. However, animal studies usually have been investigated using higher dosages of vitamin A than humans would generally be exposed to, *in vivo* effects do not always need such large concentrations of vitamin A.

III.8 Mechanism of RA effects on bone development

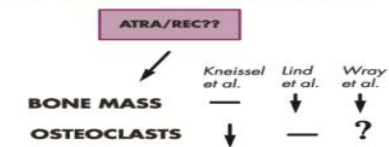
Excess vitamin A consumption might reduce BMD and thus lead to increased rates of hip fractures in humans. Vitamin D acts a principal role in calcium absorption and mineral homeostasis. Vitamin D deficiency is common, and some investigations have proposed that the risk of bone fracture and osteoporosis might be higher when elevated vitamin A consumption occurs in individuals with low vitamin D levels. It indicates the possibility that a high risk of bone fracture and osteoporosis may exist for high vitamin A consumption and/or low vitamin D consumption[224].

Increased osteoclastic resorption of periosteal bone is a well-determined *in vitro* result of excess vitamin A. In calvarial bone (a model of periosteal resorption) ATRA is a strong *in vitro* activator of RANKL and osteoclastogenesis, compared to effects in cultured calvarial bones. Periosteal resorption of cortical bone is an *in vivo* consequence of excess vitamin A in laboratory animals, as well as in humans[224]. Moreover, available evidence proposes that excess vitamin A can also reduce endosteal blood flow, decreases endosteal osteoclast formation, and leads to endosteal mineralization[224] (Figure 15). Vitamin A also causes up-regulated osteoblast differentiation and bone formation (Figure 15). Interestingly, injury-induced heterotopic ossification is able to be stopped by a RAR γ signaling-specific retinoid[351].

A. CORTICAL BONE

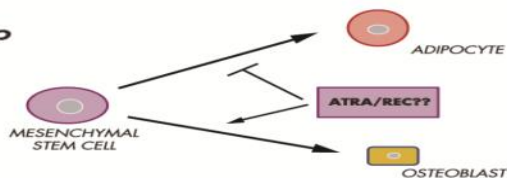


B. TRABECULAR BONE

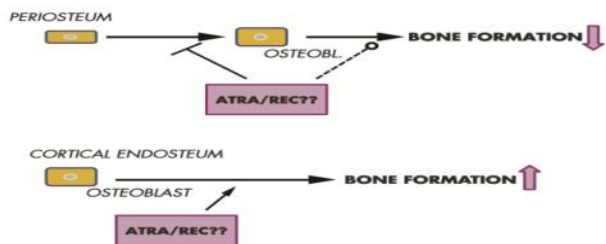


C. BONE FORMATION

IN VITRO



IN VIVO



HETEROTOPIC BONE FORMATION

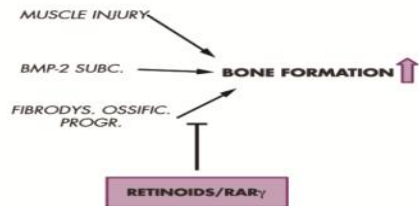


Figure 15 The model of Hypervitaminosis A.

Hypervitaminosis A leads to decreased cortical bone mass, whereas results on trabecular bone still remain unclear. Alterations in cortical bone are linked with effects on osteoclast formation, as well as on bone formation.

(A) Hypervitaminosis A increases the number of osteoclasts on periosteal surfaces. This effect is associated with an increased RANKL/OPG ratio regulated by $RAR\alpha$, probably in osteoblasts or osteocytes. At the endosteal surface of cortical bone, it appears as if vitamin A decreases osteoclasts, which might be owing to reduced numbers of microvessels in bone marrow caused by hypoxia. In other hand, this differentiation of osteoclast progenitors in bone marrow may be inhibited because of $RAR\alpha$ -mediated inhibition of RANK signaling.

(B) Effects by vitamin A on trabecular bone are less understood. A few studies propose that vitamin A has no effect on trabecular bone mass, hence excess did not alter bone mass (reviewed in [346, 347])

(C) Data studied *in vitro* propose that vitamin A inhibits adipocyte differentiation and activates osteoblast differentiation. This suggests the role of vitamin A playing synergistically with BMP2. An *in vivo* study utilizing dynamic histomorphometry shows that vitamin A reduces the number of bone-forming osteoblasts on periosteal surfaces without effect on the capacity of the remaining osteoblasts, which proposes that vitamin A has a repressing effect on periosteal bone formation. Another morphological study shows that vitamin A activates formation of atypical woven bone at the endosteal surfaces. Hence, retinoids have been described to inhibit heterotopic bone formation. (source [224])

Part IV

Dental anomalies

IV.1 Definitions

Dental anomalies refer to abnormal tooth development events. Developmental dental anomalies may exist in isolation or be associated with extraoral clinical manifestations in syndromes. They can be due to the action of teratogens and are then acquired or of genetic origin and are therefore inherited.

Dental anomalies can be classified into anomalies of:

- Tooth number (missing or extra teeth), and of tooth shape, or size (a continuum of anomalies)
- Tooth structure
- Root formation and eruption and of resorption.

Each developmental stage and event when modified is directly linked to a type of dental anomaly. Thus, any interferences with these developmental processes can lead to clinical anomalies and defects and some occasionally even result in tumours arising from dental epithelial cells (odontogenic tumours).

IV.2 Environmental factors altering tooth development

Retinoic acid is an important regulator of embryonic and fetal environment. It also extends to the potential adverse effects of chemical, nutritional, and/or hormonal effects on neonatal and early childhood development. The effects of vitamin A/retinoic acid signaling on tooth development/anomalies are interesting as the tooth through mineralization will fix the anomalies and will allow through their discovery a coming back in time to altered developmental events. Retinoids also cross path with endocrine disrupting agents some of them known to affect odontogenesis and specifically amelogenesis[352].

Endocrine disruptors or hormones may act through epigenetic mechanisms producing reversible changes, without affecting DNA sequence, however modifying gene expression. Epigenetic events such as changes in DNA methylation, histone acetylation, and phosphorylation affecting chromatin structure can modify gene activity and expression. Since these changes can be inherited, environmental alteration could produce permanent expression alterations during development.

Enamel, the hardest tissue in the body, and its synthesizing cells the ameloblasts are highly sensitive to environmental assaults during development. The disruption of ameloblast differentiation and function is thought to contribute to qualitative enamel defects that characterize these conditions[353]. A variety of environmental factors can interfere with enamel formation. These factors include infection, heat (fever), hypoxia, physical trauma, chemical exposure, fluorides, nutritional deficiencies or excesses (Table 3). In human, the most critical stage in enamel formation/maturation would be from the third trimester of pregnancy to 3 year of age[354].

Many environmental factors can play a role during tooth development and results in a disease called Molar Incisor Hypomineralization (MIH). This is a rather common developmental dental defect of permanent teeth, which manifests classically as hypoplastic/hypomineralized enamel in permanent first molars and enamel opacities in permanent incisors. The disease also exists in the primary dentition as Hypomineralised Second Primary Molars (HSPM). A high prevalence of MIH has recently been recognized by dental professionals globally[355]. From a limited number of studies, the prevalence of MIH ranges vary from 2.4% to 40.2%[355] and the prevalence of HSPM is reported to be 4.9-6.9%[356-358]. These extended enamel defects can increase the subsequent risk of secondary dental caries, infection and hospitalization[359]. Both MIH and HSPM are associated with a high burden of disease, due to a range of unique clinical challenges that predispose to treatment failure such as the adhesion to restorative material[360]. For example, given their high prevalence and burden of disease, the cost of these conditions to the general community is substantial.

Since the criteria for MIH were developed, a number of observational studies have tried to determine the associated etiological factors[361]. Studies worldwide have investigated the potential risk factors for MIH during pre-, peri-, and postnatal stages of development; and concluded in a lack of evidence, with lack of standardized outcome measurement being a major limitation[362, 363]. These studies did not include severe presentations of MIH such as post-eruptive enamel breakdown, atypical restorations and atypical extractions[364]. Finally, the results

reported are diverse and inconclusive[359, 362, 365, 366] and require more extensive investigations, both at the clinical and pre-clinical level.

In this thesis we considered the impact of RA pathway alteration on the genesis of dental/enamel and bone anomalies and retinoids as potential endocrine disrupting chemicals. One of the objectives of this PhD work was to discover novel early factors initiating and influencing enamel regulatory networks, possibly to design strategies to alleviate those tooth defects[195].

Environmental factors related to tooth formation				
Factors	Actions	Defects	Model	References
Amoxicillin	-Amoxicillin prenatal administration on dental enamel	-Clinically and histologically observed enamel disorders	Rat	-Gottberg 2014[367]
	-Chronic subcutaneous injection of amoxicillin	-Morphology and histological changes of enamel and ameloblasts	Mouse	-Mihalas 2016[368]
Aspirin	-Treatment with aspirin during pregnancy	-Microhardness of mineralized tissues of the offspring's teeth	Rabbit	-Nazir 2015[369]
	-Quantitative analysis of minerals on the developing teeth of the fetus while the mothers were treated throughout the pregnancy	-Calcium was the most affected mineral	Rabbit	-Nazir 2011[370]

Bisphenol A (BPA)	-Enamel hypomineralization by low-dose BPA -BPA has both ER-dependent and ER-independent effects on ameloblasts.	Enamel defects mimic human enamel pathologies or MIH	Rat	-Jedeon 2016[371]
Estrogen	The estrogen signaling pathway is involved in tooth development and the enamel mineralization process	Possibility of enamel differences between sexes	Rat	-Jedeon 2014[352]
Fluoride	Multiple mechanisms; -direct fluoride related effects on ameloblasts -indirect fluoride related effects on the forming matrix	Porous and discoloration of enamel	Rat, mouse, sheep, pig, rabbit, hamster, zebrafish	-Bronckers 2009[372]
Genistein and Vinclozolin	Endocrine disruptor	Hypomineralization of enamel -Modulations of <i>Klk4</i> and <i>Enamelin</i> in males -Female rats are less affected than males	Rat	-Jedeon 2016[373, 374]
Hypoxia	Upregulate the expression of	Hypoplasia with hypomineralization	Mouse	-Sidaly 2015[375]

	vascular endothelial growth factor (VEGF)	or hypomineralization without hypoplasia enamel		
Insulin	- <i>Akita</i> ^{-/-} mutant mice	-Decreased enamel matrix proteins and predisposes to excessive wearing and decay	Mouse	-Yeh 2012[376]
	-The EphB2/ephrinB1 system that govern tertiary dentin formation in vitro and in vivo	-The IGF-1/ephrinB1 axis plays significant roles in the early stages of tooth injury	Mouse	-Matsumura 2017[377]
Retinoic acid (RA)	-Availability of RA influences tooth number and size	-RA signalling play an important role in the diversification of teeth	Cyprinid fish	-Gilbert 2015[378]
	-Exposure of embryos to exogenous RA induces tooth development.	-RA is sufficient to induce anterior ectopic tooth development in zebrafish	Zebrafish	-Seritrakul 2012[379]
	-RA was supplied to pregnant mice as a food supplement	-Elevated RA signaling affects dental cell lineages and induces permanent enamel alterations.	Mouse	-Morkmued 2017[324]

Serotonin 2B receptor	Contributes to the differentiation of neuroectodermal, neural crest, and mesodermal derivatives	Enamel thickness and architecture	Mouse	-Dimitrova-Nakov 2014[380]
Smoking	The maternal passive smoking model in offspring rats	The passive smoking alters the morphological and mineralized development of lower molars	Rat	-Dong 2011[381]

Table 3 Environmental factors related to dental hard tissue formation/anomalies; pre-clinical studies.

IV.3 Dental anomalies in rare genetic diseases

Anomalies of tooth number, shape, size, structure, eruption, and resorption may exist as isolated symptoms or diseases but are often part of the clinical synopsis of numerous syndromes. Dental agenesis, either with/without size defects, is mainly a genetically driven anomaly due to alterations in many signaling pathways including TGF- β , FGF, WNT, SHH, and EDA/NF- κ B pathways. Genes and their mutations responsible for hypo/oligodontia (missing tooth) have been recently reviewed in [382].

IV.3.1 Hypodontia/Oligodontia

Congenitally missing teeth is a highly prevalent dental anomaly. Dental agenesis is classified according to the number of missing teeth[383]. Hypodontia defines less than 6 missing teeth (excluding the third molars). Oligodontia refers to six or more missing teeth (excluding the third molars) and anodontia to no teeth present (typically seen in ectodermal dysplasia).

In the primary dentition, hypodontia is rather rare, occurring at a prevalence of 0.1% - 2.4% within the population[383]. Primary tooth agenesis might be followed by permanent tooth agenesis[384-386]. The prevalence of hypodontia in the permanent dentition ranges between 0.15% -16.2%, based on studies using 200 subjects to ~100,000 patient cases[387].

Hypodontia is a result of disturbances during the early stages of development and is suggested as a mild dysplastic defect of the dental lamina[388]. Genetics plays a crucial role in dental agenesis, as confirmed by studies on monozygotic twins[389]. Hypodontia support a monogenic or polygenic mode of inheritance, with epistatic genes and environmental factors exerting some influence on the phenotypic expression of the genes involved[384, 390]. It has a remarkable variation in both penetrance and expressivity.

Genetic non-syndromic hypodontia is associated with divergent homeobox genes as seen in *MSX1* and *PAX9* mutations[391, 392]. The missing teeth follow a pattern that corresponds to the territories specified by the expression of divergent homeobox genes within the maxilla and the mandibule. *IRF6*, *FGFR1*, and *TGFA* contribute to teeth agenesis.

Non syndromic hypodontia/oligodontia can also be associated with *EDA*, *EDARADD* mutations. The same genes are responsible for non-syndromic and syndromic tooth agenesis.

Hypodontia/oligodontia may also be seen in several syndromes:

- Hypodontia might be associated to cleft/lip and palate (*MSX1*, *IRF6* genes Van der Woude syndrome),
- Ectodermal dysplasia (ED) (*EDA1*, *EDAR*, *EDARADD*, and *WNT10A* account for 90% of hypohidrotic/anhidrotic ectodermal dysplasia cases),
- Incontinentia Pigmenti, a form of ED is due to *NEMO* gene mutation,
- Carvajal/Naxos syndrome secondary to desmoplakin-dominant mutations,
- Down's syndrome.

IV.3.2 Supernumerary teeth or hyperdontia

Supernumerary teeth are defined as any supplementary tooth or tooth substance in addition to usual configuration of twenty deciduous and thirty two permanent teeth. Classification of supernumerary teeth may be based on position or morphology[393]. Truly additional (supernumerary) teeth are uncommon (in 0.8% of primary dentitions and in 2.1% of permanent dentitions). Supernumerary teeth may be found especially in the upper maxilla region and most typically occur alone in otherwise healthy individuals but are more common in the relatives of affected people than in the general population.

Expression and formation of supernumerary teeth may be seen in syndromic conditions. For examples: Multiple additional teeth are typically seen in association with Cleidocranial Dysplasia (CCD), cleft lip and cleft palate (8619981). Familial adenomatous polyposis [Gardner's], Apert, Klippel-Trenaunay-Weber, Craniometaphyseal dysplasia, Down's syndrome, Nance-Horan, Orofaciodigital syndrome (type III), Sturge-Weber, and Tricho-Rhino-Phalangeal type I syndromes[394].

IV.3.3 Microdontia

Microdontia is a rare anomaly. The term microdontia is defined as the condition of having abnormally small teeth[395]. Microdontia can be divided into different types according to the number of affected teeth and the morphological change of each tooth. This size anomaly may affect the entire dentition or a single tooth and may therefore be termed generalised or localised. The syndromes associated with microdontia are Gorlin-Chaudhry-Moss syndrome, Williams's syndrome, Turner syndrome (45X0), Trisomy 13, Rothmund-Thomson syndrome, Hallermann-Streiff, Orofaciodigital syndrome (type III), Oculo-mandibulo-facial syndrome, Tricho-Rhino-Phalangeal type I, and Branchio-oculo-facial syndrome[396].

IV.3.4 Heritable dentin conditions

Dentinogenesis Imperfecta / dentin dysplasia. Dentin anomalies are always genetic.

Dentinogenesis Imperfecta (DI) represents a group of hereditary conditions that are characterized by abnormal dentin formation. These conditions are both genetically and clinically heterogeneous and can either affect only the teeth or can be co-associated with other anomalies such as bone defects in OI conditions. DI and dentin dysplasias were classified using clinical, radiographic criteria and histopathology. DI has been subdivided based on its association with OI (Type I) (OMIM; 166240) or not (Type II) (OMIM; 125490), or being associated, within the Brandywine population isolate, with large pulp chambers (Type III) (OMIM; 125500).

In all three DI subtypes the teeth have a variable blue-gray to yellow brown discoloration that appears opalescent due to the defective, abnormally colored dentin shining through the translucent thin enamel[395]. Due to the lack of support of the poorly mineralized underlying dentin, the enamel frequently fractures leading to rapid wear and attrition of the teeth. The molecular defects in OI include numerous mutations in the pro-alpha chains of collagen type I that result in a phenotype characterized by increased bone fragility[397]. Although the dental phenotypes of DI types I and type II appear very similar, the later disorder is not associated with any of the non-dental phenotypic features of OI, and is not caused by a collagen type I defect. DI type II and type III are autosomal dominant allelic conditions due to mutations of the *DSPP* gene[398, 399], coding for the most abundant noncollagenous protein in dentin[400]

IV.3.5 Dentin Dysplasia

Two types of Dentin Dysplasia (DD) are recognized. DD type I (OMIM; 125400) is a rare dentin defect that appears to be inherited as an autosomal dominant condition with a reported frequency of 1:100,000 persons. Clinically the dental crowns appear normal while radiographically, the teeth are characterized by pulpal obliteration and short blunted roots. The teeth are generally mobile, frequently abscessed, and can be lost prematurely. There is no known specific treatment

approach for DD type I although effort to keep occlusal forces to a minimum and avoiding orthodontic treatment for the malaligned teeth may increase tooth longevity[401].

DD type II (OMIM; 125420) is also inherited as an autosomal dominant trait. DD type II appears virtually identical to DI type II in the primary dentition with yellow-brown to blue-gray discoloration of the teeth and pulpal obliteration. However, in DD II the permanent dentition is normal in color or minimally discolored, but displays abnormal pulpal morphology that can appear shaped like a thistle tube in the anterior teeth. Pulp stones also are common in the permanent teeth. Studies now show that in at least some families DD type II is caused by mutations in the *DSPP* gene which is also associated with DI type II[401].

Abnormal dentin may also be a variable feature of syndromes such as:

- Ehlers- Danlos syndrome,
- Golblatt syndrome,
- Schimke immuno-osseous dysplasia,
- Brachio-skeleto-genital syndrome,
- Osteodysplastic and primordial short stature with severe microdontia and opalescent teeth and rootless molars

IV.3.6 Amelogenesis Imperfecta

In humans Amelogenesis Imperfecta (AI) is a relatively rare heterogeneous group of inherited disorders characterized by abnormal enamel formation. The term AI is reserved for hereditary defects of enamel that are not associated with defects in other parts of the body or other health problems but this might be discussed and revised as AI are now more and more recognized as associated to other symptoms in syndromes[37].

The prevalence of these conditions has been studied in only a few populations and has been reported to range from 1 in 700 to 1 in 15,000[402]. It is most probably inaccurate considering the diversity of these diseases. In AI, the enamel defect phenotype exhibit a great variability according to the thickness, hardness and smoothness of the affected enamel[37]. These defects are described as hypoplastic

(quantitative defect of enamel), hypomature (defect in final growth and maturation of enamel crystallites eventually due to insufficient resorption of enamel matrix protein), and/or hypocalcified (defect in initial crystallite formation followed by defective growth)[403]. The enamel in both the hypomaturation and hypocalcified AI types is not mineralized to the level of normal enamel and can be described as hypomineralized. AI can be inherited either as a X-linked, autosomal dominant (AD), or autosomal recessive (AR) condition.

As the final thickness of dental enamel is established at secretory stage, disruption of this process will lead to insufficient enamel appositional growth and pathologically thin or hypoplastic enamel (hypoplastic AI). The maturation stage of amelogenesis is critical for development of enamel hardness and translucidity. Aberration of this process will cause insufficient mineral deposits on the sides of enamel crystallites and leave enamel opaque, colored and sometimes softer, a condition known as hypomaturation AI. In this case, the affected enamel is of normal thickness but easily abraded after tooth eruption due to the hardness defect. Hypocalcified AI is another form of AI in which the failure in mineralization is the most extreme. The enamel may have normal thickness but is rough, soft, and easily chipped off from tooth surfaces after eruption. Patients with AI often experience difficulty chewing and maintaining oral hygiene, have lower self-esteem due to poor dental appearance, and report compromised quality of life[404].

Defects in a number of genes have been reported to cause isolated AI, including *AMELX*, *ENAM*, *KLK4*, *MMP20*, *FAM83H*, *WDR72*, *C4orf26*, *SLC24A4*, and *LAMB3*[405]. In addition, many other genes such as *DLX3*, *CNNM4*, *ROGDI*, *FAM20A*, *STIM1*, *ORAI1*, and *LTBP3*[406] have been shown to be involved in developmental syndromes with enamel defects. These findings reveal many critical players in dental enamel formation. *AMELX* and *ENAM* are two genes encoding enamel matrix proteins that are actively secreted by ameloblasts at secretory stage. Mutations in these two genes lead to hypoplastic forms of AI[37]. *MMP20* and *KLK4* are two major enamel proteases expressed by mainly secretory-stage and maturation-stage ameloblasts respectively. While *MMP20* processes enamel matrix proteins during the secretory stage, *KLK4* is responsible for further degradation of residual proteins during the maturation stage[37, 407, 408]. Mutations in these two

genes generally cause enamel hardness defects (hypomaturation AI) due to defective protein degradation and removal[37]. Except the four mentioned genes encoding enamel matrix proteins and proteases, all of the other AI associated genes were identified through human sequence analysis of AI families[409, 410]. Often, the enamel-specific functions of many of these genes and associated proteins are largely unknown.

IV.4 A focus on rare diseases through human genetics and mimicking mouse models

On the basis of informative families recruited within the Reference Center for rare oral and dental diseases (CRMR O-Rares) of the Hôpitaux Universitaires de Strasbourg (Pôle de médecine et chirurgie bucco-dentaires) in collaboration with the Laboratoire de Génétique Médicale (Pr Hélène DOLLFUS, UDS EA3939-Avenir INSERM, INSERM U1112) and international collaborators, in the framework of Interreg IV Offensive Sciences A27 and Interreg V RARENET, ERDF funded projects, it was possible to approach via next generation sequencing (NGS) especially whole exome sequencing the genotype matching extraordinary oral phenotypes.

LTBP3 was identified as the gene responsible for Verloes Bourguignon syndrome linking short stature, platispondyly with hypoplastic amelogenesis imperfecta[129]. The characterization of the enamel phenotype was detailed in this PhD work using the *Ltbp3*^{-/-} mouse model. This work is summarized in the next part (Page 130).

A new gene *SMOC2* was also discovered as a critical regulator of tooth development and alveolar bone growth[411]. In humans *SMOC2* null mutation results in oligodontia, microdontia, thin enamel, short roots such as in dentin dysplasia type I, and shape abnormalities phenotypes. This secreted BM-40 (SPARC) family matricellular protein appears a key regulator of extracellular matrix signaling. The functional properties of *SMOC2* suggest it acts as a secreted signal inducing tooth and alveolar bone development.

The pathophysiology and role of *Smoc2* can be approach using the *Smoc2*^{-/-} mouse model. A preliminary manuscript describing the murine *Smoc2*^{-/-} mutant

phenotype, comparing it to the clinical symptoms observed in patients is reported on page 148. The summary of human rare diseases associated with orofacial manifestations described in results are summarized in Table 4.

Summary of human rare diseases discussed in this PhD work				
Gene name	Disease name	MIM and Inheritance	Clinical Phenotype	References
<i>CYP26B1</i>	-Craniosynostosis with radiohumeral fusions and other skeletal and craniofacial anomalies -Lethal occipital encephalocele-skeletal dysplasia syndrome	614416	-Skeletal and craniofacial anomalies, including fusions of long bones, calvarial bone hypoplasia, and craniosynostosis	-Laue 2011[412]
<i>DMP1</i>	- AR hypophosphatemic rickets	241520, AR	-DI type II -AR hypophosphatemia -AR hypophosphatemic rickets, osteomalacia with isolated renal phosphate-wasting associated and normocalciuria.	-Hirst 1997[413] -Lorenz-Depiereux 2006[414] -Feng 2006[415]
<i>DSPP</i>	-Deafness, autosomal dominant 39, with dentinogenesis	605594, AD	-DI type I and type II -DI with or without hearing loss	-Takagi 1988[416] -Xiao 2001[398]

	-DD, type II	125420, AD	-DI Shields type II	-Zhang 2001[399]
	-DI, Shields type II	125490, AD	-DI type II	-Rajpar 2002[417]
	-DI, Shields type III	125500, AD	-Hereditary dentin disorders and no obvious pathogenetic effects on dentin formation	-Song 2008[418]
<i>ENAM</i>	-AI, type IB	104500, AD	-AD local hypoplastic AI	-Kärman 1997[419]
			-AD smooth hypoplastic form of AI	-Rajpar 2001[420]
	-AI, type IC	204650, AR	-27% of the autosomally inherited cases of local hypoplastic form of AI	-Mårdh 2002[421]
			-AR, AI and localised enamel defects	-Hart 2003[422]
<i>FGF3</i>	Deafness, congenital with inner ear agenesis, microtia, and microdontia	610706, AR	-Type I microtia, microdontia, and profound congenital deafness associated with a complete absence of inner ear structures	-Tekin 2007[423]

			<ul style="list-style-type: none"> -Congenital sensorineural deafness, microtia and microdontia -Otodontal syndrome and associated ocular coloboma -Deafness, microtia, and microdontia 	<ul style="list-style-type: none"> -Alsmadi 2009[424] -Gregory-Evans 2007[425] -Sensi 2011[426]
<i>LTBP3</i>	Dental anomalies and short stature	601216, AR	<ul style="list-style-type: none"> -Oligodontia and short stature -Oligodontia, short stature, and mitral valve prolapsed -Brachyolmia and hypoplastic amelogenesis imperfecta 	<ul style="list-style-type: none"> -Noor 2009[127] -Dugan 2015[128] -Huckert 2015[129]
<i>RUNX2</i>	<p>-CCD (CCD, forme fruste, dental anomalies only) AND (CCD, forme fruste, with brachydactyly)</p>	119600, AD	<ul style="list-style-type: none"> -CCD with brachydactyly -Patent fontanelles, wide cranial sutures, hypoplasia of clavicles, short stature, supernumerary teeth, and other skeletal anomalies 	<ul style="list-style-type: none"> -Mundlos 1997[427] -Quack 1999[428] -Zhou 1999[429] -Bergwitz 2001[430] -Otto 2002[76] -Yoshida 2002[431]

			-Absence of the clavicles marked calvarial hypomineralization, osteoporosis, progressive kyphoscoliosis, Bowdler spurs, severe osteopenia, and low alkaline phosphatase.	-Zheng 2005[432] -Fernandez 2005[433] -Baumert 2005[434] -El-Gharbawy 2010[435]
	-Metaphyseal dysplasia with maxillary hypoplasia with or without brachydactyly	156510, AD	-Metaphyseal dysplasia with short stature, facial manifestations include beaked nose, short philtrum, thin lips, maxillary hypoplasia, dystrophic yellowish teeth	-Halal 1982[436] -Moffatt 2013[437]
<i>SFRP4</i>	-Pyle disease -Metaphyseal dysplasia, Pyle type	265900, AR	Cortical-bone thinning, limb deformity, and fractures	-Simsek Kiper 2016[438]
<i>SMOC2</i>	DD, type I, with microdontia and misshapen teeth	125400, AR	-DD phenotype with oligodontia, microdontia, and tooth shape abnormalities	-Bloch-Zupan 2011[411]

			-Oligodontia and microdontia	-Alfawaz 2013[439]
SOX3	-Mental retardation, X-linked, with isolated growth hormone deficiency	300123	-X-linked mental retardation with growth hormone deficiency	-Hamel 1996[440] -Laumonier 2002[441]
	-Panhypopituitarism X-linked	312000, XL	-Variable X-linked recessive hypopituitarism	-Solomon 2004[442] -Solomon 2007[443]
			-Spina bifida and panhypopituitarism	-Woods 2005[444] -Bowl 2005[445]
			- 46,XY individuals with X-linked hypopituitarism	-Sutton 2011[446] -Vetro 2015[447]
			-46,XX individuals with random X inactivation	-Stagi 2014[448] -Haines 2015[449] -Igarashi 2015[450]

Table 4 Human rare diseases and their phenotypes. This selection reflects the diseases linked to the genes, signaling networks discussed in this PhD work.

Résumé de la thèse

Approches cliniques, précliniques et translationnelles des anomalies bucco-dentaires associées aux maladies rares

Les anomalies bucco-dentaires et crânio-faciales sont des manifestations phénotypiques des maladies rares. Elles participent au tableau clinique des syndromes et sont susceptibles d'orienter un diagnostic. Ces anomalies que l'on peut classer en anomalies de nombre, forme, taille, structure, d'éruption et de résorption de la dent et de son parodonte, entité biologique, sont des signes diagnostiques fixés dans le temps par les phénomènes de minéralisation et témoin des altérations du développement. Ces anomalies sont d'origine génétique mais peuvent être acquises pour certaines d'entre elles en particulier les anomalies de l'émail, tant l'odontogenèse est en interaction avec l'environnement.

La dent et son parodonte sont confrontés de par leur origine embryologique et les processus de développement mis en œuvre à la problématique des crêtes neurales céphaliques, au développement des dérivés ectodermiques, aux interactions épithélio-mésenchymateuses et aux grandes voies de signalisation, aux phénomènes de minéralisation différentielle dans différents contextes et tissus (émail, dentine, cément, os alvéolaire) d'organisation variée tant à l'échelle macroscopique que microscopique, au remodelage osseux entourant les phénomènes d'éruption.

Ce doctorat combine les approches cliniques, précliniques et translationnelles en particulier par l'étude des modèles murins génétiquement modifiés reproduisant les maladies rares étudiées. Ces modèles sont choisis pour répondre aux problématiques de compréhension des processus biologiques et de prise en charge des patients maladies rares suivis au Centre de référence des maladies rares orales et dentaires (O-Rares) du Pôle de médecine et Chirurgie Bucco-dentaires des Hôpitaux Universitaires de Strasbourg.

Ce doctorat vise ainsi à identifier des gènes impliqués dans la morphogenèse et la signalisation inter-cellulaire en s'intéressant aux facteurs (i) environnementaux et (ii)

génétiques initiant et modulant le développement de la dent et la morphogénèse associée au parodonte.

Les résultats sont ici résumés :

(i) Etude des effets de l'acide rétinoïque en excès sur le développement dentaire et la formation de l'émail. Certains facteurs environnementaux peuvent altérer le développement de l'émail. Les anomalies de l'émail au cours du développement (anomalies de dépôt de la matrice extracellulaire, de la minéralisation, ou de la dégradation) peuvent exister dans un éventail de maladies génétiques, appelées *Amélogénèse Imparfait* (AI). Nous avons réalisé une étude visant à évaluer l'action d'un facteur environnemental et nutritionnel : l'acide rétinoïque (AR) - la forme active de la vitamine A - lors du développement de l'émail. Nous avons observé des défauts de l'émail chez des souris exposées *in utero* à des doses faiblement tératogéniques d'AR, par supplémentation de la nourriture maternelle, pendant 2 à 4 jours aux stades précoces du développement foetal (E12,5 à 16,5). Le profil d'expression d'enzymes impliquées dans la dégradation de l'AR (*Cyp26b1* et *Cyp26c1*) suggère qu'en condition d'excès, l'action de telles enzymes ne suffit plus à éliminer l'AR dans les cellules qui doivent être exemptes de ce signal, ce qui affecte le processus de minéralisation de l'émail. Nous avons effectué une analyse transcriptomique (séquençage d'ARN à haut débit ou RNA-seq) des cellules de bourgeons d'incisives à E14,5 et E16,5 après exposition à l'AR et avons mis en évidence de fortes réductions des niveaux d'ARN messenger (ARNm) de gènes codant pour des protéines de l'émail : *Enamelin (Enam)*, *Ameloblastin (Ambn)*, et *Odontogenic ameloblast-associated protein (Odam)*. L'administration d'AR affecte également la minéralisation osseuse crânio-faciale, avec une ossification réduite après 2 jours de traitement. Le séquençage par RNA-seq montre une réduction de *Runx2* (codant pour un facteur de transcription indispensable pour la régulation de la différenciation osseuse et de l'émail). Des gènes codant pour des facteurs de croissance de l'os (y compris des protéines BMP), des protéines de la matrice extracellulaire, ou de l'homéostasie du calcium, sont également affectés dans les bourgeons dentaires à E14.5 exposés à l'AR, alors que des gènes mutés dans les cas d'AI chez l'homme (*ENAM*, *AMBN*, *AMELX*, *AMTN*, *KLK4*) montrent une expression réduite à E16.5. Nous avons utilisé une approche bio-informatique pour

proposer un modèle expliquant comment la signalisation par l'AR aux stades E14,5-15,5 affecte les protéines de l'émail à E16.5. Ce modèle explique comment l'AR en excès peut nuire à la production de protéines de l'émail, entraînant des altérations permanentes de sa formation. Nos résultats peuvent avoir des implications cliniques, puisque des différences phénotypiques dans la sévérité de certaines AI ont été décrites entre des membres de la même famille portant des mutations identiques. Les patients atteints pourraient être sensibilisés à des altérations normalement bénignes provoquées par la consommation en excès de vitamine A (ou de médicaments contenant de l'AR), et/ou une activité sub-optimale des enzymes de catabolisme de l'AR. Les facteurs nutritionnels, tels que la vitamine A, pourraient donc moduler la pénétrance phénotypique et la gravité de maladies rares telles que l'AI et l'hypominéralisation des molaires et incisives. Ces données ont été récemment publiées dans le journal *Frontiers in physiology* (IF 4.031).

(ii) Phénotypage de modèles murins de maladies rares.

Par une collaboration entre notre équipe à l'IGBMC et le Laboratoire de Génétique Médicale (EA3939-Equipe Avenir puis Inserm U_1112) dirigé par le Professeur H. Dollfus, nous avons identifié, grâce à des familles informatives, plusieurs nouveaux gènes responsables de maladies rares, codant notamment pour : (ii-1) Latent Transforming Growth Factor Beta Binding Protein 3 (*LTBP3*) responsable, lorsqu'il est muté, de l'association AI, petite taille et anomalies vertébrales et (ii-2) *SMOC2*, un régulateur du développement de la dent et de la croissance de l'os alvéolaire.

(ii-1) Anomalies dentaires et de la formation de l'émail chez la souris mutante *Ltbp3*. *LTBP3* joue un rôle important dans la morphogénèse crânio-faciale et la minéralisation des tissus, car il est requis dans le phénomène d'activation de TGF- β . Afin d'étudier le rôle de *Ltbp3* dans la formation de l'émail, des souris adultes mutantes pour *Ltbp3* (fournies grâce à une collaboration avec le Dr D. Rifkin, New York University Medical Center, NY, États-Unis), ont été analysées par microtomographie (micro-CT) et microscopie électronique à balayage (SEM). En comparaison des témoins, les souris mutantes *Ltbp3*^{-/-} présentent des altérations de l'émail, les anomalies apparaissant dès les premiers stades de formation de la matrice amélaire. Les améloblastes (cellules produisant l'émail) sont particulièrement affectés au stade de la maturation. La minéralisation de l'émail est en conséquence

fortement réduite. La formation des racines des molaires est aussi altérée, avec la formation de masses bulbeuses irrégulières chez les mutants. Comme la signalisation par TGF- β a rôle majeur dans le développement osseux, le squelette crânio-facial est globalement affecté. Ces anomalies miment cliniquement les mutations du gène *LTBP3* produisant des phénotypes d'AI associées à des anomalies osseuses. Ces données ont été publiées dans le journal *European Journal of Oral Sciences*, (IF 1.607) en 2017.

(ii-2) Caractérisation du modèle mutant *Smoc2*^{-/-}. Les patients porteurs de mutations de ce gène, codant pour une protéine de la matrice extra-cellulaire liant le calcium (SMOC2: SPARC-related modular calcium-binding protein 2), présentent une déficience prononcée de la croissance de l'os de la mâchoire et des anomalies dentaires (oligodontie (plus de 6 dents permanentes manquantes), microdontie et/ou dents de forme et taille anormales). Les propriétés fonctionnelles de SMOC2 suggèrent que cette protéine agit comme un signal sécrété, induisant à la fois le développement osseux basal et alvéolaire. Des études récentes démontrent que SMOC2 est présent dans des populations de cellules souches (les cryptes intestinales et les lèvres cervicales des germes dentaires) où elle favorise la prolifération cellulaire et l'angiogenèse.

J'ai effectué des analyses approfondies du phénotype dentaire et crânio-facial des souris mutantes *Smoc2*^{-/-} (produites pour notre équipe de recherche par l'institut clinique de la souris). Afin d'étudier l'origine des anomalies crânio-faciales et dentaires, une étude de lignage cellulaire à l'aide d'un marqueur GFP inséré dans le gène muté est en cours. La mutation de *Smoc2* entraîne un déficit modéré de la croissance squelettique, avec une déficience de la croissance osseuse alvéolaire, ainsi qu'une dysplasie de la dentine. Ces anomalies phénocopient les altérations observées chez les patients. En plus de la microdontie, certaines souris *Smoc2*^{-/-} possèdent une molaire supplémentaire (quatrième molaire), indiquant un défaut de développement évocateur de modifications de la signalisation par la voie *Wnt*.

Pour comprendre l'étiologie et analyser les anomalies crânio-faciales et dentaires, une analyse morphométrique approfondie a été effectuée par la technologie de micro-tomographie (micro-CT), complétée par des analyses

histologiques et en microscopie électronique. Les anomalies de l'expression de gènes chez les souris *Smoc2*^{-/-} ont été explorées par la technique de RNA-seq. Les données obtenues pour les molaires au stade E14.5 révèlent chez le mutant des réductions significatives pour les gènes *Bone gamma-carboxyglutamate protein (Bglap)*, *Dentin matrix acidic phosphoprotein 1 (Dmp1)*, *Odontogenic ameloblast-associated protein (Odam)*, *Secreted frizzled-related protein 4 (Sfrp4)* et *Fgf3*. L'expression anormalement faible de gènes des voies *Wnt* et *NF-κB* pourraient aussi compromettre la formation de l'émail, de la dentine et de l'os alvéolaire. Nous avons donc identifié des cibles potentielles de *Smoc2*. Les données de RNA-seq sur le tissu mandibulaire chez le mutant *Smoc2* au jour E18.5 montrent une diminution de l'expression de gènes comme la *Dentine sialophosphoprotein (Dspp)*, une protéine de la matrice extracellulaire de la dentine impliquée dans la biominéralisation.

Au cours de ce projet, des études ont été publiées indiquant que SMOC2 fait partie du sécrétome de certains cancers. SMOC2 pourrait jouer plusieurs fonctions permettant la prolifération inflammation-dépendante de cancers, par l'intermédiaire de la signalisation *NF-κB*. Il pourrait aussi agir comme un facteur sécrété pro-métastatique, induisant la vascularisation, la prolifération des cellules néoplasiques et la métastase. Plusieurs nouvelles cibles oncogéniques (*Prap1*, *Aqp1* et *Gsdmc*) ont été découvertes dans notre analyse par RNA-seq. Les données suggèrent une fonction dans la régulation de la croissance vasculaire, en induisant localement des signaux pro-mitotiques impliquant la signalisation par la MAP-kinase. SMOC2 aurait donc un rôle crucial pour contrôler la prolifération cellulaire (expliquant les déficits de croissance observés chez les mutants).

En clinique, de nombreux patients ont besoin de traitements par implants pour remplacer des dents manquantes. Un des objectifs de recherche translationnelle serait de fournir une preuve de principe que SMOC2 régule la croissance de l'os alvéolaire, et pourrait améliorer le taux de succès des implants dentaires. Tandis que nos objectifs initiaux étaient d'élaborer des stratégies impliquant l'administration de SMOC2 pour améliorer l'adhésion des implants dentaires chez les patients avec un os alvéolaire déficient, les découvertes récentes sur les rôles pro-oncogéniques de SMOC2 nous ont amené à abandonner cette perspective et à nous concentrer sur le rôle physiologique de cette protéine. Puisque les souris *Smoc2*-nulle montrent des

défauts de la cicatrisation osseuse, lorsque celle-ci est stimulée dans un modèle d'extraction dentaire, une hypothèse formulée est que la signalisation par SMOC2 est impliquée dans les interactions réciproques entre l'épithélium et le mésenchyme de la dent et de son parodonte. Ce modèle serait conforme avec l'observation de niveaux d'expression réduits de *Dmp1* et *Dspp* chez le mutant *Smoc2*, deux facteurs importants pour l'ostéo-intégration et la cicatrisation de l'os alvéolaire. Avec l'aide de collègues de la faculté de chirurgie dentaire et de l'INSERM U_1109, j'ai développé un modèle d'extraction la première molaire de souris, pour analyser le processus de réparation et cicatrisation de l'os alvéolaire. Les données préliminaires montrent que six semaines après l'extraction, les souris *Smoc2*-nulle ne réparent pas correctement l'os alvéolaire, et au contraire présentent une résorption osseuse ectopique (phénomène d'ostéonécrose). Notre hypothèse est que SMOC2 aurait un rôle critique, se manifestant pendant le phénomène de cicatrisation, et peut-être d'autres processus pathologiques comme la fibrose. Les expériences en cours se concentrent sur cette question, en testant par exemple si les souris *Smoc2*-nulle montrent un excès de la fonction des ostéoclastes. Ces données pourront avoir des implications plus larges dans la compréhension de la régénération des tissus et des os.

En conclusion, l'investigation des bases moléculaires et génétiques du développement dentaire et crânio-facial, par des approches de recherche translationnelle, ne contribue pas seulement à la compréhension des anomalies de ce développement, mais permettra aussi de progresser dans la mise au point de traitements appropriés et de stratégies thérapeutiques applicables à la prise en charge de patients atteints de maladies rares.

RÉSULTATS (RESULTS)

(i) Environmental factors

Retinoic Acid Excess Impairs Amelogenesis Inducing Enamel Defects

Morkmued S, Laugel-Haushalter V, Mathieu E, Schuhbaur B, Hemmerlé J, Dollé P, Bloch-Zupan A, Niederreither K.

Front Physiol. 2017 Jan 6;7:673. doi: 10.3389/fphys.2016.00673

L'excès d'acide rétinoïque interfère avec l'amélogénèse provoquant des défauts de formation de l'émail.

Les anomalies de synthèse et sécrétion de protéines matricielles de l'émail, de la minéralisation de cette matrice ou de sa dégradation pendant le développement dentaire sont responsables d'un spectre d'anomalies de l'émail ou amélogénèse imparfaite (AI) rencontrées dans les maladies génétiques ou éventuellement de défauts de l'émail acquis par interaction entre ces processus et l'environnement. Pour évaluer si les facteurs environnementaux / nutritionnels peuvent exacerber les défauts de l'émail, nous avons étudié le rôle de la forme active de la vitamine A, l'acide rétinoïque (AR). Une forte expression des enzymes dégradant l'AR : Cyp26b1 et Cyp26c1 suggère qu'un excès d'AR réduirait la minéralisation des tissus durs, en affectant le développement de l'émail. Nous avons utilisé un protocole où l'AR a été donné à une souris gestante comme complément alimentaire, à une concentration n'augmentant que modérément le taux sérique d'AR. Cette supplémentation a entraîné de graves défauts d'émail observés même à l'âge adulte chez les souris nées de mères traitées, les altérations les plus sévères étant observées pour les traitements par l'AR effectués entre les jours embryonnaires (E) 12,5 à E16,5. Nous avons identifié les protéines de la matrice de l'émail, l'énameline (Enam), l'améloblastine (Ambn) et la protéine associée à l'améloblaste odontogène (Odam) comme étant des gènes cibles affectés par un excès d'AR et présentant des réductions d'ARNm plus de 20 fois supérieures dans les incisives inférieures à E16,5. Les traitements à l'AR ont également affecté la formation des os, en réduisant la minéralisation. Par conséquent, l'ossification crânio-faciale a été considérablement

réduite après 2 jours de traitement (E14.5). Le séquençage massif d'ARN (ARN-seq) a été effectué sur les incisives inférieures E14.5 et E16.5. Une diminution de l'expression de *Runx2* (un régulateur transcriptionnel clé de la différenciation des os et de l'émail) et de ses cibles a été observée à E14.5 dans les embryons exposés à l'AR. L'analyse par ARN-seq a en outre indiqué que les facteurs de croissance osseuse, la matrice extracellulaire et l'homéostasie du calcium étaient perturbés. Les gènes mutés dans l'AI chez l'homme (*ENAM*, *AMBN*, *AMELX*, *AMTN*, *KLK4*) ont vu leur expression réduite à E16.5. Nos observations appuient un modèle dans lequel une signalisation élevée d'AR aux stades fœtaux, affecterait les lignées cellulaires dentaires. Par la suite, la production de protéines de l'émail est altérée, entraînant des altérations permanentes de l'émail.



Retinoic Acid Excess Impairs Amelogenesis Inducing Enamel Defects

Supawich Morkmued^{1,2,3,4,5}, Virginie Laugel-Haushalter^{1,2,3,4}, Eric Mathieu⁶, Brigitte Schuhbauer^{1,2,3,4}, Joseph Hemmerlé⁶, Pascal Dollé^{1,2,3,4}, Agnès Bloch-Zupan^{1,2,3,4,7,8,9,10} and Karen Niederreither^{1,2,3,4,7*}

¹ Developmental Biology and Stem Cells Department, Institute of Genetics and Molecular and Cellular Biology (IGBMC), Illkirch, France, ² Centre National de la Recherche Scientifique, UMR 7104, Illkirch, France, ³ Institut National de la Santé et de la Recherche Médicale, U 964, Illkirch, France, ⁴ Université de Strasbourg, Illkirch, France, ⁵ Pediatrics Department, Faculty of Dentistry, Khon Kaen University, Khon Kaen, Thailand, ⁶ Université de Strasbourg, INSERM UMR_1121, Biomaterials and Bioengineering, Strasbourg, France, ⁷ Faculté de Chirurgie Dentaire, Université de Strasbourg, Strasbourg, France, ⁸ Faculté de Médecine, Fédération de Médecine Translationnelle de Strasbourg, Université de Strasbourg, Strasbourg, France, ⁹ Hôpitaux Universitaires de Strasbourg, Pôle de Médecine et Chirurgie Bucco-Dentaires, Centre de Référence des Manifestations Odontologiques des Maladies Rares, CRMR, Strasbourg, France, ¹⁰ Eastman Dental Institute, University College London, London, UK

OPEN ACCESS

Edited by:

Ophir D. Klein,
University of California, San Francisco,
USA

Reviewed by:

Amel Grilli-Linde,
University of Gothenburg, Sweden
Lucia Jimenez-Rojo,
University of Zurich, Switzerland

*Correspondence:

Karen Niederreither
niederre@igbmc.fr

Specialty section:

This article was submitted to
Craniofacial Biology and Dental
Research,
a section of the journal
Frontiers in Physiology

Received: 08 November 2016

Accepted: 20 December 2016

Published: 06 January 2017

Citation:

Morkmued S, Laugel-Haushalter V,
Mathieu E, Schuhbauer B, Hemmerlé J,
Dollé P, Bloch-Zupan A and
Niederreither K (2017) Retinoic Acid
Excess Impairs Amelogenesis
Inducing Enamel Defects.
Front. Physiol. 7:673.
doi: 10.3389/fphys.2016.00673

Abnormalities of enamel matrix proteins deposition, mineralization, or degradation during tooth development are responsible for a spectrum of either genetic diseases termed *Amelogenesis imperfecta* or acquired enamel defects. To assess if environmental/nutritional factors can exacerbate enamel defects, we investigated the role of the active form of vitamin A, retinoic acid (RA). Robust expression of RA-degrading enzymes *Cyp26b1* and *Cyp26c1* in developing murine teeth suggested RA excess would reduce tooth hard tissue mineralization, adversely affecting enamel. We employed a protocol where RA was supplied to pregnant mice as a food supplement, at a concentration estimated to result in moderate elevations in serum RA levels. This supplementation led to severe enamel defects in adult mice born from pregnant dams, with most severe alterations observed for treatments from embryonic day (E)12.5 to E16.5. We identified the enamel matrix proteins *enamelin* (*Enam*), *ameloblastin* (*Ambn*), and *odontogenic ameloblast-associated protein* (*Odam*) as target genes affected by excess RA, exhibiting mRNA reductions of over 20-fold in lower incisors at E16.5. RA treatments also affected bone formation, reducing mineralization. Accordingly, craniofacial ossification was drastically reduced after 2 days of treatment (E14.5). Massive RNA-sequencing (RNA-seq) was performed on E14.5 and E16.5 lower incisors. Reductions in *Runx2* (a key transcriptional regulator of bone and enamel differentiation) and its targets were observed at E14.5 in RA-exposed embryos. RNA-seq analysis further indicated that bone growth factors, extracellular matrix, and calcium homeostasis were perturbed. Genes mutated in human AI (*ENAM*, *AMBN*, *AMELX*, *AMTN*, *KLK4*) were reduced in expression at E16.5. Our observations support a model in which elevated RA signaling at fetal stages affects dental cell lineages. Thereafter enamel protein production is impaired, leading to permanent enamel alterations.

Keywords: retinoids, tooth, enamel, RNA-seq, mouse models, *enamelin*

INTRODUCTION

Enamel formation is a unique biomineralization process involving a highly organized matrix protein scaffold deposition and degradation, leading to hydroxyapatite crystal nucleation generating a dense and tightly aligned network of hydroxyapatite crystals. Mature enamel is the body's hardest tissue. Ameloblasts are cells of ectodermal origin responsible for enamel development. These cells secrete enamel proteins, which are required for correct mineralization and structural maturation. Enamel proteins self-assemble and provide a matrix organization that aligns the thin ribbons of calcium phosphate deposited during enamel appositional growth. Enamel formation is characterized by inductive, secretory, and maturation stages. During the inductive stage, the inner enamel epithelium begins to differentiate. Then at the secretory stage, polarized differentiated ameloblasts release enamel proteins, contributing to the enamel matrix (Bei, 2009). Finally at the maturation stage, ameloblasts absorb water and organic matrix. This dehydration allows dense crystal deposition. Mature enamel is thus extremely strong, because of the density and fine organization of its crystal layers (Bei, 2009; Simmer et al., 2010).

Amelogenesis imperfecta (AI) refers to a group of rare genetic diseases presenting with defects in enamel formation either as isolated trait, or in association with other symptoms. Patient cases of AI are classified into hypoplastic, hypomineralized, or hypomaturation categories based on enamel quantitative or qualitative defects, i.e., thickness, hardness, and/or color. To date, mutations in over 30 genes are associated with non-syndromic or syndromic AI (Bloch-Zupan et al., 2012). These diseases can be recapitulated in several mouse models. For example, hypoplastic or aplastic enamel deficiencies are produced by *amelogenin* (*Amel*), *ameloblastin* (*Ambn*), and *enamelin* (*Enam*) mutations, recapitulating defects in patients (Gibson et al., 2001; Fukumoto et al., 2004; Masuya et al., 2005; Hu et al., 2008, 2014). Studies in mouse models have contributed to understanding how defective ameloblast protein secretion contributes to these diseases. For a given genetic defect, interfamilial, intrafamilial, and individual intraoral variations in phenotype severity are often seen, suggesting that environmental factors come into play. Indeed, ameloblasts are highly sensitive to their environment (Simmer et al., 2010). Body stressors including high fever (Ryynänen et al., 2014), excess fluoride (Yang et al., 2015), and endocrine disrupters such as bisphenol A disrupt ameloblast function (Jedeon et al., 2014). It is likely that a variety of factors contribute to clinical heterogeneity found in AI and to acquired enamel defects such as molar incisor hypomineralization (MIH) or hypomineralized second primary molars (HSPM; Alaluusua, 2010; Jeremias et al., 2013). Our objective is to discover novel factors initiating and influencing enamel regulatory networks, with the aim of designing new strategies to alleviate dental defects. To further characterize nutritional and environmental factors regulating enamel formation, we have focused on the role of retinoic acid (RA), the main active form of vitamin A that plays key roles during vertebrate development (Niederreither and Dollé, 2008). RA is the ligand for nuclear receptors (RAR α , β , and

γ), which bind as heterodimers with RXRs to DNA regulatory elements termed RA-response elements (RAREs, Rochette-Egly and Germain, 2009). Through this mechanism, RA regulates expression of various target genes (Balmer and Blomhoff, 2002). RA distribution within embryonic tissues is tightly controlled through an interplay between enzymes involved in its synthesis (mainly retinol dehydrogenase 10 and retinaldehyde dehydrogenases [Raldh]1, 2, and 3) and catabolism (Cyp26A1, B1, and C1). As both RA deficiency and excess results in diverse developmental defects, the distribution of active retinoid signaling requires tight regulation to limit potent adverse effects (Rhinn and Dollé, 2012).

Expression of RA receptors, synthesizing, and catabolizing enzymes has been detected in the developing teeth (Bloch-Zupan et al., 1994; Berkovitz et al., 2001; Cammas et al., 2007). Severe dietary vitamin A deficiency in rats leads to hypoplastic enamel, enamel organ metaplasia, dentine dysplasia, and delayed tooth eruption (Mellanby, 1941; Punyasingh et al., 1984; McDowell et al., 1987). Hypervitaminosis A during rodent pregnancy induces exencephaly and craniofacial malformations, along with tooth fusions and supernumerary incisors (Knudsen, 1967 and references therein). These effects may reveal an evolutionary role of RA signaling in the posterior pharyngeal region controlling tooth number (Seritrakul et al., 2012). In culture, RA excess can retard molar growth (Mark et al., 1992), reduce ameloblast differentiation (Kronmiller et al., 1992), and diminish tooth alkaline phosphatase production (Jones et al., 2008). Retinoids may also regulate incisor cervical loop maturation, increasing mitosis and laminin gene expression (Bloch-Zupan et al., 1994).

In vivo models to substantiate RA actions in tooth development are lacking. Interestingly, though, *Cyp26b1* knockout mice show a defect in maxillary bone compaction around upper incisors (Maclean et al., 2009). Observing that the fetal tooth has robust expression of *Cyp26b1* and *Cyp26c1* RA-degrading enzymes, we hypothesized that *in vivo*, conditions of RA excess may have adverse effects on osteoblast and ameloblast growth regulatory networks. We report that mice born from dams exposed to RA during mid-late pregnancy using a food-based supplementation suffer adult-stage enamel hypoplasia. Effects were strongest when treatments began at the tooth dental lamina-placode stage (E12.5), and continued until early bell developmental stages. Reductions of *Enam*, *Ambn*, and *Odam* mRNA expression in E16.5 lower incisors were observed. High throughput RNA sequencing (RNA-seq) analysis of lower incisors revealed that RA excess perturbs neural crest lineage determinants and pro-ossification growth factor and transcription networks. Combinatorial changes in collagen, extracellular matrix, and calcium homeostasis genes occur at E14.5, followed by a decrease at E16.5 of transcripts encoding pre-ameloblast secretory-stage proteins. These alterations in gene expression are observed several days before the ameloblast lineage begins to differentiate. Retinoid excess targets fetal odontoblasts, along with a range of epithelial enamel protein targets. Our data provides potential avenues through which environmental and nutritional changes may alter the penetrance and expressivity of human enamel defects such as AI or MIH.

MATERIALS AND METHODS

Ethics Statement

All animals were maintained and manipulated under animal protocols in agreement with the French Ministry of Agriculture guidelines for use of laboratory animals (IGBMC protocol 2012–097) and with NIH guidelines, provided in the Guide for the Care and Use of Laboratory Animals. CD1 mice were purchased from Charles River, France. All-*trans*-RA (Sigma) suspended in ethanol (5 mg/mL) was mixed into 50 mL water and 50 g powdered food to a final concentration of 0.4 mg/g food. The RA-containing food mixture (protected from light) was left in the cage for the mice to feed *ad libitum* and changed every day. Control groups consisted of CD1 mice given a matching food treatment, but with no added RA. Equal numbers of RA-treated samples vs. controls were randomly assigned to treatment or control groups.

In situ Hybridization, Beta-Galactosidase (X-gal) Staining, and Skeletal Analysis

In situ hybridization was performed using digoxigenin-labeled RNA probes on 200 μ M vibratome sections of paraformaldehyde-fixed embryos, which were processed using an Intavis InSituPro robot, as described in detail on the website <http://empress.har.mrc.ac.uk/browser/> (Gene Expression section). To analyze patterns of RA-response, we used the *RARE-hsp68-lacZ* reporter transgenic line (Rossant et al., 1991). At least 20 randomized fetal samples from control and matching RA-treated samples were used to test each probe. All expression studies were confirmed in at least 3 independent experiments. X-gal assays were performed on 200 μ m vibratome sections. Whole-mount fetal alizarin red/alcian blue staining was carried out as described in <http://empress.har.mrc.ac.uk/browser/> (Bone, Cartilage, Arthritis, Osteoporosis section).

Real-Time Quantitative RT-PCR

RT-PCR assays were performed in duplicate on 3 RNA samples for control or RA-treated incisors dissected at E14.5 and E16.5. Total RNA (1 μ g) was subjected to real-time RT-PCR using SYBR Green Reagents (Qiagen). RNA was extracted using the RNeasy Micro-kit. Oligo-dT primed cDNAs were generated using the Superscript II kit (Invitrogen). The incorporation of SYBR Green into the PCR products was monitored in real-time with a Roche 480 LightCycler. Sequences of primers are given in supplemental Table S1. Target genes were normalized relative to the glyceraldehyde-3-phosphate dehydrogenase (*Gapdh*) housekeeping gene.

X-Ray Microtomography

Seven week-old mice were analyzed by X-ray micro-computed tomography (micro-CT) using a Quantum FX micro-CT *in vivo* Imaging System (Caliper Life Sciences), which operates at 80 kV and 160 μ A, with high-resolution at 10–80 μ m pixel size, to assay skull and tooth morphology. Data reconstructions were performed with the Analyze software (v 11.0; Biomedical Imaging Resource, Mayo Clinic, Rochester, MN).

Scanning Electron Microscopy

The lower incisors of 7 week-old control and RA-treated mice were dissected out of the alveolar bone, rinsed, dehydrated in a graded series of ethanol, and then transferred in a propylene oxide/epon resin (v/v) solution. After embedding the teeth in Epon 812 (Euromedex, Souffelweyersheim, France), they were sectioned sagittally and polished with diamond pastes (Escil, Chassieu, France). The embedded half incisors were etched with a 20% (m/v) citric acid solution for 2 min, rinsed with distilled water, dehydrated in a graded series of ethanol and dried at room temperature. The samples were then coated with a gold-palladium alloy using a HUMMER JR sputtering device (Technics, CA, USA) before performing scanning electron microscopy with a Quanta 250 ESEM (FEI Company, Eindhoven, The Netherlands) with an accelerating voltage of the electrons of 5 kV.

RNA Sequencing

Total RNA was extracted in quadruplicate from lower incisors at E14.5 and 16.5 (2 days or 4 days after RA treatment) and respective controls. The mRNA-seq libraries were prepared as detailed in the Illumina protocol (supplemental Experimental Procedures). Sequence reads mapped to the mouse reference genome mm10/NCBI37 using Tophat. Only uniquely aligned reads were retained for further analysis. Quantification of gene expression was performed with HTSeq-0.6.1. (see <http://www-huber.embl.de/users/anders/HTSeq/doc/overview.html>). For each transcript the resulting reads per kilobase of exon model per million mapped reads (RPKM) were converted to raw read counts, which were then added for each gene locus. Data normalization was performed as described (Anders and Huber, 2010) and resolved using the DESeq Bioconductor package. Resulting *p*-values were adjusted for multiple testing, according to Benjamini and Hochberg (1995). Regulated transcripts with an RPKM of >2, an adjusted *p* < 0.050, and a log₂ fold change of >0.3 and < –0.3 at E14.5 and >0.5 and < –0.5 at E16.5 were considered.

RESULTS

To analyze RA-dependent tooth alterations, we employed a protocol where RA added to the food supply was administered to pregnant CD1 mice (Niederreither et al., 2002), at a concentration of 0.4 mg/g food beginning at E12.5 or later. The treatment period began after craniofacial neural crest migration into the head was complete (Minoux and Rijli, 2010), avoiding earlier stage lethality due to exencephaly. In another study, HPLC analysis carried out after similar RA treatment at 0.1 mg/g food showed that serum RA levels were moderately increased (~20%) compared with untreated controls (Mic et al., 2003). Treated dams bore litters with 50% lethality, typically with 5–7 pups. Incisors in both groups erupted at the same age. Once the pups reached adulthood (4–7 weeks-old), we compared 100 randomized control and RA-treated groups macroscopically for dental defects. The labial side of rodent incisor (analog of the crown and covered with enamel) normally has a yellow/orange pigmentation, due to iron present at a net weight of about

0.03% in enamel (Pindborg, 1953). It gives mouse teeth a characteristic color, which is a dark orange in the upper incisors (**Figures 1A,E**). When RA treatments were performed from E12.5 to 16.5, they were found to produce a chalky lightening and length reduction of incisors, changes more pronounced in lower incisors (**Figures 1B,F**). The whiter color and less shiny surface may reflect reduced enamel thickness typical of mouse enamel hypoplasia models (Gibson et al., 2001; Masuya et al., 2005; Hu et al., 2014). Treatments performed at later stages (E13.5–16.5: **Figures 1C,G**, or E14.5–17.5: **Figures 1D,H**) had less severe effects on enamel, suggesting RA has early roles in the oral epithelium starting at the placode stage of tooth initiation.

Samples shown in **Figures 1A,E** (WT) and **B,F** (RA-treated) were analyzed by X-ray micro-computed tomography (micro-CT). This analysis confirmed lower incisor shortening (**Figures 2A,B**; Figure S1). Optical sections revealed a reduction in enamel mineral density and thickness (molars in **Figures 2C,E**; incisors in **Figures 2D,F**). Alveolar bone at the level of the molars showed greater porosity in the RA-treated animals (boxes in **Figures 2C,E**; Figure S2). Although retinoid gradients shape pharyngeal tooth evolution (Seritrakul et al., 2012), our micro-CT analysis revealed normal molar eruption and cusp morphology (Figure S3), as predicted because RA treatments

are initiated at E12.5, after neural crest has completed its migration into the jaw. This analysis also revealed no evident signs of dental attrition from both groups. **Figure 2G** shows scanning electron micrographs (SEM) of enamel prisms of control lower incisor, exhibiting a well-organized decussating pattern. This was disrupted following RA treatment. The most outer enamel was less mineralized when compared with the control tooth, as outer enamel appeared darker in RA-treated animals. Enamel rods of RA-supplemented animals were less densely packed, and as a consequence, areas normally filled with interprismatic enamel seemed empty and showed holes-like pattern (**Figure 2H**), similar to *Enam* haploinsufficient mice (Hu et al., 2014).

Histological analysis of 1-week old mice after hematoxylin-eosin staining confirmed that RA treatments produced a shorter, smaller, and disorganized layer of ameloblasts in both molars (**Figures 3A,B**) and incisors (**Figures 3C–H**). This was clearly seen in the secretory zone, where ameloblasts displayed disrupted epithelial sheet organization (**Figure 3H**). In all treated samples, ameloblast adhesion to enamel was impaired (**Figures 3B,D,G,H**). This was first seen histologically as a detachment of the basement membrane, likely causing preameloblast separation from forming odontoblasts (**Figure 3G**, red arrowhead). Non-cellular

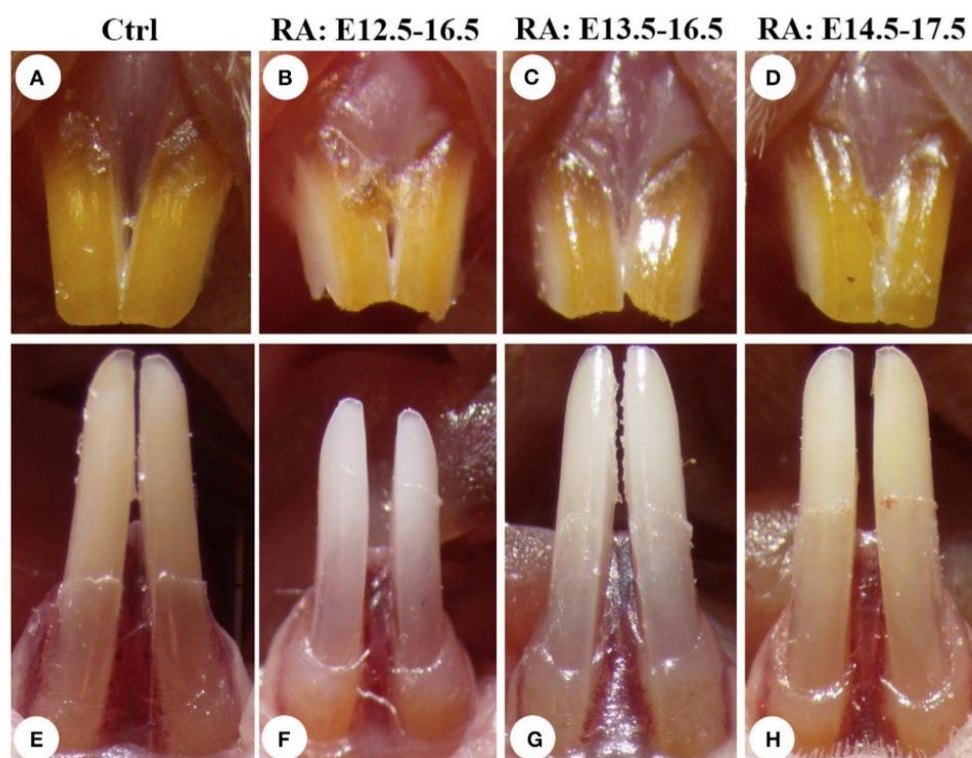
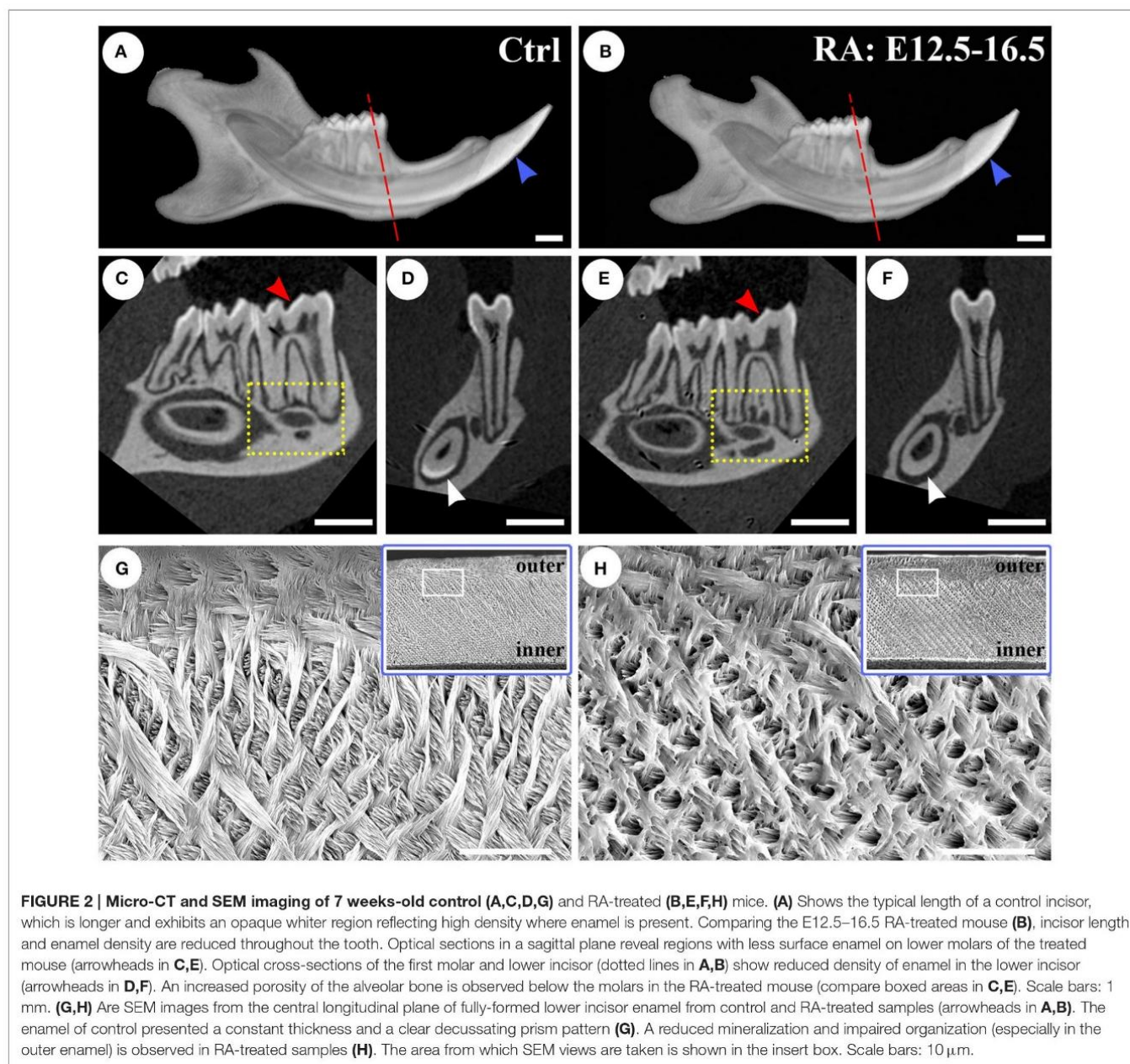


FIGURE 1 | RA excess during pregnancy produces stage-specific whitening and size reductions of mouse incisors. Enamel of the upper (**A**) and lower (**E**) incisors of 7 weeks-old CD1 control (non-RA treated) mice has a characteristic yellow/orange color, which is consistently darker in the upper incisor. Retinoic acid treatment from E12.5 to 16.5 reduces incisor length (by ~20%) and lightens enamel color (**B,F**), suggesting reduced iron accumulation typical of murine models of hypoplastic enamel formation. When RA treatment begins at E13.5 (**C,G**) or E14.5 (**D,H**), incisor length reductions and lightening of incisor color are progressively less severe.

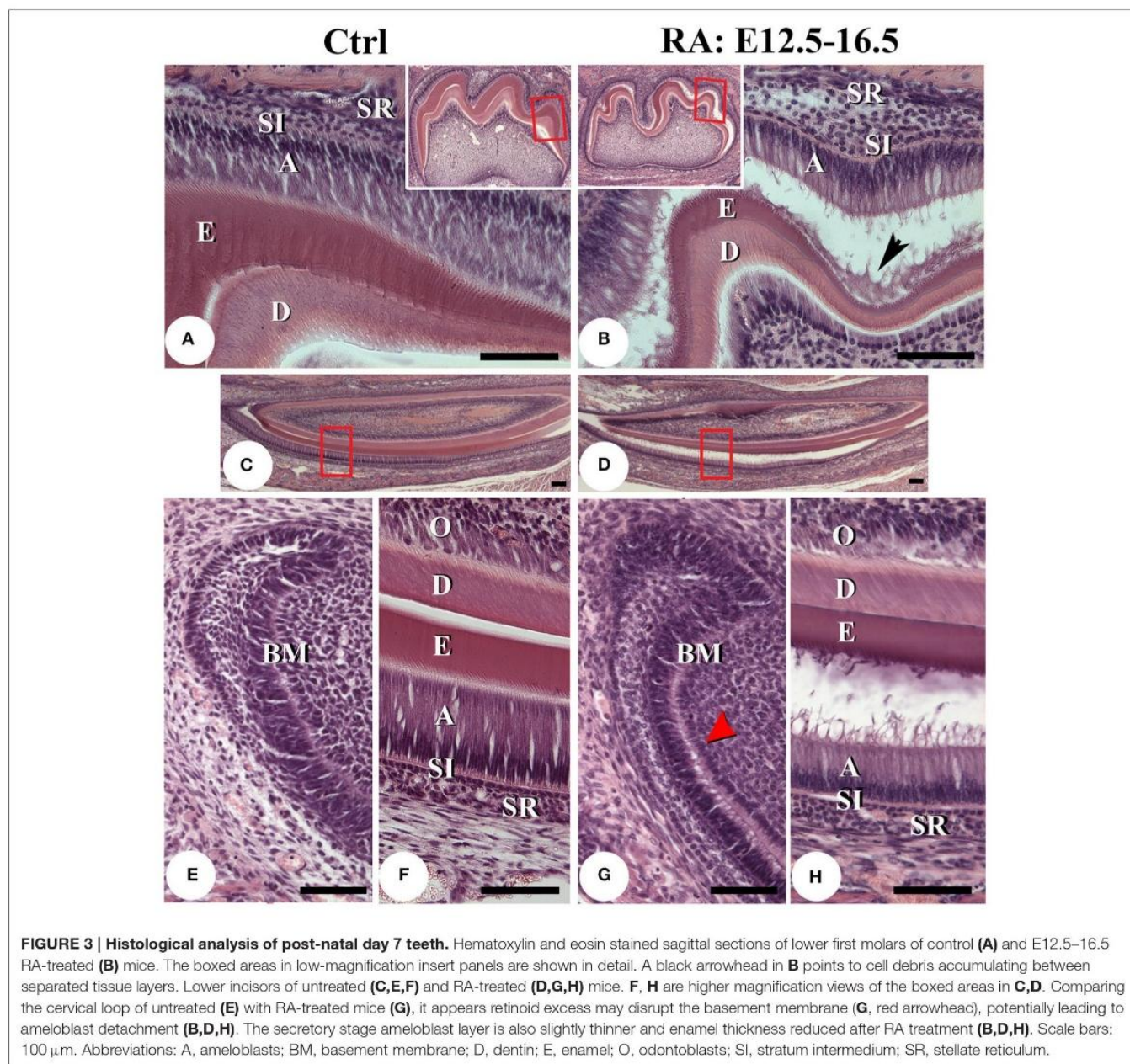


organic material was present between layers (**Figure 3B**, black arrowhead). The lower incisor secretory zone enamel layer was slightly thinner (**Figure 3H**), suggesting RA treatment delayed enamel maturation and/or reduced overall mineralization.

Enamel matrix proteins are secreted by ameloblasts and form a matrix directing enamel mineral deposition. Among these proteins, amelogenin is the most abundant (Eastoe, 1979). Enamel fails to form or is hypoplastic in amelogenin-deficient mice (Gibson et al., 2001), and in *Enam*- or *Ambn*-null mutant mice (Fukumoto et al., 2004; Masuya et al., 2005; Hu et al., 2014). Our real-time RT-PCR analysis of E16.5 lower incisors following E12.5–16.5 RA treatment

revealed up to 20-fold reductions in *Enam*, *Ambn*, and *Odam* mRNAs (**Figure 4**). Notably, no RA-induced alterations in *Enam*, *Ambn*, or *Odam* were observed at E14.5 (data not shown).

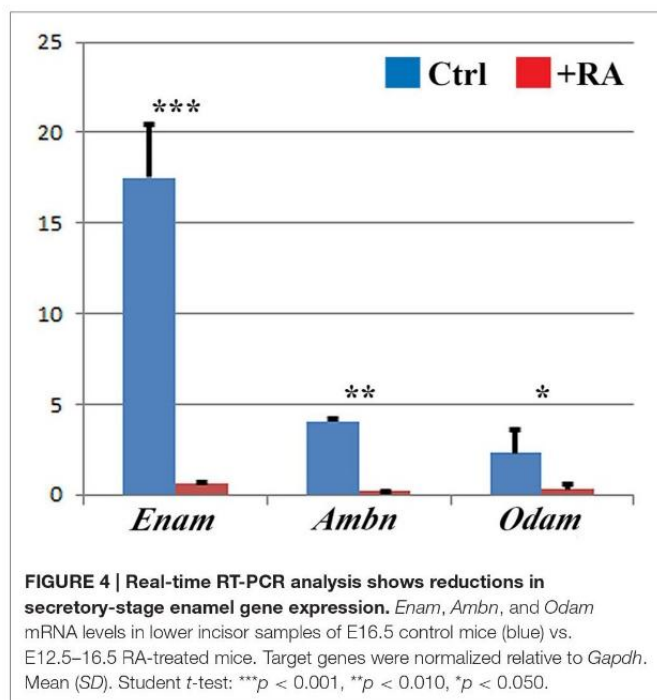
To assess if reduced enamel protein expression was linked to ectopic activation of RA signaling, we used RARE-hsp68-*lacZ* transgenic mice as a reporter for RA activity (Rossant et al., 1991). No expression was seen in the tooth germ areas at E13.5 (data not shown), although activity was found in the mandible next to the tooth germs at E14.5 (**Figures 5A,B**). This retinoid reporter transgene exhibited low level of expression in both mandible and maxilla adjacent to the growing incisors and molars in E16.5 untreated fetuses (**Figure 5C** and data not shown). In E16.5



fetuses following RA treatment from E12.5 to 16.5, domains of *RARE-lacZ* activity broadly extended into alveolar bone and surrounding mesenchyme, but appeared absent from enamel organ and dental ectomesenchyme (Figure 5D and data not shown). Note that very low levels of RA signaling may not be detected by such a reporter transgene. Proper control of RA levels is necessary for early neural crest patterning, but RA deficiency does not alter first branchial arch formation (Niederreither et al., 2000). To explore why RA activity was absent from most tissues of the tooth buds, we examined expression of CYP26 family cytochrome P450 enzymes specifically involved in RA catabolism. At E13.5, *Cyp26b1* expression (Figure 5E) was found to be prominent in mesenchyme surrounding the

forming incisors. At E14.5, *Cyp26c1* (Figure 5F) was prominently expressed in the enamel organ, whereas a low amount of *Cyp26a1* transcripts was seen in the dental papilla (Figure 5F, insert).

Excesses of vitamin A or RA lead to skeletal fragility by reducing bone formation and by stimulating bone-resorbing osteoclasts (Henning et al., 2015). In the *Cyp26b1* mutant, impaired RA catabolism causes long-bone fusions and induces premature osteoblast differentiation into mineralizing osteocytes, truncating bone development in the craniofacial region (Maclean et al., 2009). Alizarin red/alcian blue staining of E14.5 skulls 2 days into RA regime revealed shortened mandibles, and truncated regions of ossified maxilla and premaxilla in the



RA-treated animals (Figures 6A,B). The skull frontal plate was also smaller in treated animals, with less ossification. Malformed Meckel's cartilage and truncated mandibles could lead to incisor shortenings. Skeletal staining performed at E15.5 confirmed RA-reduced mineralization (Figures 6C,D). RT-PCR analysis showed reductions in *Runx2* mRNA in both lower incisor and adjacent alveolar bone at E14.5 in RA-treated animals (Figures 6E,F). A 3-fold reduction in the expression of this key target might account for reduced bone mineral deposition (Ducy and Karsenty, 1998), and its mesenchymal localization (Figure 6G) implies indirect enamel effects. To exclude systemic non-specific RA effects, we cultured isolated lower incisors or lower incisors with adjacent alveolar bone from E13.5 embryos (Figure S4). When 10^{-8} M RA was added to culture medium, *Enam* levels were dramatically reduced in isolated incisor cultures, indicating RA acted directly on tooth.

To compare global gene expression changes in control vs. RA-treated samples, E14.5 and E16.5 lower incisors were analyzed by high throughput RNA sequencing (RNA-seq). Principal component analysis (PCA plot, Figure S5) and scatter plots (Figure S6) revealed the overall changes observed at E14.5 were tightly clustered, statistically significant, yet often seen as net reductions of ~20–50% (Table 1). RNA-seq analysis confirmed broad effects of RA treatment affecting mineralization-inducing pathways, extracellular collagens, and calcium networks. Genes reduced in expression at E14.5 included *Runx*, *Dlx*, *Bmp*, and *Shh*, all known inducers of inner enamel epithelium differentiation (Bei, 2009). Net reduction in *Runx2* and *Dlx5* (Table 1) may act combinatorially to reduce the bone biomarker BGLAP (osteocalcin, (Hassan et al., 2004)), a target reduced by ~2-fold at E16.5 in RA-treated samples

(Table 2). A novel RA-inhibited target is the matricellular protein *Smoc2*, whose mutation in human produces oligodontia, microdontia, abnormal root development, dentin dysplasia, and reduced alveolar bone growth (Bloch-Zupan et al., 2011). Retinoids are known to drive uncommitted progenitor cells into neuronal lineages (Maden, 2007). Consistently, DAVID (Database for Annotation, Visualization, and Integrated Discovery) analysis revealed a functional enrichment score of 1.4×10^{-6} for neuronal differentiation pathways. Increased *Neurogenin1* (*Neurog1*), *Neurogenin2* (*Neurog2*), and the notch target *Hes5*, are typical of an RA-induced neuronal differentiation profile (Table S2). At E16.5, *Enam* was the most reduced target (Table 2), also markedly reduced by *in situ* hybridization analysis (Figure S7). Reductions in *ameloblastin*, *X-linked amelogenin*, *amelotin*, and *kallikrein-related peptidase 4* (*Klk4*), all encoding enamel proteins (Núñez et al., 2015), were observed (Table 2). Notably, these reductions at E16.5 occur much earlier than the characterized times of action of the corresponding proteins in inductive, secretory, or maturation stages of rodent enamel development. Odontoblast-originating signals control ameloblast induction (Bei, 2009). Reductions in mineralization targets (*alkaline phosphatase*), odontoblast structural proteins (*dentin matrix protein 1*, *dentin sialophosphoprotein*), ossification biomarkers (*Bglap1/osteocalcin*, *Bglap2*), and calcium homeostasis pathways (*calcitonin*, *vitamin D receptor*) were all observed in E16.5 RA-treated samples. Table S3 summarizes how RA excess at E16.5 increases the expression of genes involved in retinoid signaling (including *Cyp26b1*), Wnt signaling, and neuronal differentiation.

DISCUSSION

RA Excess Affects Enamel Matrix Protein Expression Prior to Ameloblast Differentiation

AI refers to rare, inherited diseases characterized by a defect in enamel formation with clinical heterogeneity even within the same family (Bloch-Zupan et al., 2012). These variations, also observed in acquired enamel defects, have been proposed to be due to environmental excess in fluoride (Yang et al., 2015), or to other nutritional, environmental, or behavioral changes (Li et al., 2013), along with genetic makeup of an individual. Retinoids are regulators of skeletal growth and patterning, known to lead to skeletal fragility when given in excess (Henning et al., 2015). Since reciprocal interactions between enamel organ and ectomesenchyme are necessary for alveolar bone, periodontal, and tooth differentiation, we examined if nutritional RA excess could have additional effects on developing teeth. Prior to this study, little was known about *in vivo* effects of RA on enamel cytodifferentiation. Here we find that RA treatment at a defined window of murine development resulted in permanent defects resembling human AI. Ameloblast differentiation begins at the advanced bell stage (~E18.5 in mouse), when the inner enamel epithelial originating cells express enamel secretory proteins and follow

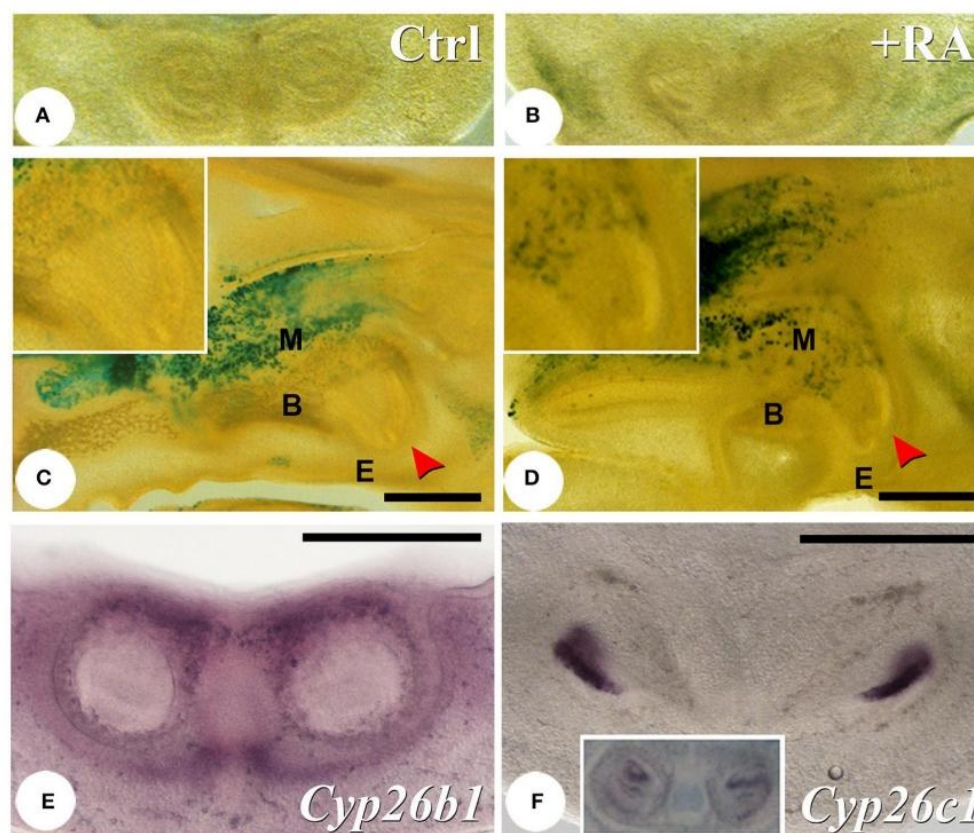


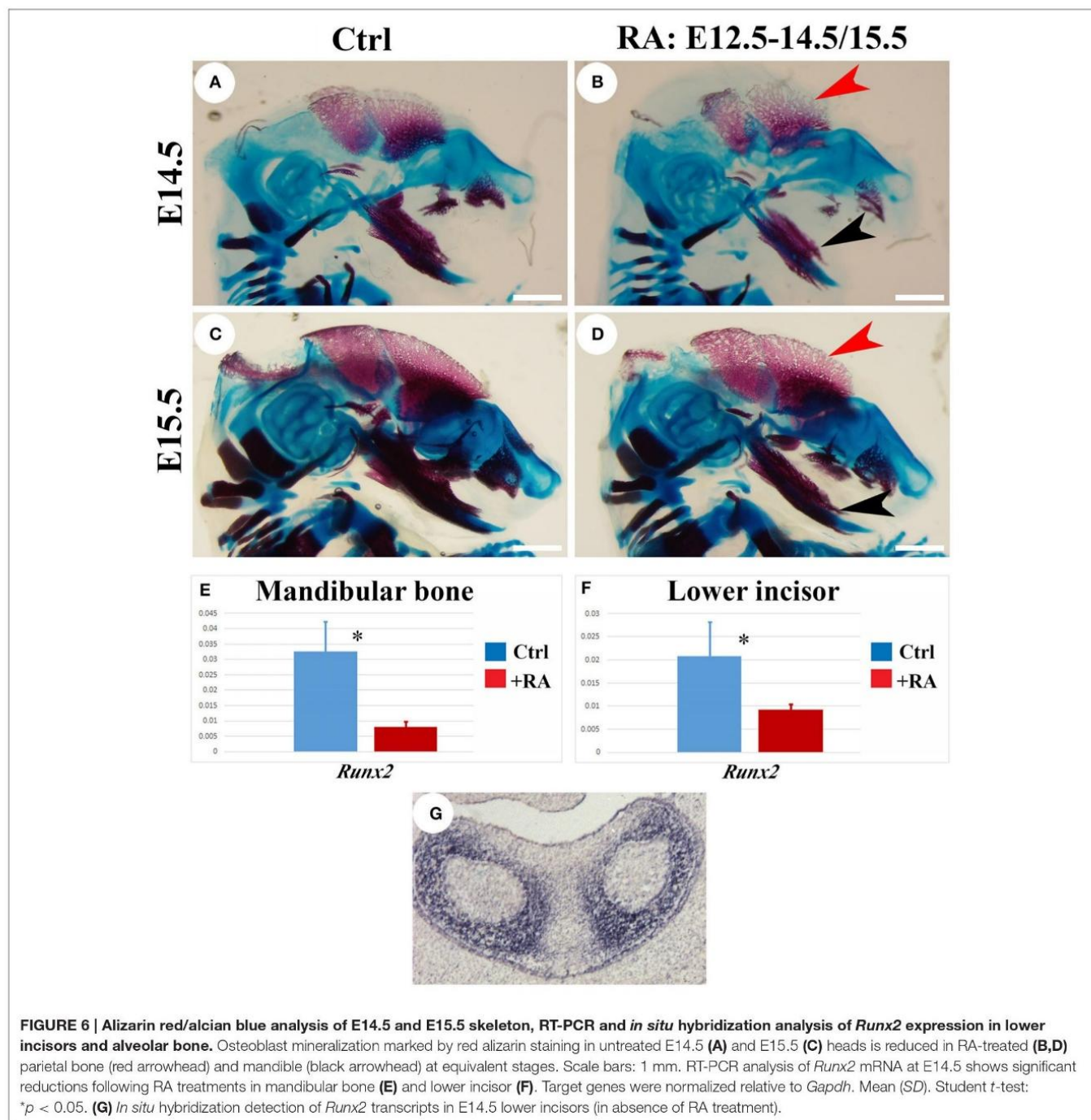
FIGURE 5 | Regions of RA activity and expression of RA-catabolizing enzymes in the developing teeth. X-gal analysis of RARE-hsp68-lacZ reporter transgene activation in E14.5 (A,B) and E16.5 (C,D) untreated and RA-treated (E12.5–16.5) mice. At E14.5 in untreated mice, transgene activity can be observed surrounding the tooth germ, and this activity is increased in treated mice. At E16.5, X-gal activity is detected in alveolar bone adjacent to upper (C,D) and lower (data not shown) incisors (arrowhead). After RA treatment, reporter activity is increased in alveolar bone, but is never seen in developing teeth (compare high magnification insert panels in C,D). At E13.5, *Cyp26b1* is expressed in mesenchyme surrounding the lower incisors (E). At E14.5 a pronounced expression of *Cyp26c1* is seen in the enamel organ (F), whereas *Cyp26a1* is expressed in the dental papilla epithelium (F, insert). Scale bars: 500 μ m. Abbreviations: B, bone; E, epithelium; M, mesenchyme.

by processing enzymes (Bei, 2009; Bloch-Zupan et al., 2012). Assuming normal rodent nocturnal feed, in our experimental protocol RA exposure would begin at the bud stage of tooth formation (E13.0). We observed that at E14.5, RA excess impairs expression of *Runx*, *Dlx*, bone morphogenetic proteins, while levels of enamel secretory proteins are not altered in either our RNA-seq analysis or RT-PCR analysis at these same stages (data not shown). RA excess changes likely occur prior to ameloblast differentiation, with molecular alterations indicating effects on pro-mineralization signaling.

Retinoids Have Early Targets in Mineralized Tissue, and Later Effects on Enamel Proteins

Enamel-reducing effects of RA supplementation at E13–14.5 coincide with the initial stages of intramembraneous ossification. An early target is *Runx2*, a master regulator of skeletal mineralization. *Runx2*^{-/-} mouse mutants have a block in endochondral and intramembraneous osteoblast maturation,

and site-specific reductions in collagen type I and alkaline phosphatase expression (Ducy and Karsenty, 1998). *Runx2*^{-/-} mutants lack differentiated odontoblast and ameloblast matrices, indicative of late bell-stage defects (D'Souza et al., 1999; Bronckers et al., 2001). We observe RA-dependent *Runx2* reductions at E14.5 bud stage incisors, but not at E16.5, suggesting earlier effects. Cleidocranial dysplasia, an autosomal dominant condition caused by mutations of *RUNX2*, likewise results in insufficient dentin and enamel mineralization (Xuan et al., 2010) and other dental anomalies (Camilleri and McDonald, 2006). Terminal ameloblast differentiation requires odontoblast-originating signals and matrix components (Balic and Thesleff, 2015). Reports of evolutionarily conserved *Runx2*-binding sites in *Enam*, *Ambn*, and *Odam* gene promoters Dhamija and Krebsbach, 2001; Lee et al., 2010, suggested a model of RA-inhibitory effects (Figure 7). Retinoid excess at E14.5 would induce relatively small, yet combined reductions in *Runx2/3*, *Dlx3/5*, and *Bmp2/3*, predominantly mesenchymal targets that surround the bud stage tooth (Figure S8). By E16.5 these factors collectively regulate early epithelial (enamel



organ) expression of *Enam*, *Ambn*, and *Amelx*. This is plausible because these enamel targets possess evolutionarily conserved binding site-motifs in their proximal promoters (Loots et al., 2002; Cartharius et al., 2005; Figure 7C; Table S4). While the bell stage tooth reacts to the high retinoid environment by up-regulating *Cyp26b1* levels (Table S3), this change is insufficient to offset strong reductions in enamel matrix protein secretion, which then induce ameloblast differentiation defects.

Many Enamel Targets Are in the Secretory Phosphoprotein-Encoding (SCPP) Gene Cluster

Our RNA-seq analysis on the whole lower incisors uncovered many genes significantly reduced at E16.5 that regulate ameloblast differentiation, enamel formation, and dentin/bone development (Table 2). Hence combinatorial deficits in enamel secretory protein expression included reductions in X-linked amelogenin (*AMELX*, OMIM: 300391) (Gibson et al., 2001;

TABLE 1 | Genes encoding regulators of bone growth, collagens, and proteins involved in calcium signaling and homeostasis, retinoid, and Shh pathways, reduced in expression in E14.5 RA-treated lower incisors.

Symbol	Name	FC log2	p-value
BONE/OSTEOBLAST GROWTH			
Bmp2	Bone morphogenetic protein 2	-0.35	1.08 E-02
Bmp3	Bone morphogenetic protein 3	-0.33	1.93 E-02
Bmp5	Bone morphogenetic protein 5	-0.43	1.72 E-02
Ostn	Osteocrin	-1.30	8,96 E-05
Sp7	Sp7 transcription factor 7	-0.80	2,62 E-05
Smoc2	SPARC modular calcium binding 2	-0.73	1,74 E-08
Runx2	Runt related transcription factor 2	-0.38	2.98 E-02
Runx3	Runt related transcription factor 3	-0.62	7.01 E-06
Dlx5	Distal-less homeobox 5	-0.58	1.64 E-03
Dlx3	Distal-less homeobox 3	-0.53	8.37 E-03
Mef2c	Myocyte enhancer factor 2C	-0.58	6.33 E-05
Ltbp2	Latent transforming growth factor β binding protein 2	-0.86	1.98 E-06
Fgf10	Fibroblast growth factor 10	-0.42	4.17 E-04
Fam20a	Family with sequence similarity 20A	-0.64	2.71 E-04
Tnn	Tenascin N	-1.18	2.01 E-10
Sox6	SRY (sex determining region Y)-box 6	-0.41	1.20 E-02
Tgfb3	Transforming growth factor β 3	-0.31	1.45 E-04
COLLAGEN			
Col1a1	Collagen, type I, α 1	-0.61	6.25 E-03
Col1a2	Collagen, type I, α 2	-0.43	3.62 E-02
Col5a1	Collagen, type V, α 1	-0.37	1,39 E-04
Col6a3	Collagen, type VI, α 3	-0.42	8.34 E-05
Col8a1	Collagen, type VIII, α 1	-0.79	3.74 E-04
Col8a2	Collagen, type VIII, α 2	-0.53	1.25 E-04
Col12a1	Collagen, type XII, α 1	-0.63	1.43 E-04
CALCIUM SIGNALING AND HOMEOSTASIS			
Capn3	Calpain 3	-1.03	1.78 E-03
Otof	Otoferlin	-0.82	3.68 E-03
Kcnma1	Potassium calcium-activated channel M α 1	-0.54	8.47 E-03
Cacna2d2	Calcium channel, voltage dependent, α 2/ β 2	-0.48	2.26 E-03
RETINOID SIGNALING			
Aldh1a1	Retinaldehyde dehydrogenase 1	-0.80	1.22 E-02
Aldh1a3	Retinaldehyde dehydrogenase 3	-0.69	2.70 E-03
Rbp2	Retinol binding protein 2	-0.86	4.68 E-02
Cyp26c1	Cytochrome P450 26c1	-0.29	3.77 E-01
SHH SIGNALING			
Ihh	Indian hedgehog	-1.40	1.84 E-06
Hhip	Hedgehog-interacting protein	-0.65	1.64 E-05
Ptch1	Patched 1	-0.42	3.04 E-02

Data are presented as log₂ fold changes in RA-treated vs. control samples; for instance, a FC log₂ value of -1.00 will correspond to a 50% mRNA level in the RA-treated samples.

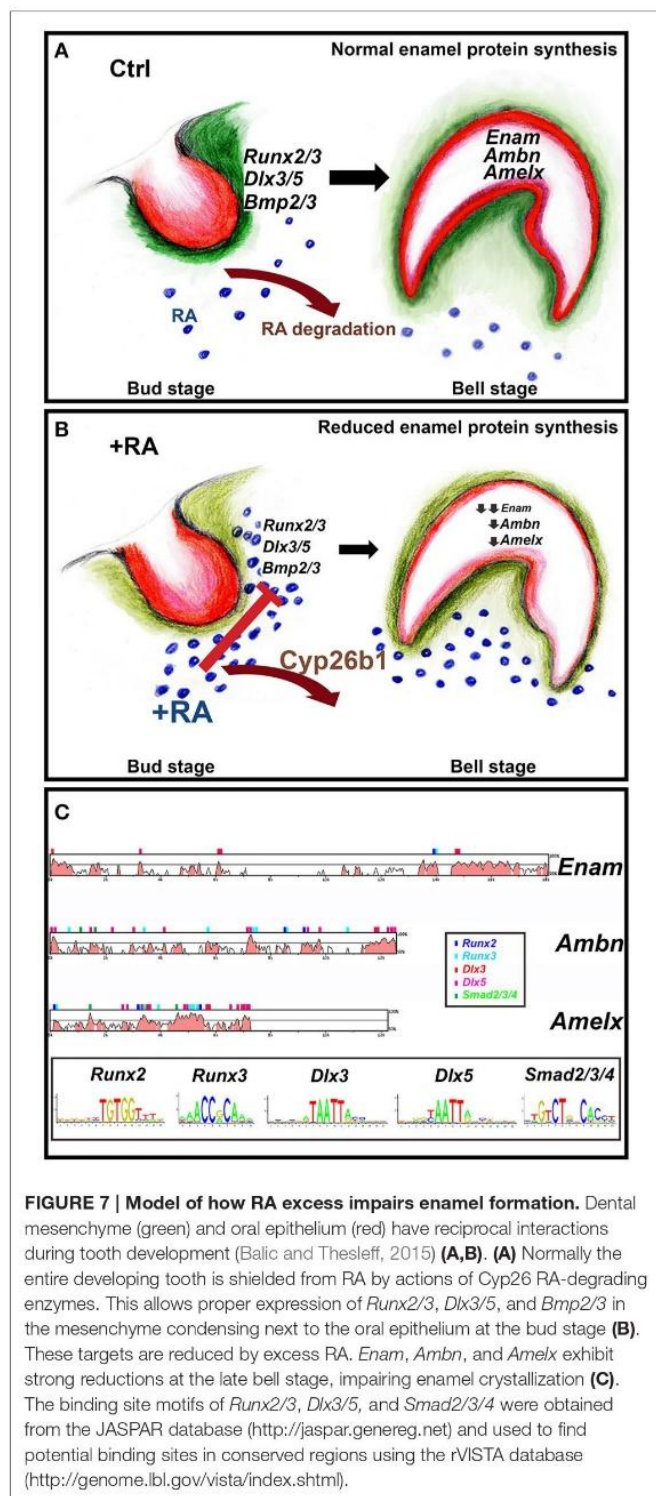
Barron et al., 2010), *AMBN* (OMIM: 601259) (Fukumoto et al., 2004), *AMTN* (OMIM: 610912) (Nakayama et al., 2015), along with *Odam* (OMIM: 614843). These genes belong to the evolutionarily-related *SCPP* gene cluster, a linked group of genes also containing members regulating skeletal mineralization (Kawasaki and Weiss, 2008). These *SCPP* enamel proteins contain structural domains promoting calcium sequestration and

TABLE 2 | Summary of genes encoding enamel proteins, extracellular matrix components, proteins involved in bone growth pathways, or calcium and iron signaling/homeostasis, all reduced in expression according to RNA-seq analysis of E16.5 RA-treated lower incisors.

Symbol	Name	FC log2	p-value
ENAMEL MATRIX PROTEINS			
Enam	Enamelin	-3.47	4.99 E-013
Amtn	Amelotin	-1.85	1.53 E-004
Amelx	Amelogenin, X-linked	-1.7	1.01 E-004
Ambn	Ameloblastin	-1.42	1.78 E-003
ENAMEL MODIFICATION			
Klk4	Kallikrein peptidase 4	-1.62	1.14 E-003
Ppara	Peroxisome proliferator activated receptor α	-0.74	1.55 E-002
Fam20c	Family with sequence similarity 20, C	-0.66	7.31 E-003
BONE GROWTH FACTOR PATHWAYS			
Bglap	Bone gamma carboxyglutamate protein	-1.67	6.06 E-004
Bglap2	Bone gamma-carboxyglutamate protein 2	-1.15	2.41 E-002
Comp	Cartilage oligomeric matrix protein	-2.89	3.00 E-013
Phex	Phosphate endopeptidase X-linked	-1.01	4.10 E-002
Alpl	Alkaline phosphatase	-0.94	5.79 E-006
Col11a1	Collagen, type XI, α 1	-1.16	4.60 E-006
Col11a2	Collagen, type XI, α 2	-1.4	5.72 E-004
Col13a1	Collagen, type XIII, α 1	-1.34	7.25 E-008
EXTRACELLULAR MATRIX			
Dmp1	Dentin matrix protein 1	-0.94	7.47 E-002
Dspp	Dentin sialophosphoprotein	-0.85	9.79 E-002
Postn	Periostin	-0.56	1.39 E-004
CALCIUM SIGNALING AND HOMEOSTASIS			
Camk2a	Calcium/calmodulin protein kinase II α	-1.31	4.72 E-005
Camk2b	Calcium/calmodulin protein kinase II β	-1.41	1.33 E-005
Smoc2	SPARC related modular calcium binding 2	-0.51	5.02 E-004
Calcr	Calcitonin receptor	-2.91	1.22 E-014
Vdr	Vitamin D receptor	-1.45	6.81 E-008
Slc8a3	Solute carrier family 8 (sodium/calcium exchanger) 3	-1.17	3.80 E-003
Pth1r	Parathyroid hormone 1 receptor	-1.00	3.31 E-006
Ramp1	Receptor (calcitonin) activity modifying protein1	-1.09	1.00 E-006
IRON HOMEOSTASIS			
Hfe2	Hemochromatosis type 2	-1.04	3.70 E-002
Tfr2	Transferrin receptor 2	-0.99	1.34 E-003

Data are presented as log₂ fold changes (FC log₂) in RA-treated vs control samples; for instance, a FC log₂ value of -1.00 will correspond to a 50% mRNA level in the RA-treated samples. Adjusted p-value takes into account a false discovery rate wherein 5% of samples with a p-value of 0,050 will result in false positives.

regulating crystal adsorption (Addison and McKee, 2010), and their mutations produce hypomineralized enamel phenotypes including altered prism patterning and increased cellular apoptosis in both patients and mouse models (Fukumoto et al., 2004; Bei, 2009; Hu et al., 2014; Núñez et al., 2015). Reductions in the *SCPP* cluster appeared specific to enamel expression. Other enamel-regulating targets included the kallikrein-related



peptidase 4, essential for removing enamel proteins and biomineralization (OMIM: 603767), the peroxisome proliferator-activated receptor (PPAR) alpha, required to achieve normal enamel mineralization (OMIM: 170998) (Sehic et al., 2009), and FAM20C, whose mutation produces severe enamel defects

in human and mouse (Wang et al., 2012; Acevedo et al., 2015).

RA Excess Alters the Osteoblast, Odontoblast, and Ameloblast Lineages

Over 80 years ago, severe nutritional vitamin A deficiency was reported to reduce enamel formation (Mellanby, 1941), but since this time no genetic models of RA deficiency have been reported with ameloblast or other primary tooth defects. No defects are observed in mouse mutants for the RA-synthesizing enzymes *Raldh2* and *Raldh3* (Dupé et al., 2003, our unpublished observations), implicating a more severe RA deficiency is required. More likely vitamin A intake levels are usually quite high, hence cellular RA levels need to be reduced during ossification. Both hypervitaminosis A and very low serum retinol levels produce skeletal fragility, poor bone health, and osteoporosis risk (Henning et al., 2015; Green et al., 2016). During mineralization, site-specific increases in CYP26 enzymes are required for bone formation (Minegishi et al., 2014). *Cyp26b1*^{-/-} mutants have truncated, under-ossified mandibles, possibly due to RA excess perturbing neural crest migration, or alternatively to defects in osteoblast maturation. Incisor defects, while noted, were not characterized (Maclean et al., 2009). Human mutations (both null and hypomorphic) for this RA-catabolizing enzyme produce calvarial hypoplasia and craniosynostosis (Laue et al., 2011). In our experiments, *Cyp26b1* is potently induced in RA-treated E16.5 incisors (Table S3). Even so, enamel defects are still observed.

The dentino-alveolar bone complex regulates tooth development. We observe rapid *in vivo* effects of RA reducing *Runx2*, and its collagenous and mineralization targets. This rapid rodent response to hypervitaminosis A (Lind et al., 2013) is similar to effects in humans (Henning et al., 2015). These RA excesses target enamel matrix protein production. Phenotypic differences in AI severity have been described between family members with identical mutations (see Prasad et al., 2016, for a recent list). Affected patients could be sensitized to otherwise benign alteration in vitamin consumption, RA catabolism pathways, or defects in the tooth and bone biosynthesis programs. Accumulating mutations might sensitize fetal development to environmental factors, including nutrition, explaining variability in AI morphogenetic phenotypes. Similar models have been proposed for RA interactions with the DiGeorge/chromosome 22q1 deletion syndrome (Maynard et al., 2013). Even physiological RA excesses, in the context of additional genetic alterations (which otherwise would produce benign changes) could have net consequences contributing to clinical variations in oral manifestations of rare diseases.

AUTHOR CONTRIBUTIONS

Study design: SM, AB, and KN. Data collection: SM, VL, EM, BS, and KN. Data analysis: SM, VL, JH, AB, and KN. Drafting manuscript: SM, PD, AB, and KN. Revising manuscript content:

SM, JH, PD, AB, and KN. Approving final version of manuscript: SM, VL, JH, EM, BS, PD, AB, and KN. KN takes responsibility for the integrity of the data analysis.

FUNDING

This work was supported by a grant from the University Hospital of Strasbourg (API, 2009–2012, “Development of the oral cavity: from gene to clinical phenotype in Human”), the EU-funded projects (ERDF) A27 “Oro-dental manifestations of rare diseases” in the framework of the RMT-TMO Offensive Sciences initiative INTERREG IV and INTERREG V No. 1.7 RARENET, the Institut d’Études Avancées (Institute of Advanced Studies) de l’Université de Strasbourg (USIAS Fellows 2015), and the grant ANR-10-LABX-0030-INRT managed by the Agence Nationale de la Recherche under the frame program Investissements d’Avenir ANR-10-IDEX-0002-02. Sequencing was performed by the IGBMC Microarray and Sequencing platform, supported

by the France Genomics National Infrastructure, funded as part of the Investissements d’Avenir program (ANR-10-INB S-0009).

ACKNOWLEDGMENTS

We wish to thank Amandine Velt, Céline Keime, Bernard Jost, Christelle Thibault-Carpentier, Doulaye Dembelé, Antonio Nanci, Greg Pratt, Rena D’Souza, Sylvain Provot, Dominique Hotton, Valérie Fraulob, Carole Haushalter, Muriel Rhinn, Anna Niewiadomska-Cimicka, and Claire Huber for gift of reagents, technical assistance, and/or knowledgeable insight.

SUPPLEMENTARY MATERIAL

The Supplementary Material for this article can be found online at: <http://journal.frontiersin.org/article/10.3389/fphys.2016.00673/full#supplementary-material>

REFERENCES

- Acevedo, A. C., Poulter, J. A., Alves, P. G., de Lima, C. L., Castro, L. C., Yamaguti, P. M., et al. (2015). Variability of systemic and oro-dental phenotype in two families with non-lethal Raine syndrome with FAM20C mutations. *BMC Med. Genet.* 16:8. doi: 10.1186/s12881-015-0154-5
- Addison, W. N., and McKee, M. D. (2010). ASARM mineralization hypothesis: a bridge to progress. *J. Bone Miner. Res.* 25, 1191–1192. doi: 10.1002/jbmr.110
- Alaluusua, S. (2010). Aetiology of molar-incisor hypomineralisation: a systematic review. *Eur. Arch. Paediatr. Dent.* 11, 53–58. doi: 10.1007/BF03262713
- Anders, S., and Huber, W. (2010). Differential expression analysis for sequence count data. *Genome Biol.* 11:R106. doi: 10.1186/gb-2010-11-10-r106
- Balic, A., and Thesleff, I. (2015). Tissue interactions regulating tooth development and renewal. *Curr. Top. Dev. Biol.* 115, 157–186. doi: 10.1016/bs.ctdb.2015.07.006
- Balmer, J. E., and Blomhoff, R. (2002). Gene expression regulation by retinoic acid. *J. Lipid Res.* 43, 1773–1808. doi: 10.1194/jlr.R100015-JLR200
- Barron, M. J., Brookes, S. J., Kirkham, J., Shore, R. C., Hunt, C., Mironov, A., et al. (2010). A mutation in the mouse Amelx tri-tyrosyl domain results in impaired secretion of amelogenin and phenocopies human X-linked *Amelogenesis imperfecta*. *Hum. Mol. Genet.* 19, 1230–1247. doi: 10.1093/hmg/ddq001
- Bei, M. (2009). Molecular genetics of ameloblast cell lineage. *J. Exp. Zool. Part B Mol. Dev. Evol.* 312B, 437–444. doi: 10.1002/jez.b.21261
- Benjamini, Y., and Hochberg, Y. (1995). Controlling the false discovery rate: a practical and powerful approach to multiple testing. *J. R. Stat. Soc. Ser. B. (Methodological)* 57, 289–300.
- Berkovitz, B. K., Maden, M., McCaffery, P., and Barrett, A. W. (2001). The distribution of retinaldehyde dehydrogenase-2 in rat and human orodental tissues. *Arch. Oral Biol.* 46, 1099–1104. doi: 10.1016/S0003-9969(01)00081-4
- Bloch-Zupan, A., Décimo, D., Lorient, M., Mark, M. P., and Ruch, J. V. (1994). Expression of nuclear retinoic acid receptors during mouse odontogenesis. *Differentiation* 57, 195–203. doi: 10.1046/j.1432-0436.1994.5730195.x
- Bloch-Zupan, A., Jamet, X., Etard, C., Laugel, V., Muller, J., Geoffroy, V., et al. (2011). Homozygosity mapping and candidate prioritization identify mutations, missed by whole-exome sequencing, in SMOC2, causing major dental developmental defects. *Am. J. Hum. Genet.* 89, 773–781. doi: 10.1016/j.ajhg.2011.11.002
- Bloch-Zupan, A., Sedano, H., and Scully, C. (2012). *Dento/Oro/Craniofacial Anomalies and Genetics*. Amsterdam: Elsevier.
- Bronckers, A. L., Engelse, M. A., Cavender, A., Gaikwad, J., and D’Souza, R. N. (2001). Cell-specific patterns of Cbfa1 mRNA and protein expression in postnatal murine dental tissues. *Mech. Dev.* 101, 255–258. doi: 10.1016/S0925-4773(00)00562-1
- Camilleri, S., and McDonald, F. (2006). Runx2 and dental development. *Eur. J. Oral Sci.* 114, 361–373. doi: 10.1111/j.1600-0722.2006.00399.x
- Cammass, L., Romand, R., Fraulob, V., Mura, C., and Dollé, P. (2007). Expression of the murine retinol dehydrogenase 10 (Rdh10) gene correlates with many sites of retinoid signalling during embryogenesis and organ differentiation. *Dev. Dyn.* 236, 2899–2908. doi: 10.1002/dvdy.21312
- Cartharius, K., Frech, K., Grote, K., Klocke, B., Haltmeier, M., Klingenhoff, A., et al. (2005). MatInspector and beyond: promoter analysis based on transcription factor binding sites. *Bioinformatics* 21, 2933–2942. doi: 10.1093/bioinformatics/bti473
- Dhamija, S., and Krebsbach, P. H. (2001). Role of Cbfa1 in ameloblastin gene transcription. *J. Biol. Chem.* 276, 35159–35164. doi: 10.1074/jbc.M010719200
- D’Souza, R. N., Aberg, T., Gaikwad, J., Cavender, A., Owen, M., Karsenty, G., et al. (1999). Cbfa1 is required for epithelial-mesenchymal interactions regulating tooth development in mice. *Development* 126, 2911–2920.
- Ducy, P., and Karsenty, G. (1998). Genetic control of cell differentiation in the skeleton. *Curr. Opin. Cell Biol.* 10, 614–619. doi: 10.1016/S0955-0674(98)80037-9
- Dupé, V., Matt, N., Garnier, J. M., Chambon, P., Mark, M., and Ghyselinck, N. B. (2003). A newborn lethal defect due to inactivation of retinaldehyde dehydrogenase type 3 is prevented by maternal retinoic acid treatment. *Proc. Natl. Acad. Sci. U.S.A.* 100, 14036–14041. doi: 10.1073/pnas.2336223100
- Eastoe, J. E. (1979). Enamel protein chemistry—past, present and future. *J. Dent. Res.* 58, 753–764. doi: 10.1177/00220345790580022701
- Fukamoto, S., Kiba, T., Hall, B., Iehara, N., Nakamura, T., Longenecker, G., et al. (2004). Ameloblastin is a cell adhesion molecule required for maintaining the differentiation state of ameloblasts. *J. Cell Biol.* 167, 973–983. doi: 10.1083/jcb.200409077
- Gibson, C. W., Yuan, Z. A., Hall, B., Longenecker, G., Chen, E., Thyagarajan, T., et al. (2001). Amelogenin-deficient mice display an *Amelogenesis imperfecta* phenotype. *J. Biol. Chem.* 276, 31871–31875. doi: 10.1074/jbc.M104624200
- Green, A. C., Martin, T. J., and Purton, L. E. (2016). The role of vitamin A and retinoic acid receptor signaling in post-natal maintenance of bone. *J. Steroid Biochem. Mol. Biol.* 155, 135–146. doi: 10.1016/j.jsbmb.2015.09.036
- Hassan, M. Q., Javed, A., Morasso, M. I., Karlin, J., Montecino, M., van Wijnen, A. J., et al. (2004). Dlx3 transcriptional regulation of osteoblast differentiation: temporal recruitment of Msx2, Dlx3, and Dlx5 homeodomain proteins to chromatin of the osteocalcin gene. *Mol. Cell. Biol.* 24, 9248–9261. doi: 10.1128/MCB.24.20.9248-9261.2004
- Henning, P., Conaway, H. H., and Lerner, U. H. (2015). Retinoid receptors in bone and their role in bone remodeling. *Front. Endocrinol.* 6:31. doi: 10.3389/fendo.2015.00031

- Hu, J. C., Hu, Y., Lu, Y., Smith, C. E., Lertlam, R., Wright, J. T., et al. (2014). Enamelin is critical for ameloblast integrity and enamel ultrastructure formation. *PLoS ONE* 9:e89303. doi: 10.1371/journal.pone.0089303
- Hu, J. C., Hu, Y., Smith, C. E., McKee, M. D., Wright, J. T., Yamakoshi, Y., et al. (2008). Enamel defects and ameloblast-specific expression in Enam knock-out/lacZ knock-in mice. *J. Biol. Chem.* 283, 10858–10871. doi: 10.1074/jbc.M710565200
- Jedon, K., Loidice, S., Marciano, C., Vinel, A., Canivenc Lavier, M. C., Berald, A., et al. (2014). Estrogen and bisphenol A affect male rat enamel formation and promote ameloblast proliferation. *Endocrinology* 155, 3365–3375. doi: 10.1210/en.2013-2161
- Jeremias, F., Koruyucu, M., Küchler, E. C., Bayram, M., Tuna, E. B., Deeley, K., et al. (2013). Genes expressed in dental enamel development are associated with molar-incisor hypomineralization. *Arch. Oral Biol.* 58, 1434–1442. doi: 10.1016/j.archoralbio.2013.05.005
- Jones, D. M., Fabian, B., and Kramer, B. (2008). The effect of retinoic acid on mouse mandibular molar development *in vitro*, using alkaline phosphatase as a molecular indicator of differentiation. *SADJ* 63, 276, 278–280.
- Kawasaki, K., and Weiss, K. M. (2008). SCPP gene evolution and the dental mineralization continuum. *J. Dent. Res.* 87, 520–531. doi: 10.1177/154405910808700608
- Knudsen, P. A. (1967). Dental malformations in rat embryos with exencephaly induced by hypervitaminosis A. *Acta Odontol. Scand.* 25, 267–287. doi: 10.3109/00016356709104023
- Kronmiller, J. E., Upholt, W. B., and Kollar, E. J. (1992). Alteration of murine odontogenic patterning and prolongation of expression of epidermal growth factor mRNA by retinol *in vitro*. *Arch. Oral Biol.* 37, 129–138. doi: 10.1016/0003-9969(92)90008-V
- Laue, K., Pogoda, H. M., Daniel, P. B., van Haeringen, A., Alanay, Y., von Ameln, S., et al. (2011). Craniosynostosis and multiple skeletal anomalies in humans and zebrafish result from a defect in the localized degradation of retinoic acid. *Am. J. Hum. Genet.* 89, 595–606. doi: 10.1016/j.ajhg.2011.09.015
- Lee, H. K., Lee, D. S., Ryoo, H. M., Park, J. T., Park, S. J., Bae, H. S., et al. (2010). The odontogenic ameloblast-associated protein (ODAM) cooperates with RUNX2 and modulates enamel mineralization via regulation of MMP-20. *J. Cell. Biochem.* 111, 755–767. doi: 10.1002/jcb.22766
- Li, Y., Konicki, W. S., Wright, J. T., Suggs, C., Xue, H., Kuehl, M. A., et al. (2013). Mouse genetic background influences the dental phenotype. *Cells Tissues Organs* 198, 448–456. doi: 10.1159/000360157
- Lind, T., Sundqvist, A., Hu, L., Pejler, G., Andersson, G., Jacobson, A., et al. (2013). Vitamin A is a negative regulator of osteoblast mineralization. *PLoS ONE* 8:e82388. doi: 10.1371/journal.pone.0082388
- Loots, G. G., Ovcharenko, I., Pachter, L., Dubchak, I., and Rubin, E. M. (2002). rVista for comparative sequence-based discovery of functional transcription factor binding sites. *Genome Res.* 12, 832–839. doi: 10.1101/gr.225502. Article published online before print in April 2002
- Maclean, G., Dollé, P., and Petkovich, M. (2009). Genetic disruption of CYP26B1 severely affects development of neural crest derived head structures, but does not compromise hindbrain patterning. *Dev. Dyn.* 238, 732–745. doi: 10.1002/dvdy.21878
- Maden, M. (2007). Retinoic acid in the development, regeneration and maintenance of the nervous system. *Nat. Rev. Neurosci.* 8, 755–765. doi: 10.1038/nrn2212
- Mark, M. P., Bloch-Zupan, A., and Ruch, J. V. (1992). Effects of retinoids on tooth morphogenesis and cytodifferentiations, *in vitro*. *Int. J. Dev. Biol.* 36, 517–526.
- Masuya, H., Shimizu, K., Sezutsu, H., Sakuraba, Y., Nagano, J., Shimizu, A., et al. (2005). Enamelin (Enam) is essential for amelogenesis: ENU-induced mouse mutants as models for different clinical subtypes of human *Amelogenesis imperfecta* (AI). *Hum. Mol. Genet.* 14, 575–583. doi: 10.1093/hmg/ddi054
- Maynard, T. M., Gopalakrishna, D., Meechan, D. W., Paronett, E. M., Newbern, J. M., and LaMantia, A. S. (2013). 22q11 Gene dosage establishes an adaptive range for sonic hedgehog and retinoic acid signaling during early development. *Hum. Mol. Genet.* 22, 300–312. doi: 10.1093/hmg/ddt429
- McDowell, E. M., Shores, R. L., Spangler, E. F., Wenk, M. L., and De Luca, L. M. (1987). Anomalous growth of rat incisor teeth during chronic intermittent vitamin A deficiency. *J. Nutr.* 117, 1265–1274.
- Mellanby, H. (1941). The effect of maternal dietary deficiency of vitamin A on dental tissues in rats. *J. Dent. Res.* 20, 489–509. doi: 10.1177/00220345410200051401
- Mic, F. A., Molotkov, A., Benbrook, D. M., and Duester, G. (2003). Retinoid activation of retinoic acid receptor but not retinoid X receptor is sufficient to rescue lethal defect in retinoic acid synthesis. *Proc. Natl. Acad. Sci. U.S.A.* 100, 7135–7140. doi: 10.1073/pnas.1231422100
- Minegishi, Y., Sakai, Y., Yahara, Y., Akiyama, H., Yoshikawa, H., Hosokawa, K., et al. (2014). Cyp26b1 within the growth plate regulates bone growth in juvenile mice. *Biochem. Biophys. Res. Commun.* 454, 12–18. doi: 10.1016/j.bbrc.2014.10.001
- Minoux, M., and Rijli, F. M. (2010). Molecular mechanisms of cranial neural crest cell migration and patterning in craniofacial development. *Development* 137, 2605–2621. doi: 10.1242/dev.040048
- Nakayama, Y., Holcroft, J., and Ganss, B. (2015). Enamel hypomineralization and structural defects in amelotin-deficient mice. *J. Dent. Res.* 94, 697–705. doi: 10.1177/0022034514566214
- Niederreither, K., and Dollé, P. (2008). Retinoic acid in development: towards an integrated view. *Nat. Rev. Genet.* 9, 541–553. doi: 10.1038/nrg2340
- Niederreither, K., Vermot, J., Schuhbauer, B., Chambon, P., and Dollé, P. (2000). Retinoic acid synthesis and hindbrain patterning in the mouse embryo. *Development* 127, 75–85.
- Niederreither, K., Vermot, J., Schuhbauer, B., Chambon, P., and Dollé, P. (2002). Embryonic retinoic acid synthesis is required for forelimb growth and anteroposterior patterning in the mouse. *Development* 129, 3563–3574.
- Núñez, S. M., Chun, Y.-H. P., Ganss, B., Hu, Y., Richardson, A. S., Schmitz, J. E., et al. (2015). Maturation stage enamel malformations in *Amtn* and *Klk4* null mice. *Matrix Biol.* 52–54, 219–233. doi: 10.1016/j.matbio.2015.11.007
- Pindborg, J. J. (1953). The pigmentation of the rat incisor as an index of metabolic disturbances. *Oral Surg. Oral Med. Oral Pathol.* 6, 780–789. doi: 10.1016/0030-4220(53)90205-9
- Prasad, M. K., Geoffroy, V., Vicaire, S., Jost, B., Dumas, M., Le Gras, S., et al. (2016). A targeted next-generation sequencing assay for the molecular diagnosis of genetic disorders with orodental involvement. *J. Med. Genet.* 53, 98–110. doi: 10.1136/jmedgenet-2015-103302
- Punyasingh, J. T., Hoffman, S., Harris, S. S., and Navia, J. M. (1984). Effects of vitamin A deficiency on rat incisor formation. *J. Oral Pathol.* 13, 40–51. doi: 10.1111/j.1600-0714.1984.tb01399.x
- Rhinn, M., and Dollé, P. (2012). Retinoic acid signalling during development. *Development* 139, 843–858. doi: 10.1242/dev.065938
- Rochette-Egly, C., and Germain, P. (2009). Dynamic and combinatorial control of gene expression by nuclear retinoic acid receptors (RARs). *Nucl. Recept. Signal.* 7:e005. doi: 10.1621/nrs.07005
- Rossant, J., Zirngibl, R., Cado, D., Shago, M., and Giguère, V. (1991). Expression of a retinoic acid response element-hsplaCZ transgene defines specific domains of transcriptional activity during mouse embryogenesis. *Genes Dev.* 5, 1333–1344. doi: 10.1101/gad.5.8.1333
- Ryynänen, H., Sahlberg, C., Lukinmaa, P. L., and Alaluusua, S. (2014). The effect of high temperature on the development of mouse dental enamel *in vitro*. *Arch. Oral Biol.* 59, 400–406. doi: 10.1016/j.archoralbio.2014.01.005
- Sehic, A., Khuu, C., Risnes, S., and Osmundsen, H. (2009). Differential gene expression profiling of the molar tooth germ in peroxisome proliferator-activated receptor-alpha (PPAR-alpha) knockout mouse and in wild-type mouse: molar tooth phenotype of PPAR-alpha knockout mouse. *Eur. J. Oral Sci.* 117, 93–104. doi: 10.1111/j.1600-0722.2009.00615.x
- Seritkrakul, P., Samarut, E., Lama, T. T., Gibert, Y., Laudet, V., and Jackman, W. R. (2012). Retinoic acid expands the evolutionarily reduced dentition of zebrafish. *FASEB J.* 26, 5014–5024. doi: 10.1096/fj.12-209304

- Simmer, J. P., Papagerakis, P., Smith, C. E., Fisher, D. C., Rountrey, A. N., Zheng, L., et al. (2010). Regulation of dental enamel shape and hardness. *J. Dent. Res.* 89, 1024–1038. doi: 10.1177/0022034510375829
- Wang, X., Wang, S., Lu, Y., Gibson, M. P., Liu, Y., Yuan, B., et al. (2012). FAM20C plays an essential role in the formation of murine teeth. *J. Biol. Chem.* 287, 35934–35942. doi: 10.1074/jbc.M112.386862
- Xuan, D., Sun, X., Yan, Y., Xie, B., Xu, P., and Zhang, J. (2010). Effect of cleidocranial dysplasia-related novel mutation of RUNX2 on characteristics of dental pulp cells and tooth development. *J. Cell. Biochem.* 111, 1473–1481. doi: 10.1002/jcb.22875
- Yang, T., Zhang, Y., Zheng, D., Hao, Y., Snead, M. L., and Duan, X. (2015). High-fluoride promoted phagocytosis-induced apoptosis in a matured ameloblast-like cell line. *Arch. Oral Biol.* 60, 84–90. doi: 10.1016/j.archoralbio.2014.09.001

Conflict of Interest Statement: The authors declare that the research was conducted in the absence of any commercial or financial relationships that could be construed as a potential conflict of interest.

The handling Editor declared a past co-authorship with the authors VL and AB and states that the process nevertheless met the standards of a fair and objective review.

Copyright © 2017 Morkmued, Laugel-Haushalter, Mathieu, Schuhbaur, Hemmerlé, Dollé, Bloch-Zupan and Niederreither. This is an open-access article distributed under the terms of the Creative Commons Attribution License (CC BY). The use, distribution or reproduction in other forums is permitted, provided the original author(s) or licensor are credited and that the original publication in this journal is cited, in accordance with accepted academic practice. No use, distribution or reproduction is permitted which does not comply with these terms.

Supplemental Material

Retinoic acid excess impairs amelogenesis inducing enamel defects

I Supplementary Text

Methods:

Incisor explant culture:

Pregnant CD1 mice were sacrificed at E13.5, and paired lower incisors (still bearing cartilage connection) were dissected, then cultured for 7 days on Costar 6-well Transwell dishes containing 1.5 mL of Advanced Dulbecco's Modified Eagle Medium F12 (DMEM F12 - GIBCO-BRL) containing 10% fetal calf serum, 1% penicillin-streptomycin (Sigma), and 20 µg/mL ascorbic acid (Sigma). All-trans retinoic acid (Sigma) at a concentration of 5 mg/mL in ethanol was diluted in media and added to cultures. Cultures were shielded from light and incubated at 37°C in 5% CO₂, and medium was changed every two days.

Histological analysis

Heads of 7 day-old control and RA-treated mice were fixed in 4% paraformaldehyde, rinsed, demineralized in 10% EDTA at room temperature for 8 days (the demineralizing solution was changed every two days). After thorough water washes, the heads were dehydrated in a graded ethanol series, cleared in Histosol, and embedded in paraffin at 60°C. Sagittal sections (8 µm) were stained with hematoxylin/eosin. A detailed histology protocol can be found at <http://www.empress.har.mrc.ac.uk> phenotyping, Necropsy Exam, Pathology, Histology section.

RNA sequencing

The mRNAseq libraries were prepared according to a modified Illumina protocol. Purified mRNA was isolated from total RNA using oligo-dT magnetic beads, and fragmented using divalent cations (95°C for 5 minutes). mRNA fragments were reverse transcribed using random primers, and second strand cDNA synthesis was performed. The cDNA fragments were blunt-ended, phosphorylated, and ligated to single-ended adapter dimers. Following PCR amplification, excess PCR primers and dimer adapters were removed using AMPure bead purification (Agencourt Biosciences Corporation). Size selection by electrophoresis in agarose gel was used to isolate DNA fragments of ~250-350 bp. These were excised and purified using QIAquick Gel Extraction Kit (Qiagen). DNA library quality and quantification

was assessed using a 2100 Bioanalyzer (Agilent). The libraries were loaded in the flowcell (at a 6 picomolar concentration) and sequenced using Illumina Genome Analyzer Iix equipment which performed single-end 54 base reads. Image analysis and base calling were performed with the 1.6 Illumina Pipeline.

***In silico* analysis of the enamel matrix protein regulatory regions**

For *in silico* comparative genomic analysis of the *Enam*, *Ambn*, and *Amelx* regulatory regions we used a combination of web-based programs. Blast searches were conducted using the National Center for Biotechnology Information programs (<https://www.ncbi.nlm.nih.gov/>). We used the whole human and mouse sequences of each gene to find evolutionarily conserved regions. Vista plot analysis was performed using the mVista program at <http://genome.lbl.gov/vista/mvista/submit.shtml>. To identify binding element motifs of the *Runx2/3*, *Dlx3/5*, and *Smad2/3/4* transcription factors we used the web-based program JASPAR (version 2016) at <http://jaspar.genereg.net>. To find transcription factor binding sites at the conserved regions both rVista and (<http://genome.lbl.gov/vista/rvista/submit.shtml>) and MatInspector (https://www.genomatix.de/online_help/help_matinspector/matinspector_help.html#seq_selection) programs were used. Gene expression databases (<http://bite-it.helsinki.fi>) and (<http://genepaint.org>) were used to verify expression domains of transcription factors potentially binding to the selected enamel matrix proteins.

II Supplementary Figures and Tables

Supplementary Figures

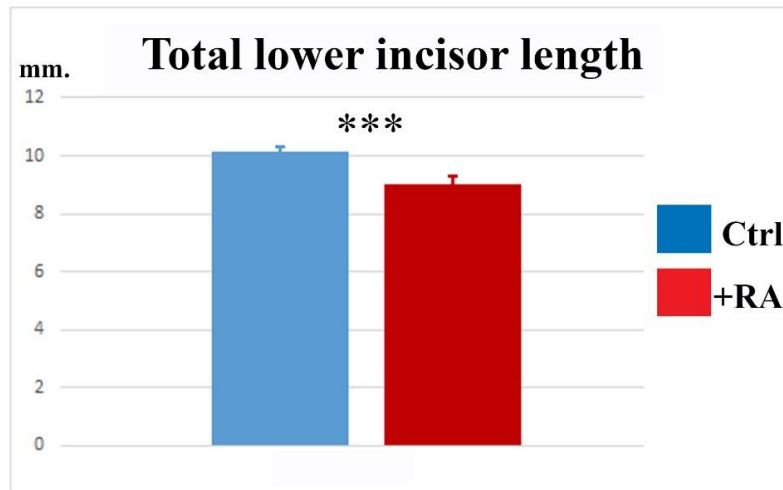


Figure S1. Mean values of total lower incisor length calculated by micro-CT analysis. Incisor length was measured from the most posterior to the tip of the incisal edge of lower incisors. In RA-treated samples, total lower incisor length is reduced by ~10% (** $p < 0.001$).

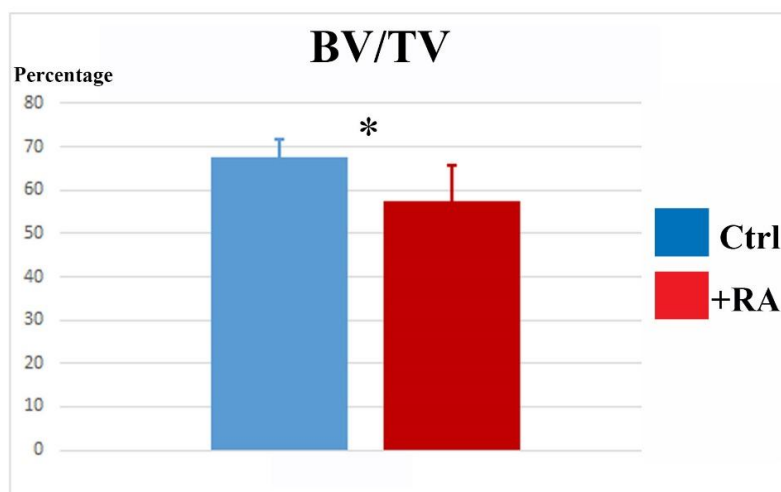


Figure S2. Mean values of bone volume/tissue volume (BV/TV) analyzed by micro-CT analysis. Percentage of alveolar bone around the lower first molar divided by total volume. In RA-treated samples, BV/TV is significantly reduced. (* $p < 0.05$).

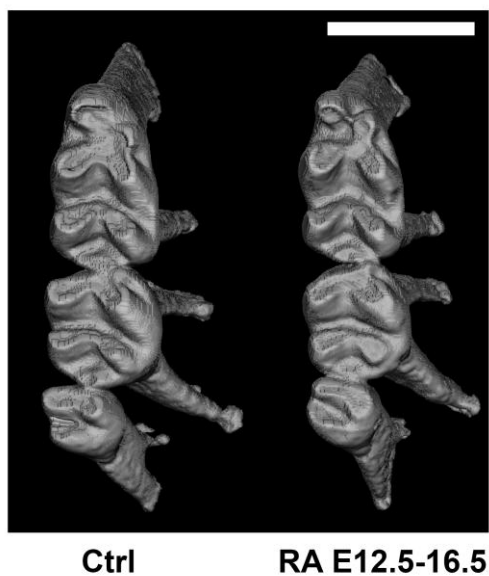


Figure S3. Micro-CT imaging comparing lower molars from 50 day-old mice: untreated (left side) and following E12.5-16.5 RA treatment (right side). Overall, the number of cusps, root morphology, and overall appearance is similar, although moderate growth reductions are observed. Scale bar: 1 mm.

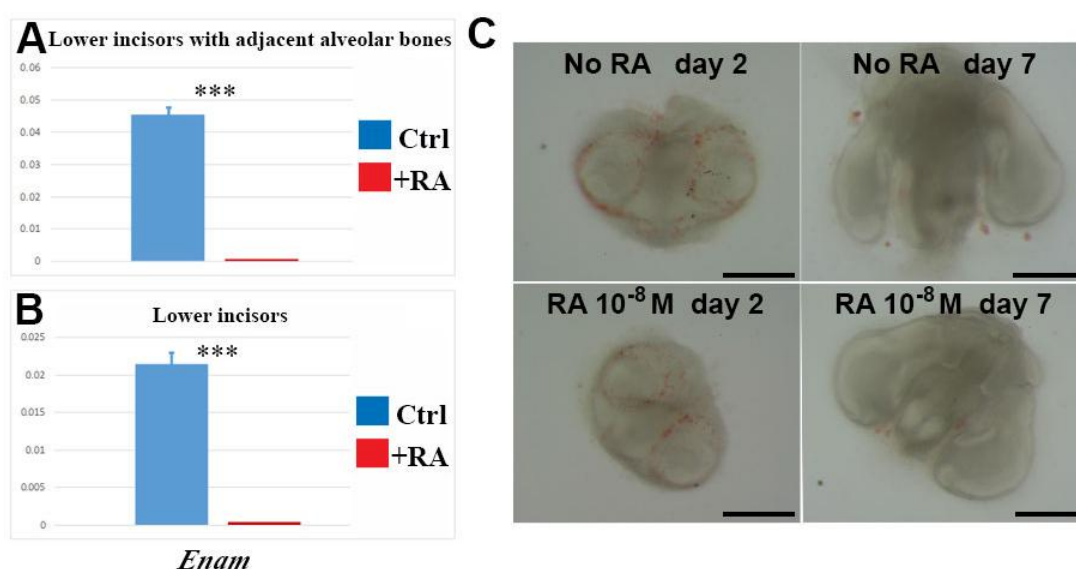


Figure S4. RT-PCR analysis of *Enam* transcripts after Transwell explant culture of E13.5 lower incisors for 7 days. Panel A shows effects of 10⁻⁸ M RA when incisors are cultured with adjacent alveolar bone. Panel B shows similar effects of RA in reducing *Enam* in isolated incisors (*** $p < 0.001$). Photos of incisor explants in culture are shown in C. Note

equivalent growth of incisors during RA treatment compared with control untreated samples.
Scale bars: 500 μm .

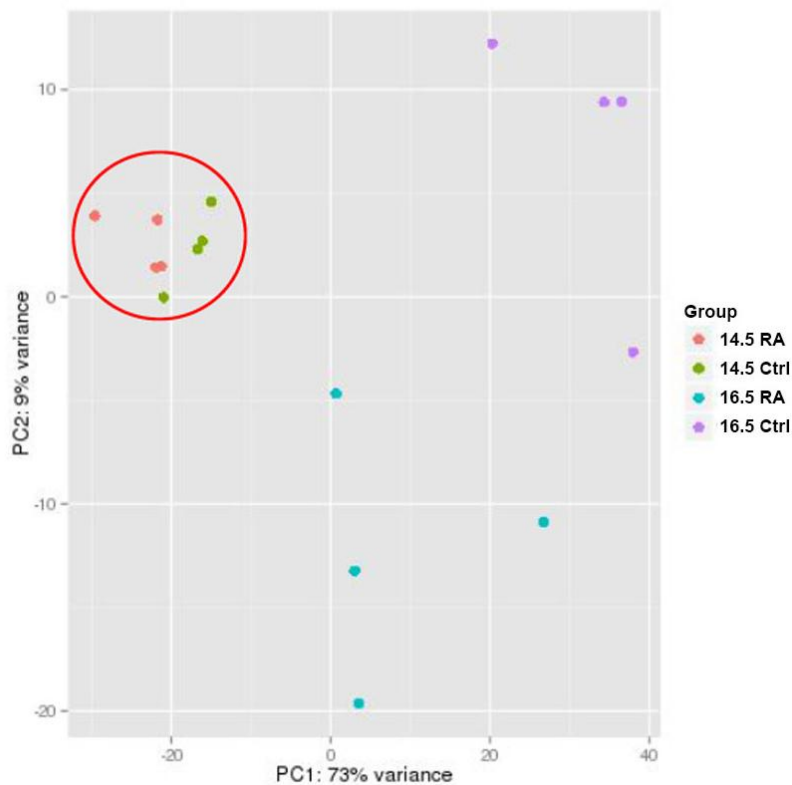


Figure S5. Principal component analysis (PCA plot) visualizing overall effect of retinoid treatments on the incisor RNA transcriptome. At E14.5, RA-treated and control samples show tight clustering. At E16.5 larger expression changes and sample disparity are observed.

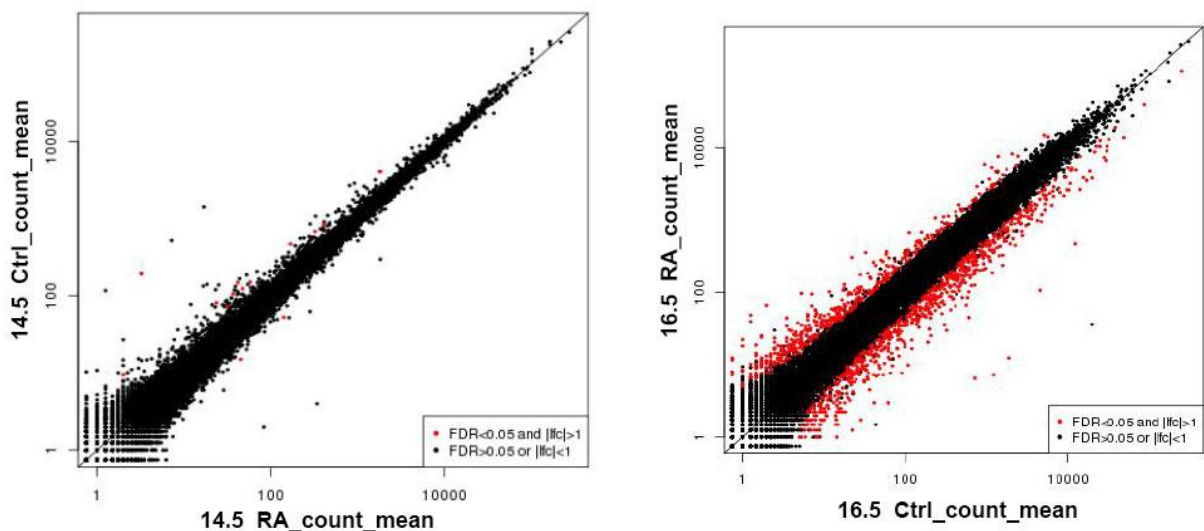


Figure S6. Comparison between E14.5 untreated and RA-treated samples (left), and E16.5 untreated and RA-treated samples (right) using scatterplot diagrams (obtained with DESeq2). At E14.5, less than 20 genes had fold-changes (\log_2) > 1 (red dots). At E16.5,

using a false discovery rate (FDR) <0.05 and \log_2 fold-change > 1 , the total number of significantly differentially expressed genes is 1375. The number of overexpressed genes is 502, whereas the number of underexpressed genes is 873.

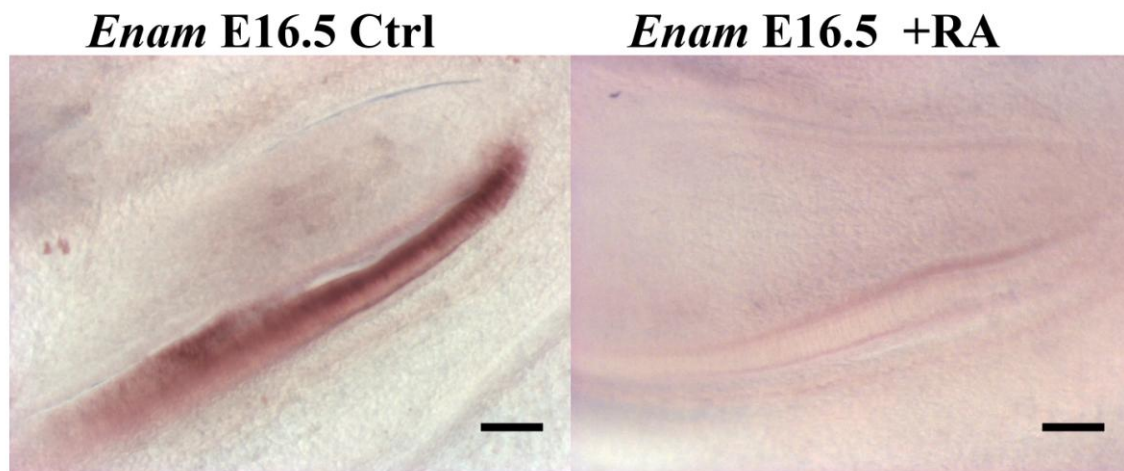


Figure S7. In situ hybridization localization of *Enam* in the lower incisor pre-secretory ameloblasts at E16.5. Marked expression of *Enam* is detected in pre-secretory stage ameloblasts. In RA-treated samples, *Enam* is significantly reduced. Scale bars: 100 μm .

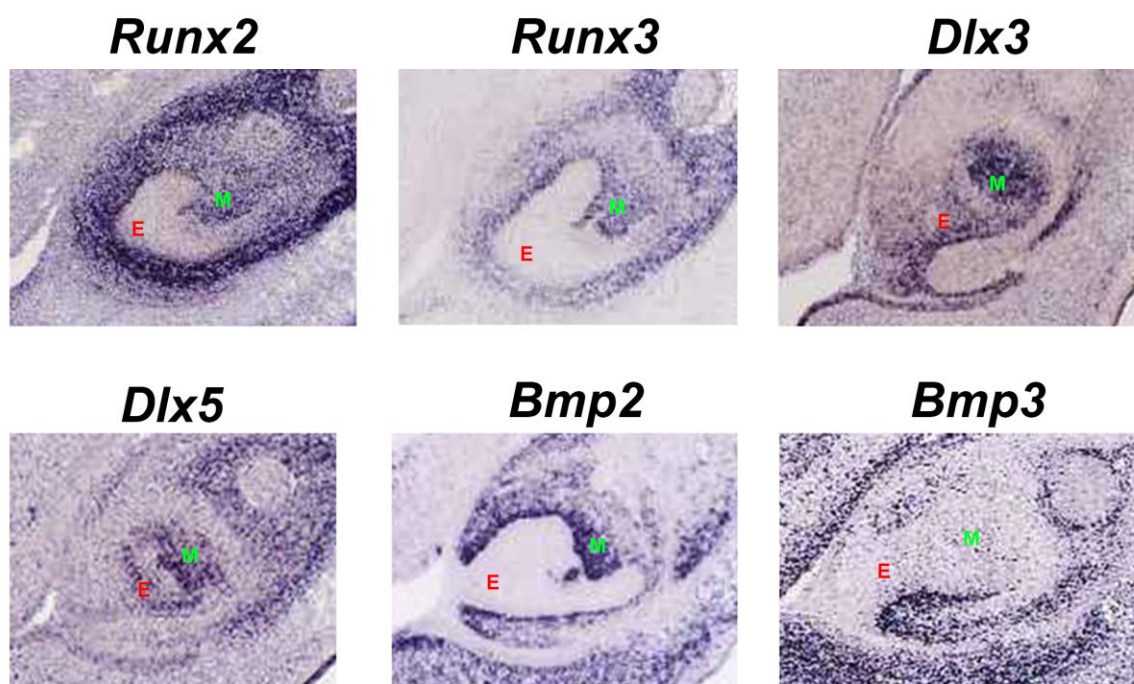


Figure S8. In situ hybridization localization of *Runx2*, *Runx3*, *Dlx3*, *Dlx5*, *Bmp2*, and *Bmp3* in lower incisors at E14.5. Marked expression of these genes is detected

predominantly in dental mesenchymal tissue. All images are obtained from the Genepaint database (<http://genepaint.org/>). Abbreviations: epithelium (E), mesenchyme (M).

Supplementary Tables

NAME	Forward Primer	Reverse Primer
<i>Enam</i>	TGC AGA AAT CCG ACT TCT CCT	CAT CTG GAA TGG CAT GGC A
<i>Ambn</i>	ATG AAG GGC CTG ATC CTG TTC	GTC TCA TTG TCT CAA GGC TCA AA
<i>Odam</i>	AGC TTT GCT GGA CTA TTC CCA	GTA CCA CAT AGG ACA TAG GGC T
<i>Runx2</i>	AGA GTC AGA TTA CAG ATC CCA GG	TGG CTC TTC TTA CTG AGA GAG G
<i>Bmp2</i>	GGG ACC CGC TGT CTT CTA GT	TCA ACT CAA ATT CGC TGA GGA C
<i>Dlx3</i>	CAC TGA CCT GGG CTA TTA CAG C	GAG ATT GAA CTG GTG GTG GTA G
<i>Dlx5</i>	TCT CTA GGA CTG ACG CAA ACA	GTT ACA CGC CAT AGG GTC GC
<i>Ihh</i>	CTC AGA CCG TGA CCG AAA TAA G	CCT TGG ACT CGT AAT ACA CCC AG
<i>Gapdh</i>	AGG TCG TGT TGA ACG GAT TTG	TGT AGA CCA TGT AGT TGA GGT CA

Table S1: Primer sequences used for real-time RT-PCR analysis.

Symbol	Name	FC log2	p-value
Retinoid signaling			
Rarb	retinoic acid receptor β	0.50	1.29 E-02
Retsat	retinol saturase (all-trans-retinol 13,14 reductase)	0.40	2.42 E-03
Rdh16	retinol dehydrogenase 16	0.32	2.38 E-01
Neuronal transcription pathway			
En2	engrailed 2	1.96	4.63 E-06
Neurog1	neurogenin 1	0.96	2.58 E-03
Neurog2	neurogenin 2	1.29	1.22 E-03
Sox1	SRY (sex determining region Y)-box 1	1.09	7.94 E-03
Hes5	hairy and enhancer of split 5	0.99	4.07 E-03
Dbx1	developing brain homeobox 1	0.93	2.38 E-02
Neurod4	neurogenic differentiation 4	0.86	2.19 E-02
Neurod1	neurogenic differentiation 1	0.83	4.11 E-02
Otx2	orthodenticle homolog 2	1.45	9.09 E-04
Cell death			
Prok1	prokineticin 1	1.20	5.98 E-03
Prokr2	prokineticin receptor 2	0.88	2.76 E-03
Hrk	harakiri, BCL2 interacting protein	0.76	1.50 E-02
Blood lineage			
Hbq1a	hemoglobin, theta 1A	0.87	3.52 E-02
Vwf	Von Willebrand factor homolog	0.73	2.96 E-06
Notch signaling			
Hey2	hairy/enhancer-of-split with YRPW motif 2	0.57	3.65 E-02
Dtx3	deltex 3 homolog	0.33	1.40 E-03

Table S2: Summary of genes increased in expression in E14.5 RA-treated lower incisors. Selected genes are members of the retinoic acid pathway, transcriptional regulators of neuronal development, or related to cell death, blood lineage commitment, or Notch signaling. Data are presented as log2 fold changes in RA-treated versus control samples: for instance, a FC log2 value of 1.00 will correspond to a 2-fold mRNA increase in the RA-treated samples.

Symbol	Name	FC log2	p-value
Retinoic acid			
Cyp26b1	cytochrome P450 26b1	2.26	2.66 E-023
Rarb	retinoic acid receptor β	1.16	2.55 E-007
Stra6	stimulated by retinoic acid gene 6	1.09	4.11 E-004
Wnt signaling			
Wnt4	wingless-type MMTV integration site 4	0.94	4.33 E-008
Wnt5a	wingless-type MMTV integration site 5 α	0.96	4.89 E-014
Wnt5b	wingless-type MMTV integration site 5 β	0.42	3.72 E-002
Wnt7b	wingless-type MMTV integration site 7 β	0.94	1.36 E-006
Wnt11	wingless-type MMTV integration site family 11	0,59	3.04 E-004
Wisp3	WNT1 inducible signaling 3	0.8	4.36 E-002
Fzd10	frizzled homolog 10	1.13	1.40 E-007
Neuronal differentiated			
Sycp21	synaptonemal complex protein 2	2.58	2.10 E-008
Cntn2	contactin 2	1.68	9.05 E-010
Fscn2	fascin homolog 2, actin-bundling protein	1.65	9.15 E-005
Gldn	gliomedin	1.57	4.54 E-007
Nps	neuropeptide S	1.51	1.36 E-003
Syt16	synaptotagmin XVI	1.48	2.08 E-008
Cacna2d3	calcium channel, voltage-dependent, $\alpha 2/\delta 3$	1.48	1.26 E-008
Kcnmb2	potassium large conductance channel M $\beta 2$	1.47	7.02 E-004
Mc5r	melanocortin 5 receptor	1.14	7.11 E-004
Scg2	secretogranin II	1.13	6.06 E-003
Grid2	glutamate receptor $\delta 2$	1.12	3.03 E-006
Stx19	syntaxin 19	1.11	6.45 E-004
Gabrg3	gamma-aminobutyric acid (GABA) A receptor, $\gamma 3$	1.11	9.48 E-005
Gprin2	G protein regulated inducer of neurite outgrowth 2	1.08	3.94 E-003

Table S3: Genes of the retinoic acid pathway, or involved in Wnt signaling or neuronal differentiation, increased in expression in E16.5 RA-treated lower incisors. Data are presented as log₂ fold changes in RA-treated versus control samples.

Seq. name	Matrix Family	Detailed Matrix info.	Position	Core sim.	Matrix sim.	Evidence	Sequence
GXP_152 236 Enam	V\$DLXF	DLX-1, -2, and -5 binding sites	95-113	1	0.982	V\$DLXF TF: Dlx3	attccagtttA ATTacgta
	V\$DLXF	DLX-1, -2, and -5 binding sites	100-118	1	0.976	V\$DLXF TF: Dlx3	gttaatacgtA ATTaaact
	V\$HAML	RUNX3, AML2	798-812	1	0.971	V\$HAML TF: Runx2	attTGTGgt gtttct
GXP_597 4669 Enam	V\$HAML	RUNX3, AML2	57-71	1	0.971	V\$HAML TF: Runx2	attTGTGgt gtttct
GXP_152 087 Ambn	V\$DLXF	Distal-less homeobox 2	71-89	1	0.937	V\$DLXF TF: Dlx3	aacacacagt AATTgtgtc
	V\$DLXF	Distal-less homeobox 5	76-94	1	0.925	V\$DLXF TF: Dlx3	tcagtgacac AATTactgt
	V\$HAML	RUNX3, AML2	381-395	1	0.947	V\$HAML TF: Runx2	ggaTGTGg tcattgg
GXP_152 088 Ambn	V\$DLXF	Distal-less homeobox 3	45-63	1	0.933	V\$DLXF TF: Dlx3	ccctagagaT AATttggg
	V\$DLXF	Distal-less 3 homeo-domain TF	206-224	1	0.912	V\$DLXF TF: Dlx3	caaacagaT AATggcttg
	V\$DLXF	Distal-less 3 homeo-domain TF	402-420	1	0.985	V\$DLXF TF: Dlx3	ggtgtggacT AATgcagg
	V\$DLXF	Distal-less homeobox 2	407-425	1	0.928	V\$DLXF TF: Dlx3	gtgctcctgc AATtagtcc
GXP_229 912 Amelx	V\$HAML	Runx2/ CBFA1	36-50	1	0.841	V\$HAML TF: Runx2	acagGTGG ttttcta
	V\$DLXF	Distal-less 3 homeo-domain TF	266-284	1	0.992	V\$DLXF TF: Dlx3	aagtaacgtT AATtgctag
	V\$DLXF	Distal-less homeobox 2	271-289	1	0.924	V\$DLXF TF: Dlx3	cagttctagcA ATTaacgt
	V\$HAML	AML1/CBF A2 Runt domain	667-681	1	0.991	V\$HAML TF: Runx2	cactGTGGt catttc
GXP_152 163 Amtn	V\$DLXF	Distal-less homeobox 3	292-310	1	0.884	0	atgcctatatA ATTttaa

Table S4: Potential transcription factor binding sites (TFBS) for *Enam*, *Ambn*, *Amelx*, and *Amtn* with *Dlx* and *Runx* families. These results were generated by MatInspector (https://www.genomatix.de/online_help/help_matinspector/matinspector_help.html).

(ii) Genetic factors

Enamel and dental anomalies in latent-transforming growth factor beta-binding protein 3 mutant mice

Morkmued S, Hemmerle J, Mathieu E, Laugel-Haushalter V, Dabovic B, Rifkin DB, Dollé P, Niederreither K, Bloch-Zupan A.
Eur J Oral Sci. 2017 Feb;125(1):8-17. doi: 10.1111/eos.12328.

Anomalies de l'émail et des dents chez les souris mutantes pour le gène *Ltbp3* (latent-transforming growth factor beta-binding protein 3).

Latent-transforming growth factor beta-binding protein 3 (LTBP-3) est important pour la morphogenèse crânio-faciale et la minéralisation des tissus durs, car il est essentiel pour l'activation du facteur de croissance TGF- β . Pour étudier le rôle de LTBP-3 dans la formation de la dent, nous avons effectué des analyses de souris adultes *Ltbp3*^{-/-} par tomodensitométrie aux rayons X (micro-CT), histologie et microscopie électronique à balayage. Les mutants *Ltbp3*^{-/-} présentent des malformations crânio-faciales uniques et une hypoplasie de l'émail qui a débuté au stade de la mise en place de la matrice amélaire. L'organisation des améloblastes en phase de maturation est gravement perturbée. Les côtés latéraux de l'incisive sont les plus affectés. Une hypominéralisation de l'émail, une modification du schéma d'organisation des prismes de l'émail et des nodules d'émail sont observés dans les incisives, par microscopie électronique à balayage. Les racines des molaires montrent des formations internes de forme bulbeuse irrégulière. L'épaisseur du ciment est réduite, et les tubules dentaires microscopiques montrent des changements mineurs à l'échelle nanostructurale. Ainsi, LTBP-3 est nécessaire pour la différenciation de l'améloblaste et pour la décussation des prismes d'émail, pour empêcher la formation de nodules d'émail et pour la morphogenèse correcte de la racine. En outre, et en cohérence avec le rôle de la signalisation TGF- β pendant la minéralisation, presque tous les éléments osseux crânio-faciaux sont affectés dans les souris *Ltbp3*^{-/-}, en particulier ceux impliquant la mâchoire supérieure et le

museau. Ce modèle de souris démontre un chevauchement phénotypique avec le syndrome de Verloes-Bourguignon, également causé par les mutations de *LTBP3*, et caractérisé par des anomalies crânio-faciales et un phénotype d'amélogenèse imparfaite.

Enamel and dental anomalies in latent-transforming growth factor beta-binding protein 3 mutant mice

Supawich Morkmued^{1,2,3},
Joseph Hemmerle⁴, Eric Mathieu⁴,
Virginie Laugel-Haushalter²,
Branka Dabovic⁵, Daniel B. Rifkin⁵,
Pascal Dollé², Karen Niederreither^{1,2},
Agnès Bloch-Zupan^{1,2,6}

Morkmued S, Hemmerle J, Mathieu E, Laugel-Haushalter V, Dabovic B, Rifkin DB, Dollé P, Niederreither K, Bloch-Zupan A. Enamel and dental anomalies in latent-transforming growth factor beta-binding protein 3 mutant mice. *Eur J Oral Sci* 2017; 125: 8–17. © 2017 The Authors. *Eur J Oral Sci* published by John Wiley & Sons Ltd

Latent-transforming growth factor beta-binding protein 3 (LTBP-3) is important for craniofacial morphogenesis and hard tissue mineralization, as it is essential for activation of transforming growth factor- β (TGF- β). To investigate the role of LTBP-3 in tooth formation we performed micro-computed tomography (micro-CT), histology, and scanning electron microscopy analyses of adult *Ltbp3*^{-/-} mice. The *Ltbp3*^{-/-} mutants presented with unique craniofacial malformations and reductions in enamel formation that began at the matrix formation stage. Organization of maturation-stage ameloblasts was severely disrupted. The lateral side of the incisor was affected most. Reduced enamel mineralization, modification of the enamel prism pattern, and enamel nodules were observed throughout the incisors, as revealed by scanning electron microscopy. Molar roots had internal irregular bulbous-like formations. The cementum thickness was reduced, and microscopic dentinal tubules showed minor nanostructural changes. Thus, LTBP-3 is required for ameloblast differentiation and for the formation of decussating enamel prisms, to prevent enamel nodule formation, and for proper root morphogenesis. Also, and consistent with the role of TGF- β signaling during mineralization, almost all craniofacial bone components were affected in *Ltbp3*^{-/-} mice, especially those involving the upper jaw and snout. This mouse model demonstrates phenotypic overlap with Verloes Bourguignon syndrome, also caused by mutation of *LTBP3*, which is hallmarked by craniofacial anomalies and amelogenesis imperfecta phenotypes.

¹Faculté de Chirurgie Dentaire, Université de Strasbourg, Strasbourg, France; ²CNRS UMR_7104, INSERM U964, Institut de Génétique et de Biologie Moléculaire et Cellulaire (IGBMC), Centre Européen de Recherche en Biologie et en Médecine (CERBM), Université de Strasbourg, Illkirch, France; ³Faculty of Dentistry, Pediatric Dentistry, Khon Kaen University, Khon Kaen, Thailand; ⁴Biomaterials and Bioengineering, Inserm UMR1121 Strasbourg, Université de Strasbourg, Strasbourg, France; ⁵Department of Cell Biology, New York University Medical Center, New York, NY, USA; ⁶Pôle de Médecine et Chirurgie Bucco-Dentaires, Centre de Référence des Manifestations Odontologiques des Maladies Rares, O Rares, Hôpitaux Universitaires de Strasbourg, Strasbourg, France

Agnès Bloch-Zupan, Institut de Génétique et de Biologie Moléculaire et Cellulaire (IGBMC), CNRS UMR 7104, INSERM U 964, Université de Strasbourg, 1 rue Laurent Fries, BP 10142, 67404 Illkirch, France

E-mail: agnes.bloch-zupan@unistra.fr

Key words: amelogenesis; enamel; *Ltbp3*; mouse; scanning electron microscopy

This is an open access article under the terms of the Creative Commons Attribution-NonCommercial-NoDerivs License, which permits use and distribution in any medium, provided the original work is properly cited, the use is non-commercial and no modifications or adaptations are made.

Accepted for publication December 2016

Enamel is the body's strongest tissue because of its dense mineralized content, which forms in a unique stage-specific process. Enamel formation is a sensitive process susceptible to environmental effects, as well as to the consequences of gene mutations, sometimes encountered in rare diseases (1). Enamel-formation defects observed in rodent genetic models are excellent systems for using to study the basis of analogous human malformations (2). Enamel formation begins when an organic protein-enriched matrix is deposited by ameloblasts during the secretory stage. This protein matrix is then modified through the transition and maturation stages (3). During the secretory stage, polarized columnar-shaped ameloblasts, adjacent to forming enamel, secrete enamel proteins, such as amelogenin,

ameloblastin, and enamelin. Tomes' processes on the distal surface of secretory ameloblasts organize the direction of enamel deposition into rods (4). During the maturation and mineralization stages, enamel matrix proteins are degraded in a stepwise manner by matrix metalloproteinase-20 (MMP-20) and kallikrein-4 (KLK-4) to form unique enamel prisms (5, 6). Murine mutations of enamel processing and degradation proteins produce enamel defects resembling human amelogenesis imperfecta (AI) phenotypes (5–8).

Transforming growth factor beta (TGF- β) is part of a superfamily of growth factors that regulate a broad range of cell growth, differentiation, and extracellular morphogenic events (9). Inhibited TGF- β signaling (by mutation of TGF- β ligands, TGF- β receptors, or

intracellular SMADs) leads to reduced enamel formation and detachment of ameloblast cells from the dentin surface, causing the secretion of bubble-like masses that form cystic structures (10, 11). For example, mice with a conditional knockout mutation for TGF- β receptor II display enamel attrition with thinner crystals (12). Both *Smad3*^{-/-} and *Smad7*^{-/-} mutations reduce enamel mineralization (13, 14). Hence, disrupted TGF- β signaling has stage-specific consequences for amelogenesis in a variety of rodent models.

Transforming growth factor- β family proteins are secreted in the form of high-molecular-mass latency complexes that contain other proteins, including latent-transforming growth factor beta-binding proteins (LTBPs) (15). To date, four members of the LTBP family (LTBP-1, LTBP-2, LTBP-3, and LTBP-4) are known. Through their interactions with other extracellular proteins, LTBPs are important regulators of the bioavailability and action of TGF- β (16). Immunoprecipitation studies using mouse pre-osteoblast MC3T3-E1 cells revealed that the LTBP polypeptide forms a complex with the TGF- β 1 precursor (16). Moreover, LTBP-3 allows latent TGF- β complexes to be targeted to connective tissue matrices and cells (17, 18). *Ltbp3*^{-/-} mice show severe skull deformities (19, 20) and an osteopetrosis-like phenotype (21), while other LTBP members have broad functions in many systems (16). Exactly how craniofacial hard-tissue defects occur under *Ltbp3* deficiency is still unclear, especially those concerning tooth and enamel malformation.

Mutations in human *LTBP3* were first observed in a consanguineous Pakistani family, in which all affected members presented with short stature, vertebral and skull bone alterations, and oligodontia (22). In another family, two sisters with homozygous-recessive truncating mutations in *LTBP3* also had oligodontia, short stature, and mitral valve prolapse (23). Our published report identified recessive hypomorphic *LTBP3* mutations (including deletion, nonsense, and aberrant splice mutations) in patients with dental anomalies and short stature (MIM; 601216) (24) or Verloes Bourguignon syndrome (25). Using the adult *Ltbp3*^{-/-} mouse model to characterize all dental hard-tissue components, we previously described very thin or absent enamel in both incisors and molars (24). More complete understanding of *Ltbp3*^{-/-} mouse dental phenotypes will allow us to address how mutations of this gene in humans produce tooth abnormalities (19, 20), and to clarify the role of LTBP-3 in modulating TGF- β bioavailability (19).

Here we explore dental and cranial morphological differences caused by *Ltbp3* deficiency using a three-dimensional (3D) imaging system [X-ray micro-computed tomography (micro-CT)], classical histology, and scanning electron microscopy. We observed (i) alterations in enamel formation and deposition of enamel nodules, (ii) maturation-stage ameloblast disruptions, (iii) small bulbous-like formations inside molar roots, and (iv) enamel prism pattern malformations and reduced cementum thickness, collectively providing a framework for investigating the genetic basis of TGF- β signaling defects.

Material and methods

Animals

Ltbp3^{-/-} mice (C57BL/6;Sv129;SW mixed background) were produced and genotyped as previously described (19, 20). All procedures with animals were performed according to the standards approved by New York University School of Medicine Institutional Animal Care and Use Committee.

Micro-CT imaging

The heads of five adult male *Ltbp3*^{-/-} mutant mice and of five corresponding age/sex-matched wild-type (WT) littermates were examined at 3.5 months of age. To investigate malformations at slightly later stages, two male 5.5-month-old *Ltbp3*^{-/-} mutants and two WT matching controls were also examined. All samples were scanned using the Quantum FX micro-CT pre-clinical in vivo imaging system (Caliper Life Sciences, Hopkinton, MA, USA), which operates at an energy of 80 kV and current intensity of 160 μ A. We found no obvious skull morphological changes with aging. Micro-CT data acquisitions (with resolution at 80, 40, 20, and 10 μ m pixel sizes for skulls, mandibles, incisors, and molars, respectively) were reconstructed using Analyze11.0 (Biomedical Imaging Resource, Mayo Clinic, Rochester, MN, USA). Bony dento-cranio-facial anatomy was sorted in coronal, transverse, and sagittal planes at skull, mandible, incisor, and molar levels. The segmented voxels were compiled to represent bony tissue and then were separated according to density to quantitate incisor and molar enamel. Cranial anatomical landmarks were analyzed using Euclidean distance matrix analysis (EDMA) for morphometric analysis (26, 27).

Histology

Samples (heads of 3.5-month-old WT and *Ltbp3*^{-/-} mice) were fixed in 10% formalin for 30 d or longer and then transferred into 70% ethanol, washed in water, and demineralized in 10% ethylenediaminetetraacetic acid (EDTA) at 37°C for 10 d (the demineralizing solution was changed every day for the first 3 d and then every other day). After thoroughly washing in water, the heads were dehydrated in graded ethanol, cleared in Histo-Clear (National Diagnostics, Atlanta, GA, USA), and embedded in paraffin at 60°C. Ten-micrometer-thick transverse sections were collected, deparaffinized, and stained with hematoxylin and eosin (H&E). A detailed histology protocol can be found at <http://www.empress.har.mrc.ac.uk>.

Scanning electron microscopy

The upper and lower murine incisors of 3.5-month-old *Ltbp3*^{-/-} and WT mice were dissected out of the alveolar bone. After rinsing with distilled water, the teeth were dehydrated in a graded series of ethanol, transferred in a solution of propylene oxide/epon resin (1:1, vol/vol), and embedded in Epon 812 (Euromedex, Souffelweyersheim, France). The teeth were sectioned into two halves along their sagittal axes using a water-cooled diamond circular saw (Bronwill Scientific, Rochester, NY, USA), and both surfaces were polished with diamond paste (Escil, Chassieu, France). One-half was etched with a 20% (wt/vol)

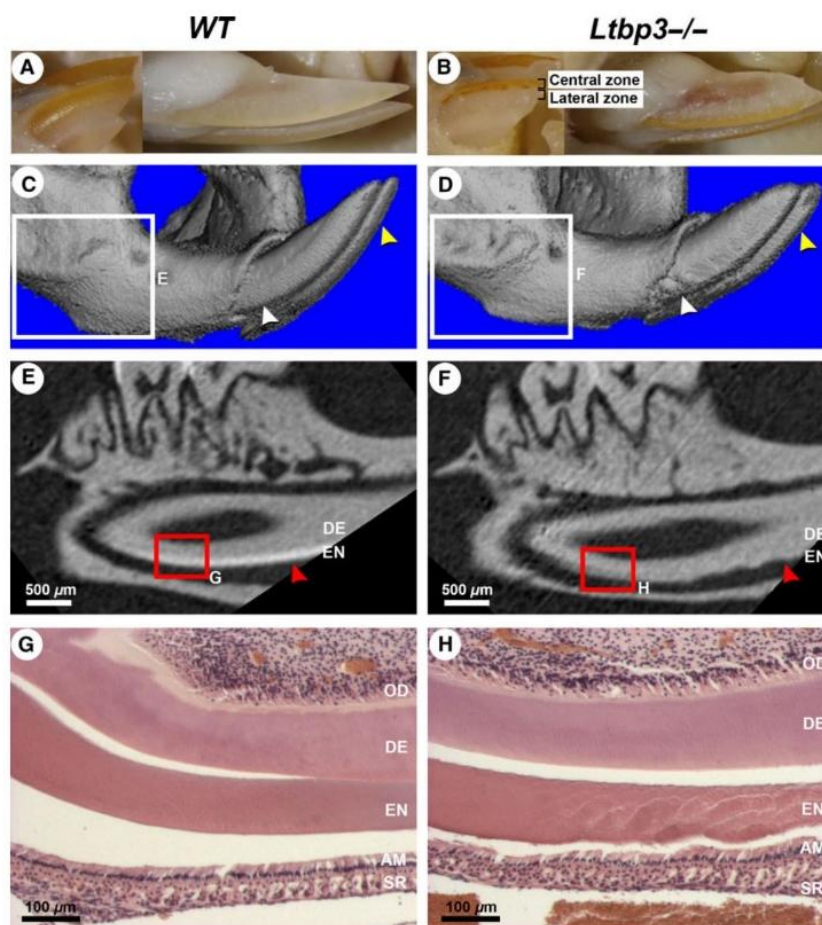


Fig. 1. External morphology, micro-computed tomography (micro-CT), and histology analysis of lower incisors of a 3.5-month-old wild-type (WT) mouse (left column of panels) or a latent transforming growth factor beta binding protein mutant (*Ltbp3*^{-/-}) mouse (right column of panels). The same WT or *Ltbp3*^{-/-} mutant is shown in all respective panels. (A, B) In external views of lower incisors, the incisors of the mutant are shorter, laterally white, and centrally orange. (C, D) Three-dimensional rendered micro-CT images of the distal part of the mandible. The surface of enamel from the *Ltbp3*^{-/-} mouse appears irregular (yellow arrows), and enamel nodules are seen near the alveolar bone crest area of the incisor (white arrows). (E, F) Two-dimensional micro-CT sagittal sections of the first lower molar and the underlying incisor (obtained from the respective boxed region in panels C and D), showing the enamel density. In the mutant the enamel layer is clearly reduced and has a rough appearance (red arrows). (G, H) Histological sections (hematoxylin and eosin staining) of the lower incisor (respective red boxed area in panels E and F) showing an irregular enamel layer (EN) in the *Ltbp3*^{-/-} mutant. The odontoblast (OD) and dentin (DE) layers show no obvious changes. AM, ameloblasts; SR, stellate reticulum.

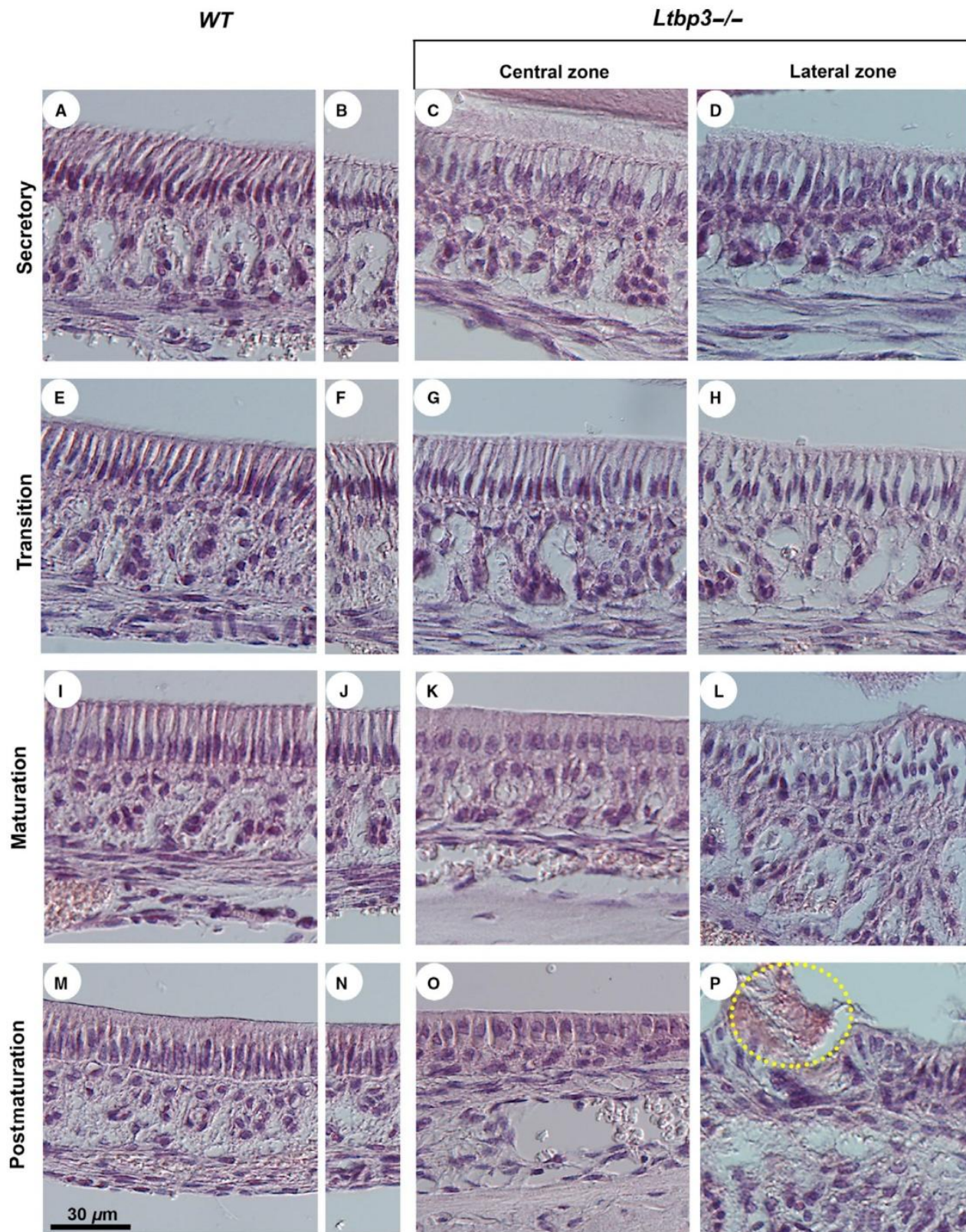
citric acid solution for 2 min, rinsed with distilled water, dehydrated in a graded series of ethanol solutions and left to dry at room temperature. The samples were coated with a gold-palladium alloy using a Hummer Jr sputtering device (Technics, Union City, CA, USA). Scanning electron microscopy assessments were performed using a Quanta 250 ESEM (FEI Company, Eindhoven, the

Netherlands) operating with an accelerating voltage of electrons of 5 kV.

Statistical analysis

Non-parametric statistical testing (using the Mann-Whitney *U*-test) was used to compare the enamel volume of

Fig. 2. Histological analysis (hematoxylin and eosin staining) of the lower incisor ameloblasts. Normal ameloblast development starts at the cervical loop region of the incisor and involves differentiation in consecutive secretory, transition, maturation, and postmaturation stages toward the incisal edge. These regions are illustrated both in central and lateral zones of the incisor in latent transforming growth factor beta binding protein (*Ltbp3*^{-/-}) mutants (right-side panels) and respective wild-type (WT) controls (left-side panels). The central (A, E, I, M) and lateral (B, F, J, N) zones of WT mice show virtually identical morphology. (A-H) Ameloblasts of *Ltbp3*^{-/-} mice show no obvious changes at the secretory and transition stages. However, the papillae underlying the ameloblasts have an irregular organization, with an increased space between each papilla. (I-L) At the maturation stage, the ameloblasts of *Ltbp3*^{-/-} mice differentiate as shorter columnar cells (K). Ameloblasts appear highly abnormal in the lateral zone (L). (M-P) At the postmaturation stage, the ameloblast layer is disorganized in the mutants (O, P), with cell disruptions localizing mainly to the lateral zone, including the detachment of enamel (circled in P).



incisor and molar enamel segmentations. The level of statistical significance was set at $P < 0.05$. For EDMA analysis, a parametric bootstrap approach was performed to

validate the statistical significance, as described previously (27). All significance points were then recalculated as length in millimeters, aiding data interpretation.

Results

Alterations in enamel formation and deposition of enamel nodules

Macroscopically, the upper and lower incisors of normal teeth (from WT mice) are naturally yellow in color and the enamel is smooth and present only on the labial side (Fig. 1A). In *Ltbp3*^{-/-} mutants, reduced coloration and irregular enamel surfaces were observed, with the lateral zones having less enamel than the central zones (Fig. 1B). The 3D rendered micro-CT images showed disrupted enamel patterns at the junction between the alveolar bone and the crown area, where numerous enamel nodules had formed laterally (Fig. 1C,D; white arrowheads). Early enamel formed at the distal part of the lower incisor showed obvious changes, as seen in two-dimensional (2D) sagittal plane reconstructions from micro-CT images (Fig. 1E,F; red arrowheads). This impaired enamel formation was confirmed by histological analysis (Fig. 1G,H). The enamel matrix in *Ltbp3*^{-/-} mutants was irregular and failed to form a steady pattern (Fig. 1H). Changes in enamel volume were not uniform throughout the tooth crown, as enamel was completely missing from the lateral side of the labial portion of the incisor. However, a band of enamel of similar thickness as in WT mice was present in the central portion of the labial crown of the incisors.

Maturation-stage ameloblast disruptions

Histological analysis of secretory, transition, maturation, and postmaturation stage ameloblasts of the lower incisors revealed striking alterations in differentiation in *Ltbp3*^{-/-} mutants (Fig. 2). At the secretory and transition stages, ameloblasts from *Ltbp3*^{-/-} mice showed no obvious morphological changes compared with ameloblasts from WT mice, although the papillary layer underneath ameloblasts appeared impaired (Fig. 2A–H). Then, during the maturation stage, ameloblasts displayed a clearly disrupted morphology in mutants, especially within the lateral region of the incisor where the most severe ameloblast differentiation defects were observed (Fig. 2L). In addition, the ameloblast columnar epithelium was reduced in thickness within the central region (Fig. 2K). All these changes were more severe at postmaturation stages (Fig. 2M–P; compare WT with *Ltbp3*^{-/-}).

Small bulbous-like formations inside molar roots

Micro-CT analysis allows us to segment each tissue according to its density, using different density thresholds. Using this method, we performed morphometric analysis of the skull and facial bones of *Ltbp3*^{-/-} mice (Figs S1, S2). We were also able to segment the enamel to calculate the enamel volume (Fig. 3A,B; Fig. S3). The enamel volume of *Ltbp3*^{-/-} mice was significantly reduced in all teeth (Fig. S3). In molars, even in the case of complete absence of enamel, the molar cusp pattern was maintained (Fig. 3C,D). As seen in Fig. 3C,D, the overall root pattern and molar surfaces, as revealed by

3D micro-CT, appear well preserved. However, irregular circles (bulbous-like structures) were seen, with an apparent random distribution on the mesial and/or distal molar roots, especially for M1 (Fig. 3H; yellow arrowhead). From histological analysis, small circle-like growths were observed within *Ltbp3*^{-/-} roots, in contrast to the smooth mineralization pattern in roots from WT mice (Fig. 3I,J; red arrows). These findings indicate that LTBP-3 is not critical for proper root formation, but has important actions in ameloblasts in regulating proper differentiation of enamel.

Enamel prism pattern malformations and reduced cementum thickness – scanning electron microscopy analysis

Figure 4 shows enamel prism patterns on sagittal views of the lower incisor, which were obtained by high-resolution scanning electron microscopy. Mineralization starts by forming an enamel ribbon, with ameloblasts in WT incisors secreting a rod-like structure. This typical pattern was not observed in the *Ltbp3*^{-/-} incisors (Fig. 4A,B). Figure 4C shows normal decussating enamel rods, with adjacent rows that criss-cross near the dentinoenamel junction. In contrast, enamel from *Ltbp3*^{-/-} mice was poorly organized, with a clearly impaired prism pattern (Fig. 4D) and almost no rod pattern at the incisal edge (Fig. 4F). At its thickest area, the enamel from *Ltbp3*^{-/-} teeth appears to be more porous (Fig. 4G,H). The whole outer enamel pattern, oriented in the opposite direction of the inner enamel, exhibited a disturbed structure (Fig. 4L; arrowhead). These observations suggest that ameloblasts from *Ltbp3*^{-/-} mice fail to complete enamel formation.

Similar alterations in enamel formation were also found in molars, consistent with the observations made for incisors (Fig. 5). Root regions in *Ltbp3*^{-/-} mutants showed a more condensed, unsteady pattern, according to the presence of bulbous-like formations (Fig. 5B; oval area shown by a broken line), and an irregular distribution of dentinal tubules beneath a reduction of cementum thickness (Fig. 5A,B, white arrowheads; Fig. 5C,D). These findings suggest that LTBP-3 is required for ameloblasts to secrete a proper enamel matrix, to establish a typical enamel rod structure, and for formation of normal dentinal tissue.

Discussion

Transforming growth factor- β proteins are thought to play a major role in the morphogenesis of developing teeth (14). Both TGF- β 1 and TGF- β 3 are produced by the enamel organ and are activated by components of the basement membrane, including those induced by odontoblast differentiation (28). Inactivation of the *Tgfbr2* gene (which encodes TGF- β receptor II) increases the proliferation of odontogenic epithelial cells (29). Both *Tgfbr2* conditional knockout mice and *Tgf β 1* over-expressing transgenic mice exhibit an abnormal tooth phenotype at early stages of enamel

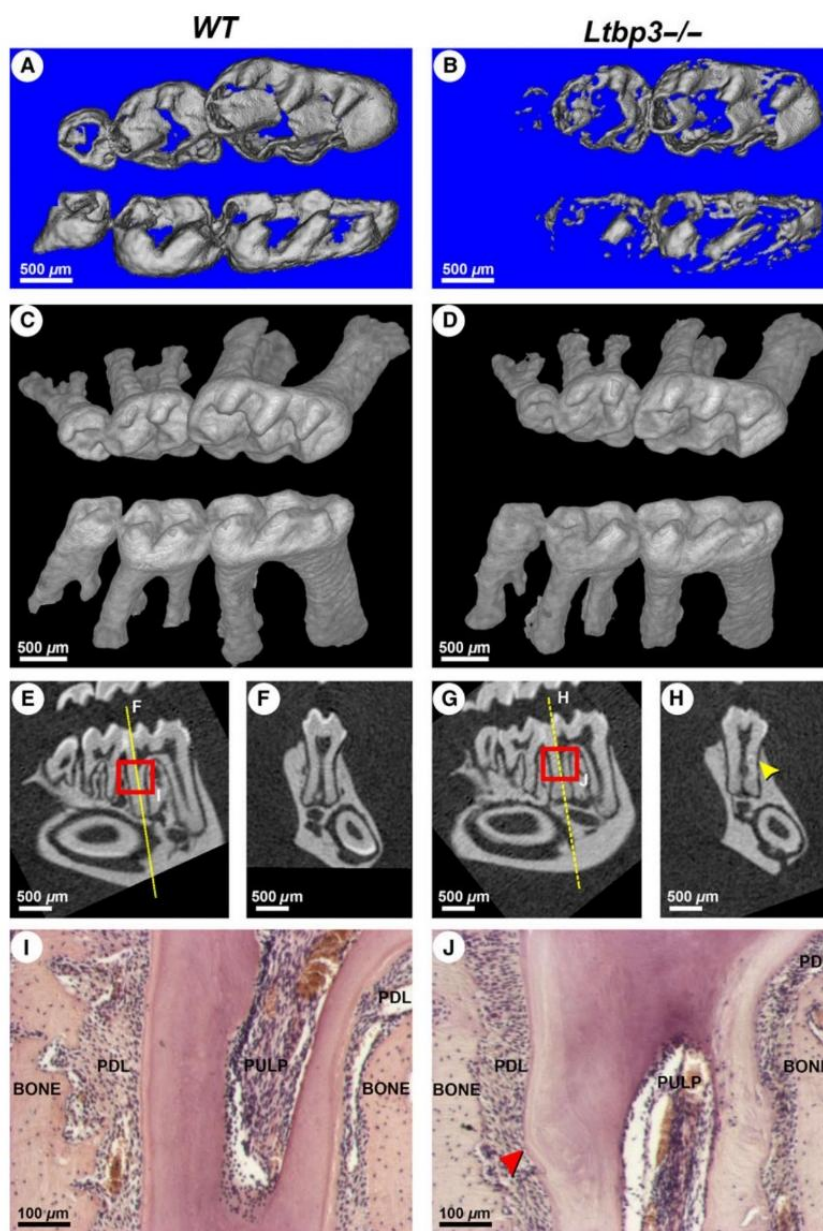


Fig. 3. Alterations of enamel in molars and the molar root phenotype in latent transforming growth factor beta binding protein mutant (*Ltbp3*^{-/-}) mice. (A, B) High-density renderings of micro-computed tomography (micro-CT) data from wild-type (WT) and *Ltbp3*^{-/-} molars, highlighting enamel structural deficits. The enamel volume of the *Ltbp3*^{-/-} molar is significantly reduced, especially at the third molar (also see Fig. S3). (C, D) Three-dimensional rendering of micro-CT images showing less density in molar crowns of *Ltbp3*^{-/-} mice. The root pattern of *Ltbp3*^{-/-} mice is similar to that of WT mice. (E–H) Two-dimensional sections confirming enamel reduction in both molars and incisors of *Ltbp3*^{-/-} mutants. Section planes (F, H) are generated at the level of the yellow line. (H) A bulbous-like structure can be found in some areas of *Ltbp3*^{-/-} molar roots (yellow arrowhead). (I, J) Histology (hematoxylin and eosin staining; regions highlighted by red boxes in E and G) showing a correctly organized root dentin in the lower molar of WT mouse, whereas irregular dentin staining is seen in the *Ltbp3*^{-/-} mutant mouse. A bulbous-like structure (red arrowhead) is also observed. The periodontium, cementum, alveolar bone, and dental pulp tissues have no obvious morphological changes at the histological scale. BONE, alveolar bone; PDL, periodontium; PULP, dental pulp tissue.

formation (11, 12). As TGF- β proteins are present in the extracellular matrix as inactive forms, the absence of the targeting LTBP probably results in reduced TGF- β activity, mirroring other *Tgf β* mouse mutant models (15). The incisors of *Ltbp3*^{-/-} mice have a partial white color, with some yellow–orange bands centrally, indicative of loss of enamel, as confirmed by

micro-CT, histology, and scanning electron microscopy analyses. In accordance with this result, TGF- β -activating SMAD2 and SMAD3, and TGF-inhibiting SMAD7, are found both in the enamel epithelium and in the dental mesenchyme, with alterations in these SMAD signaling components producing a variety of tooth phenotypes (14, 30–32).

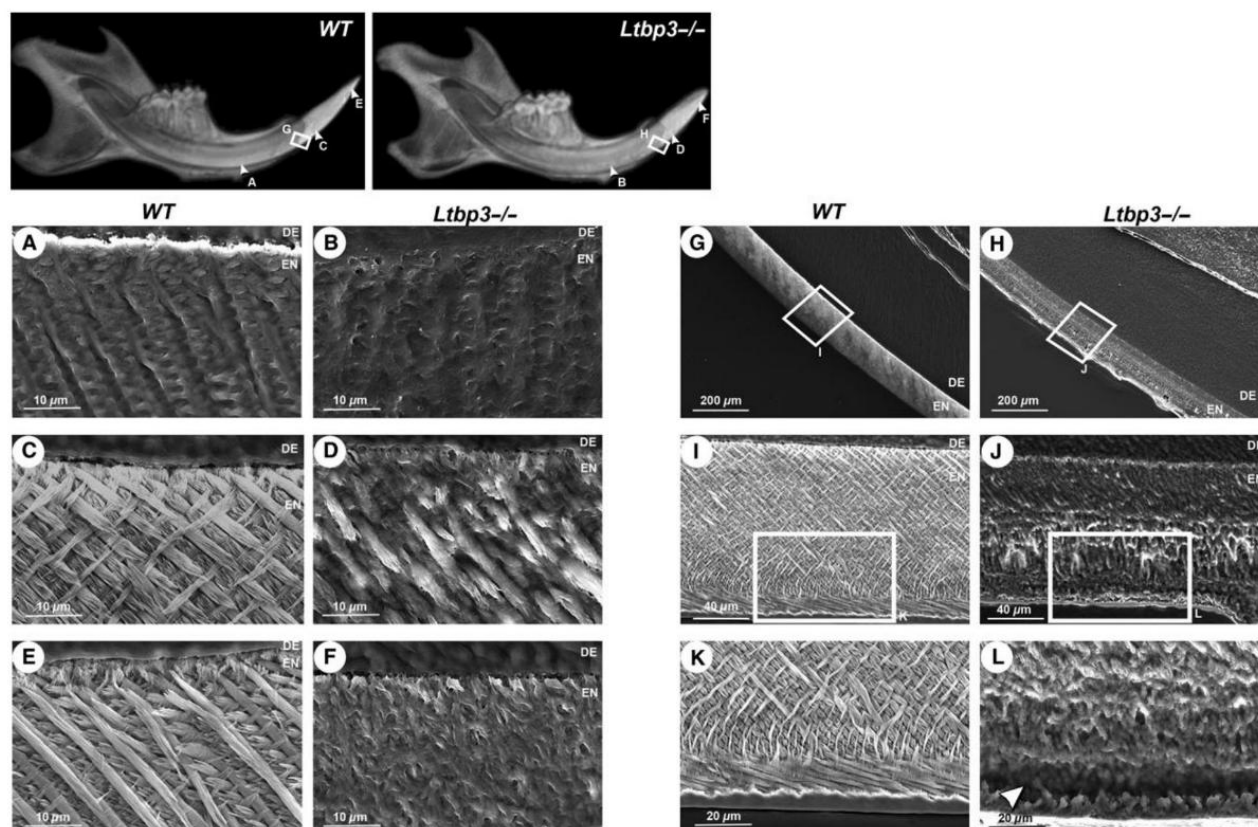


Fig. 4. Comparative scanning electron microscopy images of midsagittal sections of lower incisor enamel at various distances from the incisor extremity (the approximate location of the areas shown is given in the upper, low-magnification views), comparing teeth from wild-type (WT) (A, C, E, G, I, K) and latent transforming growth factor beta binding protein mutant (*Ltp3*^{-/-}) (B, D, F, H, J, L) mice. (A, B) Early maturation stage of enamel crystal deposition showing enamel ribbon patterns in WT mouse, whereas no clear pattern is seen in *Ltp3*^{-/-} mouse. (C, D) Junction area between the alveolar bone crest and crown analog of incisor, showing a criss-cross pattern in WT mouse, whereas a poor organization of enamel rods is observed in *Ltp3*^{-/-} mouse. (E, F) Incisal (or tip) area of incisor showing a typical enamel prism pattern in WT mouse, whereas no such pattern is observed in mutant mouse. (G, H) Fully mineralized enamel showing a rough external surface in *Ltp3*^{-/-} mouse. The enamel thickness in this zone is similar in WT and *Ltp3*^{-/-} mice. Boxed areas indicate areas shown under higher magnification in the next panels. (I, J) The enamel layer appears porous and non-decussated in *Ltp3*^{-/-} mutant mouse compared with WT mouse. (K, L) Under higher magnification, the outer enamel shows poorly organized, non-structured prism patterns (arrowhead), while an increased roughness at the outer enamel surface is also observed in the *Ltp3*^{-/-} mutant. DE, dentin; EN, enamel.

Both histological and micro-CT analyses confirmed alterations in enamel formation in the mutants, with obvious reductions in incisor and molar mineralized enamel volume. A gradient of reduced enamel mineralization seen from central to lateral zones of incisors, and from the first to the third molars, suggests site-specific or temporally defined roles of LTBP-3. In addition, some incisor enamel areas also showed enamel nodules, especially at the lateral zones near the alveolar bone crest, suggesting that enamel formation and ameloblast differentiation are not maintained throughout tooth development. Normal fully formed murine incisor enamel has a decussating mineralized rod pattern. Each rod is presumably formed from a single ameloblast, preserving a complete record of its migratory path during its formation (3). Our scanning electron microscopy analysis showed enamel defects throughout the lower and upper incisors, as the prism patterns always failed to form. Consistently, SMAD3-signaling mutants

showed alterations in enamel mineralization (13). In addition, *Klk4* is down-regulated in 7-d-old *Tgfb2* conditional mouse mutants (12). The phenotypic changes in our *Ltp3*^{-/-} mice suggest that active TGF- β signaling complexes may regulate enamel matrix protein levels and/or enamel proteases, such as KLK-4, thereby regulating dental hard-tissue mineralization.

Severe ameloblast morphological alterations are observed at the maturation stage, revealed as both shortening and severe morphological alterations of these cells. Transforming growth factor- β family members are known to regulate blood-vessel formation and hematopoiesis (33), and in our histological analysis we observed some vessel enlargements and an impaired papillary layer below the ameloblasts. This suggests that the ameloblast alterations may potentially be caused by a vascularization defect, although this hypothesis will need further analysis to be substantiated. It has been reported that transgenic over-

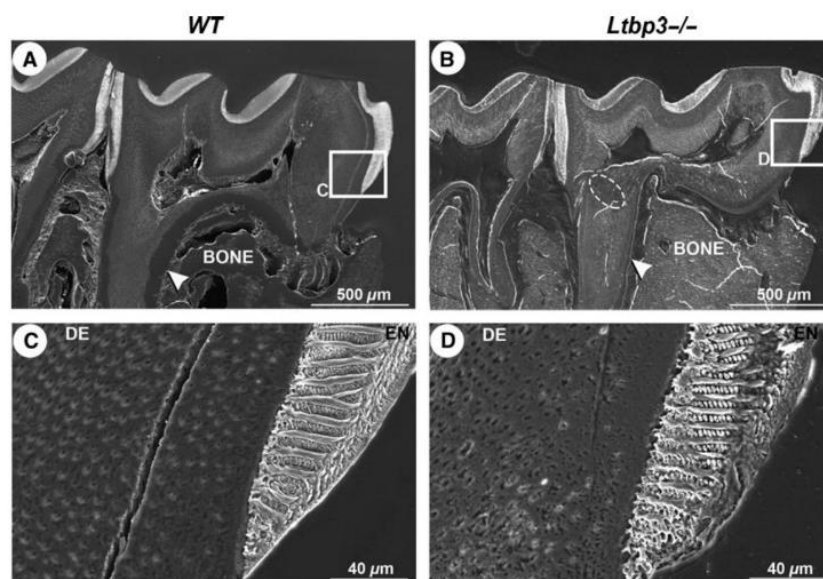


Fig. 5. Scanning electron microscopy analysis of sagittal sections of lower molars. (A, B) In this section of the mid-sagittal plane, the enamel thickness observed in the molar of latent transforming growth factor beta binding protein mutant (*Ltbp3*^{-/-}) mouse is nearly identical to that of wild-type (WT) mouse. The white arrows (A, B) indicate the cementum thickness, and the dashed oval (B) indicates a bulbous-like formation. (C, D) Higher-magnification views (boxed areas in A, B), showing an irregular organization of the enamel rods and a rough outer surface in the molar from *Ltbp3*^{-/-} mouse compared with that from WT mouse. The dentinal tubule distribution is also impaired. BONE, alveolar bone; DE, dentin.

expression of TGF- β 1 in early secretory stage ameloblasts triggers dentin adhesion and the formation of cyst-like structures and mineralized globules (11). The loss of enamel ribbon formation observed in *Ltbp3*^{-/-} mice confirms that enamel defects must start at the beginning of enamel deposition, suggesting that LTBP-3 signaling regulates enamel mineralization at early stages, with the effects continuing through amelogenesis.

Dental-targeted over-expression of TGF- β 1 (using a *Dspp-Tgfb1* transgene) results in a phenotype similar to dentin dysplasia (34), and over-expression of TGF- β 2 in the dentin matrix results in the reduction of dentin hardness and elasticity in male mice (35). Our histological analysis shows no obvious changes in dentin or odontoblasts in *Ltbp3*^{-/-} mutants. Osteodentin, which was found in teeth from *Dspp-Tgfb1* transgenic mice (11), was not found in *Ltbp3*^{-/-} mice. Even so, scanning electron microscopy analysis reveals that *Ltbp3*^{-/-} mice have an impairment of dentinal tubular patterns, suggesting an indirect effect through alterations of enamel differentiation.

Some regions of the *Ltbp3*^{-/-} molar roots have irregular bulbous-like formations under the cementum. Despite this, the overall root pattern is consistently similar to that of WT mice. *In vivo* assays of TGF- β signaling effects in ameloblasts using Ki67, a cellular marker for proliferation, showed marked proliferation in the Hertwig's epithelial root sheath (HERS) at postnatal day 7 (12). Likewise, the presence of LTBP-3 in outer dental epithelium could regulate molar proliferation (24), explaining the reduction of cementum thickness.

Ltbp3^{-/-} mice also had striking craniofacial defects, such as reductions of viscerocranium and dome-shape neurocranium, which suggests premature ossification of some cranial sutures (19). Our results are consistent with previous work on *Ltbp3*^{-/-} mice, which described craniofacial malformations (20) and a high bone-mass phenotype (21). Our measurements show that the reduction of the upper jaw is greater than that of the mandible (see molar relationship classification in Fig. S4).

Our previous study reported that four unrelated families had mutations in *LTBP3*, which probably produced AI and brachyolmia phenotypes. This highlights the role of LTBP-3 and TGF- β signaling in amelogenesis (24). Here, our findings of morphological changes within all tooth components, including enamel and ameloblasts, of *Ltbp3*-knockout mice supports multiple roles of LTBP-3 in odontogenesis. Understanding how LTBP-3 regulates hard-tissue mineralization and tooth development might provide treatment strategies for patients with a variety of craniofacial anomalies.

The *Ltbp3*^{-/-} mouse phenotype described herein is characterized by severe enamel defects and overlaps with those of human *LTBP3* mutations and mouse mutants for other genes of the TGF- β pathway. This study demonstrates that LTBP-3 is necessary for initiating and maintaining an enamel matrix, for regulating ameloblast differentiation, for complete enamel prism formation, and for establishing root mineralization.

Acknowledgements – We would like to thank Brigitte Schuhbaug and Valérie Fraulob for their help in histological procedures, Isabelle Goncalves Da Cruz for her help in micro-CT training, and Arnaud Duchon for his expertise in applying 3D landmark coordinates analysis. This work was supported by a training grant from

the Centre Européen de Recherche en Biologie et en Médecine (CERBM GIE), institutional funds from the CNRS, Inserm, and University of Strasbourg, grants from the French Ministry of Health (National Program for Clinical Research, PHRC 2005 #4266 'Amelogenesis imperfecta', HUS, API 2009-2012 'Development of the oral cavity: from gene to clinical phenotype in Human'), and IFRO (Institut Français pour la Recherche Odontologique) to Agnès Bloch-Zupan, grant CA034282 from the National Institutes of Health to Daniel B. Rifkin, and Franco-Thai and Khon Kaen University scholarships to Supawich Morkmued. This initiative is supported by the project #1.7 'RARENET: a tri-national network for education, research and management of complex and rare diseases in the Upper Rhine' co-financed by the European Regional Development Fund (ERDF) of the European Union in the framework of the INTERREG V Upper Rhine program. Agnès Bloch-Zupan is a 2015 Fellow of the Institute of Advanced Studies (USIAS) of the University of Strasbourg.

Conflicts of interest – The authors have no conflict of interest to declare.

References

- HABELITZ S. Materials engineering by ameloblasts. *J Dent Res* 2015; **94**: 759–767.
- PUGACH MK, GIBSON CW. Analysis of enamel development using murine model systems: approaches and limitations. *Front Physiol* 2014; **5**: 313.
- SIMMER JP, RICHARDSON AS, HU YY, SMITH CE, CHING-CHUN HU J. A post-classical theory of enamel biomineralization.. and why we need one. *Int. J Oral Sci* 2012; **4**: 129–134.
- SIMMER JP, PAPAGERAKIS P, SMITH CE, FISHER DC, ROUNTREY AN, ZHENG L, HU JC. Regulation of dental enamel shape and hardness. *J Dent Res* 2010; **89**: 1024–1038.
- BARTLETT JD, SIMMER JP. Kallikrein-related peptidase-4 (KLK4): role in enamel formation and revelations from ablated mice. *Front Physiol* 2014; **5**: 240.
- BARTLETT JD, SKOBE Z, NANJI A, SMITH CE. Matrix metalloproteinase 20 promotes a smooth enamel surface, a strong dentino-enamel junction, and a decussating enamel rod pattern. *Eur J Oral Sci* 2011; **119**(Suppl 1): 199–205.
- HATAKEYAMA J, FUKUMOTO S, NAKAMURA T, HARUYAMA N, SUZUKI S, HATAKEYAMA Y, SHUM L, GIBSON CW, YAMADA Y, KULKARNI AB. Synergistic roles of amelogenin and ameloblastin. *J Dent Res* 2009; **88**: 318–322.
- HU JC, HU Y, SMITH CE, MCKEE MD, WRIGHT JT, YAMAKOSHI Y, PAPAGERAKIS P, HUNTER GK, FENG JQ, YAMAKOSHI F, SIMMER JP. Enamel defects and ameloblast-specific expression in Enam knock-out/lacZ knock-in mice. *J Biol Chem* 2008; **283**: 10858–10871.
- WAN M, CAO X. BMP signaling in skeletal development. *Biochem Biophys Res Commun* 2005; **328**: 651–657.
- CHEN G, DENG C, LI YP. TGF-beta and BMP signaling in osteoblast differentiation and bone formation. *Int J Biol Sci* 2012; **8**: 272–288.
- HARUYAMA N, THYAGARAJAN T, SKOBE Z, WRIGHT JT, SEPTIER D, SREENATH TL, GOLDBERG M, KULKARNI AB. Overexpression of transforming growth factor-beta1 in teeth results in detachment of ameloblasts and enamel defects. *Eur J Oral Sci* 2006; **114**(Suppl 1): 30–34; discussion 39–41, 379.
- CHO A, HARUYAMA N, HALL B, DANTON MJ, ZHANG L, ARANY P, MOONEY DJ, HARICHANE Y, GOLDBERG M, GIBSON CW, KULKARNI AB. TGF-ss regulates enamel mineralization and maturation through KLK4 expression. *PLoS ONE* 2013; **8**: e82267.
- YOKOZEKI M, AFANADOR E, NISHI M, KANEKO K, SHIMOKAWA H, YOKOTE K, DENG C, TSUCHIDA K, SUGINO H, MORIYAMA K. Smad3 is required for enamel biomineralization. *Biochem Biophys Res Commun* 2003; **305**: 684–690.
- KLOPCIC B, MAASS T, MEYER E, LEHR HA, METZGER D, CHAMON P, MANN A, BLESSING M. TGF-beta superfamily signaling is essential for tooth and hair morphogenesis and differentiation. *Eur J Cell Biol* 2007; **86**: 781–799.
- KUBICZKOVA L, SEDLARIKOVA L, HAJEK R, SEVCIKOVA S. TGF-beta - an excellent servant but a bad master. *J Transl Med* 2012; **10**: 183.
- TODOROVIC V, RIFKIN DB. LTBP3s, more than just an escort service. *J Cell Biochem* 2012; **113**: 410–418.
- LI X, YIN W, PEREZ-JURADO L, BONADIO J, FRANCKE U. Mapping of human and murine genes for latent TGF-beta binding protein-2 (LTBP2). *Mamm Genome* 1995; **6**: 42–45.
- YIN W, SMILEY E, GERMILLER J, MECHAM RP, FLORER JB, WENSTRUP RJ, BONADIO J. Isolation of a novel latent transforming growth factor-beta binding protein gene (LTBP-3). *J Biol Chem* 1995; **270**: 10147–10160.
- DABOVIC B, CHEN Y, COLAROSSO C, OBATA H, ZAMBUTO L, PERLE MA, RIFKIN DB. Bone abnormalities in latent TGF-[beta] binding protein (Ltbp)-3-null mice indicate a role for Ltbp-3 in modulating TGF-[beta] bioavailability. *J Cell Biol* 2002; **156**: 227–232.
- DABOVIC B, CHEN Y, COLAROSSO C, ZAMBUTO L, OBATA H, RIFKIN DB. Bone defects in latent TGF-beta binding protein (Ltbp)-3 null mice; a role for Ltbp in TGF-beta presentation. *J Endocrinol* 2002; **175**: 129–141.
- DABOVIC B, LEVASSEUR R, ZAMBUTO L, CHEN Y, KARSENTY G, RIFKIN DB. Osteopetrosis-like phenotype in latent TGF-beta binding protein 3 deficient mice. *Bone* 2005; **37**: 25–31.
- NOOR A, WINDPASSINGER C, VITCU I, ORLIC M, RAFIQ MA, KHALID M, MALIK MN, AYUB M, ALMAN B, VINCENT JB. Oligodontia is caused by mutation in LTBP3, the gene encoding latent TGF-beta binding protein 3. *Am J Hum Genet* 2009; **84**: 519–523.
- DUGAN SL, TEMME RT, OLSON RA, MIKHAILOV A, LAW R, MAHMOOD H, NOOR A, VINCENT JB. New recessive truncating mutation in LTBP3 in a family with oligodontia, short stature, and mitral valve prolapse. *Am J Med Genet A* 2015; **167**: 1396–1399.
- HUCKERT M, STOETZEL C, MORKMUED S, LAUGEL-HAUSHALTER V, GEOFFROY V, MULLER J, CLAUS F, PRASAD MK, OBRY F, RAYMOND JL, SWITALA M, ALEMBIK Y, SOSKIN S, MATHIEU E, HEMMERLE J, WEICKERT JL, DABOVIC BB, RIFKIN DB, DHEEDENE A, BOUDIN E, CALUSERIU O, CHOLETTE MC, MCLEOD R, ANTEQUERA R, GELLE MP, COEURIOT JL, JACQUELIN LF, BAILLEUL-FORESTIER I, MANIERE MC, VAN HUL W, BERTOLA D, DOLLE P, VERLOES A, MORTIER G, DOLLFUS H, BLOCH-ZUPAN A. Mutations in the latent TGF-beta binding protein 3 (LTBP3) gene cause brachyolmia with amelogenesis imperfecta. *Hum Mol Genet* 2015; **24**: 3038–3049.
- VERLOES A, JAMBLIN P, KOULISCHER L, BOURGUIGNON JP. A new form of skeletal dysplasia with amelogenesis imperfecta and platyspondyly. *Clin Genet* 1996; **49**: 2–5.
- RICHTSMEIER JT, LELE S. A coordinate-free approach to the analysis of growth patterns: models and theoretical considerations. *Biol Rev Camb Philos Soc* 1993; **68**: 381–411.
- COLE III TM, LELE S, RICHTSMEIER JT. A parametric bootstrap approach to the detection of phylogenetic signals in landmark data. In: MACLEOD N, FOREY PL, eds. *Morphology, shape and phylogeny*. London: Taylor & Francis, 2002; 194–219.
- LESOT H, LISI S, PETERKOVA R, PETERKA M, MITOLO V, RUCH JV. Epigenetic signals during odontoblast differentiation. *Adv Dent Res* 2001; **15**: 8–13.
- CHAI Y, ZHAO J, MOGHAREI A, XU B, BRINGAS P Jr, SHULER C, WARBURTON D. Inhibition of transforming growth factor-beta type II receptor signaling accelerates tooth formation in mouse first branchial arch explants. *Mech Dev* 1999; **86**: 63–74.
- XU X, JEONG L, HAN J, ITO Y, BRINGAS P Jr, CHAI Y. Developmental expression of Smad1-7 suggests critical function of TGF-beta/BMP signaling in regulating epithelial-mesenchymal interaction during tooth morphogenesis. *Int J Dev Biol* 2003; **47**: 31–39.
- ITO Y, ZHANG YW. A RUNX2/PEBP2alphaA/CBFA1 mutation in cleidocranial dysplasia revealing the link between the gene and Smad. *J Bone Miner Metab* 2001; **19**: 188–194.
- FERGUSON CA, TUCKER AS, HEIKINHEIMO K, NOMURA M, OH P, LI E, SHARPE PT. The role of effectors of the activin

- signalling pathway, activin receptors IIA and IIB, and Smad2, in patterning of tooth development. *Development* 2001; **128**: 4605–4613.
33. MASSAGUE J. TGF[β] signalling in context. *Nat Rev Mol Cell Biol* 2012; **13**: 616–630.
 34. THYAGARAJAN T, SREENATH T, CHO A, WRIGHT JT, KULKARNI AB. Reduced expression of dentin sialophosphoprotein is associated with dysplastic dentin in mice overexpressing transforming growth factor- β 1 in teeth. *J Biol Chem* 2001; **276**: 11016–11020.
 35. SAEKI K, HILTON JF, ALLISTON T, HABELITZ S, MARSHALL SJ, MARSHALL GW, DENBESTEN P. Elevated TGF- β 2 signaling in dentin results in sex related enamel defects. *Arch Oral Biol* 2007; **52**: 814–821.

Supporting Information

Additional Supporting Information may be found in the online version of this article:

Fig. S1. Anatomical landmarks used for morphometric analysis.

Fig. S2. Form difference matrix analysis of skulls and mandibles.

Fig. S3. Bar graph of mean enamel volume of *WT* vs. *Ltbp3*^{-/-} mutants.

Fig. S4. Molar relationship classification: the wild-type mice have molar class I occlusions (a normal occlusion), but *Ltbp3*^{-/-} mutants have a class III molar bite (otherwise known as an anterior bite).

SUPPORTING INFORMATION

Enamel and dental anomalies in latent transforming growth factor-beta binding protein 3 (*LTBP3*) mutant mice

**MORKMUED S, HEMMERLE J, MATHIEU E, LAUGEL-HAUSHALTER V, DABOVIC B, RIFKIN DB,
DOLLÉ P, NIEDERREITHER K, BLOCH-ZUPAN A**

Université de Strasbourg, Faculté de Chirurgie Dentaire, Strasbourg, France; Université de Strasbourg, Institut de Génétique et de Biologie Moléculaire and Cellulaire, Illkirch, France; Khon Kaen University, Faculty of Dentistry, Khon Kaen, Thailand; Université de Strasbourg, Biomaterials and Bioengineering, Inserm Strasbourg, France; Department of Cell Biology, New York University Medical Center, New York, NY, USA; Hôpitaux Universitaires de Strasbourg, Strasbourg, France.

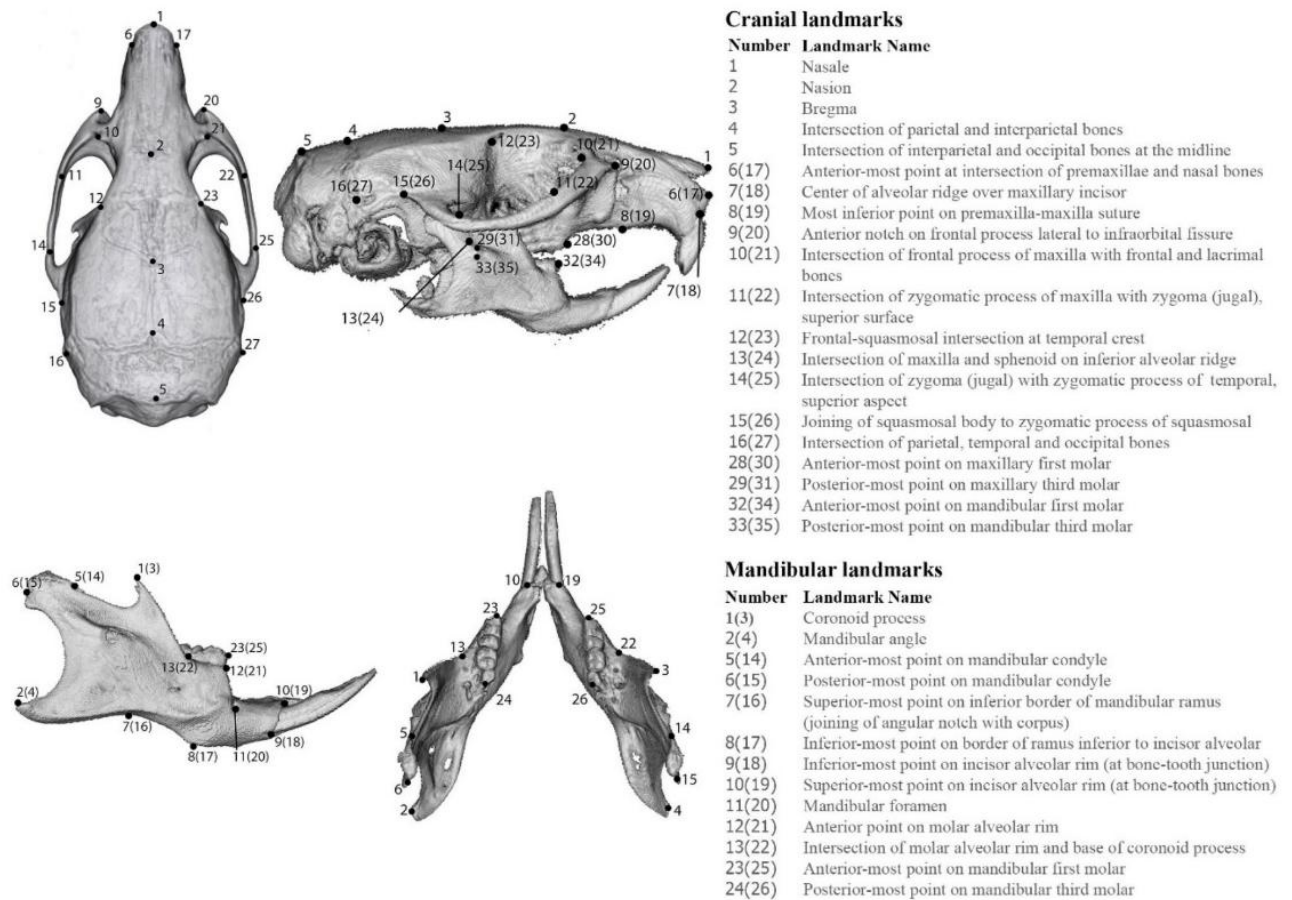


Figure S1. Anatomical landmarks used for morphometric analysis. Thirty-five points have been chosen to characterize the dimensions and the shape of the head. Twenty-six points have been chosen to characterize the mandible. For bilateral landmarks the right-side points are given in parentheses.

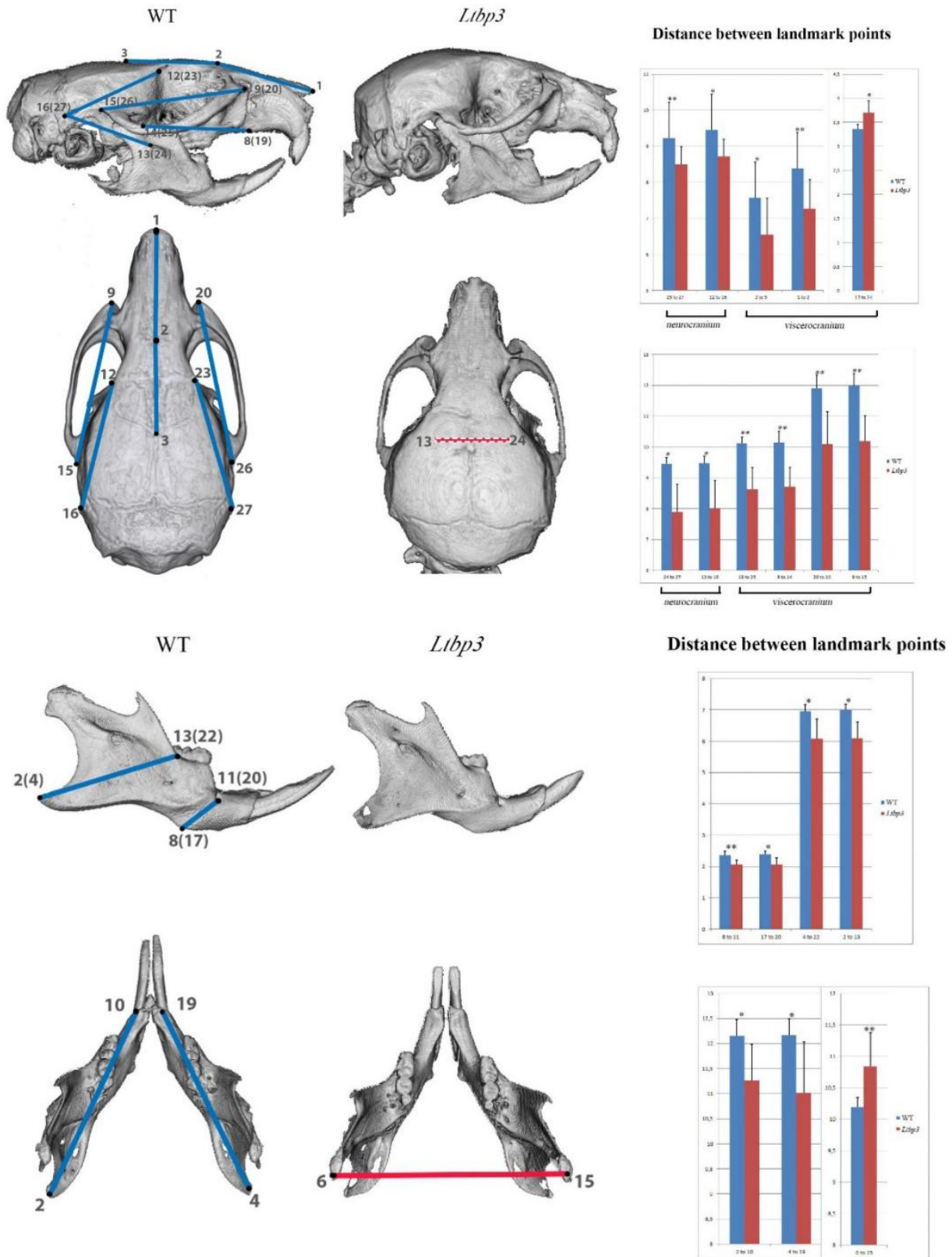


Figure S2. Form difference matrix analysis of skulls and mandibles. *WT* mice are shown in blue compared with *Ltbp3*^{-/-} mice shown in red. Neurocranium and viscerocranium (lengthwise measurements) are shorter in *Ltbp3*^{-/-} mutants. Crosswise measurements, for example taken at the mandibular condyle (between points 6 and 15) show *Ltbp3*^{-/-} mice are

wider. The bar graph shows the re-calculated length distances of the significant differences between each landmark points. * $p \leq 0.05$, ** $p \leq 0.01$, *** $p \leq 0.001$.

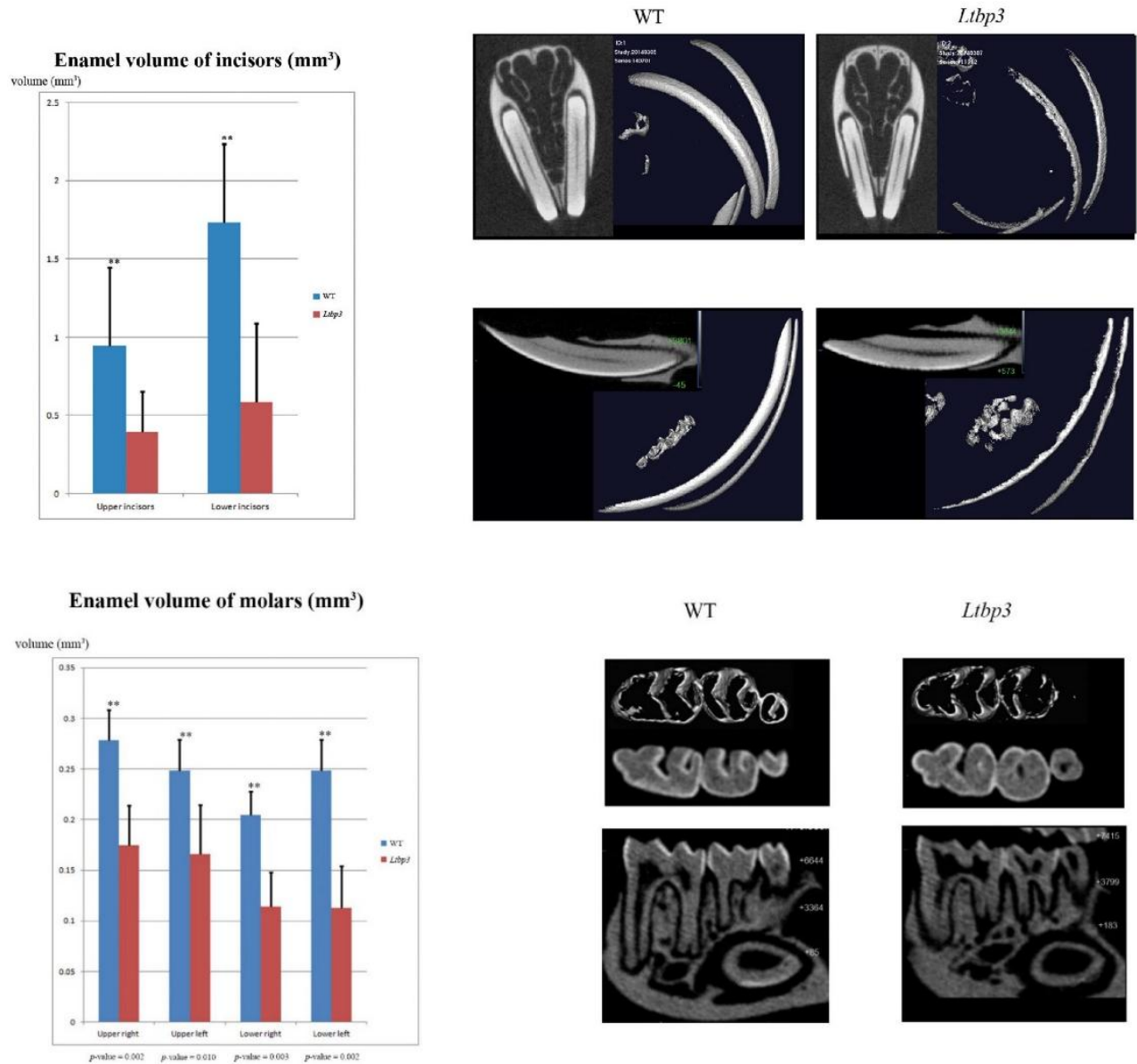


Figure S3. Bar graph of mean enamel volume of *WT* vs. *Ltbp3*^{-/-} mutants. Incisors are shown in upper graphs and molars are shown in lower graphs. The 2D and 3D images of upper and lower incisors showing enamel defects are shown in respective panels. Mutant samples are shown on the far right side. The 2D and 3D images of molars show the overall extent of *Ltbp3*^{-/-} mutant enamel defects. The enamel deficiency is most severe in M3 of the mutant.

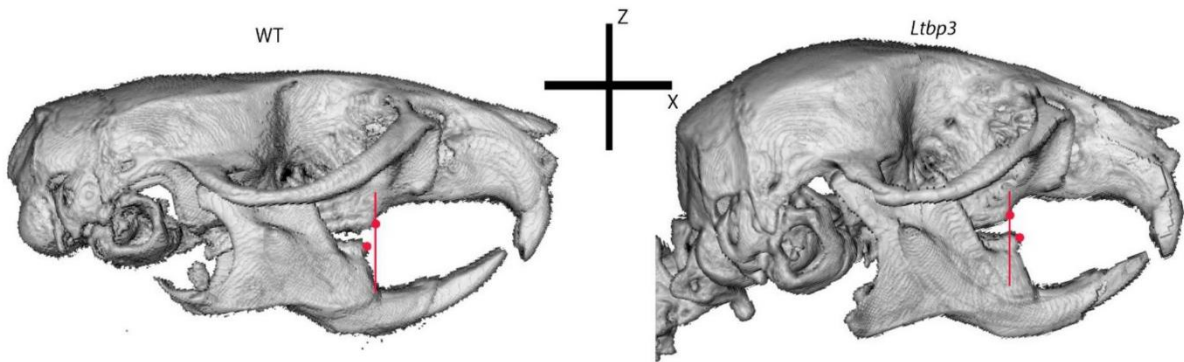


Figure S4. Molar relationship classification: the wild-type mice have molar class I occlusions (a normal occlusion), but *Ltbp3* $-/-$ mutants have a class III molar bite (otherwise known as an anterior bite).

Craniofacial and tooth abnormalities in Sparc-related modular calcium-binding protein 2 (*Smoc2*) mutant mice

Supawich Morkmued, Francois Clauss, Brigitte Schuhbaur, Valerie Fraulob, Eric Mathieu, Joseph Hemmerlé, Pascal Dollé, Karen Niederreither, and Agnès Bloch-Zupan

Craniofacial and tooth abnormalities in Sparc-related modular calcium-binding protein 2 (*Smoc2*) mutant mice

Supawich Morkmued¹⁻⁵, Francois Clauss⁶⁻⁸, Brigitte Schuhbaur¹⁻⁴, Valerie Fraulob¹⁻⁴, Eric Mathieu⁹, Joseph Hemmerlé⁹, Pascal Dollé^{1-4,10}, Karen Niederreither^{1-4,6*}, and Agnès Bloch-Zupan^{1-4,6-7,11-12*}

¹Developmental Biology and Stem Cells Department, Institute of Genetics and Molecular and Cellular Biology (IGBMC), 1 rue Laurent Fries, BP 10142, 67404 Illkirch, France

²Centre National de la Recherche Scientifique, UMR 7104, Illkirch, France

³Institut National de la Santé et de la Recherche Médicale, U 964, Illkirch, France

⁴Université de Strasbourg, Illkirch, France

⁵Faculty of Dentistry, Pediatrics Department, Khon Kaen University, Khon Kaen, Thailand

⁶Université de Strasbourg, Faculté de Chirurgie Dentaire, 8 rue Ste Elisabeth, 67000 Strasbourg, France

⁷Hôpitaux Universitaires de Strasbourg, Pôle de Médecine et Chirurgie Bucco-Dentaires, Centre de Référence des Manifestations Odontologiques des Maladies Rares, CRMR, O Rares, 1 place de l'Hôpital, 67000 Strasbourg, France

⁸Osteoarticular and Dental Regenerative NanoMedicine, Inserm UMR 1109, 11 rue Humann 67000 Strasbourg, France Hôpitaux Universitaires de Strasbourg.

⁹Université de Strasbourg, INSERM UMR_1121, Biomaterials and Bioengineering, 11 rue Humann, 67000 Strasbourg, France

¹⁰Université de Strasbourg, Faculté de Médecine, FMTS, 4 Rue Kirschleger, 67000 Strasbourg, France

¹¹Université de Strasbourg, Institut d'Études Avancées de l'Université de Strasbourg (USIAS), 5 allée du Général Rouvillois, 67083 Strasbourg, France

¹²Eastman Dental Institute, University College London, London, UK

* Correspondence:

Dr. Karen Niederreither (niederre@igbmc.fr)

Pr. Agnès Bloch-Zupan (agnes.bloch-zupan@unistra.fr)

Abstract

Secreted components of the extracellular matrix have multiple actions enabling proliferation, adhesion, and osteogenesis during craniofacial development, actions that can be reapplied during organ repair events such as wound healing. We have investigated the function of the secreted matrixcellular protein Smoc2 (SPARC related modular calcium binding 2), whose *SMOC2* human null mutation produces oral anomalies including dentin dysplasia, oligodontia, microdontia, and jaw ossification deficits. In the mouse *Smoc2-GFP* lineage tracing was performed showing dental stem-specific localization, and enrichment at other progenitor sites. We generated a mouse *Smoc2* mutation identical to that found in our patients, finding murine deletion slightly reduced tooth size, altered enamel prism pattern, and locally perturbed periodontal tissue. RNA-seq analysis indicated limited number of targets might produce these discrete defects. These included the enamel matrix protein *ODAM*, *dentin sialophosphoprotein*, integrins, and ERK signaling pathway targets that might be involved in inflammation, cell proliferation, and differentiation. To address the effects of clinical challenges, we tested osteogenic response following molar extraction. X-ray microtomography imaging revealed *Smoc2*^{-/-} mutants had reduced bone regrow and increased bone resorption around the extracted teeth, potentially due to increased inflammation and osteoclast recruitment. Molecularly SMOC2 induces cell growth via ERK-dependent signaling, cyclin-induced proliferation, proangiogenic actions, and/or NF-κB modulation of inflammation. Experiments are in progress to test probable mechanisms of SMOC2-dependent dental-induction and bone regeneration.

Introduction

Growing cells develop amidst a secreted fibrotic extracellular environment, providing not only structural support- but also having a bioactive role promoting growth and cell attachment. Here we investigate the functional roles of SMOC2 (SPARC related modular calcium binding 2 protein), a member of the secreted protein acidic/rich in cysteines (SPARCs) family of matricellular proteins. Matricellular proteins are non-structural components of extracellular matrix (ECM) often increasing growth factor signaling(Murphy-Ullrich and Sage, 2014) and promoting wound repair(Jun et al., 2015). In vitro studies suggest SMOC2 promotes keratinocyte attachment(Maier et al., 2008) and angiogenesis(Rocnik et al., 2006). Its preferential enrichment in colon(Muñoz et al., 2012), myeloid(Mommaerts et al., 2014), and dental(Bloch-Zupan et al., 2011) stem cell lineages suggests functions in progenitor maintenance and/or cell anoikis(Mommaerts et al., 2014;Brady et al., 2016;Shvab et al., 2016). Clinically high SMOC2 levels signal poor cancer survival(Su et al., 2016), marking highly aggressive metastatic cancers(Brady et al., 2016;Shvab et al., 2016). SMOC2 also induces TGF- β , in turn driving pathological fibrosis that often accompanies end-stage organ failure(Gerarduzzi et al., 2017). Strategies reducing SMOC2 levels have been suggested to have numerous therapeutic implications. Patients with homozygous *SMOC2* mutations have specific defects in the developing dentition. These include oligodontia (reduced tooth number), microdontia (small teeth), dentin dysplasia, and reduced alveolar/jaw bone density(Bloch-Zupan et al., 2011;Alfawaz et al., 2013). We generated a *Smoc2* inactivating mouse model with an intron 1 splice donor site mutation mimicking patient defects (Bloch-Zupan et al., 2011). The murine model displays small, but sustained growth reductions. In general, mouse mutants survive normally with few pathological consequences, somewhat similar to reports on *SMOC2* mutated children(Bloch-Zupan et al., 2011). Like other matricellular proteins(Jun et al., 2015), SMOC2 appears critical for the repair process. Following 1st molar extraction, *Smoc2*^{-/-} mutants had impaired bone healing (mimicking osteonecrosis). We are testing if strategies modulating the SMOC2-induced secretome/inflammation might be advantageously applied for dental treatment alleviating jaw osteonecrosis-like symptoms(Zhang et al., 2013) - a frequent derisive consequence of tooth extraction during bisphosphonate osteoporosis treatment.

Experimental Procedures/Methods

Patient

The patients with a homozygous *SMOC2* mutation were initially described (Bloch-Zupan et al., 2011) as part of a French Ministry of Health National Program for Clinical Research, PHRC 2008 HUS (Strasbourg University Hospital) N°4266 and in the INTERREG IV Offensive Sciences A27 “Orofacial manifestation of rare diseases” EU funded (ERDF) project. The 2 cousins and their family members gave informed written consent and documents for the D[4]/phenodent registry, a Diagnosing Dental Defects Database [see www.phenodent.org, to access assessment form], which is approved by CNIL (French National commission for informatics and liberty, number 908416). They were examined and followed up at the university of Strasbourg hospital such as X-ray and computed tomography (CT).

Ethics statement

All animals were maintained and manipulated under animal protocols in agreement with the French Ministry of Agriculture guidelines for use of laboratory animals (IGBMC protocol 2012–097) and with NIH guidelines, described in the Guide for the Care and Use of Laboratory Animals. *Smoc2*^{-/-} mouse line was created at the Mouse Clinical Institute (ICS) using Cre and Flp methods (Birling et al., 2012) described in Fig S1 and Table S1.

Immunofluorescence

Smoc2-EGFP-ires-CreERT2 knock-in (*Smoc2-ki*) mice, generated by homologous recombination in embryonic stem cells targeting an *EGFP-ires-CreERT2* cassette at the translational start site of *Smoc2*, from Dr. Hans Clever (Muñoz et al., 2012) were used to perform *GFP* immunofluorescence. E14.5 and E18.5 embryos fixed in 4% paraformaldehyde solution (PFA)/1X PBS for 2 hours, were embedded in melted Ultra-pure LMP agarose gel (Invitrogen, REF16520-100) at a concentration of 4% for E14.5, or 6% for E18.5 in dH₂O in Peel-A-Way embedding molds (Polysciences) prior to cutting using a Leica VT1000 vibratome (thickness = 30 μm). After incubated in blocking solution (10% normal donkey serum in PBT) for 30 min, the primary antibody (Anti-GFP antibody-ChIP Grade (ab290), Abcam) was added overnight. Secondary antibody (Donkey anti-Mouse IgG Secondary Antibody, Alexa Fluor 488) and DAPI (Sigma-D9542, Sigma-Aldrich) staining were performed. Images were acquired with a Leica Leitz DMRB fluorescence microscope.

Quantitative Real-Time (RT-PCR):

To quantitate expression alterations in tooth and bone RT-PCR was performed on age-matched RNA samples for either control or *Smoc2*^{-/-} mutants. For this, total RNA (1 μg) was extracted with the RNeasy Micro-kit and amplified using real-time RT-PCR using SYBR Green Reagents (Qiagen). cDNAs templates were generated using the Oligo-dT primed Superscript II kit (Invitrogen). The SYBR Green incorporation into amplified PCR products was detected in real-time using a Roche 480 LightCycler. Primer sequences listed in Supplemental Table 1, were obtained from “Harvard primer” website <https://pga.mgh.harvard.edu/primerbank/>,

Primerbank, or designed using the Primer3web program. Expression of all genes was normalized to glyceraldehyde-3-phosphate dehydrogenase (*Gapdh*) levels.

X-Ray Microtomography

Smoc2^{-/-} mutant samples were fixed in a 4% PFA for 10-14 days, then washed in demineralised water, then screened for tooth and bone mineral density alterations by X-ray micro-computed tomography (μ CT) imaging using the Quantum FX μ CT Imaging System (Caliper Life Sciences). The threshold to scan bone and tooth was 90 kV and 160 μ A with “Fine” scan option using a pixel size of 10–80 μ m. DICOM images were imported into Analyze software (v11.0; Biomedical Imaging Resource, Mayo Clinic, Rochester, MN) for image reconstruction and bone mineral density comparisons.

Scanning Electron Microscopy

The teeth of 8 week-old *Smoc2*^{-/-} mutants and respective controls dissected from alveolar bone were serially dehydrated in 100% ethanol, transferred into propylene oxide/epon resin (Epon 812 - Euromedex, Souffelweyersheim, France) embedding, followed by sagittal sectioning and diamond paste polishing (Escil, Chassieu, France). Briefly, samples were etched with a 20% citric acid for 2 min, rinsed, dehydrated into pure ethanol and dried. A HUMMER JR sputtering device coated teeth with gold-palladium (Technics, CA, USA). Scanning electron microscopy was then performed using a Quanta 250 ESEM system (FEI Company, Eindhoven, The Netherlands) at an accelerating electron voltage of 5 kV.

RNA Sequencing

Total RNA from female E14.5 molars, along with female E18.5 mandibular bone adjacent to the first molar was obtained from *Smoc2*^{-/-} mutants and respective *WT* controls. Supplemental Experimental Procedures describes mRNA-seq library preparation following defined Illumina protocols. Sequence mapping relative to the mm10/NCBI37 mouse reference genome were performed using Tophat. Only when unique aligned sequence reads obtained was gene expression quantification performed using HTSeq-0.6.1. (Described at <http://www-huber.embl.de/users/anders/HTSeq/doc/overview.html>). For every transcript reads per exon kilobase of model per million sequence reads (RPKM) were then converted to raw read counts, then added for each gene locus. Data normalization was as described (Anders and Huber, 2010) and resolved with the DESeq Bioconductor package. A Benjamini and Hochberg, 1995 (Klipper-Aurbach et al., 1995) -based multiple testing model provided adjusted *p*-values. Transcripts alterations with a RPKM of >1, and an adjusted *p* < 0.050 were considered.

Molar Extraction Methods:

Two to three months-old male *Smoc2*^{-/-} mutants and age-matched controls on the day of wound creation (D0), were deeply anesthetized with i.p. administration of 9% ketamine HCl+ 1% xylazine (10 μ l/g body weight). A blade number 11 scalpel was used to loosen the maxillary left first molar. The tooth was then selectively extracted, removing the crown (leaving the roots intact) by rotating clinical forceps causing the crown to crack. After removal, the

extracted crown was verified for integrity. All *Smoc2*^{-/-} mutants and age-matched controls exhibited no surgical complications following tooth extraction. At 6 weeks after extraction, 7 mice per group were sacrificed and μ CT performed.

Results:

***SMOC2* mutation in a patient produces specific dental abnormalities:**

We continued clinical monitoring of a patient, which had autosomal-recessive mutations in *SMOC2*, predicted to cause loss of gene function (Bloch-Zupan et al., 2011). Figure 1A,B shows respective frontal and lateral radiographic views of the skull of this 13 year-old patient. Extracting μ CT images revealed alveolar bone and associated upper (Fig. 1C) and lower jaw defects (Fig. 1D). For most of the permanent teeth, the lower dentition had a relatively severe oligodontia and microdontia. In addition, the right first mandibular molar had macrodontia (Fig. 1D- red arrowhead). Full-frontal views showed the lower jaw had more severe dentition deficits (Fig. 1E). The Analyze11.0 program allowed image extraction of isolated teeth, showing that a micro-root structure consistently accompanies patient microdontia (Fig. 1E).

Lineage Tracing for *Smoc2* GFP expression:

To assay for how localized *Smoc2* might enact severe tooth growth defects, we performed murine lineage tracing using a *green fluorescent protein* (*GFP*) inserted in frame into the *Smoc2* loci. The group of Dr. Hans Clevers reported germline targeting produced viable *Smoc2* null mutants, with no characterized defects (Muñoz et al., 2012). Indeed, *Smoc2*-driven *GFP* immunolocalization labeled in E14.5 mouse brain (Fig. 2A-telencephalon), eye (Fig. 2B- red arrowhead denotes perioptic mesenchyme), basement nasal epithelial (red arrowhead Fig. 2C), and first molar dental follicle mesenchymal populations (Fig. 2D- red arrowhead). At E18.5 *GFP* localized to hair follicles of the vibrissae (Fig. 2E), lingual (data not shown) and labial cervical loop of the lower incisor (Fig. 2F), and continued within the first and second molar mesenchyme (regions at the cervical loop area predicted analogous to the incisor cervical loop-Fig. 2G). During tooth development the cervical loop function a stem cell zone, functioning not only during incisor and molar development, but also in adult incisors - explaining the capacity of rodent teeth to continuously growth and produce enamel stopping tooth erosion (reviewed in (Renvoise and Michon, 2014)) Hence, with a more transient stability of *GFP* (compared to the high stability of β -galactosidase), a rather dynamic *Smoc2* expression follows organogenesis.

A novel mouse *Smoc2* mutation assimilating patient alterations:

To investigate *SMOC2* function we generated a mouse mutant with genetic alterations recapitulating patient genotype (Bloch-Zupan et al., 2011), and which were predicted to create a complete loss of function (Fig. S1, A and Table S1). Indeed, upon CMV-mediated excision targeted mutation abolished all *Smoc2* mRNA (Fig. S1, C and Table S2), yet produced viable mutants with no compensatory increases in *Smoc1* (Fig. S1, D), a homologous target whose inactivation produces lethality with severe ocular and limbs malformations (Okada et al., 2011).

Long-term monitoring of *Smoc2*^{-/-} mutant (up to 18 months) reveals comparable survival to *WT* (data not shown). Adult *Smoc2*^{-/-} showed slight (less than 5%), non-significant reductions in body weight and overall body length (data not shown). μ CT and surface rendering were

performed to completely assess morphological defects in *Smoc2*^{-/-} mice. Comparing age-matched adults, both incisor and molar number is generally maintained. Discrete cusp morphology changes were observed, nonetheless, still allowing normal dental occlusion (Fig. 3 A,C, E,F). Two dental anomalies were observed. Firstly, there was a significant (~12%, *p*-value<0.01) reduction in the 1st-3rd molar field length (compare Fig. 3E *WT*–green bar vs. Fig. 3F *Smoc2*^{-/-} red bar). In addition, an ectopic 4th molar caudal to the 3rd molar was observed (Fig. 3F –green arrowhead). Hence ~25% of *Smoc2*^{-/-} females display an extra 4th molar, appearing distally. Both molar length and volume reductions, and female the sex-biased appearance of the ectopic 4th molar is provided in Table S3. A μ CT scan screening indicated alveolar bone defect in 7 week-old *Smoc2*^{-/-} mutants (compare yellow arrowheads Fig. 3G *WT*; 3H *Smoc2*^{-/-}). When standard histology was formed on the orange-boxed scanned region, *Smoc2*^{-/-} mutants had reduced alveolar ossification (Fig. 3I *WT*; 3K *Smoc2*^{-/-} noted with yellow arrowheads). Enamel is the hardest mineralized tissue. The dense hydroxyapatite crystals composing enamel show irregular alignments and reduced compaction in *Smoc2*^{-/-} mutant (Fig. 3J *WT*; 3L *Smoc2*^{-/-} . SEM region is indicated on the μ CT scans (region indicated by a small blue box in Fig. 3G *WT*; 3H *Smoc2*^{-/-}). These alterations correlated with the slightly whiter appearance of *Smoc2*^{-/-} mutant incisors (Fig. 3A *WT*; 3C *Smoc2*^{-/-}) - reflecting a minor structural impairment.

Mouse molar extraction model show requirement for SMOC2 for bone healing:

To test the capacity of the alveolar bone to heal, two months-old male *Smoc2*^{-/-} mutants and age-matched controls were deeply anesthetized and the left 1st maxillary molar crown removed (leaving the underlying molar roots intact). Six weeks post-extraction μ CT scan images revealed *Smoc2*^{-/-} mutants displayed a loss of bone around the extracted first molar (Fig. 4A *WT*; 4B *Smoc2*^{-/-}-yellow arrowhead), propagating below the remaining 2nd molar (Fig. 4B red arrowhead). Increased bone loss in *Smoc2*^{-/-} mutants is tabulated (Fig. 4C). The extent of bone loss appeared similar to other mouse drug-induced osteonecrosis of the jaw occurring after dental-related interventions in patients undergoing treatment with bisphosphonates altering osteoclast bone re-absorptive functions, treatments known to suppress bone reformation after dental trauma/surgery(Williams et al., 2014). Mechanistically, reduced angiogenesis and/or impaired NF- κ B induction might elicit localized osteonecrosis through osteoclast honing/recruitment. *Smoc2*^{-/-} exhibit elevated serum/circulating alkaline phosphatase (IMPC database - <http://www.mousephenotype.org/data/genes/MGI:1929881>). Experiments to uncover the etiology of this preferential bone loss in mutants are in progress.

RNA –seq analysis shows novel *Smoc2* targets in E14.5 molars and E18.5 bone:

First molars from E14.5 *Smoc2*^{-/-} mutant females and respective controls were collected, stored at -80°C, and remaining (tail/head) tissue DNA extracted and used to genotype for *Smoc2* or Sry-a male-specific transcript (Table S1). Along with confirming the absence of *Smoc2* transcripts, significant reductions in *bone gamma-carboxyglutamate protein (Bglap* - also known as *osteocalcin*) (a non-collagenous protein marker of bone turnover(Murshed et al., 2004), *dentin matrix acidic phosphoprotein 1 (Dmp1)* (a regulator dental stem cell osteogenic differentiation(Rezai Rad et al., 2015), *odontogenic ameloblast-associated protein (Odam)* (a

secreted protein guiding early enamel formation), *Secreted frizzled-related protein 4 (Sfrp4)* – (a Wnt-pathway inhibitor whose human mutation produces Pyle’s disease affecting long bone and tooth (Simsek Kiper et al., 2016), and fibroblast growth factor *Fgf3* are observed as key changes listed in Table S4. RNA-seq expression changes for E18.5 microdissected mandibular bone (Table S4) revealed *Smoc2*^{-/-} mutant jaw bones have down-regulation of critical targets such as *Dspp* – a principle dentin extracellular matrix protein instructing dentin, vitamin D, and calcium signaling (Wan et al., 2016). Normally cell-adhesion induced ezrin signaling, activating NF-kappaB which binds to the proximal promoter of SMOC2 (Shvab et al., 2016). Alterations in several NF-κB targets such as *Edar*, *Cxcl13*, and *Pak7* (Table S4) indicate altered cytokine signaling. Hence, RNA seq analysis of *Smoc2*^{-/-} mutants provides numerous potential SMOC2 signaling avenues in alveolar bone, dentin, and enamel formation.

Discussion:

SMOC2 mutants reveal precise actions fine-tuning skeletal growth

While SMOC1 deletion produces severe growth deficiency, limb syndactyly, and bone hypoplasia (Okada et al., 2011), and canine SMOC2 reductions account for debilitating facial brachycephaly (Marchant et al., 2017), our mouse *Smoc2*^{-/-} mutants exhibit relatively minor initial reductions in bone mineral density and overall body length/mass. With aging, some *Smoc2* mutant mice exhibit spontaneous bone deterioration and maxillary molar root resorption, which we hypothesize is due to increase bone attrition accompanying age-dependent periodontal decay. Molecularly, reduced *Fgf3* levels, along with other SMOC2-induced pERK/MAP kinase signaling targets provide avenues of how SMOC2 induces mitosis, a role first described in cell-based assays (Liu et al., 2008). Hence overall growth deficiencies are predictable considering SMOC2 increases mitogenesis, a role linked to increased G1 phase cyclin expression and integrin-linked kinase activity promoting cell-cycle progression (Liu et al., 2008). *In vivo* roles are likely much more complex. For example, reduced *Fgf3* signaling has been associated with human hypodontia, yet several synergistic unidentified targets are believed to contribute to the etiology of this defect (Vieira et al., 2013).

A novel bone injury model:

Molar extraction elicits bone injury, inducing an acute, highly regulated inflammatory response benefiting healing. It appears *Smoc2* deficiency suppresses bone healing, dysregulating reparative osteogenesis, potentially inducing chronic inflammation- a phenomena which is quite detrimental to healing (Mountziaris and Mikos, 2008). Although the mechanisms of these actions require further clarification, it appears *Smoc2* signaling affect several events in wound/bone healing. Mesenchymal stem cell growth, fibromyeloblast transition, osteoblasts proliferation are all events having complex interactions with osteoclasts, macrophages, and monocytes targets. We are currently exploring if *Smoc2* deficiency increases osteoclast activity, induces cell death, and/or directly alters inflammatory-mediated events following post-extraction alveolar bone repair (Loi et al., 2016). Both intramembranous and alveolar bone repair also requires *de novo* coupling with angiogenesis (Vieira et al., 2015). While we do not observe fetal or adult stages vascular patterning alterations, we predict defects in injury induced revascularization in *Smoc2*^{-/-} mutants (Rocnik et al., 2006).

A unique appearance of distal supernumerary molars in *Smoc2*^{-/-} mutants:

Supernumerary teeth are occasionally observed in genetically mutant mice, for example following *Rsk2* (Laugel-Haushalter et al., 2014) or *Sprouty2, 4* (Marangoni et al., 2015) deletion. These supernumerary teeth are believed evolutionarily vestigial (reflecting evolutionary reduction in mouse tooth number), always arising in the “tooth” permissive space/field between mouse incisor and first molar. They are often found as a consequent to increased ERK/MAPK signaling, potentially reducing normal diastemal apoptosis accompanying evolutionary tooth loss (Marangoni et al., 2015). In the opposite situation, reduced ERK/MAPK levels (*Fgf3* mutant mouse) produces smaller teeth. Since extra teeth arising caudal to the 3th molar in

Smoc2^{-/-} in a region not prone to supernumerary teeth, *Smoc2*^{-/-} mutation could reveal alteration in the caudal developing cervical loop stem cell zone. The stochastic nature, aberrant location, and female-sex enriched appearance suggests *Smoc2*^{-/-} supernumerary teeth are unique, assimilating *Wnt10a* mutants - which have a similar distal supernumerary 4th molar (Yang et al., 2015). *Smoc2* actions in dental progenitor/dental lineage merit future exploration. We have no explanation for a female-sex bias of these molar duplications, which could potentially be the flip-side of in utero testosterone exposure altering 2rd/4rd digit ratios correlating with increased incidence of male aggressiveness, autism, risk taking (reviewed in (Pintzka et al., 2016)).

ACKNOWLEDGEMENTS

This work was supported by a grant from the University Hospital of Strasbourg (API, 2009–2012, “Development of the oral cavity: from gene to clinical phenotype in Human”), the EU-funded projects (ERDF) A27 “Oro-dental manifestations of rare diseases” in the framework of the RMT-TMO Offensive Sciences initiative INTERREG IV and INTERREG V No. 1.7 RARENET, the Institut d'Etudes Avancées (Institute of Advanced Studies) de l'Université de Strasbourg (USIAS Fellows 2015), and the grant ANR-10-LABX-0030-INRT managed by the Agence Nationale de la Recherche under the frame program Investissements d'Avenir ANR-10-IDEX-0002-02. Sequencing was performed by the IGBMC Microarray and Sequencing platform, supported by the France Genomics National Infrastructure, funded as part of the Investissements d'Avenir program (ANR-10-INBS-0009).

Figure legend

Figure 1. Radiographic images of a 13 year-old female patient with a homozygous *SMOC2* mutation (Bloch-Zupan et al., 2011). A,B shows respective extraoral frontal and lateral radiographic views of the skull. Cranial bones, cranial structures, cranial sutures, sella turcica, and orbit structures are normal except maxilla and mandible. C,D shows extracted μ CT images of upper and lower jaw defects revealed teeth and associated alveolar bone defects, respectively. Affected teeth are typically 15-20% smaller than normal, except for the lower right first molar (Red arrow) which is bigger. E shows full-frontal views of the dentitions, the lower dentition displaying more severe oligodontia and microdontia compared with the upper teeth. F shows the image extraction of isolated teeth (using the Analyze11.0 program) showing that a micro-root structure consistently accompanies microdontia.

Figure 2. *Smoc2*-driven *GFP* immunolocalization in the E14.5 and E18.5 mouse. *Smoc2*-driven *GFP* is diversely expressed in the telecephalon (A), localized to the perioptic mesenchyme (POM) surrounding the eye (B red arrowhead), and the molar dental follicle mesenchymal populations surrounding the outer dental epithelium (C red arrowhead). At E18.5, *Smoc2*-driven *GFP* localizes to hair follicles of the vibrissae (E), the labial cervical loop of the lower incisor (F), and the first and second molar mesenchyme (G) corresponding to the dental stem/cervical loop progenitors area.

Figure 3 *Smoc2*^{-/-} mutant mice have clear dental alterations. 7 week-old *WT* (A) versus *Smoc2*^{-/-} (C) with mutant lower incisors exhibiting slight size reductions. Scanning electron microscope (SEM) of *WT* (B) and *Smoc2*^{-/-} (D) (taken from the respective red boxed regions in panels A and C), showing mutants have alterations in both outer and inner enamel prisms structure (red arrows). E,F shows μ CT 3D renderings of the occlusal surface of all three lower molars to assess morphological defects. Mutants display a significant reduction in the 1st-3rd molar field length (compare E *WT*—green bar vs. F *Smoc2*^{-/-} red bar). Additionally, an ectopic posterior 4th molar is observed in *Smoc2* mutants (F-green arrowhead). G,H μ CT –derived mid-sagittal sectioning indicated thinner alveolar bone in *Smoc2*^{-/-} mutants (H - yellow arrowhead) vs. *WT* (G- yellow arrowhead). Standard histology (of the region indicated from orange-boxed region in G,H, respectively) shows *Smoc2*^{-/-} mutants had reduced alveolar ossification (K-yellow arrowheads). SEM (on the blue-boxed region in G,H) shows reduced enamel crystal compaction, with irregular alignments in *Smoc2*^{-/-} mutant (L-blue arrowheads).

Figure 4. 6-week post-extraction μ CT images of the two months-old *WT* (A) and *Smoc2*^{-/-} mutant (B) males showing mutants have delayed healing and a loss of bone around the extracted first molar (yellow arrowhead) and intact 2nd molar (red arrowhead) are tabulated in the bar graph (C) revealing increased bone loss in *Smoc2*^{-/-} mutants.

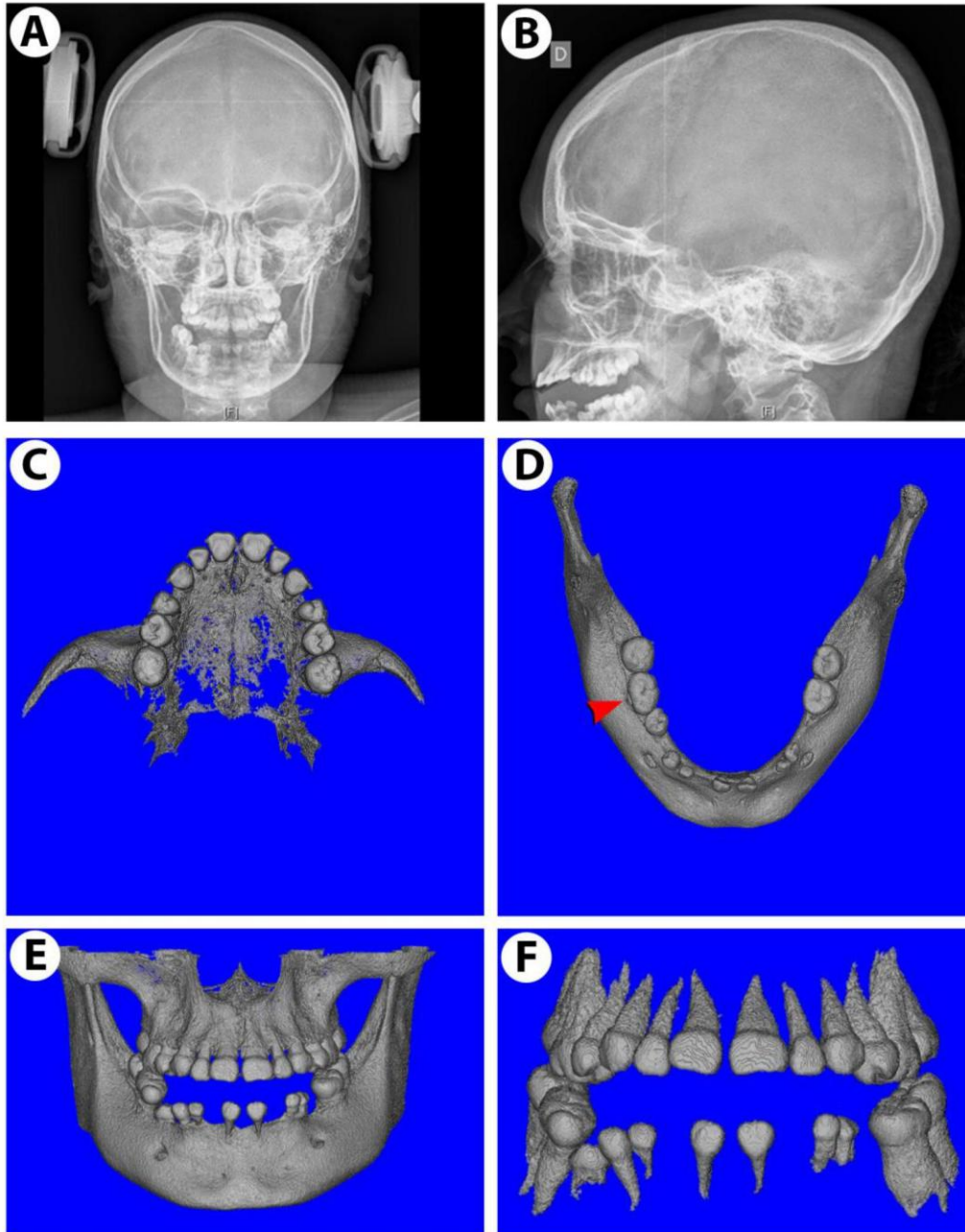
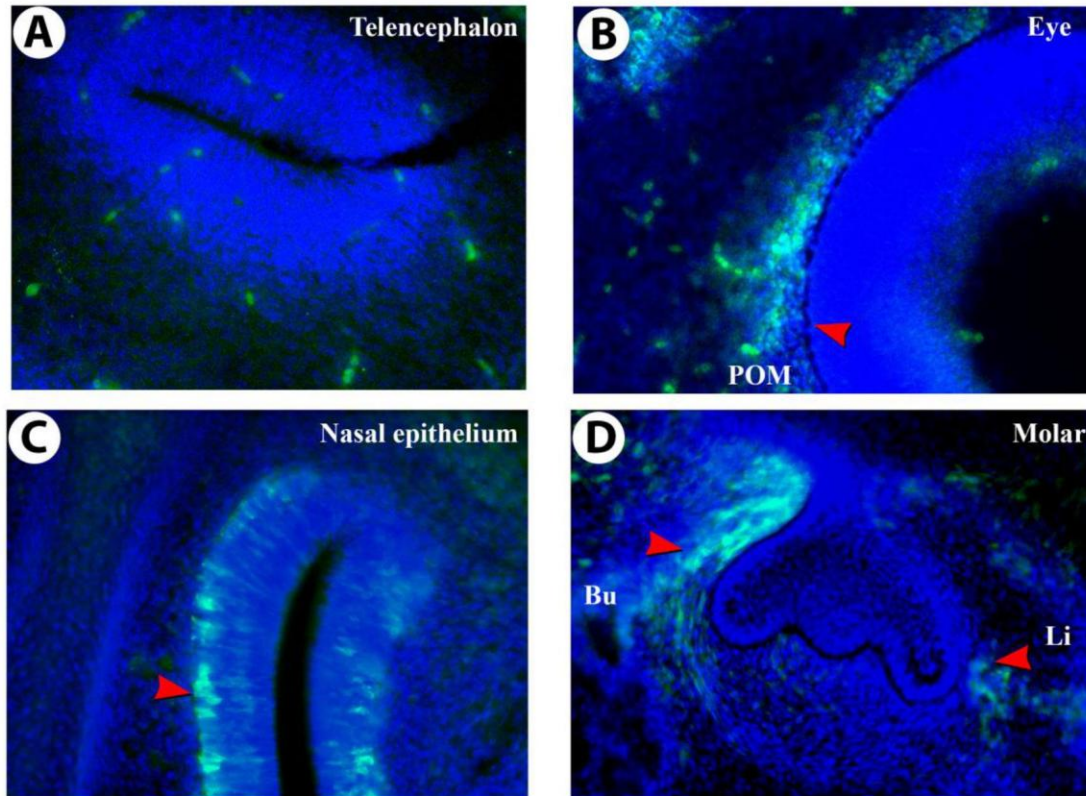


Figure 1

E14



E18

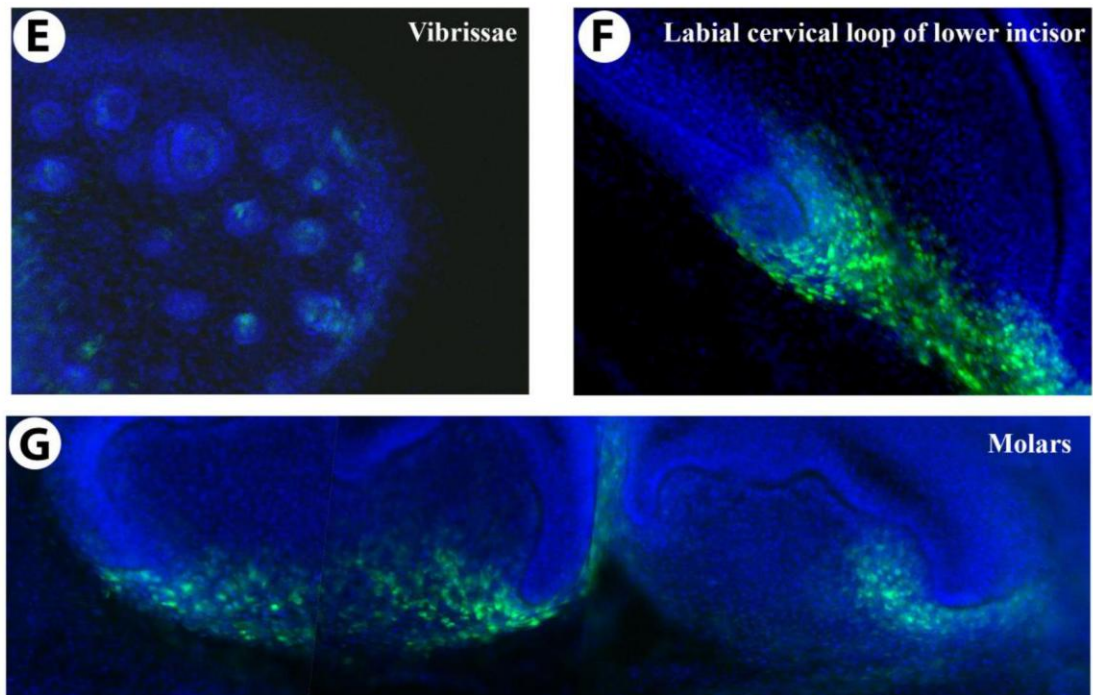


Figure 2

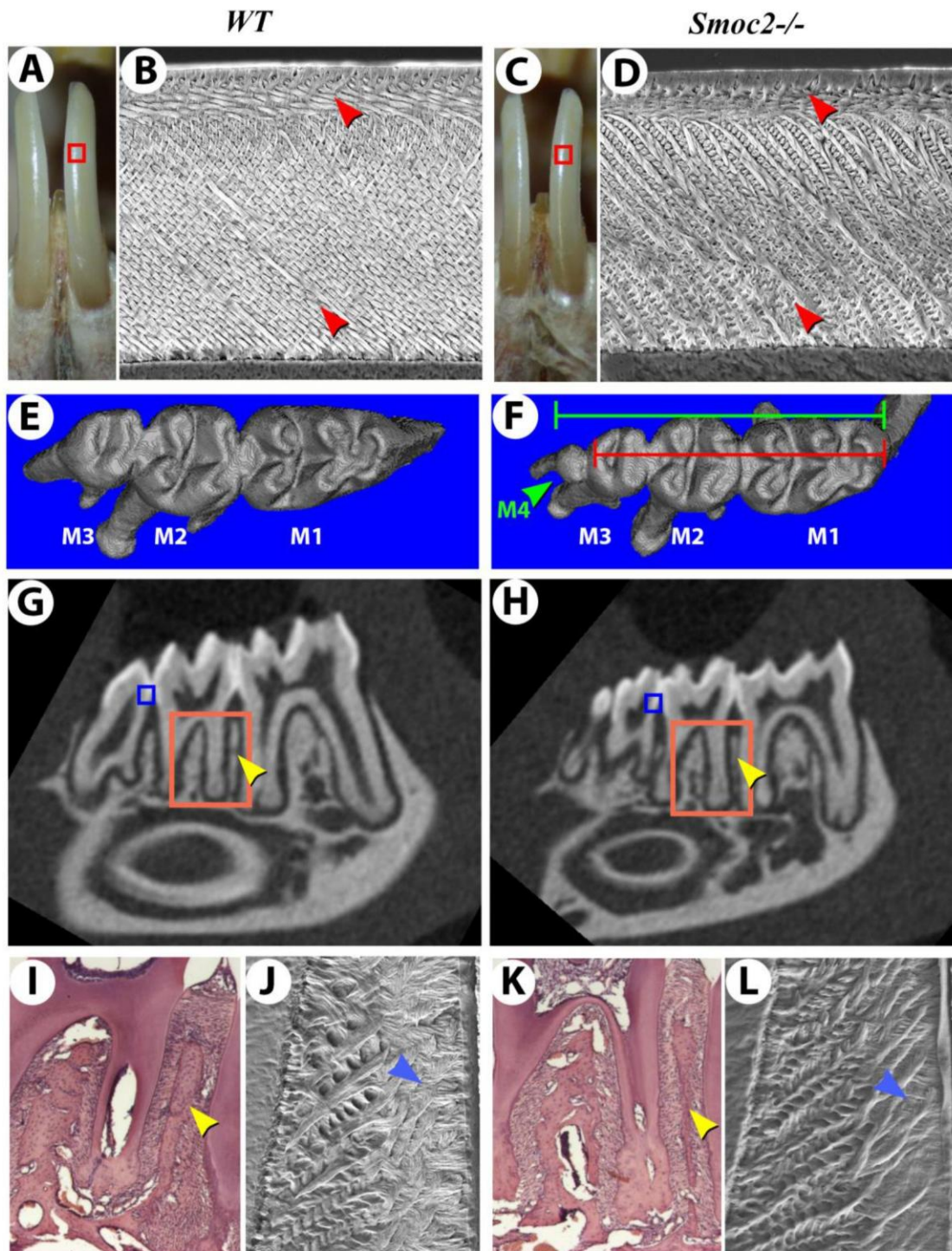
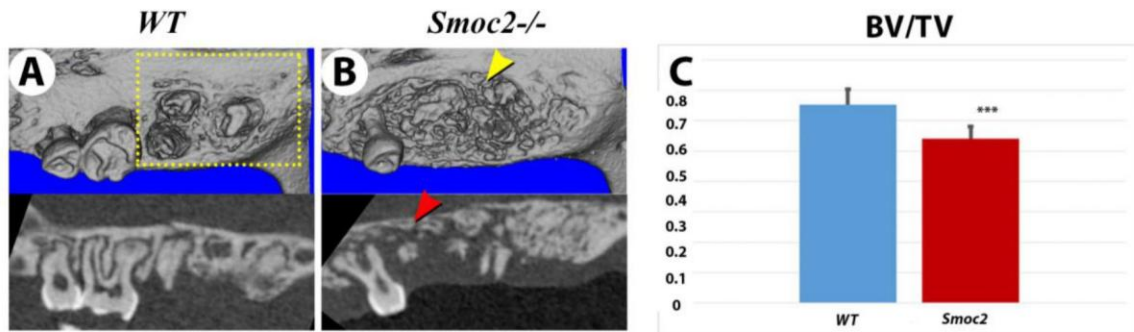


Figure 3

**Figure 4**

REFERENCES

- Alfawaz, S., Fong, F., Plagnol, V., Wong, F.S., Fearn, J., and Kelsell, D.P. (2013). Recessive oligodontia linked to a homozygous loss-of-function mutation in the SMOC2 gene. *Arch Oral Biol* 58, 462-466.
- Anders, S., and Huber, W. (2010). Differential expression analysis for sequence count data. *Genome Biol* 11, R106.
- Birling, M.C., Dierich, A., Jacquot, S., Herault, Y., and Pavlovic, G. (2012). Highly-efficient, fluorescent, locus directed cre and FlpO deleter mice on a pure C57BL/6N genetic background. *Genesis* 50, 482-489.
- Bloch-Zupan, A., Jamet, X., Etard, C., Laugel, V., Muller, J., Geoffroy, V., Strauss, J.P., Pelletier, V., Marion, V., Poch, O., Strahle, U., Stoetzel, C., and Dollfus, H. (2011). Homozygosity mapping and candidate prioritization identify mutations, missed by whole-exome sequencing, in SMOC2, causing major dental developmental defects. *Am J Hum Genet* 89, 773-781.
- Brady, J.J., Chuang, C.H., Greenside, P.G., Rogers, Z.N., Murray, C.W., Caswell, D.R., Hartmann, U., Connolly, A.J., Sweet-Cordero, E.A., Kundaje, A., and Winslow, M.M. (2016). An Arntl2-Driven Secretome Enables Lung Adenocarcinoma Metastatic Self-Sufficiency. *Cancer Cell* 29, 697-710.
- Gerarduzzi, C., Kumar, R.K., Trivedi, P., Ajay, A.K., Iyer, A., Boswell, S., Hutchinson, J.N., Waikar, S.S., and Vaidya, V.S. (2017). Silencing SMOC2 ameliorates kidney fibrosis by inhibiting fibroblast to myofibroblast transformation. *JCI Insight* 2.
- Jun, J.I., Kim, K.H., and Lau, L.F. (2015). The matricellular protein CCN1 mediates neutrophil efferocytosis in cutaneous wound healing. *Nat Commun* 6, 7386.
- Klipper-Aurbach, Y., Wasserman, M., Braunspiegel-Weintrob, N., Borstein, D., Peleg, S., Assa, S., Karp, M., Benjamini, Y., Hochberg, Y., and Laron, Z. (1995). Mathematical formulae for the prediction of the residual beta cell function during the first two years of disease in children and adolescents with insulin-dependent diabetes mellitus. *Med Hypotheses* 45, 486-490.
- Laugel-Haushalter, V., Paschaki, M., Marangoni, P., Pilgram, C., Langer, A., Kuntz, T., Demassue, J., Morkmued, S., Choquet, P., Constantinesco, A., Bornert, F., Schmittbuhl, M., Pannetier, S., Viriot, L., Hanauer, A., Dolle, P., and Bloch-Zupan, A. (2014). RSK2 is a modulator of craniofacial development. *PLoS One* 9, e84343.
- Litingtung, Y., Dahn, R.D., Li, Y., Fallon, J.F., and Chiang, C. (2002). Shh and Gli3 are dispensable for limb skeleton formation but regulate digit number and identity. *Nature* 418, 979-983.
- Liu, P., Lu, J., Cardoso, W.V., and Vaziri, C. (2008). The SPARC-related factor SMOC-2 promotes growth factor-induced cyclin D1 expression and DNA synthesis via integrin-linked kinase. *Mol Biol Cell* 19, 248-261.
- Loi, F., Córdova, L.A., Pajarinen, J., Lin, T.H., Yao, Z., and Goodman, S.B. (2016). Inflammation, fracture and bone repair. *Bone* 86, 119-130.
- Maier, S., Paulsson, M., and Hartmann, U. (2008). The widely expressed extracellular matrix protein SMOC-2 promotes keratinocyte attachment and migration. *Exp Cell Res* 314, 2477-2487.
- Marangoni, P., Charles, C., Tafforeau, P., Laugel-Haushalter, V., Joo, A., Bloch-Zupan, A., Klein, O.D., and Viriot, L. (2015). Phenotypic and evolutionary implications of modulating the ERK-MAPK cascade using the dentition as a model. *Sci Rep* 5, 11658.
- Marchant, T.W., Johnson, E.J., Mctear, L., Johnson, C.I., Gow, A., Liuti, T., Kuehn, D., Svenson, K., Bermingham, M.L., Drögemüller, M., Nussbaumer, M., Davey, M.G., Argyle, D.J., Powell, R.M., Guilherme, S., Lang, J., Ter Haar, G., Leeb, T., Schwarz,

- T., Mellanby, R.J., Clements, D.N., and Schoenebeck, J.J. (2017). Canine Brachycephaly Is Associated with a Retrotransposon-Mediated Missplicing of SMOC2. *Curr Biol* 27, 1573-1584.e1576.
- Mommaerts, H., Esguerra, C.V., Hartmann, U., Luyten, F.P., and Tylzanowski, P. (2014). Smoc2 modulates embryonic myelopoiesis during zebrafish development. *Dev Dyn* 243, 1375-1390.
- Mountziaris, P.M., and Mikos, A.G. (2008). Modulation of the inflammatory response for enhanced bone tissue regeneration. *Tissue Eng Part B Rev* 14, 179-186.
- Muñoz, J., Stange, D.E., Schepers, A.G., Van De Wetering, M., Koo, B.K., Itzkovitz, S., Volckmann, R., Kung, K.S., Koster, J., Radulescu, S., Myant, K., Versteeg, R., Sansom, O.J., Van Es, J.H., Barker, N., Van Oudenaarden, A., Mohammed, S., Heck, A.J., and Clevers, H. (2012). The Lgr5 intestinal stem cell signature: robust expression of proposed quiescent '+4' cell markers. *EMBO J* 31, 3079-3091.
- Murphy-Ullrich, J.E., and Sage, E.H. (2014). Revisiting the matricellular concept. *Matrix Biol* 37, 1-14.
- Murshed, M., Schinke, T., Mckee, M.D., and Karsenty, G. (2004). Extracellular matrix mineralization is regulated locally; different roles of two gla-containing proteins. *J Cell Biol* 165, 625-630.
- Okada, I., Hamanoue, H., Terada, K., Tohma, T., Megarbane, A., Chouery, E., Abou-Ghoch, J., Jalkh, N., Cogulu, O., Ozkinay, F., Horie, K., Takeda, J., Furuichi, T., Ikegawa, S., Nishiyama, K., Miyatake, S., Nishimura, A., Mizuguchi, T., Niikawa, N., Hirahara, F., Kaname, T., Yoshiura, K., Tsurusaki, Y., Doi, H., Miyake, N., Furukawa, T., Matsumoto, N., and Saito, H. (2011). SMOC1 is essential for ocular and limb development in humans and mice. *Am J Hum Genet* 88, 30-41.
- Pintzka, C.W.S., Evensmoen, H.R., Lehn, H., and Håberg, A.K. (2016). Changes in spatial cognition and brain activity after a single dose of testosterone in healthy women. *Behavioural Brain Research* 298, 78-90.
- Renvoise, E., and Michon, F. (2014). An Evo-Devo perspective on ever-growing teeth in mammals and dental stem cell maintenance. *Front Physiol* 5, 324.
- Rezai Rad, M., Liu, D., He, H., Brooks, H., Xiao, M., Wise, G.E., and Yao, S. (2015). The role of dentin matrix protein 1 (DMP1) in regulation of osteogenic differentiation of rat dental follicle stem cells (DFSCs). *Arch Oral Biol* 60, 546-556.
- Rocnik, E.F., Liu, P., Sato, K., Walsh, K., and Vaziri, C. (2006). The novel SPARC family member SMOC-2 potentiates angiogenic growth factor activity. *J Biol Chem* 281, 22855-22864.
- Shvab, A., Haase, G., Ben-Shmuel, A., Gavert, N., Brabletz, T., Dedhar, S., and Ben-Ze'ev, A. (2016). Induction of the intestinal stem cell signature gene SMOC-2 is required for L1-mediated colon cancer progression. *Oncogene* 35, 549-557.
- Simsek Kiper, P.O., Saito, H., Gori, F., Unger, S., Hesse, E., Yamana, K., Kiviranta, R., Solban, N., Liu, J., Brommage, R., Boduroglu, K., Bonafé, L., Campos-Xavier, B., Dikoglu, E., Eastell, R., Gossiel, F., Harshman, K., Nishimura, G., Girisha, K.M., Stevenson, B.J., Takita, H., Rivolta, C., Superti-Furga, A., and Baron, R. (2016). Cortical-Bone Fragility--Insights from sFRP4 Deficiency in Pyle's Disease. *N Engl J Med* 374, 2553-2562.
- Su, J.R., Kuai, J.H., and Li, Y.Q. (2016). Smoc2 potentiates proliferation of hepatocellular carcinoma cells via promotion of cell cycle progression. *World J Gastroenterol* 22, 10053-10063.
- Vieira, A.E., Repeke, C.E., Ferreira Junior Sde, B., Colavite, P.M., Bigueti, C.C., Oliveira, R.C., Assis, G.F., Taga, R., Trombone, A.P., and Garlet, G.P. (2015). Intramembranous bone healing process subsequent to tooth extraction in mice: micro-

- computed tomography, histomorphometric and molecular characterization. *PLoS One* 10, e0128021.
- Vieira, A.R., D'souza, R.N., Mues, G., Deeley, K., Hsin, H.Y., Küchler, E.C., Meira, R., Patir, A., Tannure, P.N., Lips, A., Costa, M.C., Granjeiro, J.M., Seymen, F., and Modesto, A. (2013). Candidate gene studies in hypodontia suggest role for FGF3. *Eur Arch Paediatr Dent* 14, 405-410.
- Wan, C., Yuan, G., Luo, D., Zhang, L., Lin, H., Liu, H., Chen, L., Yang, G., Chen, S., and Chen, Z. (2016). The Dentin Sialoprotein (DSP) Domain Regulates Dental Mesenchymal Cell Differentiation through a Novel Surface Receptor. *Sci Rep* 6, 29666.
- Williams, D.W., Lee, C., Kim, T., Yagita, H., Wu, H., Park, S., Yang, P., Liu, H., Shi, S., Shin, K.H., Kang, M.K., Park, N.H., and Kim, R.H. (2014). Impaired bone resorption and woven bone formation are associated with development of osteonecrosis of the jaw-like lesions by bisphosphonate and anti-receptor activator of NF-kappaB ligand antibody in mice. *Am J Pathol* 184, 3084-3093.
- Yang, J., Wang, S.K., Choi, M., Reid, B.M., Hu, Y., Lee, Y.L., Herzog, C.R., Kim-Berman, H., Lee, M., Benke, P.J., Lloyd, K.C., Simmer, J.P., and Hu, J.C. (2015). Taurodontism, variations in tooth number, and misshapened crowns in Wnt10a null mice and human kindreds. *Mol Genet Genomic Med* 3, 40-58.
- Zhang, Q., Atsuta, I., Liu, S., Chen, C., Shi, S., and Le, A.D. (2013). IL-17-mediated M1/M2 macrophage alteration contributes to pathogenesis of bisphosphonate-related osteonecrosis of the jaws. *Clin Cancer Res* 19, 3176-3188.

CONCLUSIONS-DISCUSSION- PERSPECTIVES

Clinical diagnosis and management of patients presenting with rare diseases and their associated orodental anomalies is challenging for health professionals and dentists, as limited knowledge and understanding of these developmental anomalies is available. Dental anomalies are excellent dysmorphic markers, providing visible evidence, through their unchanging mineralized state, of earlier developmental abnormalities, and giving warning signs that may provide sign-posts in rare disease diagnosis. They may be classified into five main groups; number (missing or supernumerary teeth), shape, size, hard tissue structure, and root formation (including eruption, resorption, and associated periodontal tissue).

Tooth development is an extraordinarily complex process, which progresses through different stages from the initial dental lamina, through bud, cap and bell stages to terminal cytodifferentiation of odontoblasts and ameloblasts synthesizing dentin and enamel matrix proteins, respectively. It encompasses a very large timeframe, from initial neural crest cell formation and migration beginning around day 22 in human embryogenesis to the completion of root formation of the third molars or wisdom teeth occurring around 20-25 years of age. Tooth development is under strict genetic control and involves continuous progressive inductive interactions between defined sites of the oral ectoderm and ectomesenchymal cells derived from the cephalic neural crest. Disruptions of the involved signaling pathways and associated transcription factors lead to dental anomalies. These are seen in human isolated rare dental genetic diseases and in numerous syndromes. Of the over 7000 genetic syndromes known more than 900 have orodental anomalies and over 250 have associated clefting. Some of these anomalies can also occur as the results of or could be modulated in their severity through teratogenic environmental factors impairing craniofacial or dental development. A differential diagnosis is indispensable.

Providing accurate information to the patient and its family is crucial. The specialist dentist is an indispensable partner of the multidisciplinary team helping these patients. He/She can also participate to the enrichment of knowledge through liaison with a clinical reference center. Thus, the pooling of expertise and cases allows the establishment of therapeutic guidelines to provide clear, concise, and evidence based recommendations about patient oral health care management.

It is therefore important to recognize, characterize, and precisely record dental anomalies and phenotypes, so that they may be integrated within the familial, medical and dental histories of the patient. Such detailed recording will reveal developmental origins and go some way towards providing additional clues for understanding underlying etiopathogenic mechanisms and unravelling a syndrome diagnosis. Identified informative families will lead to the discovery of new genes involved in these developmental processes. While patients can be sequenced to find potential loci causing clinical malformations, the molecular basis can neither be elucidated nor novel treatment approaches could be design by basing our approach solely in humans.

To go further into understanding the fundamental molecular basis of orodental patterning and morphogenesis, is it of great importance to study rare diseases mouse models. The mouse dentition is a powerful model to study the genesis of human orodental anomalies. A number of genetically modified mice generated so far display dental defects that mimic the pathology encountered in human.

This doctoral work aims at better understanding the molecular basis of rare diseases, and overcoming the inherent limitations of patient-based research. Essential to this goal was the involvement in the creation and investigation of novel mouse models of human rare diseases.

In brief summary, the first published study investigated the developmental effects of excess retinoic acid on enamel formation to gain understanding of the mechanisms by which environmental factors can alter enamel development and produce enamel defects resembling AI pathologies observed in rare diseases[405]. By assessing the actions of an environmental/nutritional factor, we have *in vivo* evidence, in mouse, that retinoic acid excess blocks craniofacial ossification 2 days after treatment. We developed a model that combined reductions in mesenchymal targets (surrounding the bud stage tooth) that are first adversely affected by excess RA. At later stages (E15.5-onward), these mesenchymal factors later blocked epithelial (enamel organ) expression of *Enam*, *Ambn*, and *Amelx*. The bell stage tooth is quite sensitive to its environment. It reacts to the high retinoid environment by up-regulating the RA-destroying enzyme *Cyp26b1*. This change, though, is insufficient to offset strong reductions in enamel matrix protein secretion caused by excess RA. Fetal retinoid exposure causes permanent ameloblast differentiation

defects. Thus, nutritional factors such as vitamin A could indeed affect human tooth and bone mineralization, and potentially modulate severity of rare diseases such as AI.

The genetics of amelogenesis and its defects was tackled by observing enamel and dental anomalies in *latent transforming growth factor-beta binding protein 3 (LTBP3)* mutant mice (*Ltbp3*^{-/-}), reported in [130]. This gene was identified as the causal gene for brachyolmia with amelogenesis imperfecta or Verloes Bourguignon syndrome[129].

LTBP3 plays an important role in craniofacial morphogenesis and hard tissue mineralization, as it is essentially required for TGF- β activation. Compared with wild-type mice, *Ltbp3*-null mutants presented a unique alteration in enamel formation, ameloblast differentiation, root formation, and dentin formation. Almost all craniofacial structures were affected in the *Ltbp3*-null mice, consistent with the important role of TGF- β signaling in this region. This change clinically mimicked the human mutation and its AI phenotypes.

Another mouse model used to study craniofacial and tooth abnormalities is the *Sparc-related modular calcium-binding protein 2 (Smoc2*^{-/-}) mutant line. This mouse model was created by A Bloch-Zupan and collaborators, following the identification of *SMOC2* in an informative human family as a gene essential for tooth development[411].

Our current goals are to understand the functional properties of *SMOC2*, based on clues that it acts as a secreted progenitor signal[451], and appears to regulate both tooth and alveolar bone, based on patient phenotypes[411]. A summary of mouse phenotypes (the manuscript to date) is presented on page 148 in this thesis. To investigate the origins and mechanisms of craniofacial defects, we performed lineage tracing of *Smoc2*-labeled dental stem cells using an engineered *GFP* expression approach. We confirmed *Smoc2*-*GFP* labeling in progenitor zones, such as the cervical loop.

We also show the *Smoc2*^{-/-} mouse mutant shows no obvious developmental changes, aside from minor (but consistent) tooth and alveolar bone phenotypes. This confirmed previous studies showing no evident developmental change in either *Smoc2*^{-/-} mutant or in *Smoc2* overexpressing mice[451, 452]. In adult mice, the International Mouse Phenotyping Consortium (IMPC) reported that their

independently created *Smoc2*^{-/-} mutant (*Smoc2*^{tm1.1(KOMP)Vlcg}) has clear bone density and body mass deficits, along with reduced coping, and grip strength defects, (<http://www.mousephenotype.org/data/genes/MGI:1929881>) (date 26/06/2017). Additionally at <http://cordis.europa.eu/docs/results/302/302314/final1-smoos-summary.pdf>, another group reported that analysis of *Smoc2*^{-/-} knockout mice was not possible, as null inactivation of this gene produced early embryonic lethality. We similarly observed what we believe as a background or mouse facility-dependent lethality from mice obtained from Dr. Hans Clevers[451]. Potentially, variations within mouse phenotypes may be due to a significant tissue-specific expression bias, a functional consequence of allele-specific transcript abundance variations, found in at least 12% of in different mouse background[453]. These differences between mouse strains, while interesting, are difficult to understand. Investigating such differences would involve comparative genomic analysis using a large set of recombinant inbred strains. In addition, we believe large inter-species variations exist. For example, Canine species studies suggest *SMOC2* disruption affects 36% of facial length variation associated with brachycephalic (in pugs, for example -[454]). Hence, the differences of phenotypes in human, canine, murine, and zebrafish models are seen, complicated by strain-specific variations in mouse mutant phenotypes.

Functionally, some clear mechanisms of *SMOC2* signaling have recently been reported. *SMOC2* appears pro-fibrotic. Indeed, its expression appears to induce fibrotic progression (characterized by TGF- β -induced type I collagen, fibronectin, and α SMA+ myofibroblastic transition), as characterized in kidney injury models[452]. This study also indicated *SMOC2* induces fibroblast migration following scratch assays.

Recently we have found a very interesting, clinically relevant phenotype in *Smoc2*^{-/-} mice following tooth extraction. This alteration—a preferential loss of bone around the extracted tooth in *Smoc2*^{-/-} mutants—is shown in results (Figure 4, page 165). We are testing the hypothesis that the bone disappearance observed in *Smoc2*^{-/-} mice following first molar extraction may be due to osteonecrosis of the alveolar bone[455]. Thus the disappearance of alveolar bone may be due to increased cell death. In patients this type of jaw osteonecrosis a frequent complication of radiotherapy, oral infections, and nitrogen-containing bisphosphonates used during treatment of osteoporosis[456]. In addition, *SMOC2*

may induce bone and tooth growth via integrin-linked Kinase (ILK) activation[457], which can induce integrin β 1 in both keratinocytes[458] and fibroblasts[452]. Integrin-based signaling may be the rationale of why SMOC2 can activate ERK and AKT signaling in hepatocytes[459] and myofibroblasts[452]. To recapitulate, integrin, ILK, and ERK signaling pathways are involved in inflammation, cell proliferation, and differentiation. Inflammation (along with cell growth and differentiation) can also be controlled by the NF- κ B factor pathway. Since NF- κ B is also SMOC2 transcriptional activator[460], we tested if inflammation contributed to bone loss in *Smoc2*^{-/-} mutants. Hence, we are currently testing possible mechanisms by which SMOC2 regulates bone growth, the inflammatory process, and a variety of other cellular events. A step-by-step experimental plan to complete this study is proposed:

1) Roles of the inflammatory process:

An obvious plan is to identify inflammatory targets enacting rescue is to screen for the levels of potential targets such as interleukin (IL), cytokines, and chemokines. This will initially be performed using RT-PCR. Potential critical targets include IL-36 and IL-17, which are both functional targets in osteomucosal tissues, which can be modulated to rescue bisphosphonate-induced osteonecrosis of the jaw (BRONJ) in rodent models[461, 462]. Mechanistically, IL-36 can suppress TGF- β mediated expression of collagen- α 1 and α -SMA, by targeting the ERK signaling pathway. IL-17 promotes IFN- γ -induced M1 macrophage polarization, inducing a cytokine/chemokine production found elevated in BRONJ lesions[462].

If time permits, the next step would be investigation of roles specific to immune cell. Isolating immune populations can be performed using fluorescence activated cell sorting (FACS) approaches with extraction socket tissues[463]. This technique can sort monocytes, macrophages, dendritic cells, natural killer cells, and eosinophils from a range of tissues, defining for example, macrophages based using CD64 vs. CD24 cell-surface antigen expression.

2) Testing osteoclast activation:

Increased disappearance of bone following extraction may be due to increased osteoclast recruitment. Bone resorption is regulated by osteoclasts, a cell-type controlled by the ratios of various cytokines and hormones such as IL. Different

osteoclasts can be derived from mesenchymal stem cells[464]. Osteoclastogenesis activators play a key role in osteoclast differentiation. Both macrophage colony stimulating factor and receptor activator of nuclear factor κ B ligand (RANKL) stimulates osteoclastogenesis[465]. The ligand RANKL increases the production of proinflammatory cytokines and chemokines[466]. This differentiation from hematopoietic stem cells requires multiple steps including: monocyte lineage commitment, preosteoclast formation, RANKL-mediated osteoclast maturation and activation.

To determine if osteoclasts function is increased, we will first quantify mature osteoclasts function using Tartrate Resistant Acid Phosphatase (TRAP) immunostaining, a technique detecting acid phosphatase- an activity highly enriched in osteoclasts and activated macrophages. Multinucleated (>3 nuclei) TRAP+ cells will be quantitated by TRAP staining ~4-10 days after tooth extraction at bone surface. We will also test for osteonecrosis caused by cell death (assaying TUNEL and activated caspase3 immunostaining as death markers). If justified, we will quantitate the osteoclast targets MMP9 and IL-36 using RT-PCR. Then, immune-cell specific changes during osteoclast recruitment can be tested by performing FACS analyses on sorted populations using different combinations of hematopoietic cell surface markers such as CD45R, CD11b, CD3, CD115, Sca-1 and CD117.

3) Potential roles of fibrosis and altered collagen formation:

To date, we have no visual clues that fibrosis is altered in the extraction socket using micro-CT analysis. Based on renal studies, *SMOC2-KO* mice appear protected from kidney fibrosis. Hence, targeting *SMOC2* using RNA interference protects against fibrosis development[452]. Targets of these events include Tgf- β , collagen type 1, candidates to be tested by RT-PCR. If *Smoc2*^{-/-} mutation augments inflammatory targets such as IL-36, these would predictably suppress TGF- β , in turn reducing collagen- α 1 and α -SMA levels. To test if these pathways are functioning during alveolar bone healing, we will assay mRNA and protein levels of α -SMA- a myelofibroblast target implicated in wound healing and cancer. Addition experiments could also be proposed to test the diverse roles of *SMOC2* in angiogenesis[467] and proliferation[457], events induced by tooth extraction (see below).

4) Angiogenesis-a target not altered in the unchallenged *Smoc2*^{-/-} mutant:

SMOC2 has clear vascular effects in endothelial cell culture and in matrigel invasion assays, according to published data[467]. In spite of this, we observed no changes in vascularization by PECAM –endothelial cell staining during normal embryonic and fetal-stage *Smoc2*^{-/-} mutant development. Potentially, a de novo/injury-based effect may exist. SMOC2 re-activation may be manifested during wound healing. To study this, *VEGF* and *Fgf3*, general inducers of vascular growth[468, 469] and PECAM levels will be determined by RT-PCR and immunohistochemistry. In addition, Tnf- α , acts as a pro-angiogenic chemokine that induces an endothelial tip-cell-like phenotype via the NF- κ B pathway[470]. This will also be tested.

5) Proliferation changes under wound repair:

Published reports suggested *SMOC2* promotes growth factor-induced expression and DNA synthesis (via increasing Cyclin D1[457]). To date, extensive RNA-Seq analysis of fetal stage *Smoc2*^{-/-} molars and bone did not reveal significant enrichment for cell cycle proliferative targets. To investigate if post-wounding proliferation events are altered, *cyclin D1* levels (RT-PCR) will be screened, followed by other cell proliferation assays (PCNA, mitosis-specific phosphorylated histone immunohistochemistry).

These investigations will define the role of *SMOC2* in injury/healing and its compensated role in normal development. Even though mice are different from humans, understanding clinically relevant targets will give a net benefit for patients, including in events such as dental implant osseointegration. In general, *SMOC2* targets may improve alveolar bone growth and dental implant surgery success rate. Regarding our results, concerning up-regulated *Smoc2* protein, it may play a role in promoting healing and bone regeneration in compromised patients. Our concerns are that systemic delivery of drugs could have numerous side effects. Specifically, *SMOC2* up-regulation appears critical in cancer metastasis[460] and *SMOC2* levels correlate with a worse prognosis in human cancer studies[471]. The possible solution might be locally treating implant surfaces, surgical placing membranes, or other biomaterials with local *SMOC2* over a short period. Ideas of combining biomaterials with *SMOC2* and/or with TGF- β to overcome osteonecrosis are needed in patients.

Thus, long-term investigations must be established to confirm rodent model outcomes, aiming treatments at a tightly restricted surgical site.

This PhD work was made possible thanks to different funding sources: the French Ministry of Health (National Program for Clinical Research, PHRC 2008 N°4266 Amelogenesis imperfecta), the EU-funded project (ERDF) A27 'Oro-dental manifestations of rare diseases,' supported by the RMT-TMO Offensive Sciences initiative, INTERREG IV Upper Rhine program and the INTERREG V RARENET program, the grant ANR-10-LABX-0030-INRT, a French State fund managed by the Agence Nationale de la Recherche under the frame program Investissements d'Avenir labelled ANR-10-IDEX-0002-02. This research was also funded by the University of Strasbourg Institute for Advanced Study (USIAS) as part of a USIAS Fellowship granted to Agnès Bloch-Zupan. The PhD is supported by Franco-Thai scholarship and Khon Kaen University granted to Supawich MORKMUED.

Future work will be based on continuous collaborations between the Faculté de Chirurgie Dentaire de l'Université de Strasbourg, the Centre de Référence Maladies Rares O-Rares, Pôle de Médecine et Chirurgie Bucco-Dentaires, Hôpitaux Universitaires de Strasbourg, France, and Khon Kaen University, Khon Kaen, Thailand. This work will focus on the genetics of rare diseases, exploring the genotypes behind families and patients showing exceptional rare orodental phenotype.

ANNEXES (APPENDIX)

Liste des annexes (List of appendix)

Autres publications (Other publications)

- Mutations in the Latent TGF-beta Binding Protein 3 (*LTBP3*) gene cause brachyolmia with amelogenesis imperfecta.....180
- RSK2 is a modulator of craniofacial development.....193
- Homozygous and Compound Heterozygous MMP20 Mutations in Amelogenesis Imperfecta.....210

Méthodes (Materials and Methods)

- Genotyping protocol.....217
- RT-PCR Protocol.....220
- Bone and cartilage staining by Alizarin red and Alcian blue.....225
- Fixation, decalcification, and paraffin embedding of whole adult mouse heads.....226
- Immunohistochemistry protocol.....227
- Tissue treatments.....230
- Synthesis of Digoxigenin-11-UTP RNA Probe for In Situ Hybridization.....233
- Whole-mount in situ hybridisation of mouse embryos.....236
- Automated whole-mount in situ hybridisation of mouse embryos.....243
- Solutions for Hybridization in situ with Digoxigenin RNA Probes on Section.....249
- Micro-CT imaging.....256
- Analyze11.0 instructions for bone and tooth analysis.....260

Mutations in the Latent TGF-beta Binding Protein 3 (*LTBP3*) gene cause brachyolmia with amelogenesis imperfecta.

Huckert M, Stoetzel C, **Morkmued S**, Laugel-Haushalter V, Geoffroy V, Muller J, Clauss F, Prasad MK, Obry F, Raymond JL, Switala M, Alembik Y, Soskin S, Mathieu E, Hemmerlé J, Weickert JL, Dabovic B, Rifkin DB, Dheedene A, Boudin E, Caluseriu O, Cholette MC, McLeod R, Antequera R, Gellé MP, Coeuriot JL, Jacquelin LF, Bailleul-Forestier I, Manière MC, Van Hul W, Bertola D, Dollé P, Verloes A, Mortier G, Dollfus H, Bloch-Zupan A.

Hum Mol Genet. 2015 Jun 1;24(11):3038-49. doi: 10.1093/hmg/ddv053. Epub 2015 Feb 10.

Les mutations du gène Latent TGF-beta Binding Protein 3 (*LTBP3*) provoquent une brachyolmie associée à une amélogénèse imparfaite.

Les malformations dentaires héréditaires constituent un groupe de troubles cliniquement et génétiquement hétérogènes. Ici, nous décrivons dans quatre familles, dont trois consanguines, un phénotype identique, caractérisé par une petite taille avec une brachyolmie et une amélogénèse imparfaite (AI) hypoplasique avec un émail presque absent. Ce phénotype a d'abord été décrit en 1996 par Verloes et *al.* comme une forme autosomique récessive de brachyolmie associée à l'AI. Le séquençage d'exome a abouti à l'identification de mutations hypomorphiques récessives, y compris des délétions, des mutations non-sens et d'épissage, dans le gène *LTBP3*, impliqué dans la voie de signalisation TGF-bêta. Nous avons également étudié l'expression de *Ltbp3* lors du développement de la souris et de la formation des dents. Des améloblastes différenciés synthétisant des protéines de matrice d'émail et des odontoblastes expriment le gène. L'étude d'un modèle de souris *Ltbp3*^{-/-} knock-out a montré que les souris mutantes présentaient un émail très mince voire absent sur les incisives et les molaires, récapitulant le phénotype d'AI observé dans ce syndrome chez l'homme.



ORIGINAL ARTICLE

Mutations in the latent TGF-beta binding protein 3 (LTBP3) gene cause brachyolmia with amelogenesis imperfecta

Mathilde Huckert^{1,2,7,†}, Corinne Stoetzel^{1,†}, Supawich Morkmued^{2,3,11}, Virginie Laugel-Haushalter³, Véronique Geoffroy¹, Jean Muller^{3,4,8}, François Clauss^{2,5,7}, Megana K. Prasad¹, Frédéric Obry^{2,7}, Jean Louis Raymond², Marzena Switala^{2,7}, Yves Alembik⁹, Sylvie Soskin¹⁰, Eric Mathieu⁶, Joseph Hemmerlé⁶, Jean-Luc Weickert³, Branka Brukner Dabovic¹², Daniel B. Rifkin¹², Annelies Dheedene¹³, Eveline Boudin¹⁴, Oana Caluseriu¹⁵, Marie-Claude Cholette¹⁵, Ross Mcleod¹⁵, Reynaldo Antequera¹⁶, Marie-Paule Gellé^{17,18}, Jean-Louis Coeuriot¹⁷, Louis-Frédéric Jacquelin¹⁷, Isabelle Bailleul-Forestier¹⁹, Marie-Cécile Manière^{2,7}, Wim Van Hul¹⁴, Debora Bertola²⁰, Pascal Dollé^{3,‡}, Alain Verloes^{21,‡}, Geert Mortier^{13,14,‡}, Hélène Dollfus^{1,9,‡} and Agnès Bloch-Zupan^{2,3,7,*}

¹Université de Strasbourg, Laboratoire de Génétique Médicale, INSERM UMR 1112, Faculté de Médecine, FMTS, 11 rue Humann 67000 Strasbourg, France, ²Université de Strasbourg, Faculté de Chirurgie Dentaire, 8 rue St Elisabeth, 67000 Strasbourg, France, ³Université de Strasbourg, Institut de Génétique et de Biologie Moléculaire et Cellulaire (IGBMC), CERBM, INSERM U 964, CNRS UMR 7104, 1 rue Laurent Fries, BP 10142, Illkirch 67404, France, ⁴Université de Strasbourg, Laboratoire ICube UMR 7357, CNRS, LBGI, Strasbourg, France, ⁵Université de Strasbourg, Osteoarticular and Dental Regenerative NanoMedicine, Inserm UMR 1109, 11 rue Humann 67000 Strasbourg, France, ⁶Université de Strasbourg, Biomaterials and Bioengineering, Inserm UMR 1121, 11 rue Humann, 67000 Strasbourg, France, ⁷Hôpitaux Universitaires de Strasbourg, Pôle de Médecine et Chirurgie Bucco-Dentaires, Reference Centre for Orofacial Manifestations of Rare Diseases, CRMR, 1 place de l'Hôpital, 67000 Strasbourg, France, ⁸Hôpitaux Universitaires de Strasbourg, Laboratoire de Diagnostic Génétique, 1 place de l'Hôpital, 67000 Strasbourg, France, ⁹Hôpitaux Universitaires de Strasbourg, Service de Génétique Médicale, 1 place de l'Hôpital, 67000 Strasbourg, France, ¹⁰Hôpitaux Universitaires de Strasbourg, Service de Pédiatrie 1, Endocrinologie Pédiatrique, 1 place de l'Hôpital, 67000 Strasbourg, France, ¹¹Faculty of Dentistry, Khon Kaen

[†] These authors contributed equally to the work.

[‡] Senior authors.

Received: November 15, 2014. Revised and Accepted: February 6, 2015

© The Author 2015. Published by Oxford University Press.

This is an Open Access article distributed under the terms of the Creative Commons Attribution Non-Commercial License (<http://creativecommons.org/licenses/by-nc/4.0/>), which permits non-commercial re-use, distribution, and reproduction in any medium, provided the original work is properly cited. For commercial re-use, please contact journals.permissions@oup.com

University, Khon Kaen, Thailand, ¹²Department of Cell Biology, NYU Langone Medical Centre, New York, USA, ¹³Center for Medical Genetics, Ghent University, Ghent University Hospital, De Pintelaan 185, Ghent 9000, Belgium, ¹⁴Department of Medical Genetics, University of Antwerp and Antwerp University Hospital, Prins Boudewijnlaan 43, Edegem 2650, Belgium, ¹⁵Department of Medical Genetics, Faculty of Medicine and Dentistry, University of Calgary, Alberta Children's Hospital, Calgary, AB, Canada, ¹⁶Dentistry Division, HC/FMUSP, São Paulo, Brazil, ¹⁷Faculté d'Odontologie, Université de Reims Champagne-Ardenne, 2 rue du Général Koenig, Reims 51100, France, ¹⁸Laboratoire EA 4691 'BIOS', 1, rue du Maréchal Juin, Reims 51100, France, ¹⁹Faculty of Dentistry, Paul Sabatier University, LU51, Pôle Odontologie, Hôpitaux de Toulouse, 3 Chemin des Maraîchers, Toulouse, France, ²⁰Unidade de Genética do Instituto da Criança, Hospital das Clínicas da Faculdade de Medicina da Universidade de São Paulo – Instituto de Biociências, Universidade de São Paulo, São Paulo, Brazil and ²¹Département de Génétique – Hôpital Robert Debré, CRMR 'Anomalies du Développement & Syndromes Malformatifs', CRMR 'Déficiences Intellectuelles de Causes Rares', 48 bd Sérurier, Paris 75019, France

*To whom correspondence should be addressed at: Faculty of Dentistry, University of Strasbourg, 8 rue St Elisabeth, 67000 Strasbourg, France. Tel: +33 368853919; Fax: +33 368853900; Email: agnes.bloch-zupan@unistra.fr

Abstract

Inherited dental malformations constitute a clinically and genetically heterogeneous group of disorders. Here, we report on four families, three of them consanguineous, with an identical phenotype, characterized by significant short stature with brachyolmia and hypoplastic amelogenesis imperfecta (AI) with almost absent enamel. This phenotype was first described in 1996 by Verloes *et al.* as an autosomal recessive form of brachyolmia associated with AI. Whole-exome sequencing resulted in the identification of recessive hypomorphic mutations including deletion, nonsense and splice mutations, in the *LTBP3* gene, which is involved in the TGF-beta signaling pathway. We further investigated gene expression during mouse development and tooth formation. Differentiated ameloblasts synthesizing enamel matrix proteins and odontoblasts expressed the gene. Study of an available knockout mouse model showed that the mutant mice displayed very thin to absent enamel in both incisors and molars, hereby recapitulating the AI phenotype in the human disorder.

Introduction

Brachyolmia (from the greek 'short trunk') refers to a heterogeneous group of skeletal dysplasias with as major clinical feature a disproportionate short stature with short trunk. Radiographic abnormalities are predominantly present in the axial skeleton and include generalized platyspondyly (i.e. flattened vertebral bodies). Amelogenesis imperfecta (AI) is a defect in enamel formation and mineralization (1). AI can be an isolated finding or occur in association with other anomalies (syndromic AI) (2). In 1996, Verloes *et al.* (3) described an autosomal recessive form of platyspondyly with AI [MIM 601216]. Absence of enamel and oligodontia were the major dental findings. Bertola *et al.* (4) subsequently published two other families, one of them with abnormal yellow coloration of primary and permanent teeth, as well as retarded dental eruption compatible with a diagnosis of AI. Here we report on four families, three of them being consanguineous, with an identical phenotype, characterized by platyspondyly (brachyolmia) and AI. Affected individuals have very thin or almost absent enamel. By using a combined strategy of homozygosity mapping and whole-exome sequencing, recessive mutations in the latent TGF-beta binding protein 3 (*LTBP3*) gene were identified. Analysis of *ltbp3* expression during mouse development and the study of dental anomalies observed in the *Ltbp3*^{-/-} knockout mouse model underscored the key role of the latent TGF-beta binding protein 3 in amelogenesis and skeletal development.

Results

Patients' phenotype

The index family 1 presented with AI and short stature. The almost complete absence of enamel in both primary and permanent

dentitions (Fig. 1A and B) led to the diagnosis of hypoplastic AI, thereby explaining the yellow, small and spaced appearance of the teeth. The panoramic radiographs confirmed the absence of enamel associated with large pulp chambers and taurodontic molars (Fig. 1C). Class III mandibular prognathism encountered in family 1 was due to maxillary underdevelopment (Fig. 1D). Radiographs of the skeleton revealed brachyolmia (Fig. 1E and F)

Subsequently, three additional families with a similar phenotype were identified. Additional bone anomalies such as osteopenia and scoliosis were present in family 4. Missing teeth (family 4) and retarded teeth eruption (family 3) were also reported.

Enamel shows quantitative and qualitative defects

The enamel structure of a permanent tooth, the left upper second premolar (25) extracted within the course of treatment of patient IV-1 of family 1 was further analyzed by scanning electron microscopy (Fig. 1G and H). With this evaluation the enamel hypoplasia was confirmed and very thin or absent enamel was noted. Dentin was normal. The initial aprismatic enamel layer was absent. A very thin shell of irregular prismatic enamel (PE), with a reduced thickness thinner than 150 µm (instead of 300 µm comparatively at the same site on a control tooth), was deposited covering the dentin scaffold. In this layer, a Hunter-Schreger band pattern, featuring the arrangement of enamel prisms, was present. In these areas, no aprismatic outer layer was deposited. However in some areas, amelogenesis continued and some 'bubbling' of non-prismatic enamel (NPE) occurred on top of this basal first enamel layer. Waves of aprismatic and prismatic enamel alternated. The outermost layer was always aprismatic in areas where enamel formation continued.

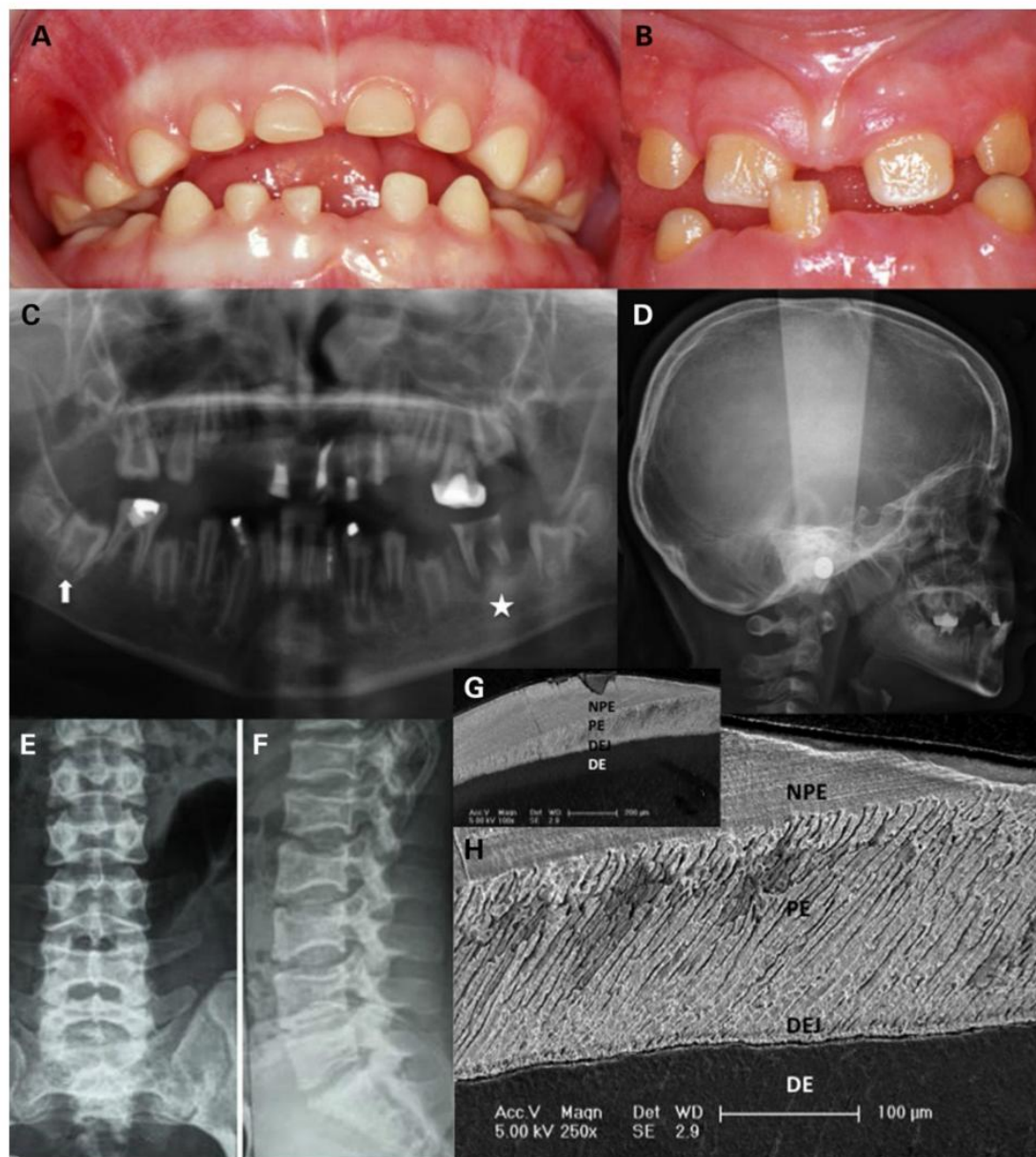


Figure 1. Phenotypic data on family 1. (A) Intraoral view of individual IV.1 (at age 5 years). All primary teeth are smaller and yellowish showing thin, almost absent, enamel. The dentition is spaced. (B) Intraoral view of individual IV.2 (at age 7 years). The erupting permanent incisors are yellow and small due to absent enamel. Primary teeth were lost after recurrent infections. (C) Panoramic radiograph of individual IV.2 (at age 9 years) showing erupted and non-erupted permanent teeth with no enamel. No teeth are missing. Pulp chambers appear large. Infection as a consequence of microbial contamination of pulp spaces is visible around the 36 (radiolucent area around the roots of the lower left first permanent molar filled star) in the absence of the protective enamel layer. The upward arrow points toward a second right lower permanent molar not yet erupted presenting with taurodontism and a large pulp chamber. (D-F) Radiographs taken from individual IV.2 (skull at age 9 years and spine at age 14 years). Skull radiograph reveals absent pneumatization of sinuses and mandibular prognathism secondary to underdevelopment of the maxilla. The spine radiographs show platyspondyly with indentations of both upper and lower vertebral endplates. (G) The enamel phenotype analyzed at the ultra-structural level through SEM revealed a thin PE layer directly starting at the dentino-enamel junction (DEJ). In some areas enamel formation continued as an aprismatic layer (NPE). Dentin (DE) was normal. (H) Close up of the PE and NPE thin layer.

Mutations in *LTBP3* underlie syndromic AI with brachyolmia

Whole-exome sequencing was performed independently (in two different labs) in families 1 and 2 and in families 3 and 4. Coverage and variant calling data for families 1 and 2 are provided in Supplementary Material, Table S1.

A single gene, *LTBP3*, was found to carry bi-allelic mutations in all affected individuals from the four families (Fig. 2A and B).

In family 1, we identified a homozygous 14 bp deletion, c.[2071_2084delTACCGGCTCAAAGC] (Table 1 and Fig. 2A). This mutation lies within a zone of homozygosity that is shared between the two affected individuals, but that is absent in the unaffected sibling and parents (Supplementary Material, Fig. S1).

In family 2 we identified compound heterozygosity for a nonsense and a splice donor site mutation c.[421C>T];[1531+1G>T]; in families 3 and 4 homozygosity for a single nucleotide deletion was found (c.[2216_2217delG] in family 3 and c.[2356_2357delG]

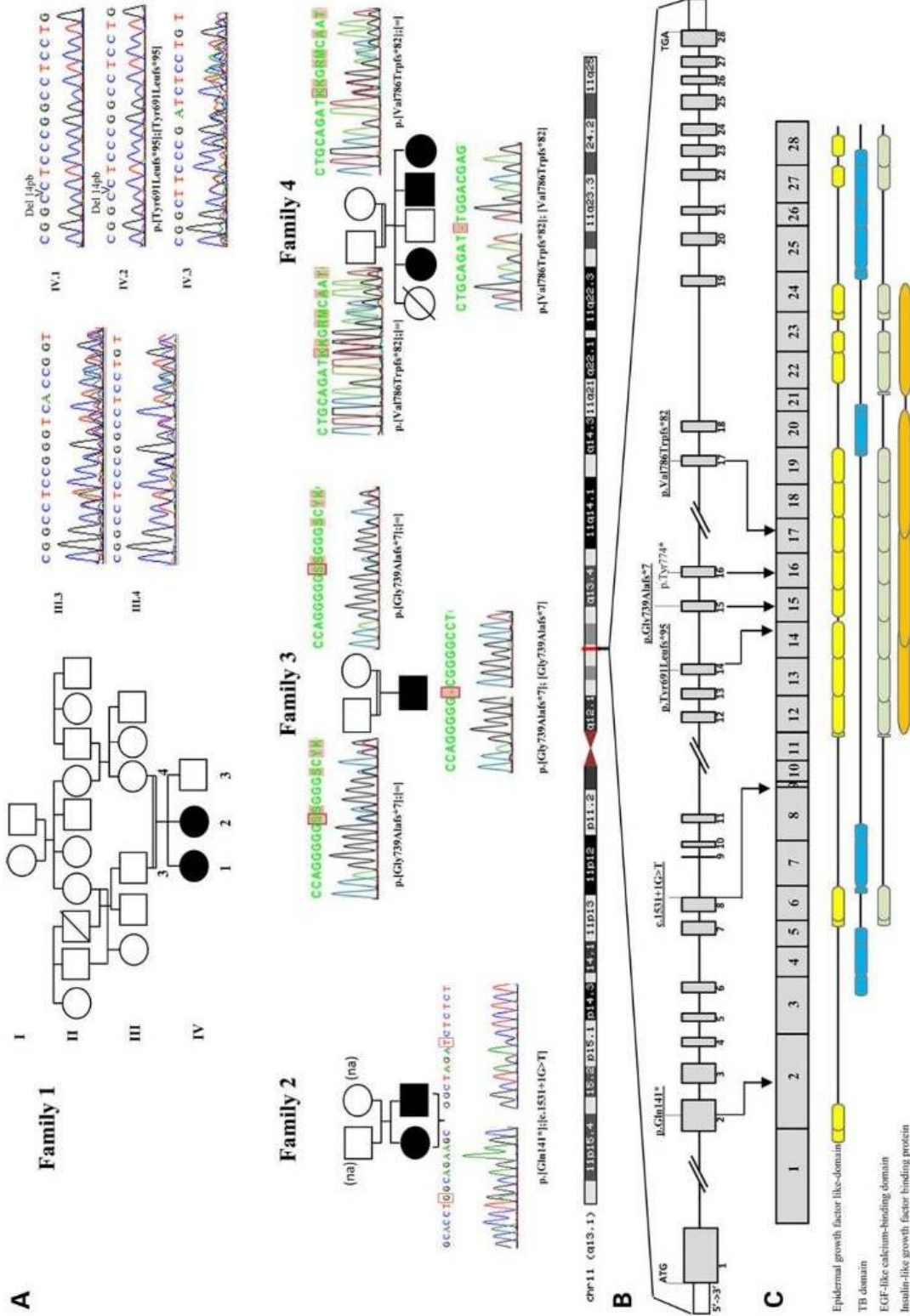


Figure 2. Detected LTBP3 mutations and corresponding protein domains. (A) Pedigrees and sequences analysis of families 1-4 (na: not available). Simplified pedigrees of family 1 demonstrates consanguinity between the parents III.3 and III.4. Electropherograms reveal a 14-bp homozygous deletion in the affected individuals IV.1 and IV.2. The parents III.3 and III.4 are heterozygous for the deletion. (B) The LTBP3 human gene is located on chr11q13.1, extends over 20 kb and contains 28 exons (vertical gray hatches); the position of the start codon (ATG) and the stop codon (TGA) are indicated. The mutations detected in this study are bold and underlined. Vertical lines indicate positions relative to exons (only the p.Tyr774* was previously described in Noor et al. [5]). (C) Arrows indicate positions relative to the cDNA and the protein domain; according to EMBL-EBI Interpro.

Table 1. Mutations described in *LTBP3* (NM_001130144.2)

Family	Affected	Ethnic origin	#Exon	Chromosomal position (hg19)	cDNA change	Protein change
1	Two siblings	Turkey	Exon 14	g.65314933	c.[2071_2084delTACCGGCTCAAAGC]; [2071_2084delTACCGGCTCAAAGC]	p.[Tyr691Leufs*95]; [Tyr691Leufs*95]
2	Two siblings	Caucasian French	Exon 2 and 8	g.65321762	c.[421C>T(;);1531+1G>T]	p.[Gln141*(;)?]
3	One boy	Brazil	Exon 15	g.65314283	c.[2216_2217delG]; [2216_2217delG]	p.[Gly739Alafs*7]; [Gly739Alafs*7]
4	Three siblings	Pakistan	Exon 17	g.65311018	c.[2356_2357delG]; [2356_2357delG]	p.[Val786Trpfs*82]; [Val786fs*82]

Mutation affecting splice are in italics.

in family 4). All mutations segregated with the disease phenotype in each family and were confirmed by Sanger sequencing (Fig. 2). In addition, they were absent in the Exome Variant Server (EVS) and the Thousand Genomes Project Catalog. Interestingly a single nucleotide insertion (c.2216_2217insG; p.Gly740Argfs*51) was tabulated in EVS in the homozygous state in 7 out of more than 6098 individuals. However, coverage information was not available for these individuals to verify if this is a false or true positive variant.

The *LTBP3* mutations identified in our families are most likely hypomorphic. The 14-bp deletion found in family 1 does not seem to result in nonsense-mediated decay because it was present in RNA extracted from a gingival biopsy of patient IV.1 (Supplementary Material, Fig. S2). The mutation most likely gives rise to a truncated protein that lacks the terminal 612 amino acids, which encode essential functional domains (epidermal growth factor like-domain, TB domain, EGF-like calcium-binding domain and insulin-like growth factor binding protein domain) of the protein (Fig. 2C). The splice-site mutation in family 2 is predicted to cause an in-frame skipping of exon 8. The remaining mutations, one nonsense mutation and two single nucleotide deletions, are expected to result in nonsense-mediated decay through the creation of a premature stop codon.

Expression pattern of *Ltbp3* in developing mouse bone and tooth

To gain insight into *Ltbp3* expression during bone and tooth development in mice, we performed an *in situ* hybridization analysis, using a digoxigenin-labeled antisense riboprobe generated from the same DNA template as previously used by the EURExpress consortium (www.eurexpress.org). Mouse embryos were analyzed at E14.5, E16.5 and E18.5. *Ltbp3* transcripts were detected in several developing tissues and organs. Expression was found in various developing bones undergoing either endochondral or intramembranous ossification (e.g. the vertebrae: Fig. 3A; mandibular bone: Fig. 3B; base of the skull bones: Fig. 3C). Expression was also detected in the ventricular and subventricular zones of the developing brain vesicles (Fig. 3D), and in cells surrounding the lumen of the neural tube (the spinal cord primordium: Fig. 3A). Discrete expression was observed in the developing inner ear (cochlea: Fig. 3C). *Ltbp3* transcripts were detected in the small and large intestine, with most conspicuous expression at the base of the intestinal crypts (Fig. 3E). Weaker expression was seen in the differentiating lung (Fig. 3F), whereas discrete expression was observed in the heart outflow tract (not shown) and in the wall of the large blood vessels such as the aorta and pulmonary artery (Fig. 3F).

Ltbp3 expression pattern was also investigated during tooth development. In a large-scale gene expression study (www.eurexpress.org), *Ltbp3* transcripts were detected at E14.5 cap

stage of tooth development (6). This also has been documented in a mouse tooth cap stage transcriptome analysis (6). Our analysis confirmed these data. In addition we investigated more precisely *Ltbp3* expression at various stages of tooth development (Fig. 3G, I and K lower incisor and H, J and L molar). *Ltbp3* transcripts were observed at E14.5 in cap stage teeth, at E16.5 in the epithelial and mesenchymal compartments of the bell stage teeth, especially in the most differentiated areas such as the molar cusp tips and the rostral part of the incisors. At E18.5 labeling was observed in differentiating ameloblasts and odontoblasts. Transcripts were scattered at the apical secretory pole of ameloblasts.

Ltbp3^{-/-} mouse dental phenotype

We further explored the dental phenotype of *Ltbp3*^{-/-} mice described in (7–9) by X-ray micro-computed tomography (microCT) and histological analysis to compare morphological phenotype in mouse (10) and human. *Ltbp3*^{-/-} mutant mice displayed enamel defects with very thin to absent enamel in both incisors and molars (Fig. 4). Hence, the *Ltbp3*^{-/-} mouse model clearly recapitulates the AI phenotype observed in our patients. Mandibular relative class III prognathism due to maxillary underdevelopment, seen in patients IV.1 and IV.2 of family 1, was also present in the mutant mouse model. Histological analysis of continuously growing incisor enamel organ revealed a cohesive, however at defined localizations, non-palisadic ameloblasts layer facing a thinner disorganized enamel matrix (Fig. 4M) confirming at the cellular level the dysfunction of amelogenesis.

Discussion

Using a combined strategy of homozygosity mapping and whole-exome sequencing in four unrelated families with the association of brachyolmia and AI, we identified the *LTBP3* (latent TGF-beta binding protein 3) gene as the underlying causal gene responsible for this rare autosomal recessive disorder [MIM 601 216]. Mutations in the *LTBP3* gene have already been reported in individuals with oligodontia (5), a dental developmental disorder defined by the absence of more than six permanent teeth. The question therefore arises if mutations in *LTBP3* can cause different dental phenotypes and how we can explain the presence of extra-dental manifestations such as brachyolmia in our families.

One gene associated with different phenotypes?

A homozygous nonsense mutation in the *LTBP3* gene was first reported in a consanguineous Pakistani family with oligodontia (5).

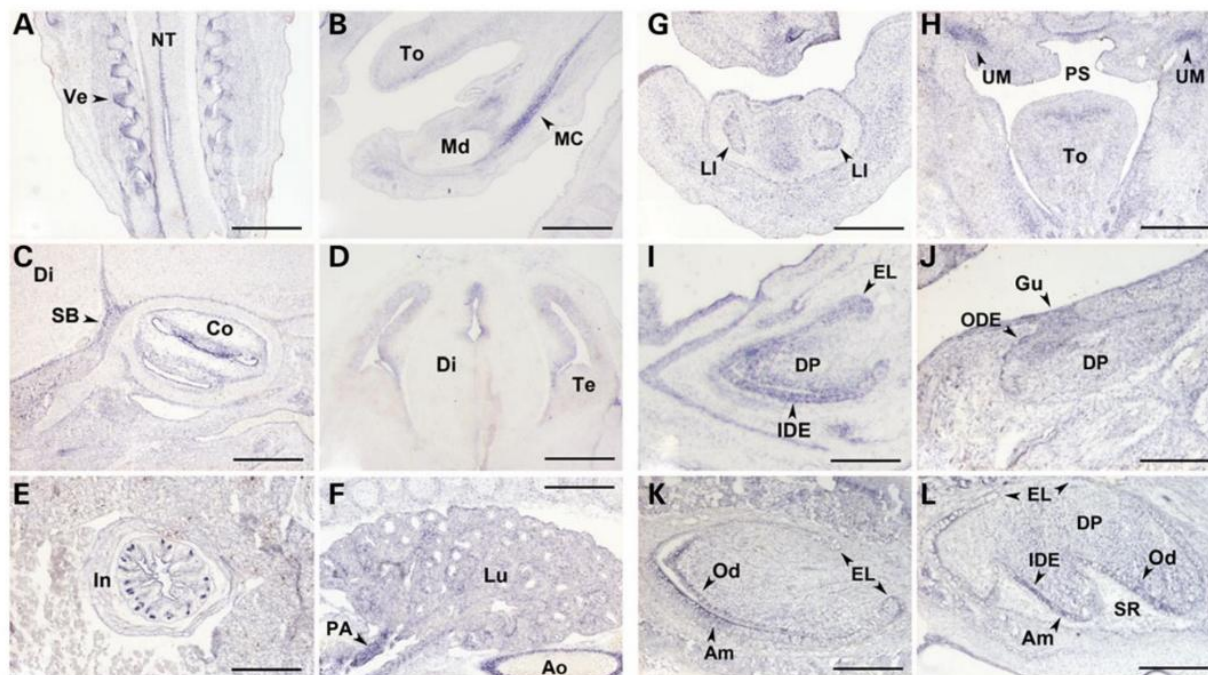


Figure 3. Analysis of mouse *Ltbp3* transcripts distribution by in situ hybridization. Selected sections illustrating *Ltbp3* expression features in the developing bone, central nervous system and viscera are shown in the left-side panels (A–F), whereas right-side panels focus on incisor (G, I and K) and molar (H, J and L) tooth development. Developmental stages and section planes are: E14.5 frontal (A, D, F, G and H), E16.5 sagittal (B, C, I and J); E18.5 sagittal (E, K and L) sections. Am, ameloblasts; Ao, aorta; Co, cochlea; Di, diencephalon; DP, dental papilla; EL, epithelial loop; Gu, gubernaculum; IDE, inner dental epithelium; In, intestine (duodenum); LI, lower incisor; Lu, lung; MC, Meckel's cartilage; Md, mandible; NT, neural tube; Od, odontoblasts; ODE, outer dental epithelium; PA, pulmonary artery; PS, palatal shelves; SB, skull bone; SR, stellate reticulum; Te, telencephalon; To, tongue; UM, upper molar; Ve, vertebrae. Scale bars: 40 μ m (B and D–H); 50 μ m (C, K and L); 80 μ m (I and J); 150 μ m (A).

Based on the available data in the report, we believe that the oligodontia phenotype in this family was either related to early loss of teeth due to enamel defects or caused by defective tooth development leading to absent teeth. Close examination of the skull X-ray of an affected patient in their published Figure 2 (5) clearly shows absent enamel and short roots in the remaining teeth, which suggests the diagnosis of an AI. Verloes *et al.* also mentioned oligodontia as a feature in his family with brachyolmia and AI (3). Missing teeth were also found in our family 4. Oligodontia may therefore be part of the clinical spectrum of this condition. The affected individuals in the consanguineous Pakistani family with oligodontia also presented with short stature. Varying degrees of scoliosis were apparently present but no other skeletal anomalies were observed. The authors do not report flattening of the vertebral bodies in their family and no lateral views of the spine are shown in their article. They only describe a higher bone mineral density in the spine found by dual-energy X-ray absorptiometry. Although we cannot judge on the presence or absence of brachyolmia as cause of the short stature in the affected individuals, we believe that this reported family with oligodontia may be affected by the same disorder given the presence of a recessive mutation in the *LTBP3* gene.

LTBP3 and TGF- β acting as partners

The *LTBP3* gene (NM_001130144.2, 11q13.1) spans 28 exons, has 20 372 base pairs and generates 22 different transcripts (only two major transcripts with CCDS number, eight without a protein and two resulting in nonsense-mediated decay).

LTBP3 codes for a protein of the extracellular matrix that is involved in regulation of TGF- β secretion, trapping and

activation (11–13). *LTBP3* (1139 amino acids, NCBI RefSeq: NP_001157738.1; 1303 amino acids NM_001130144.2) is one of the four members of the *LTBP*/fibrillin family and can form a large complex with latent TGF- β 1, 2 and 3 (14). The *LTBP* protein domain structure consists of EGF-like calcium-binding conserved domains, 4 TGF- β -binding protein-like (TB) domains also named eight cysteine repeats as well as insulin-like growth factor binding protein domains (Fig. 2). This domain structure is also found in TGF-binding protein and fibrillins.

LTBP3 and AI

TGF- β 1, 2 and 3 are growth factors involved in various biological functions such as cell growth and differentiation, extracellular matrix secretion and remodeling. TGF- β signaling is essential for hair and tooth growth especially enamel formation. Enamel is a complex structure secreted by ameloblasts presenting different successive stages during their life cycle. In mammals it is possible to recognize an initial aprismatic enamel layer at the dentin-enamel junction deposited by secreting ameloblasts without Tomes' process, then the bulk of enamel with rod and interrod compartments forms with secreting ameloblasts with Tomes' process and finally the last-formed surface aprismatic layer of enamel with the retraction of ameloblasts' Tomes' process (15). *Ltbp3* expression pattern in differentiating ameloblasts and odontoblasts is highly similar to that of TGF- β 1 (16–18). Blockade of TGF- β signaling results in a failure of ameloblasts to produce an enamel layer in incisor teeth (11). Overexpression of TGF- β 1 in teeth results in detachment of ameloblasts and enamel defects (1,19). TGF- β 1 and TGF- β receptor 1 (*TGFR1*) genes are strongly expressed in secreting

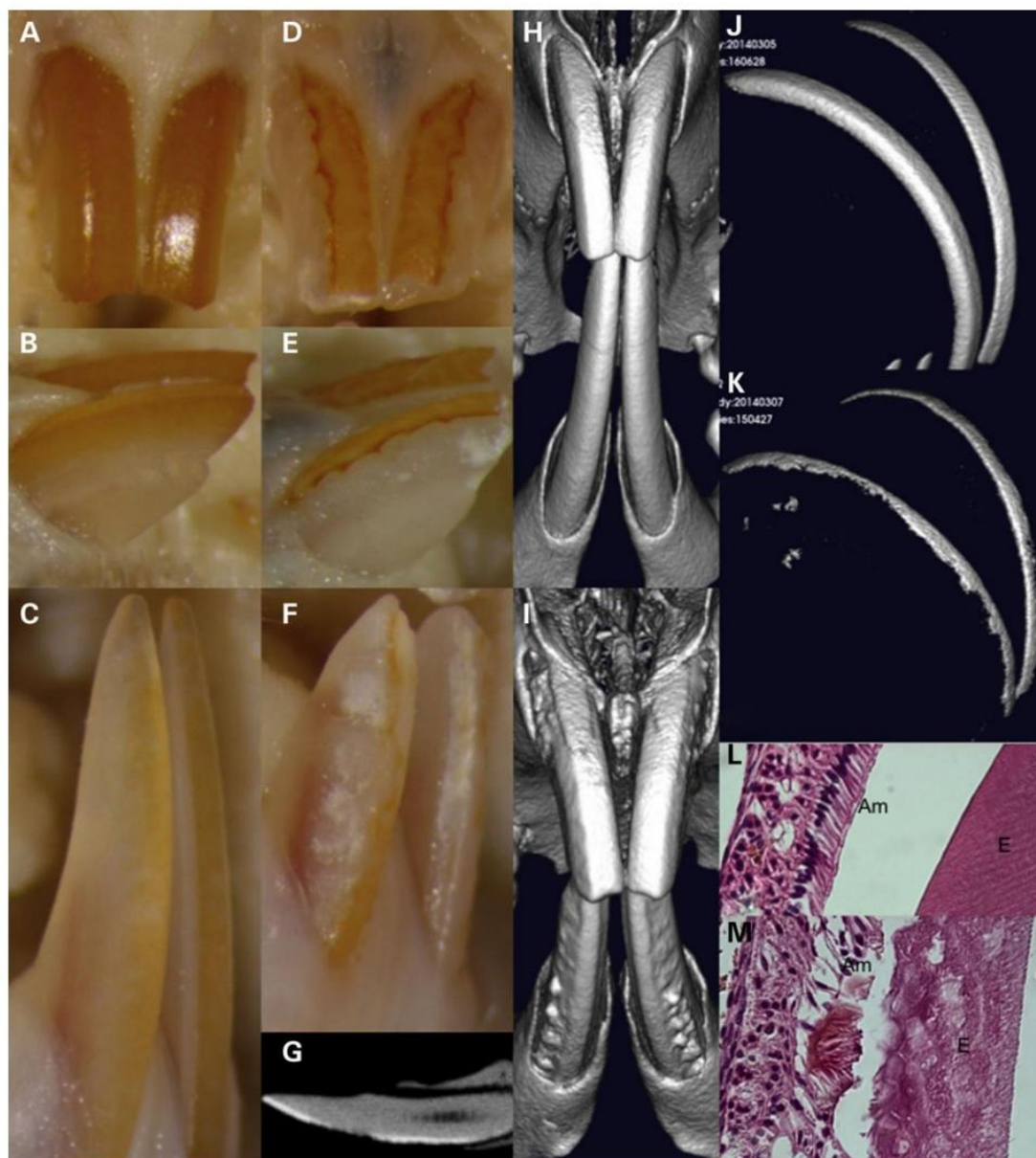


Figure 4. MicroCT and histological analysis of *Ltbp3*^{-/-} mice. The Quantum FX® microCT Pre-clinical In Vivo Imaging System is a low X-ray dose system devised for longitudinal microCT in preclinical studies (Caliper Life Sciences, Inc., Hopkinton, MA, USA). Seven *Ltbp3*^{-/-} mouse heads and seven WT littermates were analyzed. (A–C) Normal macroscopic aspect of the mouse upper (A face, B side view) and lower incisors (C: side view). Note that the teeth are naturally colored yellow that enamel is smooth and present only on the labial side. The lower incisors are twice as long as the upper. (D–F) Enamel defects encountered in *Ltbp3*^{-/-} mouse. The colored area is decreased and an irregular indented enamel surface is present. (G) Appearance of lower incisor from *Ltbp3*^{-/-} mouse as observed by X-ray imaging. Note irregular contour of thin enamel, a hypoplastic area, with limited or no enamel is seen on the labial side. (H–I) 3D reconstruction of microCT imaging demonstrating the outer surface appearance and contact between continuously growing incisors in a WT mouse (H) or *Ltbp3*^{-/-} mouse (I). The enamel surface is reduced and the tooth surface irregular. (J–K) Normal (J: WT) and reduced (in size and density) enamel layer (K: *Ltbp3*^{-/-} mouse), as observed when isolated from dentin through its highest mineralization and therefore X-ray density degree. (L) Normal ameloblasts (Am) layer facing a highly organized decalcified enamel (E) matrix. (M) In the *Ltbp3*^{-/-} mouse, in certain area, the ameloblast layer became erratic, like blubbing and laid out a differently organized thinner enamel matrix.

ameloblasts where they promote the expression of MMP20, an enamel matrix protease (20). TGF- β 1 is also expressed later in the maturation-stage ameloblasts and seems to play an important role in ameloblast apoptosis (21). In addition, TGF- β 1 is able to induce *KLK4* (a protease degrading enamel proteins to increase mineralization) expression (22,23). TGF- β 1 may also control cell layer integrity for odontoblasts (24).

The enamel defects, observed in our families, at the ultrastructural level (Fig. 1) with both the absence of the initial aprismatic enamel layer and the abnormal secretion of non-prismatic bulk enamel, strongly suggest a role of *LTPB3* during the life cycle of ameloblasts especially at the secretory stages with Tomes process formation/modulation. The molecular mechanisms that control the formation, function and retraction of Tomes' process

are not well understood. However clear molecular differences exist between NPE and PE (25) and this may involve TGF-beta signaling. Transgenic mice presenting with enamel defects such as the amelotin (AMTN) overexpression model also exhibit enamel defects in relation with the disappearance of Tomes' process (26). We therefore formulate the hypothesis that TGF-beta signaling is involved in the modulation of Tomes' process and the deposition of a decussating prisms enamel pattern. Interestingly, the *Klk4* ablated mice display rod/interrod anomalies besides enamel maturation defects (27).

LTBP3 and brachyolmia

LTBP3 is also involved in bone formation and remodeling. Inactivation of LTBP3 reduces TGF-beta activation and therefore diminishes associated cell proliferation and osteogenic differentiation (28). TGF-beta is the most abundant growth factor in bone playing a major role in bone development and skeletogenesis, especially during endochondral ossification but also later in adult bone homeostasis and remodeling (29). Deregulation of the TGF-beta signaling pathway is likely to interfere with axial skeleton patterning (30).

Ltbp3 is expressed in cartilage primordia especially in developing vertebrae (7). Recently, genes such as TRPV4 (transient receptor potential cation channel, subfamily V, member 4 gene) have been identified in autosomal dominant brachyolmia (31) and PAPSS2 (3'-phosphoadenosine 5'-phosphosulfate synthase 2) in autosomal recessive brachyolmia (32). A direct relationship may exist between the TGF-beta signaling pathway and the TRPV4 and PAPSS2 genes. TRPV4 regulates cardiac fibroblast differentiation to myofibroblasts by integrating signals from TGF-beta1 and mechanical factors (33). Altered responsiveness to TGF-beta results in reduced *Papss2* expression and alterations in the biomechanical properties of mouse articular cartilage (34).

The role of LTBP3 in bone development is also exemplified by the *Ltbp3*^{-/-} knockout mouse phenotype (7,8,35,36). These animals show growth retardation, obliteration of the skull synchondrosis within 2 weeks of birth, osteopetrosis of long bones and vertebrae and osteoarthritis. Thoracic kyphosis (curvature of the cervical and thoracic vertebrae) and distorted ribcage were also observed in the mutant mice. The high bone mass was related to a defect in bone resorption with compromised osteoclast function and decreased bone turnover (9). Platyospondyly however was not observed in the *Ltbp3*^{-/-} knockout mice.

A wider phenotype

A previous report has described expression of LTBP3 in various human tissues and cell lines, predominantly in heart, skeletal muscle, prostate and ovaries, as well as testis and small intestine (14). *Ltbp3* was also found to be expressed in the rat brain, with a partially overlapping expression with several other TGF-beta family members (37). Basioccipital-basisphenoid synchondrosis of P1 mouse expressed *Ltbp3* in prehypertrophic chondrocytes. *Ltbp3* transcripts were also present in adult mouse tissues in heart, brain, lung and kidney (7,8). We also report the transcription of *ltbp3* in brain vesicles, in cells surrounding the lumen of the neural tube, in the developing inner ear, in the small and large intestine, in the differentiating lung, in heart outflow tract and in the wall of the large blood vessels (Fig. 3).

It is surprising that the mutations of LTBP3 in human seem to affect only two organ systems, the skeleton and the teeth. It will be very important to follow over time the cohort of patients to assess the clinical relevance of this in situ hybridization data and to

record any additional occurring illness that may extend the phenotype spectrum.

Ltbp3^{-/-} knockout mouse model display an enamel phenotype

Analyzing further the *Ltbp3*^{-/-} knockout mouse with respect to the craniofacial and orodental phenotypes was of importance to convince that LTBP3 is indeed the causative gene behind brachyolmia associated with AI.

As described in refs. (7-9) craniofacial malformations were identified in *Ltbp3*^{-/-} mice at postnatal day 12. By 3 months of age mutant mice displayed a pronounced rounding of the cranial vault, extension of the mandible beyond the maxilla and kyphosis. The altered skull shape with occipital bossing was believed to be caused by the premature ossification of the cranial base synchondroses. Shortened skull base and disproportionately short upper jaw were evident. The external facial appearance was characterized by a rounded head and a shortened snout. Our analysis indicated that almost all craniofacial structures were affected in the *Ltbp3*-null mice. Alterations were observed in intramembranous and endochondral bones, along with in teeth. Compared with wild-type (WT) mice, *Ltbp3*-null mutants presented with an overall reduction in craniofacial size and modifications of the shape of various parts of the craniofacial skeleton. Modifications of viscerocranium, neurocranium and mandible were prominent changes.

Some of the skeletal and growth anomalies observed in the *Ltbp3*^{-/-} mice were also present in our patients (short maxilla, mandibular prognathism) but others (such as the increased bone density) were not present, underscoring the fact that the mouse phenotype is not always recapitulating the human phenotype. We do know secreting ameloblasts express *Ltbp3*. The enamel was clearly defective in the mouse mutant. It was thinner, less mineralized and exhibited an unusual wavy pattern with alternating area of presence/absence. Both incisors and molars were affected. *Ltbp3*^{-/-} ameloblasts as seen on histological sections of continuously growing incisor enamel organ were, in spotted area, able to synthesize an extruding NPE matrix confirming at the cellular level the impaired amelogenesis and the wavy pattern appearance.

This knockout-mice is now to be inscribed in the list of animal models presenting with enamel defects (38) and will likely serve as an important model to study further brachyolmia with AI (39).

In conclusion, the study of four unrelated families with the association of AI and brachyolmia has led to the identification of LTBP3 as causal gene. Our study not only confirms the existence of this rare, autosomal recessive disorder but also highlights the role of LTBP3 and TGF-beta signaling in amelogenesis, both in humans and mice. It also adds another member to the growing list of genes causing isolated and syndromic forms of brachyolmia. Study of additional families is warranted for better understanding of the phenotypic spectrum of this disorder given the wide expression of the LTBP3 gene.

Materials and Methods

Patients

In Family 1, two sisters born from a consanguineous family of Turkish origin were referred to the Reference Center for Rare Oro-dental Diseases at the Strasbourg University Hospital because of pain and enamel defects (Fig. 1). Besides short stature (140 cm adult height, -4.2 SD), they also showed facial dysmorphism with large forehead, thick eyebrows, almond shaped eyes,

myopia and mild learning difficulties. Radiographs of the skeleton revealed brachyolmia (Fig. 1E and F) and there were no signs of a generalized skeletal dysplasia. Bone age was considered as normal.

Their orodental findings were documented using the D[4]/phenodent Diagnosing Dental Defects Database registry (www.phenodent.org).

Enamel was almost absent (hypoplastic AI) in both primary and permanent dentitions (Fig. 1A and B). The teeth were yellow, small and spaced. Several teeth were surgically extracted because of recurrent infections. On orthopantomogram, no enamel was observed, pulp chambers were large and molars were taurodontic (Fig. 1C). Lateral cephalogram showed somewhat thickened cortical plates of the frontal bone and an absence of pneumatization of the frontal and sphenoid sinuses. Posterior clinoid apophyses of the sphenoid were abnormally shaped. Class III mandibular prognathism was due to maxillary underdevelopment (Fig. 1D).

Family 2 consisted of two sibs born to non-consanguineous, unrelated Caucasian parents. The female proband (III.6) is the sixth child. Birth weight was 2.760 g, birth length 46 cm and head circumference was 33 cm at 39 weeks of gestation. She had normal psychomotor development and no general health problems. Primary teeth were small and yellowish with a poor square morphology and rounded cusps without pronounced fissures. The enamel was smooth and showed external crown resorption before molars erupted. She suffered of repeated dental abscesses, leading to the extraction of several teeth at ages 2½ and 5 years. When seen at age 8, she had clearly hypoplastic AI, microdontia and taurodontism. At age 13, she was 149 cm tall (−1.5 SD), weighed 42 kg and had an occipital-frontal circumference of 51 cm. She had a triangular face with retraction of the midface. She had short hands with stubby interphalangeal joints. Pro- and supination movements were limited. Osteotendinous reflexes in the lower limbs were jerky. Single nucleotide polymorphism (SNP)-array was normal (Illumina CytoSNP-12 v2) and did not reveal homozygosity stretches. Radiographs showed mild platyspondyly. Her brother (III.7) was the seventh sib of the family. He was prematurely born at 28 weeks of gestation and remained in the intensive neonatal care unit for 3 months, without major cardiopulmonary or neurological complication. Inguinal herniae were surgically corrected. He walked at age 14 months and his first words were delayed to 2½ years. He required speech therapy. When examined at age 5½ year-old, he was 101 cm tall (−3 SD), weighed 16 kg and had a head circumference of 48.5 cm. His teeth were small and yellow lacking enamel. He had a triangular face, converging squint, a narrow thorax with prominent sternum and hypermobile small joints. The family history was unremarkable. Parents had normal height (175 cm for the father and 170 for the mother) and teeth. The six other sibs were normal.

Family 3 has been described previously by Bertola *et al.* (4). The proband is a 12-year-old boy from consanguineous and healthy parents. The patient sat unsupported at 8 months of age, walked at 12 months, said his first words at 2 years. Although the mother refers some difficulties in learning, he attends a regular school (currently last year of high school). He presented with short stature (height at −3 SD for age) and enamel defects in the primary and permanent dentition. A panoramic radiograph revealed taurodontic pulp chambers of the permanent teeth. Skeletal survey showed mild flattening of the vertebral bodies with minimal posterior scalloping and no evidence of a generalized epi- or metaphyseal dysplasia. Mother and father have normal height (145 and 162.5 cm, respectively) and dental status. This was confirmed by clinical and X-ray examinations.

Family 4 includes three affected sibs in a sibship of five children born to first cousin parents of Pakistani origin. The three affected children, two girls and one boy of, respectively, 16, 9 and 12 years of age, presented with short stature (height ranging from −2 to −5 SD). They were disproportionate with short trunk due to a generalized platyspondyly. Radiographs showed osteopenia and mild vertebral flattening with posterior scalloping and superior and inferior indentations in the posterior third of the lumbar vertebrae. The oldest girl underwent surgery for an S-shaped scoliosis. The scoliosis in the two other children was rather mild. Recurrent dental abscesses were noted and the dental practitioner confirmed a diagnosis of AI with missing teeth.

None of the family members had intellectual disability. The father's height was 165.2 cm (3rd–10th centile), and the mother's height was 149.4 cm (>3rd centile). None of the unaffected member of the family have skeletal nor dental anomalies.

Genetic analyses

This study was approved by the ethics committee of the Strasbourg University Hospital (ClinicalTrials.gov Identifier: NCT01746121). Informed consent and DNA samples were obtained from all participating individuals. Genomic DNA was isolated either from blood using the Flexigene DNA kit (Qiagen, Courtaboeuf, France) or from saliva using the prepIT-L2P OG-250 Oragene[®] DNA kit (DNA Genotek Inc., ON, Canada). Whole-exome sequencing was performed by IntegraGen (Evry, France). The coding parts of the genome were captured using the SureSelect Human All Exon Kits V5+UTR 70 Mb (Agilent, Massy, France) and the resulting libraries were sequenced as paired-end 75 base pair reads on a HiSeq 2000 (Illumina, San Diego, USA). Image analysis and base calling were performed using the Real Time Analysis (RTA) Pipeline version 1.9 with default parameters (Illumina). The bioinformatic analysis of sequencing data was based on the CASAVA.1.8 pipeline (Illumina). CASAVA performs alignment and detects variants (SNPs and indels) based on the allele calls and read depth. The variants were annotated and prioritized using an in-house pipeline VaRank (<http://lbg.fr/VaRank/>, (40) (41).

Sanger sequencing (GATC Biotech, Applied Biosystems ABI 3730xl[™], Konstanz, Germany) was used to validate the mutations and verify segregation using the primers shown in Supplementary Material, Table S2.

Homozygosity mapping via GeneChip Human 250 K SNP Affymetrix was performed as previously described (42) in family 1 on affected individuals IV.1, IV.2, on the unaffected individual IV.3 and both parents III.3 and III.4 (Supplementary Material, Fig. S1).

cDNA analysis

RNA was extracted from fibroblasts of patient IV.1 (gingival biopsy) and one unrelated control by using a RiboPure[™] Kit, followed by a DNase treatment with the TURBO DNA-free[™] Kit (Life Technologies, Carlsbad, CA). RNA integrity was assessed by gel electrophoresis and RNA concentration was measured with the Eppendorf Biophotometer Plus[™] with the Hellma[®] TrayCell[™] (Eppendorf, Hamburg, Germany). Reverse transcription of 1 µg total RNA to cDNA was performed using the iScript[™] cDNA Synthesis Kit (BioRad, Hercules, CA). Reverse transcription polymerase chain reaction was performed to determine the exon content of the cDNA from the patient. Primers used for reverse transcription polymerase chain reaction are shown in Supplementary Material, Table S2.

Scanning electron microscopy

The permanent left upper second premolar (25) of patient IV2, family 1, as well as an identical control tooth, were available for the comparative study of enamel AI/control ultrastructure. After extraction, the teeth were rinsed with tap water and immersed in a sodium hypochlorite solution (1.2 chlorometric degree) for 24 h. After a rinsing with distilled water the tooth was dehydrated in a graded series of ethanol, transferred in a solution of propylene oxide/epon resin (v/v) for 24 h, then embedded in Epon 812 (Euro-medex, Souffelweyersheim, France). The tooth was sectioned into two halves along its vertical axis using a water-cooled diamond circular saw (Bronwill, NY, USA) and both surfaces were polished with diamond paste (Escil, Chassieu, France). One half was then etched with a 20% (m/v) citric acid solution for 2 min, rinsed with distilled water, dehydrated in a graded series of ethanol solutions and finally left to dry at room temperature. The samples were coated with a gold-palladium alloy using a HUMMER JR sputtering device (Technics, CA, USA). Scanning electron microscope assessments and microanalysis (Energy dispersive X-ray) were performed with a XL SIRION 200 FEG SEM (FEI company, Eindhoven, The Netherlands) operating with an electron accelerating voltage of 5 kV.

In situ hybridization

Sample preparation

Mouse embryos/fetuses were collected at E12.5, E14.5, E16.5 and E18.5, after natural mating between C57BL6 mice. All experiments were carried out in accordance with the European Community Council Directive of 24 November 1986 (86/609/EEC). The project was approved by the ICS/IGBMC animal experimentation ethics committee (2012-097). For E14.5 and older samples, the whole body was embedded in OCT 4583 medium (Tissue-TEK, Sakura) and frozen on the surface of dry ice. E12.5 embryos were fixed overnight in 4% paraformaldehyde (pH 7.5, w/v) in phosphate buffered saline (PBS), cryoprotected by overnight incubation in 20% sucrose (w/v) in PBS and cryoembedded as described above. Cryosections (Leica CM3050S cryostat) at 10 μ m were collected on Superfrost plus slides and stored at -80°C until hybridization. E12.5 and E14.5 samples were sectioned in a frontal plane, whereas other stages were sectioned sagittally.

Probe synthesis

The *Ltbp3* probe was synthesized from PCR-generated DNA templates kindly provided by the EURExpress consortium (<http://www.eurexpress.org>). The template sequence is given in Supplementary Material, Fig. S3. DIG-labeled antisense riboprobe was transcribed *in vitro* by incubation for 2 h at 37°C using 1 μ g of the PCR product, 20 U SP6 RNA polymerase, 5 \times transcription buffer (Promega), 10 \times DIG RNA labeling Mix (Roche), 0.5 M 1,4-Dithiothreitol, 20 U RNase inhibitor (Roche) in a 20- μ l volume. The reaction was stopped with 2 μ l EDTA (0.2 M, pH 8), and RNA was precipitated with 1 μ l yeast tRNA (10 mg/ml), 2.5 μ l LiCl (4 M) and 75 μ l absolute ethanol, followed by an incubation for 30 min at -80°C and centrifugation at 12 000 rpm (30 min at 4°C). The pellet was washed with 0.5 ml ethanol (70%) and re-centrifuged. The supernatant was discarded and the pellet was allowed to dry. The probe was then diluted in 20 μ l sterile H_2O . The quality of the probe was verified by electrophoresis in a 1% agarose gel. If no smear was observed and the size was as expected, the probe was considered to be ready for use. The quantity of RNA was evaluated by Nanodrop (ND-1000

Spectrophotometer, Labtech) and adjusted to 150 ng/ μ l in hybridization buffer, then stored at -20°C until use.

In situ hybridization

In situ hybridization was performed as previously described (43).

MicroCT imaging

Fixed in ethanol heads of 7 (5 \times 3.5 months-old and 2 \times 5.5 months-old) mutant *Ltbp3*^{-/-} mice and 7 WT littermates were analyzed through X-ray micro-CT using Quantum FX[®] microCT Pre-clinical In Vivo Imaging System (Caliper Life Sciences, Inc., Hopkinton, MA, USA), which operates at an energy of 80 kV and current intensity of 160 μ A, with high-resolution detection at 10–295 μ m pixel size. 3D data reconstructions were performed using Analyze software (v 11.0; Biomedical Imaging Resource, Mayo Clinic, Rochester, MN). Animals necropsy material was kindly provided by B. Dabovic and D.B. Rifkin, Department of Cell Biology, NYU Langone Medical Center, New York, NY.

Histological analysis

Fixed in 10% formalin and then transferred in 70% ethanol, heads of 3.5 months-old WT and *Ltbp3*^{-/-} mice were washed in water and then demineralized in EDTA 10% in H_2O at 37°C for 10 days (the demineralizing solution was changed every day for the first 3 days and then every other day). After thorough water washes, the heads were dehydrated in graded ethanol, cleared in histosol and embedded in paraffin at 60°C . 10 μ m transversal sections were stained with hematoxylin/eosin. A detailed histology protocol can be found at <http://www.empress.har.mrc.ac.uk>.

Supplementary Material

Supplementary Material is available at HMG online.

Acknowledgements

We would like to thank the patients and families for their participation. We are grateful to Nadia Messaddeq from the IGBMC Imaging centre for her help and support and to Yann Héroult and Isabelle Goncalves da Cruz from the Mouse Clinical Institute for facilitating access to the Micro-CT imaging. We thank Vanessa Stoehr for her efficient management of the INTERREG project. All contributors have read and approved the submitted manuscript.

Conflict of Interest statement. None declared.

Funding

This work was supported by grants from the University of Strasbourg, the French Ministry of Health (National Program for Clinical Research, PHRC 2008 No. 4266 Amelogenesis imperfecta), the Hôpitaux Universitaires de Strasbourg (API, 2009-2012, 'Development of the oral cavity: from gene to clinical phenotype in Human'), IFRO (Institut Français pour la Recherche Odontologique) and the EU-funded project (ERDF) A27 'Oro-dental manifestations of rare diseases', supported by the RMT-TMO Offensive Sciences initiative, INTERREG IV Upper Rhine program www.genosmile.eu. Work performed at IGBMC was supported by the grant ANR-10-LABX-0030-INRT, a French State fund managed by the Agence Nationale de la Recherche under the frame programme Investissements d'Avenir labelled ANR-10-IDEX-0002-02. Funding was also received under the European Commission Seventh

Framework Programme (SYBIL project; grant number 602300). E.B. holds a post-doctoral fellowship of the FWO (Fund for Scientific Research—Flanders). B.B.D. and D.B.R. are funded by National Institutes of Health: NIH R01 CA034282. Funding to pay the Open Access publication charges for this article was provided by the EU-funded project (ERDF) A27 “Oro-dental manifestations of rare diseases”, supported by the RMT-TMO Offensive Sciences initiative, INTERREG IV Upper Rhine program www.genosmile.eu.

Web Resources

The URLs for data presented herein are as follows:

1000 Genome Browser, <http://browser.1000genomes.org>
 BDGP, <http://www.fruitfly.org>
 D[4]/phenodent Diagnosing Dental Defects Database, www.phenodent.org
 dbSNP, <http://www.ncbi.nlm.nih.gov/projects/SNP>
 Ensembl Genome Browser, <http://www.ensembl.org>
 Eurexpress, <http://www.eurexpress.org/ee/>
 Exome Variant Server (EVS) <http://evs.gs.washington.edu/EVS/>
 GenBank, <http://www.ncbi.nlm.nih.gov/Genbank>
 GeneHub-GEPIS, <http://www.cgl.ucsf.edu/Research/genentech/genehub-gepis/genehubgepis-search.html>
 Gene expression in tooth, <http://bite-it.helsinki.fi>
 GenePaint, <http://www.genepaint.org>
 HSF2.4.1, <http://www.umd.be/HSF>
 NCBI, <http://www.ncbi.nlm.nih.gov/>
 Online Mendelian Inheritance in Man (OMIM), <http://www.omim.org>
 UCSC Genome Browser, <http://genome.ucsc.edu/cgi-bin/hgGateway>
 UniGene, <http://www.ncbi.nlm.nih.gov/unigene>
 VaRank, <http://lbgf.fr/VaRank/>
 EMBL-EBI Interpro, <http://www.ebi.ac.uk/interpro/>
 EMPReSS, <http://www.empress.har.mrc.ac.uk>

References

- Crawford, P.J., Aldred, M. and Bloch-Zupan, A. (2007) Amelogenesis imperfecta. *Orphanet J. Rare Dis.*, **2**, 17.
- Bloch-Zupan, A., Sedano, H. and Scully, C. (2012) *Dento/Oro/Craniofacial Anomalies and Genetics*. Elsevier Inc., London.
- Verloes, A., Jamblin, P., Koulischer, L. and Bourguignon, J.P. (1996) A new form of skeletal dysplasia with amelogenesis imperfecta and platyspondyly. *Clin. Genet.*, **49**, 2–5.
- Bertola, D.R., Antequera, R., Rodvalho, M.J., Honjo, R.S., Albano, L.M., Furquim, I.M., Oliveira, L.A. and Kim, C.A. (2009) Brachyolmia with amelogenesis imperfecta: further evidence of a distinct entity. *Am. J. Med. Genet. A*, **149A**, 532–534.
- Noor, A., Windpassinger, C., Vitcu, I., Orlic, M., Rafiq, M.A., Khalid, M., Malik, M.N., Ayub, M., Alman, B. and Vincent, J.B. (2009) Oligodontia is caused by mutation in LTBP3, the gene encoding latent TGF-beta binding protein 3. *Am. J. Hum. Genet.*, **84**, 519–523.
- Laugel-Haushalter, V., Paschaki, M., Thibault-Carpentier, C., Demele, D., Dolle, P. and Bloch-Zupan, A. (2013) Molars and incisors: show your microarray IDs. *BMC Res. Notes*, **6**, 113.
- Dabovic, B., Chen, Y., Colarossi, C., Zambuto, L., Obata, H. and Rifkin, D.B. (2002) Bone defects in latent TGF-beta binding protein (Ltbp)-3 null mice; a role for Ltbp in TGF-beta presentation. *J. Endocrinol.*, **175**, 129–141.
- Dabovic, B., Chen, Y., Colarossi, C., Obata, H., Zambuto, L., Perle, M.A. and Rifkin, D.B. (2002) Bone abnormalities in latent TGF-[beta] binding protein (Ltbp)-3-null mice indicate a role for Ltbp-3 in modulating TGF-[beta] bioavailability. *J. Cell Biol.*, **156**, 227–232.
- Dabovic, B., Levasseur, R., Zambuto, L., Chen, Y., Karsenty, G. and Rifkin, D.B. (2005) Osteopetrosis-like phenotype in latent TGF-beta binding protein 3 deficient mice. *Bone*, **37**, 25–31.
- Nieman, B.J., Wong, M.D. and Henkelman, R.M. (2011) Genes into geometry: imaging for mouse development in 3D. *Curr. Opin. Genet. Dev.*, **21**, 638–646.
- Klopčič, B., Maass, T., Meyer, E., Lehr, H.A., Metzger, D., Chambon, P., Mann, A. and Blessing, M. (2007) TGF-beta superfamily signaling is essential for tooth and hair morphogenesis and differentiation. *Eur. J. Cell Biol.*, **86**, 781–799.
- Annes, J.P., Munger, J.S. and Rifkin, D.B. (2003) Making sense of latent TGFbeta activation. *J. Cell Sci.*, **116**, 217–224.
- Hyttiäinen, M., Penttinen, C. and Keski-Oja, J. (2004) Latent TGF-beta binding proteins: extracellular matrix association and roles in TGF-beta activation. *Crit. Rev. Clin. Lab. Sci.*, **41**, 233–264.
- Penttinen, C., Saharinen, J., Weikkolainen, K., Hyttiäinen, M. and Keski-Oja, J. (2002) Secretion of human latent TGF-beta-binding protein-3 (LTBP-3) is dependent on co-expression of TGF-beta. *J. Cell Sci.*, **115**, 3457–3468.
- Inage, T., Fujita, M., Kobayashi, M., Wakao, K., Saito, N., Shibuya, H., Shimada, M. and Takagi, K. (1990) Ultrastructural differentiation in the distal ends of ameloblasts from the pre-secretory zone to the early secretory zone. *J. Nihon Univ. Sch. Dent.*, **32**, 259–269.
- Zhu, Q., Fan, M., Bian, Z., Chen, Z., Zhang, Q. and Peng, B. (2000) In situ hybridization analysis of transforming growth factor-beta 1 RNA expression during mouse tooth development. *Chin. J. Dent. Res.*, **3**, 21–25.
- Fan, M.W., Bian, Z. and Gao, Y.G. (1998) Immunohistochemistry and in situ hybridization investigation of transforming growth factor-beta: during odontoblast and ameloblast differentiation. *Chin. J. Dent. Res.*, **1**, 17–21.
- Khan, Q.E., Sehic, A., Khuu, C., Risnes, S. and Osmundsen, H. (2013) Expression of Clu and Tgfb1 during murine tooth development: effects of in-vivo transfection with anti-miR-214. *Eur. J. Oral Sci.*, **121**, 303–312.
- Haruyama, N., Thyagarajan, T., Skobe, Z., Wright, J.T., Septier, D., Sreenath, T.L., Goldberg, M. and Kulkarni, A.B. (2006) Overexpression of transforming growth factor-beta1 in teeth results in detachment of ameloblasts and enamel defects. *Eur. J. Oral Sci.*, **114**(Suppl 1), 30–34.
- Gao, Y., Li, D., Han, T., Sun, Y. and Zhang, J. (2009) TGF-beta1 and TGFBR1 are expressed in ameloblasts and promote MMP20 expression. *Anat. Rec. (Hoboken)*, **292**, 885–890.
- Tsuchiya, M., Sharma, R., Tye, C.E., Sugiyama, T. and Bartlett, J.D. (2009) Transforming growth factor-beta1 expression is up-regulated in maturation-stage enamel organ and may induce ameloblast apoptosis. *Eur. J. Oral Sci.*, **117**, 105–112.
- Suzuki, M., Shin, M., Simmer, J.P. and Bartlett, J.D. (2014) Fluoride Affects Enamel Protein Content via TGF-beta1-mediated KLK4 Inhibition. *J. Dent. Res.*, **93**, 1022–1027.
- Cho, A., Haruyama, N., Hall, B., Danton, M.J., Zhang, L., Arany, P., Mooney, D.J., Harichane, Y., Goldberg, M., Gibson, C.W. et al. (2013) TGF-ss regulates enamel mineralization and maturation through KLK4 expression. *PLoS One*, **8**, e82267.
- Tjaderhane, L., Koivumäki, S., Paakkonen, V., Ilvesaro, J., Soini, Y., Salo, T., Metsikko, K. and Tuukkanen, J. (2013) Polarity of mature human odontoblasts. *J. Dent. Res.*, **92**, 1011–1016.
- Sehic, A., Risnes, S., Khan, Q.E., Khuu, C. and Osmundsen, H. (2010) Gene expression and dental enamel structure in developing mouse incisor. *Eur. J. Oral Sci.*, **118**, 118–130.
- Lacruz, R.S., Nakayama, Y., Holcroft, J., Nguyen, V., Somogyi-Ganss, E., Snead, M.L., White, S.N., Paine, M.L. and Ganss, B.

- (2012) Targeted overexpression of amelotin disrupts the microstructure of dental enamel. *PLoS One*, **7**, e35200.
27. Bartlett, J.D. and Simmer, J.P. (2014) Kallikrein-related peptidase-4 (KLK4): role in enamel formation and revelations from ablated mice. *Front. Physiol.*, **5**, 240.
 28. Koli, K., Ryyanen, M.J. and Keski-Oja, J. (2008) Latent TGF-beta binding proteins (LTBPs)-1 and -3 coordinate proliferation and osteogenic differentiation of human mesenchymal stem cells. *Bone*, **43**, 679–688.
 29. Kanaan, R.A. and Kanaan, L.A. (2006) Transforming growth factor beta1, bone connection. *Med. Sci. Monit.*, **12**, RA164–RA169.
 30. Alliston, T., Piek, E. and Derynck, R. (2008) 22 TGF- β Family Signaling in Skeletal Development, Maintenance, and Disease. In Derynck, R. and Miyazono, K. (eds), *The TGF-Beta Family*. Cold Spring Harbor Monograph Archive, North America, 50. Available at: <https://cshmonographs.org/index.php/monographs/article/view/3854> (last accessed, 17 February 2015).
 31. Grigelioniene, G., Geiberger, S., Horemuzova, E., Mostrom, E., Jantti, N., Neumeyer, L., Astrom, E., Nordenskjold, M., Nordgren, A. and Makitie, O. (2014) Autosomal dominant brachyolmia in a large Swedish family: phenotypic spectrum and natural course. *Am. J. Med. Genet. A*, **164**, 1635–1641.
 32. Iida, A., Simsek-Kiper, P.O., Mizumoto, S., Hoshino, T., Elcioglu, N., Horemuzova, E., Geiberger, S., Yesil, G., Kayserili, H., Utine, G.E. et al. (2013) Clinical and radiographic features of the autosomal recessive form of brachyolmia caused by PAPSS2 mutations. *Hum. Mutat.*, **34**, 1381–1386.
 33. Adapala, R.K., Thoppil, R.J., Luther, D.J., Paruchuri, S., Meszaros, J.G., Chilian, W.M. and Thodeti, C.K. (2013) TRPV4 channels mediate cardiac fibroblast differentiation by integrating mechanical and soluble signals. *J. Mol. Cell. Cardiol.*, **54**, 45–52.
 34. Ramaswamy, G., Sohn, P., Eberhardt, A. and Serra, R. (2012) Altered responsiveness to TGF-beta results in reduced Paps2 expression and alterations in the biomechanical properties of mouse articular cartilage. *Arthritis Res. Ther.*, **14**, R49.
 35. Colarossi, C., Chen, Y., Obata, H., Jurukovski, V., Fontana, L., Dabovic, B. and Rifkin, D.B. (2005) Lung alveolar septation defects in *Ltbp-3*-null mice. *Am. J. Pathol.*, **167**, 419–428.
 36. Chen, Y., Dabovic, B., Colarossi, C., Santori, F.R., Lilic, M., Vukmanovic, S. and Rifkin, D.B. (2003) Growth retardation as well as spleen and thymus involution in latent TGF-beta binding protein (*Ltbp*)-3 null mice. *J. Cell. Physiol.*, **196**, 319–325.
 37. Dobolyi, A. and Palkovits, M. (2008) Expression of latent transforming growth factor beta binding proteins in the rat brain. *J. Comp. Neurol.*, **507**, 1393–1408.
 38. Pugach, M.K. and Gibson, C.W. (2014) Analysis of enamel development using murine model systems: approaches and limitations. *Front. Physiol.*, **5**, 313.
 39. Fleischmannova, J., Matalova, E., Tucker, A.S. and Sharpe, P.T. (2008) Mouse models of tooth abnormalities. *Eur. J. Oral Sci.*, **116**, 1–10.
 40. Geoffroy, V., Pizot, C., Redin, C., Piton, A., Vasli, N., Stoetzel, C., Blavier, A., Laporte, J. and Muller, J. (2015) VaRank: a simple and powerful tool for ranking genetic variants. *PeerJ*. in press.
 41. Redin, C., Le Gras, S., Mhamdi, O., Geoffroy, V., Stoetzel, C., Vincent, M.C., Chiurazzi, P., Lacombe, D., Ouertani, I., Petit, F. et al. (2012) Targeted high-throughput sequencing for diagnosis of genetically heterogeneous diseases: efficient mutation detection in Bardet-Biedl and Alstrom syndromes. *J. Med. Genet.*, **49**, 502–512.
 42. Bloch-Zupan, A., Jamet, X., Etard, C., Laugel, V., Muller, J., Geoffroy, V., Strauss, J.P., Pelletier, V., Marion, V., Poch, O. et al. (2011) Homozygosity mapping and candidate prioritization identify mutations, missed by whole-exome sequencing, in *SMOC2*, causing major dental developmental defects. *Am. J. Hum. Genet.*, **89**, 773–781.
 43. Laugel-Haushalter, V., Langer, A., Marrie, J., Fraulob, V., Schuhbaur, B., Koch-Phillips, M., Dolle, P. and Bloch-Zupan, A. (2012) From the transcription of genes involved in ectodermal dysplasias to the understanding of associated dental anomalies. *Mol. Syndromol.*, **3**, 158–168.

RSK2 is a modulator of craniofacial development.

Laugel-Haushalter V, Paschaki M, Marangoni P, Pilgram C, Langer A, Kuntz T, Demassue J, **Morkmued S**, Choquet P, Constantinesco A, Bornert F, Schmittbuhl M, Pannetier S, Viriot L, Hanauer A, Dollé P, Bloch-Zupan A.

PLoS One. 2014 Jan 8;9(1):e84343. doi: 10.1371/journal.pone.0084343. eCollection 2014

RSK2 est un modulateur du développement crânio-facial.

CONTEXTE:

Le gène *RSK2* est responsable du syndrome de Coffin-Lowry, un trouble génétique transmis selon le mode dominant lié à X qui provoque un retard mental, un retard de croissance squelettique, des anomalies crânio-faciales et des doigts typiquement associées à ce syndrome. Les anomalies crânio-faciales et dentaires rencontrées dans cette maladie rare ont été insuffisamment caractérisées.

MÉTHODOLOGIE / PRINCIPAUX CONSTATS:

Nous avons examiné, en utilisant l'analyse microtomographique à rayons X, la dysmorphie crânio-faciale variable et les anomalies dentaires présentes chez les souris *Rsk2* knock-out (inactivée), modèles du syndrome de Coffin-Lowry, ainsi que chez les mutants triple knock-out pour *Rsk1,2,3*. Nous rapportons que la mutation de *Rsk* produit des dents surnuméraires de la ligne médiane / mésiale de la première molaire. Ce phénotype très pénétrant récapitule des structures dentaires plus ancestrales perdues au cours de l'évolution. Très probablement, cela entraîne une réduction du diastème maxillaire. Les anomalies de forme des molaires sont généralement limitées à la partie mésiale des premières molaires supérieures et inférieures (M1). L'analyse du patron expression des quatre gènes *Rsk* (*Rsk1, 2, 3 et 4*) a été réalisée à différents stades de l'odontogenèse chez des souris de type sauvage (WT). *Rsk2* est exprimé dans le compartiment mésenchymateux, dérivé de la crête neurale, en corrélation avec les zones prolifératives des dents en développement. Ceci est cohérent avec le fonctionnement de RSK2 dans le contrôle du cycle cellulaire et la régulation de la croissance, des fonctions potentiellement responsables de phénotypes dentaires sévères. Pour découvrir les voies moléculaires impliquées dans l'étiologie de ces défauts, nous avons effectué une analyse comparative transcriptomique (puce à ADN (microarray)) entre les molaires

mandibulaires de type sauvage et *Rsk2*^{-/-}. Nous avons également démontré une dérégulation de plusieurs gènes critiques, en utilisant une stratégie d'inactivation par shARN anti *Rsk2* dans les germes dentaires molaires cultivés *in vitro*.

CONCLUSIONS:

Cette étude révèle que RSK2 régule le développement crânio-facial, y compris le développement dentaire et le modelage via de nouvelles cibles transcriptionnelles.

RSK2 Is a Modulator of Craniofacial Development

Virginie Laugel-Haushalter¹, Marie Paschaki¹, Pauline Marangoni², Coralie Pilgram³, Arnaud Langer³, Thibaut Kuntz³, Julie Demassue³, Supawich Morkmued^{1,3,7}, Philippe Choquet⁴, André Constantinesco⁴, Fabien Bornert^{3,6}, Matthieu Schmittbuhl^{3,5,6}, Solange Pannetier¹, Laurent Viriot², André Hanauer¹, Pascal Dollé¹, Agnès Bloch-Zupan^{1,3,5*}

1 Institute of Genetics and Molecular and Cellular Biology (IGBMC), Centre National de la Recherche Scientifique (UMR 7104), Institut National de la Santé et de la Recherche Médicale (U 964), University of Strasbourg, Illkirch, France, **2** Team «Evo-Devo of Vertebrate Dentition», Institut de Génétique Fonctionnelle de Lyon, Unité Mixte de Recherche 5242 Centre National de la Recherche Scientifique, Ecole Normale Supérieure de Lyon, Claude Bernard Lyon 1 University, Lyon, France, **3** Faculty of Dentistry, University of Strasbourg, Strasbourg France, **4** UF6237 Preclinical Imaging Lab, Biophysics and Nuclear Medicine, Hôpitaux Universitaires de Strasbourg (HUS), Strasbourg, France; ICube, CNRS, University of Strasbourg, Strasbourg, France, **5** Reference Centre for Orofacial Manifestations of Rare Diseases, Pôle de Médecine et Chirurgie Bucco-dentaires, Hôpitaux Universitaires de Strasbourg (HUS), Strasbourg, France, **6** INSERM U1121, "Biomaterials and Bioengineering", University of Strasbourg, Strasbourg, France, **7** Faculty of Dentistry, Khon Kaen University, Khon Kaen, Thailand

Abstract

Background: The *RSK2* gene is responsible for Coffin-Lowry syndrome, an X-linked dominant genetic disorder causing mental retardation, skeletal growth delays, with craniofacial and digital abnormalities typically associated with this syndrome. Craniofacial and dental anomalies encountered in this rare disease have been poorly characterized.

Methodology/Principal Findings: We examined, using X-Ray microtomographic analysis, the variable craniofacial dysmorphism and dental anomalies present in *Rsk2* knockout mice, a model of Coffin-Lowry syndrome, as well as in triple *Rsk1,2,3* knockout mutants. We report *Rsk* mutation produces supernumerary teeth midline/mesial to the first molar. This highly penetrant phenotype recapitulates more ancestral tooth structures lost with evolution. Most likely this leads to a reduction of the maxillary diastema. Abnormalities of molar shape were generally restricted to the mesial part of both upper and lower first molars (M1). Expression analysis of the four *Rsk* genes (*Rsk1*, 2, 3 and 4) was performed at various stages of odontogenesis in wild-type (WT) mice. *Rsk2* is expressed in the mesenchymal, neural crest-derived compartment, correlating with proliferative areas of the developing teeth. This is consistent with RSK2 functioning in cell cycle control and growth regulation, functions potentially responsible for severe dental phenotypes. To uncover molecular pathways involved in the etiology of these defects, we performed a comparative transcriptomic (DNA microarray) analysis of mandibular wild-type versus *Rsk2*-Y molars. We further demonstrated a misregulation of several critical genes, using a *Rsk2* shRNA knock-down strategy in molar tooth germs cultured *in vitro*.

Conclusions: This study reveals RSK2 regulates craniofacial development including tooth development and patterning via novel transcriptional targets.

Citation: Laugel-Haushalter V, Paschaki M, Marangoni P, Pilgram C, Langer A, et al. (2014) RSK2 Is a Modulator of Craniofacial Development. PLoS ONE 9(1): e84343. doi:10.1371/journal.pone.0084343

Editor: Yann Gibert, Deakin School of Medicine, Australia

Received: May 21, 2013; **Accepted:** November 21, 2013; **Published:** January 8, 2014

Copyright: © 2014 Laugel-Haushalter et al. This is an open-access article distributed under the terms of the Creative Commons Attribution License, which permits unrestricted use, distribution, and reproduction in any medium, provided the original author and source are credited.

Funding: This work was supported by grants (to AB-Z) from the University of Strasbourg, the Hôpitaux Universitaires de Strasbourg (API, 2009-2012, "Development of the oral cavity: from gene to clinical phenotype in Human"), IFRO (Institut Français pour la Recherche Odontologique), by institutional funds from the Centre National de la Recherche Scientifique (CNRS) and Institut National de la Santé et de la Recherche Médicale (INSERM). This project, A27 "Orofacial manifestations of rare diseases", selected by the Offensive Sciences of the Trinationnal Metropolitan Area Upper Rhine (TMR), is co-financed by the European Regional Development Fund (ERDF) of the European Union, in the framework of the INTERREG IV Upper Rhine programme. VL-H was the recipient of a PhD fellowship from the Ministère Français de la Recherche. MP was supported by a grant from the Agence Nationale de la Recherche (to PD). The funders had no role in study design, data collection and analysis, decision to publish, or preparation of the manuscript.

Competing Interests: The authors have declared that no competing interests exist.

* E-mail: agnes.bloch-zupan@unistra.fr

Introduction

The ribosomal S6 family of serine/threonine kinases is composed of 4 highly related members in mammals: RSK1 (human chromosome 3), RSK2 (*RPS6KA3*, Xp22.2-p22.1), RSK3 (chromosome 6) and RSK4 (Xq21), which are 75% homologous and are implicated in several important cellular events including proliferation, differentiation, cellular stress response and apoptosis. Mutations in *RSK2* cause X-linked Coffin-Lowry syndrome (OMIM #303600) characterized by psychomotor and growth

retardation, with typical facial and digital abnormalities and progressive skeletal malformations like delayed bone development, spinal kyphosis/scoliosis, and sternum/rib protrusions (pectus carinatum) or depression (excavatum) [1,2,3]. Orofacial findings include a high narrow palate, a midline lingual furrow, malocclusion, hypodontia, and peg shaped incisors (Fig. 1). Premature loss of the primary dentition was also observed, and wide spaced teeth and large medial incisors were reported [1,4,5].

RSKs are Ser/Thr protein kinases that act at the distal end of the Mitogen-Activated Protein Kinase/Extracellular signal-Regu-

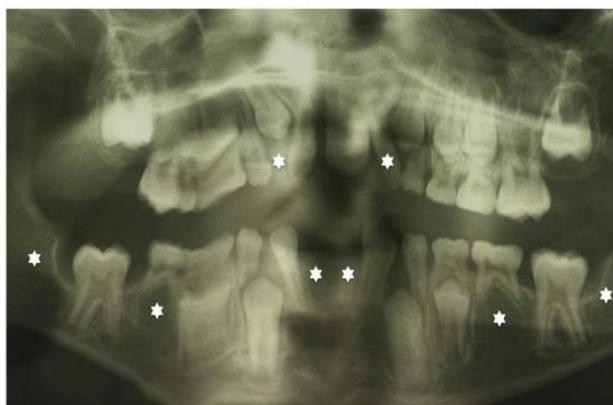


Figure 1. Dental anomalies encountered in Coffin-Lowry syndrome. This panoramic radiograph shows oligodontia (more than six permanent missing teeth (white stars: 12, 22, 41, 31, 45, 35, 47, 37). The deformations observed on this panoramic radiograph are linked to movements during the X-Ray acquisition process and difficulties for handicapped patient to remain still during the procedure. doi:10.1371/journal.pone.0084343.g001

lated Kinase (MAPK/ERK) signalling pathway. The various RSK proteins are widely expressed, with many cell types expressing several members. RSKs are directly phosphorylated and activated by ERK1/2 in response to several growth factors [6]. In the cytosol, RSK proteins have been shown to phosphorylate substrates including GSK3, L1CAM, the Ras GEF-Sos, Ikb, the p34cdc2-inhibitory kinase Myt1, the translation factors eEF2 and eIF4B, and the pro-apoptotic protein BAD [7,8]. Moreover, upon activation a fraction of the cytosolic RSKs translocate to the nucleus where they are thought to regulate gene expression through phosphorylation of transcription factors such as CREB1, ERa, Nurr77 and SRF, as well as histones [7]. The contribution of each RSK family member to the *in vivo* activation of most of these substrates is currently not well defined.

RSK orthologues have been identified in mouse, rat, chicken, *Xenopus* and *Drosophila* [9]. *Rsk2* knockout mice display spatial learning and memory impairment [10] and develop a progressive osteopenia due to impaired osteoblast function [11]. Lack of phosphorylation of the transcription factor ATF4 is responsible for the skeletal abnormalities in *Rsk2* knockout mice [10]. Murine *Rsk2* is highly expressed during somitogenesis, suggesting skeletal and muscle growth and/or patterning roles, potentially leading to the numerous skeletal abnormalities encountered in the human syndrome [12]. It is interesting to note that *Rsk2* shows specific developmental patterns of expression in the maxillary and the mandibular components of the first branchial arch [12], and that craniofacial and dental anomalies are present in the clinical synopsis of Coffin-Lowry syndrome.

The mouse dentition is a powerful and useful model to study the mechanisms leading to human dental anomalies, despite some intrinsic differences. The mouse has a monophyodont dentition that encompasses only four permanently growing incisors and 12 molars separated by a diastema [13]. Most mutant mouse models for human syndromic and non-syndromic genetic disorders displaying dental defects mimicking human pathologic phenotypes [14], although some discrepancies have been reported [15]. In this study, we describe the craniofacial and orodental phenotype of *Rsk2*-/*Y* knockout mice, as well as triple *Rsk1,2,3*-/- mutants. By employing several additional approaches (expression analysis by *in situ* hybridization, comparative transcriptomic analysis, shRNA

knock-down in tooth germ explants) we establish RSK2 regulates defined processes in odontogenesis and craniofacial growth.

Results

Rsk2-/*Y* craniofacial phenotype

The craniofacial phenotype was assessed by X-Ray microtomographic imaging and analyzed through euclidean distances measurement and comparison. This phenotype was variable, ranging from normality (mutant mice 702, 731) to obvious craniofacial dysmorphism (mutant mice 150, 700) (Fig. 2). Some mutant mice show an intermediate phenotype, with skulls smaller in length but not in width.

An overall skull length reduction from the nasal to the occipital bone was a collective measure of the sum defects in the nasal, frontal, parietal, interparietal/occipital bones. The frontal bone always exhibited the greatest reductions in length of all skull bones. The interparietal/occipital bones were the least affected (distances 1-4, 1-5, 2-3, 2-4, 2-5 being more reduced than 1-2 or 1-3: see Table 1; measurements were performed according to anatomical landmarks detailed in Fig. S1). A nasal deviation was observed in some mutant mice (Fig. 2B,C,E; Table 1). Craniofacial microtomographic analysis of *Rsk1,2,3*-/- mice was not performed, due to rare availability of these triple mutants. Analysis thus focused on *Rsk2*-/*Y* mice, a defined genetic model of human Coffin-Lowry syndrome.

Rsk2-/*Y* and *Rsk1,2,3*-/- dental phenotype

Phenotype of molar tooth rows. We analyzed 15 *Rsk2*-/*Y* mice and 9 *Rsk1,2,3*-/- mutant mice (see Table 2 and Fig. 3). Supernumerary teeth (ST) occurred in all specimens except for two *Rsk2*-/*Y* mice (702, 731). ST were aligned with the molar tooth row and located just in front and at the contact of the first molars (M1).

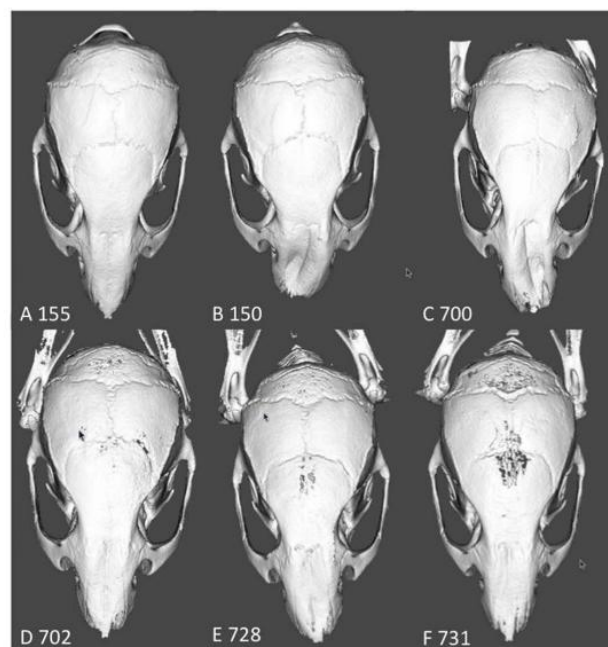


Figure 2. Craniofacial phenotype of *Rsk2*-/*Y* mice assessed by X-Ray microtomography. The craniofacial phenotype is highly variable, ranging from an almost normal-shaped cranium (mutant 155), although smaller in length, to a very dysmorphic appearance with a lateral nasal deviation. For mutant identification see Table 1. doi:10.1371/journal.pone.0084343.g002

Table 1. Distances between skull landmarks on wild-type and *Rsk2*-/*Y* mutant mice.

Distances	Mean WT	STD WT	Mean <i>Rsk2</i> mutants	STD <i>Rsk2</i> mutants	p-value
Between 1 and 2	7.10	0.59	6.84	0.35	0.03
Between 1 and 3	15.05	0.46	13.92	0.59	0.01
Between 1 and 4	18.59	0.41	17.24	0.57	0.005
Between 1 and 5	21.87	0.49	20.48	0.48	0.005
Between 2 and 3	8.07	0.45	7.25	0.47	0.005
Between 2 and 4	11.72	0.38	10.69	0.45	0.005
Between 2 and 5	15.21	0.35	14.13	0.31	0.005
Between L and R 6	12.08	0.17	12.16	0.13	0.47
Between L and R 7	6.42	0.21	6.45	0.27	0.68
Between L and R 8	4.77	0.11	4.79	0.73	0.22
Between L and R 9	6.27	0.25	6.13	0.12	0.06
Between L and R 10	0.74	0.06	0.71	0.08	0.47
Between L and R 11	1.05	0.05	1.13	0.11	0.29
Between L and R 12	10.08	0.37	10.22	0.28	0.29
Between L and R 15	4.53	0.19	4.72	0.51	0.37
Between L and R 16	2.29	0.22	2.23	0.23	0.57
Between 1 and 6R	15.24	0.34	14.39	0.52	0.008
Between 1 and 6L	15.20	0.32	14.47	0.31	0.008
Between 1 and 7R	7.92	0.28	7.18	0.58	0.008
Between 1 and 7L	7.89	0.22	7.24	0.34	0.005
Between 1 and 8R	6.90	0.24	6.29	0.46	0.88
Between 1 and 8L	6.90	0.25	6.35	0.29	0.68
Between 1 and 9R	20.65	0.47	19.55	0.46	0.008
Between 1 and 9L	20.62	0.48	19.56	0.32	0.008

In bold are distances significantly different between wild-type (WT) and mutants (all these distances were shorter in mutants). Anatomical landmarks are explained in Fig. S1 (supplementary information). All distances are in millimeters. STD: standard deviation; L: left; R: right.
doi:10.1371/journal.pone.0084343.t001

The phenotype penetrance was higher in the upper dentition (65% in *Rsk2*-/*Y* mice, 83% in *Rsk1,2,3*-/- mice) than in the lower dentition (31% and 11%, respectively). Shape and size of the supernumerary teeth were variable and ranged from a monocuspid tooth to a well-shaped molar-like tooth. ST were always smaller in size than the adjacent first molars, and they were sometimes, especially in the *Rsk1,2,3*-/- upper rows, as big as the M2. Inactivation of *Rsk2* alone was sufficient to generate the phenotype. When a ST was present, the mesial part of the first molar displayed altered crown morphology (Fig. 3). Even when the phenotype looked almost normal, a significant reduction in M1-M3 length was observed (Table 3). When ST occurred, the length mean value was always reduced for both M1 and M2 (Table 3). ST were always longer than M3. Molar width remained stable for M1, but was reduced for M2 and M3, except when only 3 molars were present in the mandible (Table 4). Shape abnormalities mainly occurred in mesial parts of the first lower (M1) and first upper (M1) molars in *Rsk2*-/*Y* mice. In upper M1, the central cusp of the mesial crest tended to be reduced, and the crest itself was more flattened (see red dotted circles in Fig. 3). Accordingly the mesial crest of the lower M1 also had an abnormal shape, because this crest tended to be strongly reduced when a ST occurred (see yellow dotted circles in Fig. 3). In triple mutants without ST (e.g. 789), the lower M1 displayed a mesial crest with vestibular cusp bigger than in WT.

The length of the molar row was significantly reduced in both the lower and upper jaws when no ST was present. When a ST

occurred, the length of the molar row was almost normal in the mandible, but was significantly higher in the maxilla when compared to WT (Table 3). Some *Rsk1,2,3*-/- mouse specimens displayed 3 upper postcanine teeth, as in the WT, but the dental row encompassed maxillary ST-M1-M2, and lacked the M3. Consequently, the second tooth (M1) was bigger than neighbouring teeth ST and M2 (Fig. 3, specimen 1283).

Incisor phenotype. No statistically significant differences were revealed between right and left incisors in both groups ($p > 0.05$). As a consequence, results from right and left incisors were merged (Table 5). No statistical difference was observed between WT and *Rsk2*-/*Y* ($p > 0.05$). No obvious incisor anomaly was detected. Analysis of the incisor phenotype in *Rsk1,2,3*-/- mice was not performed due to a reduced number of available animals, visual inspection however did not reveal any incisor dental defects. The existence of incisor anomalies in *Rsk1,2,3*-/- cannot be ruled out.

Abnormal molar root development in *Rsk2*-/*Y* mice. Both the number and shape of molar roots also reflect the tooth identity. In WT mice the mandibular molars M1 and M2 have 2 roots, whereas M3 has only one root. The maxillary molars M1 and M2 have 3 roots. Variations in the root number of M3 occur both within and among various WT strains. The upper M3 molar usually has 2 or 3 roots, although sometimes it has only 1 root. Thus, the total number of molar roots is 5 per hemi-mandible, whereas it can vary from 7 to 9 per hemi-maxillary. In *Rsk2*-/*Y* mice, hemi-mandibles harbouring a ST had a total root number of 6, with the ST always having a single root. In the

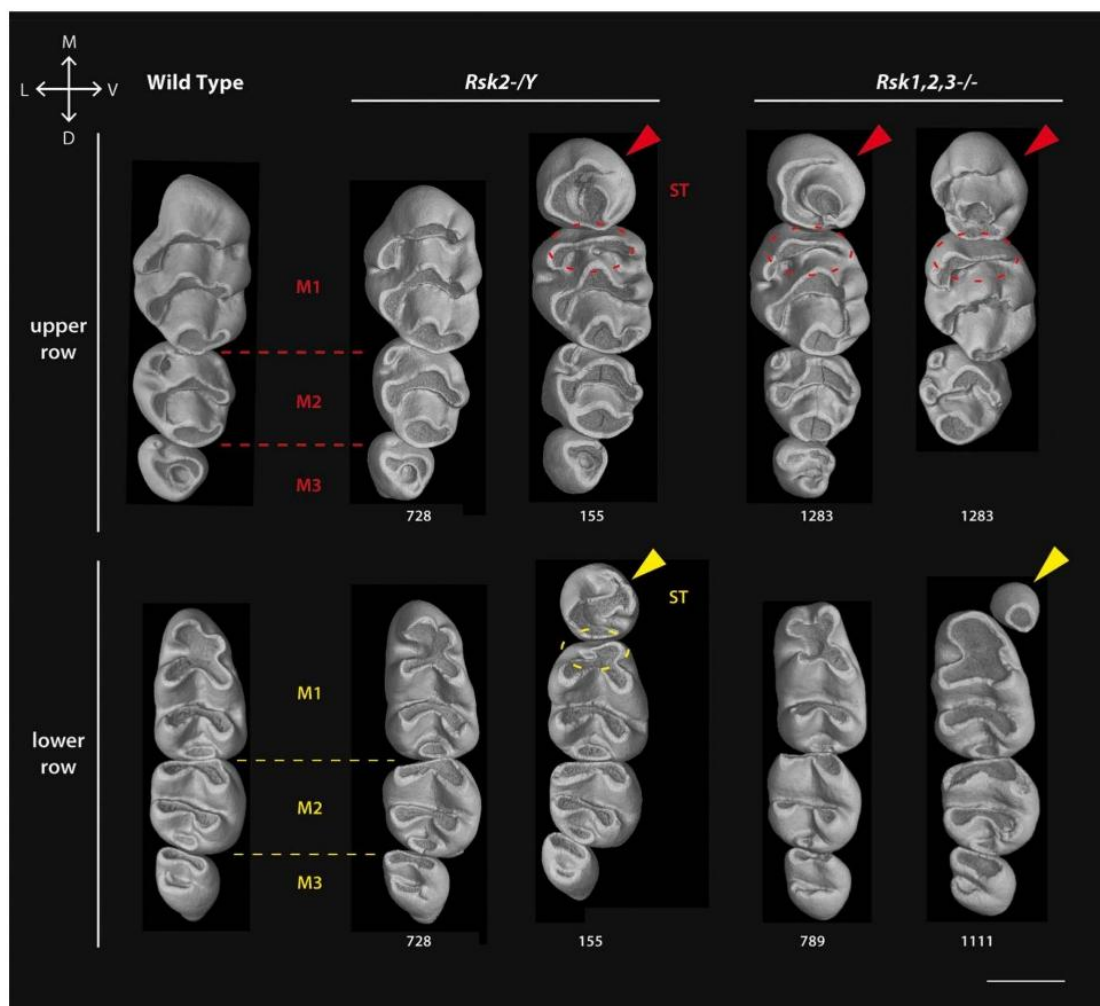


Figure 3. Variation of molar shape, size and number in *Rsk2*^{-/-} and *Rsk1,2,3*^{-/-} mice analyzed by X-Ray microtomography. All molar rows are oriented in the same manner (top corresponds to mesial and left to lingual side). At the left are wild-type molars, other rows are mutants as indicated. Arrowheads point to the supernumerary teeth ST; dotted ellipses show the reduction of the mesial-most affected cusp. Scale bar: 0.7 μ m. doi:10.1371/journal.pone.0084343.g003

maxillary quadrant, the total root number varied from 8 to 9 when a ST was present. ST could have 1 or 2 roots, M1 had 2 roots, but the M2 root number remained stable with 3 roots (Table S1 in File S1). The presence of maxillary M1 with only 2 roots probably correlates with the occurrence of ST, often associated to a compression and a reduction of the mesial part of M1.

***Rsk2*^{-/-} and the diastema.** The maxillary diastema was significantly reduced in *Rsk2*^{-/-} mice harbouring ST (Table 6). This was not the case for the mandibular diastema, whatever the number of teeth.

Expression patterns of *Rsk* genes during mouse odontogenesis

To investigate whether the dental anomalies observed in the *Rsk*-deficient mice may correlate with distinct patterns of expression of *Rsk* genes during odontogenesis, we performed an *in situ* hybridization analysis of *Rsk1*, *Rsk2*, *Rsk3* and *Rsk4* mRNA transcripts at various stages of tooth development. All four genes were found to be expressed in specific areas of the tooth anlagen, as illustrated in Fig. 4

for the developing first molars, and Fig. 5 for the mandibular incisors. Their expression features are summarized in Table 7.

Rsk2 transcripts were mainly localized in the mesenchymal compartment or dental papilla from E12.5 (dental lamina stage) to E19.5 (late bell stage). At E16.5 (bell stage), the transcripts were scattered in the area facing the epithelial loops or at the base of the cusps; the second molar dental mesenchyme was uniformly labelled. In the incisors the transcripts were also located in the mesenchyme, and the signal was more intense in the labial area and posterior area.

The expression of *Rsk1* and *Rsk4* was mainly epithelial, marking the inner dental epithelium and especially the epithelial loop areas. A faint signal was also observed for *Rsk4* in the posterior mesenchymal area facing the epithelial loops especially the labial loop for incisors (E16.5 and 19.5).

Rsk3 transcripts were mainly visible in the dental papilla at E14.5 (cap stage), E16.5 (bell stage) and E19.5 (Figs. 4, 5 and Table 7). At E19.5 the transcripts were concentrated in the cervical part of the papilla for the first molar and had a wider distribution in the second molar mesenchyme.

Table 2. Presence (+) of a supernumerary tooth (mesial to the first molar) in *Rsk* mutant mice.

Mouse	Genotype	Upper Right	Upper Left	Lower Right	Lower Left
11	<i>Rsk2</i> - <i>Y</i>	+ (4)	+ (4)	+ (4)	N
25	<i>Rsk2</i> - <i>Y</i>	+ (4)	+ (4)	N	+ (4)
37	<i>Rsk2</i> - <i>Y</i>	+ (4)	+ (4)	+ (4)	N
39	<i>Rsk2</i> - <i>Y</i>	+ (4)	+ (4)	N	N
46	<i>Rsk2</i> - <i>Y</i>	+ (4)	N	N	N
61	<i>Rsk2</i> - <i>Y</i>	+ (4)	+ (4)	N	N
62	<i>Rsk2</i> - <i>Y</i>	N	+ (4)	N	N
150	<i>Rsk2</i> - <i>Y</i>	+ (4)	+ (4)	+ (4)	+ (4)
155	<i>Rsk2</i> - <i>Y</i>	+ (4)	+ (4)	+ (4)	+ (4)
184	<i>Rsk2</i> - <i>Y</i>	+ (4)	+ (4)	+ (4)	+ (4)
185	<i>Rsk2</i> - <i>Y</i>	+ (4)	+ (4)	N	N
700	<i>Rsk2</i> - <i>Y</i>	N	N	N	+ (4)
702	<i>Rsk2</i> - <i>Y</i>	N	N	N	N
728	<i>Rsk2</i> - <i>Y</i>	+ (4)	N	N	N
731	<i>Rsk2</i> - <i>Y</i>	N	N	N	N
789	<i>Rsk1,2,3</i> -/-	+ (4)	+ (4)	N	N
793	<i>Rsk1,2,3</i> -/-	+ (4)	N	N	N
860	<i>Rsk1,2,3</i> -/-	+ (4)	N	+ (4)	N
883	<i>Rsk1,2,3</i> -/-	+ (4)	+ (3)	N	N
1105	<i>Rsk1,2,3</i> -/-	+ (4)	N	N	N
1111	<i>Rsk1,2,3</i> -/-	+ (3)	+ (3)	+ (4)	N
1283	<i>Rsk1,2,3</i> -/-	+ (3)	+ (4)	N	N
1139	<i>Rsk1,2,3</i> -/-	+ (3)	+ (4)	N	N
1159	<i>Rsk1,2,3</i> -/-	+ (4)	+ (3)	N	N

N: normal pattern of 3 molars M1, M2, M3. (3) means the presence of only 3 molars but the size of the second one is bigger (most probably there is a supernumerary tooth ST in front of M1, and M3 is missing). doi:10.1371/journal.pone.0084343.t002

Rsk2-*Y* supernumerary tooth is associated with an extra mesial placode

An extra tooth placode, and subsequent enamel knot labelled with *Sonic hedgehog* (*Shh*) as a marker, was clearly visible at E14.5, mesially to M1 in *Rsk2*-*Y* mice when compared to WT littermates (Fig. 6). The presence of this extra placode was seen in nearly 30% of the analysed embryo and was not always simultaneously present on right and left sides of the jaw. During WT development the three molars (M1, M2 and M3) are forming from a unique molar placode. The presence of an additional dental placode mesially to the M1 placode likely corresponds to the primordium of ST developing in *Rsk2*-*Y* mutants.

Rsk2-*Y* transcriptome analysis

We performed a comparative transcriptomic analysis (Affymetrix GeneChips) of wild-type and *Rsk2*-*Y* mice, analyzing RNA isolated from dissected E14.5 mandibular molar tooth germs. By using a principal component analysis (PCA), it was possible to discriminate between the molar samples according to their genotype (wild-type versus *Rsk2*-*Y*) (Fig. 7). 504 genes were retrieved as being differentially expressed, with fold changes exceeding ± 1.2 and a false discovery rate below 0.1. The fold changes were however rather low, ranking between +2.044 and

-1.98, suggesting that rather minimal molecular changes, at the transcriptome level, were taking place. These changes could be also minimized by a heterogeneous sampling for *Rsk2*-*Y* molars, with putative phenotypes ranking as previously described between normality and a 3 molars with a supernumerary tooth phenotype; this phenotype was not known at the E14.5 cap stage, when molar germs were pooled for transcriptomic analysis. The most affected ("top ten") genes, and a selection of additional genes being up- or down-regulated, are listed in Table 8 and Table 9.

The *Rdh1* gene encoding retinol dehydrogenase (RDH) 1 was found to be the most up-regulated gene in *Rsk2*-*Y* mutant mice. In addition to retinol dehydrogenase activity, this enzyme has strong 3 α -hydroxy steroid dehydrogenase- and weak 17 β -hydroxy steroid dehydrogenase- activities. *Rdh1* exhibits widespread and intense mRNA expression in many embryonic tissues including the neural tube, gut, and neural crest, as well as in adult mice [16]. Interestingly, retinoic acid (the end product of retinol oxidation initiated by RDH enzymes) is involved in tooth morphogenesis and differentiation, and abnormal retinoic acid levels can lead to dental anomalies [17,18,19,20].

Sectm1b, encoding secreted and transmembrane protein 1B, was the most down-regulated gene in *Rsk2*-*Y* mutant mice. This gene and protein had never been described previously as potentially involved in odontogenesis.

Among the differentially expressed genes selected (Table 9) as belonging to signalling pathways acting during tooth development (TGF-beta, FGF, Wnt, NF-kappaB) and/or cell cycle progression, *Eaf2* is a proto-oncogene acting together with Wnt4 in an autoregulatory feedback loop [21]. Inactivation of this gene causes numerous tumours in mice [22]. *Eaf2* was down-regulated in *Rsk2*-*Y* mutants.

We tried unsuccessfully to confirm those results on a selection of genes by qRT-PCR, comparing three *Rsk2*-*Y* and three WT molar RNA samples. This negative result might be explained by the heterogeneous nature of the *Rsk2*-*Y* phenotype (as described above), the relative low level of expression changes, and may not invalidate the microarray data.

Rsk2 inactivation *in vitro*

In order to overcome the potential problem of *Rsk2*-*Y* molar samples heterogeneity we decided to use an *in vitro* system, and inactivated *Rsk2* by microinjection and electroporation of shRNA in E14.5 molar tooth germs. *In vivo* electroporation in the mandible, as previously described by [23] was not suitable for our study, because of the lack of precision on the targeted zone and our aim to inactivate the gene directly within the tooth anlagen.

We optimized the experimental settings to inject and electroporate *Rsk2* shRNA in cap stage molars explanted and cultured *ex vivo*. Control explants were electroporated with a random shRNA construct. After electroporation the explants were placed into collagen drop culture to maintain their morphology [24] and kept in a defined culture medium for 24 h, before being processed for qRT-PCR analysis. Tooth morphology was preserved and neither apoptosis nor cell death were induced, as shown by activated caspase3 and TUNEL assays (data not shown).

Rsk2 shRNA electroporation efficiently diminished *Rsk2* expression by 75% (Fig. 8A). We then analyzed *Eaf2* and *Rdh1* expression, and found that *Eaf2* expression was down-regulated (75% decrease) (Fig. 8B), while *Rdh1* expression was up-regulated (50% increase) (Fig. 8C). These results were in accordance with the microarray data. The new combined technique allowed us not only to optimize a protocol for studying the molecular mechanisms of early tooth development, but also to set up a new approach for microarray validation.

Table 3. Comparison of each molar length, of the total molar field length, and the total length of M1+ M2, between wild-type (WT) mice and *Rsk2*- γ mutant mice with 3 or 4 molars.

	Mandibular molars WT	Mandibular molars Mutant 3M	Mandibular molars Mutant 4M	Maxillary molars WT	Maxillary molars Mutant 3M	Maxillary molars Mutant 4M
Mean ST			0.60			0.74
STD			0.01			0.02
Mean M1	1.44	1.37	1.14	1.56	1.38	1.14
STD	0.03	0.11	0.05	0.07	0.10	0.09
p-value		0.23	0.0004		0.01	0.001
Mean M2	0.89	0.85	0.79	0.92	0.85	0.82
STD	0.03	0.02	0.03	0.02	0.04	0.05
p-value		0.003	0.004		0.02	0.01
Mean M3	0.59	0.53	0.49	0.60	0.63	0.63
STD	0.02	0.03	0.04	0.03	0.03	0.05
p-value		0.0002	0.0004		0.96	0.15
Total	2.93	2.75	2.88	3.08	2.85	3.31
STD	0.04	0.15	0.28	0.10	0.13	0.06
p-value		0.0008	0.36		0.01	0.001
M1+ M2	2.33	2.10	2.15	2.48	2.30	1.96
STD	0.04	0.16	0.21	0.08	0.14	0.13
p-value		0.03	0.004		0.002	0.001

M1 size is reduced in mutants with 4 molars both in mandible and maxilla, but only in the maxilla of mutants showing 3 molars. M2 is reduced both in maxilla and mandible whatever the molar mutant phenotype. M3 mesiodistal dimension is reduced only in the mandible, irrespective of the presence of 3 or 4 molars. The total size of the molar field is reduced in the mandible and maxilla in mutant with 3 molars. The total size of the molar field is significantly increased in the maxilla in mutants with 4 molars. The total size of M1+M2 was always reduced when compared to the wild type value. All distances are in millimeters. Significant p-values are shown in bold. M1 : molar 1; M2 : molar 2; M3 : molar 3; ST : supplementary tooth in front of M1; STD : standard deviation; Mutant 3M : mutant with 3 molars; Mutant 4M : mutant with 4 molars; Total : total length of all molars in the molar field.
doi:10.1371/journal.pone.0084343.t003

Discussion

A peculiar dental phenotype

Mice are commonly studied mammals for investigating the mechanisms of tooth development and evolution. The orodental

phenotype of mouse models of human genetic disorders also often mimics dental anomalies encountered in human rare diseases [14]. Basal placental mammals had a dental formula including three incisors, one canine, four premolars, and three molars per dentition quadrant [13,25]. Through evolution, almost all

Table 4. Comparison of each molar width (vestibulolingual dimension) between wild-type and *Rsk2*- γ mutant mice with 3 or 4 molars.

	Mandibular molars WT	Mandibular molars Mutants 3M	Mandibular molars Mutants 4M	Maxillary molars WT	Maxillary molars Mutants 3M	Maxillary molars Mutants 4M
Mean ST			0.59			0.76
STD			0.09			0.04
Mean M1	0.79	0.77	0.82	1.04	1.01	1.06
STD	0.02	0.04	0.03	0.05	0.05	0.02
p-value		0.19	0.12		0.19	0.56
Mean M2	0.85	0.85	0.81	0.90	0.86	0.86
STD	0.02	0.02	0.03	0.02	0.05	0.03
p-value		0.89	0.02		0.03	0.02
Mean M3	0.60	0.57	0.58	0.61	0.58	0.54
STD	0.02	0.02	0.05	0.03	0.02	0.04
p-value		0.006	0.06		0.02	0.01

In mutants the width of M1 was not modified. The width of the maxillary M2 and M3 was reduced. In the mandible the width of M2 was lower only when 4 molars were present, and the width of M3 was lower only in mutants with 3 molars (all distances in millimeters; significant p-values in bold).
M1 : molar 1; M2 : molar 2; M3 : molar 3; ST : supplementary tooth in front of M1; STD : standard deviation; Mutant 3M : mutant with 3 molars; Mutant 4M : mutant with 4 molars.
doi:10.1371/journal.pone.0084343.t004

Table 5. Morphological analysis of mandibular incisors in WT and *Rsk2*^{-Y} mice.

		Li (mm)	hi (mm)	Hi (mm)	li (mm)	ti (mm)	lpa (mm ²)
WT	Mean	11.33	1.11	2.96	9.38	0.65	10.36
	STD	2.34	0.07	0.20	1.56	0.02	1.07
<i>Rsk2</i> ^{-Y}	Mean	11.29	1.14	2.97	9.05	0.65	10.18
	STD	1.66	0.05	0.21	1.65	0.03	1.33

No statistically significant differences were revealed between right and left incisors in both groups ($p > 0.05$). As a consequence, results from right and left incisors were merged. No statistical difference was observed between WT and *Rsk2*^{-Y} ($p > 0.05$).

(Li) length of the longest and external bow, (hi) height of median part of the incisor, (Hi) total height of the incisor, (li) horizontal length of the incisor joining the tip to the distal extremity of the root, (lpa) projected area in lateral view of the incisor, (ti) thickness the median part of the incisor. For more explanations on the measured distances, see Figure S3. STD : standard deviation.

doi:10.1371/journal.pone.0084343.t005

mammals reduced their dental formulas, but lost functional teeth sometimes remaining as rudiments that begin to develop and then abort. The dentition of the mouse comprises 4 functional teeth in each quadrant (1 incisor and 3 molars separated by a toothless space called diastema). Rudimentary tooth primordia have been reported to develop in the distal part of the diastema through the initial stages of odontogenesis of WT mice. However their development ceases before the cap stage and they regress by apoptosis [26,27,28]. The tooth phenotype encountered in the *Rsk2*^{-Y} mutant mouse is remarkable by the occurrence of supernumerary teeth at the positions of the fourth premolars. Fourth premolars are still present in certain rodent groups such as squirrels, and have been lost through murid rodent evolution [13].

Rsk2 phenotype is similar to the tabby phenotype

Supernumerary teeth within the diastema were described in other mouse mutants for *ectodin*, *Irf4*, *Sprouty2/4*, *Wise*, *Polaris*, and *Gas1* [29,30,31,32,33,34,35,36]. Dysfunctions of the FGF, Shh, Wnt, and/or NF-kappaB signalling pathways are thought to induce formation of these supernumerary teeth within the diastema, indicating that the mouse maintains genetic potentialities that could be stimulated and induce the formation of supernumerary teeth [37,38].

Ectopic teeth in the diastema are also observed in mice misexpressing *Eda* (ectodysplasin A; also known as Ta; Ed1; EDA1; XLHED; tabby) and *Eda* receptor (Edar) [39,40,41,42].

The dental phenotype of the *Rsk2*^{-Y} mouse resembles that encountered in the *tabby* mouse (a model for X-linked hypohidrotic ectodermal dysplasia- an ectodermal dysplasia characterized by an absence or dystrophic development of hair, nail, sweat- lacrymal-mammary- glands and tooth; OMIM #305100). Mutations in the human X-linked gene *EDI* (the *Eda* orthologue) are responsible for this disorder [43,44,45,46]. Ontogenetic and phylogenetic data together suggest that the occurrence of functional supernumerary teeth in *tabby* mice diastema is caused by the persistence of the premolar rudiments that usually regress in WT mice. It has thus been proposed that this phenotype may represent an evolutionary throwback or atavism [43,44,45,46].

Recently it has been shown that the number of teeth is regulated by fine-tuning of the level of receptor-tyrosine kinase signalling [32]. Known cytosolic RSK substrates include I-kappaB alpha [7,47,48], a member of the NF-kappaB pathway. This pathway is involved in development and in some human disorders including ectodermal dysplasias that affect ectodermal derivatives like the teeth, hair, salivary, mammary glands and skin. I-kappaB alpha has specifically been associated with an autosomal dominant form of anhidrotic ectodermal dysplasia and with T cell immunodeficiency [49]. The fact that I-kappaB alpha can be phosphorylated by RSKs, leading to increase of NF-kappaB activity, may therefore explain some of the dental anomalies encountered in the *Rsk2*^{-Y} transgenic mice and in Coffin-Lowry syndrome patients. However, the downstream signalling pathway(s) of *Eda*/*Edar* involved in tooth formation in the diastema are not yet known.

The phenotype in the light of Coffin-Lowry syndrome

The mouse model for Coffin-Lowry syndrome, obtained by inactivation of the *Rsk2* gene and used in this study, was previously described by [11]. Mutant mice weigh 10% less and are 14% shorter than their wild-type littermates. This is in agreement with a role of RSK2 in organismal growth. These mice exhibit impaired learning and poor coordination, providing evidence that RSK2 plays similar roles at least for cognitive functions, in mouse and human. No previous description of the craniofacial or dental phenotype was so far reported. The craniofacial features described in Coffin-Lowry syndrome include a thick calvarium, hyperplastic supra-orbital ridges, hypertelorism, a flat malar region, and a prominent mandible. Clearly it is difficult in the light of our present observations, to relate the *Rsk*-knockout craniofacial phenotype to the anomalies encountered in patients. The small size of the skull could be associated to the general growth defect. However it is interesting to notice that in Coffin-Lowry patients, teeth agenesis and/or hypodontia is described. An apparent opposite phenotype between human patients and a mouse model has already been described in another rare disease, the cleidocranial dysplasia syndrome, which is characterized by skeletal

Table 6. Upper and lower diastema size in wild-type and *Rsk2*^{-Y} mutant mice with 3 or 4 molars.

	Mean size (mm)	STD	p-value
Mandibular diastema Wild-type	2.99	0.09	
Mandibular diastema Mutants with 3 molars	2.83	0.21	0.22
Mandibular diastema Mutants with 4 molars	2.71	0.1	0.26
Maxillary diastema Wild-type	5.45	0.18	
Maxillary diastema Mutants with 3 molars	5.33	0.21	0.49
Maxillary diastema Mutants with 4 molars	5.01	0.21	0.0019

Only the upper (maxillary) diastema from mutants with 4 molars was significantly smaller compared to wild-type (bold). STD : standard deviation.

doi:10.1371/journal.pone.0084343.t006

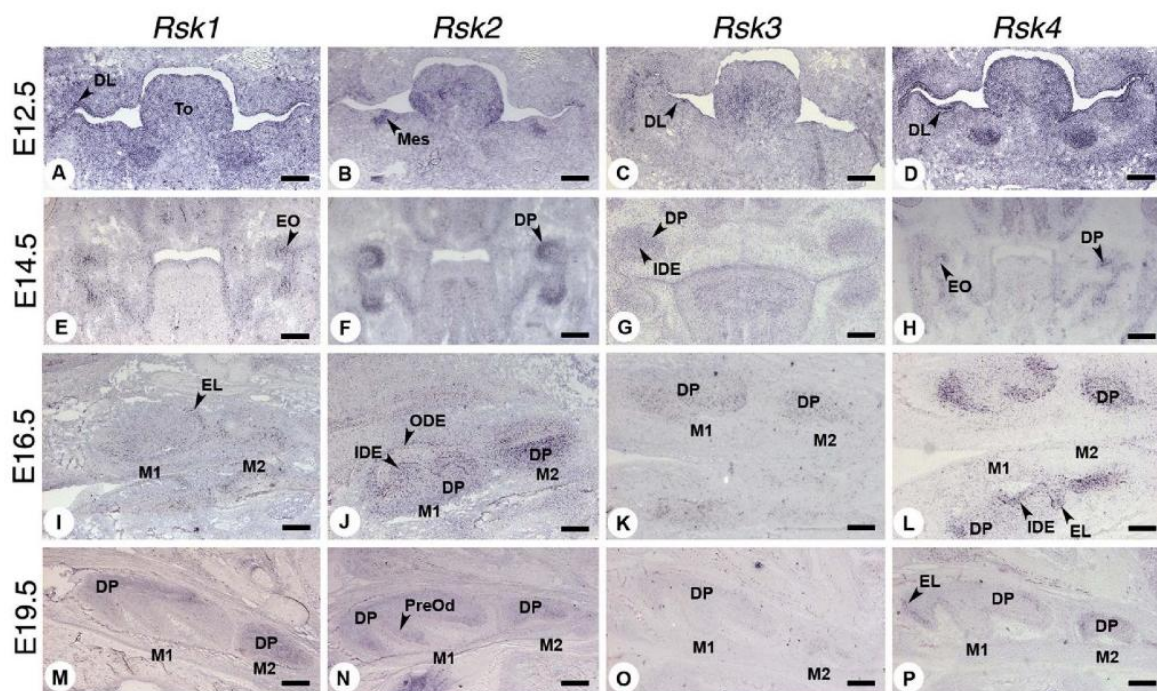


Figure 4. Expression patterns of *Rsk* genes during mouse molar odontogenesis at E12.5 (dental lamina), E14.5 (cap), E16.5 (bell) and E19.5 (late bell) stages, analyzed by *in situ* hybridization. Abbreviations: DL dental lamina, DP dental papilla, EL epithelial loop, EO enamel organ, IDE inner dental epithelium, M1 first molar, M2 second molar, Mes ectomesenchyme, ODE outer dental epithelium, PreOd preodontoblasts, To tongue. Scale bars 140 μ m (A,B,C,D,I,J,K and L) and 250 μ m (E,F,G,H,M,N,O and P). doi:10.1371/journal.pone.0084343.g004

defects, numerous supernumerary teeth, and delayed tooth eruption. The mouse model of this disease (*Cbfa1*-KO) exhibits arrested tooth development [15]. Mostly loss of function mutations

in *RSK2* both in human and mouse are responsible for the phenotype. Despite striking similarities mouse and human tooth development, cross-species comparison of mouse/human denti-

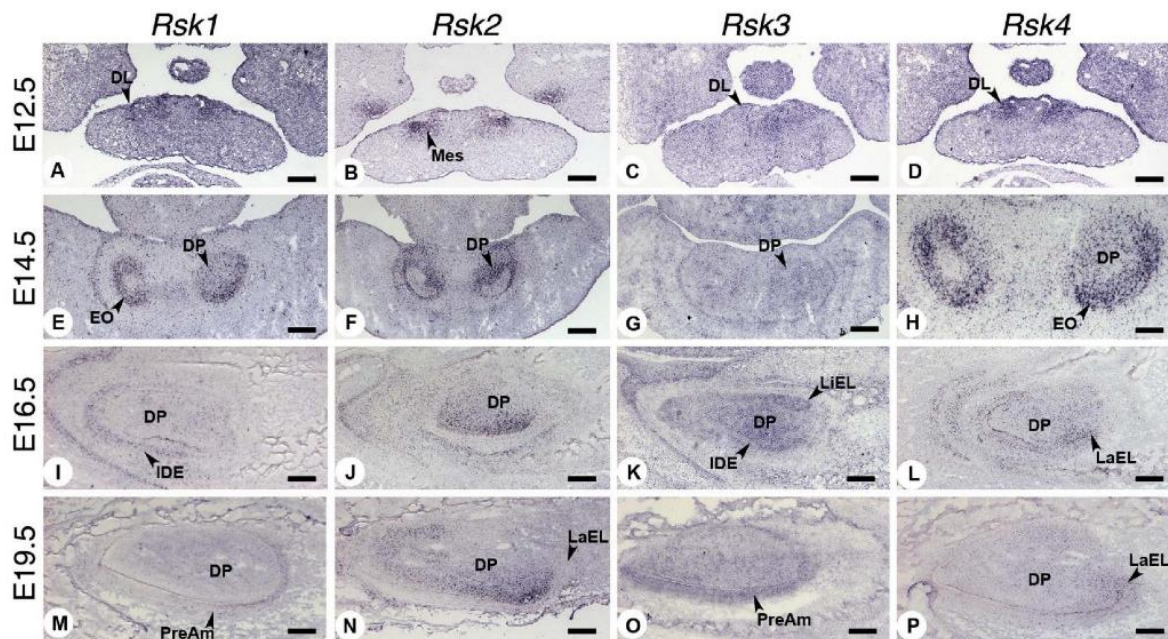


Figure 5. Expression patterns of *Rsk* genes during incisor odontogenesis at E12.5 (dental lamina), E14.5 (cap), E16.5 (bell) and E19.5 (late bell) stages analyzed by *in situ* hybridization. Abbreviations: DL dental lamina, DP dental papilla, EL epithelial loop, EO enamel organ, IDE inner dental epithelium, LaEL labial epithelial loop, LiEL lingual epithelial loop, Mes ectomesenchyme, PreAm preameloblasts. Scale bars 140 μ m (A,B and C), 200 μ m (D,E, F,G,I, J, K and L), 250 μ m (M,N,O and P) and 50 μ m (H). doi:10.1371/journal.pone.0084343.g005

Table 7. *Rsk*s expression patterns during odontogenesis.

	<i>Rsk1</i>			<i>Rsk2</i>			<i>Rsk3</i>			<i>Rsk4</i>		
	Inc	M1	M2	M3	Inc	M1	M2	M3	Inc	M1	M2	M3
E12.5												
Oral epithelium	+	+							+			+
Dental lamina	+	+						+ faint	+	+		+
Mesenchyme					+	+			+	+		
E14.5												
Enamel organ	+	+										+
IDE	+					+			+	+		
Enamel knot												
Dental Papilla	+ π faint				+	+		+	+			+
Dental sac					+							
E16.5												
ODE	+					+	+					
IDE	+	+	+			+	+			+		+
Epithelial loop	+	+	+				+			+		+
Dental Papilla	+ lab				+	+	+	π	+	+	+	+
E19.5												
ODE												
SR												
SI												
IDE								+		+		+
PreAm	+							+				
Am												
Epithelial loop	+	+					+			+	lab	+
Od												
PreOd							+					
Dental papilla	+	+	+		+	lab	+	+	+	+	lab	+
Dental sac					+							

+ : positive signal; lab: labial; π posterior area

IDE: inner dental epithelium; ODE: outer dental epithelium; SR: stellate reticulum; SI: stratum intermedium; PreAm: preameloblasts; Am: ameloblasts; Od: odontoblasts, PreOd: Preodontoblasts

doi:10.1371/journal.pone.0084343.t007

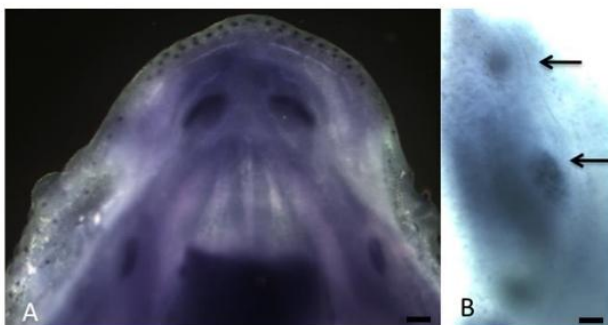


Figure 6. Whole mount in situ hybridization showing the molar and incisor placodes within the mandible at E14.5 in a wild-type mouse (A) and *Rsk2*-*Y* mouse (B: detail of the right-side mandible) labelled with a *Shh* riboprobe. Two molar placodes are clearly visible in B (arrows) Scale bars 200 μ m (A), 100 μ m (B). doi:10.1371/journal.pone.0084343.g006

tions show they are clearly not alike. This suggests differential output and involvement of identical or superimposed pathways. These differences may account for this apparently opposite in nature dental phenotype i.e. hypodontia in human versus supernumerary teeth in mouse.

Cell cycle progression and cell proliferation

It has been shown that tooth number, size, and shape are linked to cell proliferation and apoptosis events [50,51,52,53]. It is interesting to note that *Rsk*s genes are expressed throughout tooth development, especially in proliferating areas (this study, Figs. 4 and 5), either in the mesenchyme (*Rsk2*, *Rsk3*) or in the epithelial loops (*Rsk1*, *Rsk4*). The expression patterns described for the *Rsk* genes in other embryonic regions [12,54,55] also indicate a correlation with proliferative areas. *Rsk1* is highly expressed in tissues harbouring highly proliferating cells like liver, lung, thymus, and olfactory and respiratory epithelia. Particularly intense *Rsk1* expression is observed in the gut epithelium. *Rsk2* is expressed at very low levels throughout mouse development in dorsal root ganglia, thyroid gland, kidney, lung, liver and skeletal muscles. *Rsk3* is mainly expressed in the nervous system, but also in the

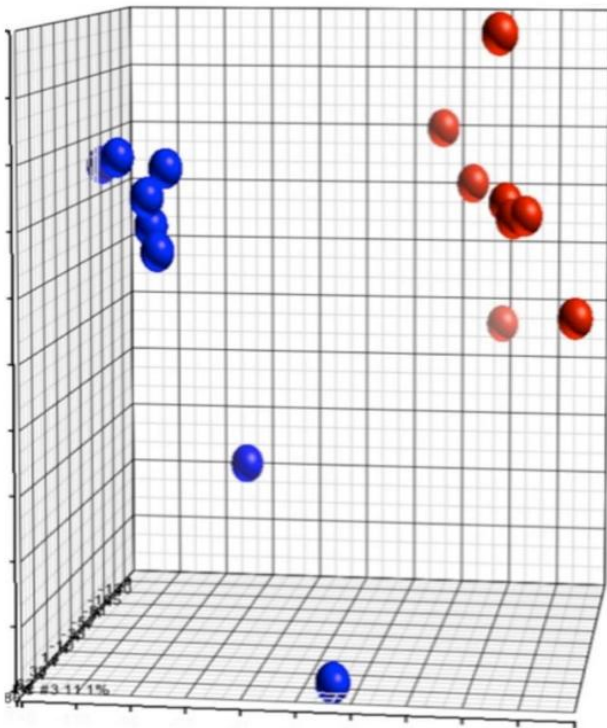


Figure 7. Principal component analysis (PCA) of transcriptomic data of wild-type versus *Rsk2*^{-/-} mandibular molars samples. Wild-type samples are represented in blue (X, Y and Z units are arbitrary units created by the software). The units are data-dependent and are generated by the software, which gives coordinates to each sample according to three axes that relate to the weight (inertia) of the decomposition into 3 principal components. For this analysis, samples segregate in two distinct groups, showing relevant transcriptional differences between WT and *Rsk2*^{-/-} samples. doi:10.1371/journal.pone.0084343.g007

thyroid gland and testis cords. RSK3 may regulate proliferation and seems linked to cellular differentiation of neuroepithelial cells during development [55]. *Rsk4* ubiquitous low expression was observed throughout development. In teeth *Rsk4* expression was rather specifically marking the epithelial loops.

It is well established that RSKs control cell proliferation through the regulation of mediators of the cell cycle [7]. RSK2 for example promotes cell cycle progression by phosphorylating c-Fos, a transcription factor regulating the expression of cyclin D1 during G1/S transition. RSK2 activates and phosphorylates p53 *in vitro* and *in vivo* and colocalizes with p53 in the nucleus. The RSK2-p53-histone H3 complex may likely contribute to chromatin remodelling and cell cycle regulation [56]. A list of phosphorylation substrates of the RSK isoforms was reported by [7] including c-Fos, NHE-1, Er α , p27^{kip1}, Sos1, RanBP13, YB-1, Erp1, eIF4B, rpS6, Bad, DAPK, Nur77, NFAT3, TIF-1A, ATF4, ATF1, MEF2c, Filamin A, Raptor, CCT β , CRHSP24, Shank. Interestingly, alterations in the expression of a number of genes involved in cell cycle control (*Cna1*, *Hmgb1*, *Mdm2*, *Tpd52*) or in cell growth (*Ngf*, *Bdkrb1*, *Amhr2*) is shown in our microarray analysis.

Increased proliferation and decreased apoptosis are necessary to develop supernumerary teeth, as seen by differential regulation of *Sprouty* genes [57]. The localisation of *Rsk*s genes in proliferative

areas, their role in the regulation of proliferation and apoptosis [58] as well as the interconnection of the involved pathways could explain that the deletion of *Rsk2* gene could induce the formation of supernumerary teeth and therefore reveal ancestral stages of murine dental evolution.

RSK and the Ras/MAPK pathway

Altered ERK/MAPK signalling (with abnormally increased phosphorylation of ERK1/2) was recently reported in the hippocampus of the *Rsk2*^{-/-} mice [59]. RSK2 was also proven to exert a feedback inhibitory effect on the ERK1/2 pathway. Our microarray data did not indicate a similar trend at the level of the developing molar. *Ngf* was the only gene detected by our microarray analysis, known to be regulated at the transcriptional level by ERK1/2 and involved in tooth development [60].

Unravelling target genes and involved pathways

The heterogeneity of the molar samples and the variability of the *Rsk2*^{-/-} molar phenotype has certainly interfered with the analysis of the microarray data and may have prevented the confirmation of target gene expression by qRT-PCR. However, genes involved in TGF-beta receptor signalling (*Amhr2*), or in the FGF (*Fgfbp3*) and Wnt (*Sfrp5*) pathways, were shown to be affected by the inactivation of *Rsk2*. These pathways are known to be involved in tooth development [61] and, when affected, are responsible for dental anomalies both in mouse models and human [62]. The *in vitro* assay we have developed, involving micro-injection and electroporation of a *Rsk2* shRNA in explanted molar tooth germs, proved to be a valuable system to assess quantitative changes in target gene expression.

Conclusions

Analysis of *Rsk2*^{-/-} mutant mice revealed an important role of *Rsk2* in craniofacial development, especially in dentition development and patterning. The loss of function of *Rsk2* allows the reappearance of supernumerary diastemal teeth considered as remnants of teeth lost over evolution. Our *in situ* hybridization analysis indicated that *Rsk2* expression pattern may correlate with proliferative areas of the developing teeth, consistent with a biological function of RSK2 in cell-cycle control and cell growth. Transcriptome profiling analysis was difficult because of the heterogeneity and variability of the *Rsk2*^{-/-} dental phenotype, however it provided candidate genes and pathways potentially involved in this phenotype. *In vitro* inactivation of *Rsk2* using shRNA was found to be a promising approach to address target genes and showed, in particular, an interference with an enzyme involved in the retinoid/steroid biosynthesis pathway. The fact that the regression of the fourth premolar seen in mouse is not found in all mammals, and is never observed in humans, may provide an explanation for the divergent phenotypes in *Rsk2*^{-/-} and human patients.

Materials and Methods

Patients and Ethics Statement

Patients attending the Reference centre for orodental manifestations of rare diseases, Pôle de médecine et chirurgie bucco-dentaire, Hôpitaux Universitaires de Strasbourg, or their legal representatives (parents, next of kin, caretakers or guardians) if minor and/or not in capacity to provide his or her own consent, give written informed consent for the use and publication of medical data. The picture proposed as figure 1 was uploaded in D4/phenodent database (CCTIRS positive report 11/09/2008, CNIL authorization 18/05/

Table 8. Overview of top ten genes differentially expressed in *Rsk2*-*Y* and wild-type developing mandibular molars.

Top ten up-regulated genes	Fold change	P-value	Name
<i>Rdh1</i>	2.04458	5.22E-11	retinol dehydrogenase 1 (all trans)
<i>Dip2c</i>	1.82248	4.50E-11	DIP2 disco-interacting protein 2 homolog C (<i>Drosophila</i>)
<i>1700001J11Rik</i>	1.6761	2.92E-08	-
<i>Olf319</i>	1.66441	1.56E-08	olfactory receptor 319
<i>Myh1</i>	1.64957	1.91E-06	myosin. heavy polypeptide 1 skeletal muscle
<i>Acaa1b</i>	1.62775	1.64E-07	acetyl-Coenzyme A acyltransferase 1B
<i>6430550D23Rik</i>	1.62394	3.80E-08	-
<i>Hmgb1</i>	1.61691	4.11E-10	high mobility group box 1
<i>4930555K19Rik</i>	1.58002	2.16E-09	-
<i>9630041A04Rik</i>	1.57948	3.38E-09	-
<i>BC022713</i>	1.57732	2.80E-07	cDNA sequence
<i>Gm9968</i>	1.56689	4.24E-12	predicted gene 9968
<i>Gm6718</i>	1.56677	4.74E-07	predicted gene 6718
<i>Naip2</i>	1.56543	3.72E-09	NLR family, apoptosis inhibitory protein 2
Top ten down-regulated genes	Fold change	P-value	Name
<i>Glycam1</i>	-1.55694	1.83E-10	glycosylation dependent cell adhesion molecule 1
<i>Sfrp5</i>	-1.5577	2.67E-06	secreted frizzled-related sequence protein 5
<i>Olf459</i>	-1.56115	8.07E-10	olfactory receptor 459
<i>Fgl2</i>	-1.59412	7.32E-08	fibrinogen-like protein 2
<i>Ttc29</i>	-1.59842	6.35E-10	tetratricopeptide repeat domain 29
<i>2510003E04Rik</i>	-1.61995	2.51E-10	-
<i>Tas2r117</i>	-1.63064	9.61E-12	taste receptor, type 2, member 117
<i>4930529M08Rik</i>	-1.65052	1.67E-07	-
<i>4930529M08Rik</i>	-1.65555	3.89E-11	-
<i>Rnf39</i>	-1.6586	7.87E-09	ring finger protein 39
<i>LOC100134990</i>	-1.67412	2.18E-09	selenoprotein K pseudogene
<i>Muc19</i>	-1.68802	5.59E-07	mucin 19
<i>Tpd52</i>	-1.74912	1.10E-10	tumor protein D52
<i>Sectm1b</i>	-1.9796	2.54E-06	secreted and transmembrane 1B

The table is highlighting genes showing the highest degree of enrichment (positive values) or down-regulation (negative values).
doi:10.1371/journal.pone.0084343.t008

2009 (N°908416). A copy of the consent form can be downloaded at <http://www.phenodent.org/consentement.php>

Animals and Ethics Statement

Rsk2 gene targeting was previously described [11]. As in human, the mouse *Rsk2* gene is located on the X chromosome. Analyses were performed on *Rsk2*-*Y* ("knockout") male mice, with littermate wild-type (*Rsk2*+*Y*) males used as control animals. Triple *Rsk1,2,3*^{-/-} mutant mice were obtained by breeding of single knockout mice, themselves obtained by excision of exons three and four (*RSK1* knockout) or exon two (*RSK2* and *RSK3* knockouts) of the corresponding genes, leading to frameshift mutations [11]. The experiments were performed in accordance with the French national and European Laws and Directives Concerning Laboratory Animal Housing, Welfare and Experimentation and after approval from the CERBM-GIE: ICS/IGBMC Ethical Research Board.

X-Ray microtomography

A cohort of 6 mutant *Rsk2*-*Y* male mice (#150, 155, 700, 702, 728, 731) and 6 wild-type (WT) littermates (#149, 154, 699, 727,

729, 730), as well as 7 *Rsk1,2,3* compound mutant male mice (#789, 860, 883, 1105, 1111, 1139, 1283), were analyzed through X-ray micro-computed tomography (micro-CT) (GE eXplore Vision CT120 (General Electric, Waukesha, USA) for craniofacial exploration and Phoenix Nanotom (General Electric measurement and control, Billerica, USA) for tooth analysis). For craniofacial exploration the micro-CT was performed using 220 projections with an angle increment of 0.877 degrees (Parker mode) and one average frame per projection (70.0 kV, 32 mA, and exposition time of 16 milliseconds). 3D-reconstructions were done using a Feldkamp algorithm giving voxels of 100×100×100 μm³. For teeth a second micro-CT acquisition was performed with a smaller reconstructed voxel size (3×3×3 μm³) using 2 000 projections and three average frames per projection (100.0 kV, 70 μA, and exposure time of 500 ms). 3D-reconstructions were done using datos|x software and algorithm including beam hardening correction and ring artefact reduction.

Anatomical landmarks were identified as remarkable points (for instance cranial sutures) that could be easily recognized on each specimen. Fig. S1 (supplementary material) illustrates this step, showing on a 3D isosurface rendering the landmarks (red points)

Table 9. Overview of other genes differentially expressed in *Rsk2*-Y and wild-type developing mandibular molars.

Up-regulated genes	Fold change	P-value	Name
<i>Mdm2</i>	1.42143	6.43E-07	p53 E3 ubiquitin protein ligase homolog oncoprotein
<i>Neurog3</i>	1.39695	4.46E-08	neurogenin 3
<i>Pou6f2</i>	1.38695	2.35E-07	POU domain class 6 transcription factor 2
<i>Dffa</i>	1.38653	4.93E-10	DNA fragmentation factor alpha subunit
<i>Bdkrb1</i>	1.38509	4.15E-08	bradykinin receptor beta 1
<i>Ofd1</i>	1.37103	4.33E-08	oral-facial-digital syndrome 1 gene homolog; ciliogenic protein
<i>Zfp759</i>	1.35236	5.23E-07	zinc finger protein 759
<i>Cflar</i>	1.32394	7.32E-07	CASP8 and FADD-like apoptosis regulator
<i>Aak1</i>	1.23472	3.15E-06	AP2 associated kinase 1 positive regulation of Notch signaling pathway
Down-regulated genes	Fold change	P-value	Name
<i>Pde4a</i>	-1.20556	1.57E-07	phosphodiesterase 4A cAMP specific
<i>Eaf2/U19</i>	-1.23309	1.52E-06	ELL associated factor 2, ehrllich S-II transcriptional activator factor testosterone regulated apoptosis inducer and tumor suppressor
<i>Sp3</i>	-1.24825	9.34E-08	trans-acting transcription factor 3
<i>Ndufaf4</i>	-1.26049	5.41E-08	NADH dehydrogenase (ubiquinone) 1 alpha subcomplex. assembly factor 4
<i>Wnt11</i>	-1.28904	3.63E-08	wingless-related MMTV integration site 11
<i>Fgfbp3</i>	-1.30479	5.46E-07	fibroblast growth factor binding protein 3
<i>Ccna1</i>	-1.31914	9.33E-09	cyclin A1
<i>Trim69</i>	-1.35725	5.04E-08	tripartite motif-containing 69
<i>Npy5r</i>	-1.37768	5.33E-10	neuropeptide Y receptor Y5
<i>Zfp78</i>	-1.38882	1.95E-09	zinc finger protein 78
<i>Amhr2</i>	-1.46255	5.42E-09	anti-Mullerian hormone type 2 receptor transforming growth factor beta receptor signalling pathway
<i>L3mbtl4</i>	-1.48069	4.21E-08	l(3)mbt-like 4
<i>Zkscan17</i>	-1.48573	4.10E-08	zinc finger with KRAB and SCAN domains 17
<i>Ngf</i>	-1.49018	1.63E-08	nerve growth factor
<i>Nlr5</i>	-1.53839	1.64E-08	NLR family. CARD domain containing 5 negative regulation of NF-kappaB transcription factor activity

The table is highlighting genes selected on the basis of their known involvement in pathways regulating odontogenesis.
doi:10.1371/journal.pone.0084343.t009

and their anatomical definitions. A similar approach was used for molar analysis (Fig. S2).

Calculation involved euclidean distances between selected pairs of points that could be compared to identify statistical significant

differences between WT and mutant mice. The methodology is based upon previously described work [63,64]. To avoid any bias in landmarks position, landmarks were placed two times by one investigator (intra-investigator reproducibility) and one time by

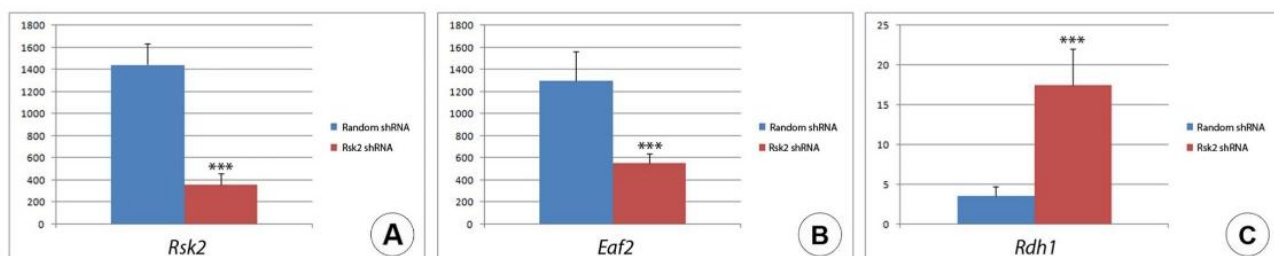


Figure 8. Summary of experiments involving *in vitro* inactivation of *Rsk2* and its consequences on target gene expression, as observed after microinjection in E14.5 mandibular molar explants of a *Rsk2* shRNA, followed by qRT-PCR analysis 24 h after injection. A: *Rsk2* was down regulated 4.01 fold after electroporation. B: *Eaf2* was significantly down-regulated, and C: *Rdh1* was up-regulated after electroporation. Histograms show expression levels in molars electroporated with the random shRNA (blue) and microinjected-electroporated explants with the *Rsk2* shRNA (red), with values normalized with respect to *Gapdh* expression. Data (mean \pm SEM) were analyzed with Student t-test; *** $p < 0.001$; ** $p < 0.01$; * $p < 0.05$.
doi:10.1371/journal.pone.0084343.g008

another (inter-investigator reproducibility). As no statistical differences were observed between distances measured within or in between investigators, we decided to base our study on the average of the three measured distances. Statistical analysis comparing WT and mutant mice was performed using Mann-Whitney non parametric test. P-values lower than 0.05 were considered as significant.

Analysis of incisor morphology

All image processing tasks were done using MicroView (GE Healthcare, Waukesha, USA). Right and left mandibular incisors were isolated by manual segmentation from mandible micro-CT acquisitions of the two mouse groups (6 *Rsk2*^{-/-} and 6 WT mice). Several measurements were achieved for morphology description, on the lateral and dorsal views of a 3D isosurface rendering of incisors (threshold value = 700 Hounsfield units): the length of the longest and external bow (Li), the height of median part of the incisor (hi), the total height (Hi), the horizontal length joining the tip of the incisor and the distal extremity of the root (li), projected area in lateral view of the incisor (lpa) and the thickness of the median part of the incisor (ti) (Fig. S3). A Wilcoxon-Mann Whitney test was used to compare both groups.

In situ hybridization on cryosections

In situ hybridizations were performed according to an automatized procedure described in [65], using cDNA plasmids described in Table S2 in File S1. Mouse embryos/fetuses (C57BL6) were collected at E12.5, E14.5, E16.5, and at the day of birth (referred to as E19.5). For E14.5 and older samples, the whole head was embedded in OCT 4583 medium (Tissue-TEK, Sakura) and frozen on the surface of dry ice. E12.5 embryos were fixed overnight in 4% paraformaldehyde (pH 7.5, w/v) in phosphate-buffered saline (PBS), cryo-protected by overnight incubation in 20% sucrose (w/v) in PBS, and cryo-embedded as described above. Cryosections (Leica CM3050S cryostat) at 10 μ m were collected on Superfrost plus slides and stored at -80°C until hybridization. E12.5 and E14.5 samples were sectioned in a frontal plane, whereas other stages were sectioned sagittally.

Whole mount in situ hybridization

Whole mount in situ hybridization of mandibles collected at E14.5 was performed with a digoxigenin-labeled *Shh* riboprobe as described [66], using an Intavis InSituPro robot (for details, see <http://www.empress.har.mrc.ac.uk/browser/>, Gene Expression section). The *Shh* template plasmid was kindly provided by A. McMahon (Harvard University).

DNA microarray analysis

Tissue preparation. Embryos at E14.5 were dissected and mandibular molars were isolated. The tail was used for embryo genotyping. Individual tissue samples were frozen in liquid nitrogen and kept at -80°C until genotyping results were available and further used.

Microarray hybridization. To obtain enough RNA for hybridization on DNA microarrays, total RNA was extracted from molar tooth germs dissected manually (pooling samples from two independent wild-type or *Rsk2*^{-/-} embryos). Total RNA was extracted with the RNeasy micro Kit (Qiagen). RNA quality was verified by analysis on the 2100 Bioanalyzer (Agilent). All samples displayed a RNA Integrity Number greater than 9.8. Eight *Rsk2*^{-/-} and 8 WT samples were hybridized and compared.

Biotinylated single strand cDNA targets were prepared, starting from 300 ng of total RNA, using the Ambion WT Expression Kit (Cat #4411974) and the Affymetrix GeneChip WT Terminal Labeling Kit (Cat #900671), according to Affymetrix recommendations. Following fragmentation and end-labeling, 1.9 μ g of cDNAs were hybridized for 16 h at 45°C on GeneChip Mouse Gene 1.0 ST arrays (Affymetrix) interrogating 28,853 genes represented by approximately 27 probes spread across the full length of the gene. The chips were washed and stained in the GeneChip Fluidics Station 450 (Affymetrix) and scanned with the GeneChip Scanner 3000 7G (Affymetrix). Finally, raw data (.CEL Intensity files) were extracted from the scanned images using the Affymetrix GeneChip Command Console (AGCC) version 3.1. See also [67].

The data discussed in this publication have been deposited in NCBI's Gene Expression Omnibus (GEO) [68] and are accessible through GEO Series accession number GSE51034. (<http://www.ncbi.nlm.nih.gov/geo/query/acc.cgi?acc=GSE51034>)

Microarray analysis. CEL files were further processed with the Partek software to obtain principal component analysis (PCA) and to select and consider only genes with a signal value above 5 (20th percentile of all expression values) in at least one sample. Genes were considered as differentially expressed if the false discovery rate from Benjamini and Hochberg test was under 0.1 and if the fold change was greater than 1.2 or lower than -1.2.

In vitro culture and shRNA inactivation

E14.5 tooth germs were dissected and cultured in chemically defined culture medium as previously described [19]. The tooth explant consisted of both the enamel organ (epithelial component) and the attached dental mesenchyme. A DNA solution containing 1 μ g of *Rsk2* shRNA (SABiosciences SureSilencing shRNA Plasmid for Mouse Rps6kA3 clone ID1– linearized pGeneclip Neomycin vector, insert sequence TGATGATACTCCAGAGGAAT) or a random shRNA (insert sequence GGAATCTCATTCGATGCATAC), 0.5% sucrose, and Fast Green (Sigma; 1/10,000) was injected into the developing molars with a Femtojet Eppendorf device ($t=0.2$ s, $P=61$ hPa). Two platinum needle electrodes (0.1 mm tip, Sonidel) were inserted into the tissue lying in a cover round platinum flat electrode (Sonidel). DNA was then transferred into the cells using an ECM 830 Electroporation System (BTX Harvard Apparatus), applying 1 set of 5 pulses. Electroporation settings were set to 5 V for 50 ms, spaced by 50 ms intervals. As negative control, explants were electroporated with a random shRNA sequence.

After electroporation, the explants were embedded into 14 μ l rat collagen drops (BD Biosciences) containing 0.2 ng laminin (BD Biosciences), 50 μ l DMEM 10x concentrated, 5 μ l HEPES (1 mM), 60 μ l 7.5% NaHCO_3 (adapted from [24]). The collagen drops were kept on ice to prevent them from polymerizing. The collagen was then polymerized at 37°C for 10–15 min before addition of the culture medium.

All explants were subsequently cultured for 24 hours in a DMEM-HAM F12 medium supplemented with Vitamin C (18 mg/ml); L-Glutamine (200 mM); Streptomycin (1000 U/ml) and 20% fetal calf serum for optimal tooth growth. Explants were then processed for RT-qPCR analysis.

Real-time quantitative RT-PCR

RT-PCR assays were performed in duplicate, comparing 3 wild-type and 3 *Rsk2*^{-/-} RNA samples (4 teeth were used in each sample for validation of microarray data), or 6 molar samples electroporated with *Rsk2* shRNA and 6 control samples (for shRNA experiments). RNA extractions were performed as previously described (ref. [67]). Oligo-dT primed cDNAs were generated

using the Superscript II kit (Invitrogen) according to the manufacturer's protocol. Quantitative real-time PCR was achieved using SybrGreen and LightCycler 480 (Roche). The sequences of primers used for the various tested genes are given in Table S3 in File S1. A probe set for detection of mouse *Gapdh* mRNA (encoded by a housekeeping gene) was used for normalization. For each sample the ratio between signals for the gene of interest and *Gapdh* was calculated to normalize concentration values. To verify if genes were differentially expressed between electroporated and control samples, the average of ratios were then compared.

Statistical tests

Data, presented as means \pm SEM, were compared using Student t-test (for 2 groups comparison). P-values below 0.05 were considered as significant.

Supporting Information

Figure S1 Description of the craniofacial anatomical landmarks used for X-Ray microtomographic analysis of *Rsk* mutant mice.

(TIF)

Figure S2 Molar landmarks used for the analysis of X-Ray tomography images.

(TIF)

Figure S3 Three-dimensional isosurface rendering of a right mandibular incisor from a wild-type mouse, in lateral

(A) and dorsal (B) views, depicting the distances measured for the morphometric analysis.

(TIF)

File S1 Supporting Information file containing Tables S1–S3. Table S1 in file S1. Molar root numbers in WT and *Rsk2*^{-/-} mice. UR: upper right. UL: upper left. LR: lower right. LL: lower left. M1: first molar. M2: second molar. M3: third molar. ST: supernumerary tooth. Table S2 in file S1. Template plasmids used for *in situ* hybridization. Table S3 in file S1. Sequences of primers used for quantitative RT-PCR experiments. (DOCX)

Acknowledgments

The authors are grateful to the patients and families attending the Reference centre for orodental manifestations of rare diseases, IJUS, Strasbourg, France, and to Dr. Karen Niederreither for proofreading of the manuscript. They also wish to thank Cathy Herouard-Molina, Doulaye Dembele, and Christelle Thibault from the IGBMC Microarray and sequencing platform.

Author Contributions

Conceived and designed the experiments: VH-L MP PC AC LV AH PD AB-Z. Performed the experiments: VL-H MP PM AL TK JD SM FB SP. Analyzed the data: VL-H LV PD AB-Z. Contributed reagents/materials/analysis tools: CP AL TK JD MS FB SP. Wrote the paper: VL-H MP LV AH PD AB-Z.

References

- Hanauer A, Young ID (2002) Coffin-Lowry syndrome: clinical and molecular features. *J Med Genet* 39: 705–713.
- Temtamny SA, Miller JD, Hussels-Maumenee I (1975) The Coffin-Lowry syndrome: an inherited faciocardiac mental retardation syndrome. *J Pediatr* 86: 724–731.
- Temtamny SA, Miller JD, Dorst JP, Hussels-Maumenee I, Salinas C, et al. (1975) The Coffin-Lowry syndrome: a simply inherited trait comprising mental retardation, faciocardiac anomalies and skeletal involvement. *Birth Defects Orig Artic Ser* 11: 133–152.
- Igari K, Hozumi Y, Monma Y, Mayanagi H (2006) A case of Coffin-Lowry syndrome with premature exfoliation of primary teeth. *Int J Paediatr Dent* 16: 213–217.
- Day P, Cole B, Welbury R (2000) Coffin-Lowry syndrome and premature tooth loss: a case report. *ASDC J Dent Child* 67: 148–150.
- Frodin M, Gammeltoft S (1999) Role and regulation of 90 kDa ribosomal S6 kinase (RSK) in signal transduction. *Mol Cell Endocrinol* 151: 65–77.
- Romeo Y, Zhang X, Roux PP (2012) Regulation and function of the RSK family of protein kinases. *Biochem J* 441: 553–569.
- Tan Y, Ruan H, Demeter MR, Comb MJ (1999) p90(RSK) blocks bad-mediated cell death via a protein kinase C-dependent pathway. *J Biol Chem* 274: 34859–34867.
- Hauge C, Frodin M (2006) RSK and MSK in MAP kinase signalling. *J Cell Sci* 119: 3021–3023.
- Poirier R, Jacquot S, Vaillend C, Southiphong AA, Libbey M, et al. (2007) Deletion of the Coffin-Lowry Syndrome Gene *Rsk2* in Mice is Associated With Impaired Spatial Learning and Reduced Control of Exploratory Behavior. *Behav Genet* 37: 31–50.
- Yang X, Matsuda K, Bialek P, Jacquot S, Masuoka HC, et al. (2004) ATF4 is a substrate of RSK2 and an essential regulator of osteoblast biology; implication for Coffin-Lowry Syndrome. *Cell* 117: 387–398.
- Kohn M, Hameister H, Vogel M, Kehrer-Sawatzi H (2003) Expression pattern of the *Rsk2*, *Rsk4* and *Pdk1* genes during murine embryogenesis. *Gene Expr Patterns* 3: 173–177.
- Viriot L, Peterkova R, Peterka M, Lesot H (2002) Evolutionary implications of the occurrence of two vestigial tooth germs during early odontogenesis in the mouse lower jaw. *Connect Tissue Res* 43: 129–133.
- Fleischmannova J, Matalova E, Tucker AS, Sharpe PT (2008) Mouse models of tooth abnormalities. *Eur J Oral Sci* 116: 1–10.
- Aberg T, Cavender A, Gaikwad JS, Bronckers AL, Wang X, et al. (2004) Phenotypic Changes in Dentition of Runx2 Homozygote-null Mutant Mice. *J Histochem Cytochem* 52: 131–140.
- Zhang M, Chen W, Smith SM, Napoli JL (2001) Molecular characterization of a mouse short chain dehydrogenase/reductase active with all-trans-retinol in intact cells, mRDH1. *J Biol Chem* 276: 44083–44090.
- Bloch-Zupan A, Decimo D, Lorient M, Mark MP, Ruch JV (1994) Expression of nuclear retinoic acid receptors during mouse odontogenesis. *Differentiation* 57: 195–203.
- Bloch-Zupan A, Mark MP, Weber B, Ruch JV (1994) In vitro effects of retinoic acid on mouse incisor development. *Arch Oral Biol* 39: 891–900.
- Mark MP, Bloch-Zupan A, Ruch JV (1992) Effects of retinoids on tooth morphogenesis and cytodifferentiation, in vitro. *Int J Dev Biol* 36: 517–526.
- Mark MP, Bloch-Zupan A, Wolf C, Ruberte E, Ruch JV (1991) Involvement of cellular retinoic acid-binding proteins I and II (CRABPI and CRABPII) and of the cellular retinol-binding protein I (CRBPI) in odontogenesis in the mouse. *Differentiation* 48: 89–98.
- Wan X, Ji W, Mei X, Zhou J, Liu JX, et al. (2010) Negative feedback regulation of Wnt4 signaling by EAF1 and EAF2/U19. *PLoS One* 5: e9118.
- Xiao W, Zhang Q, Habermacher G, Yang X, Zhang AY, et al. (2008) U19/Eaf2 knockout causes lung adenocarcinoma, B-cell lymphoma, hepatocellular carcinoma and prostatic intraepithelial neoplasia. *Oncogene* 27: 1536–1544.
- Wise GE, He H, Gutierrez DL, Ring S, Yao S (2011) Requirement of alveolar bone formation for eruption of rat molars. *Eur J Oral Sci* 119: 333–338.
- Wright TJ, Ladher R, McWhirter J, Murre C, Schoenwolf GC, et al. (2004) Mouse FGF15 is the ortholog of human and chick FGF19, but is not uniquely required for otic induction. *Dev Biol* 269: 264–275.
- Ji Q, Luo ZX, Yuan CX, Wible JR, Zhang JP, et al. (2002) The earliest known eutherian mammal. *Nature* 416: 816–822.
- Peterka M, Vonesch JL, Ruch JV, Cam Y, Peterkova R, et al. (2000) Position and growth of upper and lower tooth primordia in prenatal mouse—3D study. *J Craniofac Genet Dev Biol* 20: 35–43.
- Viriot L, Lesot H, Vonesch JL, Ruch JV, Peterka M, et al. (2000) The presence of rudimentary odontogenic structures in the mouse embryonic mandible requires reinterpretation of developmental control of first lower molar histomorphogenesis. *Int J Dev Biol* 44: 233–240.
- Peterkova R, Peterka M, Lesot H (2003) The developing mouse dentition: a new tool for apoptosis study. *Ann N Y Acad Sci* 1010: 453–466.
- Pornaveetus T, Ohazama A, Choi HY, Herz J, Sharpe PT (2011) Wnt signaling in the murine diastema. *Eur J Orthod*.
- Ohazama A, Blackburn J, Pornaveetus T, Ota MS, Choi HY, et al. (2010) A role for suppressed incisor cuspal morphogenesis in the evolution of mammalian heterodont dentition. *Proc Natl Acad Sci U S A* 107: 92–97.
- Klein OD, Minowada G, Peterkova R, Kangas A, Yu BD, et al. (2006) Sprouty genes control diastema tooth development via bidirectional antagonism of epithelial-mesenchymal FGF signaling. *Dev Cell* 11: 181–190.
- Charles C, Hovorakova M, Ahn Y, Lyons DB, Marangoni P, et al. (2011) Regulation of tooth number by fine-tuning levels of receptor-tyrosine kinase signaling. *Development* 138: 4063–4073.

33. Ohazama A, Haycraft CJ, Seppala M, Blackburn J, Ghafoor S, et al. (2009) Primary cilia regulate Shh activity in the control of molar tooth number. *Development* 136: 897–903.
34. Kassai Y, Munne P, Hotta Y, Penttila E, Kavanagh K, et al. (2005) Regulation of mammalian tooth cusp patterning by ectodin. *Science* 309: 2067–2070.
35. Murashima-Suginami A, Takahashi K, Sakata T, Tsukamoto H, Sugai M, et al. (2008) Enhanced BMP signaling results in supernumerary tooth formation in USAG-1 deficient mouse. *Biochem Biophys Res Commun* 369: 1012–1016.
36. Ohazama A, Johnson EB, Ota MS, Choi HY, Pomtaveetus T, et al. (2008) Lrp4 modulates extracellular integration of cell signaling pathways in development. *PLoS One* 3: e4092.
37. Hacohen N, Kramer S, Sutherland D, Hiromi Y, Krasnow MA (1998) sprouty encodes a novel antagonist of FGF signaling that patterns apical branching of the Drosophila airways. *Cell* 92: 253–263.
38. Kim HJ, Bar-Sagi D (2004) Modulation of signalling by Sprouty: a developing story. *Nat Rev Mol Cell Biol* 5: 441–450.
39. Tucker AS, Headon DJ, Courtney JM, Overbeck P, Sharpe PT (2004) The activation level of the TNF family receptor, Edar, determines cusp number and tooth number during tooth development. *Dev Biol* 268: 185–194.
40. Pispas J, Mikkola ML, Mustonen T, Thesleff I (2003) Ectodysplasin, Edar and TNFRSF19 are expressed in complementary and overlapping patterns during mouse embryogenesis. *Gene Expr Patterns* 3: 675–679.
41. Mustonen T, Pispas J, Mikkola ML, Pummila M, Kangas AT, et al. (2003) Stimulation of ectodermal organ development by Ectodysplasin-A1. *Dev Biol* 259: 123–136.
42. Peterkova R, Lesot H, Viriot L, Peterka M (2005) The supernumerary cheek tooth in tabby/EDA mice—a reminiscence of the premolar in mouse ancestors. *Arch Oral Biol* 50: 219–225.
43. Peterkova R, Kristenova P, Lesot H, Lisi S, Vonesch JL, et al. (2002) Different morphotypes of the tabby (EDA) dentition in the mouse mandible result from a defect in the mesio-distal segmentation of dental epithelium. *Orthod Craniofac Res* 5: 215–226.
44. Lesot H, Peterkova R, Kristenova P, Lisi S, Peterka M (2003) [Effect of the Tabby mutation on the dentition of mice]. *Bull Group Int Rech Sci Stomatol Odontol* 45: 1–11.
45. Charles C, Pantalacci S, Peterkova R, Tafforeau P, Laudet V, et al. (2009) Effect of eda loss of function on upper jugal tooth morphology. *Anat Rec (Hoboken)* 292: 299–308.
46. Kristenova P, Peterka M, Lisi S, Gendralut JL, Lesot H, et al. (2002) Different morphotypes of functional dentition in the lower molar region of tabby (EDA) mice. *Orthod Craniofac Res* 5: 205–214.
47. Ghoda L, Lin X, Greene WC (1997) The 90-kDa ribosomal S6 kinase (pp90rsk) phosphorylates the N-terminal regulatory domain of IkkappaBalpha and stimulates its degradation in vitro. *J Biol Chem* 272: 21281–21288.
48. Schouten GJ, Vertegaal AC, Whiteside ST, Israel A, Toebes M, et al. (1997) IkkappaB alpha is a target for the mitogen-activated 90 kDa ribosomal S6 kinase. *Embo J* 16: 3133–3144.
49. Courtois G, Smahi A, Reichenbach J, Doffinger R, Cancrini C, et al. (2003) A hypermorphic IkkappaBalpha mutation is associated with autosomal dominant anhidrotic ectodermal dysplasia and T cell immunodeficiency. *J Clin Invest* 112: 1108–1115.
50. Boran T, Lesot H, Peterka M, Peterkova R (2005) Increased apoptosis during morphogenesis of the lower cheek teeth in tabby/EDA mice. *J Dent Res* 84: 228–233.
51. Coin R, Lesot H, Vonesch JL, Haikel Y, Ruch JV (1999) Aspects of cell proliferation kinetics of the inner dental epithelium during mouse molar and incisor morphogenesis: a reappraisal of the role of the enamel knot area. *Int J Dev Biol* 43: 261–267.
52. Lesot H, Peterkova R, Viriot L, Vonesch JL, Tureckova J, et al. (1998) Early stages of tooth morphogenesis in mouse analyzed by 3D reconstructions. *Eur J Oral Sci* 106 Suppl 1: 64–70.
53. Viriot L, Peterkova R, Vonesch JL, Peterka M, Ruch JV, et al. (1997) Mouse molar morphogenesis revisited by three-dimensional reconstruction. III. Spatial distribution of mitoses and apoptoses up to bell-staged first lower molar teeth. *Int J Dev Biol* 41: 679–690.
54. Guimiot F, Delezoide AL, Hanauer A, Simonneau M (2004) Expression of the RSK2 gene during early human development. *Gene Expr Patterns* 4: 111–114.
55. Zeniou M, Ding T, Trivier E, Hanauer A (2002) Expression analysis of RSK gene family members: the RSK2 gene, mutated in Coffin-Lowry syndrome, is prominently expressed in brain structures essential for cognitive function and learning. *Hum Mol Genet* 11: 2929–2940.
56. Cho YY, He Z, Zhang Y, Choi HS, Zhu F, et al. (2005) The p53 protein is a novel substrate of ribosomal S6 kinase 2 and a critical intermediary for ribosomal S6 kinase 2 and histone H3 interaction. *Cancer Res* 65: 3596–3603.
57. Lagronova-Churava S, Spoutil F, Vojtechova S, Lesot H, Peterka M, et al. (2013) The dynamics of supernumerary tooth development are differentially regulated by Sprouty genes. *J Exp Zool B Mol Dev Evol* 320: 307–320.
58. Liu Z, Li T, Reinhold ML, Naski MC (2012) MEK1-RSK2 contributes to hedgehog signaling by stabilizing GLI2 transcription factor and inhibiting ubiquitination. *Oncogene*.
59. Schneider A, Mehmood T, Pannetier S, Hanauer A (2011) Altered ERK/MAPK signaling in the hippocampus of the msk2_KO mouse model of Coffin-Lowry syndrome. *J Neurochem* 119: 447–459.
60. Mitsiadis TA, Luukko K (1995) Neurotrophins in odontogenesis. *Int J Dev Biol* 39: 195–202.
61. Tummers M, Thesleff I (2009) The importance of signal pathway modulation in all aspects of tooth development. *J Exp Zool B Mol Dev Evol* 312B: 309–319.
62. Bloch-Zupan A, Sedano H, Scully C (2012) *Dento/Oro/Craniofacial Anomalies and Genetics*. London: Elsevier Inc.
63. Richtsmeier JT, Paik CH, Elfert PC, Cole TM 3rd, Dahlman HR (1995) Precision, repeatability, and validation of the localization of cranial landmarks using computed tomography scans. *Cleft Palate Craniofac J* 32: 217–227.
64. Richtsmeier JT, Baxter LL, Reeves RH (2000) Parallels of craniofacial maldevelopment in Down syndrome and Ts65Dn mice. *Dev Dyn* 217: 137–145.
65. Diez-Roux G, Banfi S, Sultan M, Geffers L, Anand S, et al. (2011) A high-resolution anatomical atlas of the transcriptome in the mouse embryo. *PLoS Biol* 9: e1000582.
66. Chotteau-Lelievre A, Dolle P, Gofflot F (2006) Expression analysis of murine genes using in situ hybridization with radioactive and nonradioactively labeled RNA probes. *Methods Mol Biol* 326: 61–87.
67. Laugel-Haushalter V, Paschaki M, Thibault-Carpentier C, Demele D, Dolle P, et al. (2013) Molars and incisors: show your microarray IDs. *BMC Res Notes* 6: 113.
68. Edgar R, Domrachev M, Lash AE (2002) Gene Expression Omnibus: NCBI gene expression and hybridization array data repository. *Nucleic Acids Res* 30: 207–210.

Homozygous and Compound Heterozygous MMP20 Mutations in Amelogenesis Imperfecta.

Gasse B, Karayigit E, Mathieu E, Jung S, Garret A, Huckert M, **Morkmued S**, Schneider C, Vidal L, Hemmerlé J, Sire JY, Bloch-Zupan A.

J Dent Res. 2013 Jul;92(7):598-603. doi: 10.1177/0022034513488393. Epub 2013 Apr 26.

Des mutations *MMP20* homozygotes et hétérozygotes composites dans l'amélogénèse imparfaite.

Dans cet article, nous nous concentrons sur l'amélogénèse imparfaite de type hypomature autosomique-récessive (type IIA2) et décrivons 2 nouvelles mutations du gène codant pour la Métalloprotéinase de la matrice 20 (*MMP20*) retrouvées dans deux familles non apparentées: une mutation non sens p.T130I à l'état homozygote et des mutations hétérozygotes composites, avec la même mutation combinée à une délétion nucléotidique, conduisant à un codon stop prématuré (p.N120fz * 2). Nous avons caractérisé la structure de l'émail de ce dernier cas en utilisant une analyse par microscopie électronique à balayage et une microanalyse (Spectroscopie de rayons X à énergie dispersive, EDX) et confirmé l'amélogénèse imparfaite de type hypomature, comme indiqué dans le diagnostic clinique. Le contenu minéralisé est légèrement diminué, avec remplacement du magnésium par le calcium dans la structure cristalline. Les anomalies ont affecté l'émail avec épaisseur minimale et des cristaux d'apatite perpendiculaires aux prismes d'émail, ce qui suggère un nouveau rôle possible de la *MMP20* dans la formation de l'émail.

RESEARCH REPORTS

Clinical

B. Gasse¹, E. Karayigit^{2,8}, E. Mathieu³,
S. Jung⁴, A. Garret⁴, M. Huckert^{4,7},
S. Morkmued^{4,6}, C. Schneider^{2,4},
L. Vidal⁵, J. Hemmerlé³, J.-Y. Sire¹,
and A. Bloch-Zupan^{2,4,8*}

¹Research group "Evolution & Développement du Squelette-EDS", UMR 7138-SAE, Université Pierre et Marie Curie, Paris, France; ²Reference Center for Orofacial Manifestations of Rare Diseases, Pôle de Médecine et Chirurgie Bucco-Dentaires, Hôpitaux Universitaires de Strasbourg (HUS), Hôpital Civil, 1 place de l'Hôpital, 67000 Strasbourg Cedex, France; ³INSERM U1121, "Biomatériaux et Bioingénierie", Université de Strasbourg, France; ⁴Faculty of Dentistry, University of Strasbourg, France; ⁵Université de Haute-Alsace, Institut de Science des Matériaux de Mulhouse (IS2M), CNRS UMR 7361, Mulhouse, France; ⁶Faculty of Dentistry, University of Khon Kaen, Thailand; ⁷Laboratoire de Génétique Médicale, INSERM U 1112, Faculté de Médecine, Université de Strasbourg, France; and ⁸Institut de Génétique et de Biologie Moléculaire et Cellulaire (IGBMC), INSERM U 964, CNRS-Université de Strasbourg UMR7104, Illkirch, France; *corresponding author, agnes.bloch-zupan@unistra.fr

J Dent Res 92(7):598-603, 2013

ABSTRACT

In this article, we focus on hypomaturation autosomal-recessive-type amelogenesis imperfecta (type IIA2) and describe 2 new causal Matrix metalloproteinase 20 (*MMP20*) mutations validated in two unrelated families: a missense mutation p.T130I at the expected homozygous state, and a compound heterozygous mutation having the same mutation combined with a nucleotide deletion, leading to a premature stop codon (p.N120fz*2). We characterized the enamel structure of the latter case using scanning electron microscopy analysis and microanalysis (Energy-dispersive X-ray Spectroscopy, EDX) and confirmed the hypomaturation-type amelogenesis imperfecta as identified in the clinical diagnosis. The mineralized content was slightly decreased, with magnesium substituting for calcium in the crystal structure. The anomalies affected enamel with minimal inter-rod enamel present and apatite crystals perpendicular to the enamel prisms, suggesting a possible new role for *MMP20* in enamel formation.

KEY WORDS: rare disease, dental anomalies, enamel, human, gene, scanning electron microscopy.

DOI: 10.1177/0022034513488393

Received November 5, 2012; Last revision April 8, 2013; Accepted April 9, 2013

A supplemental appendix to this article is published electronically only at <http://jdr.sagepub.com/supplemental>.

© International & American Associations for Dental Research

Homozygous and Compound Heterozygous *MMP20* Mutations in Amelogenesis Imperfecta

INTRODUCTION

Amelogenesis imperfecta (AI) consists of a heterogeneous group of rare genetic diseases that affect the formation/mineralization of tooth enamel and are transmitted according to various modes of inheritance (X-linked, autosomal-dominant, autosomal-recessive) (Crawford *et al.*, 2007). These disorders exist either in isolation, with clinical manifestations limited to the oral cavity, or associated with other symptoms in syndromes. Mutations occur in many genes coding for either enamel matrix proteins (EMPs), enamel-matrix-degrading proteins, or proteins involved in hydroxyapatite formation and growth and mineralization and have been identified as being responsible for the clinical phenotypes (hypoplastic, hypomineralization, or hypomaturation) of AI (Bloch-Zupan *et al.*, 2012).

The matrix metalloproteinase 20 (*MMP20*) gene codes for the developing-tooth-specific proteinase enamelysin (Kawasaki and Suzuki, 2011; Meredith *et al.*, 2011) that degrades the EMPs, amelogenin and ameloblastin, during the secretory stage of enamel formation (Yamakoshi *et al.*, 2011). Enamelysin plays an important role in tooth enamel formation (Simmer and Hu, 2002), by promoting and controlling mineralization (Uskokovic *et al.*, 2011) through the replacement of the organic matrix with mineral crystals, and generating a hypermineralized enamel layer. *MMP20* regulates crystal elongation, normal architecture of the dentin-enamel junction, and the organization and maintenance of enamel rods (Lu *et al.*, 2008). *MMP20* is expressed during enamel development in both ameloblasts (Caterina *et al.*, 2000) and odontoblasts (Bartlett *et al.*, 1998; Bègue-Kim *et al.*, 1998; Hu *et al.*, 2002). Its expression is initiated prior to the onset of dentin mineralization and continues throughout the secretory stage of amelogenesis (Simmer and Hu, 2002).

Mutations in *MMP20* (11q22.3-q23) cause the autosomal-recessive hypomaturation type of AI—type IIA2, AI2A2, OMIM #612529 (Kim *et al.*, 2005)—which is characterized by a hypomineralized, mottled grayish-brown discoloration appearance of the enamel, which has a rougher surface and is duller and less reflective than normal but has normal thickness, leading to crowns of normal sizes and shapes. The enamel is slightly soft and detaches

Table. MMP20 Mutations Associated with Amelogenesis Imperfecta

Mutation	Location	Mode of Inheritance	References
g.115g>a; c.102g>a; p.W34X	exon 1	AR	Papagerakis <i>et al.</i> , 2008 Chan <i>et al.</i> , 2011
g.8,506delA; c.359delA; p.N120Ifs*2	exon 2	AR	Present study
g.13,444c>t; c.389c>t; p.T130I	exon 3	AR	Present study
g.15,390; c.611A>G; p.H204R	exon 4	AR	Wang <i>et al.</i> , 2013
g.16,250T>A; c.678T>A; p.H226Q	exon 5	AR	Ozdemir <i>et al.</i> , 2005 Wright <i>et al.</i> , 2011
g.18,755G>A; c.910G>A; p.A304T	exon 6	AR	Lee <i>et al.</i> , 2010
g.30,574A>T; c.954-2A>T; p.I319Ffs*19	intron 6	AR	Kim <i>et al.</i> , 2005, 2006 Wright <i>et al.</i> , 2011

The nomenclature follows <http://www.hgvs.org/mutnomen/>, and the RefSeqs of Gene/mRNA/protein are NG_012151.1/NM_004771.3/NP_004762.2. AR: autosomal recessive.

easily from the dentin. Radiographs show a lack of contrast between enamel and dentin (Witkop, 1988; Crawford *et al.*, 2007; Bloch-Zupan *et al.*, 2012). The prevalence of this specific form of AI is not known.

In this article, we focus on the hypomaturational autosomal-recessive type of AI and describe 2 new causal MMP20 mutations, which have been validated in 2 unrelated families. Five MMP20 mutations associated with AI have been reported in the literature (Table), but for the first time a compound heterozygous mutation is identified and the resultant AI enamel ultrastructure described.

MATERIALS & METHODS

Patients

The patients and their families were selected from the pool of patients participating in the French Ministry of Health National Program for Clinical Research, PHRC 2008 HUS (Strasbourg University Hospital) N°4266, Amelogenesis Imperfecta. For our study, we selected two patients from two unrelated cases with clinical diagnoses matching the possible underlying MMP20 mutations. Affected and unaffected family members gave informed consent. All clinical and molecular studies were approved by the Local Ethics Committee of the Strasbourg University Hospital. Patients were examined clinically by dentists in the Reference Center for Orofacial Manifestations of Rare Diseases, Pôle de Médecine et Chirurgie Bucco-Dentaires, Hôpitaux Universitaires, Strasbourg, France. The dental phenotypes were documented using the D[4]/phenodent registry: a Diagnosing Dental Defects Database (see www.phenodent.org, to access assessment form). This registry allows for the standardization of data collection and assists in orofacial phenotyping. It also facilitates providing clinical care to patients, a basis for genotype/orofacial phenotype correlations, and sharing of data and clinical material between/among clinicians.

Mutation Analysis

Genomic DNA was isolated from the saliva of patients and unaffected family members by means of the Oragene[®]-DNA (OG-250)

saliva kit (DNA Genotek Inc., Ontario, Canada) following the manufacturer's protocol. MMP20 genomic and transcript reference sequences NG_012151.1 and NM_004771.3, respectively, were used to design the primers (Appendix Table 1). Mutational analysis was performed for the 10 exons of MMP20, including exon-intron boundaries (see Appendix Table 1 for detailed process). PCR products were sent to GATC Biotech for purification and sequencing in both directions, to minimize sequencing artifacts. The sequences were aligned manually with the reference sequence NG_012151.1 using Se-AI v2.0a11 software.

Comparative Material

The MMP20 sequences of 36 species, representative of mammalian lineages, were extracted from GenBank (Appendix Table 2), translated into protein sequences, and aligned with the human MMP20 sequence to localize sensitive positions, *i.e.*, residues which have been unchanged during 200 million years of mammalian evolution.

Specimen Preparation

The first primary right upper molar tooth (FDI World Dental Federation notation #54) of patient 2, as well as an identical control primary tooth (#54), were available for the comparative study of enamel AI/control ultrastructure. The control tooth was obtained from a donor patient of the same age and gender as patient 2, attending the pediatric dentistry department of the Pôle de Médecine et Chirurgie Bucco-Dentaires, Hôpitaux Universitaires de Strasbourg (HUS), for treatment.

After extraction, the teeth were rinsed with tap water and immersed in a sodium hypochlorite solution (1.2 chlorometric degree) for 24 hrs. After being rinsed with distilled water, the tooth was dehydrated in a graded series of ethanols, transferred in a solution of propylene oxide/epon resin (v/v) for 24 hrs, then embedded in Epon 812 (Euromedex, Souffelweyersheim, France). The tooth was sectioned into 2 halves along its vertical axis by means of a water-cooled circular diamond saw (Bronwill Scientific, Rochester, NY, USA), and both surfaces were polished with diamond paste (Escil, Chassieu, France). The 2 halves were then left to dry at room temperature.



Figure 1. Clinical phenotypes associated with the 2 new *MMP20* mutations. **(A-C)** Patient 1. **(A)** 5 years old; **(B)** 8 years old; **(C)** panoramic radiograph (8 years old). **(A)** In the primary dentition, the enamel is opaque and chalky white, and some post-eruptive enamel breakdown is visible on the incisal edges of primary upper incisors and on the occlusal surfaces of primary molars. **(B)** The morphology of the newly erupted permanent upper incisors is normal, but enamel defects are visible. The enamel has an opaque and creamy appearance, and some isolated enamel pits are visible on the vestibular surface of 11. **(C)** On the panoramic radiograph, tooth germs show a normal morphology; the enamel is indeed present but shows limited contrast when compared with dentin, underlying its undermineralized status. **(D-H)** Patient 2. **(D)** 6 years old; **(E)** 8 years old; **(F)** 10 years old; **(G)** 14 years old; **(H)** 11 years old. **(D)** The appearance of the enamel on the permanent teeth is similar to that observed in patient 1. **(E)** The structural defect involves the whole enamel layer and is still visible when the surface of enamel is removed to prepare the tooth for composite veneers. **(F, G)** Newly erupted teeth have a normal morphology and appear orange. The enamel is rather rough. **(H)** No contrast is visible between enamel and dentin on this panoramic radiograph. A globular aspect of the crowns and a cervical constriction are present. The first permanent molars appear taurodontic.

Scanning Electron Microscopy

The samples were coated with gold-palladium alloy by means of a HUMMER JR sputtering device (Anatech/Technics, Union City, CA, USA). Scanning electron microscopy assessments and microanalysis (Energy-dispersive x-ray) were performed with a Quanta 400 ESEM (FEI company, Eindhoven, The Netherlands) operating with an electron accelerating voltage of 30 kV.

RESULTS

Clinical Phenotype

Patient 1

This female patient is the third child born from consanguineous first-cousin parents. One previous miscarriage was reported. Two male children died early in life, presenting with multiple malformations and brain anomalies. *In utero*, the absence of fetal movements was mentioned in the medical records. The caryotypes of all family 1 members were normal. The female patient 1 presented at birth with a cheek hemangioma and suffered from deafness secondary to multiple serous otitis, somnambulism, learning deficit, and behavioral disorder.

The orodental clinical phenotype, assessed through oral clinical and radiographic (panoramic radiograph) examination, revealed no abnormalities of tooth number, shape, or size, but abnormalities of tooth structure were obvious, with AI affecting both the primary and permanent dentitions (Figs. 1A-1C). The chalky white color of the enamel and the overall intact morphology of unerupted and erupted teeth suggested the clinical diagnosis of hypomaturation type AI. The enamel surface was hard, and the enamel loss was related to secondary enamel breakdown. Some true hypoplastic enamel areas (pits) were also present. On the panoramic radiograph, a differential but limited contrast was visible between enamel and dentin. Early eruption of permanent lower incisors was reported by the parents, but the dental age seemed to match the physical age at subsequent visits. No tooth was available for SEM analysis for patient 1.

Patient 2

This female patient was born prematurely at 30 weeks' gestation from non-consanguineous parents; there was a history of the *in utero* death of her twin sister at 26 wks of gestation, due to twin-to-twin transfusion syndrome. A previous female fetus had died at 8 mos *in utero* with no specific diagnosis. Patient 2 had asthma from 3 to 10 yrs old but no other significant health problems.

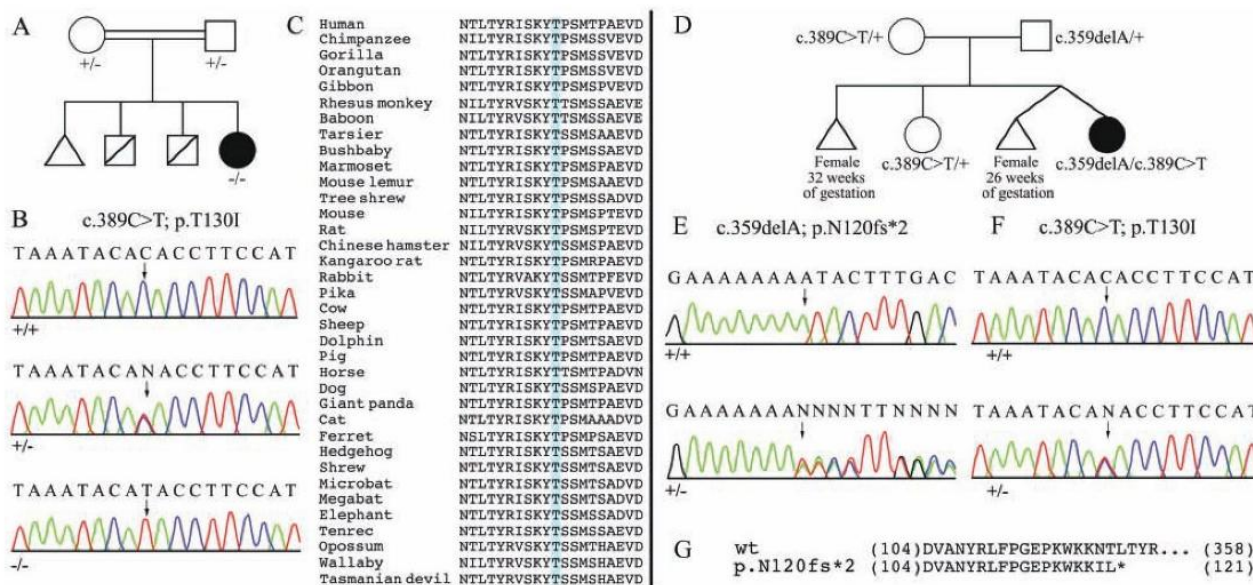


Figure 2. Mutational analysis of the 2 new *MMP20* mutations. (A-C) Patient 1. (A) Pedigree of the AI kindred with the homozygous mutation (c.389C>T; p.T130I). (B) DNA sequencing chromatograms of control (+/+), and of heterozygous (+/-) and homozygous (-/-) mutations. The mutation site is indicated with arrows. (C) Sequence alignment of 36 mammalian *MMP20* in the target region encoded by exon 3. The affected threonine (blue background) is unchanged in all species. (D-G) Patient 2. (D) Pedigree of the AI kindred with the compound heterozygous mutation (c.359delA / c.389C>T). (E, F) Mutational analyses. DNA sequencing chromatograms of control (+/+) and of heterozygous (+/-) mutation. Arrows point to the mutation sites. (G) Alignment of the wild-type *MMP20* sequence with the truncated protein resulting from the p.N120fs*2 mutation.

Oral clinical and radiographic (panoramic radiograph) examination (Figs. 1D-1H) revealed no abnormalities in tooth number in the primary or permanent dentition, but there were abnormalities of tooth shapes/sizes (crowns rather bulbous with a cervical constriction, roots thin and short, and molars possibly taurodontic). The tooth structure demonstrated hypomaturational AI affecting both the primary and permanent dentitions. Early tooth eruption was reported in mandibular permanent second molars and premolars. The eruption of maxillary teeth seemed normal and matched her chronological age. This girl required extensive restorative crown treatment, with only a few teeth being intact. The enamel defects in patient 2 were more pronounced than those in patient 1. The enamel of primary teeth was white, opaque, and chalky, with sites of post-eruptive enamel loss and wear. The color change of permanent teeth was more intense (orange), with a hard but rough enamel surface. The teeth were sensitive, the soft porous enamel having no protective barrier effect. There was almost invisible radiographic contrast between enamel and dentin (in comparison with that seen in patient 1). The first primary right upper molar was available for SEM analysis.

Genotype

Patient 1: Homozygous Mutation c.389C>T

We identified a missense mutation in exon 3 of *MMP20* of patient 1. The mutation is referred to as g.13,444C>T; c.389C>T; p.T130I. The female proband was homozygous for the mutation, while both unaffected parents were heterozygous (Figs. 2A, 2B). The mutation occurred at a threonine residue that is unchanged in the 36 *MMP20* mammalian sequences studied (Fig. 2C). This finding indicates a putative important function for this amino acid

and validates the homozygous mutation as being responsible for the AI phenotype. The presence of several unchanged residues (e.g., lysine 128, tyrosine 129, serine 132, methionine 133) in this region suggests a putative functional/structural domain.

Patient 2: Compound Heterozygous Mutation c.389C>T and c.359delA

We identified the same missense mutation c.389C>T; p.T130I in patient 2. The female proband was heterozygous for the mutation, as were her unaffected mother and her sibling (Figs. 2D, 2F). We also identified a nucleotide deletion in *MMP20* exon 2 that causes a frame shift and leads to a premature stop codon. The mutation is referred to as g.8,506delA; c.359delA; p.N120Ifs*2 (Figs. 2D, 2E). The female proband was heterozygous for the mutation, as was her unaffected father. Neither her mother nor her sibling was a carrier of this deletion. This case of compound heterozygosity is responsible for the AI phenotype because both alleles possess a valid mutation.

Electron Microscopy Data

Clinical hypomaturational as well as localized hypoplasia were noticed for the AI tooth (first primary right upper molar of patient 2). The thickness of the enamel layer seemed not to be affected (Figs. 3A, 3B). In the area of hypoplastic enamel, it was possible to observe a non-prismatic outer layer. This confirms that the hypoplastic defect is neither artifactual nor due to secondary enamel breakdown, but is *per se* a primary anomaly (Fig. 3B). The anomalies mostly affected secondary enamel structures: In pre-natal enamel (Fig. 3C), crystals were less well-defined than in post-natal enamel (Fig. 3D); and apatite crystals were amazingly

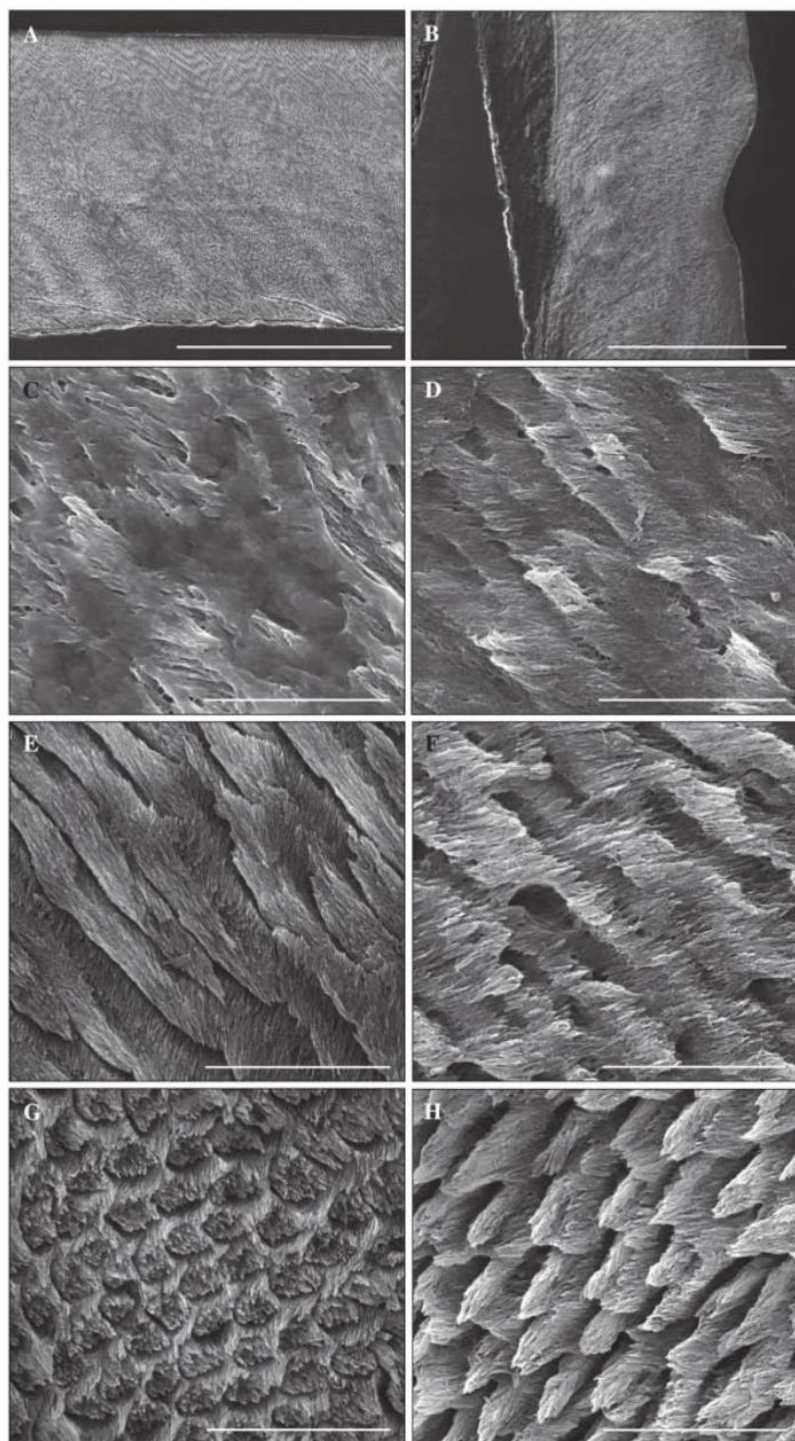


Figure 3. Ultrastructural features of amelogenesis imperfecta (AI) enamel in patient 2. **(A)** Normal enamel in a control tooth showing characteristic Hunter-Schreger bands. **(B)** AI enamel of the first upper molar from the hypoplastic area. The surface of the tooth is not flat as compared that of the control (in A), and there is a localized depression of enamel. Note that the prismless subsurface enamel layer is present and continuous. We called this lack of enamel a hypoplastic defect. The darker layer corresponds to pre-natal enamel, and the difference in enamel crystals between pre- and post-natal enamel is unique for the AI tooth. **(C)** Enlargement of the pre-natal enamel from the darker area in B. **(D-H)** Post-natal enamel. **(D)** Enlargement of the post-natal enamel from the darker area in B. **(E)** Enamel crystal alignment within the enamel rods of the control tooth. **(F)** Enamel crystal direction within the rods in the AI tooth. **(G)** Presence of inter-rod enamel in the normal tooth. **(H)** Absence or loss of interprismatic enamel in the AI tooth. Scale bars: A,B, 500 μm ; C-H, 20 μm .

perpendicular to enamel prisms (Fig. 3F). These structural features differ from the normal crystal formation parallel to prism direction (Fig. 3E) and have not, to our knowledge, been previously described in the literature. Abnormal (almost absent) inter-rod enamel was noticed (Fig. 3H). Incremental lines did not show the typical features of striae of Retzius as in normal enamel. They were irregularly spaced.

Microanalysis (EDX) disclosed $\text{Ca/P} = 1.671 \pm 0.009$ (atomic %) for normal enamel and $\text{Ca/P} = 1.647 \pm 0.002$ (atomic %) for AI enamel. Moreover, we recorded a magnesium content of 0.39% (weight) in the AI enamel. Crystallographically, the AI enamel appeared slightly calcium-deficient compared with normal enamel. This calcium deficiency was related to magnesium substitutions in the enamel crystal structure.

DISCUSSION

The new mutations identified in the 2 unrelated European families increase to 7 the *MMP20* mutations known to date as being responsible for hypomaturation AI (Table). Previously described mutations are homozygous mutations, like the T130I mutation found in patient 1. This mutation was validated because it affects a residue conserved in all mammalian species through natural selection. Such substitutions of an AI-associated residue were validated in previous studies for 2 EMPs, amelogenin (Delgado *et al.*, 2007) and enamelin (Al-Hashimi *et al.*, 2009). The mutation in patient 2 is the first report of a compound heterozygous mutation of a gene involved in autosomal-recessive AI, meaning that 2 different allelic mutations occurred at the same locus. Such a compound mutation favored the appearance of this rare disease in a heterogeneous, non-consanguineous population. This occurrence would mean that *MMP20* mutations could be more frequently present in the general population than expected. Therefore, it will be of great importance to scrutinize patient cohorts for future molecular diagnosis of this specific AI.

In the 2 mutations described, we speculate that the protein is translated and secreted, even if non-functional, because the mutation is located far from the ATG. This explains the observed enamel defects. The enamel phenotype was basically the same in the two patients, although enamel defects were more pronounced in patient 2: hypomineralized, opaque enamel from whitish to brown-orange, with local areas of hypoplasia and post-eruptive enamel loss on molars, possibly indicative of a faulty dentino-enamel junction. This phenotype is similar to previous descriptions of *MMP20*-associated

type IIA2 AI (Lee *et al.*, 2010; Wang *et al.*, 2013) and is reminiscent of the observation in *Mmp20*^{-/-} mice with enamel hypoplasia coupled with hypomineralization (Caterina *et al.*, 2002). In particular, the ultrastructural features of AI enamel observed in the primary tooth from patient 2 are similar to those described in mouse *Mmp20*^{-/-} enamel, the only descriptions of submicroscopic alterations of enamel available so far (Bartlett *et al.*, 2006, 2011). It is worth noting that because the KO mouse is a loss-of-function model, the phenotype should be different from that reported here, as resulting from point mutations, which, however, significantly reduce enamelysin function. In patient 1, T130I substitution occurred in a region that was not yet identified as being functionally important, although the resulting enamel defaults indicate an important role. However, this threonine is not predicted as being phosphorylated but is conserved in several MMPs (JYS, personal observations), which suggests a more general function. In patient 2, the allele with the one base-pair deletion encodes a largely truncated protein that misses the catalytic domain (zinc-binding site) of MMP20. This mutation (i) confirms the crucial role of the catalytic domain for the correct function of MMP20 since the phenotype mimics that of the loss of function in the KO mouse, and (ii) indicates that the more severe phenotype observed in patient 2 when compared with patient 1 results from the compound heterozygous mutation, including the truncated protein encoded by one mutant allele.

These findings shed some light on MMP20 function, although further in-depth exploration is needed. The other anomalies of tooth form (cervical constriction, thin roots, taurodontic molars), which were also found in patient 2, are unlikely to be due to *MMP20* mutation.

ACKNOWLEDGMENTS

The authors thank the two families for their participation and contributions and are grateful to Prof. R.K. Hall (University of Melbourne, Australia) for critical reading of the manuscript. This work was supported by grants from the University of Strasbourg, the French Ministry of Health (National Program for Clinical Research, PHRC 2005 N°4266 Amelogenesis imperfecta), the Hôpitaux Universitaires de Strasbourg (API, 2009-2012, "Development of the oral cavity: from gene to clinical phenotype in Human"), Institut Français pour la Recherche Odontologique (IFRO), and the EU-funded project (ERDF) A27 "Oro-dental manifestations of rare diseases", and by the RMT-TMO Offensive Sciences initiative, INTERREG IV Upper Rhine program. S.M was the recipient of a Master fellowship from the University of Khon Kaen, Faculty of Dentistry, Thailand. The authors declare no potential conflicts of interest with respect to the authorship and/or publication of this article.

REFERENCES

- Al-Hashimi N, Sire JY, Delgado S (2009). Evolutionary analysis of mammalian enamelin, the largest enamel protein, supports a crucial role for the 32-kDa peptide and reveals selective adaptation in rodents and primates. *J Mol Evol* 69:635-656.
- Bartlett JD, Ryu OH, Xue J, Simmer JP, Margolis HC (1998). Enamelysin mRNA displays a developmentally defined pattern of expression and encodes a protein which degrades amelogenin. *Connect Tissue Res* 39:101-109.
- Bartlett JD, Skobe Z, Lee DH, Wright JT, Li Y, Kulkarni AB, *et al.* (2006). A developmental comparison of matrix metalloproteinase-20 and amelogenin null mouse enamel. *Eur J Oral Sci* 114(Suppl 1):18-23.
- Bartlett JD, Skobe Z, Nanci A, Smith CE (2011). Matrix metalloproteinase 20 promotes a smooth enamel surface, a strong dentino-enamel junction, and a decussating enamel rod pattern. *Eur J Oral Sci* 119(Suppl 1):199-205.
- Bègue-Kirn C, Krebsbach PH, Bartlett JD, Butler WT (1998). Dentin sialoprotein, dentin phosphoprotein, enamelysin and ameloblastin: tooth-specific molecules that are distinctively expressed during murine dental differentiation. *Eur J Oral Sci* 106:963-970.
- Bloch-Zupan A, Sedano H, Scully C (2012). *Dento/oro/craniofacial anomalies and genetics*. 1st ed. London, UK: Elsevier Inc.
- Caterina J, Shi J, Sun X, Qian Q, Yamada S, Liu Y, *et al.* (2000). Cloning, characterization, and expression analysis of mouse enamelysin. *J Dent Res* 79:1697-1703.
- Caterina JJ, Skobe Z, Shi J, Ding Y, Simmer JP, Birkedal-Hansen H, *et al.* (2002). Enamelysin (matrix metalloproteinase 20)-deficient mice display an amelogenesis imperfecta phenotype. *J Biol Chem* 277:49598-49604.
- Chan HC, Estrella NM, Milkovich RN, Kim JW, Simmer JP, Hu JC (2011). Target gene analyses of 39 amelogenesis imperfecta kindreds. *Eur J Oral Sci* 119 (Suppl 1):311-23.
- Crawford PJ, Aldred M, Bloch-Zupan A (2007). Amelogenesis imperfecta. *Orphanet J Rare Dis* 2:17.
- Delgado S, Ishiyama M, Sire JY (2007). Validation of amelogenesis imperfecta inferred from amelogenin evolution. *J Dent Res* 86:326-330.
- Hu JC, Sun X, Zhang C, Liu S, Bartlett JD, Simmer JP (2002). Enamelysin and kallikrein-4 mRNA expression in developing mouse molars. *Eur J Oral Sci* 110:307-315.
- Kawasaki K, Suzuki T (2011). Molecular evolution of matrix metalloproteinase 20. *Eur J Oral Sci* 119(Suppl 1):247-253.
- Kim JW, Simmer JP, Hart TC, Hart PS, Ramaswami MD, Bartlett JD, *et al.* (2005). MMP-20 mutation in autosomal recessive pigmented hypomaturation amelogenesis imperfecta. *J Med Genet* 42:271-275.
- Kim JW, Simmer JP, Lin BP, Scymen F, Bartlett JD, Hu JC (2006). Mutational analysis of candidate genes in 24 amelogenesis imperfecta families. *Eur J Oral Sci* 114(Suppl 1):3-12.
- Lee SK, Scymen F, Kang HY, Lee KE, Gencay K, Tuna B, *et al.* (2010). MMP20 hemopexin domain mutation in amelogenesis imperfecta. *J Dent Res* 89:46-50.
- Lu Y, Papagerakis P, Yamakoshi Y, Hu JC, Bartlett JD, Simmer JP (2008). Functions of KLK4 and MMP-20 in dental enamel formation. *Biol Chem* 389:695-700.
- Meredith RW, Gatesy J, Cheng J, Springer MS (2011). Pseudogenization of the tooth gene enamelysin (MMP20) in the common ancestor of extant baleen whales. *Proc Biol Sci* 278:993-1002.
- Ozdemir D, Hart PS, Ryu OH, Choi SJ, Ozdemir-Karatas M, Firatli E, *et al.* (2005). MMP20 active-site mutation in hypomaturation amelogenesis imperfecta. *J Dent Res* 84:1031-1035.
- Papagerakis P, Lin HK, Lee KY, Hu Y, Simmer JP, Bartlett JD, *et al.* (2008). Premature stop codon in MMP20 causing amelogenesis imperfecta. *J Dent Res* 87:56-59.
- Simmer JP, Hu JC (2002). Expression, structure, and function of enamel proteinases. *Connect Tissue Res* 43:441-449.
- Uskokovic V, Khan F, Liu H, Witkowska HE, Zhu L, Li W, *et al.* (2011). Hydrolysis of amelogenin by matrix metalloproteinase-20 accelerates mineralization in vitro. *Arch Oral Biol* 56:1548-1559.
- Wang SK, Hu Y, Simmer JP, Scymen F, Estrella NM, Pal S, *et al.* (2013). Novel KLK4 and MMP20 mutations discovered by whole-exome sequencing. *J Dent Res* 92:266-271.
- Witkop CJ Jr (1988). Amelogenesis imperfecta, dentinogenesis imperfecta and dentin dysplasia revisited: problems in classification. *J Oral Pathol* 17:547-553.
- Wright JT, Torain M, Long K, Seow K, Crawford P, Aldred MJ, *et al.* (2011). Amelogenesis imperfecta: genotype-phenotype studies in 71 families. *Cells Tissues Organs* 194:279-283.
- Yamakoshi Y, Richardson AS, Nuncz SM, Yamakoshi F, Milkovich RN, Hu JC, *et al.* (2011). Enamel proteins and proteases in *Mmp20* and *Klk4* null and double-null mice. *Eur J Oral Sci* 119(Suppl 1):206-216.

Extended methods and protocols

Genotyping protocol:

- On a small tail (1-3 mm) or fetal membrane samples (DNA)
- Add : 250 μ l **NaOH** 50mM
- 40 min 95°C → +4°C (using PCR machine)
- Then add 25 μ l **Tris pH8 1M**
- Vigorously vortex several seconds
- Centrifuge 5 min at 13000 trs/min
- *Use 1-2 μ l of supernatant per reaction*

Calculation formula for 20 μ l mix/ PCR tube

Reaction of PCR	96	60	45	30	20	15	10
H2O (μ l)	1702	1280	850	570	425	285	143
10xPCR (μ l) buffer(ROCHE)	200	150	100	66,6	50	33,3	17
dNTPs (μ l) 5 mg each	40	30	20	13,3	10	6,6	3,3
BSA (μ l) 10mg/ml	20	15	10	6,6	5	3,3	1,7
TAQ(ROCHE) (μ l)	20	15	10	6,6	5	3,3	1,7
Primer 1 mg/ml (each) (μ l)	6 each	4,5 each	3 each	2 each	1,5 each	1 each	0,5 Each
+ 1-2 μ l DNA							

- Add 20 μ l mix per PCR tube + 1 to 2 μ l supernatant (DNA)
- Place tubes in the PCR Machine (A preset program (**VANVB**) has standard PCR conditions listed below).

PCR conditions:

-94°C : 4 mins

-94°C : 1 mins

-61°C : 1 mins

-72°C : 1 mins

2 CYCLES

-94°C : 30 sec

-61°C : 30 sec

-72°C : 40 sec

31 CYCLES

-72°C : 5 min → -4°C

Gel preparation

Agarose gel (1.5%) 400 ml.

- TAE 1x 200 ml in « Gel » bottle
- Add "Agarose powder" 6 g.
- Microwave ~2 mins cap loosely covered
- Add TAE 1x 200 ml
- Add 3 ul ethidium bromide (EtBr in cold room) Caution: Highly mutagenic
- Rinse tip into the gel under the hood
- Preparing the gel box before use

Sex genotyping in mice

While adult mice can be readily sexed using anatomical features, young male and female mouse embryos are not yet sufficiently developed to assess their sex. In fact, their genital tubercles look superficially identical. At E16 (3-4 days before birth), the genital tubercle looks like this embedded image:

To determine sex a PCR genotyping for Sry – a gene found exclusively on the Y chromosome can be performed.

Common male-specific PCRs

Sry Sex-determining region of the Y chromosome

forward SRY F : TTG TCT AGA GAG CAT GGA GGG CCA TGT CAA

reverse SRY R : CCA CTC CTC TGT GAC ACT TTA GCC CTC CGA

PCR product: 273 base pair

Primer source: Uni Washington, St. Louis, Mouse Genetics Core

Alternate strategy:

Forward sry1 AACAACTGGGCTTTGCACATTG

Reverse sry2 GTTTATCAGGGTTTCTCTCTAGC

PCR product: 146/166 bp doublet

Genotyping protocol from Mutant Mouse Resource and Research Centers (www.mmrrc.or), including Sry primers.

RT-PCR Protocol

First-Strand cDNA Synthesis Using SuperScript II RT

RNA Extraction protocol by using RNeasy Micro Kit;

Before starting: 12 tubes are prepared

- Beta-Mercaptoethanol (β -ME) 10 μ l + Buffer RLT 1 ml (1,000 μ l)

* For example: 350 μ l per tube x 13 = Preparing 5 ml just before you use

DNase I stock solution preparation and RNA extraction: please follow the protocol provide from the kit

cDNA preparation: 20 μ l per tube, 1 tube contains 1 μ g of RNA

MIX 1

- 50-250 μ g random primer 1 μ l
- RNA 1 μ g (1000 ng) added to sterile, distilled water, TOTAL RNA + H₂O = 9 μ l
- 1 μ l dNTP 5mM 2 μ l

MIX 2

- 5X First-Strand Buffer 4 μ l
- 0.1 M DTT 2 μ l
- RNaseOUT (40 units/ μ l) 1 μ l
- SuperScript (SS) 1 μ l

At the last step add 1 μ l (200 units) of SuperScript II P.T and mix by gently pipetting up and down.

****Prepare the thermocycler** (Eppendorf, Thermomixer comfort) before starting!
(65°C / 42°C)

A 20- μ l reaction volume can be used for 1 ng-5 μ g of total RNA or 1-500 ng of mRNA.

1. Add the following components to a nuclease-free microcentrifuge tube:
MIXED1
2. Heat mixture to 65°C for 5 min and quick chill on ice. Collect the contents of the tube by **brief centrifugation and add MIXED2**
3. Incubate at 42°C for 50 min

4. Inactivate the reaction by heating at 70°C for 15 min.
5. Add 20 µl H₂O and store at -20°C (Can add 20 µl H₂O after start the RT-PCR)

RT-PCR plate preparation

*Prepare every tube before (Standards for three different proportion AND cDNAs of samples)

Standard preparation

Using the same proportions as samples, but prepare 5x more mix + RNA for samples (5 µg of RNA per tube). The RNA for the standard is made from control for these experiments.

Dilute 1 → 1+9H₂O for 0.1

Use 0.1 and → 1+9H₂O for 0.001 OR 2+8 for 0.02

All standard tubes have to be ready before!

Use only 10% of the first-strand reaction for PCR.

MilliQ autoclaved water can use for diluting Control.

1. Add the following to each PCR tube/hole;
 - 6 µl SyberGreen (more viscous than dH₂O)
 - 3 µl H₂O
 - 1 µl Primer

For 12 columns, prepare enough (eg. x13 for each of the 3 solutions).

 - 2 µl of cDNA (After already add 20 µl H₂O)

1 µl Primer; Prepare by

- Primer Forward 10 µl
- Primer Reverse 10 µl
- H₂O 80 µl

***SyberGreen.** (**THE LAST** to add) should quickly keep in refrigerator and should be the last to add in tube.

Start

- Add 3x13 µl H₂O in tubes
- Add 2µl cDNA in holes
- Prepare primer tube 10-10-80, add 1x13 in tubes that have H₂O
- Add solution with 6x13 µl SyberG.

RT-PCR running on the machine (ROCHE, LightCycler 480 II):

Open the computer before starting– Log-in the computer entering username and password (written on the computer).

Then, Click on the LightCycler 480 machine program icon

Username : Dolle

Password : Stemcell1

Each new experiment:

Apply template at the bottom

1. Run template > templates > run template > carole marie 2011
2. Click “save” before start machine, after insert PCR plate in the Dolle experiment.
3. Save > Dolle > experiment > name_date_type
4. Running time 1.15 h.

RT-PCR analysis on office computer:

LightCycler program

Username: admin

Password: LightCycler480

Click icon to shows the navigator

Select – experiment Then click import below the screen

Select – SubsetEditor on the left side---- add experiment by click (+) below

Put the name of the “primer” and select the holes that corresponded after that ---- click “apply”

Select – SampleEditor on the left side---- click “Absolute quantification”**** before give all the names.

Select the type Standard and give the concentration.

Primer selecting and ordering

Primer design

Using “Harvard primer” website <https://pga.mgh.harvard.edu/primerbank/>

Primerbank, then finding all the primers

- Search by keyword, then select- mouse
- Amplicon size \geq 150
- Length, T_m (melting tempature) = nearly the same
- Give A, B, C if buy 2-3 primers

Primer3web for checking our primer

If an established primer set is not available for a given gene, you can design you own primers in the following manner. Find the species-appropriate nucleotide sequence from Pubmed Nucleotide <https://www.ncbi.nlm.nih.gov/nucleotide/>. Take the entire coding cDNA in its Fasta format and paste this into Primer3web as follows:

```

1 atgctgccgc cacagctgtg ctggctgccg ctgctcgtg ccttgctgcc gccggtgcc
61 gcgcagaagt ttcagcgcct cacgttcttg agagtcgata aagacaaaga cagagactgc
121 agcctggact gcccaagctc ccctcagaag ccactctgtg cctcggacgg gaggacctc
181 ctgtcccgat gtgagttcca gcgggccaag tgcaaagatc cacagctgga gatcgcctac
241 cgtgggaatt gcaaagatgt gtccagggtg gtggctgaga ggaagtatac ccaggagcag
301 gcccggaagg agtccagca agtgttcatt ccagaatgca atgatgacgg cacctacagt
361 caggctcagt gtcacagcta cacaggatac tgttggtgtg ttacaccaa tggaagacc
421 atcagtggca ctgctgtggc ccacaagaca cccaggtgcc ccggttcaat aatgaaaag
481 gtgccgcagc ggaaggagc agggaaagca gatgatgctg cagccccagc attggagact
541 cagcccaag gagatgaaga agatattgcc tcacgctacc ctacactctg gaccgagcaa
601 gtaagagtc ggcagaaca gaccaataa aattcagcat cctcctgtga tcaggagcat
661 cagtcagctc ttgaggaagc caagcagccc aagaatgaca atgtagtat cccgagtg
721 gcacatggtg gtctctaca gccagtgcaa tgccatccat ccaccggata ctgctggtg
781 gtgctagtgg aactggacg gccattccc gggacctcca caaggtatga gcaacctaa
841 tgtgacaaca cagcccagc tcaccagcg aaggcccggg acctgtaca gaacaggcca
901 ctgcagggtt gtctggtgc caaaaagc gagtttctga caagtctct ggatgcgctc
961 tccacagaca tggttcatgc cgtctctgac cctcttct cttctggcag gctgtcagag
1021 ccagaccca gccacaccct ggaggagagg gttgtacatt ggtactcaa gctgctgat

```


1081 aagaactcta gtggagacat tggcaagaag gagatcaaac cctttaagag gttcctgcga
1141 aagaaatcca agcccacaaa gtgtgtgaag aagtttggg agtactgcga catgaacaat
1201 gacaagtcca tcaccgtgca ggagctcatg ggctgcttgg gtgcaccag agaggagggt
1261 aaagccaaca ccaggaagcg ccacaccccc agaggaaatg ctgaaagttc ttcttctaat
1321 agacagccca ggaaacaagg atga

Define a primer size range (typically 18-23 nt), a melting temperature (T_m) (typically T_m 57-62), and a desired size of amplification (~180-230 nucleotides).

*From the suggested list pick primers, which can be ordered at Sigma (<http://www.sigmaldrich.com/france.html>)

Bone and cartilage staining by Alizarin red and Alcian blue

- Fix tissue overnight (O/N) in 95% ethanol (or in the SAINTE-MARIE fixation)
- Color in 80 ml 95% ethanol + 20 ml acetic acid + 15 mg Alcian blue powder for approximately 48 hours depending on fetal stage (~24-72 hours)
 - E14 – 24-48 hours
 - E16 – 72 hours
- Dehydrate in 95% ethanol for 24 hours or more (during week-end)
- Put in 1% KOH in dH₂O, until bones are visible (several hours, up to a day)
 - E14 – 2 hours
 - E16 – 3-6 hours
- Coloration O/N in 15mg Alizarin red powder diluted in 100 ml 1% KOH in dH₂O
- Decoloration about 1-2 weeks in 20% glycerol + 1% KOH in dH₂O. Further dissection of samples can be performed if needed.
- Dehydrating in: 70% Ethanol-Glycerol (1:1), absolute Ethanol-Glycerol (1:1), Glycerol.

Solution preparations;

- Alcian blue 8GX CI74240 SIGMA 25g A-3157
- Alizarin red: Alizarin Sodium Sulforate CI58005 SIGMA 100g A-3757
- SAINTE-MARIE fixation: 1% acetic acid in 95% ethanol

General Histological Procedures:**Fixation, decalcification, and paraffin embedding of whole adult mouse heads**

Procedure:

1. Cut off the head, remove all skin and muscles and place in a 50 ml plastic tube containing 45 ml of 4% paraformaldehyde in 1X PBS, fix during 7 days.
2. Wash in demineralized water for 1 hour (keep in same tube), using a rocking platform at room temperature.
3. Decalcify for 24 hours in 10% EDTA pH 7.3, under gentle agitation, on a rocking platform. This step can be increase or accelerated by putting samples at 37°C (placed in warm room about few weeks for adult heads, changing out the EDTA solution ~every 2 days.
4. Wash in demineralized water for 1 hour, replace tube on the rocking platform.
5. Dehydrate in graded alcohol series.
 - 70% ethanol: 1 day
 - 95% ethanol: 2 changes, 1 day each;
 - 100% ethanol: 3 changes (8 hours; overnight, 8 hours)
6. Transfer to Histosol: 3 changes (8 hours; overnight, 8 hours)
7. Infiltrate with paraffin (8 hours; overnight, 8 hours) at 60°C under vacuum (retort is maintained at -70kPa)
8. Orient the head to produce frontal sections, and embed in paraffin

Immunohistochemistry protocol

Preparation of vibratome sections:

- Embryos/fetuses are immediately fixed in 4% PFA/in 1X PBS (PECAM) or 8% PFA/in 1X PBS (p-ERK) for 4-8 hours, then stored in 1X PBS prior to cutting using a Leica VT1000 vibratome. It is preferable to have tissue sectioned several days after collection

Prepare embryonic/fetal sections using the vibratome as follows:

- Sample thickness is set as 30 μm (thinnest section for which acceptable sections are obtained)
- Samples are embedded in dissolved Ultra-pure LMP agarose gel (Invitrogen, REF16520-100) at a concentration of 4% for E12.5-14.5, or 6% for E16.5-E18.5 in dH₂O, correctly oriented in Peel-A-Way embedding molds (Polysciences). Note agarose density should approximate the density of the tissue to be sectioned. Note: A lower quality agarose can destroy mRNA/proteins under analysis. Sections are selected under a stereoscopic microscope. Since our focus is dental development, E14.5—15.5 are typically in the section plane of the eye for molar frontal sections. In sagittal sections, both incisors and molars are located in the oral plane. The samples are re-fixed immediately following section in a solution of 4% formaldehyde in 1X PBS for up to 2 hours, then serial removal of fixative is performed using 2- 3 PBT rinses (PBS 1X / 0.1% Tween 20), followed by serial dehydration in methanol (25 %, 50%, 75% and finally 100%). The sections then can be stored for several months at -20 ° C.
- Processing sections the day immunohistochemistry is performed:
- Rehydrate the samples serially using graded methanol solutions until at a final solution of 100% PBT solution (25% PBT/75% methanol, 50% PBT/50% methanol, 75%/25% methanol and then 100% PBT).
- 2.0 μl aliquots of each antibody and control tubes (lacking the primary antibody) are prepared solution: typically 1/500 dilutions or 1 μl antibody per 500 μl

- Composition of antibody staining solution (2-10% species-specific serum/ 1X PBT/ + primary antibody).

Antibody procedure:

Blocking solution:

It is important to select an appropriate species-specific blocking solution. Both the primary and secondary antibody should be blocked using the same species in which the antibody was obtained.

Examples of blocking solutions are as follows:

- 10% normal goat serum (NGS) in PBT
- 10% normal donkey serum in PBT
- 2% Fetal Bovine Serum (BSA) for phosphorylated antibodies

Typical blocking solution preparation:

- 50µl of NGS
- 450µl PBT (Dulbecco's Phosphate Buffered Saline Solution)

Blocking solution is equilibrated to room temperature before use. Sample blocking is performed at RT for 30 minutes or more.

- Add 1µl of primary antibody and except in the control tube (negative control).

Primary antibodies include:

- PERK: p44 / 42 MAPK (Erk1 / 2) Antibody, Cell Signaling Technology, # 9102
- PECAM: Purified Rat Anti-Mouse CD31, (PECAM-1), BD Pharmingen™, # 550274

Incubation with the primary antibody is performed overnight at 4°C (with gentle agitation for vibratome sections).

- Wash with a solution of 1000µl of PBT. Pipette 500µl of solution thoroughly by tilting the tube to avoid pipetting the cuts samples. Agitate for ~30 minutes. Repeat the operation 6 times. Remove the remaining PBT solution.

- Add 500-1000µl of NGS solution (diluted to 10% in a PBT solution) depending on the dilution of the secondary antibody (1:500-1:1000).

- In the pERK tube: 1µl of the secondary anti-rabbit antibody (red fluorochrome) or Goat anti Rabbit 594

- In the PECAM tube: 1µl of the 2nd anti-rat antibody (green fluorochrome) or Goat anti Rat 488

- In the control tube: 1µl of the 2nd anti-rabbit antibody (red fluorochrome) or Goat anti Rabbit 594
- Add 0.1 µl DAPI to stain all cell nuclei (DAPI =blue fluorochrome). Incubate from few hours/overnight.

Fluorescence microscope:

Immunohistochemistry reactions were documented using a Leica Leitz DMRB fluorescence microscope under semi-darkroom conditions. The procedure involved warning up the microscope and the fluorescence light generator for at least 10 minutes. The fluorescence source was kept on (to avoid excessive heating by turning off and on the device.) Processed samples (and respective controls) were oriented on slides, and Aqua-poly/mount (Polysciences) used to secure coverslips. A complementary colored filter is used to observe specific signal position, which in all cases is compared to match to control sections (lacking primary antibody). Note: Filter No. 1 = red fluorochrome (pERK), Filter No. 2 = green fluorochrome (PECAM), Filter No. 3 = blue fluorochrome (DAPI), Filter No. 4=brightfield.

Tissue treatments

All dissections are performed at room temperature in sterile Phosphate Buffer Saline (PBS) [1x] (made with sterilized milliQ water). All solution changes are done under gentle agitation and at room temperature unless specified.

1). Whole embryos.

- Fix in Paraformaldehyde 4 % (w/v) in sterile PBS [1x] over-night at 4°C (samples can be kept much longer for mRNA in situ analysis).
- Rinse in sterile PBT (PBS with 0.1 % v/v Tween-20) ~2 x 10 min.
- Gradually rehydrate in Methanol 100 % (50% methanol/ 50% PBT ~3 min.; 75% methanol/ 25% PBT ~3 min; 100% methanol ~5 min).
- Store at -20°C.

2). For tissue sectioning.

Paraplast embedding:

- Fix in Paraformaldehyde 4 % (w/v) in sterile PBS [1x] over-night at 4°C (do not over-fix as this destroys quality of sections).
 - Rinse in sterile PBS [1x] 1 x 30 min.
 - Dehydrate in Ethanol 70 % (made with sterile milliQ water) 1 x 30 min, samples can be stored at sterile milliQ water) 1 x 30 min, samples can be stored 4°C at this step.
 - Ethanol 95 % 1 x 30 min.
 - Ethanol 100 % 2 x 30 min.
 - Histosol Plus 2 x 30 min.
- (If the embryos are older than E12.5, repeat PBS washing. Fetuses older than E16.5 samples also need to be skinned and decalcified)
- Paraplast 1 x 1 h then overnight or 3 x 1 h at 56°C.
 - Pour Paraplast into Histomolds on a heating plate, transfer samples (e.g. with heated glass pipette or quickly with blue tip) and orientate them with a heated needle or tweezers.
 - Allow to cool at room temperature.
 - Store the blocks at 4°C.

- The thickness of Paraplast sections is 7 μm . Superfrost Plus slides are stored at 4°C.

Freeze embedding:

Unfixed tissue:

- Orientate sample in a histomold, remove excess of PBS (with a twisted corner of a Kleenex). Using Shandon™ Cryomatrix (Thermo-Fisher Scientific) to completely cover tissue/sample.
- Check the final orientation.
- Solidify on dry ice (Cryomatrix becomes white) at least 15 min, then store at -80°C.

Fixation for large fetuses/organs:

- Dissect fetuses or organs directly in a petri dish (without PBS).
- Dip samples in a beaker containing isopentane (2-Methyl-butane) and place on dry ice. Let the samples freeze (several minutes), and store them in a 50 ml Falcon tube at -80°C.
- Mouse fetuses are placed in a 14 ml Falcon tube (cut at the bottom) to keep them straight during freezing.

Cryoprotection tissue:

- Fix samples previously fixed in paraformaldehyde 4 % (w/v) in 1X PBS overnight at 4°C or less for early stages (E8.5 = 1 h; E9.5 = 1h30; E10.5 = 2h). Note: over-night fixation can be used for all stages.
- Rinse in sterile PBS [1x] 3 x 10 min.
- Cryoprotect: ~over-night at 4°C in sterile Sucrose 20% (w/v) in PBS [1x], until tissue sinks to bottom (hence equilibrated with sucrose). (Sucrose solution is sterilized at 0.5 atmosphere or filtered through a 0.2 μm filter.)
- Put the tissue directly in a Histomold, removing excess sucrose (20%) with a Pipetman and a twisted Kleenex. Cover with Cryomatrix and orientate.
- Follow steps described above for unfixed tissue.

The thickness of cryostat sections is typically 10 μm . sections are placed on Superfrost Plus™ slides are stored at -80°C.

Solution preparation;

- PBS w/o Calcium w/o Magnesium: SIGMA CHIMIE Ref.: D-5652, 10l
- Formaldehyde 16% ultrapure methanol free: EUROMEDEX Ref.: 15710, 10x10ml
- Histosol Plus ininflammable: THERMO ELECTRON DIVISION HYSTOLOGIE-CYTOLOGIE: Ref.: 67740000, 4x5l
- Paraplast normal bulk: LABONORD SA: Ref.: 069-48-421, 4x5kg
- Sucrose minimum 99.5% RNase activity < 0.0005 Kunitz: SIGMA CHIMICAL : Ref.: S-9378, 1kg
- Cryomatrix: THERMO ELECTRON DIVISION HISTOLOGY-CYTOLOGIE: Ref.: S6769006, 4x120ml
- Histomold : LEICA MICROSYSTEMES SA: Ref.: 14702218313 for 13x19mm, Ref.: 14702218311 for 6x8mm, /10
- Slides Superfrost Plus 25x75x1mm: VWR INTERNATIONAL SAS: Ref.: 631-9483, /72

- Assembled the components of the reaction at room temperature to avoid the precipitation of the DNA template by placing Spermidine in the Transcription Buffer.

- Mix.

Reaction.

16 μ l	Buffer A
1 μ g	linearized template DNA (use 0.5 μ g DNA if PCR product)
1 μ l	RNA Polymerase T3, T7 or SP6 20 u/ μ l
Up to 20 μ l (2 μ l sterile milliQ H ₂ O if 1 μ l of DNA).	

- Mix and centrifuge briefly.
- Incubate 2 h at 37°C for T3 and T7, at 40°C for SP6.

Analysis of labelled RNA.

Estimate quantity and quality of transcript by a 1% agarose gel in TAE Electrophoresis Buffer [1x] (1 μ l of the transcription reaction and 1 μ l at the end of the purification).

Purification.

1. Stop reaction by adding 2 μ l EDTA 0.2 M, pH 8.0
2. Add a carrier 1 μ l tRNA 10 mg/ml
3. Precipitate RNA with 2.5 μ l Lithium Chloride (LiCl) 4 M (do not use Ammonium Acetate) 75 μ l cold Ethanol 100%
4. Mix well.
5. Incubate the mixture at -80°C for 15 min (not more) or at -20°C for 30 min (do not store probe over-night at this stage).
6. Centrifuge 30 min at 14,000 rpm at 4°C.
7. Remove the supernatant carefully.
8. Re-suspend the pellet in 22 μ l H₂O milliQ sterile
9. Re-precipitate RNA with 2.5 μ l LiCl 4 M + 75 μ l cold Ethanol 100%
10. Mix.
11. Put at -80°C for 15 min (not more) or at -20°C for 30 min (you can stop here and store it at -20°C).
12. Centrifuge 30 min at 14,000 rpm at 4°C.
13. Remove the supernatant carefully.

14. Wash the pellet with 0.5 ml cold Ethanol 70% (diluted with sterile milliQ H₂O)
15. Centrifuge 15 min at 14,000 rpm at 4°C.
16. Remove the supernatant carefully.
17. Air dry.
18. Dissolve in 20 µl of H₂O milliQ sterile and take 1 µl to check the final quantity of a gel.

Storage

- Dissolve in 100 to 200 µl Hybridization Buffer according to the quantity of transcript.
- Store at -20°C.

The day of use, put the tube 5 min at 37°C and vortex briefly.

Whole-mount *in situ* hybridisation of mouse embryos.

Precautions should be taken to avoid the degradation of RNA probes and of cellular mRNA during all steps preceding the hybridisation reaction. Gloves should be regularly changed throughout experimentation. All supplies must be treated with RNase inactivation agents. Instruments (spatulas, dissection tools, magnetic stirrers etc.) and glassware must be washed clean and oven-baked for 4 hours at 200°C. Following hybridisation, the probe-mRNA duplexes are nuclease-resistant and it is not essential to work in RNase-free conditions.

General notes:

The procedure described herein is validated for E7.5-11.5 whole mouse embryos, fixed overnight in 4% paraformaldehyde in PBS. We have found storage in 4% PFA at 4°C maintains RNA over the course of months. Similarly storage in absolute ethanol at -20°C after steps of graded dehydration can be performed. Storage in methanol works equally well.

The formamide used for pre-hybridisation and hybridisation steps *must* be of 'molecular grade', while 'proanalysis' formamide is sufficient for post-hybridisation washes. Alternatively, deionise with proanalysis formamide for pre-hybridisation steps. Prepare by gently stirring Dowex XG8 resin beads (5 g/100 ml formamide) for 1 hour (at room temperature) followed by filtration through Whatman N°1 paper. Deionised formamide can be stored in aliquots at -20°C.

The permeabilisation step with proteinase K, prior to hybridisation is critical. The exact concentration and length of the incubation should be optimised for: (i) each developmental stage, and (ii) each new batch of proteinase K. Proteinase K (17 mg/ml) from Roche is found to be stable at 4°C and generates reproducible results. This enzyme is validated at the following concentrations: 2.5 µg/ml for 5 minutes with E8.5 embryos; 2.5 µg/ml for 10 minutes with E9.5 embryos; 5 µg/ml for 15 minutes for E10.5 embryos; and 10 µg/ml for 15 minutes for older embryos.

Optimisation:

The anti-DIG antibody is a polyclonal antibody, thus a step of pre-adsorption with embryo powder can be performed in order to prevent non-specific binding to

embryonic tissues and to reduce background. Pre-absorption may be helpful for large (E9.5 and older) embryos.

1. Embryo powder: Collect E12.5-14.5 mouse embryos and homogenise them in a small volume of cold PBS (2-3 ml), using a douncer.
2. Add 4 x the volume of acetone and mix.
3. Incubate on ice for 30 minutes.
4. Centrifuge at 10000 g for 10 minutes and discard the supernatant.
5. Wash the pellet with cold acetone.
6. Centrifuge at 10000 g for 10 minutes and discard the supernatant.
7. Spread the pellet and grind it to a fine powder using a blade on a filter paper to absorb the acetone.
8. Store the powder at 4°C.
9. Pre-adsorb antibody: Add 18 mg of the embryo powder to 2 ml of TBST and heat to 70°C for 30 minutes.
10. Cool on ice and add 30 µl of blocking solution and 9 µl of anti-DIG antibody.
11. Gently agitate at 4°C for 1 hour.
12. Centrifuge for 10 minutes at 4°C to pellet the embryo powder.
13. Recover the supernatant and dilute it in 13 ml of blocking solution. The antibody is ready to use.

Expected range of results:

According to the probe, the time required for staining can be highly variable ranging from 1 hour to between 12-24 hours. If staining does not appear within the day (3-4 hours), samples must be washed in NTMT and stored overnight at 4°C. On the following day, the staining reaction can be resumed with freshly made solutions. Staining can also efficiently be resumed after several days of storage in PBT.

Staining can be terminated when sufficiently stained, and washed with PBT, as embryos can be observed and photographed in PBT (can be stored for a few weeks in PBT at 4°C). An additional bleaching step with absolute ethanol can also be performed. This results in bleaching of non-labelled tissue (from pinkish to white) and a change of colour (purple to blue) for the signal. Overall, this increases the signal/background ratio. Embryos are then transferred into a mix of glycerol/PBT that allows conservation almost indefinitely at 4°C. Tissues are more translucent in

glycerol, and this can improve the observation of the signal and quality of the pictures (see Figure M1).

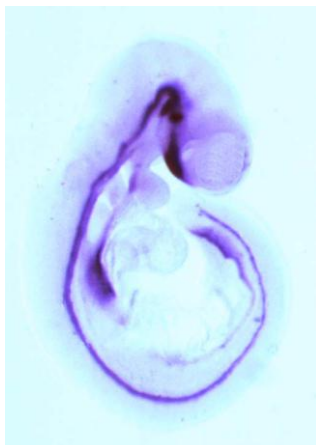


Figure M1 E9.5 mouse embryo hybridised with a *Sonic Hedgehog* RNA probe from <http://empress.har.mrc.ac.uk/>.

Quality Control:

Appropriate controls must always be included for an experimental group, to ensure both the sensitivity of detection and specificity of the signals. These should include positive controls to test for the quality of the tissue samples (mRNA preservation) and hybridisation procedure, as well as negative controls to assess for non-specific (background) and/or artificial labelling.

Positive controls should include sample(s) known to contain the mRNA of interest and/or, if the expression pattern of the gene studied is unknown, the use of additional probe(s) whose expression pattern has already been characterised in the tissue(s) studied.

Negative controls are samples devoid of the mRNA of interest (although one should be aware that background levels may vary according to the tissue). Sense probes are also commonly used to evaluate non-specific background labelling. Other valuable technical controls to evaluate the specificity of a signal are the omission of either the probe or the antibody, or the pre-treatment of sections with RNase A.

Supplies:

Pre-treatments and hybridisation:

- Tissue culture plates (24-well)
- Dulbecco's phosphate-buffered saline (PBS) (Sigma-Aldrich):

Prepare a 10X stock solution by diluting the powder with 1L of water, and autoclave. The stock solution is diluted to 1X in water before use.

- PBT: PBS 1X with 0.1% Tween 20
- Absolute ethanol and 25%, 50% and 75% dilutions in PBT
- Proteinase K: Stock solution at 17.7 mg/ml (Roche), diluted before use with PBT to 2.5, 5 or 10 µg/ml
- Glycine: Stock solution at 100 mg/ml, stored at -20°C. Dilute to 2 mg/ml in PBT before use.
- Paraformaldehyde (PFA): Prepare a stock 8% (w/v) solution in PBS 1X pre-warmed to 85-95°C under a safety hood. Cool using ice and store at -20°C. PFA stocks are thawed on the day of use, kept at 4% on ice and used within 24 hours.
- Glutaraldehyde 25% (Sigma), stored in aliquots at -20°C.
Post-fixation mix: 4% PFA, 0.2% glutaraldehyde in PBS 1X.
- Hydrogen peroxide (H₂O₂): Stock solution at 30%, stored at 4°C in dark. Dilute to 6% in PBT before use.
- Formamide: 'molecular grade' or deionised.
- SSC 20X (175.3 g NaCl, 88.2 g sodium citrate per 1L of water). Adjust to pH 5 and autoclave.
- SDS (electrophoresis grade) 20% (w/v) in water. Adjust pH to 7.2. Do not autoclave.
- tRNA from baker's yeast, 10 mg/ml (Sigma), stored at -20°C.
- Heparin, sodium salt (Grade I-A, from Porcine intestinal mucosa, Sigma), stock solution at 100mg/ml, stored at -20°C.
- Pre-hybridisation mix: 50% formamide, 5X SSC, 50 µg/ml tRNA, 1% SDS, 50 µg/ml heparin. Prepare on the day of use.
- DIG-labelled probe stock solution.

Post-hybridisation washes and immunocytochemistry:

- Formamide: molecular biology grade.
- Washing solution 1: 50% formamide, 5X SSC, 1% SDS. Prepare on the day of use.
- Washing solution 2: 50% formamide, 2X SSC. Prepare on the day of use.
- RNase buffer (0.5 M NaCl, 10 mM Tris-HCl pH 7.5, 0.1% Tween 20 in water).

-RNase A: Stock solution at 100 mg/ml in 10 mM Tris-HCl pH 7.5, 15 mM NaCl, stored at -20°C in aliquots.

-TBST 10X stock solution: 1.5 M NaCl, 1 M Tris-HCl pH 7.5, 1% Tween 20 in water. Autoclave and store at room temperature. Dilute to 1X with water the day of use.

-Blocking solution: Blocking reagent for nucleic acid hybridisation (Roche), diluted to 1.5% (w/v) in TBST.

-Anti-DIG antibody, alkaline phosphatase conjugated, Fab fragment (Roche). Store at 4°C. Dilute to 1/1000 in blocking solution just before use.

Staining reaction and bleaching:

-TBST 1X

-NTMT: 0.1 M NaCl, 0.1 M Tris-HCl pH 9.5, 50 mM MgCl₂, 0.1% Tween 20 in water. This solution is unstable and must be prepared the day of use.

-BCIP: 5-bromo-4-chloro-3-indolyl-phosphate (Roche). Stock solution of 50 mg/ml in 100% dimethylformamide, stored in dark at -20°C.

-NBT: Nitroblue tetrazolium chloride (Roche). Stock solution of 75 mg/ml in 70% dimethylformamide, stored in dark at -20°C.

-Staining solution: NTMT with 3.5 µl/ml BCIP and 3.5 µl/ml NBT
PBT

-Absolute ethanol and 25%, 50% and 75% dilutions in PBT

-Glycerol 50% in PBT

Protocol:

Pre-treatments and hybridisation:

1. Rehydrate the embryos on ice, in a graded series of ethanol diluted in PBT (75%, 50%, and 25%) for 5-10 minutes each.
2. Wash with PBT 3 x 5 for minutes, working on ice.
3. Open the cavities (amniotic cavity, yolk sac, brain ventricles, and heart) under a stereomicroscope by piercing with a needle or Dumont forceps, and transfer the embryos into the 24-well tissue culture plates.
4. Permeabilise the samples by treatment with proteinase K (2.5-10 µg/ml), for 5-10 minutes on ice.
5. Incubate in glycine (2 mg/ml) on ice for 5 minutes to cease digestion.

6. Wash with PBT 3 x for 5 minutes, working on ice.
7. Post-fix the samples in the post fixation mix (containing 4% PFA and 0.2% glutaraldehyde in PBS 1X) for 20 minutes on ice.
8. Wash with PBT 2 x for 5 minutes at room temperature.
9. Incubate in pre-warmed PBT for 30 minutes at 70°C.
10. Bleach with 6% H₂O₂ in PBT for 1 hour at room temperature.
11. Wash with PBT 3 x for 5 minutes at room temperature.
12. Incubate with pre-hybridisation buffer in the hybridisation oven set at 70°C and gentle agitation, for a minimum of 1 hour.
13. Replace the pre-hybridisation buffer with the solution containing the RNA probe, and incubate at 70°C overnight, with gentle agitation. Empirically test the optimal probe concentration, which should usually vary between 500-1000 ng/ml.

a. Post-hybridisation washes and immunocytochemistry:

- a.1 Wash the samples in pre-warmed *washing solution 1*, 3 x for 30 minutes at 70°C and gentle agitation.
- a.2 Wash in a (1:1) mix of *washing solution 1* or RNase buffer for 10 minutes at room temperature.
- a.3 Wash in RNase buffer for 10 minutes at room temperature.
- a.4 Incubate in RNase buffer containing 100 µg/ml RNase A for 1 hour at 37°C.
- a.5 Wash with RNase buffer for 10 minutes at room temperature.
- a.6 Wash with *washing solution 2*, 3 x for 30 minutes at 65°C, with gentle agitation.
- a.7 Wash with TBST, 3 x for 5 minutes at room temperature.
- a.8 Incubate in blocking solution, for a minimum of 1 hour at room temperature.
- a.9 Incubate overnight at 4°C in anti-DIG-AP-conjugated antibody.

b. Staining and bleaching:

- b.1 Wash with TBST 3 x for 5 minutes.
- b.2 Wash with TBST 5 x for 1 hour.
- b.3 Wash with NTMT 3 x for 10 minutes.
- b.4 Incubate in the staining solution with gentle agitation, protecting from light. Assess the colour reaction regularly.

b.5 Wash with NTMT 3 x for 10 minutes.

b.6 Wash with PBT for 10 minutes.

b.7 Dehydrate in a graded series of ethanol diluted in PBT (25%, 50%, 75%), for 5-10 minutes each.

b.8 Bleach in absolute ethanol for 1 hour.

b.9 Dehydrate in a graded series of ethanol diluted in PBT for 5-10 minutes each.

b.10 Wash with PBT for 10 minutes.

- Wash with 25% glycerol in PBT for 5-10 minutes.

- Store at 4°C in 50% glycerol diluted with PBT.

Automated whole-mount *in situ* hybridisation of mouse embryos.

Instrument maintenance:

- The cleaning, dismantling, maintenance, adjustment and repair of the automated instrument *InsituPro* should only be performed by trained personnel.
- The aspiration needle, columns and outlet needles must be regularly inspected and replaced when necessary.
- Service staff from Intavis should perform maintenance and calibration.

7.0 Equipment:

InsituPro instrument (Intavis AG, Bioanalytical instruments) see Figure M2

Software '*InsituPro* WIN editor' for method development.

Water bath or heating plate

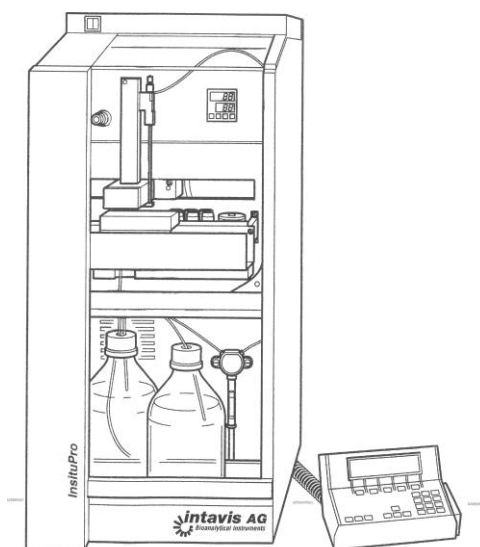


Figure M2 Schematic representation of the *InsituPro* instrument.

Supplies:

For a full run:

1. Medium sized columns, with sealing caps and outlet needles (x 30)
2. Yellow stopper caps (x 30)
3. Probe tubes (x 30)
4. Tubes and bottles for buffers and reagents
5. Tissue culture plates (24-well)

Solutions in accordance to the position in the solvent rack (see Figure M3):

- A** PBT: PBS with 0.1% Tween 20
- B** Methanol 50% in PBT
- K** Hydrogen peroxide 6% in PBT
- G** Proteinase K, 5 µg/ml in PBT
- I** Glycine 2 mg/ml in PBT
- H** Paraformaldehyde 4% with Glutaraldehyde 0.2% in PBT
- C** Hybridisation buffer
- D** Washing solution 1
- E** RNase buffer
- J** RNase A 100 µg/ml in RNase buffer
- F** Washing solution 2
- A2** TBST
- L** Blocking reagent at 1% (w/v) in TBST
- M** Anti-DIG antibody, alkaline phosphatase conjugated, and Fab fragment (Roche), diluted 1:1000 in blocking reagent.
- F2** NTMT

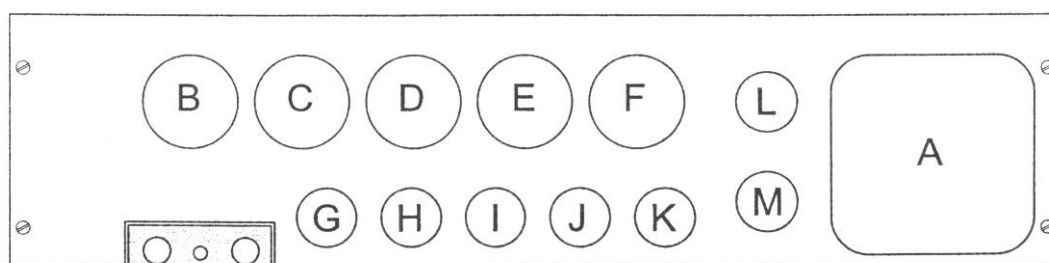


Figure M3 Solvent rack, top view.

1. Dulbecco's phosphate-buffered saline (PBS) (Sigma-Aldrich, D-5652-10L): Prepare a 10X stock solution by diluting the powder with 1 L of water, and autoclave. The stock solution should be diluted to 1X in water immediately before use.
2. Proteinase K, stock solution at 17.7 mg/ml (Roche),
Dilute to 5 µg/ml in PBT
3. Glycine, stock solution at 10 mg/ml
Dilute to 2mg/ml in PBT

4. Paraformaldehyde:

Prepare a 20 % (w/v) stock solution in PBS 1X pre-warmed at 65°C. Use a magnetic stirrer for complete dissolution. Cool on ice and store at -20°C. Warm to 65°C and dilute with PBS to 4% on the day of use. Keep 4% PFA on ice, use within 24 hours.

5. Paraformaldehyde 4% with Glutaraldehyde 0.2% in PBT:

Mix 80 µl of 25% glutaraldehyde stock solution with 10 ml of paraformaldehyde 4% in PBT.

6. SSC 20X stock solution:

Dissolve 175.3 g NaCl, 88.2 g sodium citrate for 1 L water. Adjust to pH 5 and autoclave.

7. SDS 20% stock solution:

Dissolve 100g electrophoresis-grade sodium dodecyl sulfate for 500 ml water. Adjust pH to 7.2. **Do not autoclave.*

8. tRNA from baker's yeast, 10 mg/ml (Sigma, R-8759), stored at -20°C

9. Heparin (sodium salt (Grade I-A) from Porcine intestinal mucosa, (Sigma).

10. Hybridisation Buffer:

Solution of formamide 50% (molecular grade or deionised – see 5.3), 5X SSC, 10 µg/ml tRNA, 1% SDS, 50 µg/ml heparin. Aliquot and store at -20°C. Pre-warm for 30 minutes to 65°C on the day of use.

11. Washing solution 1: 50% formamide (proanalysis), 5X SSC, and 1% SDS in water. Prepare the day of use.

12. RNase buffer: NaCl 0.5M, Tris-HCl 10 mM pH 7.5, 0.1% Tween 20 in water.

13. RNase A, stock solution.

14. Washing solution 2: 50% formamide (pro-analysis), 2X SSC in water

15. TBST:

Solution of 0.14 M NaCl, 2.7 mM KCl, 25 mM Tris-HCl pH 7.5, 0.1% Tween 20 in water. A 10X concentrated solution can be prepared and stored at room temperature once autoclaved.

16. Blocking reagent for nucleic acid hybridisation (Roche). Prepare a stock solution at 10% in MAB (Maleic acid 0.1M, NaCl 0.15M, pH 7.5) and keep at -20°C

17. Anti-DIG antibody, alkaline phosphatase conjugated, and Fab fragment (Roche)

18. NTMT:

Solution of 0.1 M NaCl, 0.1 M Tris-HCl pH 9.5, 50 mM MgCl₂, 0.1% Tween 20 in water. This solution is unstable and should be prepared on the day of use.

Staining solutions:

- BCIP: 5 – bromo – 4 – chloro – 3 - indolyl-phosphate (Roche). Stock solution containing 50 mg/ml in 100% dimethylformamide, stored in the dark at -20°C.
- NBT: Nitroblue tetrazolium chloride (Roche). Stock solution containing 75 mg/ml in 70% dimethylformamide, stored in the dark at -20°C.
- Staining solution: NTMT with 3.5 µl/ml of BCIP and 3.5 µl/ml of NBT
- PBT
- Absolute ethanol and 25%, 50% and 75% dilutions in PBT
- Glycerol 50% in PBT

Other solutions:

- Dilution reservoir: sterile milliQ water
- DIG-labelled probe stock solution

Procedure:**1. Writing the method:**

Note: *The procedure described below is an adaptation of a template provided by the manufacturer (Stand4.xcp) and stored under the name of 'mouse.xcp' on a floppy disk (available upon request). To view and modify this method you will need a computer equipped with the software 'InsituPro WIN editor'*

1.1 Open the experimental file and adapt it with respect to the following:

- The number of samples in the experimental session.
- The proteinase K treatment. Duration for permeabilisation with proteinase K may vary between different sub-zones (sub_A, sub_B, sub_C, sub_D and sub_E – see Figure M4). While proteinase K remains at a concentration of 5 µg/ml define the incubation time for each individual sub-zone according to the developmental stage of the embryos. Incubation times should vary between 2 and 15 minutes:

2 minutes for E8.5 embryos

5 minutes for E9.5 embryos

10 minutes for E10.5 embryos

15 inutes for older embryos

- Group embryos of a given developmental stage in the same sub-zone(s).
Alter steps 15, 18, 21, 24 and 27 accordingly of the automated procedure.

1.2 Save the customized method onto a floppy disk as a method file (*.xcp) that can now be read by the instrument.

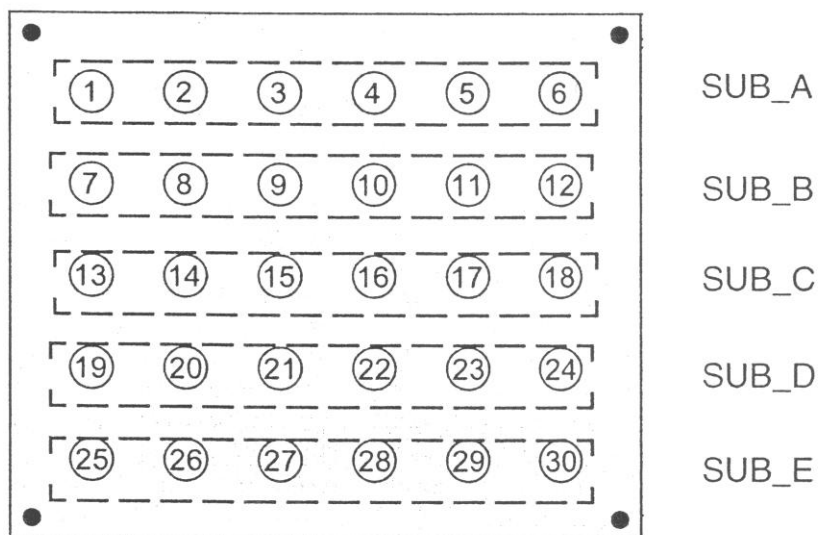


Figure M4 Identification of sub-zones in the work area.

2. Preparation and loading of the samples:

2.1 Assemble the columns with the yellow stopper and place them on a tube rack.

Label the columns according to their position on the work area (e.g. A1, A2, B1, B2 etc.).

2.2 Load the embryos into the columns using a plastic holding pipette (a 3.5 ml transfer pipette). The embryos are in 200 µl of 100% methanol.

2.3 Mount the sealing caps without closing the centre hole to allow air escape through it.

2.4 Loading the columns within the instrument:

- Close the hole in the sealing cap using a finger (to prevent air escape and leakage of methanol from the bottom).
- Remove the yellow stopper and replace with an outlet needle.
- Position the column at the correct position within the sample rack area.
- Finally release your finger from the cap.

- Check that methanol is not leaking from the column. Adjust the needle firmly if necessary or replace it with a new one.

3. Preparation and loading of probes:

- 3.1 Prepare the probe tubes (one tube for each column). Label the tubes according to the position of the work area and to the probe.
- 3.2 Pre-warm the hybridisation buffer for 30 minutes at 70°C.
- 3.3 Add 400 µl of the hybridisation buffer to each tube.
- 3.4 Dilute the probe in the hybridisation buffer. Empirically test the optimal probe concentration, which should usually vary between 500-1000 ng/ml.
- 3.5 Place the tubes on the probe rack and load the probe rack in the instrument.

4. *In situ*Pro Measurement:

- 4.1 Insert the floppy disk with the customised method into the disk drive.
- 4.2 Switch on the *In situ*Pro instrument and follow the instructions to begin automated *in situ* hybridisation of digoxigenin-labelled riboprobes.
- 4.3 The instrument will perform a series of washes and undergo the necessary incubation periods for *in situ* hybridisation automatically.

5. Staining and bleaching:

- 5.1 Following the experimental session, the samples remain in the NTMT buffer. Take the columns out of the sample rack, and recover the samples from the columns.
- 5.2 Transfer the samples using a plastic holding pipette into a 24-well tissue culture plate(s) for the colour reaction.
- 5.3 Incubate in the staining solution with gentle agitation, protecting from light. Assess the colour reaction regularly.
- 5.4 When the staining reaction is finished, wash in PBT for 10 minutes at room temperature.
- 5.5 Dehydrate samples in a graded series of ethanol in PBT (25%, 50%, 75%), for 5-10 minutes each.
- 5.6 Bleach in absolute ethanol for 1 hour at room temperature with gentle agitation. Embryos may be stored in ethanol at 4°C until documentation of expression patterns or proceed to 9.5.10.
- 5.7 Rehydrate in a graded series of ethanol in PBT for 5-10 minutes each.

5.8 Wash in PBT for 10 minutes at room temperature.

5.9 Wash with 25% glycerol in PBT for 5-10 minutes at room temperature.

5.10 Store at 4°C in 50% glycerol in PBT.

Solutions for Hybridization in situ with Digoxigenin RNA Probes on Section.

Proteinase K (prot K):

Stock solution Proteinase K 20 mg/ml in sterile milliQ water, aliquot in 100 µl and store at -20°C.

Stock Proteinase K Buffer [10x]:

	Stock solution	For 1 l
Tris-HCl 0.5 M pH 8.0	1 M	500 ml
EDTA 50 mM pH 8.0	0.5 M	100 ml
milliQ water		to 1 l

Autoclave, store at 4°C.

Proteinase K Buffer is used [1x]: 10 ml sterile Proteinase K Buffer [10x]

for 90 ml sterile milliQ water.

Triethanolamine (TEA):

	Stock solution	For 200 ml	For 1l
Triethanolamine 0,1 M	3.75 M	5.33 ml	26.66 ml
add HCl to pH 8.0	37%	333.33 µl	1666.66 µl
Anhydride Acetic 1/400		0.5 ml	2.5 ml
Sterile milliQ water		194 ml	969.2 ml

Prepare the solution the day of use but add the Anhydride Acetic just before the slides.

Triethanolamine 7.5 M is viscous that's the reason we dilute it half in sterile milliQ water.

Phosphate Buffer Saline (PBS) [10x]:

Dissolve the powder PBS perused for 10 l of PBS [1x] in 1 l of milliQ water, autoclave and store at 4°C.

PBS is used [1x]: 100 ml sterile PBS 10x for 900 ml sterile milliQ water.

Paraformaldehyde:

Stock solution Paraformaldehyde 4% (w/v) in sterile PBS [1x]:

Weigh PFA under hood, add sterile PBS [1x], heat at nearly 60°C until it dissolves but do not boil. Let cool on ice, store at -20°C in aliquots ready to use.

Stock solution Paraformaldehyde 20% (w/v) in sterile PBS [1x]:

Weigh PFA under hood, add sterile PBS [1x], heat at nearly 40°C until it dissolves but do not boil. Let cool on ice, aliquot in 10 or 35 ml and store at -20°C.

PFA is used at 4%: 10 ml PFA 20% for 40 ml sterile PBS [1x].

35 ml PFA 20% for 140 ml sterile PBS [1x].

Stock solution Paraformaldehyde 16% in Di distilled Water from Electron Microscopy Sciences:

(10ml ampoule sealed under inert gas diluted Cat. #15710)

PFA is used at 4%: 10 ml PFA 16% for 4 ml sterile PBS [10x] and 26 ml sterile water.

Hybridization Buffer:

Salt 10x:

	For 1 l	
NaCl	114 g	(1.95 M)
Tris-HCl	14.04 g	(Tris 0.1 M pH 7.2)
Tris-Base	1.34 g	
NaH ₂ PO ₄ , 2H ₂ O	7.8 g	(NaH ₂ PO ₄ , 1H ₂ O: 6.9 g) 0.05M
Na ₂ HPO ₄	7.1 g	(Na ₂ HPO ₄ , 12H ₂ O: 17.9 g) 0.05M
EDTA 0.5 M pH 8.0	100 ml	(0.05 M)
Sterile milliQ water	to 1 l	

Autoclave and store at 4°C.

Dextran Sulphate 50% (w/v):

Weigh directly in a sterile bottle 50 g of the powder; adjust to a final volume of 100 ml with sterile milliQ water. Put under agitation at 60°C and let it over-night until dissolution. Aliquot in 50 ml and store at -20°C.

t RNA 10 mg/ml:

Stock solution t RNA (Yeast or Wheat Germ) 10 mg/ml in sterile milliQ water.

Check purity 260/280nm=2. Aliquot in 10 ml and store at -20°C.

Denhardt's Solution[50x]:

Ficoll 400	5 g
Polyvinylpyrrolidone	5 g
Bovine Serum Albumin, Pentax fraction 5 (BSA)	5 g
Sterile milliQ water	to 500 ml

Filter through a 0.22 µm filter. Aliquot in 5 ml and store at -20°C.

Hybridization Buffer:

	Dilution	Stock solution	For 50 ml
Sterile milliQ water			4 ml
Salt [1x]	10x	[10 x]	5 ml
Dextran Sulphate 10%	5x	50%	10 ml
t RNA 1 mg/ml	10x	10 mg/ml	5 ml
Denhardt's [1x]	50x	[50x]	1 ml
Deionized Formamide 50%	2x	100%	25 ml

Aliquot in 50 ml and store at -20°C.

Washing Probe Solution:**Saline Sodium Citrate (SSC) 20x:**

	PM	For 2 l
NaCl 3M	58.44 g	350.64 g
Na Citrate 0.3M	294.1 g	176.46 g
milliQ water		to 2 l

We do not adjust the pH. Autoclave and store at room temperature.

Tween-20 (T) 10% (v/v):

Stock solution Tween-20; 10% (v/v) in milliQ water. Aliquot in 50 ml, autoclave, protect from light and store at 4°C.

Washing Probe Solution with Formamide:

	Dilution	Stock solution	For 1 l	For 800 ml
Formamide 50%	2x	100%	500 ml	400 ml
SSC [1x]	20x	[20x]	50 ml	40 ml
Tween-20 0,1%	100x	10%	10 ml	8 ml
milliQ water			to 1 l	to 800 ml

Washing Probe Solutions without Formamide:

	Dilution	Stock solution	For 1 l	For 800 ml
SSC 5x	4x	20x	250 ml	200 ml
SSC 0,2x	100x	20x	10 ml	8 ml

Washing Antibody Solution: Maleic Acid Buffer Tween (MABT) [1x]:

Sodium Hydroxide (NaOH) 10 N:

The preparation of 10 N NaOH (PM 40,0 g) involves a highly exothermic reaction, which can cause breakage of glass containers. Prepare this solution with extreme care in 2 liters plastic beakers. To 800 ml of sterile milliQ water, slowly add 400 g of

NaOH pellets, stir. When the pellets have dissolved completely, adjust the volume to 1 l. Storage at room temperature, sterilization is not necessary.

Maleic Acid Buffer (MAB) [5x]:

	Stock solution	For 2 l
Maleic Acid 0,5 M	PM 116,1 g	116. 1 g
add NaOH to pH 7,5 (20°C)	10 N	160 to 200 ml
NaCl 0,75 M	PM 58,44 g	87.66 g
milliQ water		to 2 l

Adjust the pH with a pH meter, be careful adding NaOH, first you'll observe a precipitation until pH6.0 that will disappear and then the pH will change very rapidly at 7.0. Check the final pH when the solution is at 20°C.

Only after adjusting the pH, add NaCl and complete with milliQ water.

Do not autoclave but filter through a 0.2 µm filter to avoid a flocculate precipitate.

Washing Antibody Solution: Maleic Acid Buffer Tween (MABT) [1x]:

	Dilution	Stock solution	For 2 l
MAB [1x]	5x	[5x]	400 ml
Tween-20 0.1%	100x	10%	20 ml
milliQ water			to 2 l

Blocking Solution:

Blocking Reagent (BR) 10% (w/v) in MAB:

Blocking Reagent is dissolved in Maleic Acid Buffer (without Tween) to a final concentration of 10% (w/v) with shaking and eating on a heating block. This stock solution is autoclaved at 0.5 atm, aliquoted in 10 ml and stored at -20°C.

Heat inactivated Normal Goat Serum (NGS):

Normal Goat Serum is defreezed on ice and heated during 30 min at 56°C in a water bath. Let cool on ice, aliquot in 10 ml and store at -20°C. The purpose of this is to denature any remaining immunoglobulins in the serum.

Blocking Solution:

	Dilution	Stock solution	For 10 ml	
MAB [0.8x]	6,25x	[5x]	1.6 ml	(6.25x dilution
BR 2%	5x	10%	2 ml	because MAB
in MAB [0.2x]		[1x]		in BR)
NGS 20%	5x	100%	2 ml	
Tween-20 0.1%	100x	10%	0.1 ml	
milliQ water			4.3 ml	

Alkaline Phosphatase Buffer (NTMT) [1x]:**Sodium Chloride (NaCl) 5 M:**

	PM	For 1 l	For 2 l
NaCl 5 M	58.44 g	292.2 g	584.4 g
milliQ water		to 1 l	to 2 l

Autoclave and store at room temperature.

Tris 1M pH 9,5:

	Stock solution	For 1 l	For 2 l
Tris-Base 1 M	PM 121.1 g	121.1 g	242.2 g
add HCl to pH 9.5	37%	~ 4.5 ml	~ 8.5 to 20 ml
milliQ water		to 1 l	to 2 l

Adjust the pH with a pHmeter. Aliquot in 100 ml, autoclave and store at 4°C.

Magnesium Chloride (MgCl₂, 6H₂O) 1 M:

	PM	For 1 l
MgCl ₂ , 6H ₂ O 1 M	203,3 g	203,3 g
milliQ water		to 1 l

Aliquot in 100 ml, autoclave and store at 4°C.

Alkaline Phosphatase Buffer (NTMT) [1x]:

	Dilution	Stock solution	For 1 l	For 200 ml	For 800 ml
NaCl 100 mM	50x	5 M	20 ml	4 ml	16 ml
Tris 100 mM pH 9,5	10x	1 M	100 ml	20 ml	80 ml
MgCl ₂ , 6H ₂ O 50 mM	20x	1 M	50 ml	10 ml	40 ml
Tween-20 0,1%	100x	10%	10 ml	2 ml	8 ml
milliQ water			to 1 l	to 200 ml	to 800 ml

Make freshly from stocks on the day of use, since otherwise the pH can change due to the absorption of CO₂.

Alkaline Phosphatase Staining Buffer:

	Stock solution	For 1 ml
NTMT [1x]		1 ml
NBT 0.35 mg/ml	100 mg/ml	3.5 µl
BCIP 0.175 mg/ml	50 mg/ml	3.5 µl
Levamisole 5 mM (4 drops / 5 ml)	125 mM	40 µl

Make with fresh NTMT. Mix after adding each product. Protect from light.

In some cases a precipitate may occur in NBT stock solution which is easily brought into solution by briefly warming the substrate at 37°C before using it.

Micro-CT imaging

Principle: X-ray microtomography (μ CT) uses X-rays to create cross-sections of a physical object that can be used to re-create a 3D virtual model noninvasively.

Quantum FX μ CT System Components

The Quantum FX μ CT is a CT imaging system that consists of a moveable sample holder surrounded by a rotating gantry (Figure M5). The gantry has an X-ray source and a flat panel detector mounted on it. The detector and slide can be moved radially to change the magnification. Two bore sizes are available depending on the magnification chosen: 70 or 200 mm.

Quantum FX micro-CT Technical Specifications

Maximum Energy	90kV with 0.2 mA
Focal spot	5 μ m - 30 μ m
High resolution X-ray detector	127 μ m pixel 14 bit X-ray
	flat panel detector
X-ray detector type	Amorphous Silicon
Detector Speed	Up to 30 fps
Bore size	193 mm ϕ (standard) 113 mm ϕ (medium), or 65 mm ϕ (High resolution)
Longitudinal travel	200 mm
Field of view	10 mm ϕ to 73 mm ϕ (120 mmj axially with image stitching)
Pixel size	10 μ m - 295 μ m
Standard scan time	Standard: 17 seconds, 26 seconds Fine: 2 min, 3 min, 4.5 min
Dimensions	Height 1,450 mm
	Width 980 mm
	Depth 930 mm
	Weight 470 kg




Figure M5 PerkinElmer's Quantum FX microCT Pre-clinical In Vivo Imaging System, Caliper, Life Sciences.


After dissection, samples were fixed in a 4% paraformaldehyde solution (PFA) for 10-14 days. These samples were then washed in demineralised water several times to remove all traces of fixative (because PFA is a neurotoxic crosslinking agent). After each scan, samples can be used for other procedures such as histology, scanning electron microscopy (SEM), or in-situ hybridization (ISH).

To operate Quantum FX system μ CT:

Open the computer of Quantum FX system control software μ CT: Identifier: "CT admin" and password: "ct2admin". The machine door needs to be in a proper closed position before opening the program. The micro-CT key then opens the machine.

When the program is running, the control panel and the dialog box will appear as Figure M6. Warm up is required before performing the scan. Click on the warm up

button  to start so the machine will generate x-ray about 15 minutes. Every time before the machine performs an x-ray, it will ask for your permission for the safety reason. After warming up is completed, the "Stand by" will appear and the "Live

mode” button  will appear on the control panel instead of warm-up button (Figure M6).

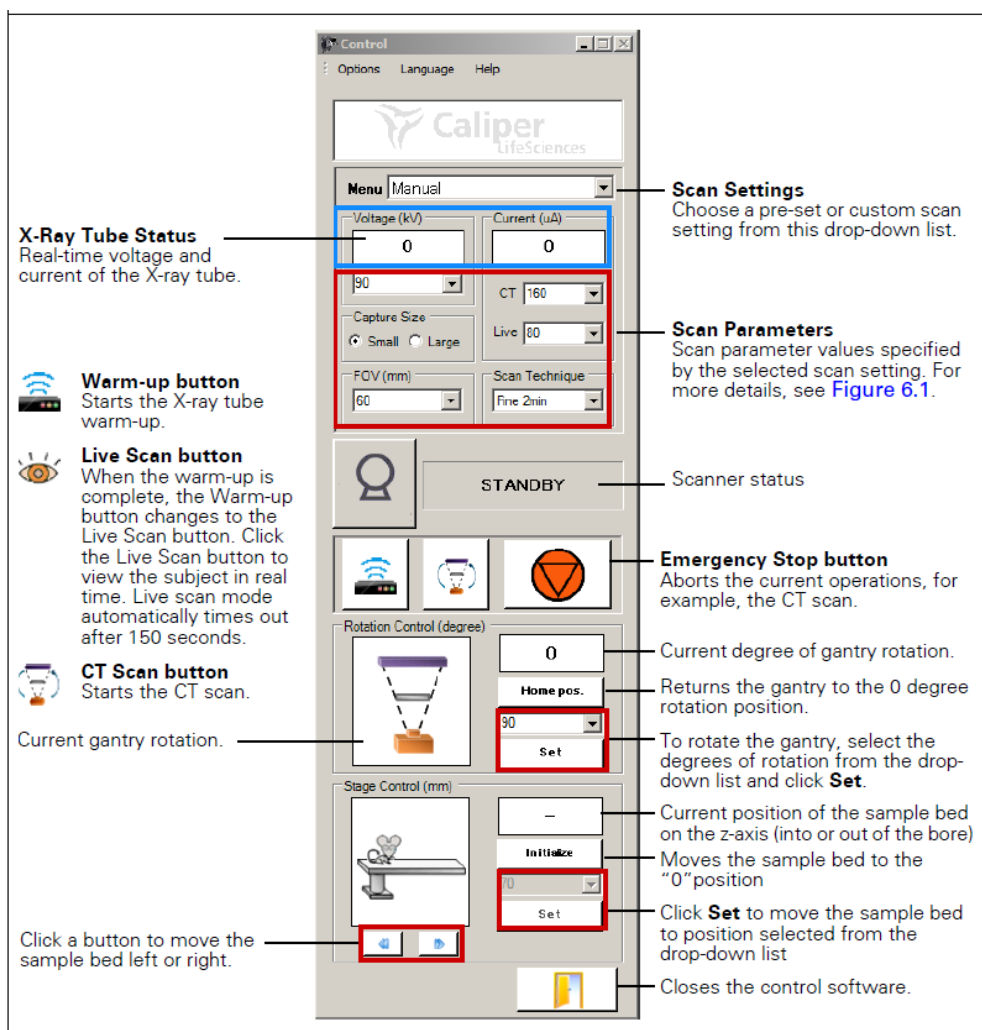


Figure M6 The control panel of the Quantum FX microCT machine from https://www.perkinelmer.com/Content/LST_Software_Downloads/9092.pdf.

To create or select a database:

Defining where the images (series) are to be saved, use the create or select database function. Then, creating the sample and describing any information such as name, gender, date of birth, age, type, and number.

To adjust the acquisition conditions:

This system allows the user to adjust the voltage and the amperage. The recommend threshold to scan bone and tooth is 90 kV and 160 µA with “Fine” scan technique.

To perform a scan:

Open the door of the Quantum FX μ CT and remove the sample table. Place the subject in the sample chamber, on the bed. Each head is placed in the actual position so that each tooth is in its well-arranged position. For the acquisitions to be standardized, we placed the samples in the same manner. First, the head of the mouse is placed muzzle forward, taking care to place the teeth around a wooden bit. The holder is oriented in its usual place (indicated by the more worn/dirty area of the platform). A transparent plastic bag was placed surrounded the bed and the samples to reduce contamination of the machine and sample. Then push the sample table into the rail and close the door, so that the locking system is engaged.

Center the subject in the capture window X:

Turn on the "Live Mode". In the capture window X, we chose a field of view of 20 mm. The subject appears in real time to be able to center the image. Use the axis control by pressing the "Fast" button and the right or left arrow to mobilize the sample. Check the position in the capture window. Orient at 90 ° in the frontal and sagittal plan, correctly centering the molars and incisors.

Start scanning CT: press "Start". Note the entry number (ex: no. 145338). After the complete acquisition, double-click on the series to automatically visualize the 3D image. Allow 2-3 minutes for scanning and 2 minutes for rebuilding

In order to standardize the acquisitions and make a comparable image analysis, the scanning technique was strictly the same for each sample, side by side, namely: overall view with whole head, molars and upper incisors straight, molars and lower right incisors, Upper molars and incisors left, molars and incisors lower left, head of the femur, knee, head of the tibia and whole leg.

Export the images to the file in DICOM format

Bone fenestration removes the surrounding soft tissue. Repeat the scans as many times as there are samples to be analyzed.

To further analysis data obtained from micro-CT machine, please refer to **Analyze11.0 instructions listed below.**

Analyze11.0 instructions for bone and tooth analysis

Analysis of micro-CT data using AnalyzeDirect program:

Analysis of 3D reconstructions.

Open file: Open the file concerned in DICOM format in the "Caliper Analyze" program. A window opens: "Caliper microCT Analysis Tools by Analysis". In the working window, create a new tab by clicking "new" or select the file already created.

The data acquisition heads of mutant and corresponding age/sex- matched WT controls were analyzed importing files in the following order:

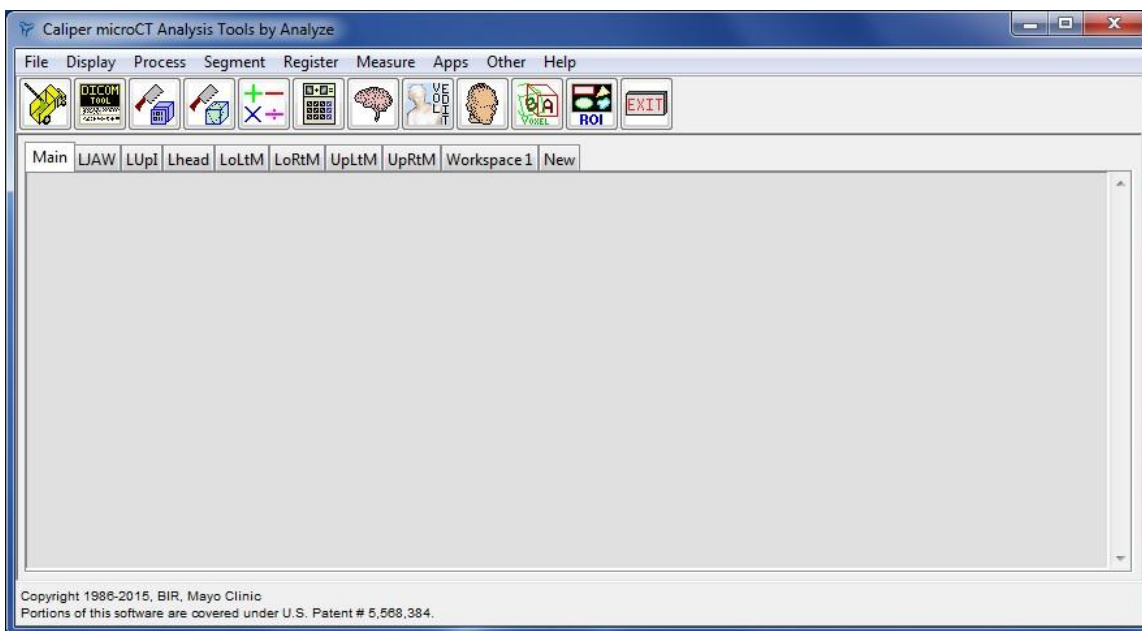
- Total head scan
- Upper molar –right side
- Lower molar-right side
- Upper molar- left side
- Lower molar- left side

DICOM tool

Files are exported in DICOM format and named as Month-day-year with the operation time. For formatting DICOM databases see <https://youtu.be/R35MLj8QIOI> for information on how to upload files.

Typically image data is loaded into Analyze using one of the load modules (Load, Load As, DICOM Tool, or Import/Export) from the 'File' menu. In our procedure, we use DICOM data because this file is normally used in the clinic and Analyze11.0 has a specific function for this format.

In the main Analyze window, each u-CT scan has 512 images in each DICOM folder. The default import to workspace is to open files in Drive C of the PC. Right-click to open the work space directory D/temp/___ where files are stored in drive D.



Import all micro-CT data needed for the analysis by using the DICOM button. Firstly, create a new DICOM Tool by =>File create database=>save in Drive D

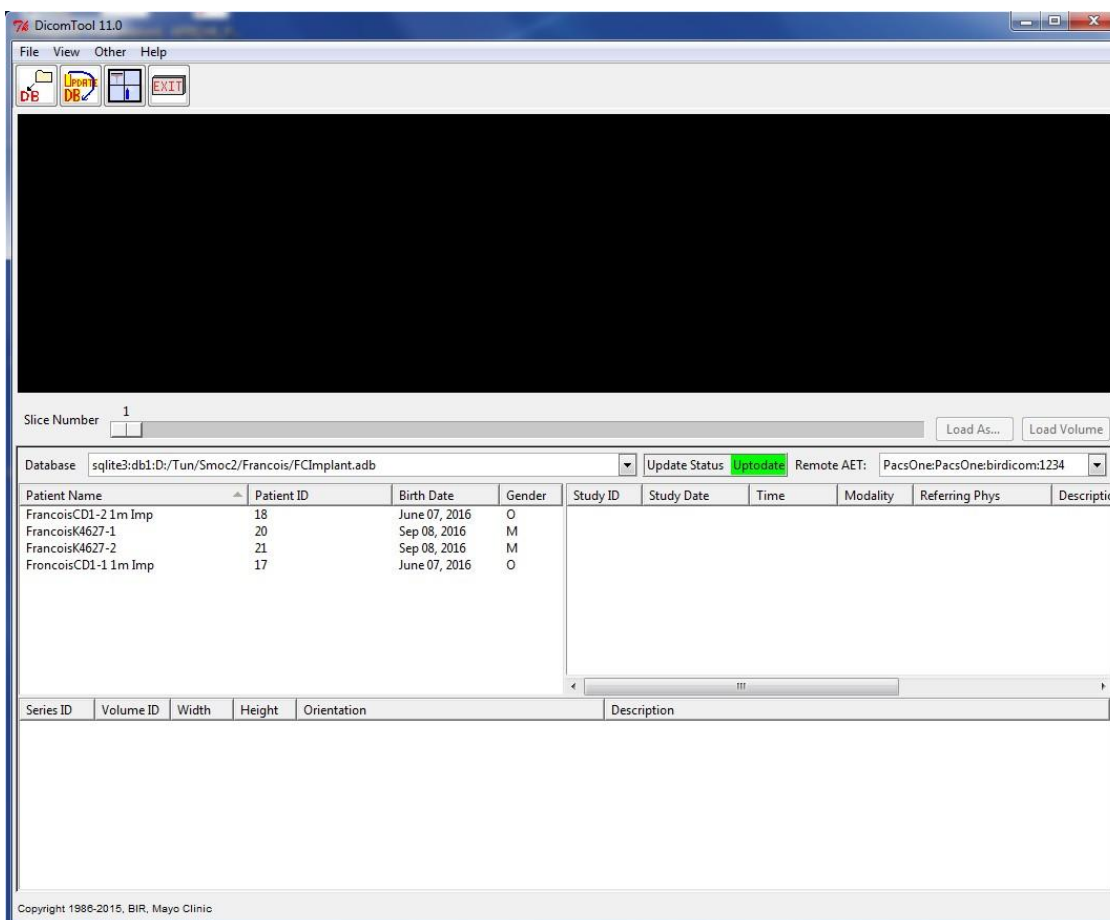


Image Database

Local Database Name: PC1-1029-A_5679

Local Database Directory: [Empty]

Dicom Receiver

Configure DICOM Receiver:

Dicom Receiver AET: PC1-1029-A_5679

Dicom Receiver Port: 5679

DCMTK path: C:/BIR/DCMTK-3.5.4/PC_NT64/bin

Database Server

Configure Database Server:

Service Name: PC1-1029-A_5680

Host System: PC1-1029-A

Port Number: 5680

Update Frequency: 5

Server Logging:

Source of Initial images: [Empty]


Buttons: Done, Create Local Database

Import files in the following order:

- 1) Total head scan
- 2) Upper molar –right side
- 3) Lower molar-right side
- 4) Upper molar- left side
- 5) Lower molar- left side

(Head of femur, tibia, and leg scans are analyzed separately). Then create local database.

Afterwards, import the DICOM files, the data save from micro-CT machine, by

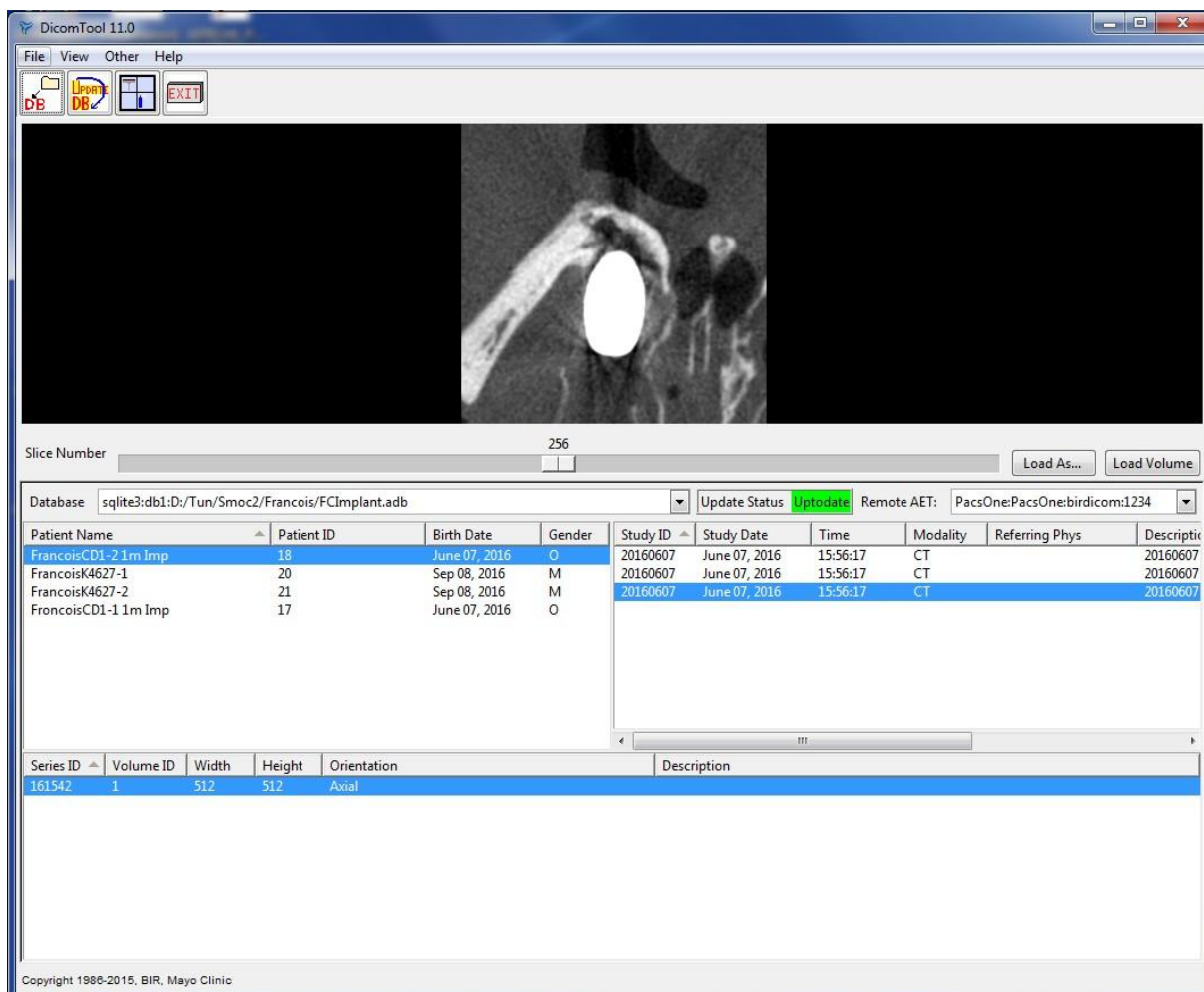
clicking on . Then select each folder contains DICOM data.

At this step, no need to change image parameters because all are exported from the same source and the machine is set the same parameter.



After import DICOM folder, these data will be available in DICOM tools and will arrange in different patients regarding to the name of the sample.

Clicking on "Up to date". A new database appears: "Patient name". Import the images in the order of the digitized samples (i.e. overall view with whole head, upper right molar, lower right molar, upper left molar, left lower molar, femur head, knee, tibial head and whole leg). The name of the folder is entered in "Patient name" (ex: No19KO1Y for upper right molar of mutant mice). Open each DICOM file, load all the images by clicking on "Load volume". The images appear in the workspace. Close the dialog once the images are imported.




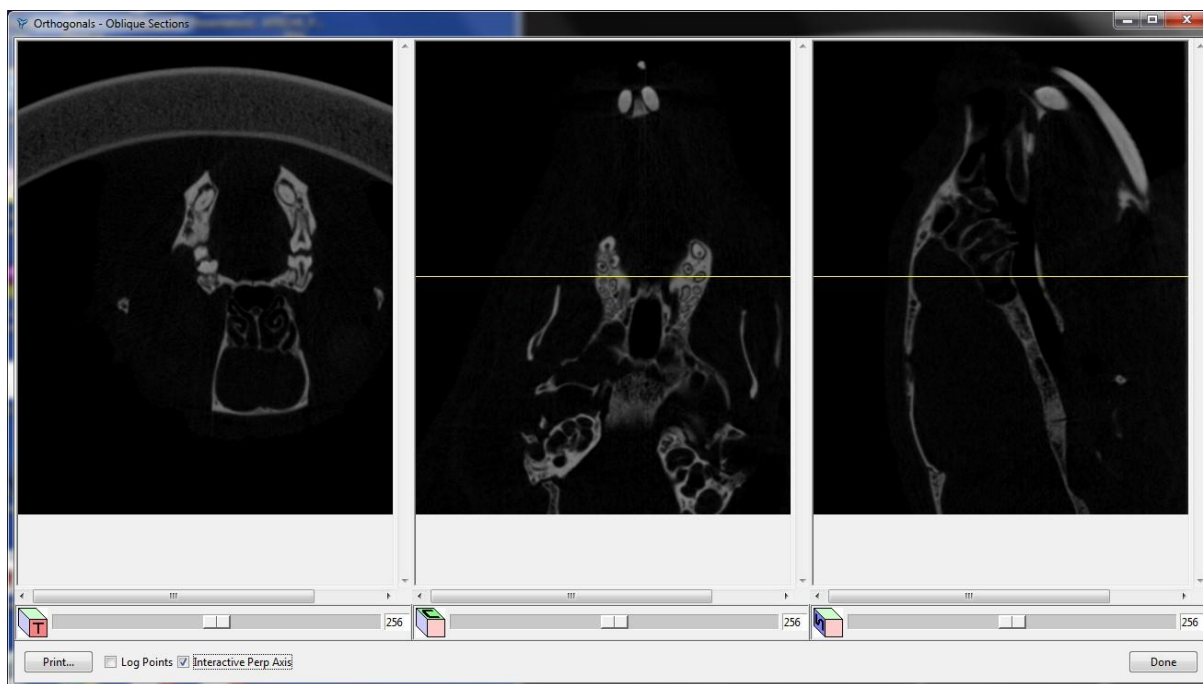
Close DICOM window and go back to the Analyze workspace.

Oblique section

Changing the orientation and re-arrangement the CT slides by using **Oblique section**




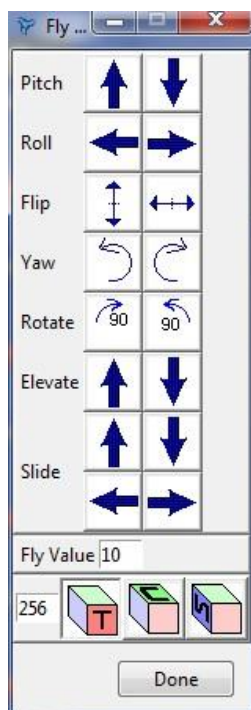
Click on  to initially select the cutting plane for your prefer section. The new window will show the μ CT data in 3 planes.



On this window, select on “Interactive Prep Axis” to show the yellow line for locating the cutting plane. Then put the yellow line through the interested plane by click+hold the mouse left button. Put this line through the organ you want to see for example upper and lower molars (M1+M2+M3). The result image will show on the main panel of oblique sections tool. Close this window after selected.

The images still needed to nicely arrange to get the highest consistency between

different data. This can be done using the next tool .



The new small window will show the tools to move the cutting line and the object.

Pitch – to move the cutting line up or down

Roll - to move the cutting line left or right

Flip – to flip the cutting line

Yaw – to rotate/turn the cutting line clockwise or anti-clockwise

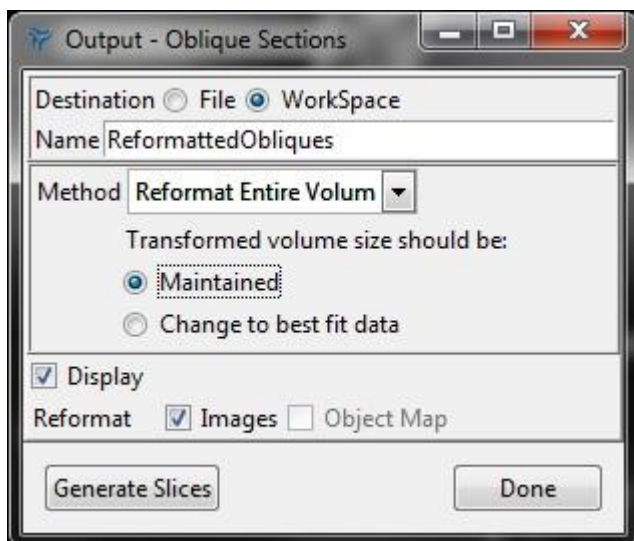
Rotate – to rotate the cutting line 90 degree

Elevate – to elevate or descend the cutting line

Slide – to slide the object into four directions

Fly Value – to set the value of all these movements

After getting the right section plane, to save it to the workspace, select on “file” and “output”



Use the “Reformat Entire Volume” method and select on “Maintained” the volume size to get new data which still has the same size (512 slides).

Click on generate slices and the new data will appear in the workspace.

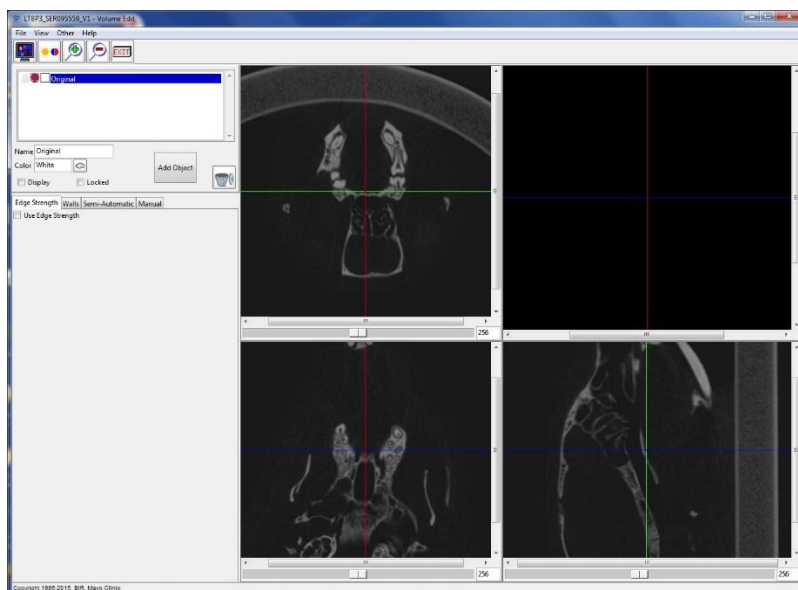


Volume Edit – Object segmentation

This tool allows you to click on object to select the ROI from micro-CT data.

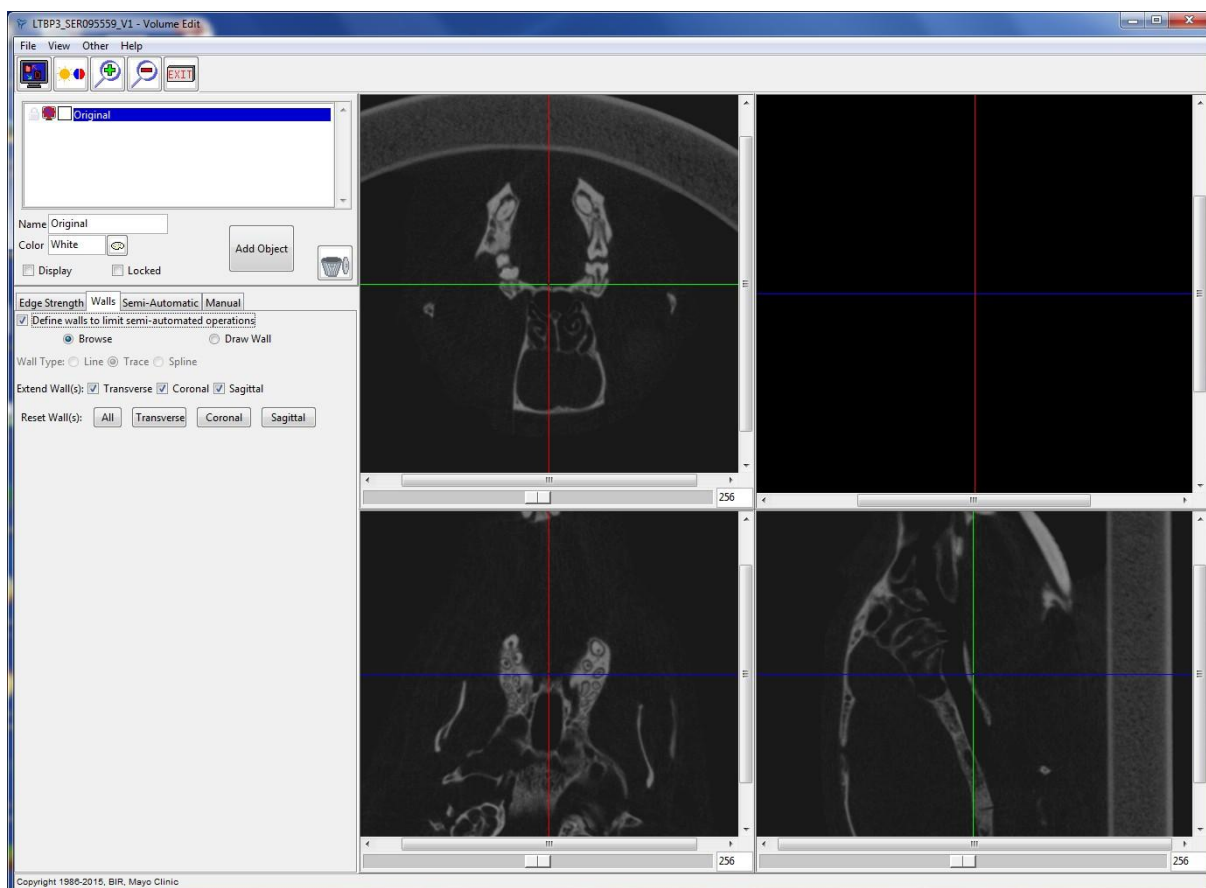
- Edge strength; to define the overall border of the CT data which allows the program to separate each object.


The value of the strength can be adjust.

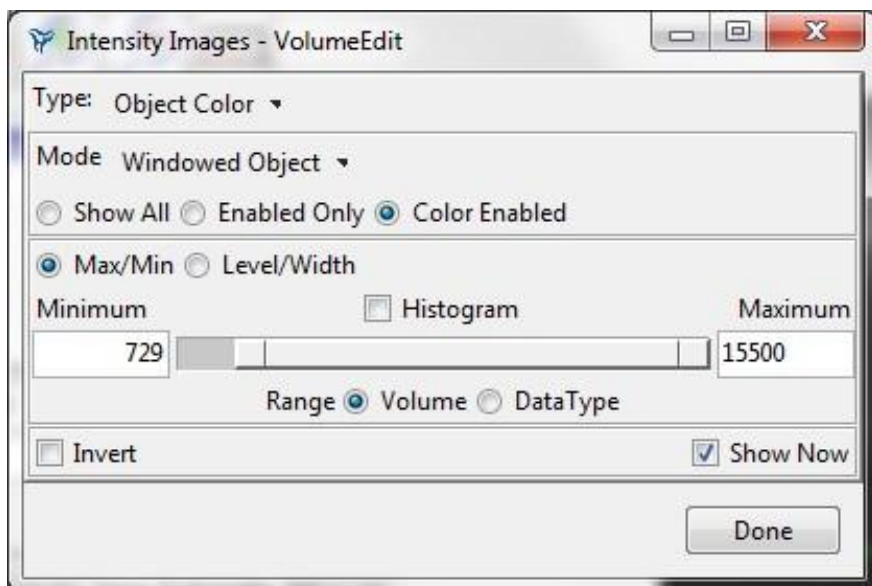


- Wall; to define the wall to limit the semi-automated functions.

For example, draw the wall on three planes covering molars or alveolar bone.



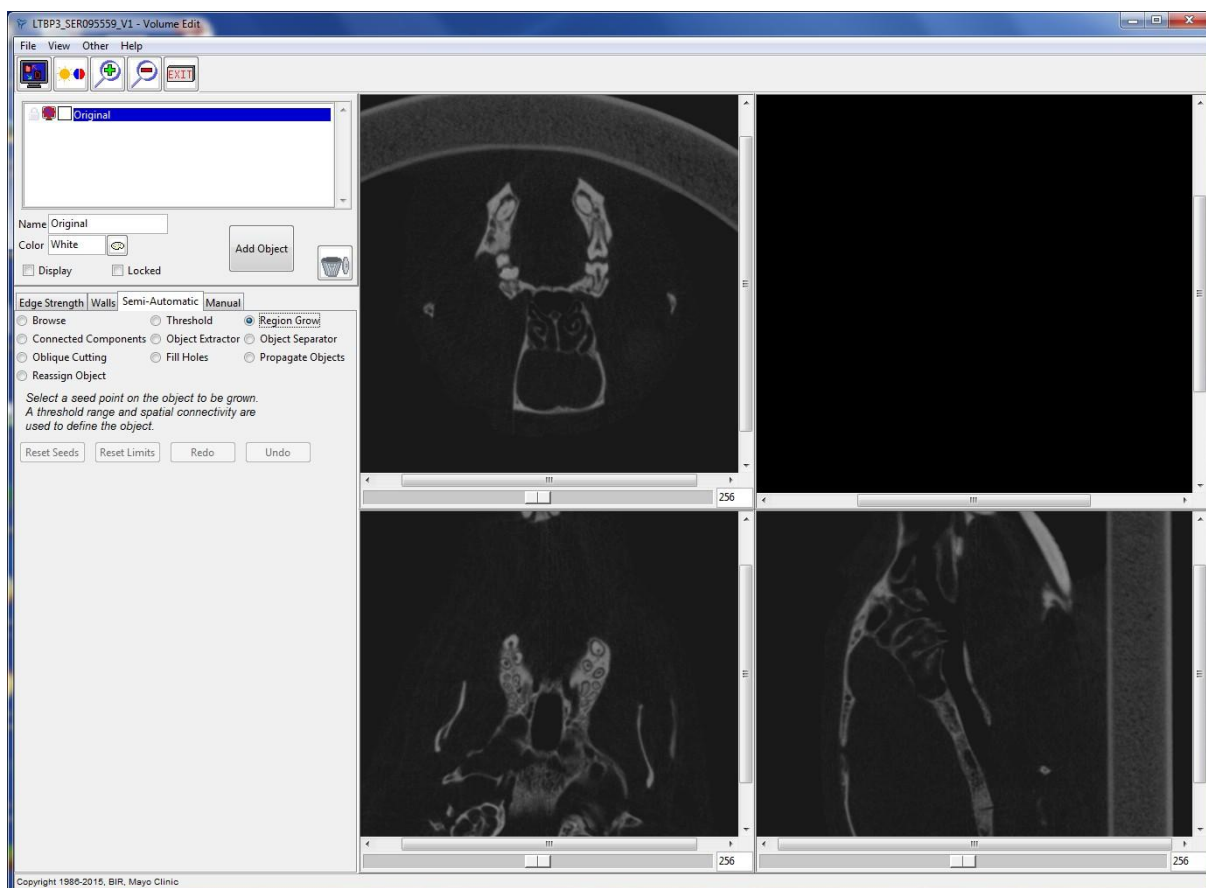
Intensity  can be adjusted to change the contrast of the x-ray image.



Low intensity – air, liquid, and soft tissue.

High intensity – bone, dentin, and enamel.

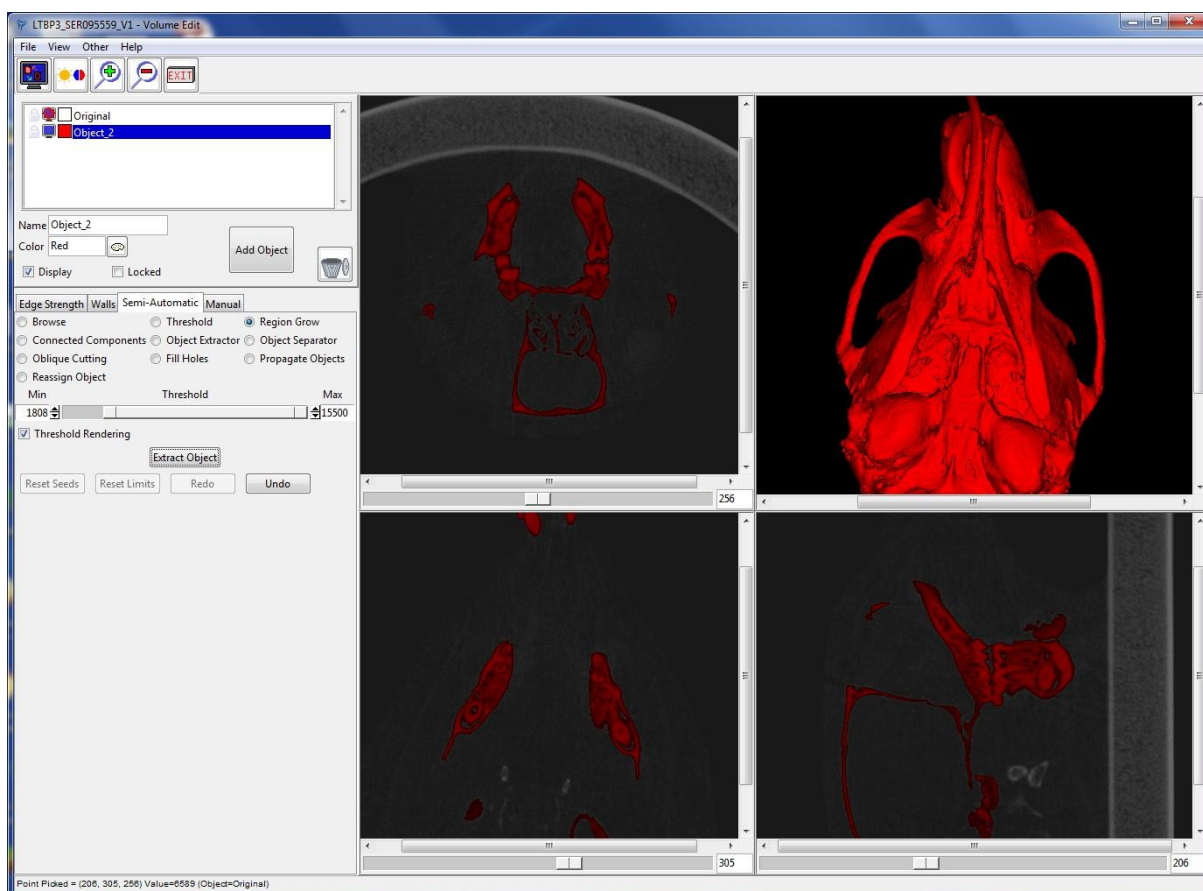
Exclude the lowest intensity value. This will take off the air and soft tissue.



- Semi-Automatic; to segment the object by different setting commands.

Region growth

For the head scans we select the upper incisor, for the molar scans we select the enamel of the second molar. After selecting the site use the volume editor to define the minimum (~2900) and maximum (highest level ~10,000+). The aim for the head is to extract all of the bones (leaving no major holes). Be careful to adjust the minimum extraction lower limit for Smoc2 mutants (~2600) which have low bone pixel densities otherwise they will have obvious hole appearing in the total head scan. The whole head sometimes the minimum threshold is around 1700.

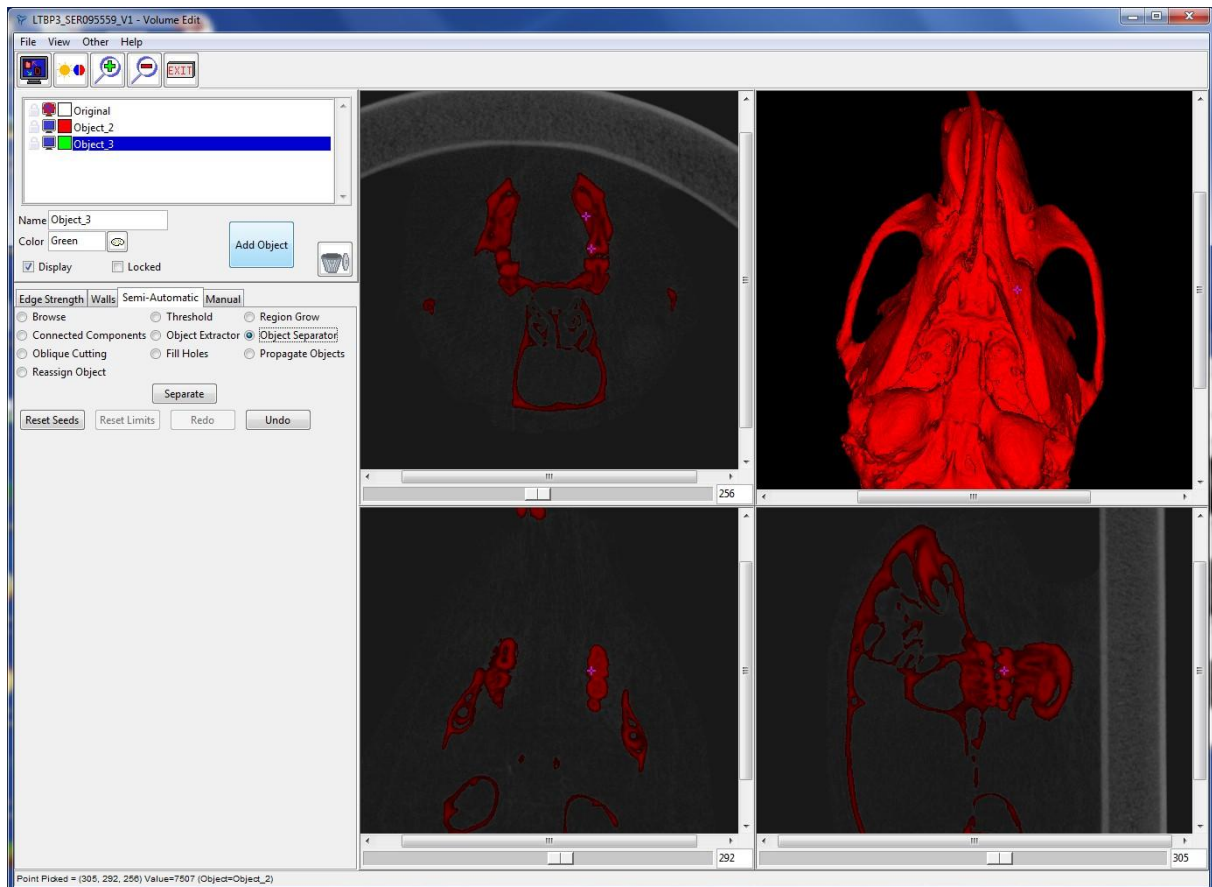


Object separator

To separate the 1st object into another object such as upper and lower jaw or molars and alveolar bone.

When the 1st object has been defined, create the new object by "Add Object".

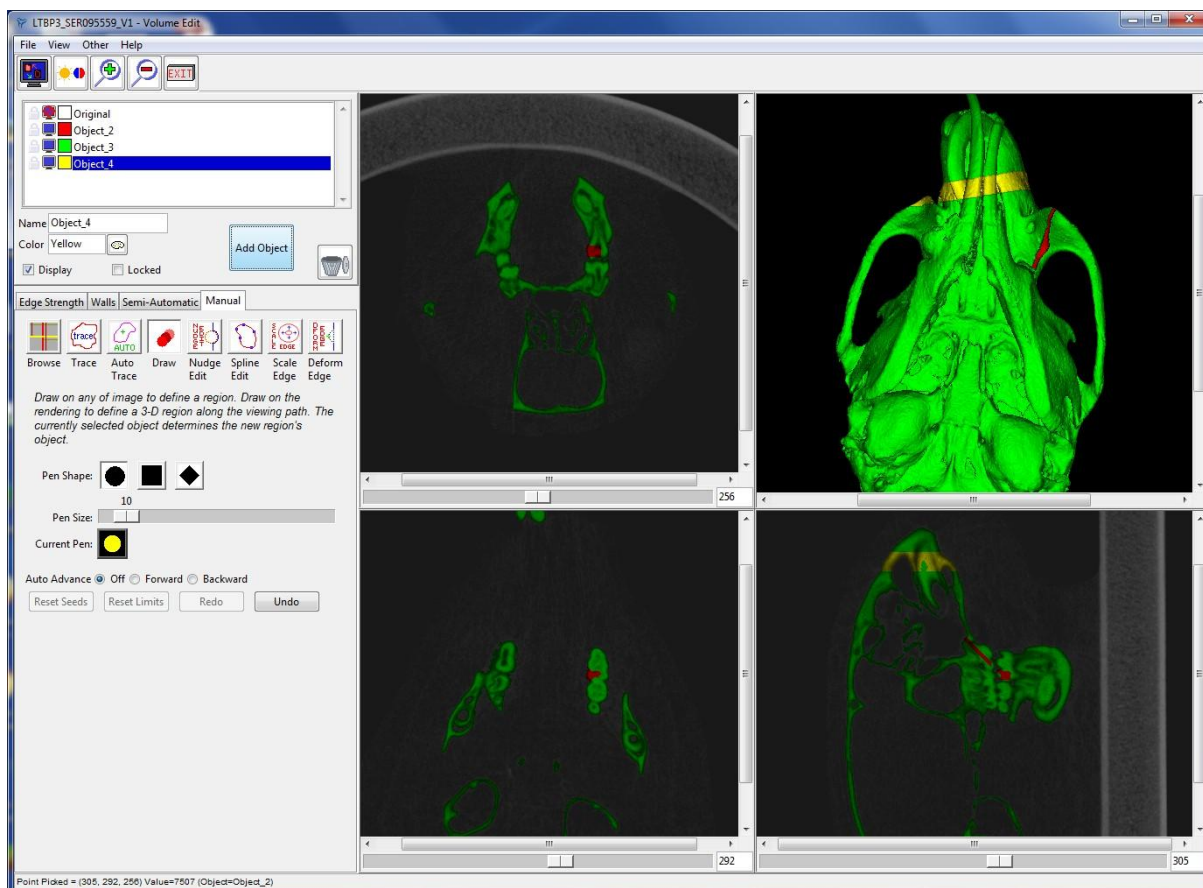
Put the two seed points within this object, the future objects will separate between these two points.



- Manual; to define and segment the object manually.

Draw

To define the object by using the pen to paint on the data manually. This pen can select on both 2D plane and 3D rendering object.



Then push **extract** button.

If there is sufficient space between the maxillary and jaw the images will be imported as two separate regions.

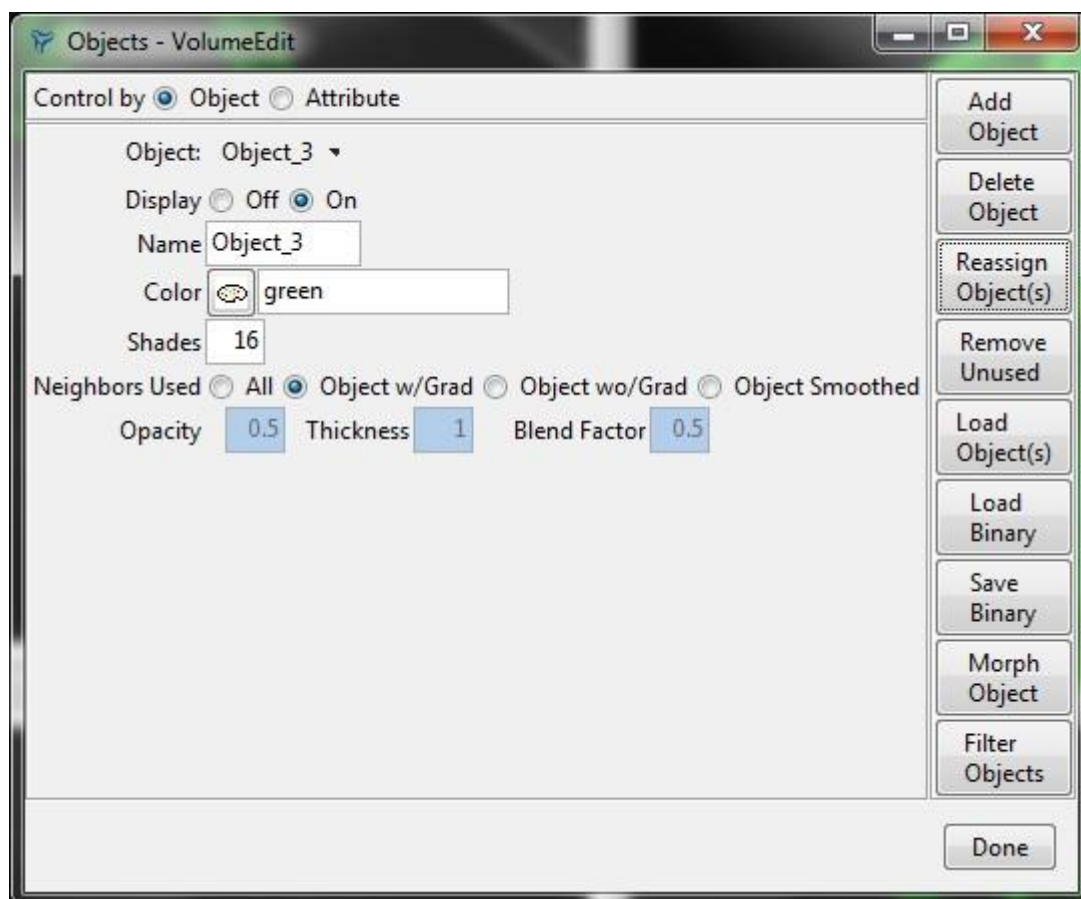
Save as name of the object (Crane, Maxillary, Jaw WT/KO/ 1yr/M etc.)

Extract the density & area-selected image (which will be color coded –red, green, etc.) Hence, the object can be rename and recolor on this window.

Segmented objects can also be reassigned on the object tool.

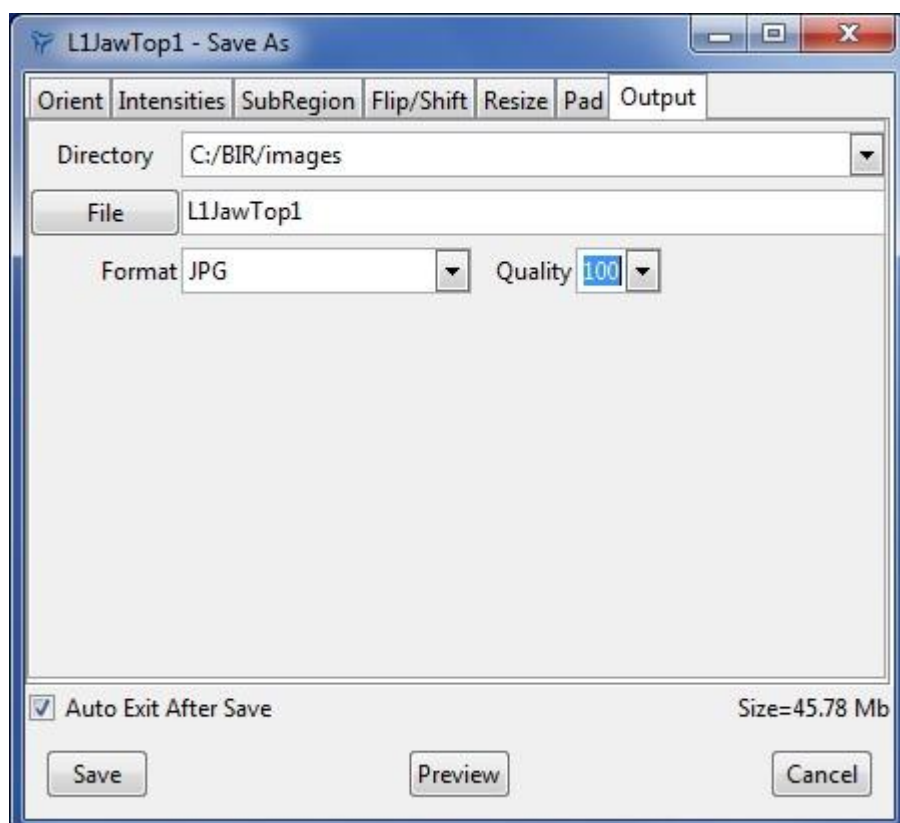
Manipulating Objects

9. In the **Objects** window (View > Objects) (figure 4), click **Reassign Object(s)**.
10. In the window returned (figure 5), select: **BlueObject** from the Reassign from list. From the drop down menu to the right select: **YellowObject**. Click **Apply** and then **OK** to dismiss the window. Note the update in the Preview window.
11. Click **Remove Unused** in the **Objects** window to remove 'BlueObject'. Click **OK** in the dialog box returned.



After images is extracted open the file (in saved regions).

Save image.



Segmentation of the object manual.

Extract areas of interest: To extract images of the areas of interest to be analyzed, click on the "Volume editor" tab to segment the volume of the object. On the "Semi automatic" tab, several filters are possible. Select "Region grow" (ex: bone). On the display, 4 dials are displayed; Top left: the coronal cut in the upper right: the 3D reconstruction, bottom left: the axial section, bottom right sagittal section. Here we have selected the root zone of the 2nd molar. It is also possible to set the pixel density threshold.

In our experiment, the bone density threshold was between 2900 and the maximum pixel density (between 2300 and the maximum density for mutant mice). For enamel, the density threshold was between 6000 and 10000 pixel density. To visualize the reconstructions in 3D, it was enough to keep the key of the keyboard "Control" while mobilizing the cursor of the mouse and to repeat the procedure to extract a second zone (for example, the mandible). The first selected area then appeared in red and the second in green. It was not necessary to change the density threshold of the pixels since it was prerecorded. Save the selection. Close the window.

Extract the elements of interest: to analyze the teeth in particular, separate the bone of the teeth by clicking on "Object separator". Select 2 points of the same object (bone and tooth). Then click on "Separate"

Repeat as long as bone tissue remains around the selected teeth until the sample to be analyzed is devoid of virtual bone tissue.

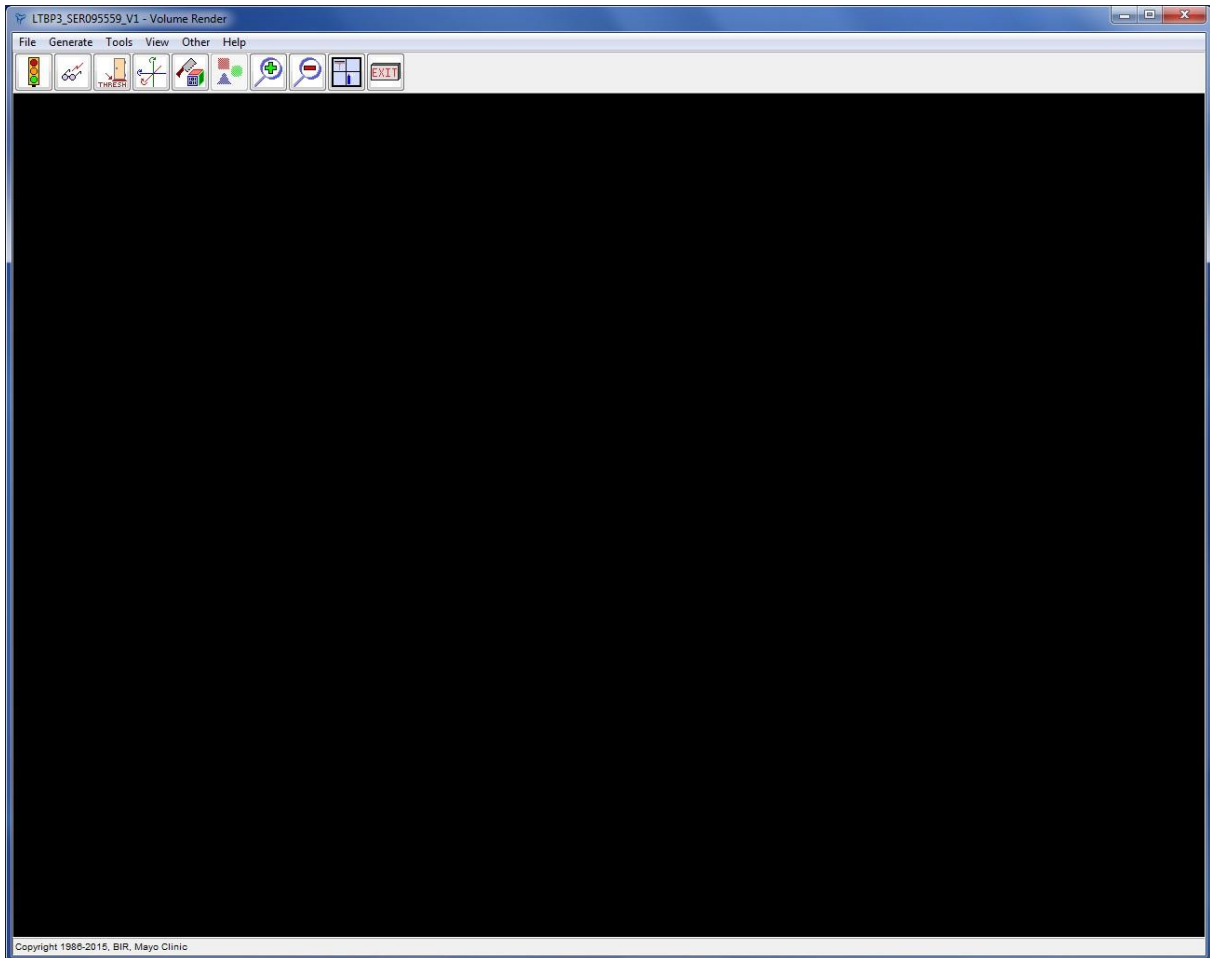
You can modify using volume render => adjust orientation

For **Volume rendering** (button with Face image) File=>load object

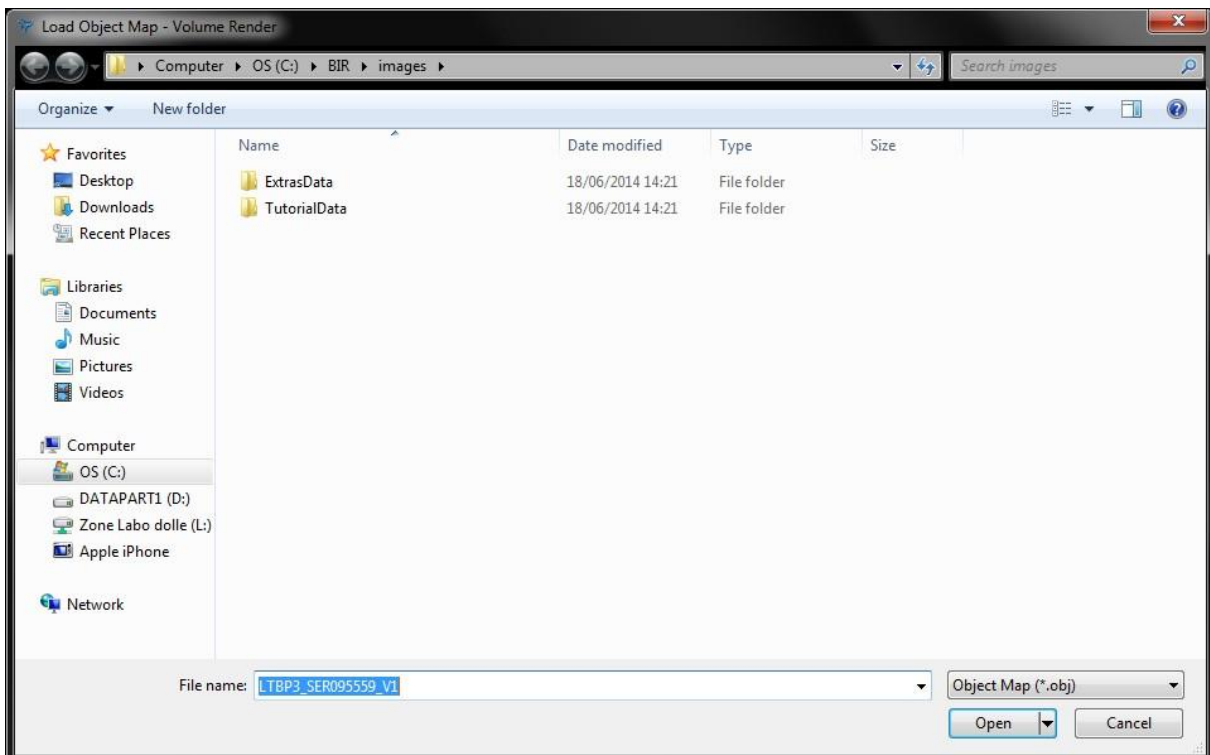
Set Rendering Type



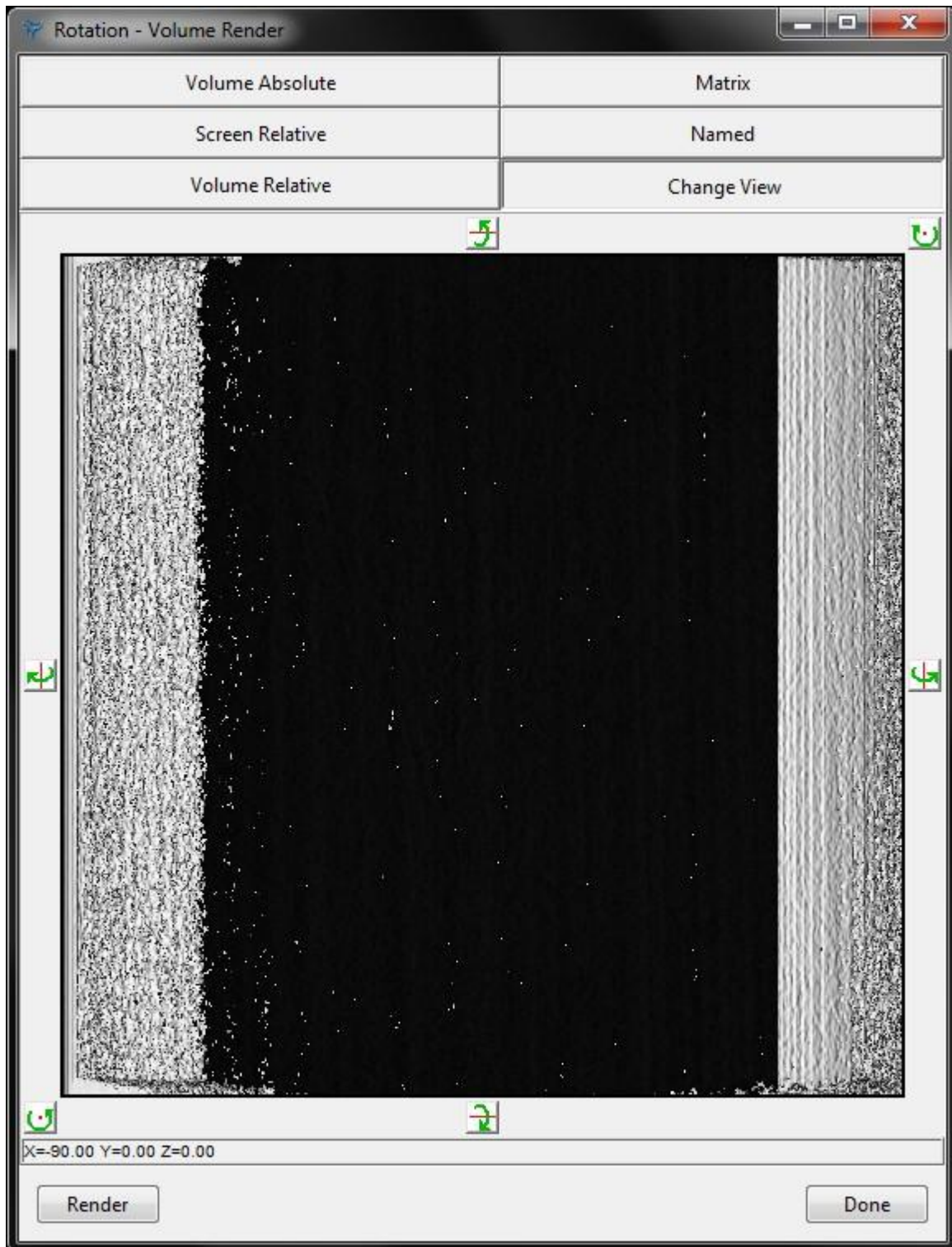
1. Load the **Cubic_CT_Head.awv** data set from the **\$:\BIR\images\TutorialData** directory.
2. Open the **Volume Render** module (**Display > Volume Render**).
3. Press the **Render** PowerBar button or choose **Generate > Render**.
4. Open the **Preview** window (**Generate > Preview**).
5. To rotate the image data in this window, click and drag the mouse.



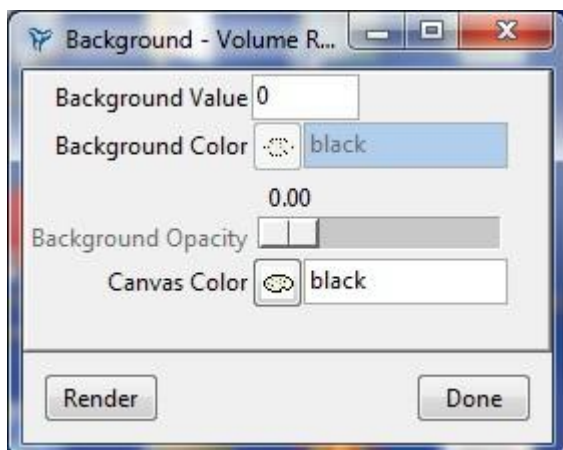
Loading object which already extracted



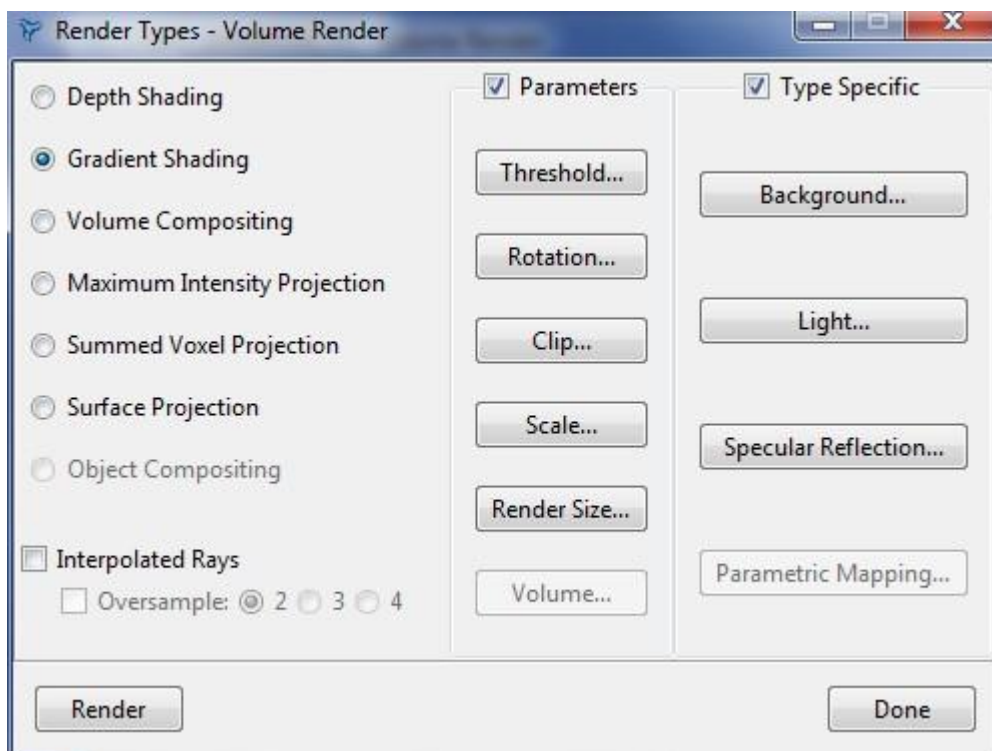
Position of the object can be adjust by using this tool.



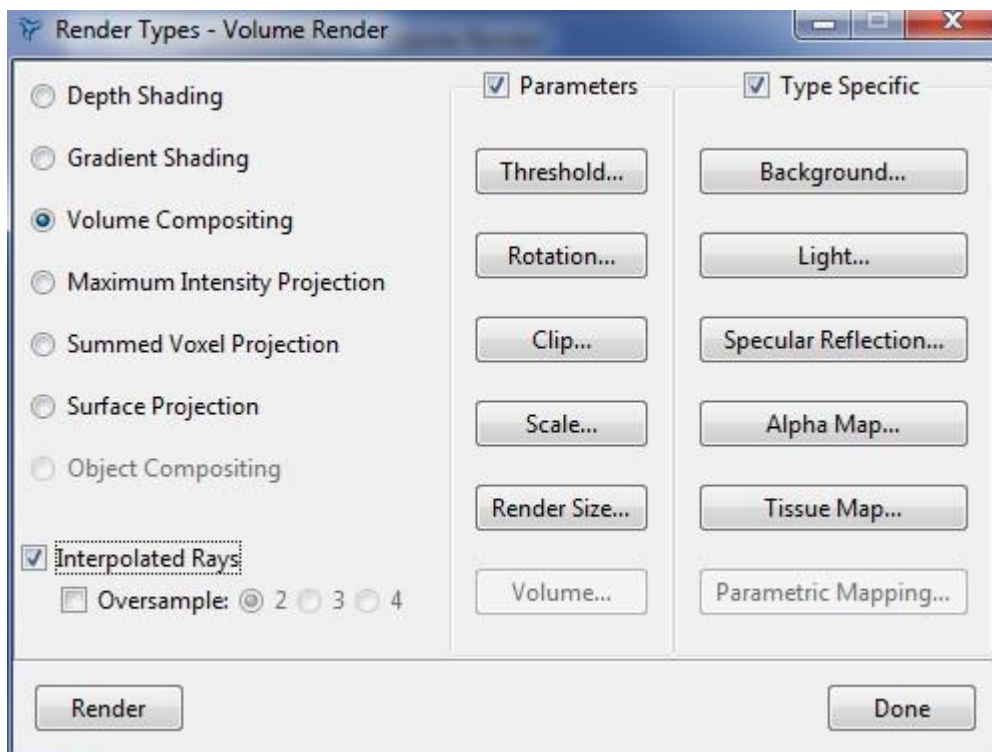
Background color can be modified on "Generate" → "Background"



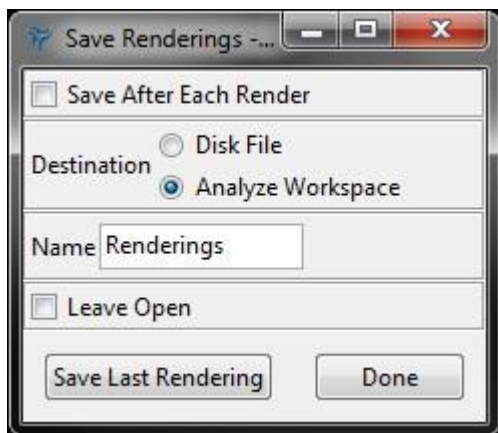
The appearance of the object can be modified on “Generate”→”Render type”



Using the 3-color buttons & selecting the object. The best quality image is usually obtained by selecting **Volume Composition & Interpolated Rays** (oversampling option).



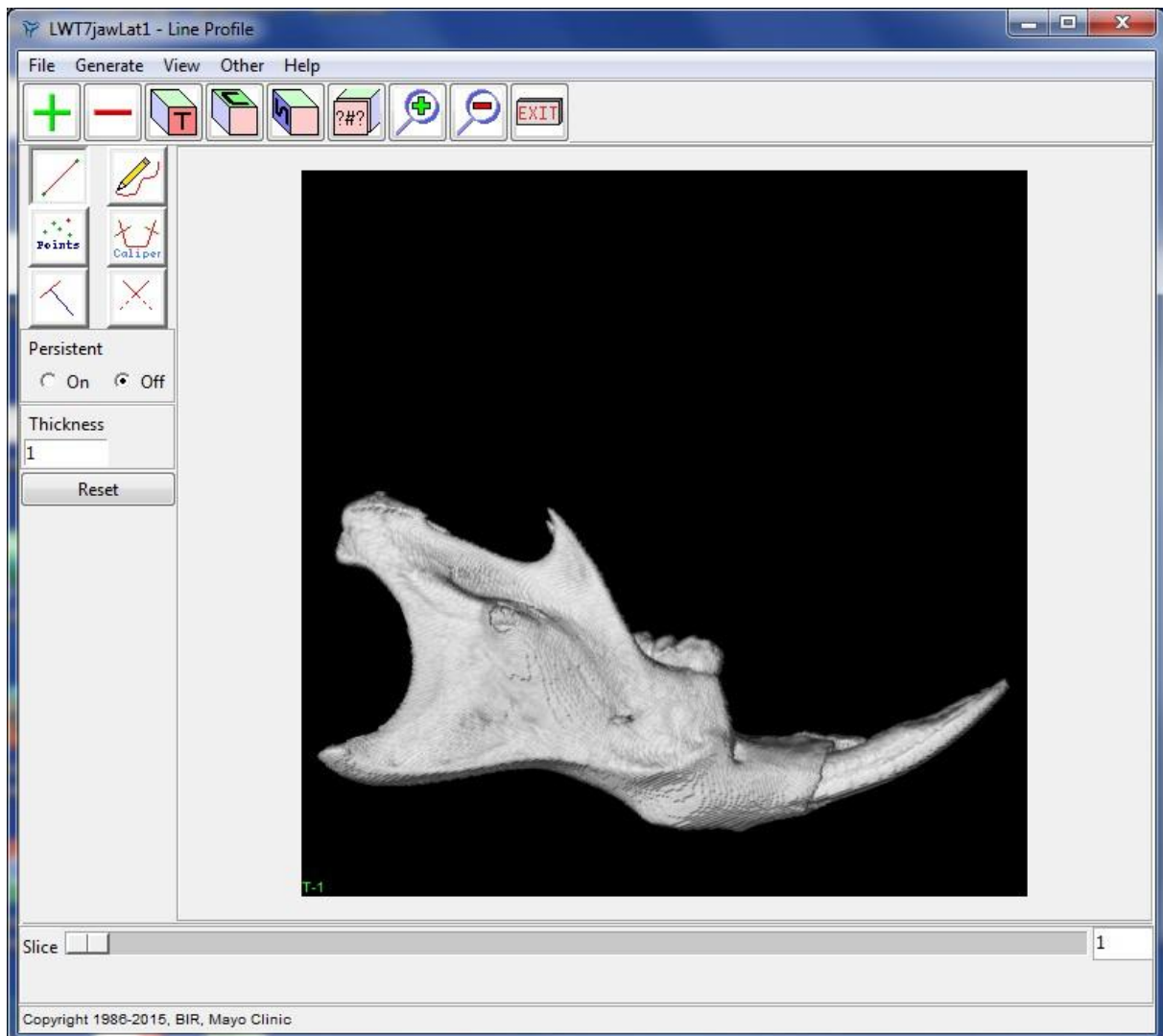
Save rendering on Analyze workspace.



Volume rendering manual

Image preview options: To modify the images (colors ...) and adjust the orientation, retrieve the recording in the appropriate file, click on "Generate" then "Render types", select the "Volume compositing" and "Interpolated rays" with 4 samples. Save the changes ("Rendering") on the work area, then save the images in the computer in JPEG format. Repeat the procedure for all items to compare in order.

Measurements: To analyze the images, take the files recorded in the "Caliper micro-CT analysis tools by analysis" and measure the length and width of the teeth of the sample.

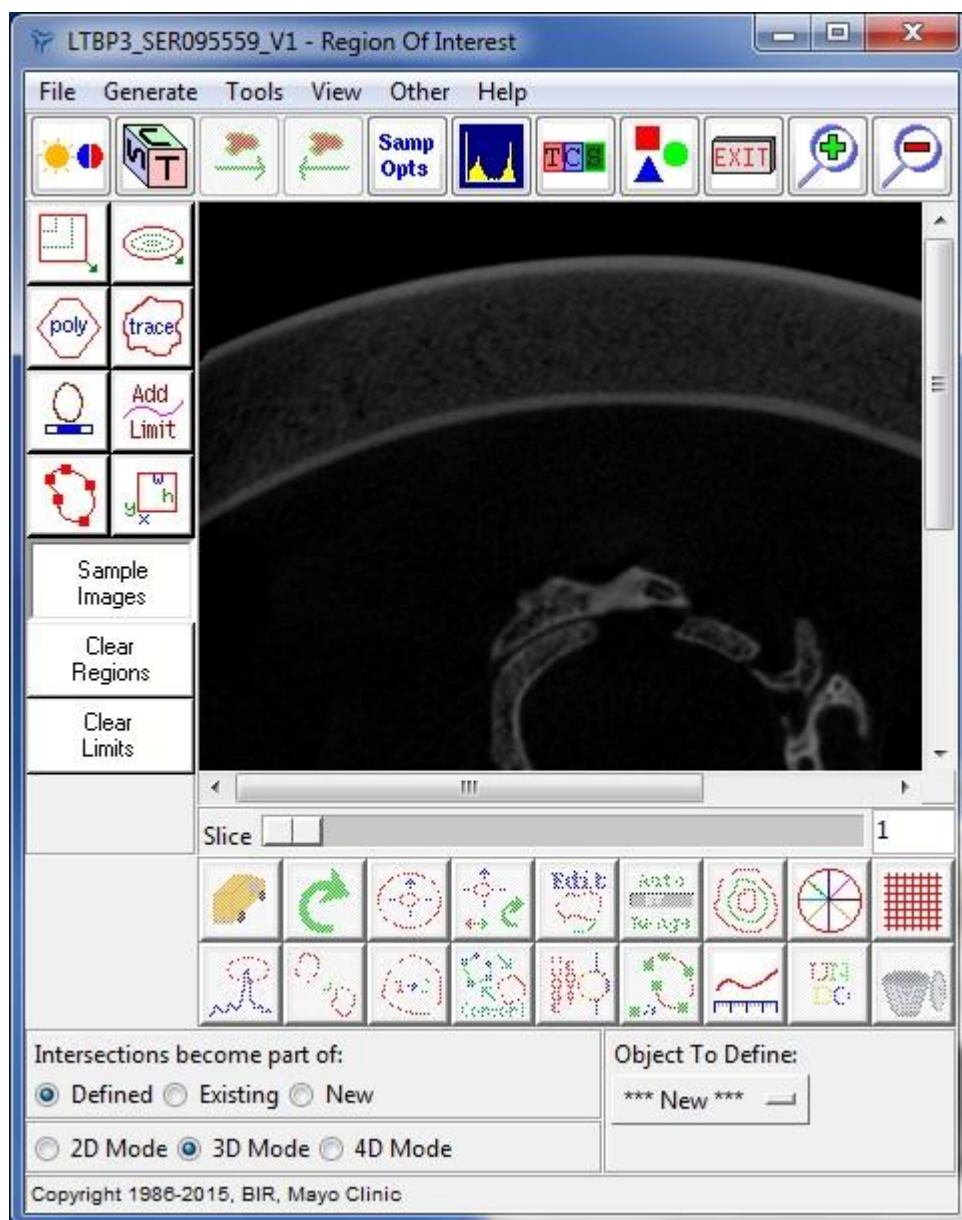


To do this, on the "Line profile" tab in "Measure", right-click on the image to be analyzed, then use "Line tool" and hold the left click from one end to the other. Here, the first molar, then the second molar, and then the third molar are to be measured in its greatest length and then its largest width.

Data report: Since the measurement technique is subjective, in order to avoid a dependent operator measurement bias, each length and width of each tooth to be analyzed has been measured 3 times by 3 different operators in order to calculate the means of measurements and then allow Exploitation of results.

In addition, the "Line profile" can also measure on both 3D segmented object as described and on 2D data.

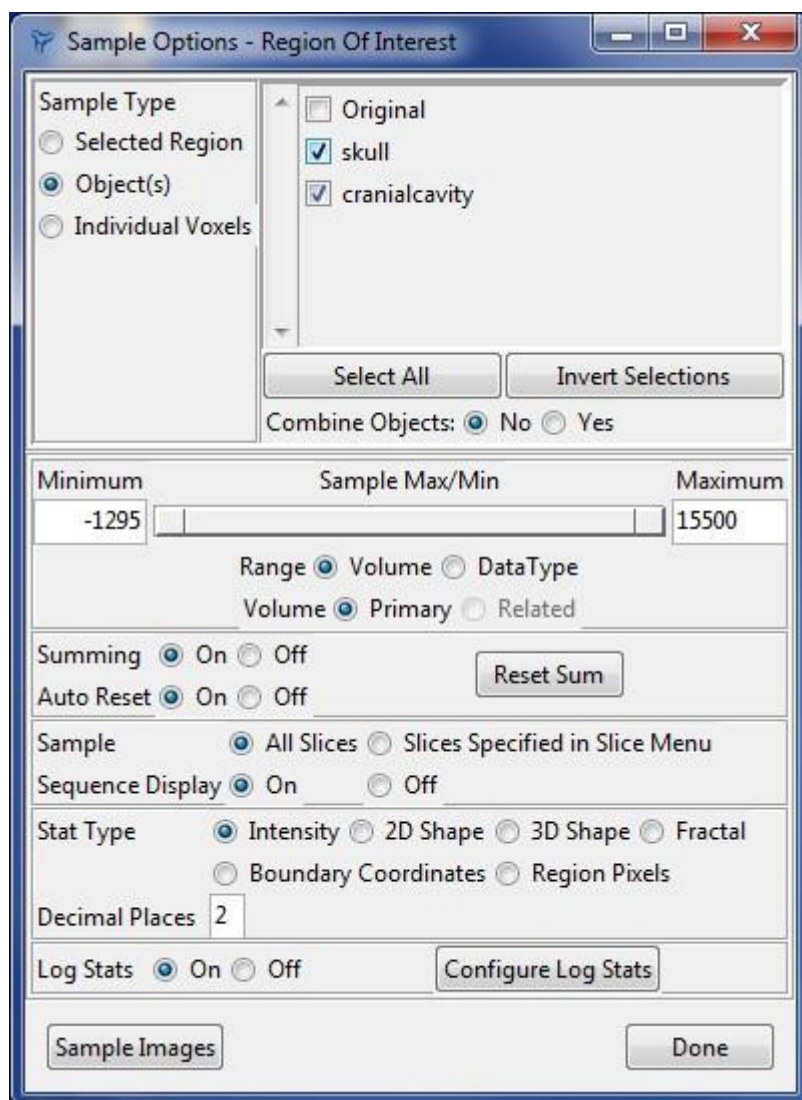
Measure ROI



Load the previous segmented object.

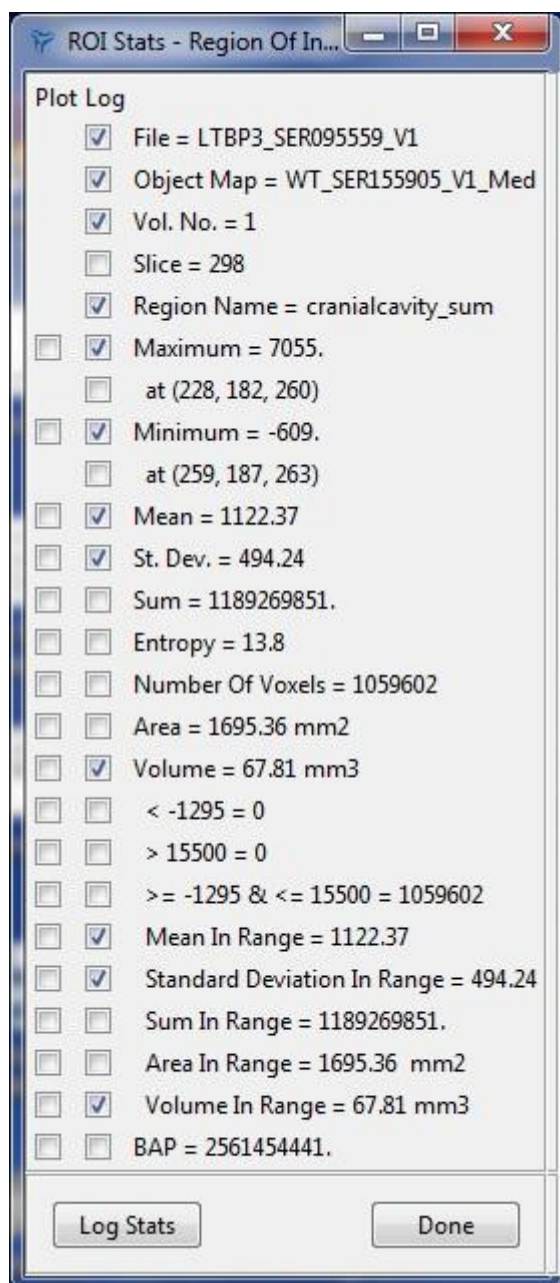


Then click on sample option . The new window will appear.



Select the object you want to calculate. Sequence display can be turned off to reduce operating time.

Configure Log stats tool is used to modify/select the appropriated result.



Result shows all parameters in a table and can be export to excel format.

ROI Stat Log - Region Of Interest

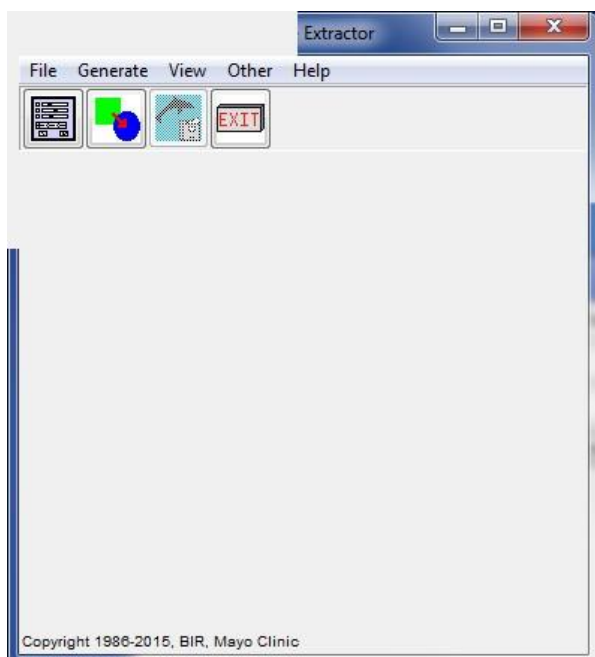
```
# Mon Nov 14 17:06:00 CET 2016
# VolumeFile= LTBP3_SER095559_v1
# SampleMax= 15500 SampleMin= -1295
# ExamNumber= 20140307 ScanDate= 20140307 PatientID= 2 Name= LTBP3 VoxelWidth= 0.040000000000000001 VoxelHeight= 0.040000000000000001
```

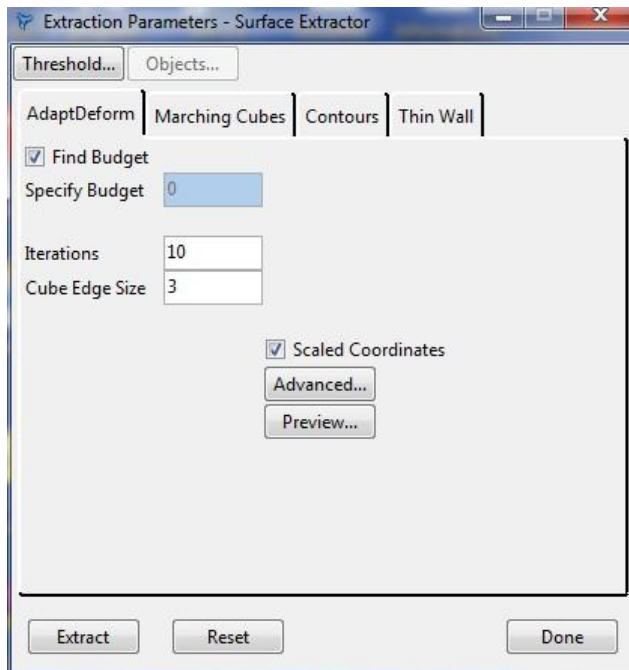
Vol_#	Name	MaxVal	MinVal	Mean	Std.Dev.	Vol_mm3	RngMean	RngSDev	Rng Vol
1	skull_sum	9492	-928	1477.86	1320.73	51.17	1477.86	1320.73	51.17 LTBP3_SER095559_v1
1	cranialcavity_sum	7055	-609	1122.37	494.24	67.81	1122.37	494.24	67.81 LTBP3_SER095559_v1

Save Done

Surface extraction

This is a tool to create the segmented object into 3D object files. The 3D object file can be view by any 3D program and analyze (locate the anatomical land mark points or 3D printing)





For bone mineral density (BMD) calculations; please follow the procedure from the AnalyzeDirect website (<https://analyzedirect.com/micro-ct/>).

RÉFÉRENCES BIBLIOGRAPHIQUES
(REFERENCES)

1. Hirasawa, T. and S. Kuratani, *Evolution of the vertebrate skeleton: morphology, embryology, and development*. Zoological Lett, 2015. **1**: p. 2.
2. Hennekam, R.C., *A newborn with unusual morphology: some practical aspects*. Semin Fetal Neonatal Med, 2011. **16**(2): p. 109-13.
3. Cohen, M.M., Jr., *The new bone biology: pathologic, molecular, and clinical correlates*. Am J Med Genet A, 2006. **140**(23): p. 2646-706.
4. Schofield, P.N., R. Hoehndorf, and G.V. Gkoutos, *Mouse genetic and phenotypic resources for human genetics*. Hum Mutat, 2012. **33**(5): p. 826-36.
5. Bei, M., *Molecular genetics of ameloblast cell lineage*. J Exp Zool B Mol Dev Evol, 2009. **312B**(5): p. 437-44.
6. Fleischmannova, J., et al., *Mouse models of tooth abnormalities*. Eur J Oral Sci, 2008. **116**(1): p. 1-10.
7. Moss-Salentijn, L., *Studies on dentin. 2. Vestigial lacteal incisor teeth of the rat*. Acta Anat (Basel), 1975. **92**(3): p. 329-50.
8. Hovorakova, M., et al., *Shh expression in a rudimentary tooth offers new insights into development of the mouse incisor*. J Exp Zool B Mol Dev Evol, 2011. **316**(5): p. 347-58.
9. Jheon, A.H., et al., *From molecules to mastication: the development and evolution of teeth*. Wiley Interdiscip Rev Dev Biol, 2013. **2**(2): p. 165-82.
10. Zhang, Z., et al., *Antagonistic actions of Msx1 and Osr2 pattern mammalian teeth into a single row*. Science, 2009. **323**(5918): p. 1232-4.
11. Wang, X.P., et al., *Runx2 (Cbfa1) inhibits Shh signaling in the lower but not upper molars of mouse embryos and prevents the budding of putative successional teeth*. J Dent Res, 2005. **84**(2): p. 138-43.
12. Jussila, M. and I. Thesleff, *Signaling networks regulating tooth organogenesis and regeneration, and the specification of dental mesenchymal and epithelial cell lineages*. Cold Spring Harb Perspect Biol, 2012. **4**(4): p. a008425.
13. Jernvall, J. and I. Thesleff, *Reiterative signaling and patterning during mammalian tooth morphogenesis*. Mech Dev, 2000. **92**(1): p. 19-29.
14. Jernvall, J., *Linking development with generation of novelty in mammalian teeth*. Proc Natl Acad Sci U S A, 2000. **97**(6): p. 2641-5.
15. Salazar-Ciudad, I. and J. Jernvall, *A gene network model accounting for development and evolution of mammalian teeth*. Proc Natl Acad Sci U S A, 2002. **99**(12): p. 8116-20.
16. Kangas, A.T., et al., *Nonindependence of mammalian dental characters*. Nature, 2004. **432**(7014): p. 211-4.
17. Kassai, Y., et al., *Regulation of mammalian tooth cusp patterning by ectodin*. Science, 2005. **309**(5743): p. 2067-70.
18. Carlson, B.M., *Chapter 14 - Head and Neck*, in *Human Embryology and Developmental Biology (Fifth Edition)*. 2014, W.B. Saunders: Philadelphia. p. 294-334.
19. Pispas, J. and I. Thesleff, *Mechanisms of ectodermal organogenesis*. Dev Biol, 2003. **262**(2): p. 195-205.
20. Mucchielli, M.L., et al., *Mouse Otlx2/RIEG expression in the odontogenic epithelium precedes tooth initiation and requires mesenchyme-derived signals for its maintenance*. Dev Biol, 1997. **189**(2): p. 275-84.
21. Balic, A. and I. Thesleff, *Tissue Interactions Regulating Tooth Development and Renewal*. Curr Top Dev Biol, 2015. **115**: p. 157-86.

22. Mina, M. and E.J. Kollar, *The induction of odontogenesis in non-dental mesenchyme combined with early murine mandibular arch epithelium*. Arch Oral Biol, 1987. **32**(2): p. 123-7.
23. Lumsden, A.G., *Spatial organization of the epithelium and the role of neural crest cells in the initiation of the mammalian tooth germ*. Development, 1988. **103 Suppl**: p. 155-69.
24. Kollar, E.J. and G.R. Baird, *Tissue interactions in embryonic mouse tooth germs. II. The inductive role of the dental papilla*. J Embryol Exp Morphol, 1970. **24**(1): p. 173-86.
25. Kollar, E.J. and G.R. Baird, *The influence of the dental papilla on the development of tooth shape in embryonic mouse tooth germs*. J Embryol Exp Morphol, 1969. **21**(1): p. 131-48.
26. Häärä, O., et al., *Ectodysplasin regulates activator-inhibitor balance in murine tooth development through Fgf20 signaling*. Development, 2012. **139**(17): p. 3189-99.
27. Keränen, S.V., et al., *Gene expression patterns associated with suppression of odontogenesis in mouse and vole diastema regions*. Dev Genes Evol, 1999. **209**(8): p. 495-506.
28. Dahmann, C. and K. Basler, *Compartment boundaries: at the edge of development*. Trends Genet, 1999. **15**(8): p. 320-6.
29. Jiménez-Rojo, L., et al., *Stem Cell Fate Determination during Development and Regeneration of Ectodermal Organs*. Front Physiol, 2012. **3**: p. 107.
30. Jernvall, J., S.V. Keränen, and I. Thesleff, *Evolutionary modification of development in mammalian teeth: quantifying gene expression patterns and topography*. Proc Natl Acad Sci U S A, 2000. **97**(26): p. 14444-8.
31. Linde, A. and M. Goldberg, *Dentinogenesis*. Crit Rev Oral Biol Med, 1993. **4**(5): p. 679-728.
32. Magloire, H., et al., *Odontoblast primary cilia: facts and hypotheses*. Cell Biol Int, 2004. **28**(2): p. 93-9.
33. Butler, W.T., J.C. Brunn, and C. Qin, *Dentin extracellular matrix (ECM) proteins: comparison to bone ECM and contribution to dynamics of dentinogenesis*. Connect Tissue Res, 2003. **44 Suppl 1**: p. 171-8.
34. Fisher, L.W. and N.S. Fedarko, *Six genes expressed in bones and teeth encode the current members of the SIBLING family of proteins*. Connect Tissue Res, 2003. **44 Suppl 1**: p. 33-40.
35. Goldberg, M., et al., *Dentin: structure, composition and mineralization*. Front Biosci (Elite Ed), 2011. **3**: p. 711-35.
36. Simmer, J.P., et al., *Regulation of dental enamel shape and hardness*. J Dent Res, 2010. **89**(10): p. 1024-38.
37. Hu, J.C., et al., *Enamel formation and amelogenesis imperfecta*. Cells Tissues Organs, 2007. **186**(1): p. 78-85.
38. Hu, J.C. and J.P. Simmer, *Developmental biology and genetics of dental malformations*. Orthod Craniofac Res, 2007. **10**(2): p. 45-52.
39. Smith, C.E. and A. Nanci, *Protein dynamics of amelogenesis*. Anat Rec, 1996. **245**(2): p. 186-207.
40. Pashley, D.H., *Dynamics of the pulpo-dentin complex*. Crit Rev Oral Biol Med, 1996. **7**(2): p. 104-33.
41. Tziafas, D., *Basic mechanisms of cytodifferentiation and dentinogenesis during dental pulp repair*. Int J Dev Biol, 1995. **39**(1): p. 281-90.
42. Solheim, T., *Amount of secondary dentin as an indicator of age*. Scand J Dent Res, 1992. **100**(4): p. 193-9.

43. Kim, T.H., et al., *Osterix regulates tooth root formation in a site-specific manner*. J Dent Res, 2015. **94**(3): p. 430-8.
44. Nakatomi, M., et al., *Sonic hedgehog signaling is important in tooth root development*. J Dent Res, 2006. **85**(5): p. 427-31.
45. Rakian, A., et al., *Bone morphogenetic protein-2 gene controls tooth root development in coordination with formation of the periodontium*. Int J Oral Sci, 2013. **5**(2): p. 75-84.
46. Wang, Y., et al., *Inactivation of Tgfbr2 in Osterix-Cre expressing dental mesenchyme disrupts molar root formation*. Dev Biol, 2013. **382**(1): p. 27-37.
47. Hirose, N., et al., *Ameloblastin in Hertwig's epithelial root sheath regulates tooth root formation and development*. PLoS One, 2013. **8**(1): p. e54449.
48. Xiong, J., et al., *Epithelial cell rests of Malassez contain unique stem cell populations capable of undergoing epithelial-mesenchymal transition*. Stem Cells Dev, 2012. **21**(11): p. 2012-25.
49. Ohazama, A., et al., *A role for suppressed incisor cuspal morphogenesis in the evolution of mammalian heterodont dentition*. Proc Natl Acad Sci U S A, 2010. **107**(1): p. 92-7.
50. Neubüser, A., et al., *Antagonistic interactions between FGF and BMP signaling pathways: a mechanism for positioning the sites of tooth formation*. Cell, 1997. **90**(2): p. 247-55.
51. St Amand, T.R., et al., *Antagonistic signals between BMP4 and FGF8 define the expression of Pitx1 and Pitx2 in mouse tooth-forming anlage*. Dev Biol, 2000. **217**(2): p. 323-32.
52. Bei, M. and R. Maas, *FGFs and BMP4 induce both Msx1-independent and Msx1-dependent signaling pathways in early tooth development*. Development, 1998. **125**(21): p. 4325-33.
53. Tissier-Seta, J.P., et al., *Barx1, a new mouse homeodomain transcription factor expressed in cranio-facial ectomesenchyme and the stomach*. Mech Dev, 1995. **51**(1): p. 3-15.
54. Grigoriou, M., et al., *Expression and regulation of Lhx6 and Lhx7, a novel subfamily of LIM homeodomain encoding genes, suggests a role in mammalian head development*. Development, 1998. **125**(11): p. 2063-74.
55. Qiu, M., et al., *Role of the Dlx homeobox genes in proximodistal patterning of the branchial arches: mutations of Dlx-1, Dlx-2, and Dlx-1 and -2 alter morphogenesis of proximal skeletal and soft tissue structures derived from the first and second arches*. Dev Biol, 1997. **185**(2): p. 165-84.
56. Sharpe, P.T., *Homeobox genes and orofacial development*. Connect Tissue Res, 1995. **32**(1-4): p. 17-25.
57. Tucker, A. and P. Sharpe, *The cutting-edge of mammalian development; how the embryo makes teeth*. Nat Rev Genet, 2004. **5**(7): p. 499-508.
58. Grimes, D.T. and R.D. Burdine, *Left-Right Patterning: Breaking Symmetry to Asymmetric Morphogenesis*. Trends Genet, 2017.
59. Mitsiadis, T.A., et al., *Expression of the transcription factors Otlx2, Barx1 and Sox9 during mouse odontogenesis*. Eur J Oral Sci, 1998. **106 Suppl 1**: p. 112-6.
60. Lu, M.F., et al., *Function of Rieger syndrome gene in left-right asymmetry and craniofacial development*. Nature, 1999. **401**(6750): p. 276-8.
61. Conte, D., et al., *The apical ectodermal ridge of the mouse model of ectrodactyly Dlx5;Dlx6^{-/-} shows altered stratification and cell polarity, which are restored by exogenous Wnt5a ligand*. Hum Mol Genet, 2016. **25**(4): p. 740-54.

62. Stock, D.W., W.R. Jackman, and J. Trapani, *Developmental genetic mechanisms of evolutionary tooth loss in cypriniform fishes*. *Development*, 2006. **133**(16): p. 3127-37.
63. Thomas, B.L., et al., *Role of Dlx-1 and Dlx-2 genes in patterning of the murine dentition*. *Development*, 1997. **124**(23): p. 4811-8.
64. Jackman, W.R. and D.W. Stock, *Transgenic analysis of Dlx regulation in fish tooth development reveals evolutionary retention of enhancer function despite organ loss*. *Proc Natl Acad Sci U S A*, 2006. **103**(51): p. 19390-5.
65. Duverger, O., et al., *Neural crest deletion of Dlx3 leads to major dentin defects through down-regulation of Dspp*. *J Biol Chem*, 2012. **287**(15): p. 12230-40.
66. Zhang, Z., et al., *Transcriptional factor DLX3 promotes the gene expression of enamel matrix proteins during amelogenesis*. *PLoS One*, 2015. **10**(3): p. e0121288.
67. Jain, P., et al., *Tricho-dento-osseous syndrome and precocious eruption*. *J Clin Exp Dent*, 2017. **9**(3): p. e494-e497.
68. Nieminen, P., et al., *DLX3 homeodomain mutations cause tricho-dento-osseous syndrome with novel phenotypes*. *Cells Tissues Organs*, 2011. **194**(1): p. 49-59.
69. Rux, D.R. and D.M. Wellik, *Hox genes in the adult skeleton: Novel functions beyond embryonic development*. *Dev Dyn*, 2017. **246**(4): p. 310-317.
70. Satokata, I. and R. Maas, *Msx1 deficient mice exhibit cleft palate and abnormalities of craniofacial and tooth development*. *Nat Genet*, 1994. **6**(4): p. 348-56.
71. Kratochwil, K., et al., *Lef1 expression is activated by BMP-4 and regulates inductive tissue interactions in tooth and hair development*. *Genes Dev*, 1996. **10**(11): p. 1382-94.
72. Chen, Y., et al., *Msx1 controls inductive signaling in mammalian tooth morphogenesis*. *Development*, 1996. **122**(10): p. 3035-44.
73. Jernvall, J., et al., *The life history of an embryonic signaling center: BMP-4 induces p21 and is associated with apoptosis in the mouse tooth enamel knot*. *Development*, 1998. **125**(2): p. 161-9.
74. Mammoto, T., et al., *Mechanochemical control of mesenchymal condensation and embryonic tooth organ formation*. *Dev Cell*, 2011. **21**(4): p. 758-69.
75. D'Souza, R.N., et al., *Cbfa1 is required for epithelial-mesenchymal interactions regulating tooth development in mice*. *Development*, 1999. **126**(13): p. 2911-20.
76. Otto, F., H. Kanegane, and S. Mundlos, *Mutations in the RUNX2 gene in patients with cleidocranial dysplasia*. *Hum Mutat*, 2002. **19**(3): p. 209-16.
77. Ryoo, H.M. and X.P. Wang, *Control of tooth morphogenesis by Runx2*. *Crit Rev Eukaryot Gene Expr*, 2006. **16**(2): p. 143-54.
78. Aberg, T., et al., *Phenotypic changes in dentition of Runx2 homozygote-null mutant mice*. *J Histochem Cytochem*, 2004. **52**(1): p. 131-9.
79. Aberg, T., et al., *Runx2 mediates FGF signaling from epithelium to mesenchyme during tooth morphogenesis*. *Dev Biol*, 2004. **270**(1): p. 76-93.
80. Kwon, H.J., et al., *Deletion of Osr2 Partially Rescues Tooth Development in Runx2 Mutant Mice*. *J Dent Res*, 2015. **94**(8): p. 1113-9.
81. Yi, R., et al., *Morphogenesis in skin is governed by discrete sets of differentially expressed microRNAs*. *Nat Genet*, 2006. **38**(3): p. 356-62.
82. Yi, R., et al., *A skin microRNA promotes differentiation by repressing 'stemness'*. *Nature*, 2008. **452**(7184): p. 225-9.
83. Andl, T., et al., *The miRNA-processing enzyme dicer is essential for the morphogenesis and maintenance of hair follicles*. *Curr Biol*, 2006. **16**(10): p. 1041-9.
84. Cao, H., et al., *MicroRNAs play a critical role in tooth development*. *J Dent Res*, 2010. **89**(8): p. 779-84.

85. Jevnaker, A.M. and H. Osmundsen, *MicroRNA expression profiling of the developing murine molar tooth germ and the developing murine submandibular salivary gland*. Arch Oral Biol, 2008. **53**(7): p. 629-45.
86. Michon, F., et al., *Tooth morphogenesis and ameloblast differentiation are regulated by micro-RNAs*. Dev Biol, 2010. **340**(2): p. 355-68.
87. Jheon, A.H., et al., *Expression of microRNAs in the stem cell niche of the adult mouse incisor*. PLoS One, 2011. **6**(9): p. e24536.
88. Kawahara, Y., *Human diseases caused by germline and somatic abnormalities in microRNA and microRNA-related genes*. Congenit Anom (Kyoto), 2014. **54**(1): p. 12-21.
89. Vainio, S., et al., *Identification of BMP-4 as a signal mediating secondary induction between epithelial and mesenchymal tissues during early tooth development*. Cell, 1993. **75**(1): p. 45-58.
90. Nie, X., K. Luukko, and P. Kettunen, *BMP signalling in craniofacial development*. Int J Dev Biol, 2006. **50**(6): p. 511-21.
91. Morrell, N.W., et al., *Targeting BMP signalling in cardiovascular disease and anaemia*. Nat Rev Cardiol, 2016. **13**(2): p. 106-20.
92. Salazar, V.S., L.W. Gamer, and V. Rosen, *BMP signalling in skeletal development, disease and repair*. Nat Rev Endocrinol, 2016. **12**(4): p. 203-21.
93. ten Dijke, P. and H.M. Arthur, *Extracellular control of TGFbeta signalling in vascular development and disease*. Nat Rev Mol Cell Biol, 2007. **8**(11): p. 857-69.
94. Andl, T., et al., *Epithelial Bmpr1a regulates differentiation and proliferation in postnatal hair follicles and is essential for tooth development*. Development, 2004. **131**(10): p. 2257-68.
95. Ferguson, C.A., et al., *Activin is an essential early mesenchymal signal in tooth development that is required for patterning of the murine dentition*. Genes Dev, 1998. **12**(16): p. 2636-49.
96. Li, L., et al., *Bmpr1a is required in mesenchymal tissue and has limited redundant function with Bmpr1b in tooth and palate development*. Dev Biol, 2011. **349**(2): p. 451-61.
97. Wang, Y., et al., *BMP activity is required for tooth development from the lamina to bud stage*. J Dent Res, 2012. **91**(7): p. 690-5.
98. Tucker, A.S., K.L. Matthews, and P.T. Sharpe, *Transformation of tooth type induced by inhibition of BMP signaling*. Science, 1998. **282**(5391): p. 1136-8.
99. Plikus, M.V., et al., *Morphoregulation of teeth: modulating the number, size, shape and differentiation by tuning Bmp activity*. Evol Dev, 2005. **7**(5): p. 440-57.
100. Kavanagh, K.D., A.R. Evans, and J. Jernvall, *Predicting evolutionary patterns of mammalian teeth from development*. Nature, 2007. **449**(7161): p. 427-32.
101. Kantaputra, P.N., et al., *GREMLIN 2 Mutations and Dental Anomalies*. J Dent Res, 2015. **94**(12): p. 1646-52.
102. Vogel, P., et al., *Malformation of incisor teeth in Grem2^{-/-} mice*. Vet Pathol, 2015. **52**(1): p. 224-9.
103. Chen, S., et al., *Bone morphogenetic protein 2 mediates dentin sialophosphoprotein expression and odontoblast differentiation via NF-Y signaling*. J Biol Chem, 2008. **283**(28): p. 19359-70.
104. Li, J., et al., *SMAD4-mediated WNT signaling controls the fate of cranial neural crest cells during tooth morphogenesis*. Development, 2011. **138**(10): p. 1977-89.
105. Wang, X.P., et al., *Follistatin regulates enamel patterning in mouse incisors by asymmetrically inhibiting BMP signaling and ameloblast differentiation*. Dev Cell, 2004. **7**(5): p. 719-30.

106. Wang, X.P., et al., *An integrated gene regulatory network controls stem cell proliferation in teeth*. PLoS Biol, 2007. **5**(6): p. e159.
107. Wan, M. and X. Cao, *BMP signaling in skeletal development*. Biochem Biophys Res Commun, 2005. **328**(3): p. 651-7.
108. Huang, X.F. and Y. Chai, *TGF- β signalling and tooth development*. Chin J Dent Res, 2010. **13**(1): p. 7-15.
109. Klopčič, B., et al., *TGF-beta superfamily signaling is essential for tooth and hair morphogenesis and differentiation*. Eur J Cell Biol, 2007. **86**(11-12): p. 781-99.
110. Lesot, H., et al., *Epigenetic signals during odontoblast differentiation*. Adv Dent Res, 2001. **15**: p. 8-13.
111. Chen, G., C. Deng, and Y.P. Li, *TGF- β and BMP signaling in osteoblast differentiation and bone formation*. Int J Biol Sci, 2012. **8**(2): p. 272-88.
112. Haruyama, N., et al., *Overexpression of transforming growth factor-beta1 in teeth results in detachment of ameloblasts and enamel defects*. Eur J Oral Sci, 2006. **114 Suppl 1**: p. 30-4; discussion 39-41, 379.
113. Chai, Y., et al., *Inhibition of transforming growth factor-beta type II receptor signaling accelerates tooth formation in mouse first branchial arch explants*. Mech Dev, 1999. **86**(1-2): p. 63-74.
114. Cho, A., et al., *TGF- β regulates enamel mineralization and maturation through KLK4 expression*. PLoS One, 2013. **8**(11): p. e82267.
115. Yokozeki, M., et al., *Smad3 is required for enamel biomineralization*. Biochem Biophys Res Commun, 2003. **305**(3): p. 684-90.
116. Thyagarajan, T., et al., *Reduced expression of dentin sialophosphoprotein is associated with dysplastic dentin in mice overexpressing transforming growth factor-beta 1 in teeth*. J Biol Chem, 2001. **276**(14): p. 11016-20.
117. Saeki, K., et al., *Elevated TGF-beta2 signaling in dentin results in sex related enamel defects*. Arch Oral Biol, 2007. **52**(9): p. 814-21.
118. Kubickova, L., et al., *TGF-beta - an excellent servant but a bad master*. J Transl Med, 2012. **10**: p. 183.
119. Todorovic, V. and D.B. Rifkin, *LTBPs, more than just an escort service*. J Cell Biochem, 2012. **113**(2): p. 410-8.
120. Li, X., et al., *Mapping of human and murine genes for latent TGF-beta binding protein-2 (LTBP2)*. Mamm Genome, 1995. **6**(1): p. 42-5.
121. Yin, W., et al., *Isolation of a novel latent transforming growth factor-beta binding protein gene (LTBP-3)*. J Biol Chem, 1995. **270**(17): p. 10147-60.
122. Dabovic, B., et al., *Bone abnormalities in latent TGF-[beta] binding protein (Ltbp)-3-null mice indicate a role for Ltbp-3 in modulating TGF-[beta] bioavailability*. J Cell Biol, 2002. **156**(2): p. 227-32.
123. Drews, F., et al., *Disruption of the latent transforming growth factor-beta binding protein-1 gene causes alteration in facial structure and influences TGF-beta bioavailability*. Biochim Biophys Acta, 2008. **1783**(1): p. 34-48.
124. Cheung, C.L., et al., *Identification of LTBP2 on chromosome 14q as a novel candidate gene for bone mineral density variation and fracture risk association*. J Clin Endocrinol Metab, 2008. **93**(11): p. 4448-55.
125. Urban, Z., et al., *Mutations in LTBP4 cause a syndrome of impaired pulmonary, gastrointestinal, genitourinary, musculoskeletal, and dermal development*. Am J Hum Genet, 2009. **85**(5): p. 593-605.
126. Kubickova, L., et al., *TGF- β - an excellent servant but a bad master*. J Transl Med, 2012. **10**: p. 183.

127. Noor, A., et al., *Oligodontia is caused by mutation in LTBP3, the gene encoding latent TGF-beta binding protein 3*. Am J Hum Genet, 2009. **84**(4): p. 519-23.
128. Dugan, S.L., et al., *New recessive truncating mutation in LTBP3 in a family with oligodontia, short stature, and mitral valve prolapse*. Am J Med Genet A, 2015. **167**(6): p. 1396-9.
129. Huckert, M., et al., *Mutations in the latent TGF-beta binding protein 3 (LTBP3) gene cause brachyolmia with amelogenesis imperfecta*. Hum Mol Genet, 2015. **24**(11): p. 3038-49.
130. Morkmued, S., et al., *Enamel and dental anomalies in latent-transforming growth factor beta-binding protein 3 mutant mice*. Eur J Oral Sci, 2017. **125**(1): p. 8-17.
131. Ornitz, D.M. and N. Itoh, *The Fibroblast Growth Factor signaling pathway*. Wiley Interdiscip Rev Dev Biol, 2015. **4**(3): p. 215-66.
132. Ornitz, D.M. and P.J. Marie, *Fibroblast growth factor signaling in skeletal development and disease*. Genes Dev, 2015. **29**(14): p. 1463-86.
133. Corn, P.G., et al., *Targeting fibroblast growth factor pathways in prostate cancer*. Clin Cancer Res, 2013. **19**(21): p. 5856-66.
134. Trumpp, A., et al., *Cre-mediated gene inactivation demonstrates that FGF8 is required for cell survival and patterning of the first branchial arch*. Genes Dev, 1999. **13**(23): p. 3136-48.
135. De Moerlooze, L., et al., *An important role for the IIIb isoform of fibroblast growth factor receptor 2 (FGFR2) in mesenchymal-epithelial signalling during mouse organogenesis*. Development, 2000. **127**(3): p. 483-92.
136. Jernvall, J., et al., *Evidence for the role of the enamel knot as a control center in mammalian tooth cusp formation: non-dividing cells express growth stimulating Fgf-4 gene*. Int J Dev Biol, 1994. **38**(3): p. 463-9.
137. Kettunen, P., I. Karavanova, and I. Thesleff, *Responsiveness of developing dental tissues to fibroblast growth factors: expression of splicing alternatives of FGFR1, -2, -3, and of FGFR4; and stimulation of cell proliferation by FGF-2, -4, -8, and -9*. Dev Genet, 1998. **22**(4): p. 374-85.
138. Harada, H., et al., *FGF10 maintains stem cell compartment in developing mouse incisors*. Development, 2002. **129**(6): p. 1533-41.
139. Jackman, W.R., B.W. Draper, and D.W. Stock, *Fgf signaling is required for zebrafish tooth development*. Dev Biol, 2004. **274**(1): p. 139-57.
140. Klein, O.D., et al., *An FGF signaling loop sustains the generation of differentiated progeny from stem cells in mouse incisors*. Development, 2008. **135**(2): p. 377-85.
141. Klein, O.D., et al., *Sprouty genes control diastema tooth development via bidirectional antagonism of epithelial-mesenchymal FGF signaling*. Dev Cell, 2006. **11**(2): p. 181-90.
142. Marangoni, P., et al., *Phenotypic and evolutionary implications of modulating the ERK-MAPK cascade using the dentition as a model*. Sci Rep, 2015. **5**: p. 11658.
143. Charles, C., et al., *Regulation of tooth number by fine-tuning levels of receptor-tyrosine kinase signaling*. Development, 2011. **138**(18): p. 4063-73.
144. Tauriello, D.V., et al., *Wnt/ β -catenin signaling requires interaction of the Dishevelled DEP domain and C terminus with a discontinuous motif in Frizzled*. Proc Natl Acad Sci U S A, 2012. **109**(14): p. E812-20.
145. Baron, R. and M. Kneissel, *WNT signaling in bone homeostasis and disease: from human mutations to treatments*. Nat Med, 2013. **19**(2): p. 179-92.
146. Järvinen, E., et al., *Continuous tooth generation in mouse is induced by activated epithelial Wnt/ β -catenin signaling*. Proc Natl Acad Sci U S A, 2006. **103**(49): p. 18627-32.

147. Nakamura, T., et al., *Transcription factor epiprofin is essential for tooth morphogenesis by regulating epithelial cell fate and tooth number*. J Biol Chem, 2008. **283**(8): p. 4825-33.
148. Wang, X.P., et al., *Apc inhibition of Wnt signaling regulates supernumerary tooth formation during embryogenesis and throughout adulthood*. Development, 2009. **136**(11): p. 1939-49.
149. Liu, F., et al., *beta-Catenin initiates tooth neogenesis in adult rodent incisors*. J Dent Res, 2010. **89**(9): p. 909-14.
150. Liu, F., et al., *Wnt/beta-catenin signaling directs multiple stages of tooth morphogenesis*. Dev Biol, 2008. **313**(1): p. 210-24.
151. Zhou, P., et al., *Lymphoid enhancer factor 1 directs hair follicle patterning and epithelial cell fate*. Genes Dev, 1995. **9**(6): p. 700-13.
152. Kuraguchi, M., et al., *Adenomatous polyposis coli (APC) is required for normal development of skin and thymus*. PLoS Genet, 2006. **2**(9): p. e146.
153. Ahn, Y., et al., *Inhibition of Wnt signaling by Wise (Sostdc1) and negative feedback from Shh controls tooth number and patterning*. Development, 2010. **137**(19): p. 3221-31.
154. Murashima-Suginami, A., et al., *Rudiment incisors survive and erupt as supernumerary teeth as a result of USAG-1 abrogation*. Biochem Biophys Res Commun, 2007. **359**(3): p. 549-55.
155. Lammi, L., et al., *Mutations in AXIN2 cause familial tooth agenesis and predispose to colorectal cancer*. Am J Hum Genet, 2004. **74**(5): p. 1043-50.
156. Bohring, A., et al., *WNT10A mutations are a frequent cause of a broad spectrum of ectodermal dysplasias with sex-biased manifestation pattern in heterozygotes*. Am J Hum Genet, 2009. **85**(1): p. 97-105.
157. Tardieu, C., et al., *Dental and extra-oral clinical features in 41 patients with WNT10A gene mutations: A multicentric genotype-phenotype study*. Clin Genet, 2017.
158. Courtney, J.M., J. Blackburn, and P.T. Sharpe, *The Ectodysplasin and NFkappaB signalling pathways in odontogenesis*. Arch Oral Biol, 2005. **50**(2): p. 159-63.
159. Mikkola, M.L., *TNF superfamily in skin appendage development*. Cytokine Growth Factor Rev, 2008. **19**(3-4): p. 219-30.
160. Lefebvre, S. and M.L. Mikkola, *Ectodysplasin research--where to next?* Semin Immunol, 2014. **26**(3): p. 220-8.
161. Kere, J., et al., *X-linked anhidrotic (hypohidrotic) ectodermal dysplasia is caused by mutation in a novel transmembrane protein*. Nat Genet, 1996. **13**(4): p. 409-16.
162. Pispas, J., et al., *Cusp patterning defect in Tabby mouse teeth and its partial rescue by FGF*. Dev Biol, 1999. **216**(2): p. 521-34.
163. Ohazama, A., et al., *Traf6 is essential for murine tooth cusp morphogenesis*. Dev Dyn, 2004. **229**(1): p. 131-5.
164. Tucker, A.S., et al., *Edar/Eda interactions regulate enamel knot formation in tooth morphogenesis*. Development, 2000. **127**(21): p. 4691-700.
165. Charles, C., et al., *Effect of eda loss of function on upper jugal tooth morphology*. Anat Rec (Hoboken), 2009. **292**(2): p. 299-308.
166. Doffinger, R., et al., *X-linked anhidrotic ectodermal dysplasia with immunodeficiency is caused by impaired NF-kappaB signaling*. Nat Genet, 2001. **27**(3): p. 277-85.
167. Sofaer, J.A., *The teeth of the "sleek" mouse*. Arch Oral Biol, 1977. **22**(4): p. 299-301.
168. Mustonen, T., et al., *Stimulation of ectodermal organ development by Ectodysplasin-A1*. Dev Biol, 2003. **259**(1): p. 123-36.

169. Tucker, A.S., et al., *The activation level of the TNF family receptor, Edar, determines cusp number and tooth number during tooth development.* Dev Biol, 2004. **268**(1): p. 185-94.
170. Charles, C., et al., *Distinct impacts of Eda and Edar loss of function on the mouse dentition.* PLoS One, 2009. **4**(4): p. e4985.
171. Harris, M.P., et al., *Zebrafish eda and edar mutants reveal conserved and ancestral roles of ectodysplasin signaling in vertebrates.* PLoS Genet, 2008. **4**(10): p. e1000206.
172. Blackburn, J., et al., *Excess NF- κ B induces ectopic odontogenesis in embryonic incisor epithelium.* J Dent Res, 2015. **94**(1): p. 121-8.
173. Li, J., et al., *Effects of canonical NF- κ B signaling pathway on the proliferation and odonto/osteogenic differentiation of human stem cells from apical papilla.* Biomed Res Int, 2014. **2014**: p. 319651.
174. Shiotani, A., Y. Shibasaki, and T. Sasaki, *Localization of receptor activator of NFkappaB ligand, RANKL, in periodontal tissues during experimental movement of rat molars.* J Electron Microsc (Tokyo), 2001. **50**(4): p. 365-9.
175. Zuo, J., et al., *Nuclear factor kappaB p65 phosphorylation in orthodontic tooth movement.* J Dent Res, 2007. **86**(6): p. 556-9.
176. Marigo, V., et al., *Cloning, expression, and chromosomal location of SHH and IHH: two human homologues of the Drosophila segment polarity gene hedgehog.* Genomics, 1995. **28**(1): p. 44-51.
177. Bitgood, M.J. and A.P. McMahon, *Hedgehog and Bmp genes are coexpressed at many diverse sites of cell-cell interaction in the mouse embryo.* Dev Biol, 1995. **172**(1): p. 126-38.
178. Hardcastle, Z., et al., *The Shh signalling pathway in tooth development: defects in Gli2 and Gli3 mutants.* Development, 1998. **125**(15): p. 2803-11.
179. Dassule, H.R. and A.P. McMahon, *Analysis of epithelial-mesenchymal interactions in the initial morphogenesis of the mammalian tooth.* Dev Biol, 1998. **202**(2): p. 215-27.
180. Malhotra, G.K., et al., *Shared signaling pathways in normal and breast cancer stem cells.* J Carcinog, 2011. **10**: p. 38.
181. Cobourne, M.T., Z. Hardcastle, and P.T. Sharpe, *Sonic hedgehog regulates epithelial proliferation and cell survival in the developing tooth germ.* J Dent Res, 2001. **80**(11): p. 1974-9.
182. Peterková, R., et al., *Development of the vestigial tooth primordia as part of mouse odontogenesis.* Connect Tissue Res, 2002. **43**(2-3): p. 120-8.
183. Turecková, J., et al., *Apoptosis is involved in the disappearance of the diastemal dental primordia in mouse embryo.* Int J Dev Biol, 1996. **40**(2): p. 483-9.
184. Cobourne, M.T., I. Miletich, and P.T. Sharpe, *Restriction of sonic hedgehog signalling during early tooth development.* Development, 2004. **131**(12): p. 2875-85.
185. Prochazka, J., et al., *Patterning by heritage in mouse molar row development.* Proc Natl Acad Sci U S A, 2010. **107**(35): p. 15497-502.
186. Jackman, W.R., J.J. Yoo, and D.W. Stock, *Hedgehog signaling is required at multiple stages of zebrafish tooth development.* BMC Dev Biol, 2010. **10**: p. 119.
187. Sarkar, L., et al., *Wnt/Shh interactions regulate ectodermal boundary formation during mammalian tooth development.* Proc Natl Acad Sci U S A, 2000. **97**(9): p. 4520-4.
188. Dassule, H.R., et al., *Sonic hedgehog regulates growth and morphogenesis of the tooth.* Development, 2000. **127**(22): p. 4775-85.
189. Gritli-Linde, A., et al., *Shh signaling within the dental epithelium is necessary for cell proliferation, growth and polarization.* Development, 2002. **129**(23): p. 5323-37.

190. Cho, S.W., et al., *Interactions between Shh, Sostdc1 and Wnt signaling and a new feedback loop for spatial patterning of the teeth*. *Development*, 2011. **138**(9): p. 1807-16.
191. Mitsiadis, T.A., et al., *BMPs and FGFs target Notch signalling via jagged 2 to regulate tooth morphogenesis and cytodifferentiation*. *Development*, 2010. **137**(18): p. 3025-35.
192. Harada, H., et al., *Stratum intermedium lineage diverges from ameloblast lineage via Notch signaling*. *Biochem Biophys Res Commun*, 2006. **340**(2): p. 611-6.
193. Balmer, J.E. and R. Blomhoff, *Gene expression regulation by retinoic acid*. *J Lipid Res*, 2002. **43**(11): p. 1773-808.
194. Maden, M., *Retinoic acid in the development, regeneration and maintenance of the nervous system*. *Nat Rev Neurosci*, 2007. **8**(10): p. 755-65.
195. Metzler, M.A. and L.L. Sandell, *Enzymatic Metabolism of Vitamin A in Developing Vertebrate Embryos*. *Nutrients*, 2016. **8**(12).
196. Thielitz, A., et al., *Topical retinoids in acne--an evidence-based overview*. *J Dtsch Dermatol Ges*, 2008. **6**(12): p. 1023-31.
197. Pechère, M., et al., *Antibacterial activity of retinaldehyde against Propionibacterium acnes*. *Dermatology*, 1999. **199 Suppl 1**: p. 29-31.
198. Coombs, C.C., M. Tavakkoli, and M.S. Tallman, *Acute promyelocytic leukemia: where did we start, where are we now, and the future*. *Blood Cancer J*, 2015. **5**: p. e304.
199. Lo-Coco, F., et al., *Retinoic acid and arsenic trioxide for acute promyelocytic leukemia*. *N Engl J Med*, 2013. **369**(2): p. 111-21.
200. Das, B.C., et al., *Retinoic acid signaling pathways in development and diseases*. *Bioorg Med Chem*, 2014. **22**(2): p. 673-83.
201. Magoulas, G.E., et al., *Syntheses, antiproliferative activity and theoretical characterization of acitretin-type retinoids with changes in the lipophilic part*. *Eur J Med Chem*, 2011. **46**(2): p. 721-37.
202. Wada, A., et al., *Preparation and biological evaluation of 5-substituted retinoic acids*. *Bioorg Med Chem*, 2008. **16**(18): p. 8471-81.
203. Wada, A., et al., *Efficient synthesis and biological evaluation of demethyl geranylgeranoic acid derivatives*. *Bioorg Med Chem*, 2010. **18**(16): p. 5795-806.
204. Patel, J.B., et al., *Novel retinoic acid metabolism blocking agents endowed with multiple biological activities are efficient growth inhibitors of human breast and prostate cancer cells in vitro and a human breast tumor xenograft in nude mice*. *J Med Chem*, 2004. **47**(27): p. 6716-29.
205. Long, B., et al., *Synthesis, characterization and in vitro antiproliferative activities of new 13-cis-retinoyl ferrocene derivatives*. *Eur J Med Chem*, 2009. **44**(6): p. 2572-6.
206. Gediya, L.K., et al., *Design, synthesis, and evaluation of novel mutual prodrugs (hybrid drugs) of all-trans-retinoic acid and histone deacetylase inhibitors with enhanced anticancer activities in breast and prostate cancer cells in vitro*. *J Med Chem*, 2008. **51**(13): p. 3895-904.
207. Gurkan-Alp, A.S., et al., *Synthesis, anticancer activities and molecular modeling studies of novel indole retinoid derivatives*. *Eur J Med Chem*, 2012. **58**: p. 346-54.
208. Mizuno, C.S., et al., *Synthesis and biological evaluation of retinoid-chalcones as inhibitors of colon cancer cell growth*. *Bioorg Med Chem Lett*, 2010. **20**(24): p. 7385-7.
209. Sun, S.Y., et al., *Identification of retinamides that are more potent than N-(4-hydroxyphenyl)retinamide in inhibiting growth and inducing apoptosis of human head*

- and neck and lung cancer cells*. *Cancer Epidemiol Biomarkers Prev*, 2001. **10**(6): p. 595-601.
210. Jubinsky, P.T., et al., *Design, synthesis, and biological activity of novel Mags inhibitors*. *Bioorg Med Chem Lett*, 2011. **21**(11): p. 3479-82.
 211. Grunwald, C., *Foliar Fatty Acids and Sterols of Soybean Field Fumigated with SO₂*. *Plant Physiol*, 1981. **68**(4): p. 868-71.
 212. Wang, W., et al., *An imageable retinoid acid derivative to detect human cancer xenografts and study therapeutic dosing to reduce its toxicity*. *Contrast Media Mol Imaging*, 2011. **6**(4): p. 200-8.
 213. Tsuchiya, H., et al., *Retinoids ameliorate insulin resistance in a leptin-dependent manner in mice*. *Hepatology*, 2012. **56**(4): p. 1319-30.
 214. Kawahara, K., et al., *Oral administration of synthetic retinoid Am80 (Tamibarotene) decreases brain beta-amyloid peptides in APP23 mice*. *Biol Pharm Bull*, 2009. **32**(7): p. 1307-9.
 215. Ding, Y., et al., *Retinoic acid attenuates beta-amyloid deposition and rescues memory deficits in an Alzheimer's disease transgenic mouse model*. *J Neurosci*, 2008. **28**(45): p. 11622-34.
 216. Gudas, L.J. and J.A. Wagner, *Retinoids regulate stem cell differentiation*. *J Cell Physiol*, 2011. **226**(2): p. 322-30.
 217. Yokoo, T., A. Fukui, and E. Kobayashi, *Application of regenerative medicine for kidney diseases*. *Organogenesis*, 2007. **3**(1): p. 34-43.
 218. Li, P., M. Pashmfroush, and H.M. Sucov, *Retinoic acid regulates differentiation of the secondary heart field and TGFbeta-mediated outflow tract septation*. *Dev Cell*, 2010. **18**(3): p. 480-5.
 219. Ptaszek, L.M., et al., *Towards regenerative therapy for cardiac disease*. *Lancet*, 2012. **379**(9819): p. 933-42.
 220. Uitto, J., *Regenerative medicine for skin diseases: iPS cells to the rescue*. *J Invest Dermatol*, 2011. **131**(4): p. 812-4.
 221. Osanai, M., *Cellular retinoic acid bioavailability in various pathologies and its therapeutic implication*. *Pathol Int*, 2017. **67**(6): p. 281-291.
 222. Daftarian, N., S. Kiani, and A. Zahabi, *Regenerative therapy for retinal disorders*. *J Ophthalmic Vis Res*, 2010. **5**(4): p. 250-64.
 223. Peng, J. and X. Zeng, *The role of induced pluripotent stem cells in regenerative medicine: neurodegenerative diseases*. *Stem Cell Res Ther*, 2011. **2**(4): p. 32.
 224. Conaway, H.H., P. Henning, and U.H. Lerner, *Vitamin a metabolism, action, and role in skeletal homeostasis*. *Endocr Rev*, 2013. **34**(6): p. 766-97.
 225. Dollé, P. and K. Niederreither, *The Retinoids: Biology, Biochemistry, and Disease*. 2015: Wiley.
 226. Harrison, E.H., *Mechanisms involved in the intestinal absorption of dietary vitamin A and provitamin A carotenoids*. *Biochim Biophys Acta*, 2012. **1821**(1): p. 70-7.
 227. D'Ambrosio, D.N., R.D. Clugston, and W.S. Blaner, *Vitamin A metabolism: an update*. *Nutrients*, 2011. **3**(1): p. 63-103.
 228. Blomhoff, R. and K. Wake, *Perisinusoidal stellate cells of the liver: important roles in retinol metabolism and fibrosis*. *FASEB J*, 1991. **5**(3): p. 271-7.
 229. Blaner, W.S., et al., *Lipoprotein lipase hydrolysis of retinyl ester. Possible implications for retinoid uptake by cells*. *J Biol Chem*, 1994. **269**(24): p. 16559-65.
 230. Blomstrand, R. and B. Werner, *Studies on the intestinal absorption of radioactive beta-carotene and vitamin A in man. Conversion of beta-carotene into vitamin A*. *Scand J Clin Lab Invest*, 1967. **19**(4): p. 339-45.

231. Harrison, E.H. and M.M. Hussain, *Mechanisms involved in the intestinal digestion and absorption of dietary vitamin A*. J Nutr, 2001. **131**(5): p. 1405-8.
232. Cooper, A.D., *Hepatic uptake of chylomicron remnants*. J Lipid Res, 1997. **38**(11): p. 2173-92.
233. Wang, Z., et al., *Retinoic acid regulates morphogenesis and patterning of posterior foregut derivatives*. Dev Biol, 2006. **297**(2): p. 433-45.
234. Episkopou, V., et al., *Disruption of the transthyretin gene results in mice with depressed levels of plasma retinol and thyroid hormone*. Proc Natl Acad Sci U S A, 1993. **90**(6): p. 2375-9.
235. AM, v.B., et al., *Biochemical basis for depressed serum retinol levels in transthyretin-deficient mice*. J Biol Chem, 2001. **276**(2): p. 1107-13.
236. Kawaguchi, R., et al., *A membrane receptor for retinol binding protein mediates cellular uptake of vitamin A*. Science, 2007. **315**(5813): p. 820-5.
237. Wilson, J.G., C.B. Roth, and J. Warkany, *An analysis of the syndrome of malformations induced by maternal vitamin A deficiency. Effects of restoration of vitamin A at various times during gestation*. Am J Anat, 1953. **92**(2): p. 189-217.
238. Mark, M., N.B. Ghyselinck, and P. Chambon, *Function of retinoid nuclear receptors: lessons from genetic and pharmacological dissections of the retinoic acid signaling pathway during mouse embryogenesis*. Annu Rev Pharmacol Toxicol, 2006. **46**: p. 451-80.
239. Kastner, P., et al., *Genetic evidence that the retinoid signal is transduced by heterodimeric RXR/RAR functional units during mouse development*. Development, 1997. **124**(2): p. 313-26.
240. Durston, A.J., et al., *Retinoic acid causes an anteroposterior transformation in the developing central nervous system*. Nature, 1989. **340**(6229): p. 140-4.
241. Simeone, A., et al., *Retinoic acid induces stage-specific antero-posterior transformation of rostral central nervous system*. Mech Dev, 1995. **51**(1): p. 83-98.
242. White, R.J., et al., *Complex regulation of cyp26a1 creates a robust retinoic acid gradient in the zebrafish embryo*. PLoS Biol, 2007. **5**(11): p. e304.
243. Maden, M., *Retinoids and spinal cord development*. J Neurobiol, 2006. **66**(7): p. 726-38.
244. Thaller, C. and G. Eichele, *Identification and spatial distribution of retinoids in the developing chick limb bud*. Nature, 1987. **327**(6123): p. 625-8.
245. Maden, M., *Retinoic acid and limb regeneration--a personal view*. Int J Dev Biol, 2002. **46**(7): p. 883-6.
246. Schneider, R.A., et al., *Local retinoid signaling coordinates forebrain and facial morphogenesis by maintaining FGF8 and SHH*. Development, 2001. **128**(14): p. 2755-67.
247. Halilagic, A., et al., *Retinoids control anterior and dorsal properties in the developing forebrain*. Dev Biol, 2007. **303**(1): p. 362-75.
248. Ribes, V., et al., *Retinaldehyde dehydrogenase 2 (RALDH2)-mediated retinoic acid synthesis regulates early mouse embryonic forebrain development by controlling FGF and sonic hedgehog signaling*. Development, 2006. **133**(2): p. 351-61.
249. Matt, N., et al., *Retinoic acid-dependent eye morphogenesis is orchestrated by neural crest cells*. Development, 2005. **132**(21): p. 4789-800.
250. Molotkov, A., N. Molotkova, and G. Duester, *Retinoic acid guides eye morphogenetic movements via paracrine signaling but is unnecessary for retinal dorsoventral patterning*. Development, 2006. **133**(10): p. 1901-10.
251. Romand, R., P. Dollé, and E. Hashino, *Retinoid signaling in inner ear development*. J Neurobiol, 2006. **66**(7): p. 687-704.

252. Niederreither, K., et al., *Embryonic retinoic acid synthesis is essential for heart morphogenesis in the mouse*. *Development*, 2001. **128**(7): p. 1019-31.
253. Batourina, E., et al., *Vitamin A controls epithelial/mesenchymal interactions through Ret expression*. *Nat Genet*, 2001. **27**(1): p. 74-8.
254. Martín, M., et al., *Dorsal pancreas agenesis in retinoic acid-deficient Raldh2 mutant mice*. *Dev Biol*, 2005. **284**(2): p. 399-411.
255. Bouillet, P., et al., *Developmental expression pattern of Stra6, a retinoic acid-responsive gene encoding a new type of membrane protein*. *Mech Dev*, 1997. **63**(2): p. 173-86.
256. Pasutto, F., et al., *Mutations in STRA6 cause a broad spectrum of malformations including anophthalmia, congenital heart defects, diaphragmatic hernia, alveolar capillary dysplasia, lung hypoplasia, and mental retardation*. *Am J Hum Genet*, 2007. **80**(3): p. 550-60.
257. Niederreither, K. and P. Dollé, *Retinoic acid in development: towards an integrated view*. *Nat Rev Genet*, 2008. **9**(7): p. 541-53.
258. Molotkov, A., et al., *Stimulation of retinoic acid production and growth by ubiquitously expressed alcohol dehydrogenase Adh3*. *Proc Natl Acad Sci U S A*, 2002. **99**(8): p. 5337-42.
259. Sandell, L.L., et al., *RDH10 is essential for synthesis of embryonic retinoic acid and is required for limb, craniofacial, and organ development*. *Genes Dev*, 2007. **21**(9): p. 1113-24.
260. Cammas, L., et al., *Expression of the murine retinol dehydrogenase 10 (Rdh10) gene correlates with many sites of retinoid signalling during embryogenesis and organ differentiation*. *Dev Dyn*, 2007. **236**(10): p. 2899-908.
261. Dupé, V., et al., *A newborn lethal defect due to inactivation of retinaldehyde dehydrogenase type 3 is prevented by maternal retinoic acid treatment*. *Proc Natl Acad Sci U S A*, 2003. **100**(24): p. 14036-41.
262. Niederreither, K., et al., *Embryonic retinoic acid synthesis is essential for early mouse post-implantation development*. *Nat Genet*, 1999. **21**(4): p. 444-8.
263. Rossant, J., et al., *Expression of a retinoic acid response element-hsplacZ transgene defines specific domains of transcriptional activity during mouse embryogenesis*. *Genes Dev*, 1991. **5**(8): p. 1333-44.
264. Haskell, G.T. and A.S. LaMantia, *Retinoic acid signaling identifies a distinct precursor population in the developing and adult forebrain*. *J Neurosci*, 2005. **25**(33): p. 7636-47.
265. Niederreither, K., et al., *Restricted expression and retinoic acid-induced downregulation of the retinaldehyde dehydrogenase type 2 (RALDH-2) gene during mouse development*. *Mech Dev*, 1997. **62**(1): p. 67-78.
266. Mic, F.A., et al., *Novel retinoic acid generating activities in the neural tube and heart identified by conditional rescue of Raldh2 null mutant mice*. *Development*, 2002. **129**(9): p. 2271-82.
267. Mic, F.A., I.O. Sirbu, and G. Duester, *Retinoic acid synthesis controlled by Raldh2 is required early for limb bud initiation and then later as a proximodistal signal during apical ectodermal ridge formation*. *J Biol Chem*, 2004. **279**(25): p. 26698-706.
268. Niederreither, K., et al., *Retinoic acid synthesis and hindbrain patterning in the mouse embryo*. *Development*, 2000. **127**(1): p. 75-85.
269. Niederreither, K., et al., *Embryonic retinoic acid synthesis is required for forelimb growth and anteroposterior patterning in the mouse*. *Development*, 2002. **129**(15): p. 3563-74.

270. Sirbu, I.O. and G. Duyster, *Retinoic-acid signalling in node ectoderm and posterior neural plate directs left-right patterning of somitic mesoderm*. *Nat Cell Biol*, 2006. **8**(3): p. 271-7.
271. Vermot, J., et al., *Retinoic acid controls the bilateral symmetry of somite formation in the mouse embryo*. *Science*, 2005. **308**(5721): p. 563-6.
272. Gale, E., M. Zile, and M. Maden, *Hindbrain respecification in the retinoid-deficient quail*. *Mech Dev*, 1999. **89**(1-2): p. 43-54.
273. Vermot, J. and O. Pourquié, *Retinoic acid coordinates somitogenesis and left-right patterning in vertebrate embryos*. *Nature*, 2005. **435**(7039): p. 215-20.
274. White, J.A., et al., *Identification of the retinoic acid-inducible all-trans-retinoic acid 4-hydroxylase*. *J Biol Chem*, 1996. **271**(47): p. 29922-7.
275. MacLean, G., et al., *Cloning of a novel retinoic-acid metabolizing cytochrome P450, Cyp26B1, and comparative expression analysis with Cyp26A1 during early murine development*. *Mech Dev*, 2001. **107**(1-2): p. 195-201.
276. Tahayato, A., P. Dollé, and M. Petkovich, *Cyp26C1 encodes a novel retinoic acid-metabolizing enzyme expressed in the hindbrain, inner ear, first branchial arch and tooth buds during murine development*. *Gene Expr Patterns*, 2003. **3**(4): p. 449-54.
277. Niederreither, K., et al., *Genetic evidence that oxidative derivatives of retinoic acid are not involved in retinoid signaling during mouse development*. *Nat Genet*, 2002. **31**(1): p. 84-8.
278. Abu-Abed, S., et al., *The retinoic acid-metabolizing enzyme, CYP26A1, is essential for normal hindbrain patterning, vertebral identity, and development of posterior structures*. *Genes Dev*, 2001. **15**(2): p. 226-40.
279. Sakai, Y., et al., *The retinoic acid-inactivating enzyme CYP26 is essential for establishing an uneven distribution of retinoic acid along the antero-posterior axis within the mouse embryo*. *Genes Dev*, 2001. **15**(2): p. 213-25.
280. Yashiro, K., et al., *Regulation of retinoic acid distribution is required for proximodistal patterning and outgrowth of the developing mouse limb*. *Dev Cell*, 2004. **6**(3): p. 411-22.
281. Duyster, G., *Retinoic acid synthesis and signaling during early organogenesis*. *Cell*, 2008. **134**(6): p. 921-31.
282. Raverdeau, M., et al., *Retinoic acid induces Sertoli cell paracrine signals for spermatogonia differentiation but cell autonomously drives spermatocyte meiosis*. *Proc Natl Acad Sci U S A*, 2012. **109**(41): p. 16582-7.
283. Kurokawa, R., et al., *Polarity-specific activities of retinoic acid receptors determined by a co-repressor*. *Nature*, 1995. **377**(6548): p. 451-4.
284. Chen, J.D. and R.M. Evans, *A transcriptional co-repressor that interacts with nuclear hormone receptors*. *Nature*, 1995. **377**(6548): p. 454-7.
285. Weston, A.D., B. Blumberg, and T.M. Underhill, *Active repression by unliganded retinoid receptors in development: less is sometimes more*. *J Cell Biol*, 2003. **161**(2): p. 223-8.
286. Janesick, A., et al., *Active repression by RAR γ signaling is required for vertebrate axial elongation*. *Development*, 2014. **141**(11): p. 2260-70.
287. Nagy, L., et al., *Nuclear receptor repression mediated by a complex containing SMRT, mSin3A, and histone deacetylase*. *Cell*, 1997. **89**(3): p. 373-80.
288. Jepsen, K., et al., *Combinatorial roles of the nuclear receptor corepressor in transcription and development*. *Cell*, 2000. **102**(6): p. 753-63.
289. Gillespie, R.F. and L.J. Gudas, *Retinoid regulated association of transcriptional co-regulators and the polycomb group protein SUZ12 with the retinoic acid response*

- elements of Hoxa1, RARbeta(2), and Cyp26A1 in F9 embryonal carcinoma cells.* J Mol Biol, 2007. **372**(2): p. 298-316.
290. McInerney, E.M., et al., *Determinants of coactivator LXXLL motif specificity in nuclear receptor transcriptional activation.* Genes Dev, 1998. **12**(21): p. 3357-68.
291. Kashyap, V. and L.J. Gudas, *Epigenetic regulatory mechanisms distinguish retinoic acid-mediated transcriptional responses in stem cells and fibroblasts.* J Biol Chem, 2010. **285**(19): p. 14534-48.
292. Rochel, N., et al., *Common architecture of nuclear receptor heterodimers on DNA direct repeat elements with different spacings.* Nat Struct Mol Biol, 2011. **18**(5): p. 564-70.
293. Kumar, S. and G. Duester, *Retinoic acid controls body axis extension by directly repressing Fgf8 transcription.* Development, 2014. **141**(15): p. 2972-7.
294. Studer, M., et al., *Role of a conserved retinoic acid response element in rhombomere restriction of Hoxb-1.* Science, 1994. **265**(5179): p. 1728-32.
295. Umesono, K., et al., *Direct repeats as selective response elements for the thyroid hormone, retinoic acid, and vitamin D3 receptors.* Cell, 1991. **65**(7): p. 1255-66.
296. Predki, P.F., et al., *Ordered binding of retinoic acid and retinoid-X receptors to asymmetric response elements involves determinants adjacent to the DNA-binding domain.* Mol Endocrinol, 1994. **8**(1): p. 31-9.
297. Moutier, E., et al., *Retinoic acid receptors recognize the mouse genome through binding elements with diverse spacing and topology.* J Biol Chem, 2012. **287**(31): p. 26328-41.
298. Balmer, J.E. and R. Blomhoff, *A robust characterization of retinoic acid response elements based on a comparison of sites in three species.* J Steroid Biochem Mol Biol, 2005. **96**(5): p. 347-54.
299. Phan, T.Q., M.M. Jow, and M.L. Privalsky, *DNA recognition by thyroid hormone and retinoic acid receptors: 3,4,5 rule modified.* Mol Cell Endocrinol, 2010. **319**(1-2): p. 88-98.
300. Cunningham, T.J. and G. Duester, *Mechanisms of retinoic acid signalling and its roles in organ and limb development.* Nat Rev Mol Cell Biol, 2015. **16**(2): p. 110-23.
301. Rochette-Egly, C. and P. Germain, *Dynamic and combinatorial control of gene expression by nuclear retinoic acid receptors (RARs).* Nucl Recept Signal, 2009. **7**: p. e005.
302. Mic, F.A., et al., *Retinoid activation of retinoic acid receptor but not retinoid X receptor is sufficient to rescue lethal defect in retinoic acid synthesis.* Proc Natl Acad Sci U S A, 2003. **100**(12): p. 7135-40.
303. Chawla, A., et al., *Nuclear receptors and lipid physiology: opening the X-files.* Science, 2001. **294**(5548): p. 1866-70.
304. Dollé, P., *Developmental expression of retinoic acid receptors (RARs).* Nucl Recept Signal, 2009. **7**: p. e006.
305. Mark, M., N.B. Ghyselinck, and P. Chambon, *Function of retinoic acid receptors during embryonic development.* Nucl Recept Signal, 2009. **7**: p. e002.
306. Mahony, S., et al., *Ligand-dependent dynamics of retinoic acid receptor binding during early neurogenesis.* Genome Biol, 2011. **12**(1): p. R2.
307. Marshall, H., et al., *Retinoids and Hox genes.* FASEB J, 1996. **10**(9): p. 969-78.
308. Rhinn, M. and P. Dollé, *Retinoic acid signalling during development.* Development, 2012. **139**(5): p. 843-58.
309. Niewiadomska-Cimicka, A., et al., *Genome-wide Analysis of RAR β Transcriptional Targets in Mouse Striatum Links Retinoic Acid Signaling with Huntington's Disease and Other Neurodegenerative Disorders.* Mol Neurobiol, 2017. **54**(5): p. 3859-3878.

310. Humphrey, J.H., K.P. West, and A. Sommer, *Vitamin A deficiency and attributable mortality among under-5-year-olds*. Bull World Health Organ, 1992. **70**(2): p. 225-32.
311. Peck, G.L., et al., *Prolonged remissions of cystic and conglobate acne with 13-cis-retinoic acid*. N Engl J Med, 1979. **300**(7): p. 329-33.
312. Siddikuzzaman, C. Guruvayoorappan, and V.M. Berlin Grace, *All trans retinoic acid and cancer*. Immunopharmacol Immunotoxicol, 2011. **33**(2): p. 241-9.
313. Furr, H.C., et al., *Vitamin A concentrations in liver determined by isotope dilution assay with tetradeuterated vitamin A and by biopsy in generally healthy adult humans*. Am J Clin Nutr, 1989. **49**(4): p. 713-6.
314. Ballew, C., et al., *Serum retinol distributions in residents of the United States: third National Health and Nutrition Examination Survey, 1988-1994*. Am J Clin Nutr, 2001. **73**(3): p. 586-93.
315. Gillespie, C., et al., *Intraindividual variation in serum retinol concentrations among participants in the third National Health and Nutrition Examination Survey, 1988-1994*. Am J Clin Nutr, 2004. **79**(4): p. 625-32.
316. Tanumihardjo, S.A., *Vitamin A: biomarkers of nutrition for development*. Am J Clin Nutr, 2011. **94**(2): p. 658S-65S.
317. Penniston, K.L. and S.A. Tanumihardjo, *The acute and chronic toxic effects of vitamin A*. Am J Clin Nutr, 2006. **83**(2): p. 191-201.
318. Croquet, V., et al., *Hepatic hyper-vitaminosis A: importance of retinyl ester level determination*. Eur J Gastroenterol Hepatol, 2000. **12**(3): p. 361-4.
319. Krasinski, S.D., et al., *Relationship of vitamin A and vitamin E intake to fasting plasma retinol, retinol-binding protein, retinyl esters, carotene, alpha-tocopherol, and cholesterol among elderly people and young adults: increased plasma retinyl esters among vitamin A-supplement users*. Am J Clin Nutr, 1989. **49**(1): p. 112-20.
320. Ballew, C., et al., *Serum retinyl esters are not associated with biochemical markers of liver dysfunction in adult participants in the third National Health and Nutrition Examination Survey (NHANES III), 1988--1994*. Am J Clin Nutr, 2001. **73**(5): p. 934-40.
321. Hollander, D. and V. Dadufalza, *Influence of aging on vitamin A transport into the lymphatic circulation*. Exp Gerontol, 1990. **25**(1): p. 61-5.
322. Olson, J.A., *Hypovitaminosis A: contemporary scientific issues*. J Nutr, 1994. **124**(8 Suppl): p. 1461S-1466S.
323. Lascari, A.D., *Carotenemia. A review*. Clin Pediatr (Phila), 1981. **20**(1): p. 25-9.
324. Morkmued, S., et al., *Retinoic Acid Excess Impairs Amelogenesis Inducing Enamel Defects*. Front Physiol, 2016. **7**: p. 673.
325. Nallamshetty, S., et al., *Deficiency of retinaldehyde dehydrogenase 1 induces BMP2 and increases bone mass in vivo*. PLoS One, 2013. **8**(8): p. e71307.
326. Feskanich, D., et al., *Vitamin A intake and hip fractures among postmenopausal women*. JAMA, 2002. **287**(1): p. 47-54.
327. Michaëlsson, K., et al., *Serum retinol levels and the risk of fracture*. N Engl J Med, 2003. **348**(4): p. 287-94.
328. Forsmo, S., S.K. Fjeldbo, and A. Langhammer, *Childhood cod liver oil consumption and bone mineral density in a population-based cohort of peri- and postmenopausal women: the Nord-Trøndelag Health Study*. Am J Epidemiol, 2008. **167**(4): p. 406-11.
329. Lim, L.S., et al., *Vitamin A intake and the risk of hip fracture in postmenopausal women: the Iowa Women's Health Study*. Osteoporos Int, 2004. **15**(7): p. 552-9.
330. Macdonald, H.M., et al., *Nutritional associations with bone loss during the menopausal transition: evidence of a beneficial effect of calcium, alcohol, and fruit*

- and vegetable nutrients and of a detrimental effect of fatty acids.* Am J Clin Nutr, 2004. **79**(1): p. 155-65.
331. Melhus, H., et al., *Excessive dietary intake of vitamin A is associated with reduced bone mineral density and increased risk for hip fracture.* Ann Intern Med, 1998. **129**(10): p. 770-8.
332. Opotowsky, A.R., J.P. Bilezikian, and N.I.f.-u. study, *Serum vitamin A concentration and the risk of hip fracture among women 50 to 74 years old in the United States: a prospective analysis of the NHANES I follow-up study.* Am J Med, 2004. **117**(3): p. 169-74.
333. Penniston, K.L., et al., *Serum retinyl esters are not elevated in postmenopausal women with and without osteoporosis whose preformed vitamin A intakes are high.* Am J Clin Nutr, 2006. **84**(6): p. 1350-6.
334. Promislow, J.H., et al., *Retinol intake and bone mineral density in the elderly: the Rancho Bernardo Study.* J Bone Miner Res, 2002. **17**(8): p. 1349-58.
335. Barker, M.E., et al., *Serum retinoids and beta-carotene as predictors of hip and other fractures in elderly women.* J Bone Miner Res, 2005. **20**(6): p. 913-20.
336. Houtkooper, L.B., et al., *Nutrients, body composition and exercise are related to change in bone mineral density in premenopausal women.* J Nutr, 1995. **125**(5): p. 1229-37.
337. Maggio, D., et al., *Marked decrease in plasma antioxidants in aged osteoporotic women: results of a cross-sectional study.* J Clin Endocrinol Metab, 2003. **88**(4): p. 1523-7.
338. Maggio, D., et al., *Low levels of carotenoids and retinol in involutional osteoporosis.* Bone, 2006. **38**(2): p. 244-8.
339. Ballew, C., D. Galuska, and C. Gillespie, *High serum retinyl esters are not associated with reduced bone mineral density in the Third National Health And Nutrition Examination Survey, 1988-1994.* J Bone Miner Res, 2001. **16**(12): p. 2306-12.
340. Kaptoge, S., et al., *Effects of dietary nutrients and food groups on bone loss from the proximal femur in men and women in the 7th and 8th decades of age.* Osteoporos Int, 2003. **14**(5): p. 418-28.
341. Kawahara, T.N., et al., *Short-term vitamin A supplementation does not affect bone turnover in men.* J Nutr, 2002. **132**(6): p. 1169-72.
342. Rejnmark, L., et al., *No effect of vitamin A intake on bone mineral density and fracture risk in perimenopausal women.* Osteoporos Int, 2004. **15**(11): p. 872-80.
343. Sowers, M.F. and R.B. Wallace, *Retinol, supplemental vitamin A and bone status.* J Clin Epidemiol, 1990. **43**(7): p. 693-9.
344. Vestergaard, P., L. Rejnmark, and L. Mosekilde, *High-dose treatment with vitamin A analogues and risk of fractures.* Arch Dermatol, 2010. **146**(5): p. 478-82.
345. Wolf, R.L., et al., *Lack of a relation between vitamin and mineral antioxidants and bone mineral density: results from the Women's Health Initiative.* Am J Clin Nutr, 2005. **82**(3): p. 581-8.
346. Green, A.C., T.J. Martin, and L.E. Purton, *The role of vitamin A and retinoic acid receptor signaling in post-natal maintenance of bone.* J Steroid Biochem Mol Biol, 2016. **155**(Pt A): p. 135-46.
347. Henning, P., H.H. Conaway, and U.H. Lerner, *Retinoid receptors in bone and their role in bone remodeling.* Front Endocrinol (Lausanne), 2015. **6**: p. 31.
348. Wu, A.M., et al., *The relationship between vitamin A and risk of fracture: meta-analysis of prospective studies.* J Bone Miner Res, 2014. **29**(9): p. 2032-9.

349. Noyes, J.J., et al., *Premature Epiphyseal Closure of the Lower Extremities Contributing to Short Stature after cis-Retinoic Acid Therapy in Medulloblastoma: A Case Report*. *Horm Res Paediatr*, 2016. **85**(1): p. 69-73.
350. Kneissel, M., et al., *Retinoid-induced bone thinning is caused by subperiosteal osteoclast activity in adult rodents*. *Bone*, 2005. **36**(2): p. 202-14.
351. Shimono, K., et al., *Potent inhibition of heterotopic ossification by nuclear retinoic acid receptor-gamma agonists*. *Nat Med*, 2011. **17**(4): p. 454-60.
352. Jedeon, K., et al., *Estrogen and bisphenol A affect male rat enamel formation and promote ameloblast proliferation*. *Endocrinology*, 2014. **155**(9): p. 3365-75.
353. Farah, R.A., et al., *Protein content of molar-incisor hypomineralisation enamel*. *J Dent*, 2010. **38**(7): p. 591-6.
354. AlQahtani, S.J., M.P. Hector, and H.M. Liversidge, *Brief communication: The London atlas of human tooth development and eruption*. *Am J Phys Anthropol*, 2010. **142**(3): p. 481-90.
355. Jälevik, B., *Prevalence and Diagnosis of Molar-Incisor- Hypomineralisation (MIH): A systematic review*. *Eur Arch Paediatr Dent*, 2010. **11**(2): p. 59-64.
356. Negre-Barber, A., et al., *Hypomineralized Second Primary Molars as Predictor of Molar Incisor Hypomineralization*. *Sci Rep*, 2016. **6**: p. 31929.
357. Mittal, N. and B.B. Sharma, *Hypomineralised second primary molars: prevalence, defect characteristics and possible association with Molar Incisor Hypomineralisation in Indian children*. *Eur Arch Paediatr Dent*, 2015. **16**(6): p. 441-7.
358. Ghanim, A., et al., *Prevalence of demarcated hypomineralisation defects in second primary molars in Iraqi children*. *Int J Paediatr Dent*, 2013. **23**(1): p. 48-55.
359. Silva, M.J., et al., *Etiology of molar incisor hypomineralization - A systematic review*. *Community Dent Oral Epidemiol*, 2016. **44**(4): p. 342-53.
360. Jälevik, B. and G.A. Klingberg, *Dental treatment, dental fear and behaviour management problems in children with severe enamel hypomineralization of their permanent first molars*. *Int J Paediatr Dent*, 2002. **12**(1): p. 24-32.
361. Weerheijm, K.L., et al., *Judgement criteria for molar incisor hypomineralisation (MIH) in epidemiologic studies: a summary of the European meeting on MIH held in Athens, 2003*. *Eur J Paediatr Dent*, 2003. **4**(3): p. 110-3.
362. Alaluusua, S., *Aetiology of Molar-Incisor Hypomineralisation: A systematic review*. *Eur Arch Paediatr Dent*, 2010. **11**(2): p. 53-8.
363. Crombie, F., D. Manton, and N. Kilpatrick, *Aetiology of molar-incisor hypomineralization: a critical review*. *Int J Paediatr Dent*, 2009. **19**(2): p. 73-83.
364. Clarkson, J. and D. O'Mullane, *A modified DDE Index for use in epidemiological studies of enamel defects*. *J Dent Res*, 1989. **68**(3): p. 445-50.
365. Vieira, A.R. and E. Kup, *On the Etiology of Molar-Incisor Hypomineralization*. *Caries Res*, 2016. **50**(2): p. 166-9.
366. Allazzam, S.M., S.M. Alaki, and O.A.S. El Meligy, *Molar Incisor Hypomineralization, Prevalence, and Etiology*. *International Journal of Dentistry*, 2014. **2014**: p. 8.
367. Gottberg, B., et al., *Prenatal effects by exposing to amoxicillin on dental enamel in Wistar rats*. *Med Oral Patol Oral Cir Bucal*, 2014. **19**(1): p. e38-43.
368. Mihalaş, E., et al., *The Role of Chronic Exposure to Amoxicillin/Clavulanic Acid on the Developmental Enamel Defects in Mice*. *Toxicol Pathol*, 2016. **44**(1): p. 61-70.
369. Nazir, S., A. Ali, and S. Zaidi, *Micro Hardness of Dental Tissues Influenced by Administration of Aspirin During Pregnancy*. *International Journal of Morphology*, 2015. **33**(2).

370. Nazir, S., et al., *Effect of aspirin on the developing teeth of neonates*. Int. j. morphol, 2011. **29**(1): p. 278-285.
371. Jedeon, K., et al., *Chronic Exposure to Bisphenol A Exacerbates Dental Fluorosis in Growing Rats*. J Bone Miner Res, 2016. **31**(11): p. 1955-1966.
372. Bronckers, A.L., D.M. Lyaruu, and P.K. DenBesten, *The impact of fluoride on ameloblasts and the mechanisms of enamel fluorosis*. J Dent Res, 2009. **88**(10): p. 877-93.
373. Jedeon, K., A. Berdal, and A. Babajko, *Impact of three endocrine disruptors, Bisphenol A, Genistein and Vinclozolin on female rat enamel*. Bull Group Int Rech Sci Stomatol Odontol, 2016. **53**(1): p. e28.
374. Jedeon, K., et al., *Enamel hypomineralization due to endocrine disruptors*. Connect Tissue Res, 2014. **55 Suppl 1**: p. 43-7.
375. Sidaly, R., et al., *The effect of hypoxia on the formation of mouse incisor enamel*. Arch Oral Biol, 2015. **60**(11): p. 1601-12.
376. Yeh, C.K., et al., *Hyperglycemia and xerostomia are key determinants of tooth decay in type 1 diabetic mice*. Lab Invest, 2012. **92**(6): p. 868-82.
377. Matsumura, S., et al., *IGF-1 Mediates EphrinB1 Activation in Regulating Tertiary Dentin Formation*. J Dent Res, 2017: p. 22034517708572.
378. Gibert, Y., et al., *Altered retinoic acid signalling underpins dentition evolution*. Proc Biol Sci, 2015. **282**(1802).
379. Seritrakul, P., et al., *Retinoic acid expands the evolutionarily reduced dentition of zebrafish*. FASEB J, 2012. **26**(12): p. 5014-24.
380. Dimitrova-Nakov, S., et al., *Deletion of serotonin 2B receptor provokes structural alterations of mouse dental tissues*. Calcif Tissue Int, 2014. **94**(3): p. 293-300.
381. Dong, Q., et al., *The morphology and mineralization of dental hard tissue in the offspring of passive smoking rats*. Arch Oral Biol, 2011. **56**(10): p. 1005-13.
382. Prasad, M.K., et al., *A targeted next-generation sequencing assay for the molecular diagnosis of genetic disorders with orodental involvement*. J Med Genet, 2016. **53**(2): p. 98-110.
383. Rakhshan, V., *Meta-Analysis of Observational Studies on the Most Commonly Missing Permanent Dentition (Excluding the Third Molars) in Non-Syndromic Dental Patients or Randomly-Selected Subjects, and the Factors Affecting the Observed Rates*. J Clin Pediatr Dent, 2015. **39**(3): p. 199-207.
384. Nunn, J.H., et al., *The interdisciplinary management of hypodontia: background and role of paediatric dentistry*. Br Dent J, 2003. **194**(5): p. 245-51.
385. Polder, B.J., et al., *A meta-analysis of the prevalence of dental agenesis of permanent teeth*. Community Dent Oral Epidemiol, 2004. **32**(3): p. 217-26.
386. Fekonja, A., *Hypodontia in orthodontically treated children*. Eur J Orthod, 2005. **27**(5): p. 457-60.
387. Rakhshan, V., *Congenitally missing teeth (hypodontia): A review of the literature concerning the etiology, prevalence, risk factors, patterns and treatment*. Dent Res J (Isfahan), 2015. **12**(1): p. 1-13.
388. Galluccio, G. and A. Pilotto, *Genetics of dental agenesis: anterior and posterior area of the arch*. Eur Arch Paediatr Dent, 2008. **9**(1): p. 41-5.
389. Militi, D., et al., *Genetic basis of non syndromic hypodontia: a DNA investigation performed on three couples of monozygotic twins about PAX9 mutation*. Eur J Paediatr Dent, 2011. **12**(1): p. 21-4.
390. Thesleff, I., *The genetic basis of tooth development and dental defects*. Am J Med Genet A, 2006. **140**(23): p. 2530-5.

391. Frazier-Bowers, S.A., et al., *A novel mutation in human PAX9 causes molar oligodontia*. J Dent Res, 2002. **81**(2): p. 129-33.
392. De Muynck, S., et al., *A novel MSXI mutation in hypodontia*. Am J Med Genet A, 2004. **128A**(4): p. 401-3.
393. Rajab, L.D. and M.A. Hamdan, *Supernumerary teeth: review of the literature and a survey of 152 cases*. Int J Paediatr Dent, 2002. **12**(4): p. 244-54.
394. Lubinsky, M. and P.N. Kantaputra, *Syndromes with supernumerary teeth*. Am J Med Genet A, 2016. **170**(10): p. 2611-6.
395. Koch, G., *Pediatric dentistry: a clinical approach*. 2017: John Wiley & Sons.
396. AlZamel, G., S. Odell, and M. Mupparapu, *Developmental Disorders Affecting Jaws*. Dent Clin North Am, 2016. **60**(1): p. 39-90.
397. Forlino, A. and J.C. Marini, *Osteogenesis imperfecta*. Lancet, 2016. **387**(10028): p. 1657-71.
398. Xiao, S., et al., *Dentinogenesis imperfecta 1 with or without progressive hearing loss is associated with distinct mutations in DSPP*. Nat Genet, 2001. **27**(2): p. 201-4.
399. Zhang, X., et al., *DSPP mutation in dentinogenesis imperfecta Shields type II*. Nat Genet, 2001. **27**(2): p. 151-2.
400. Yamakoshi, Y., *Dentin Sialophosphoprotein (DSPP) and Dentin*. J Oral Biosci, 2008. **50**(1): p. 33-44.
401. de La Dure-Molla, M., B. Philippe Fournier, and A. Berdal, *Isolated dentinogenesis imperfecta and dentin dysplasia: revision of the classification*. Eur J Hum Genet, 2015. **23**(4): p. 445-51.
402. Backman, B., *Amelogenesis imperfecta--clinical manifestations in 51 families in a northern Swedish county*. Scand J Dent Res, 1988. **96**(6): p. 505-16.
403. Seow, W., *Developmental defects of enamel and dentine: challenges for basic science research and clinical management*. Australian dental journal, 2014. **59**(s1): p. 143-154.
404. Coffield, K.D., et al., *The psychosocial impact of developmental dental defects in people with hereditary amelogenesis imperfecta*. J Am Dent Assoc, 2005. **136**(5): p. 620-30.
405. Smith, C.E.L., et al., *Amelogenesis Imperfecta; Genes, Proteins, and Pathways*. Front Physiol, 2017. **8**: p. 435.
406. Cobourne, M.T. and P.T. Sharpe, *Diseases of the tooth: the genetic and molecular basis of inherited anomalies affecting the dentition*. Wiley Interdiscip Rev Dev Biol, 2013. **2**(2): p. 183-212.
407. Bartlett, J.D., *Dental enamel development: proteinases and their enamel matrix substrates*. ISRN Dent, 2013. **2013**: p. 684607.
408. Bartlett, J.D. and C.E. Smith, *Modulation of cell-cell junctional complexes by matrix metalloproteinases*. J Dent Res, 2013. **92**(1): p. 10-7.
409. Chan, H.C., et al., *Target gene analyses of 39 amelogenesis imperfecta kindreds*. Eur J Oral Sci, 2011. **119** Suppl 1: p. 311-23.
410. Kim, J.W., et al., *Mutational analysis of candidate genes in 24 amelogenesis imperfecta families*. Eur J Oral Sci, 2006. **114** Suppl 1: p. 3-12; discussion 39-41, 379.
411. Bloch-Zupan, A., et al., *Homozygosity mapping and candidate prioritization identify mutations, missed by whole-exome sequencing, in SMOC2, causing major dental developmental defects*. Am J Hum Genet, 2011. **89**(6): p. 773-81.
412. Laue, K., et al., *Craniosynostosis and multiple skeletal anomalies in humans and zebrafish result from a defect in the localized degradation of retinoic acid*. Am J Hum Genet, 2011. **89**(5): p. 595-606.

413. Hirst, K.L., et al., *Elucidation of the sequence and the genomic organization of the human dentin matrix acidic phosphoprotein 1 (DMP1) gene: exclusion of the locus from a causative role in the pathogenesis of dentinogenesis imperfecta type II*. Genomics, 1997. **42**(1): p. 38-45.
414. Lorenz-Depiereux, B., et al., *DMP1 mutations in autosomal recessive hypophosphatemia implicate a bone matrix protein in the regulation of phosphate homeostasis*. Nat Genet, 2006. **38**(11): p. 1248-50.
415. Feng, J.Q., et al., *Loss of DMP1 causes rickets and osteomalacia and identifies a role for osteocytes in mineral metabolism*. Nat Genet, 2006. **38**(11): p. 1310-5.
416. Takagi, Y. and S. Sasaki, *A probable common disturbance in the early stage of odontoblast differentiation in Dentinogenesis imperfecta type I and type II*. J Oral Pathol, 1988. **17**(5): p. 208-12.
417. Rajpar, M.H., et al., *Mutation of the signal peptide region of the bicistronic gene DSPP affects translocation to the endoplasmic reticulum and results in defective dentine biomineralization*. Hum Mol Genet, 2002. **11**(21): p. 2559-65.
418. Song, Y.L., et al., *Dentin phosphoprotein frameshift mutations in hereditary dentin disorders and their variation patterns in normal human population*. J Med Genet, 2008. **45**(7): p. 457-64.
419. Kärman, C., et al., *Mapping of the locus for autosomal dominant amelogenesis imperfecta (AIH2) to a 4-Mb YAC contig on chromosome 4q11-q21*. Genomics, 1997. **39**(2): p. 164-70.
420. Rajpar, M.H., et al., *Mutation of the gene encoding the enamel-specific protein, enamelin, causes autosomal-dominant amelogenesis imperfecta*. Hum Mol Genet, 2001. **10**(16): p. 1673-7.
421. Mårdh, C.K., et al., *A nonsense mutation in the enamelin gene causes local hypoplastic autosomal dominant amelogenesis imperfecta (AIH2)*. Hum Mol Genet, 2002. **11**(9): p. 1069-74.
422. Hart, T.C., et al., *Novel ENAM mutation responsible for autosomal recessive amelogenesis imperfecta and localised enamel defects*. J Med Genet, 2003. **40**(12): p. 900-6.
423. Tekin, M., et al., *Homozygous mutations in fibroblast growth factor 3 are associated with a new form of syndromic deafness characterized by inner ear agenesis, microtia, and microdontia*. Am J Hum Genet, 2007. **80**(2): p. 338-44.
424. Alsmadi, O., et al., *Syndromic congenital sensorineural deafness, microtia and microdontia resulting from a novel homoallelic mutation in fibroblast growth factor 3 (FGF3)*. Eur J Hum Genet, 2009. **17**(1): p. 14-21.
425. Gregory-Evans, C.Y., et al., *SNP genome scanning localizes oto-dental syndrome to chromosome 11q13 and microdeletions at this locus implicate FGF3 in dental and inner-ear disease and FADD in ocular coloboma*. Hum Mol Genet, 2007. **16**(20): p. 2482-93.
426. Sensi, A., et al., *LAMM syndrome with middle ear dysplasia associated with compound heterozygosity for FGF3 mutations*. Am J Med Genet A, 2011. **155A**(5): p. 1096-101.
427. Mundlos, S., et al., *Mutations involving the transcription factor CBFA1 cause cleidocranial dysplasia*. Cell, 1997. **89**(5): p. 773-9.
428. Quack, I., et al., *Mutation analysis of core binding factor A1 in patients with cleidocranial dysplasia*. Am J Hum Genet, 1999. **65**(5): p. 1268-78.
429. Zhou, G., et al., *CBFA1 mutation analysis and functional correlation with phenotypic variability in cleidocranial dysplasia*. Hum Mol Genet, 1999. **8**(12): p. 2311-6.

430. Bergwitz, C., et al., *Identification of novel CBFA1/RUNX2 mutations causing cleidocranial dysplasia*. J Inherit Metab Dis, 2001. **24**(6): p. 648-56.
431. Yoshida, T., et al., *Functional analysis of RUNX2 mutations in Japanese patients with cleidocranial dysplasia demonstrates novel genotype-phenotype correlations*. Am J Hum Genet, 2002. **71**(4): p. 724-38.
432. Zheng, Q., et al., *Dysregulation of chondrogenesis in human cleidocranial dysplasia*. Am J Hum Genet, 2005. **77**(2): p. 305-12.
433. Fernandez, B.A., et al., *Holoprosencephaly and cleidocranial dysplasia in a patient due to two position-effect mutations: case report and review of the literature*. Clin Genet, 2005. **68**(4): p. 349-59.
434. Baumert, U., et al., *Cleidocranial dysplasia: molecular genetic analysis and phenotypic-based description of a Middle European patient group*. Am J Med Genet A, 2005. **139A**(2): p. 78-85.
435. El-Gharbawy, A.H., et al., *Severe cleidocranial dysplasia and hypophosphatasia in a child with microdeletion of the C-terminal region of RUNX2*. Am J Med Genet A, 2010. **152A**(1): p. 169-74.
436. Halal, F., et al., *Metaphyseal dysplasia with maxillary hypoplasia and brachydactyly*. Am J Med Genet, 1982. **13**(1): p. 71-9.
437. Moffatt, P., et al., *Metaphyseal dysplasia with maxillary hypoplasia and brachydactyly is caused by a duplication in RUNX2*. Am J Hum Genet, 2013. **92**(2): p. 252-8.
438. Simsek Kiper, P.O., et al., *Cortical-Bone Fragility--Insights from sFRP4 Deficiency in Pyle's Disease*. N Engl J Med, 2016. **374**(26): p. 2553-62.
439. Alfawaz, S., et al., *Recessive oligodontia linked to a homozygous loss-of-function mutation in the SMOC2 gene*. Arch Oral Biol, 2013. **58**(5): p. 462-6.
440. Hamel, B.C., et al., *Familial X-linked mental retardation and isolated growth hormone deficiency: clinical and molecular findings*. Am J Med Genet, 1996. **64**(1): p. 35-41.
441. Laumonier, F., et al., *Transcription factor SOX3 is involved in X-linked mental retardation with growth hormone deficiency*. Am J Hum Genet, 2002. **71**(6): p. 1450-5.
442. Solomon, N.M., et al., *Array comparative genomic hybridisation analysis of boys with X linked hypopituitarism identifies a 3.9 Mb duplicated critical region at Xq27 containing SOX3*. J Med Genet, 2004. **41**(9): p. 669-78.
443. Solomon, N.M., et al., *Array comparative genomic hybridisation analysis of boys with X-linked hypopituitarism identifies a 3.9 Mb duplicated critical region at Xq27 containing SOX3*. J Med Genet, 2007. **44**(4): p. e75.
444. Woods, K.S., et al., *Over- and underdosage of SOX3 is associated with infundibular hypoplasia and hypopituitarism*. Am J Hum Genet, 2005. **76**(5): p. 833-49.
445. Bowl, M.R., et al., *An interstitial deletion-insertion involving chromosomes 2p25.3 and Xq27.1, near SOX3, causes X-linked recessive hypoparathyroidism*. J Clin Invest, 2005. **115**(10): p. 2822-31.
446. Sutton, E., et al., *Identification of SOX3 as an XX male sex reversal gene in mice and humans*. J Clin Invest, 2011. **121**(1): p. 328-41.
447. Vetro, A., et al., *Testis development in the absence of SRY: chromosomal rearrangements at SOX9 and SOX3*. Eur J Hum Genet, 2015. **23**(8): p. 1025-32.
448. Stagi, S., et al., *A SOX3 (Xq26.3-27.3) duplication in a boy with growth hormone deficiency, ocular dyspraxia, and intellectual disability: a long-term follow-up and literature review*. Hormones (Athens), 2014. **13**(4): p. 552-60.

449. Haines, B., et al., *Interchromosomal insertional translocation at Xq26.3 alters SOX3 expression in an individual with XX male sex reversal*. J Clin Endocrinol Metab, 2015. **100**(5): p. E815-20.
450. Igarashi, M., et al., *SOX3 Overdosage Permits Normal Sex Development in Females with Random X Inactivation*. Sex Dev, 2015. **9**(3): p. 125-9.
451. Muñoz, J., et al., *The Lgr5 intestinal stem cell signature: robust expression of proposed quiescent '+4' cell markers*. EMBO J, 2012. **31**(14): p. 3079-91.
452. Gerarduzzi, C., et al., *Silencing SMOC2 ameliorates kidney fibrosis by inhibiting fibroblast to myofibroblast transformation*. JCI Insight, 2017. **2**(8).
453. Keane, T.M., et al., *Mouse genomic variation and its effect on phenotypes and gene regulation*. Nature, 2011. **477**(7364): p. 289-94.
454. Marchant, T.W., et al., *Canine Brachycephaly Is Associated with a Retrotransposon-Mediated Missplicing of SMOC2*. Curr Biol, 2017. **27**(11): p. 1573-1584.e6.
455. Jeong, H.G., et al., *Risk factors of osteonecrosis of the jaw after tooth extraction in osteoporotic patients on oral bisphosphonates*. Imaging Sci Dent, 2017. **47**(1): p. 45-50.
456. Pazianas, M., *Osteonecrosis of the jaw and the role of macrophages*. J Natl Cancer Inst, 2011. **103**(3): p. 232-40.
457. Liu, P., et al., *The SPARC-related factor SMOC-2 promotes growth factor-induced cyclin D1 expression and DNA synthesis via integrin-linked kinase*. Mol Biol Cell, 2008. **19**(1): p. 248-61.
458. Maier, S., M. Paulsson, and U. Hartmann, *The widely expressed extracellular matrix protein SMOC-2 promotes keratinocyte attachment and migration*. Exp Cell Res, 2008. **314**(13): p. 2477-87.
459. Su, J.R., J.H. Kuai, and Y.Q. Li, *Smoc2 potentiates proliferation of hepatocellular carcinoma cells via promotion of cell cycle progression*. World J Gastroenterol, 2016. **22**(45): p. 10053-10063.
460. Shvab, A., et al., *Induction of the intestinal stem cell signature gene SMOC-2 is required for L1-mediated colon cancer progression*. Oncogene, 2016. **35**(5): p. 549-57.
461. Kim, S., et al., *IL-36 Induces Bisphosphonate-Related Osteonecrosis of the Jaw-Like Lesions in Mice by Inhibiting TGF- β -Mediated Collagen Expression*. J Bone Miner Res, 2017. **32**(2): p. 309-318.
462. Zhang, Q., et al., *IL-17-mediated M1/M2 macrophage alteration contributes to pathogenesis of bisphosphonate-related osteonecrosis of the jaws*. Clin Cancer Res, 2013. **19**(12): p. 3176-88.
463. Yu, Y.R., et al., *A Protocol for the Comprehensive Flow Cytometric Analysis of Immune Cells in Normal and Inflamed Murine Non-Lymphoid Tissues*. PLoS One, 2016. **11**(3): p. e0150606.
464. Heinemann, C., et al., *Development of an osteoblast/osteoclast co-culture derived by human bone marrow stromal cells and human monocytes for biomaterials testing*. Eur Cell Mater, 2011. **21**: p. 80-93.
465. Kozopas, K.M., et al., *MCLI, a gene expressed in programmed myeloid cell differentiation, has sequence similarity to BCL2*. Proc Natl Acad Sci U S A, 1993. **90**(8): p. 3516-20.
466. Seshasayee, D., et al., *A novel in vivo role for osteoprotegerin ligand in activation of monocyte effector function and inflammatory response*. J Biol Chem, 2004. **279**(29): p. 30202-9.
467. Rocnik, E.F., et al., *The novel SPARC family member SMOC-2 potentiates angiogenic growth factor activity*. J Biol Chem, 2006. **281**(32): p. 22855-64.

468. De Smet, F., et al., *Mechanisms of vessel branching: filopodia on endothelial tip cells lead the way*. *Arterioscler Thromb Vasc Biol*, 2009. **29**(5): p. 639-49.
469. Vitorino, P. and T. Meyer, *Modular control of endothelial sheet migration*. *Genes Dev*, 2008. **22**(23): p. 3268-81.
470. Sainson, R.C., et al., *TNF primes endothelial cells for angiogenic sprouting by inducing a tip cell phenotype*. *Blood*, 2008. **111**(10): p. 4997-5007.
471. Brady, J.J., et al., *An Arntl2-Driven Secretome Enables Lung Adenocarcinoma Metastatic Self-Sufficiency*. *Cancer Cell*, 2016. **29**(5): p. 697-710.

Supawich MORKMUED

Clinical, preclinical and translational approaches of orodontal anomalies associated with rare diseases

Résumé

Les anomalies bucco-dentaires et crânio-faciales sont des manifestations phénotypiques des maladies rares. Ce doctorat combine les approches cliniques, précliniques et translationnelles en particulier par l'étude des modèles murins génétiquement modifiés reproduisant les maladies rares étudiées. Ce doctorat vise ainsi à identifier des gènes impliqués dans la morphogenèse et la signalisation inter-cellulaire en s'intéressant aux facteurs environnementaux et génétiques. Une étude détaille les effets d'un facteur d'environnement l'acide rétinoïque en excès sur du développement dentaire et la formation de l'émail. Les anomalies dentaires et de la formation de l'émail sont analysées dans des modèles murins, de maladies rares génétiques, inactivés pour *Ltbp3* et *Smoc2*. Ces résultats permettent une meilleure compréhension du développement dentaire et crânio-facial, pourraient déboucher sur la mise au point et l'amélioration de traitements appropriés et de stratégies thérapeutiques applicables à la prise en charge de patients atteints de maladies rares. L'approche via les modèles murins des maladies rares est tout à fait pertinente pour suivre la régénération osseuse et les pathologies associées.

Mots-clés : dent, génétique, syndrome, environnement, souris, développement, anomalies

Résumé en anglais

The goal of this thesis is to investigate genetic and environmental factors, both initiating and influencing signaling centers that regulate tooth development and thus producing associated defects. Essentially, my research program utilizes patient-based rare disease phenotypes to create novel mouse models. This study also involved investigating the developmental effects of excess retinoic acid on enamel formation to gain understanding of the mechanisms by which environmental factors can alter enamel development. Other studies investigated enamel and dental anomalies in *Ltbp3* and *Smoc2* mutant mice. These results advance our understanding of tooth development, and may translate towards optimizing clinical diagnosis, and improving treatment strategies for several human rare diseases. An improved understanding of rare disease models and our testing of clinically relevant approaches using rodent models is a feasible approach to address bone degeneration problems.

Key words: tooth, genetic, syndromes, environment, mouse, development, abnormalities